Identifying hominin remains in Siberia using peptide mass fingerprinting (ZooMS)

Dissertation

der Mathematisch-Naturwissenschaftlichen Fakultät

der Eberhard Karls Universität Tübingen

zur Erlangung des Grades eines

Doktors der Naturwissenschaften

(Dr. rer. nat.)

vorgelegt von

Samantha Brown

aus Mulgrave, Australien

Tübingen

2021

Gedruckt mit Genehmigung der Mathematisch-Naturwissenschaftlichen Fakultät der Eberhard Karls Universität Tübingen.

Tag der mündlichen Qualifikation:	26.02.2021
Stellvertretender Dekan:	Prof. Dr. József Fortágh
1. Berichterstatter:	Prof. Nicholas Conard
2. Berichterstatter:	Dr. Katerina Douka

Table of Contents

Acknowledgements

This research would not be possible without the substantial international network of people and organisations which have given their time and expertise to making it possible. In no particular order I would like to thank;

Katerina Douka and Tom Higham, you have supported me from the beginning of this journey and trusted me to do this work. I am incredibly grateful to you both for your guidance not only in this dissertation but during my MSc as well. Katerina, being your PhD student has been such a fantastic experience, I thank you for encouraging me throughout. I have grown so much as a researcher over the last three years and this is in large part because of you.

The Max Planck Institute for the Science of Human History and all of my colleagues. I have loved my time at the institute and consider myself very lucky to have worked here. I have been inspired every day by conversations with colleagues and have worked alongside people I respect and admire. Thank you to all who have supported me over the past three years, this dissertation would not have been possible without the support of so many people here. While it is impossible to thank everyone individually here, I would especially like to thank Nils Vanwezer, Shevan Wilkin, and Elizabeth Nelson.

Institute for Archeology and Ethnography for the Siberian branch of the Russian Academy of Sciences. In particular, I would like to thank Maxim Kozlikin, Michael Shunkov, Anatoly Derevianko, Andrei Krivoshapkin, Kseniya Kolobova, and Svetlana Schnaider. Thank you for trusting me to carry out this work and for lending your expertise to so much of my research.

The University of Oxford, particularly the Research Laboratory for Archaeology and the History of Art. Since the beginning of my MSc, the researchers and staff at RLAHA have been a constant source of support. Thank you for teaching me and lending support and advice whenever I needed it.

The staff and researchers of the University of Tübingen. Thank you for welcoming me and offering me so much support. It is such a privilege to submit my dissertation to the University.

To my family, Jeneine Walsh-Hevey, Eric Brown, Michael Hevey, Sharon Challen, Joshua Brown, Jarryd Brown, Jordyn Brown, Bianca Anstis, Blake Brown, Quinn Brown, and Sally Jope. I would not be the person I am today without you all. Being so far away from all of you, especially during this horrible pandemic, has been really tough. I miss you all every day and this dissertation is dedicated to all of you.

Finally, Blair Jope. I don't really know how to thank you for everything you have done for me. You're my champion and my best friend. Love you always.

It's been an incredible three years, thank you all.

Summary

The scarcity of human remains from Pleistocene Northern Asia is a significant limiting factor in understanding the course of human evolution in this part of the world. The high degree of fragmentation of bones in Siberia has limited our ability to identify and better understand the hominin groups present in the region between 300 – 50 ka (thousand years ago). In this dissertation, I address the dearth of human fossils in the region by screening thousands of non-diagnostic bone fragments using a peptide mass fingerprinting method known as Zooarchaeology by Mass Spectrometry (ZooMS). ZooMS allows for efficient and reliable taxonomic identification of bone collagen and here I apply it to six sites from Middle and Late Pleistocene contexts. In total, 8,921 unidentified bone fragments were analysed using ZooMS and resulted in the discovery of nine new hominin fragments including the oldest known Denisovan fossils (Denisova 18, 19, 20, 21), two Middle Palaeolithic Neanderthals (Denisova 15 and Denisova 17), two hominins linked with Upper Palaeolithic assemblages (Denisova 14 and Denisova 16), and one which had been previously misidentified as a bear parietal fragment (Denisova 7).

Parallel to the search for human fossils, large assemblages of faunal remains were also identified. These were compared against the zooarchaeological record of Denisova Cave which was established previously using traditional methods. The comparison helped identify the potential biological, depositional, and taphonomic factors responsible for the accumulation and fragmentation of the bones at the site. Bones identified using ZooMS from Denisova Cave were also used to create isotopic baselines, essential for studying Pleistocene hominin diet in the Altai Mountains. This revealed instances of extreme isotopic variation especially with regards to some of the humans, leading to the identification of the highest C and N isotope values currently reported for Neanderthals.

Finally, a subset of bones (2,501) were used to map glutamine deamidation and test the efficacy of this technique in understanding protein degradation as a function of time and as means of assessing the relative age of the hominin fossils. This technique

has been used recently to test the antiquity of unprovenanced fossils, however, our results revealed that too much variability is observed even within a single layer to be able to securely identify intrusive or unprovenanced fossils.

This work is the largest application of ZooMS on an archaeological assemblage and the results confirm our hypothesis that bone assemblages which are routinely excavated from Pleistocene-age sites, in Siberia and elsewhere, present an important untapped source of archaeological information. The data reported in this dissertation stem solely from fragmented bones that could not be identified on the basis of morphology. High throughput analysis of such material has the potential for groundbreaking discoveries and should become a routine component of the archaeological tool kit.

Zusammenfassung

Der Mangel menschlicher Überreste aus dem pleistozänen Nordasien erschwert das Verständnis über den Verlauf der menschlichen Evolution in diesem Teil der Welt. Der hohe Fragmentierungsgrad der Knochen in Sibirien stellte oftmals ein Problem für Archäolog*innen dar, die die Präsenz menschlicher Gruppen in dieser Region vor 300-50 ka (tausend Jahren) untersuchten. Ziel dieser Dissertation ist die Bearbeitung (dieses Forschungsdesiderats), durch die Untersuchung tausender nicht-diagnostischer Knochenfragmente mit Hilfe einer *peptides mass fingerprinting*-Methode, bekannt *als Zooarchaeology by Mass Spectrometry (ZooMS)*. ZooMS ermöglicht eine effiziente und zuverlässige taxonomische Identifizierung von Knochenkollagen aus Kontexten des Mittel- und Spätpleistozäns. Insgesamt wurden 8921 nicht morphologisch identifizierbare Knochenfragmente mittels ZooMS analysiert, was zur Entdeckung von neun neuen menschlichen Fragmenten geführt hat, inklusive der ältesten bekannten Denisova-Fragmente (Denisova 18, 19, 20, 21), zwei mittelpaläolithischer Neanderthaler (Denisova 15 und Denisova 17), zwei Überreste, die mit Assemblagen des Jungpaläolithikums verbunden sind (Denisova 14 und Denisova 16) und eines, welche vorher fälschlicherweise als parietales Bärenfragment identifiziert worden war (Denisova 7).

Parallel zu den menschlichen Knochenfragmenten wurden auch große Ansammlungen von Faunaresten identifiziert. Die Ergebnisse wurden mit den bisherigen zooarchälogischen Daten von Denisova verglichen. Der Vergleich half dabei, potenzielle biologische, ablagerungsbedingte und taphonomische Faktoren zu identifizieren, die für die Anhäufung von Knochenfragmenten an dieser Stelle verantwortlich sind. Darüber hinaus wurde die identifizierte Fauna aus der Denisova-Höhle dafür verwendet, die Ernährungsweise von pleistozänen Menschen im Altaigebirge via Isotopenanalyse zu erforschen. Dies führte zu den bisherig belegten Höchstwerten der C- und N-Isotopen bei Neanderthalern. Zusätzlich wurde eine Teilmenge von Knochen (2501) verwendet, um die Glutamindeamidierung zu erfassen und die Aussagekraft solcher Techniken beim Verständnis der Proteindegradierung als Funktion der Zeit für die relative Datierung menschlicher Knochen zu testen.

Solche Techniken wurden kürzlich verwendet, um das Alter von unstratifizierten Überresten zu bestimmen. Die vorliegenden Ergebnisse zeigen jedoch, dass selbst innerhalb einer einzelnen Schicht eine zu hohe Variabilität vorliegt, um intrusive Fragmente oder Knochen ohne gesicherte Herkunft, eindeutig zu identifizieren.

Diese Arbeit bildet die größte archäologische Assemblage ab, die jemals mittels ZooMS untersucht wurde. Die Ergebnisse bestätigen die Hypothese, dass Knochenassemblagen, die routinemäßig an pleistozänen Fundstellen in Sibirien und anderswo ausgegraben werden, eine wichtige Quelle an archäologischer Information darstellen. Die Daten dieser Dissertation wurden ausschließlich von fragmentierten Knochen gewonnen, die morphologisch nicht identifiziert werden konnten. Die *high-throughput*-Anwendung bei solchem Material hat das Potential für bahnbrechende Entdeckungen und sollte eine Routineanwendung im archäologischen Methodenspektrum werden.

List of Publications

Accepted Manuscripts (Appendix 1)

Manuscript A - 2019. Douka, K., Slon, V., Jacobs, Z., Ramsey, C.B., Shunkov, M.V., Derevianko, A.P., Mafessoni, F., Kozlikin, M.B., Li, B., Grün, R., Comeskey, D., Devièse, T., Brown, S., Viola, B., Kinsley, L., Buckley, M., Meyer, M., Roberts, R.G., Pääbo, S., Kelso, J., Higham, T. Age estimates for hominin fossils and the onset of the Upper Palaeolithic at Denisova Cave. Nature 565, 640–644.

Manuscript B - 2020. Brown., S., Douka, K., Collins, M., Richter, K. On the standardization of ZooMS nomenclature. Journal of Proteomics.

Submitted Manuscripts (Appendix 2)

Manuscript C - submitted. Brown, S., Massilani, D., Kozlikin, M., Shunkov, M., Derevianko, A., Stoessel, A., Jope-Street, B., Meyer, M., Kelso, J., Pääbo, S., Higham, T., Douka, K. The earliest Denisovans and their cultural adaptation. Nature Ecology and Evolution.

Manuscripts ready for submission (Appendix 3)

Manuscript D - in prep. Brown, S., Wang, N., Oertle, A., Comeskey, D., Jope-Street, B., Harvey, V., Pal Chowdury, M., Kozlikin, M., Shunkov, M., Derevianko, A., Buckley, M., Higham, T., Douka, K. Zooarchaeology through the lens of collagen fingerprinting at Denisova Cave.

Manuscript E - in prep. Brown, S., Wang, N., Oertle, A., Jope-Street, B., Kozlikin, M., Shunkov, M., Derevianko, A., Higham, T., Douka, K., Richter, K. Examining collagen preservation through glutamine deamidation at Denisova Cave.

Manuscript F - in prep. Brown, S., Larsen, T., Roberts, P., Comeskey, D., Kozlikin, M., Shunkov, M., Derevianko, A., Higham, T., Douka, K. Isotopic evidence for the diets of Neanderthals and Denisovans in Siberia.

Contributions

Manuscript A - (Douka et al., 2019) I analysed 2,212 bones from the Main and East chambers of Denisova Cave. I drilled and prepared the samples at the Research Laboratory for Archaeology and the History of Art, School of Archaeology, University of Oxford and extracted and analysed their collagen at the University of Manchester. This work led to the identification of three new hominin bones which were used to create the detailed chronology for the site presented in this paper. I taxonomically identified the samples from the Main Chamber and created the figure for the third hominin identified (Denisova 16). I co-wrote Section 8 of the Supplementary Information with Michael Buckley of the University of Manchester.

Manuscript B - (Brown et al., 2020) I co-developed the proposed ZooMS nomenclature system presented in this paper. I wrote the manuscript and created the tables with the input of all other authors. I created Figure 2 and assisted with the creation of all other figures.

Manuscript C - (Brown et al., submitted) I identified five new hominin fossils from the fragmented bone assemblage of Denisova Cave using ZooMS. Lab work was carried out at the Max Planck Institute for the Science of Human History in Jena. I wrote the manuscript, created the tables, and created the figures with the assistance of all other authors.

Manuscript D - (Brown et al., in prep) I taxonomically identified 5,938 fragmented bones from the East Gallery of Denisova Cave at the Max Planck Institute for the Science of Human History using ZooMS and I analysed the data. I wrote the manuscript and created the figures with the assistance of all other authors.

Manuscript E - (Brown et al., in prep) I prepared and analysed 2,501 peptide mass fingerprints for their deamidation measurements. I prepared the models and wrote the manuscript with the input and assistance of all authors. I created the figures and tables.

Manuscript F - (Brown et al., in prep) I performed the lab work for 266 bulk stable and isotope measurements at the Max Planck Institute for the Science of Human History

and the Research Laboratory for Archaeology and the History of Art, School of Archaeology, University of Oxford. I analysed the data, created the models, and created the figures and tables. I wrote the manuscript with the input and assistance of all authors.

1. Introduction

Identifying the fossils of ancient human populations remains a constant hurdle in Pleistocene archaeological research. Population numbers were likely low, purposeful burials were exceptional, and ideal preservational conditions for bone over hundreds of thousands of years is rare. This scarcity of human fossils across large tracts of the globe has fueled new methods for identifying the traces of their activities, for instance through the identification of their DNA in sediments (Slon et al., 2017a; Zhang et al., 2020) or through metabarcoding (Grealy et al., 2015; Murray et al., 2013). These approaches however fail to address the central problem, that there are too few actual human fossils available for the biomolecular (e.g. genetic, proteomic and isotopic) and anthropological analysis required to better understand the Pleistocene hominin record and human evolution as a whole.

The use of peptide mass fingerprinting (PMF), specifically Zooarchaeology by Mass Spectrometry (ZooMS), has presented itself as an efficient means of screening thousands of bone fragments and taxonomically identifying them. In a handful of cases, it has been used to identify human remains in the archaeological record (Brown et al., 2016; Buckley and Kansa, 2011; Charlton et al., 2016; Devièse et al., 2017; Welker et al., 2016), and it forms the backbone of this dissertation.

Siberia has one of the most complex Pleistocene hominin records outside of Africa, with evidence for multiple overlapping Neanderthal and Denisovan populations throughout the Middle and Upper Pleistocene, followed by the arrival of modern humans in the region (Derevianko et al., 2013; Fu et al., 2014; Krause et al., 2010b; Mafessoni et al., 2020; Peter, 2020; Reich et al., 2010). The intersection of these hominin populations presents a rare opportunity to study their interactions prior to the eventual disappearance of Neanderthals and Denisovans from the archaeological record. However, physical remains of these populations are rarely discovered in Siberia, largely due to the fact that bone assemblages are highly fragmented. As such, despite evidence for the presence of numerous groups of Neanderthals, Denisovans,

and modern humans, large gaps still exist in our understanding of their interactions and migrations throughout the region and in Asia as a whole.

Over that last two decades Asia has (re)emerged as a hotspot of human origins with the identification of at least three new human species identified in Siberia and the Tibetan Plateau (Denisovans) and on island Southeast Asia (*Homo floresiensis*, *Homo luzonensis*). Coupled with the persistence of *Homo erectus* as late as ~110 ka (thousand years ago) (Rizal et al., 2020), and the possible early migrations of archaic modern humans in the region as early as ~120 ka (Bae et al., 2017), there is a critical need to investigate and add to the archaeological and palaeoanthropological records of the continent.

1.1 Fossil evidence for hominins in Siberia

Neanderthals

Neanderthal fossils were first excavated in Siberia at Okladnikov Cave in 1984, located in the northwestern Altai (Figure 1). These excavations identified Mousterian-like lithic technologies, which would come to be known as the Sibiryachikha variant, and the remains of at least four individuals (Derevianko, 2007; Derevianko and Markin, 1992; Derevianko et al., 2013). Genetic analysis, followed by morphological assessment, unequivocally identified these remains as Neanderthals, extending the then known range for the population more than 1500 km to the east (Buzhilova, 2011; Krause et al., 2007; Mednikova, 2011). Neanderthal fossils have subsequently been located at Chagyrskaya Cave and Denisova Cave (Figure 1), indicating that they were present within the Altai Mountains as early as 130 ka (Douka et al., 2019b; Jacobs et al., 2019; Kolobova et al., 2020; Mafessoni et al., 2020; Peter, 2020). Neanderthals at Chagyrskaya Cave share closer technological affinities with the European Micoquian (Kolobova et al., 2020) and are genetically similar to the Neanderthals at Vindija Cave, Croatia (Mafessoni et al., 2020). Multiple populations of Neanderthals are known for Denisova Cave. The mitochondrial DNA for one individual, Denisova 11, is closely related to Neanderthals at Okladnikov Cave. Another individual however, Denisova 5, forms its own clade, separate from other Neanderthals located in the region (Prüfer et

al., 2014). The relationship between these Neanderthal populations and their movement in and out of Siberia is unclear with further fossil evidence necessary to unravel the driving forces behind this.

Denisovans

Denisova Cave is the only site in Siberia in which Denisovans, a sister population to Neanderthals which diverged from their common ancestor approximately 390 ka, have been identified (Krause et al., 2010b; Meyer et al., 2012; Prüfer et al., 2017; Reich et al., 2010; Slon et al., 2018). Denisovans are believed to have inhabited northern, eastern, and south-eastern Asia, and the Pacific where modern day people still carry their DNA (Browning et al., 2018; Jacobs et al., 2019). Genetic evidence has revealed that multiple populations of Denisovans existed and persisted throughout the Pleistocene (Browning et al., 2018; Jacobs et al., 2019). However, the tropical, arid, and windswept regions they inhabited have notoriously poor preservation of bone meaning that, prior to the research presented in this dissertation, only five fossils could be attributed to the Denisovans on the basis of genetic evidence: three molars (Denisova 2, Denisova 4, and Denisova 8), a distal phalanx (Denisova 3), and a piece of fragmentary bone identified using ZooMS (Denisova 11) (Brown et al., 2016; Krause et al., 2010b; Reich et al., 2010; Sawyer et al., 2015; Slon et al., 2018, 2017b). Mitochondrial DNA recovered from these fossils indicates they fall into two broad Denisovan clades, with Denisova 2 (194 – 122 ka) and Denisova 8 (136 – 105 ka) more closely related to one another in comparison with the clade formed by the younger Denisova 3 (76 – 51 ka) and Denisova 4 (84 – 60 ka) fossils (Douka et al., 2019b). Interestingly, nuclear DNA extracted from Denisova 11 indicated that this individual was a first generation offspring of a Neanderthal and a Denisovan (Brown et al., 2016; Slon et al., 2018).

Outside Denisova Cave, a mandible thought to come from Baishiya Cave, Tibet, has been putatively identified as Denisovan on the basis of proteomic evidence (Chen et al., 2019). While several other fossils have been suggested as potential Denisovan candidates (Chen et al., 2019; Li et al., 2017; Xing et al., 2015; Zanolli et al., 2018), there is no DNA evidence to support this.

Understanding who the Deniosvans were, how they interacted with their landscapes, and when they eventually disappeared therefore presents a very different challenge than early research into Neanderthals. Analysis of environmental DNA from soil samples tentatively suggest that they were the earliest inhabitants at Denisova Cave (Slon et al., 2017a), potentially arriving in Siberia around 200 ka or before (Jacobs et al., 2019). Despite their longevity their remains are rarely discovered, necessitating new approaches.

Early Modern Humans

Early modern human remains have so far only been found at a single site in the Altai Mountains, Strashnaya Cave (Figure 1). There, several teeth belonging to juvenile modern humans between 7 – 9 years of age, have been identified in the Upper Palaeolithic Layer 3_1a, which is the youngest Palaeolithic layer for the site dated to ~20 ka (Krivoshapkin et al., 2018; Zubova et al., 2017). The fossils were identified alongside bladelet technology, bone tools, and ornamentation, including red deer incisor pendants and bone needles (Krivoshapkin et al., 2018). This Upper Palaeolithic assemblage is similar to the one found at Denisova Cave where the oldest known bone points and pendants in Eurasia were identified, dated to approximately 48 – 42 ka (Douka et al., 2019b). Excavators at the site have suggested that it could be attributed to the Denisovans themselves (Derevianko et al., 2020) however, the arrival of the Upper Palaeolithic coincides with the estimated age for another modern human fossil, a femur, found at Ust'-Ishim in Western Siberia (Douka et al., 2019b; Fu et al., 2014). This human fossil was located on the banks of the Irtysh River, eroding out of alluvial deposits where Pleistocene fossils are regularly discovered. The Ust'-Ishim femur therefore lacks any archaeological context, however direct radiocarbon analysis and genetic age estimates confirm the femur dates to 45 ka (Fu et al., 2014).

The initial Upper Palaeolithic (IUP), a transitional technology, retaining Levallois productions types alongside novel forms of blade production, as well as the appearance of personal ornamentation and bone tools (Hublin, 2012; Kuhn and Zwyns, 2014), has become an important potential hallmark for modern human presence across northern Asia (Kuhn and Zwyns, 2014). In the Altai Mountains, the IUP is

located at open-air sites Kara-Bom and Ust'-Karakol (Derevianko, 2010; Derevianko and Rybin, 2003; Kuzmin et al., 2004). Further east, in the Transbaikal region of Siberia, the IUP is widespread and located at several sites including Kamenka, Khotyk, and Podzvonkaya (Figure 1). In Siberia, the IUP is thought to appear between 47 – 32 ka (Derevianko and Rybin, 2003; Kuhn and Zwyns, 2014; Kuzmin et al., 2006, 2004) which coincides with the estimated age for the Ust'-Ishim individual. As yet, no hominin fossils have been found in association with the IUP and, despite tantalising suggestions that it coincides with the arrival of humans (Hublin, 2012), at present it is not possible to positively identify who the makers of this transitional technology were. Finding additional modern human fossils in Siberia is key to understanding when and how they arrived in the region, before eventually replacing Neanderthal and Denisovan populations.

1.2 The challenges and approaches to identifying new hominin fossils in Siberia

Preservational issues abound for discovering hominin fossils at Siberian archaeological sites. The identification of hominin fossils at open-air sites for instance is notoriously rare, not only in Siberia but also throughout Europe and the Levant (see for example, Been et al., 2017; Faivre et al., 2014). Open-air sites are subjected to natural weathering processes over time which will typically destroy organic material unless anthropogenic or natural processes lead to their rapid burial. As there is no evidence for anthropogenic burial of hominin remains in Pleistocene Siberia, this problem is further exacerbated.

Cave sites in the Altai often have high levels of hominin and carnivore activity which significantly increases the fragmentation of bone. Butchery practices, bone tool production, carnivore gnawing and digestion, and mechanical pressure, such as compaction and trampling, all exaggerate the extent of bone fragmentation often beyond the point of morphological identification (Shunkov et al., 2020). As a result, large assemblages of non-diagnostic bone fragments are routinely excavated from cave sites in the region. Excavations in the East Chamber of Denisova Cave between 2005 and 2013 for instance, recovered approximately 177,000 bones, 95% of which

had lost all morphologically distinguishing features to allow for taxonomic identification (Jacobs et al., 2019; Vasiliev et al., 2013).

Pilot studies investigating biomolecular approaches as a way of discovering human bones have revealed the worth of screening large assemblages of fragmented bones using ZooMS (i.e. Brown et al., 2016). The aim of this dissertation is to broaden this research to include additional sites and samples in order to increase the number of hominin bones known for Pleistocene Siberia (Douka et al., 2019a).

1.3 Zooarchaeology by Mass Spectrometry (ZooMS)

ZooMS is a biomolecular approach and a form of PMF that is used to assign a taxonomic identification to extracted collagen (Buckley et al., 2009). In mammals, taxonomic resolution using ZooMS usually reaches genus and family levels, however species specific determinations are possible (Buckley et al., 2016, 2014, 2009; Harvey et al., 2019; Welker et al., 2016). The method has become increasingly important in archaeological (i.e. Coutu et al., 2016; Desmond et al., 2018) and cultural heritage studies (i.e. (Fiddyment et al., 2015; Kirby et al., 2013) as it provides a fast, reliable, and relatively cost effective means of identifying samples which can not be identified using traditional zooarchaeological, osteological or other macroscopic analysis.

ZooMS analysis specifically targets type I collagen (COL1), a highly abundant protein in the bone. Typically, between 5 to 20mg of material is sufficient for the successful application of ZooMS with novel non-destructive and minimally destructive protocols requiring even less (Fiddyment et al., 2015; McGrath et al., 2019). Aside from abundance, the structure of COL1 itself makes it highly robust. COL1 is a helical protein composed of three alpha chains which form tightly packed fibrils. These fibrils are interconnected, creating fibres which are further strengthened by hydroxylysine cross-linkages (Henriksen and Karsdal, 2019; Shoulders and Raines, 2009). The helical structure of COL1 is created by a repeating pattern of amino acids, G-X-Y, in which every third amino acid is a glycine. It is this structure which allows it to survive so abundantly in the archaeological record, far beyond the upper limits of other biomolecules including DNA (Hendy et al., 2018). In fact, collagen has been

successfully extracted from animal fossil remains as old as 3.4 Ma and analysed using ZooMS (Rybczynski et al., 2013). The time-and-cost-efficiency, its reproducibility, and the robust nature of collagen, render ZooMS a valuable tool for a suite of archaeological applications.

In most ZooMS protocols, collagen is extracted either using hydrochloric acid or ammonium bicarbonate (Buckley et al., 2009; van der Sluis et al., 2014; van Doorn et al., 2011; Welker et al., 2015). The extracted collagen is then enzymatically digested using trypsin and the resulting peptides are measured using soft ionisation mass spectrometry, typically a matrix-assisted laser desorption/ionisation mass spectrometer (MALDI-TOF MS; Figure 2). The resulting spectrum is then compared against a reference library of known peptide markers which allows for the taxonomic identification of a sample (Bradfield et al., 2018; Buckley et al., 2017a, 2016, 2014, 2009; Harvey et al., 2019, 2018; Janzen et al., submitted.; Welker et al., 2016). Initial studies focused on its potential as a zooarchaeological tool and ZooMS was used, for example, to differentiate Neolithic sheep (*Ovis sp.*) from goat (*Capra sp.*) (Buckley et al., 2010), the brown rat (*Rattus norvegicus*) from the black rat (*Rattus rattus*) (Buckley et al., 2016), and various marine mammals (Buckley et al., 2014). In recent years, the method has been for a more complete understanding of complex processes, such as subsistence strategies (i.e. Evans et al. 2016; Hofman et al. 2018), artefact production (i.e. Bradfield et al. 2018; Desmond et al. 2018), and trade (i.e. Coutu et al. 2016; Figure 3). In addition, the technique has been used as a screening tool to assess collagen preservation in bone (van der Sluis et al. 2014; Welker et al. 2015; Buckley 2015), and as a means of better understanding art objects and curatorial practices (i.e. Kirby et al. 2013; Fiddyment et al. 2015).

1.4 Assessing glutamine deamidation as a measure of relative decay

Once the bones have been identified using ZooMS there are other avenues through which the PMF data can be investigated. The use of glutamine deamidation as a means of assessing relative decay has become increasingly popular (Sinet-Mathiot et al., 2019; van Doorn et al., 2012; Wilson et al., 2012) and, for instance, was recently

used to verify the antiquity of unprovenanced fossils in Tibet (Chen et al., 2019). While collagen preservation, assessed through glutamine deamidation, is unable to provide a direct age of a fossil in the same way as radiometric dating techniques can, it has been presented as being a means to relatively assess the decay rate and preservation of samples.

The degradation of collagen can occur through a variety of pathways, including a post translational modification known as deamidation. Deamidation is a process through which glutamine converts into glutamic acid and asparagine converts into aspartic acid or their respective isomers (Figure 4). In archaeological bones, the rate at which deamidation can occur is heavily influenced by the thermal history of the sample (van Doorn et al., 2012; Wilson et al., 2012) including, climate and temperature of the burial environment, pH of the soil, and fluctuation of the water table (Robinson and Rudd, 1974; Scotchler and Robinson, 1974). As such, the deamidation of glutamine has been proposed as a marker of relative age (Hill et al., 2015; Orlando et al., 2013; van Doorn et al., 2012; Wilson et al., 2012), specifically within PMF datasets (Chen et al., 2019; Sinet-Mathiot et al., 2019; Welker et al., 2017). This assertion however has been challenged, with some studies indicating that the variation in preservation of bones from similar or the same contexts are too high to provide secure ages or relative decay rates when studying bulk collagen deamidation (Pal Chowdhury et al., 2019; Schroeter and Cleland, 2016). As the method continues to be used in order to determine the antiquity of unprovenanced fossils, understanding the limitations and utility of deamidation measurements from PMF spectra is of increasing importance. The large numbers of samples included in this dissertation offer an opportunity to determine if patterns of glutamine deamidation can be reliably detected.

1.5 Exploring dietary adaptation in Siberia using stable isotopes and amino acid compound specific analysis

The biomolecular study of diet for the Pleistocene typically focuses on the role of bulk carbon ($\delta^{13}C$) and nitrogen ($\delta^{15}N$) in the bone collagen of ancient hominins. Measurements of bulk $\delta^{13}C$ are typically used to assess the kinds of plant resources

either being directly consumed by an individual or indirectly by their prey (Ambrose and Norr, 1993; Nakamura et al., 1982; Tieszen and Boutton, 1989). Bulk $\delta^{15}N$ is used to indicate an individual's place within a food web, where consumers will exhibit an elevation of ~3‰ over the consumed (Ambrose, 2002; Deniro and Epstein, 1981; O'Connel and Hedges, 1999; Sponheimer et al., 2003). Elevated $\delta^{15}N$ values can also indicate that an individual has undergone prolonged illness or nutritional stress (Beaumont and Montgomery, 2016; Doi et al., 2017, 2007) or be an indicator of age as breastfeeding and weaning (Schurr, 1998; Tsutaya and Yoneda, 2015) will elevate an individual's bulk isotopic composition. As a result of the slow turnover of bone, these measurements represent several years of an individual's lifetime, allowing for a broad picture of the most dominant aspects of their diet and health (Ambrose and Norr, 1993). The use of bulk $\delta^{13}C$ and $\delta^{15}N$ relies heavily on the creation of appropriate faunal and foraging baselines in order to make assessments about likely food sources or detect environmental factors which might be elevating or depleting their isotopic values. Recently, compound specific isotope analysis of amino acids (CSIA) has been used to refine these models. $\delta^{13}C$ CSIA allows for the quantification of aquatic inputs into diet and has successfully been used to confirm or dismiss the inclusion of freshwater and marine resources from diets of prehistoric people. This is based on the relationship between the carbon measurement of essential amino acids (alanine (Ala), asparagine/aspartate (Asx), glutamine\glutamate (Glx), glycine (Gly), proline (Pro), serine (Ser), tyrosine (Tyr)) as opposed to non-essential amino acids (isoleucine (Ile), leucine (Leu), lysine (Lys), phenylalanine (Phe), threonine (Thr), and valine (Val)) (Jarman et al., 2017; Larsen et al., 2013). In the case of a European Neanderthal from Les Cottes, CSIA was used to cement the dietary reliance of Neanderthals on large herbivores (Jaouen et al., 2019).

At present only one study on Pleistocene hominin diet using stable isotope analysis has been carried out with a focus on the Neanderthals excavated from Okladnikov Cave (Dobrovolskaya and Tiunov, 2013; Tiunov and Dobrovoldskaya, 2011). This preliminary investigation suggests that Siberian Neanderthal subsistence strategies may have differed from groups living in Europe as they display far more elevated bulk

nitrogen values, between 13.4–13.8‰. Denisova 11, the daughter of a Neanderthal mother and a Denisovan father (Slon et al., 2018), displays the most elevated bulk nitrogen values measured for a Pleistocene hominin (16.4‰) (Brown et al., 2016). This measurement was made during radiocarbon dating of the fossil and has not been investigated further (Brown et al., 2016). Applying CSIA to hominins in Siberia could therefore reveal why elevated isotopic values have been detected in individuals from Okladnikov and Denisova caves.

2. Objectives and expected outcome of doctoral research

There are two primary objectives of this dissertation. The first is the identification of new hominin remains from six Pleistocene sites from Siberia through the high throughput analysis of fragmented bones using ZooMS. The diversity of hominin populations in Northern Asia and their interactions are only just beginning to be understood and identifying their remains is crucial to this research. With high rates of fragmentation for the region, ZooMS presents one of the most effective means of solving this problem and identifying Pleistocene hominin remains in the archaeological record.

The second objective is the further study of any hominins identified, including dietary studies to better understand the adaptations of hominin populations in Siberia in comparison with those found in Europe. This would be a significant contribution to biomolecular research for the region, where attention has mainly been placed on stable isotope analysis for the Holocene and the emergence of agriculture. In addition, the studied bones will be used to test the efficacy of glutamine deamidation research which has been used as a means of relatively assessing the age of bones through their collagen preservation. If successful, the method could be used to identify intrusive fossils or help to determine the age of fossils when direct dating is not possible or they lack archaeological context.

Additionally, as the method grows and ZooMS becomes central to the archaeological science toolkit, it is becoming increasingly important to evaluate the methods that we are using and their appropriateness in supporting this expansion. At the outset of this dissertation, very few labs were applying ZooMS. A major hindrance to the expansion of the method was the lack of standardisation in the ways in which protocols were reported and the need for a cohesive and accessible reference library. The research presented here aims to stimulate discussions surrounding the growth of ZooMS and provide practical approaches to this.

3. Materials and Methods

3.1 Sites and Samples

Fragmented bones from six Pleistocene sites in Northern Asia were included in this research, three from the Lake Baikal region: Podzvonkaya (n=170), Khotyk (n=224), and Kamenka (n=341); and three from the Altai Mountains: Denisova Cave (n=5,938), Strashnaya Cave (n=2,141), and Ust-Karakol (n=107; Appendix 4). In total, 8,921 bone fragments were analysed, all collected during sampling trips I undertook in 2017 and 2018 to the Institute for Archeology and Ethnography for the Russian Academy of Sciences in Novosibirsk and the Institute of Mongolian, Buddhist and Tibetan Studies in Ulan-Ude. These bones were specifically chosen because they bore no diagnostic markers which would allow for their identification using traditional morphological analysis. The use of ZooMS at these sites was not aimed at replacing the work already being done by zooarchaeologists and physical anthropologists, but rather to utilise the large assemblages of fragmented bones which are routinely excavated and stored, in the hopes that they contain rare fossil remains which are otherwise missed.

The majority of samples analysed were excavated from the Pleistocene layers of Denisova Cave. The site, situated in the Altai Mountains of Russian Siberia, is unique in its hominin record as the only site where both Neanderthal and Denisovan fossils have been identified (Krause et al., 2010a; Mednikova, 2011; Prüfer et al., 2014; Reich et al., 2010). Despite particularly favorable conditions that ensure a high degree of biomolecular preservation at the site, some parts of its stratigraphy have high rates of bone fragmentation, owing to the frequent occupation by humans and carnivores alike (Morley et al., 2019). On average, less than 5% of bones excavated from the site can be macroscopically identified (Agadjanian and Serdyuk, 2005; Jacobs et al., 2019; Vasiliev, et al. 2013, 2017, 2018; Vasiliev and Shunkov, 2009).

A brief description of all of the other sites included in this dissertation can be found in Appendix 4.

3.2 ZooMS Analysis

In total, 8,921 bone fragments were analysed using ZooMS. Samples were drilled in preparation for analysis at the MPI-SHH and the Oxford Radiocarbon Accelerator Unit (ORAU). From each bone a small fragment, approximately 20mg, was removed using a diamond covered disc. Care was taken to clean the discs using a sand blaster after each sample was drilled.

Analysis of the majority of samples was carried out at the ZooMS facility of the Department of Archaeology at the MPI-SHH. A smaller collection of samples were also analysed at the Manchester Institute of Biotechnology at the University of Manchester, UK. Samples analysed at the MPI-SHH followed published protocols using ammonium bicarbonate as the means of collagen extraction (Brown et al., 2020a; van Doorn et al., 2011). Samples which failed initial analysis were re-analysed using an acid soluble protocol (Brown et al., 2020c; van der Sluis et al., 2014). The same acid soluble protocol was followed for all samples analysed at the University of Manchester.

Samples at the MPI-SHH were analysed using a Bruker AutoFlex LRF Speed (Bruker) and those at the University of Manchester were analysed using a Bruker Ultraflex II (Bruker). Samples were peak picked with a signal to noise ratio of 3.5 after baseline correction, smoothing, and deisotoping with the default parameters. The resulting spectra were analysed with flexAnalysis 3.4 (Bruker Daltonics) and mMass software (Strohalm et al., 2008). The spectra were compared against a reference library of known peptide markers (Buckley et al., 2010, 2009; Buckley and Kansa, 2011; Welker et al., 2016).

3.3 Collagen Deamidation Measurement

In order to determine if patterns of glutamine deamidation could be identified at Denisova Cave, bone collagen was measured using two methods. Bulk measurement of glutamine deamidation used PMF data was compiled as part of the ZooMS analysis for the East Chamber of the site (Manuscript D, Appendix 3). Deamidation from the PMF data was measured using the Q2E R package (Wilson et al., 2012). Soft

ionisation mass spectrometry is unable to deconvolute the overlapping non-deamidated (m/z 1105.5) and deamidated (m/z 1105.6) peak for peptide COL1α1 508-519. Q2E uses a genetic algorithm to achieve this by comparing the theoretical distribution for the non-deamidated peptide against the measured MALDI TOF spectra (Wilson et al., 2012). A peptide which appears to have no deamidation returns a score (Est%Gln) of 1 while an entirely deamidated peptide returns a score of 0 (Wilson et al., 2012).

In order to ensure only high quality data were included in this study several qualifying factors were used to include/exclude samples. The first was the extraction protocol utilised. While multiple methods have been used to extract collagen for PMF research at Denisova Cave (Manuscript A and C), only collagen which was extracted using an ammonium bicarbonate protocol, which is specifically designed to avoid artificially deamidating peptides during collagen extraction (Brown et al., 2020a; van Doorn et al., 2011), were included in this study. Secondly, only samples which could be taxonomically identified using ZooMS analysis were included (Manuscript C). Thirdly, as our lab does not typically average our PMF spectra, only samples for which all three replicates passed measurement for bulk glutamine deamidation were included. In total 2,501 PMF samples qualified for this study (Supplementary Materials), spanning seven archaeological layers of the site's East Chamber and ~240 ka of the Pleistocene for Northern Asia (Douka et al., 2019b; Jacobs et al., 2019).

Additionally, site specific measurements of deamidation were made using LC MS/MS data and the recently published deamiDATE (Ramsøe et al., 2020) using 15 of the same samples that were included in PMF analysis. DeamiDATE allows for both bulk and site specific analysis of glutamine deamidation, giving a far higher degree of precision in comparison with measurements created with MALDI-TOF spectra (Ramsøe et al., 2020). Beyond glutamine deamidation, deamiDATE is used to verify if a sample is ancient and identify modern contamination within the proteins examined. Each non-deamidated asparagine and glutamine position within a sample is compared with the number of their deamidated forms to create a relative remaining intensity. Site specific deamidation looks at both the sequence-dependent deamidation rate of each

occurrence of asparagine and glutamine within a sample, as well as the relative intensity of the deamidating protein, in a similar manner to the bulk measurement (Ramsøe et al., 2020).

3.3 Stable Isotopes Analysis

In total 282 bones were measured for their bulk carbon and nitrogen isotope values. Nine hominins, and associated fauna from layers 9.3 (n= 53), 11.4 (n= 101), and 12 (n= 119) of the East Gallery of Denisova Cave were analysed. Depending on how much material remained for each of the hominin bones, the pretreatment protocol varied. For Denisova 11 (D11) (Brown et al., 2016) and Denisova 15 (D15) (Manuscript A) previously extracted and lyophilised collagen for radiocarbon dating was utilised for the isotopic study. For Denisova 7 (D7), Denisova 17 (D17), Denisova 18 (D18), Denisova 19 (D19), Denisova 20 (D20) and Denisova 21 (D21) collagen was extracted using a modified version of recently published protocols which require only 100mg of bone (Fewlass et al., 2019). For these, bone chips were demineralised in 0.5M HCl for 1-2 days. The demineralised bone chips were then rinsed in ultrapure water, treated with NaCl and rinsed again. The HCl supernatant was ultra-filtered in 30kda filters with ultrapure water. The ultra-filtered supernatant was added to the rinsed and demineralised bone chip and the entire sample was incubated at 70°C. The resulting gelatine was run through an Ezee filter and freeze dried. D17 failed to produce any collagen. All other samples produced enough for measurement.

Faunal remains were prepared at the MPI-SHH and the ORAU following established protocols for collagen extraction (Longin, 1971). Samples were demineralised in 0.5M HCl for a period of 1-5 days, rinsed in Milli Q water, treated with pH 3 water, and demineralised at 70℃ for 24 hours. The resulting supernatant was filtered using Ezee Filters and freeze dried.

The $\delta^{13}C$ and $\delta^{15}N$ ratios of the bone collagen were analysed at the Isotope Laboratory, MPI-SHH, Jena and determined using a Thermo Scientific Flash 2000 Elemental Analyser coupled to a Thermo Delta V Advantage mass spectrometer. Isotopic values are reported as the ratio of the heavier isotope to the lighter isotope

(13C/12C or 15N/14N) as δ values in parts per mill (‰) relative to international standards, VPDB for δ13C and atmospheric N2 (AIR) for δ15N. Results were calibrated against international standards of (IAEA-CH-6: δ13C = −10.80 ± 0.47‰, IAEA-N-2: δ15N = 20.3 ± 0.2‰, and USGS40: δ13C = −26.38 ± 0.042‰, δ15N = 4.5 ± 0.1‰) and a laboratory standard (fish gelatin: δ13C = ~−15.1‰, δ15N = ~14.3‰). Based on replicate analyses long-term machine error over a year is ±0.2‰ for δ13C and ±0.2‰ for δ15N. Overall measurement precision was studied through the measurement of repeats of fish gelatin (±0.2‰ for δ13C and ±0.2‰ for δ15N). The faunal (n = 266) and human (n = 7) bone collagen results from are presented in Supplementary Table 2 (Manuscript F). Samples with a C/N ratio between 2.9–3.6 were carried forward for interpretation.

4. Results

4.1 Identifying fragmented bone assemblages using ZooMS (Manuscripts A, C and D)

Manuscript A - 2019. Douka, K., Slon, V., Jacobs, Z., Ramsey, C.B., Shunkov, M.V., Derevianko, A.P., Mafessoni, F., Kozlikin, M.B., Li, B., Grün, R., Comeskey, D., Devièse, T., **Brown, S**., Viola, B., Kinsley, L., Buckley, M., Meyer, M., Roberts, R.G., Pääbo, S., Kelso, J., Higham, T. Age estimates for hominin fossils and the onset of the Upper Palaeolithic at Denisova Cave. *Nature* 565, 640–644.

Synopsis

This paper (Appendix 1) reports the identification of three new hominin remains identified from amongst an assemblage of 2,212 bones using ZooMS. These hominin remains were then radiocarbon dated alongside 50 other bone samples from Denisova Cave. The manuscript combines these radiocarbon measurements with OSL dates and genetic age estimations into a series of Bayesian models. The results provide robust evidence for the earliest occupation of the site (~200 ka) by Denisovans, offers age estimates for 10 hominin remains from the site, and identifies some of the earliest forms of Upper Palaeolithic bone tool industry and personal ornamentation, likely the oldest in Eurasia (48 – 42 ka). The three hominin bones identified were derived from layers 9.3 (Denisova 14) and 11.4 (Denisova 15) of the East Chamber and layer 9.1 (Denisova 16) of the Main Chamber.

Subsequent mtDNA analysis for Denisova 14 (D14) and Denisova 16 (D16) failed to identify their hominin populations. Direct radiocarbon dating of D14 returned an age of 45.9 – 50 ka. D16 was unfortunately too small for radiocarbon dating. Denisova 15 (D15) was located in one of the final Middle Palaeolithic layers for the East Chamber, estimated to be ~91 – 130 ka, and was determined to carry Neanderthal mtDNA. The mtDNA of D15 forms a clade with Denisova 5 (90.9 – 130 ka) which had previously been unrelated to any other known Neanderthal populations (Prüfer et al., 2014).

Manuscript C - submitted. **Brown, S**., Massilani, D., Kozlikin, M., Shunkov, M., Derevianko, A., Stoessel, A., Jope-Street, B., Meyer, M., Kelso, J., Pääbo, S., Higham, T., Douka, K. The earliest Denisovans and their cultural adaptation. *Nature Ecology and Evolution.*

Synopsis

This manuscript (Appendix 2) reports the analysis of 3,791 bones using ZooMS from the East Gallery of Denisova Cave. This resulted in the identification of five new hominin bones were identified. One bone from layer 12 (DC4969; Denisova 17) and four bones from layer 15 (DC7277, Denisova 18; DC7795, Denisova 20; DC8591, Denisova 21; and DC8846, Denisova 19) bore peptide mass fingerprints with the characteristic markers corresponding to Hominidae. Four of these contained sufficient genetic material for mtDNA analysis. Denisova 17 was found to carry mtDNA of the Neanderthal type whilst Denisova 19, 20 and 21 carried mtDNA of the Denisovan type. Excluding the three positions not covered in the mtDNA of the Denisova 19 individual, its sequence is identical to that of Denisova 21, meaning these bones either belong to the same individual or maternal relatives. It is likely that the Denisova 18 specimen has mtDNA of the Denisovan type, but due to the small number of mtDNA sequences cross-contamination from the other Denisovan specimens during the DNA processing cannot be ruled out. Denisova 17 is the third individual from layer 12 with mtDNA of the Neanderthal type however in a maximum parsimony tree, the mtDNA Denisova 17 is not closely related to the mtDNAs of other Neanderthals from Denisova Cave.

Manuscript D - in prep. **Brown, S**., Wang, N., Oertle, A., Comeskey, D., Jope-Street, B., Harvey, V., Pal Chowdury, M., Kozlikin, M., Shunkov, M., Derevianko, A., Buckley, M., Higham, T., Douka, K. Zooarchaeology through the lens of collagen fingerprinting at Denisova Cave.

Synopsis

In this manuscript (Appendix 3) we report the results for 8,253 bones from Denisova Cave analysed using ZooMS. Through the integration of bones identified using ZooMS

with previously reported macroscopically-identified fauna we are able to create a holistic picture of the zooarchaeological fossil record of the site. Our analysis highlights trends associated with climate variability throughout the Middle and Upper Pleistocene, elucidates the reasons behind fragmentation of the fauna, and informs hominin hunting practices from ~200 – 50 ka.

This work combines ZooMS analyses carried out for manuscripts A and C (Appendix 1 and 2) (n= 5,938) and Brown et al., 2016 (n= 2,315) in which only the hominin remains were discussed in detail. This is the largest single archaeological assemblage that has been studied using proteomics. Overall, of the 8,253 analysed fragments, 74% could be assigned to a specific ZooMS taxon and an additional 5% produced low quality spectra which could only be identified to family or order. The South Chamber had a high rate of samples which failed to produce enough collagen for taxonomic identification (28%), in comparison with lower rates of failure for the East (16%) and Main (17%) chambers. Where morphological analysis of bones from the site have identified a high proportion of carnivore remains (30.2%), we find they account for only 7.6% of bones identified using ZooMS. Rather it is large mammals which dominate the bones identified here, as they are between 3-5 times more abundant in the fragmented bone assemblage. Our analysis reveals a cyclical pattern in fragmentation of bones with hominins using percussive based tools and carnivores likely furthering this initial fragmentation through gnawing and digestion. The application of ZooMS at Denisova Cave has significantly improved our understanding of the site's faunal record and taphonomy. This research is illustrative of the potential of the method not only for screening large numbers of bones for the identification of hominin fossils, but as a complementary tool for comparing ZooMS datasets with traditional zooarchaeological practices.

4.2 Dietary adaptation in Siberia (Manuscript F)

Manuscript F - in prep. **Brown, S**., Larsen, T., Roberts, P., Comeskey, D., Kozlikin, M., Shunkov, M., Derevianko, A., Higham, T., Douka, K. Elevated stable carbon and nitrogen isotopes at Denisova Cave and Siberian palaeoenvironments.

Synopsis

This is the most systematic palaeodietary investigation for Pleistocene Siberia. In total, 270 fossils (seven hominins and 263 animals) were measured for their bulk isotope values. The $\delta^{13}C$ values for hominins varied by only 2‰, with D11 (Neanderthal-Denisovan offspring) the most elevated at -17.6‰ and Denisova 7 (D7; *Homo* sp.) the most depleted at -19.6‰. The range in $\delta^{15}N$ was far more significant, with 5‰ separating the most elevated (D11; 16.6‰) from the most depleted (D20, Denisovan; 11.6‰). D7, D11, and D14 (*Homo* sp.) have the most elevated $\delta^{15}N$ values at 16.3, 16.6, and 16.5‰, respectively. Two of the ~200 ka hominins, D18 (*Homo* sp.) and D20, exhibit the most depleted $\delta^{15}N$ values at 11.6 and 11.7‰ respectively.

There is a large amount of variability in $\delta^{15}N$ and $\delta^{13}C$ values measured for herbivores. Bos/Bison remains from layer 11.3, for instance, exhibit δ15N values ranging from 4.1 to 13.1‰ and Cervidae/Gazella/Saiga range from 4.4 to 12.2‰. In fact, some of the herbivores exhibit $\delta^{15}N$ values as elevated as carnivores.

The unprecedented isotopic values of herbivores measured from Denisova Cave and the hominins which were targeting them provide important evidence for the prevailing effect of the palaeoenvironment on dietary studies. We have attempted to explore and subsequently eliminate all other variables which may be driving the observed isotopic trends. To do so, we carried out compound specific isotopic analysis for the hominin remains. Without the inclusion of CSIA their unusual $\delta^{15}N$ values could easily have been attributed to reflect the inclusions of aquatic resources in their diet. Instead, we have identified the effects of hunting at high altitudes, glaciation, and repeated thaw cycles on the daily lives of hominins in the Altai Mountains.

4.3 ZooMS developmental work (Manuscript B and E)

Manuscript B - 2020. **Brown., S**., Douka, K., Collins, M., Richter, K. On the standardization of ZooMS nomenclature. *Journal of Proteomics.*

Synopsis

This article (Appendix 1) examines the need for standardisation in ZooMS research, particularly in the way peptide markers are discussed and reported. Peptide markers suitable for taxonomic discrimination are initially identified through MALDI-TOF mass spectrometry and then verified using tandem mass spectrometry (LC-MS/MS). Initially, ZooMS identifications relied on the presence/absence of seven tryptic peptide markers, labelled A-G and based upon increasing mass-to-charge (m/z) ratios (Buckley et al., 2009). Over the past decade however new markers which fall in between the masses of peptides labeled with the A-G system have been identified. Several varying nomenclature systems have been used to describe these new markers with little consistency between research groups and publications. Further, the original A-G nomenclature system does not inform the reader on the peptides being used for taxonomic identification nor where the peptides are situated within the protein sequence. The lettering system also inherently hinders the possibility for incrementally labelling newly identified peptide markers which, for instance, could fall between the masses of B (typically m/z 1400–1500) and C (m/z 1500–1600).

In this manuscript, we propose a naming system for collagen peptides based on the beginning of the helical region of COL1α1, COL1α2, and COL1α3. This corresponds to the start of the collagen-specific three letter repeating pattern (G-X-Y). We label ZooMS peptide markers with the gene (COL1α1, COL1α2, or COL1α3), followed by the start position of the peptide in reference to the first amino acid of the helical region, followed by the end position of the peptide in reference to the first amino acid of the helical region (Table 1). This system provides consistent nomenclature of peptide markers for all vertebrates, a significant advantage over tryptic digestion labels and other positional labels. The adoption of this method avoids the problem of duplicate

names appearing in the literature and, unlike the letter-based nomenclature, allows markers to be named consecutively within the COL1 sequence. Their position can easily be located using existing alignment software.

Manuscript E - in prep. **Brown, S**., Wang, N., Oertle, A., Jope-Street, B., Kozlikin, M., Shunkov, M., Derevianko, A., Higham, T., Douka, K., Richter, K. Examining collagen preservation through glutamine deamidation at Denisova Cave.

Synopsis

Measurements of glutamine deamidation were made for 2,501 samples, which were initially analysed as part of taxonomic identifications for the East Gallery of Denisova Cave in Manuscript C.

Results (Appendix 3) revealed that while a large dataset will show an overall pattern of decreasing collagen preservation, that pattern is not statistically different and could not be used in the relative assessment of the age of bones. Similarly, identifying intrusive elements into a stratigraphic layer was not possible given the variability of collagen preservation within a single layer, despite the large chronological difference between archaeological contexts in the East Chamber of Denisova Cave. Measurements of collagen deamidation made using LC-MS/MS data confirmed that the samples were ancient, but were unable to detect a pattern in their overall preservation status based on provenance and/or estimated age.

5. Discussion

5.1 ZooMS Identifications (Manuscripts A, C, D, and F)

Denisova Cave represents the bulk of ZooMS work carried out as part of this dissertation. 5,938 bones were analysed from the East (n=3,993), Main (n=1,123), and South (n= 822) chambers. For the first time, these were combined with an additional 2,315 bones analysed as part of my MSc dissertation (Brown et al., 2016) which had not been discussed previously within published research. All of this dat was collated in Manuscript D (Appendix 3). The work now accounts for the analysis of 8,253 non-diagnostic bone fragments which were excavated from all three chambers of Denisova Cave.

Denisova Cave was the only site studied as part of this dissertation in which hominin fragments were identified. Many of the sites included in this study only had a few hundred fragmented bones available for analysis, either because environmental conditions had not allowed for the preservation of large quantities of bone (4 out of 5 are open-air sites) or because non-diagnostic bones had not been stored. At Denisova Cave, a site which appears to have been occupied intensively, human remains are identified at a 1 in 1200 ratio. ZooMS analysis identified nine new hominin bones from Denisova Cave (Figure 5, Figure 6; Appendix 4), eight from amongst the fragmented bone assemblage and one that had erroneously been identified as a bear parietal fragment (Denisova 7). ZooMS-identified fossils now account for the majority of hominin remains discovered at Denisova Cave (10 out of 18; 55%). Denisova 11 (D11) (Brown et al., 2016) was identified as part of my MSc Dissertation.

The oldest fossils identified in this dissertation from Denisova Cave were the four bones from layer 15 of the East Chamber, Denisova 18 (D18), 19 (D19), 20, (D20), and 21 (D21). While all four contained the ZooMS peptide markers necessary for attribution as *Hominidae*, only three could be securely identified as Denisovan on the basis of mtDNA (D19, D20 and D21). These are the oldest human remains identified using ZooMS to date and the oldest known Denisovan fossils. The newly identified

Denisovans form a clade with Denisova 2 (D2), a lower deciduous molar from the Main Chamber (Slon et al., 2017b; Turner, 1990).

Arriving into the Altai Mountains during the Cherepet Interglacial (MIS 7), these Denisovans clearly preferred to hunt deer, as attested by the bone assemblages of roe deer (*Capreolus pygargus*), Siberian red deer (*Cervus elaphus*), and giant deer (*Megaloceros giganteus*) found throughout the stratigraphic contexts associated with their occupation of the site (Manuscript C; Jacobs et al. 2019; Vasiliev et al. 2013). While only a small number of bones have cutmarks, the abundance of deer remains illustrates a clear hunting preference, as well as informing us of the availability of fauna and the environmental settings in the proximity of the cave. Roe deer live in both forest and steppe habitats, preferring tall-grass meadows and floodplains. Red deer have a diverse habitat, showing preference for open deciduous and mixed forests, open grasslands and meadows, river valleys and floodplains. Giant deer preferred semi-open, mixed environments where they could both browse and graze (Lister and Stuart, 2019). They would have been abundant in the proximity of Denisova Cave where all such habitats would have been present in interglacial conditions (Chlachula 2001).

Humans however were not the only occupants of Denisova Cave during this period. About a quarter of the morphologically identified faunal assemblage from Layer 15 comprised carnivore remains, predominantly *Canis lupus* and *Cuon alpinus* (Jacobs et al., 2019; Vasiliev et al., 2013). This high proportion of carnivore taxa suggests that Denisovans may have been actively competing with these predators over resources and perhaps the cave itself.

The next arrivals to Denisova Cave were Neanderthals. The fossils identified in this dissertation, Denisova 15 (D15) and Denisova 17 (D17) represent some of the earliest Neanderthals in the Altai Mountains, arriving in the region between ~120 – 90 ka during MIS 5. Despite being similar in age, their mtDNA differs significantly from one another. D15 however forms a clade with Denisova 5 (D5), the proximal pedal phalanx of another Neanderthal individual, which had previously been unrelated to any other known Neanderthal populations (Manuscript A; Prüfer et al., 2014). With the inclusion

of Denisova 11 (D11), at least three distinct maternal lineages for Neanderthals can now be identified at Denisova Cave. Their presence within the Altai appears to be discontinuous, perhaps moving in and out of the region with glacial and interglacial periods.

Denisova 14 (D14) and Denisova 16 (D16) are the only hominin fossils which have been identified for the Upper Palaeolithic layers of the East and Main chambers of the site. High levels of contamination however, have prevented their association with a specific hominin population using genetic analysis. This is unfortunate as the makers of the Upper Palaeolithic technologies at Denisova Cave continue to be disputed (Manuscript A; Derevianko et al., 2020) as many of the technologies present at the site appear to develop continuously from the Middle Palaeolithic. At present D14 and D16 seem unlikely to resolve who the makers of the Upper Palaeolithic were.

Denisova 7 (D7) was the final hominin identified as part of this dissertation. D7 is a parietal fragment which was excavated in 2008 from layer 11.3, the final Middle Palaeolithic layer for the East Chamber (Shunkov et al., 2020). A small proportion (14.1%) of the artefacts found in this layer can be attributed to Upper Palaeolithic tool types, including end-scrapers and burins (Shunkov et al., 2020). D7 was excavated in the same year that the first Denisovan fossil (Denisova 3) was located. High levels of environmental contamination had initially been a hurdle in identifying this fragment as a hominin fossil. This was furthered by its unusual coronal plane and lack of meningeal grooves which are typically used for the identification of human parietal bones (Manuscript A). ZooMS analysis however was able to confirm this bone was in fact a hominin (Manuscript F). Genetic analysis is underway again to try and determine which population it comes from. If a population can be attributed to D7 it will go some way to unravelling the transition from the Middle to the Upper Palaeolithic for Denisova Cave.

The high number of samples analysed for Denisova Cave allowed for trends to be identified within a ZooMS dataset in comparison with zooarchaeological assemblages. The most notable difference between the zooarchaeological assemblages and the ZooMS-IDed component is the abundance of predators in comparison with herbivores.

In the morphological assemblage of all three chambers of Denisova Cave predator groups account for ~30% of all identified bones (Agadjanian and Serdyuk, 2005; Jacobs et al., 2019; Vasiliev, et al., 2013, 2017 2018; Vasiliev and Shunkov, 2009), in comparison with the ZooMS identified component where predators account for only 7.6%. As such, some processes of accumulation for the high rates of fragmented bone can be unraveled through the comparison of zooarchaeological and archaeological data for the site. Layers 14 and 15, the earliest archaeological layers for the East Gallery of Denisova Cave, display evidence for intensive processing of carcasses by hominins, likely the group of Denisovans identified in this dissertation (D19, D20, and D21). Throughout the Pleistocene layers for the site, carnivores appear to have only occasionally been targeted by hominins for their skins and hides and therefore their bones are less likely to suffer similar fragmentation rates as hominins process carcasses using percussive tools. The behaviours of carnivores at the site, including Crocuta/Panthera and Canidae, is also extensive, particularly in the Upper Palaeolithic layers for the site. Gnawing and digestion marks on bones alongside an assemblage of their coprolites reveals much of the fragmented assemblage can be attributed to these predators. Based on this evidence, the fragmented bone assemblage appears to reflect the alternating occupation of the site and the hunting and carcass processing practices of humans and carnivores alike. Hence, while a typical zooarchaeological assemblage at Denisova Cave will contain a higher percentage of macroscopically identifiable carnivore bones, smaller non-diagnostic fragmented bones will include more prey/herbivore species.

Two groups dominate the identified prey in the ZooMS assemblage. Cervidae/Gazella/Saiga, which likely represents red deer (*C. elaphus*), irish elk (*M. giganteus*), elk (*Alces cf. alces*), saiga (*S. borealis*), Siberian roe deer (*C. pygargus*), and gazelle (*G. guttursza*), and Bos/Bison, likely steppe bison (*Bison priscus*) and the less common Baikal yak (*Poëphagus mutus*), account for 15% and 26% of the assemblage, respectively. Despite the wide variety of taxa Cervidae/Gazella/Saiga encompasses they do not surpass the abundance of Bos/Bison except for the earliest layers which correspond to MIS 9-7 (337 - 191 ka). The majority of bones from this

phase were excavated in layer 15 which is attributed to MIS 7 and the Penultimate Interglacial, and coincides with the arrival of the first Denisovans to the site (Manuscript C; Shunkov et al., 2020; Slon et al., 2017a). As discussed earlier, cervids were clearly favoured by these early inhabitants of the cave, an observation which remains in stark contrast to the faunal record of all later periods documented at the site. During the period in which Bos/Bison remains dominate the ZooMS-IDed component (MIS 6-2) the environment was going through cyclical warm and cool climatic phases (Manuscript A; Jacobs et al., 2019). During interglacial periods warm and humid conditions allowed for the expansion of mixed and coniferous forests, whereas glacial periods were cold and arid, promoting steppe and tundra environments. Despite steppe bison and Baikal yak favouring steppe and forest steppe environments (Vasiliev, 2008; Vasiliev et al., 2013) their remains continue to dominate the ZooMS-IDed component during interglacial periods. This suggests that rather than the environment and availability being a driving force behind the abundance of fragmented bovine remains, predators, likely hominins, were preferentially targeting them and mirroring a trend identified in other large Pleistocene ZooMS assemblages (Sinet-Mathiot et al., 2019).

While ZooMS has been applied to larger assemblages and older individual faunal samples (Buckley et al., 2017b; Rybczynski et al., 2013), the work carried out at Denisova Cave represents the largest assemblage of fragmented bones with an archaeological association to be analysed using ZooMS. The oldest archaeological layers studied were 14 and 15, dating to between 217 - 163 ka (Jacobs et al., 2019). For layer 15, the oldest of the two, from which nearly 1000 bones were analysed, the success rate was 86% and four hominin bones were identified. This is particularly encouraging and opens up significant opportunities for the analysis of bone material of similar, or greater, antiquity from other sites.

5.2 Environmental Adaptation in Siberia (Manuscript A, C, F)

In order to understand if subsistence strategies differed for hominins living and adapting to life in the Altai Mountains, in comparison with groups living at the same

time in Europe, we carried out a dietary isotope analysis, measuring carbon ($\delta^{13}C$) and nitrogen ($\delta^{15}N$) values for hominins and fauna at Denisova Cave. Our results indicated an unusual elevation in isotopic measurements for many of the individuals studied.

All of the hominins identified as part of this dissertation lived throughout interglacial periods, perhaps with the exception of D7 who was found in a layer which covers the interglacial MIS 5 and the glacial MIS 4 periods (Figure 7). More secure age estimations for this individual would be necessary to be certain. The interglacial periods in the Altai Mountains represent times in which forests begin to expand (Bolikhovskaya and Shunkov, 2014; Chlachula, 2001) with humid conditions allowing for the meltwater from glaciers and permafrost to move into the lowlands of the Altai Mountains and the Ob River Valley. As a result of these humid conditions, rain would have become more common, replacing frequent snowfall during the cold and arid glacial periods. Water in glaciers and permafrost has a high nitrogen content which becomes trapped in glacial ice either through the atmosphere or through microbial weathering processes (Burpee et al., 2018; Williams et al., 2007). Measurable increases in nitrogen from rivers and tundras, fed by glacial and permafrost water can be observed today in places like the Arctic, Switzerland, and Tibet where regular thaw cycles provide much needed nutrients to ecosystems (Beermann et al., 2017; Göransson et al., 2016; Keuper et al., 2017; Mao et al., 2020; Wadham et al., 2016).

The elevated isotope values of the fauna and hominins (Figure 7; Manuscript F) may also be attributed to the altitude and topography of the Altai Mountains. Measurements of soil and plants in the Dongling Mountains and the Himalayas have recorded increasing $\delta^{15}N$ and $\delta^{13}C$ values with altitude (Liu et al., 2010; Tashi et al., 2016). Increasing altitude coupled with forested environments with nutrient rich soils was found to increase $\delta^{15}N$ values at elevations above 1350m a.s.l. (height above sea level). Denisova Cave itself however, sits at 700m a.s.l however, present day forests and tundra-forests in the Altai Mountains are situated as high as 2300-2500 a.s.l (Timoshok et al., 2016). Nonetheless, it is not improbable that some of the hominin groups occupying the cave may have been moving much higher into the Altai Mountains to hunt and forage. Over the past decade genetic evidence has shown that

Denisovans may have been well adapted to higher altitudes based on the identification of the EPAS1 gene variant, a transcription factor that regulates the response to hypoxia, that is found in modern Tibetans (Huerta-Sánchez et al., 2014). Interestingly, the second occurence of Denisovans outside Denisova Cave is in Tibetan Plateau at 3820 m a.s.l. (Chen et al., 2019; Zhang et al., 2020)

As it is not possible to measure plants from this period from the Altai Mountains we must rely on faunal baselines and the elimination of all other factors which may have contributed to the unusual $\delta^{15}N$ and $\delta^{13}C$ measurements. Bos/Bison and Cervidae/Gazella/Saiga are as much as 4 – 5‰ more elevated in comparison with their European counterparts (Manuscript F). This is the same rate of elevation for D7, D11, and D14 over the average $\delta^{15}N$ expected for European Pleistocene hominins (Figure 7). Therefore, based on the environmental evidence for the region, isotopic measurements for fauna and hominins, and CSIA we suggest that high altitudes and glaciation coupled with increasing meltwater during interglacial periods drove increasing nitrogen values in Pleistocene food webs in the Altai Mountains. Such research highlights the need for robust environmental baselines in dietary isotope studies. Without the inclusion of CSIA carried out for the hominins from Denisova Cave, their unusual $\delta^{15}N$ values could easily have been attributed to the inclusion of aquatic resources in their diet. Instead, we have identified the effects of a dynamic and changing environment on the daily lives of hominins in the Altai Mountains.

5.3 Deamidation as a Means of Assessing Relative Age (Manuscript E)

Providing secure and reliable chronologies for Pleistocene-age fossils is crucial for addressing questions surrounding human evolution, human-animal-climate interactions, and ecological reconstructions. The age of several of the fossils identified in this dissertation can only be ascertained using relative techniques like OSL because they fall outside the upper limits of radiocarbon dating. Genetic age estimations were also not possible for D7, D14, and D16 because they were too contaminated with environmental DNA for analysis. PMF data was used to create a glutamine deamidation map for Denisova Cave (Manuscript E), aimed at identifying intrusive

fossils in stratigraphic layers and assessing the relative age of fossils through collagen decay rates (Figure 8). This data was then compared with LC-MS/MS results. Bulk collagen deamidation measurements from PMF spectra show that while large numbers of samples show a pattern of decreasing preservation for the site, that pattern is not distinct enough to allow for an assessment of the relative age of these bones. As a consequence, identifying intrusive elements into a stratigraphic layer is likely not possible given the variability of collagen preservation within a single layer (Figure 8). This is despite the large chronological differences between the archaeological contexts in the East Chamber of Denisova Cave, that span more than 210 ka. Measurements of collagen deamidation made using LC-MS/MS data confirmed that the samples were ancient, but again were unable to detect a pattern in their preservational state based on age (Figure 9).

One of the most interesting result stemming from this work was the large intra-layer variability. While it is possible that some bones may have moved through the stratigraphy the hypothetical extent of such movement required to result in the levels of intra-layer variability, evident in glutamine deamidation values, would be completely out of step with all other chronological and stratigraphic studies carried out for the site (Douka et al., 2019b; Jacobs et al., 2019; Morley et al., 2019; Shunkov et al., 2020).

Layer 9 contains the largest intra-layer variability, as well as samples with the least and most deamidation values for the PMF analysis. While bones attributed to layer 9 are at least 230 ka younger than those from layer 17.1, 34% of samples appear more deamidated than the most deamidated sample from layer 17.1 (DC10782, Est%Gln= 0.43; Figure 8). The massive intra-layer variability in the PMF glutamine deamidation results for layer 9 matches what is known archaeologically for the context. Layer 9 is attributed to the Upper Palaeolithic, yet its sedimentology mirrors the overlying Holocene stratigraphy (Shunkov et al., 2020). In the uppermost Holocene layers of the East Chamber, a high saturation of organic matter has triggered chemical transformations of the underlying layers, including layer 9, resulting in heavy phosphatisation of sediments (Shunkov et al., 2020, 2018). As a result there are no reliable OSL dates for the Upper Pleistocene layers (Jacobs et al., 2019) and the only

reliable radiocarbon age comes from the hominin fossil identified within layer 9.3, Denisova 14 (50 - 45.9 ka) (Manuscript A). It is therefore not surprising that glutamine deamidation is so varied within this context, highlighting a need for a good understanding of the thermal history of bones before they are included in a study like this.

The phosphatisation of soils for layer 9 and the resulting acceleration in deamidation appears to have caused a flip in the expected relationship between glutamine and asparagine, with asparagine less deamidated than glutamine (Figure 9). This flip in expected values could provide an important indicator for artificial or chemical deamidation as a result of poor burial conditions or other factors accelerating glutamine degradation. The unexpected asparagine values reinforce the preservational issues surrounding samples from layer 9 and the likelihood that on-going proteomic and genetic analyses of bones from this layer will continue to be challenging.

Deamidation measured through PMF spectra provides an overall means for assessing collagen preservation and could be useful in identifying samples which are likely to be successful in other biomolecular methods such as DNA analysis or radiocarbon dating. The results presented here however reveal caution should be taken when attempting to connect these results with relative decay rates or an assessment of relative age.

5.4 Standardising ZooMS (Manuscript B)

In establishing the ZooMS lab at the MPI-SHH and applying the techinque to an increasingly wide variety of projects, several hurdles were identified in training and broader communication. One of the driving factors behind the establishment of this lab and the FINDER Project was making ZooMS more accessible to those aiming to apply the method to their own research (Douka et al., 2019a). At present there are no standard ZooMS protocols, with several different approaches in use depending on the various labs and publications. In order to effectively communicate our protocols and provide a much needed template for new labs to follow, we published our full ZooMS protocols. These are based on previously published methods (Brandt et al., 2018;

Buckley et al., 2009; van der Sluis et al., 2014; van Doorn et al., 2011; Welker et al., 2016), however for the first time we have made step-by-step guides for those who wish to apply ZooMS in their own labs. This includes protocols that use gentle buffer collagen extraction for well preserved and modern samples (Brown et al., 2020a), hydrochloric acid (HCl) extraction protocols for low collagen samples (Brown et al., 2020b, 2020c), and protocols for leather/skin/hide identification (Brown et al., 2020d).

To further this goal of creating standardisation within the ZooMS community we proposed a new nomenclature system. This proposal would allow all published ZooMS markers, which are labelled following several different theories, to be renamed under a single nomenclature system. With its the implementation, all-encompassing reference libraries can be created that allow for the insertion of new peptide markers sequentially and will more thoroughly inform the reader of the peptides used to make an identification. Additionally, reference libraries can combine markers for mammals, birds, and reptiles, something which had not previously been possible. The standardisation of nomenclature and the publication of protocols is one significant step towards the standardisation and opening-up of the ZooMS method.

6. Conclusion

The use of fragmented bones at Denisova Cave has resulted in the identification of nine new hominin fossils, the establishment of a large faunal baseline for bulk and carbon isotopic measurements for the region, and the creation of a deamidation map for ~210 ka of the East Gallery's stratigraphy. This work relied solely on the vast collections of non-diagnostic bone fragments excavated from Denisova Cave in the past 15 years and other sites in the region. The ability for high-throughput ZooMS analysis to taxonomically identify thousands of bone fragments opens up a huge amount of informational potential for sites with high rates of fragmentation like Denisova Cave, where despite hundreds of thousands of bones being excavated less than 5% can be morphologically identified.

The hominin fossils identified using ZooMS at Denisova Cave as part of this dissertation include the oldest known Denisovan fossils (D19, D20, and D21), a Neanderthal whose mtDNA population had not previously been known (D17), a parietal fragment which had been misidentified as a bear (D7), and the first individuals in association with the Upper Palaeolithic layers of the site (D14 and D16). The fauna identified revealed patterns in hominin behaviour and their switching preferences in prey, alongside evidence for the driving forces behind fragmentation itself. Further, this work has resulted in a collection of thousands of taxonomically identified bones which can and have gone on to multiple projects, creating research avenues which do not require destructive sampling of morphologically important faunal remains. The fragmented bone assemblage has now been used to create the first isotopic food web for the Pleistocene of the Altai Mountains, revealing the prevailing effect of the palaeoenvironment on their dietary values. This work highlights a need for a greater appreciation for environmental factors which might be placing pressures on ecosystems, reflected in what are often thought of as straightforward dietary isotope studies.

As a result of establishing new ZooMS facilities at the MPI-SHH and through the growth of projects, step-by-step lab protocols and a proposed nomenclature system have

been developed in order to cross many of the hurdles we have encountered. ZooMS is quickly becoming part of the standard analysis of archaeological materials and its role in projects such as these, as a high throughput screening tool for fragmented bones, demonstrates clearly its ability to drive forward archaeological research.

Figures

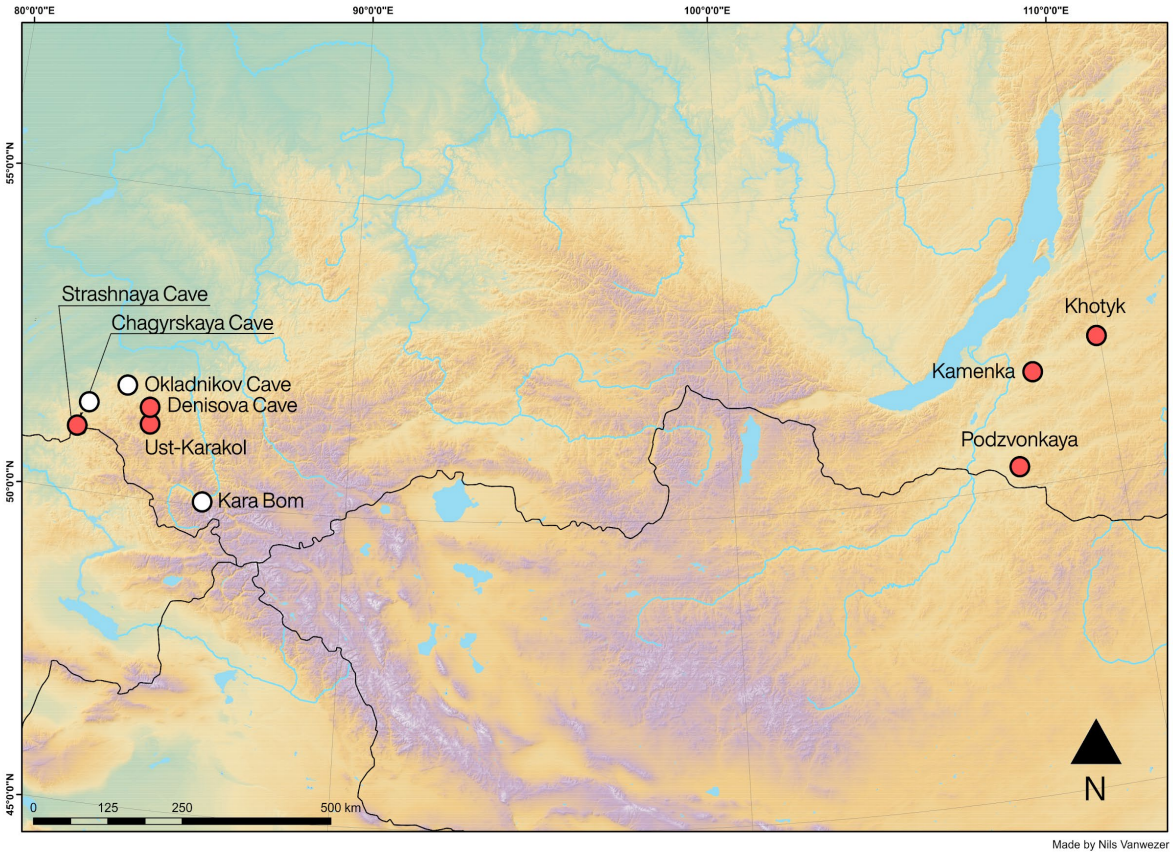

Figure 1: Map of all the sites discussed in the Russian Siberia Altai Mountains and the Transbaikal. ZooMS analysis of fragmented bone assemblages carried out for sites highlighted in red.

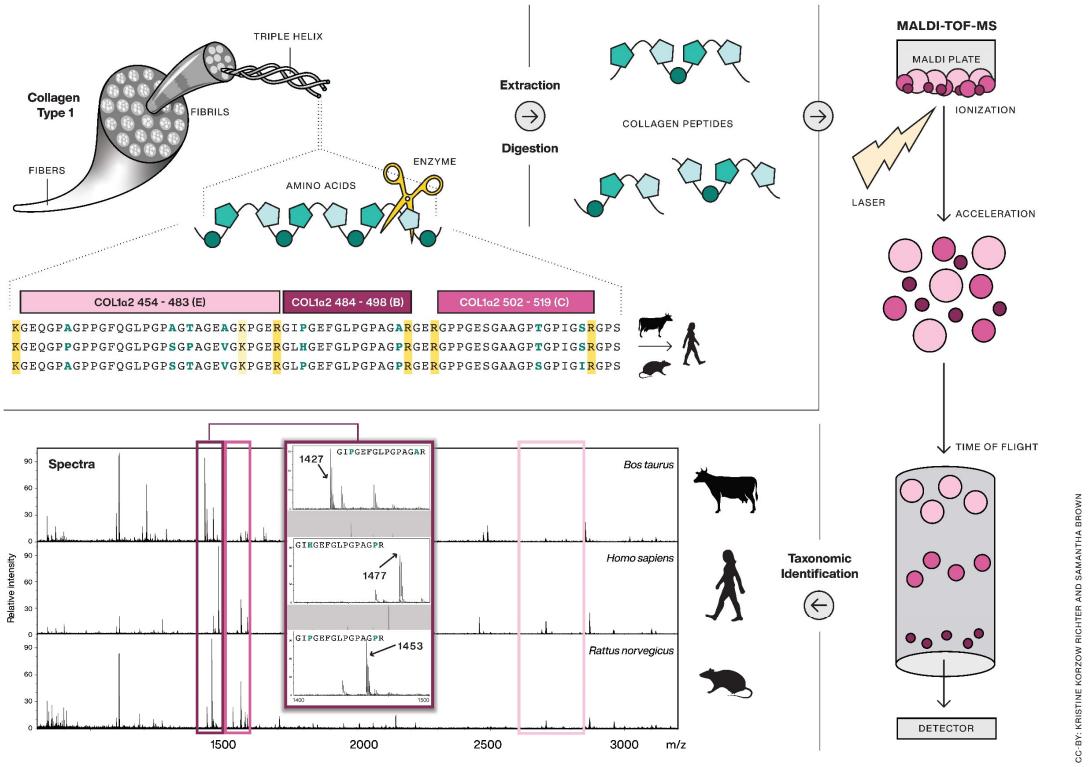

Figure 2: Schematic diagram of ZooMS and sequence alignment. ZooMS gelatinizes fibrillar collagen type I, which contains a characteristic three amino acid repeating pattern of G-X-Y (shaded green shapes). Digestion is typically conducted with the enzyme trypsin, which cuts on the C-terminal side of arginine and lysine (highlighted in yellow in the sequence data). Analysis by MALDI-TOF-MS results in spectra which can be identified based on unique patterns of peaks. The zoomed-in spectral images indicate differences between the three species in the marker COL1α2 484-498. Marker peptides are indicated in the sequence data, MALDI-TOF-MS and the spectra in shades of pink based upon mass. The sequence data is a partial alignment of COL1α2 from Bos taurus (UniProt: P024650), Homo sapiens (UniProt: P08123), and Rattus norvegicus (UniProt: P02466). Collagen image from smart.servier.com.

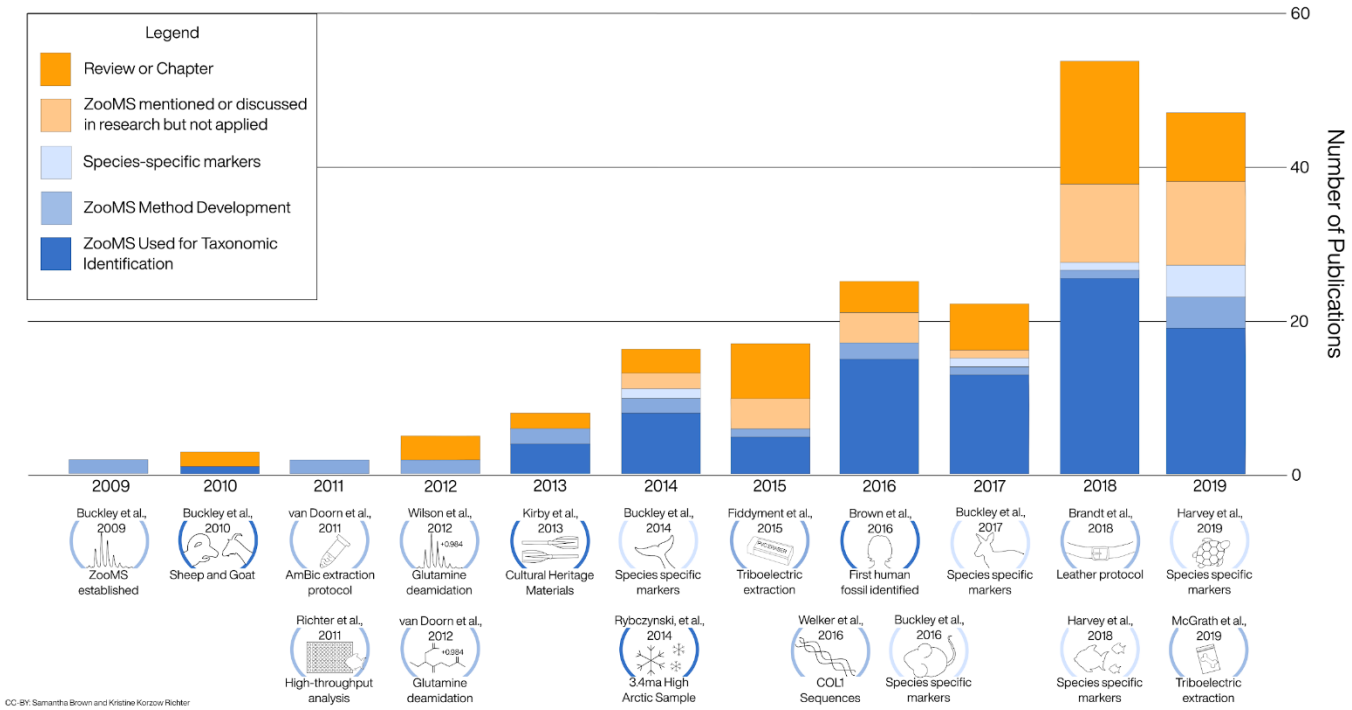

Figure 3: Number of papers which mention “Zooarchaeology by Mass Spectrometry” in the decade after the method was established according to Google Scholar. Major milestones for the method are referenced in circles below the year they were published (Brandt et al., 2018; Brown et al., 2016; Buckley et al., 2014, 2010, 2009; Fiddyment et al., 2015; Harvey et al., 2019, 2018; McGrath et al., 2019; Richter et al., 2011; Rybczynski et al., 2013; van Doorn et al., 2011; Welker et al., 2016).

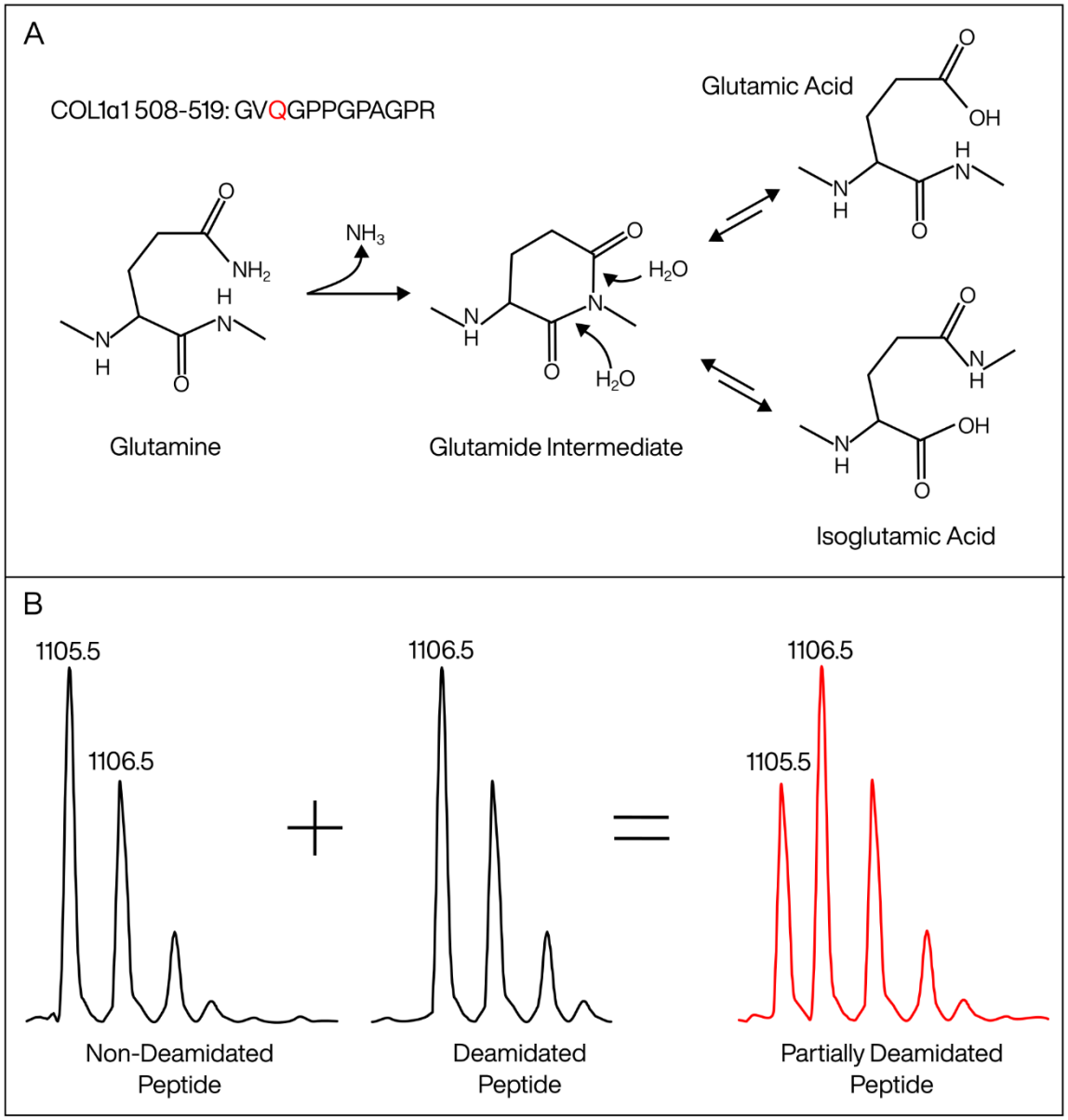

Figure 4: 1a graphical illustration of glutamine deamidating into glutamic acid through a cyclical glutarimide intermediate, adapted (Li et al., 2010). Although it is more common for glutamine deamidation to proceed through direct hydrolysis, when followed in the sequence by a glycine (G) the mechanism likely proceeds through the cyclical intermediate as shown here. 1b illustration of deamidation effects identified in a MALDI-TOF spectrum. The non-deamidated peak (COL1α1 508-519) is measured at 1105.6 m/z and the deamidated peak is measured at 1106.5 m/z. This theoretical

distribution of COL1α1 508-519 is used to determine the extent of glutamine deamidation in PMF spectra. The final “partially deamidated peptide” displays the overlapping distribution of COL1α1 508-519 when there are both non-deamidated and deamidated state peptides present.

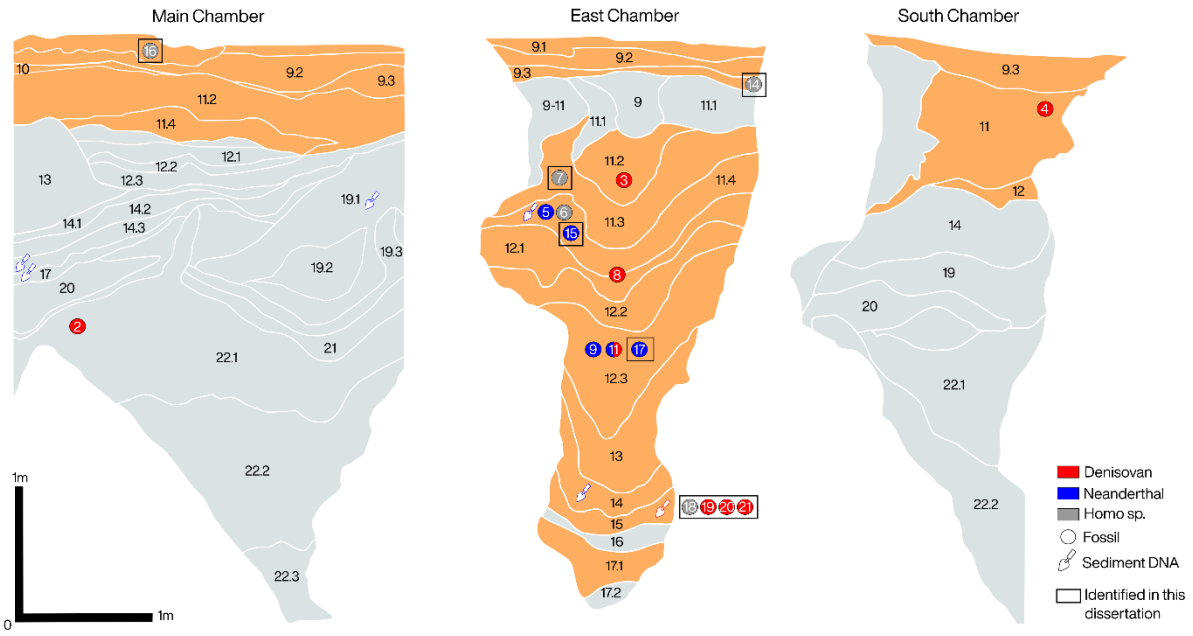

Figure 5: The hominin record at Denisova Cave. Stratigraphy of the Main, East, and South chambers of Denisova Cave. The position of hominin fossils (circles) and sediment DNA (trowel) is shown on the stratigraphic column. Newly identified hominin fossils, Denisova 7, Denisova 14, Denisova 15, Denisova 16, Denisova 17, Denisova 18, Denisova 19, Denisova 20, and Denisova 21 are shown in black boxes.

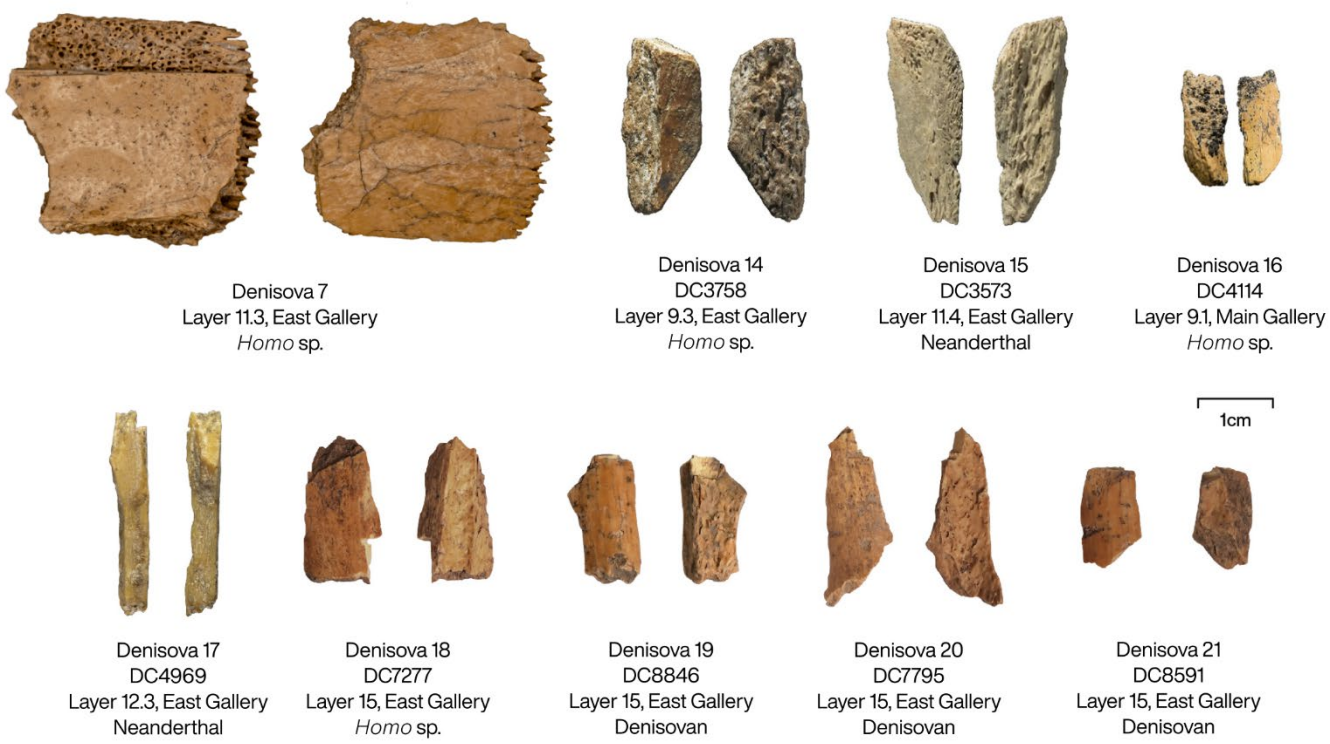

Figure 6: Photographs of each of the hominin bones identified as part of this dissertation. Photographs taken by Ian Cartwright (University of Oxford), Michelle O'Reilly (MPI-SHH) and Hans Sell (MPI-SHH).

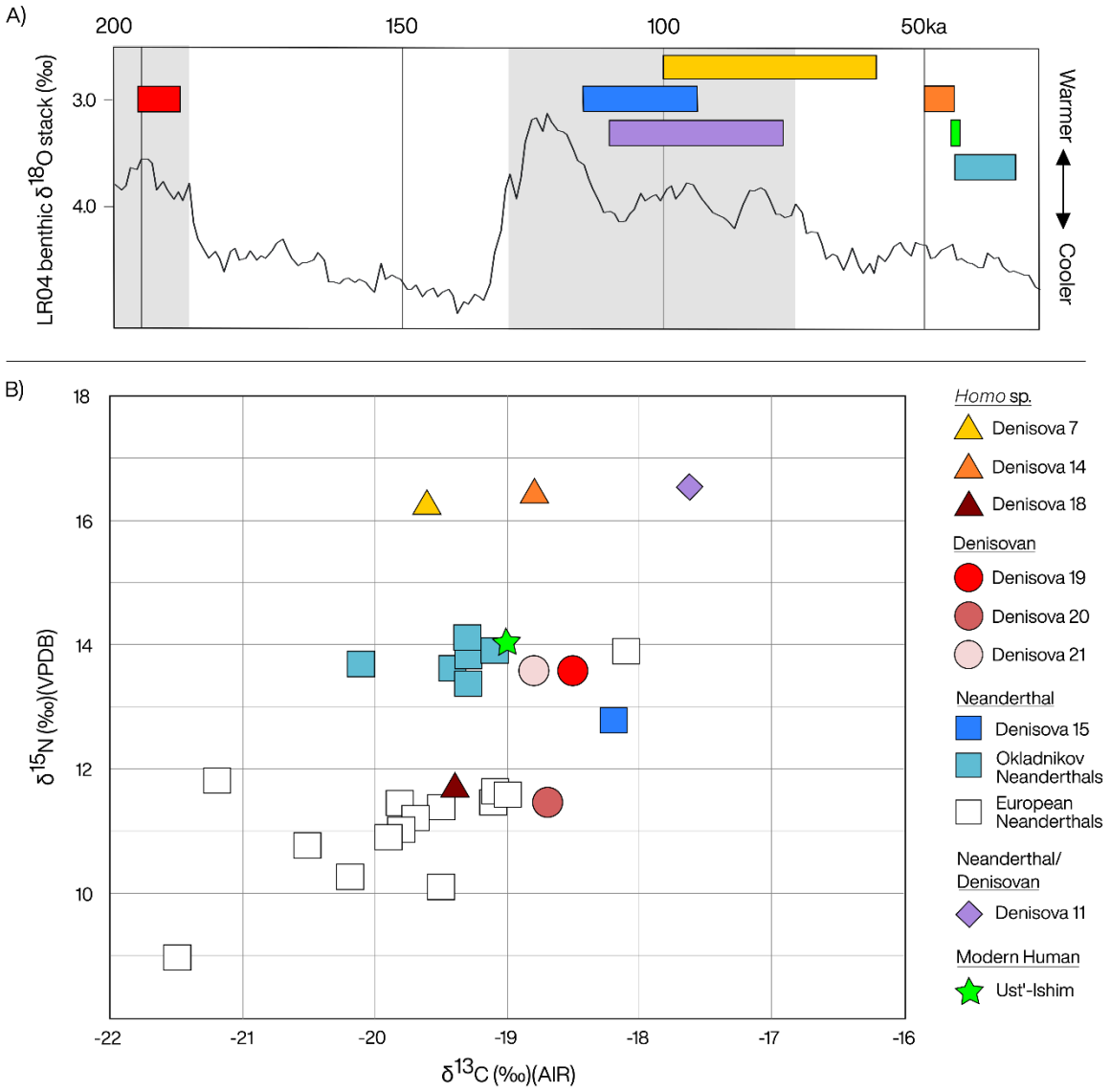

Figure 1: Measured dietary isotopes for Pleistocene hominins including two Homo sp. (D7 and D14), four Denisovans (D18, D19, D20, and D21), Neanderthals from Denisova Cave (D15), Okladnikov Cave, and Europe, the Neanderthal/Denisovan D11, and an early modern human (Ust'-Ishim). **1a**: The marine-oxygen isotope curve compiled from benthic $\delta^{18}O$ records (Lisiecki and Raymo, 2005); the Last and Penultimate Interglacial periods (Marine Isotope Stages 5 and 7) that include some of the warmest parts of the last 200 ka are highlighted. Coloured bars correspond to age estimations for the hominins included in Figure 1b (Derevianko et al., 2013; Douka et al., 2019; Fu et al., 2014).

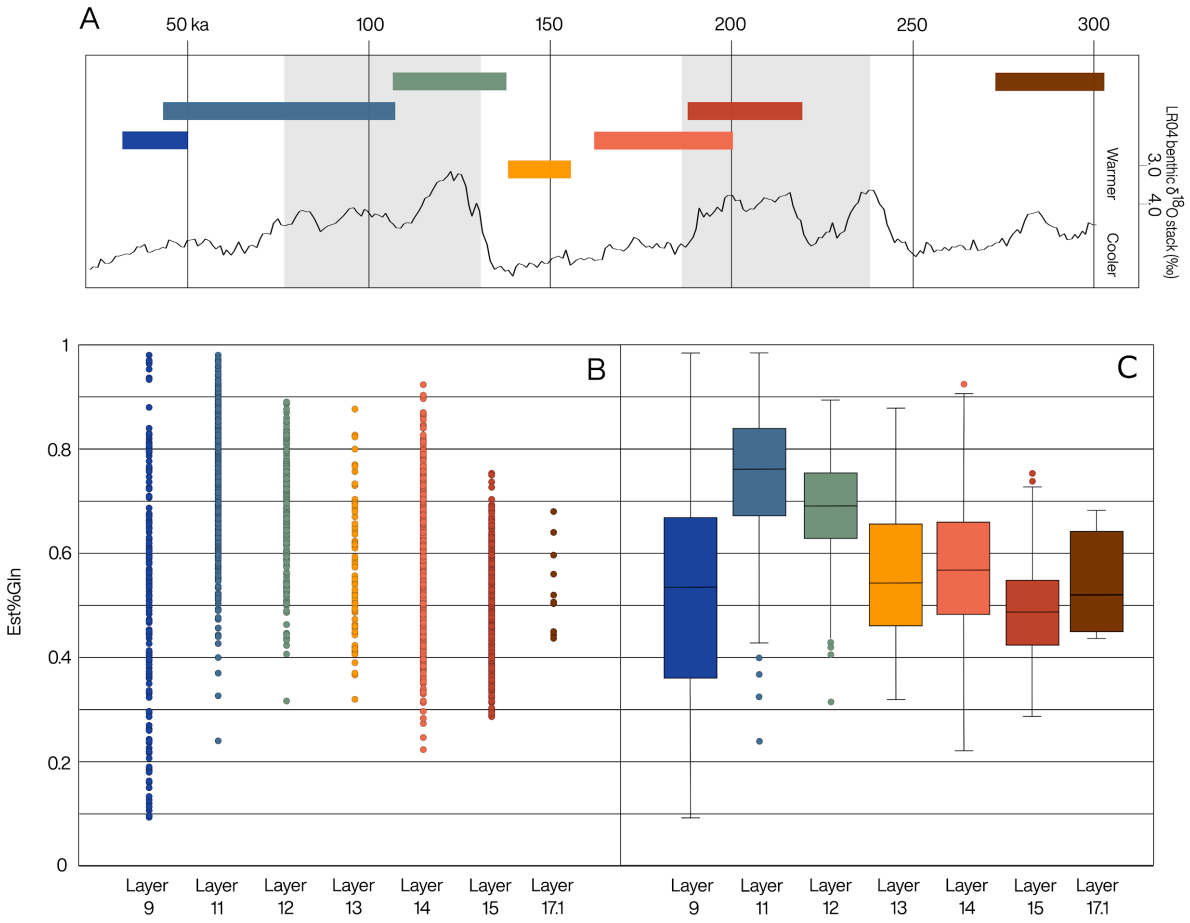

Figure 8: Results of glutamine deamidation measurements for the East Gallery of Denisova Cave. Glutamine deamidation measurements by layer using PMF spectra and Q2E (Wilson et al., 2012), an entirely non-deamidated value is represented by 1, and a completely deamidated value is represented by 0. 1a: The marine-oxygen isotope curve compiled from benthic δ18O records (Lisiecki and Raymo, 2005); the Last and Penultimate Interglacials (Marine Isotope Stages 5 and 7) that were the warmest parts of the last 300 ka are shown in grey. The age range for each of the layers included in this study are shown as coloured bars corresponding to the graphs (1b and 1c) below. 1b: individual bone measurements of glutamine deamidation using Q2E for layers 9 (n=169), 11 (n=518), 12 (n=296), 13 (n=76), 14 (n=688), 15 (n=743), and 17.1 (n=11). 1c: box-and-whisker plots for all PMF measurements by layer, identifying outliers for layers 11, 12, 14, and 15.

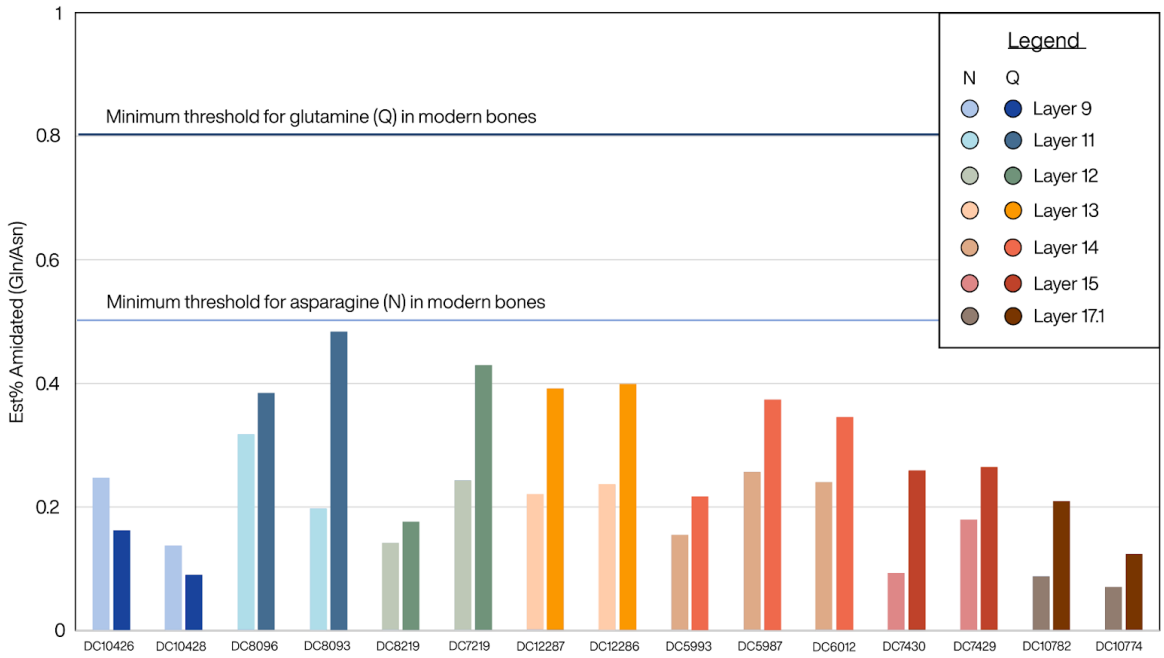

Figure 9: Bulk deamidation measured using LC-MS/MS data with deadmiDATE against modern collagen preservation levels reported in Ramsøe et al. (2020). An entirely non-deamidated value is represented by 1, and a completely deamidated value is represented by 0. All samples fall below the expected values for glutamine (Q) and asparagine (N) deamidation for modern samples.

References

Agadjanian, A.K., Serdyuk, N.V., 2005. The history of mammalian communities and paleogeography of the Altai Mountains in the Paleolithic. Paleontol. J. 39, 645–821.

Ambrose, S.H., 2002. Controlled Diet and Climate Experiments on Nitrogen Isotope Ratios of Rats, in: Ambrose, S.H., Katzenberg, M.A. (Eds.), Biogeochemical Approaches to Paleodietary Analysis. Springer US, Boston, MA, pp. 243–259.

Ambrose, S.H., Norr, L., 1993. Experimental Evidence for the Relationship of the Carbon Isotope Ratios of Whole Diet and Dietary Protein to Those of Bone Collagen and Carbonate, in: Lambert, J.B., Grupe, G. (Eds.), Prehistoric Human Bone: Archaeology at the Molecular Level. Springer Berlin Heidelberg, Berlin, Heidelberg, pp. 1–37.

Antonova, Y.E., Tashak, V.I., Kobylkin, D.V., 2020. Palaeoenvironmental and hunting activity of the Upper Palaeolithic population in Western Transbaikalia: A case study on the Podzvonkaya Settlement, South Siberia. Int J Osteoarchaeol 30, 131–144.

Astakhov, V.I., 2006. Evidence of Late Pleistocene ice-dammed lakes in West Siberia. Boreas.

Astakhov, V.I., 1992. The last glaciation in West Siberia. Sveriges Geologiska Unders. okning, Ser. Ca 81, 21–30.

Astakhov, V.I., 1989. Late Pleistocene sedimentary environments in West Siberia. Trudy Inst. Geol. and Geophys. , Siberian Branch Acad Sci. USSR 118–126.

Bae, C.J., Douka, K., Petraglia, M.D., 2017. On the origin of modern humans: Asian perspectives. Science 358.

Baryshnikov, G., 1999. Large mammals and Neanderthal paleoecology in the Altai mountains (Central Asia, Russia). Préhistoire européenne.

Beaumont, J., Montgomery, J., 2016. The Great Irish Famine: Identifying Starvation in the Tissues of Victims Using Stable Isotope Analysis of Bone and Incremental Dentine Collagen. PLoS One 11, e0160065.

Beauval, C., Lacrampe-Cuyaubère, F., Maureille, B., Trinkaus, E., 2006. Direct radiocarbon dating and stable isotopes of the neandertal femur from Les Rochers-

de-Villeneuve (Lussac-les-Châteaux, Vienne). Bulletins et mémoires de la Société d'Anthropologie de Paris, 18 (1-2) | 2006 2006(1-2) 35–42.

Been, E., Hovers, E., Ekshtain, R., Malinski-Buller, A., Agha, N., Barash, A., Mayer, D.E.B.-Y., Benazzi, S., Hublin, J.-J., Levin, L., Greenbaum, N., Mitki, N., Oxilia, G., Porat, N., Roskin, J., Soudack, M., Yeshurun, R., Shahack-Gross, R., Nir, N., Stahlschmidt, M.C., Rak, Y., Barzilai, O., 2017. The first Neanderthal remains from an open-air Middle Palaeolithic site in the Levant. Sci. Rep. 7, 2958.

Beermann, F., Langer, M., Wetterich, S., Strauss, J., Boike, J., Fiencke, C., Schirrmeister, L., Pfeiffer, E.-M., Kutzbach, L., 2017. Permafrost thaw and liberation of inorganic nitrogen in eastern Siberia. Permafrost Periglacial Processes 28, 605–618.

Bocherens, H., Billiou, D., Mariotti, A., Toussaint, M., Patou-Mathis, M., Bonjean, D., Otte, M., 2001. New isotopic evidence for dietary habits of Neandertals from Belgium. J. Hum. Evol. 40, 497–505.

Bocherens, H., Drucker, D., Billiou, D., Moussa, I., 2005. Une nouvelle approche pour évaluer l'état de conservation de l'os et du collagène pour les mesures isotopiques (datation au radiocarbone, isotopes stables du carbone et de l'azote). L'Anthropologie.

Bocherens, H., Fizet, M., Mariotti, A., Lange-Badre, B., Vandermeersch, B., Borel, J.P., Bellon, G., 1991. Isotopic biogeochemistry (13C,15N) of fossil vertebrate collagen: application to the study of a past food web including Neandertal man. J. Hum. Evol. 20, 481–492.

Bolikhovskaya, N.S., Shunkov, M.V., 2014. Pleistocene Environments of Northwestern Altai: Vegetation and Climate1. Archaeology, Ethnology and Anthropology of Eurasia 42, 2–17.

Bradfield, J., Forssman, T., Spindler, L., Antonites, A.R., 2018. Identifying the animal species used to manufacture bone arrowheads in South Africa. Archaeol. Anthropol. Sci. 11, 2419–2434.

Brandt, L.Ø., Haase, K., Collins, M.J., 2018. Species identification using ZooMS, with reference to the exploitation of animal resources in the medieval town of Odense. Danish Journal of Archaeology 7, 139–153.

Browning, S.R., Browning, B.L., Zhou, Y., Tucci, S., Akey, J.M., 2018. Analysis of Human Sequence Data Reveals Two Pulses of Archaic Denisovan Admixture. Cell 173, 53–61.e9.

Brown, S., Hebestreit, S., Wang, N., Boivin, N., Douka, K., Richter, K., 2020a. Zooarchaeology by Mass Spectrometry (ZooMS) for bone material - AmBiC protocol v1 (protocols.io.bffdjji6).

Brown, S., Hebestreit, S., Wang, N., Boivin, N., Douka, K., Richter, K., 2020b. Zooarchaeology by Mass Spectrometry (ZooMS) for bone material - Acid insoluble protocol (protocols.io.bf43jqyn).

Brown, S., Hebestreit, S., Wang, N., Nicole Boivin, Douka, K., Richter, K., 2020c. Zooarchaeology by Mass Spectrometry (ZooMS) for bone material - Acid soluble protocol (protocols.io.bf5bjq2n).

Brown, S., Hebestreit, S., Wang, N., Nicole Boivin, Douka, K., Richter, K., 2020c. Zooarchaeology by Mass Spectrometry (ZooMS) for leather/skin/hide material (protocols.io.private.482A866B96BE9422470B1A5D07FBA657)

Brown, S., Higham, T., Slon, V., Pääbo, S., Meyer, M., Douka, K., Brock, F., Comeskey, D., Procopio, N., Shunkov, M., Derevianko, A., Buckley, M., 2016. Identification of a new hominin bone from Denisova Cave, Siberia using collagen fingerprinting and mitochondrial DNA analysis. Sci. Rep. 6, 23559.

Brown, S., Massilani, D., Kozlikin, M.B., Shunkov, M.V., Derevianko, A.P., Stoessel, A., Jope, B., Meyer, M., Kelso, J., Pääbo, S., Higham, T., Douka, K., submitted. Earliest evidence for Denisovans identified using peptide mass fingerprinting and mitochondrial DNA analysis. Nat. Eco. Evo.

Buckley, M., Collins, M., Thomas-Oates, J., Wilson, J.C., 2009. Species identification by analysis of bone collagen using matrix-assisted laser desorption/ionisation time-of-flight mass spectrometry. Rapid Commun. Mass Spectrom. 23, 3843–3854.

Buckley, M., Cosgrove, R., Garvey, J., Prideaux, G.J., 2017a. Identifying remains of extinct kangaroos in Late Pleistocene deposits using collagen fingerprinting. J. Quat. Sci. 32, 653–660.

Buckley, M., Fraser, S., Herman, J., Melton, N.D., Mulville, J., Pálsdóttir, A.H., 2014. Species identification of archaeological marine mammals using collagen fingerprinting. J. Archaeol. Sci. 41, 631–641.

Buckley, M., Gu, M., Shameer, S., Patel, S., Chamberlain, A.T., 2016. High-throughput collagen fingerprinting of intact microfaunal remains; a low-cost method for distinguishing between murine rodent bones. Rapid Commun. Mass Spectrom. 30, 805–812.

Buckley, M., Harvey, V.L., Chamberlain, A.T., 2017b. Species identification and decay assessment of Late Pleistocene fragmentary vertebrate remains from Pin Hole Cave (Creswell Crags, UK) using collagen fingerprinting. Boreas 46, 402–411.

Buckley, M., Kansa, S.W., 2011. Collagen fingerprinting of archaeological bone and teeth remains from Domuztepe, South Eastern Turkey. Archaeol. Anthropol. Sci. 3, 271–280.

Buckley, M., Whitcher Kansa, S., Howard, S., Campbell, S., Thomas-Oates, J., Collins, M., 2010. Distinguishing between archaeological sheep and goat bones using a single collagen peptide. J. Archaeol. Sci. 37, 13–20.

Burpee, B.T., Anderson, D., Saros, J.E., 2018. Assessing ecological effects of glacial meltwater on lakes fed by the Greenland Ice Sheet: The role of nutrient subsidies and turbidity. Arct. Antarct. Alp. Res. 50, S100019.

Buzhilova, A.P., 2011. Odontometry of homo deciduous teeth from late pleistocene layers of altai caves, siberia 24–39.

Charlton, S.J.L., Alexander, M., Collins, M.J., Milner, N., Craig, O.E., 2016. Finding Britain's last hunter-gatherers: A new biomolecular approach to "unidentifiable" bone fragments utilising bone collagen 73, 55–61.

Chen, F., Welker, F., Shen, C.-C., Bailey, S.E., Bergmann, I., Davis, S., Xia, H., Wang, H., Fischer, R., Freidline, S.E., Yu, T.-L., Skinner, M.M., Stelzer, S., Dong, G., Fu, Q., Dong, G., Wang, J., Zhang, D., Hublin, J.-J., 2019. A late Middle Pleistocene Denisovan mandible from the Tibetan Plateau. Nature 569, 409–412.

Chlachula, J., 2001. Pleistocene climate change, natural environments and palaeolithic occupation of the Altai area, west-central Siberia. Quat. Int. 80-81, 131–167.

Conard, N.J., Malina, M., Münzel, S.C., 2009. New flutes document the earliest musical tradition in southwestern Germany. Nature 460, 737–740.

Coutu, A.N., Whitelaw, G., le Roux, P., Sealy, J., 2016. Earliest Evidence for the Ivory Trade in Southern Africa: Isotopic and ZooMS Analysis of Seventh–Tenth Century ad Ivory from KwaZulu-Natal. African Archaeological Review 33, 411–435.

Deniro, M.J., Epstein, S., 1981. Influence of diet on the distribution of nitrogen isotopes in animals. Geochim. Cosmochim. Acta 45, 341–351.

Derevianko, A., 2007. K probleme obitaniya neandertaltsev v Tsentralnoi Azii i Sibiri. Izd. IAE SO RAN, Novosibirsk.

Derevianko, A., Markin, S.V., 1992. Mustye gornogo Altaya (po materialam peschery im. Okladnikova). Nauka, Novosibirsk.

Derevianko, A.P., 2010. Three Scenarios of the Middle to Upper Paleolithic Transition: Scenario 1: The Middle to Upper Paleolithic Transition in Northern Asia. Archaeology, Ethnology and Anthropology of Eurasia 38, 2–32.

Derevianko, A.P., Markin, S.V., Shunkov, M.V., 2013. The Sibiryachikha Facies of the Middle Paleolithic of the Altai. Archaeology, Ethnology and Anthropology of Eurasia 41, 89–103.

Derevianko, A.P., Postnov, A.V., Rybin, E.P., Kuzmin, Y.V., Keates, S.G., 2005. The Pleistocene Peopling of Siberia: a review of environmental and behavioural aspects. Indo-Pacific Prehistory Association Bulletin 25.

Derevianko, A.P., Rybin, E.P., 2003. The earliest representations of symbolic behavior by Paleolithic humans in the Altai Mountains. Archaeology, Ethnology and Anthropology of Eurasia 27–50.

Derevianko, O.P., Shunkov, M.V., Kozlikin, M.B., 2020. Who Were the Denisovans? Archaeology, Ethnology & Anthropology of Eurasia 48, 3–32.

Desmond, A., Barton, N., Bouzouggar, A., Douka, K., Fernandez, P., Humphrey, L., Morales, J., Turner, E., Buckley, M., 2018. ZooMS identification of bone tools from the North African Later Stone Age. J. Archaeol. Sci. 98, 149–157.

Devièse, T., Karavanić, I., Comeskey, D., Kubiak, C., Korlević, P., Hajdinjak, M., Radović, S., Procopio, N., Buckley, M., Pääbo, S., Higham, T., 2017. Direct dating of

Neanderthal remains from the site of Vindija Cave and implications for the Middle to Upper Paleolithic transition. Proc. Natl. Acad. Sci. U. S. A. 114, 10606–10611.

Dobrovolskaya, M.V., Tiunov, A.V., 2013. The Neanderthals of Okladnikov Cave Altai: Environment and Diet Based on Isotopic Analysis*. Archaeology, Ethnology and Anthropology of Eurasia 41, 78–88.

Doi, H., Akamatsu, F., González, A.L., 2017. Starvation effects on nitrogen and carbon stable isotopes of animals: an insight from meta-analysis of fasting experiments. R Soc Open Sci 4, 170633.

Doi, H., Kikuchi, E., Takagi, S., Shikano, S., 2007. Changes in carbon and nitrogen stable isotopes of chironomid larvae during growth, starvation and metamorphosis. Rapid Commun. Mass Spectrom. 21, 997–1002.

Douka, K., Brown, S., Higham, T., Pääbo, S., Derevianko, A., Shunkov, M., 2019a. FINDER project: collagen fingerprinting (ZooMS) for the identification of new human fossils. Antiquity 93.

Douka, K., Slon, V., Jacobs, Z., Ramsey, C.B., Shunkov, M.V., Derevianko, A.P., Mafessoni, F., Kozlikin, M.B., Li, B., Grün, R., Comeskey, D., Devièse, T., Brown, S., Viola, B., Kinsley, L., Buckley, M., Meyer, M., Roberts, R.G., Pääbo, S., Kelso, J., Higham, T., 2019b. Age estimates for hominin fossils and the onset of the Upper Palaeolithic at Denisova Cave. Nature 565, 640–644.

Faivre, J.-P., Maureille, B., Bayle, P., Crevecoeur, I., Duval, M., Grün, R., Bemilli, C., Bonilauri, S., Coutard, S., Bessou, M., Limondin-Lozouet, N., Cottard, A., Deshayes, T., Douillard, A., Henaff, X., Pautret-Homerville, C., Kinsley, L., Trinkaus, E., 2014. Middle pleistocene human remains from Tourville-la-Rivière (Normandy, France) and their archaeological context. PLoS One 9, e104111.

Fewlass, H., Tuna, T., Fagault, Y., Hublin, J.-J., Kromer, B., Bard, E., Talamo, S., 2019. Pretreatment and gaseous radiocarbon dating of 40-100 mg archaeological bone. Sci. Rep. 9, 5342.

Fiddyment, S., Holsinger, B., Ruzzier, C., Devine, A., Binois, A., Albarella, U., Fischer, R., Nichols, E., Curtis, A., Cheese, E., Teasdale, M.D., Checkley-Scott, C., Milner, S.J., Rudy, K.M., Johnson, E.J., Vnouček, J., Garrison, M., McGrory, S., Bradley, D.G.,

Collins, M.J., 2015. Animal origin of 13th-century uterine vellum revealed using noninvasive peptide fingerprinting. Proc. Natl. Acad. Sci. U. S. A. 112, 15066–15071.

Fizet, M., Lange-Badré, B., 1995. δ13C et δ15N du collagène des mammifères: Reconstitution des relations trophiques et du paléoenvironnement du gisement de Marillac (France, Pléistocène supérieur). Geobios. 28(1), 167–181.

Fu, Q., Li, H., Moorjani, P., Jay, F., Slepchenko, S.M., Bondarev, A.A., Johnson, P.L.F., Aximu-Petri, A., Prüfer, K., de Filippo, C., Meyer, M., Zwyns, N., Salazar-García, D.C., Kuzmin, Y.V., Keates, S.G., Kosintsev, P.A., Razhev, D.I., Richards, M.P., Peristov, N.V., Lachmann, M., Douka, K., Higham, T.F.G., Slatkin, M., Hublin, J.-J., Reich, D., Kelso, J., Viola, T.B., Pääbo, S., 2014. Genome sequence of a 45,000-year-old modern human from western Siberia. Nature 514, 445–449.

Göransson, H., Welc, M., Bünemann, E.K., Christl, I., Venterink, H.O., 2016. Nitrogen and phosphorus availability at early stages of soil development in the Damma glacier forefield, Switzerland; implications for establishment of N2-fixing plants. Plant Soil 404, 251–261.

Grealy, A.C., McDowell, M.C., Scofield, P., Murray, D.C., Fusco, D.A., Haile, J., Prideaux, G.J., Bunce, M., 2015. A critical evaluation of how ancient DNA bulk bone metabarcoding complements traditional morphological analysis of fossil assemblages. Quat. Sci. Rev. 128, 37–47.

Harvey, V.L., Daugnora, L., Buckley, M., 2018. Species identification of ancient Lithuanian fish remains using collagen fingerprinting. J. Archaeol. Sci. 98, 102–111.

Harvey, V.L., LeFebvre, M.J., deFrance, S.D., Toftgaard, C., Drosou, K., Kitchener, A.C., Buckley, M., 2019. Preserved collagen reveals species identity in archaeological marine turtle bones from Caribbean and Florida sites. R Soc Open Sci 6, 191137.

Hendy, J., Welker, F., Demarchi, B., Speller, C., Warinner, C., Collins, M.J., 2018. A guide to ancient protein studies. Nat Ecol Evol 2, 791–799.

Henriksen, K., Karsdal, M.A., 2019. Type I collagen. in Biochemistry of Collagens, Laminins and Elastin. p. 1–12. Academic Press.

Higham, T., Basell, L., Jacobi, R., Wood, R., Ramsey, C.B., Conard, N.J., 2012. Testing models for the beginnings of the Aurignacian and the advent of figurative art and music: the radiocarbon chronology of Geißenklösterle. J. Hum. Evol. 62, 664–676.

Higham, T., Ramsey, C.B., Karavanić, I., Smith, F.H., Trinkaus, E., 2006. Revised direct radiocarbon dating of the Vindija G1 Upper Paleolithic Neandertals. Proc. Natl. Acad. Sci. U. S. A. 103, 553–557.

Hill, R.C., Wither, M.J., Nemkov, T., Barrett, A., D'Alessandro, A., Dzieciatkowska, M., Hansen, K.C., 2015. Preserved Proteins from Extinct Bison latifrons Identified by Tandem Mass Spectrometry; Hydroxylysine Glycosides are a Common Feature of Ancient Collagen. Mol. Cell. Proteomics 14, 1946–1958.

Hublin, J.-J., 2012. The earliest modern human colonization of Europe. Proc. Natl. Acad. Sci. U. S. A.

Huerta-Sánchez, E., Jin, X., Asan, Bianba, Z., Peter, B.M., Vinckenbosch, N., Liang, Y., Yi, X., He, M., Somel, M., Ni, P., Wang, B., Ou, X., Huasang, Luosang, J., Cuo, Z.X.P., Li, K., Gao, G., Yin, Y., Wang, W., Zhang, X., Xu, X., Yang, H., Li, Y., Wang, J., Wang, J., Nielsen, R., 2014. Altitude adaptation in Tibetans caused by introgression of Denisovan-like DNA. Nature 512, 194–197.

Jacobs, G.S., Hudjashov, G., Saag, L., Kusuma, P., Darusallam, C.C., Lawson, D.J., Mondal, M., Pagani, L., Ricaut, F.-X., Stoneking, M., Metspalu, M., Sudoyo, H., Lansing, J.S., Cox, M.P., 2019. Multiple Deeply Divergent Denisovan Ancestries in Papuans. Cell 177, 1010–1021.e32.

Jacobs, Z., Li, B., Shunkov, M.V., Kozlikin, M.B., Bolikhovskaya, N.S., Agadjanian, A.K., Uliyanov, V.A., Vasiliev, S.K., O'Gorman, K., Derevianko, A.P., Roberts, R.G., 2019. Timing of archaic hominin occupation of Denisova Cave in southern Siberia. Nature 565, 594–599.

Janzen, A., Richter, K.K., Mwebi, O., Brown S Onduso, Gatwiri, F., Ndiema, E., Katongo, M., Goldstein, S.T., Douka, K., Boivin, N., submitted. Distinguishing African bovids using Zooarchaeology by Mass Spectrometry (ZooMS): New peptide markers and assessments of Iron Age economies in Zambia. PLoS One.

Jaouen, K., Richards, M.P., Le Cabec, A., Welker, F., Rendu, W., Hublin, J.-J., Soressi, M., Talamo, S., 2019. Exceptionally high δ15N values in collagen single amino acids confirm Neandertals as high-trophic level carnivores. Proc. Natl. Acad. Sci. U. S. A. 116, 4928–4933.

Jarman, C.L., Larsen, T., Hunt, T., Lipo, C., Solsvik, R., Wallsgrove, N., Ka'apu-Lyons, C., Close, H.G., Popp, B.N., 2017. Diet of the prehistoric population of Rapa Nui (Easter Island, Chile) shows environmental adaptation and resilience. Am. J. Phys. Anthropol. 164, 343–361.

Keuper, F., Dorrepaal, E., van Bodegom, P.M., van Logtestijn, R., Venhuizen, G., van Hal, J., Aerts, R., 2017. Experimentally increased nutrient availability at the permafrost thaw front selectively enhances biomass production of deep-rooting subarctic peatland species. Glob. Chang. Biol. 23, 4257–4266.

Kirby, D.P., Buckley, M., Promise, E., Trauger, S.A., Holdcraft, T.R., 2013. Identification of collagen-based materials in cultural heritage. Analyst 138, 4849–4858.

Kolobova, K.A., Roberts, R.G., Chabai, V.P., Jacobs, Z., Krajcarz, M.T., Shalagina, A.V., Krivoshapkin, A.I., Li, B., Uthmeier, T., Markin, S.V., Morley, M.W., O'Gorman, K., Rudaya, N.A., Talamo, S., Viola, B., Derevianko, A.P., 2020. Archaeological evidence for two separate dispersals of Neanderthals into southern Siberia. Proc. Natl. Acad. Sci. U. S. A. 117, 2879–2885.

Krause, J., Briggs, A.W., Kircher, M., Maricic, T., Zwyns, N., Derevianko, A., Pääbo, S., 2010a. A complete mtDNA genome of an early modern human from Kostenki, Russia. Curr. Biol. 20, 231–236.

Krause, J., Fu, Q., Good, J.M., Viola, B., Shunkov, M.V., Derevianko, A.P., Pääbo, S., 2010b. The complete mitochondrial DNA genome of an unknown hominin from southern Siberia. Nature 464, 894–897.

Krause, J., Orlando, L., Serre, D., Viola, B., Prüfer, K., Richards, M.P., Hublin, J.-J., Hänni, C., Derevianko, A.P., Pääbo, S., 2007. Neanderthals in central Asia and Siberia. Nature 449, 902–904.

Krivoshapkin, A., Shalagina, A., Baumann, M., Shnaider, S., Kolobova, K., 2018. Between Denisovans and Neanderthals: Strashnaya Cave in the Altai Mountains. Antiquity 92. https://doi.org/10.15184/aqy.2018.221

Kuhn, S.L., Zwyns, N., 2014. Rethinking the initial Upper Paleolithic. Quat. Int. 347, 29–38.

Kuzmin, Y.V., Brantingham, P.J., Kuhn, S.L., Kerry, K.W., 2004. Origin of the Upper Paleolithic in Siberia. The Early Upper Paleolithic Beyond Western Europe. Los Angeles: University of California Press. p 196–206.

Kuzmin, Y.V., Lbova, L.V., Jull, A.J.T., Cruz, R.J., 2006. The Middle-to-Upper-Paleolithic transition in Transbaikal, Siberia: the Khotyk site chronology and archaeology. Current Research in the Pleistocene 23.

Larsen, T., Ventura, M., Andersen, N., O'Brien, D.M., Piatkowski, U., McCarthy, M.D., 2013. Tracing carbon sources through aquatic and terrestrial food webs using amino acid stable isotope fingerprinting. PLoS One 8, e73441.

Lbova, L., 2010. Evidence of Modern Human Behavior in the Baikal Zone during the Early Upper Paleolithic Period. Bulletin of the Indo-Pacific Prehistory Association 30, 9–13.

Lbova, L., 2008. Chronology and paleoecology of the Early Upper Paleolithic in the Transbaikal region (Siberia). Eurasian Prehistory 5.

Lbova, L., Kozhevnikova, D., Volkov, P., 2010. Musical instruments in Siberia (Early stage of the Upper Paleolithic). Ac-tes du Congrès de l'IFRAO, Tarascon-sur-Ariége 2011, 324–325.

Lbova, L.V., 2000. Paleolit severnoj zony Zapadnogo Zabajkal'ja. Izdat. Burjatskogo Naučnogo Centra SO RAN.

Lbova, L.V., 1999. The palaeoecological model of the Upper Palaeolithic site Kamenka (Buryatia-Siberia). Anthropozoikum 23, 181–191.

Lisiecki, L.E., Raymo, M.E., 2005. A Pliocene-Pleistocene stack of 57 globally distributed benthic δ18O records. Paleoceanography 20.

Lister, A.M., Stuart, A.J., 2019. The extinction of the giant deer Megaloceros giganteus (Blumenbach): New radiocarbon evidence. Quat. Int. 500, 185–203.

Li, X., Lin, C., O'Connor, P.B., 2010. Glutamine deamidation: differentiation of glutamic acid and gamma-glutamic acid in peptides by electron capture dissociation. Anal. Chem. 82, 3606–3615.

Li, Z.-Y., Wu, X.-J., Zhou, L.-P., Liu, W., Gao, X., Nian, X.-M., Trinkaus, E., 2017. Late Pleistocene archaic human crania from Xuchang, China. Science 355, 969–972.

Liu, X., Wang, G., Li, J., Wang, Q., 2010. Nitrogen isotope composition characteristics of modern plants and their variations along an altitudinal gradient in Dongling Mountain in Beijing. Sci. China Ser. D Earth Sci. 53, 128–140.

Longin, R., 1971. New method of collagen extraction for radiocarbon dating. Nature 230, 241–242.

Mafessoni, F., Grote, S., de Filippo, C., Slon, V., Kolobova, K.A., Viola, B., Markin, S.V., Chintalapati, M., Peyrégne, S., Skov, L., Skoglund, P., Krivoshapkin, A.I., Derevianko, A.P., Meyer, M., Kelso, J., Peter, B., Prüfer, K., Pääbo, S., 2020. A high-coverage Neandertal genome from Chagyrskaya Cave. Proc. Natl. Acad. Sci. U. S. A. 117(26) 15132–15136.

Mao, C., Kou, D., Chen, L., Qin, S., Zhang, D., Peng, Y., Yang, Y., 2020. Permafrost nitrogen status and its determinants on the Tibetan Plateau. Glob. Chang. Biol. 26(9) 5290–5302.

McGrath, K., Rowsell, K., Gates St-Pierre, C., Tedder, A., Foody, G., Roberts, C., Speller, C., Collins, M., 2019. Identifying Archaeological Bone via Non-Destructive ZooMS and the Materiality of Symbolic Expression: Examples from Iroquoian Bone Points. Sci. Rep. 9, 11027.

Mednikova, M., 2011. Postcranial morphology and taxonomy of representatives of the genus Homo from Okladnikov cave in Altai (in Russian), Institute of Archeology and Ethnography Publishing House, Novosibirsk.

Mednikova, M.B., 2011. A proximal pedal phalanx of a Paleolithic hominin from denisova cave, Altai. Archaeology, Ethnology and Anthropology of Eurasia 39, 129–138.

Meyer, M., Kircher, M., Gansauge, M.-T., Li, H., Racimo, F., Mallick, S., Schraiber, J.G., Jay, F., Prüfer, K., de Filippo, C., Sudmant, P.H., Alkan, C., Fu, Q., Do, R., Rohland, N., Tandon, A., Siebauer, M., Green, R.E., Bryc, K., Briggs, A.W., Stenzel, U., Dabney, J., Shendure, J., Kitzman, J., Hammer, M.F., Shunkov, M.V., Derevianko, A.P., Patterson, N., Andrés, A.M., Eichler, E.E., Slatkin, M., Reich, D., Kelso, J., Pääbo, S., 2012. A high-coverage genome sequence from an archaic Denisovan individual. Science 338, 222–226.

Morley, M.W., Goldberg, P., Uliyanov, V.A., Kozlikin, M.B., Shunkov, M.V., Derevianko, A.P., Jacobs, Z., Roberts, R.G., 2019. Hominin and animal activities in the

microstratigraphic record from Denisova Cave (Altai Mountains, Russia). Sci. Rep. 9, 13785.

Motuzaite Matuzeviciute, G., Kiryushin, Y.F., Rakhimzhanova, S.Z., Svyatko, S., Tishkin, A.A., O'Connell, T.C., 2016. Climatic or dietary change? Stable isotope analysis of Neolithic–Bronze Age populations from the Upper Ob and Tobol River basins. Holocene 26, 1711–1721.

Murray, D.C., Haile, J., Dortch, J., White, N.E., Haouchar, D., Bellgard, M.I., Allcock, R.J., Prideaux, G.J., Bunce, M., 2013. Scrapheap challenge: a novel bulk-bone metabarcoding method to investigate ancient DNA in faunal assemblages. Sci. Rep. 3, 3371.

Nakamura, K., Schoeller, D.A., Winkler, F.J., Schmidt, H.L., 1982. Geographical variations in the carbon isotope composition of the diet and hair in contemporary man. Biomed. Mass Spectrom. 9, 390–394.

O'Connel, T.C., Hedges, R.E.M., 1999. Isotopic comparison of hair and bone: Archaeological analysis. J. Archaeol. Sci. 26, 661–665.

Orlando, L., Ginolhac, A., Zhang, G., Froese, D., Albrechtsen, A., Stiller, M., Schubert, M., Cappellini, E., Petersen, B., Moltke, I., Johnson, P.L.F., Fumagalli, M., Vilstrup, J.T., Raghavan, M., Korneliussen, T., Malaspinas, A.-S., Vogt, J., Szklarczyk, D., Kelstrup, C.D., Vinther, J., Dolocan, A., Stenderup, J., Velazquez, A.M.V., Cahill, J., Rasmussen, M., Wang, X., Min, J., Zazula, G.D., Seguin-Orlando, A., Mortensen, C., Magnussen, K., Thompson, J.F., Weinstock, J., Gregersen, K., Røed, K.H., Eisenmann, V., Rubin, C.J., Miller, D.C., Antczak, D.F., Bertelsen, M.F., Brunak, S., Al-Rasheid, K.A.S., Ryder, O., Andersson, L., Mundy, J., Krogh, A., Gilbert, M.T.P., Kjær, K., Sicheritz-Ponten, T., Jensen, L.J., Olsen, J.V., Hofreiter, M., Nielsen, R., Shapiro, B., Wang, J., Willerslev, E., 2013. Recalibrating Equus evolution using the genome sequence of an early Middle Pleistocene horse. Nature 499, 74–78.

Orlova, L.A., Kuzmin, Y.V., Lbova, L.V., 2005. Radiocarbon Dates of the Paleolithic and Mesolithic Sites in Transbaikal and Mongolia. The Paleolithic Cultures of Transbaikal and Mongolia: New Facts, Methods, and Hypotheses, p. 88–92.

Pal Chowdhury, M., Wogelius, R., Manning, P.L., Metz, L., Slimak, L., Buckley, M., 2019. Collagen deamidation in archaeological bone as an assessment for relative decay rates. Archaeometry 61, 1382–1398.

Panin, A.V., Astakhov, V.I., Lotsari, E., Komatsu, G., Lang, J., Winsemann, J., 2020. Middle and Late Quaternary glacial lake-outburst floods, drainage diversions and reorganization of fluvial systems in northwestern Eurasia. Earth-Sci. Rev. 201, 103069.

Peter, B.M., 2020. 100,000 years of gene flow between Neandertals and Denisovans in the Altai mountains. bioRxiv.

Prüfer, K., de Filippo, C., Grote, S., Mafessoni, F., Korlević, P., Hajdinjak, M., Vernot, B., Skov, L., Hsieh, P., Peyrégne, S., Reher, D., Hopfe, C., Nagel, S., Maricic, T., Fu, Q., Theunert, C., Rogers, R., Skoglund, P., Chintalapati, M., Dannemann, M., Nelson, B.J., Key, F.M., Rudan, P., Kućan, Ž., Gušić, I., Golovanova, L.V., Doronichev, V.B., Patterson, N., Reich, D., Eichler, E.E., Slatkin, M., Schierup, M.H., Andrés, A.M., Kelso, J., Meyer, M., Pääbo, S., 2017. A high-coverage Neandertal genome from Vindija Cave in Croatia. Science 358, 655–658.

Prüfer, K., Racimo, F., Patterson, N., Jay, F., Sankararaman, S., Sawyer, S., Heinze, A., Renaud, G., Sudmant, P.H., de Filippo, C., Li, H., Mallick, S., Dannemann, M., Fu, Q., Kircher, M., Kuhlwilm, M., Lachmann, M., Meyer, M., Ongyerth, M., Siebauer, M., Theunert, C., Tandon, A., Moorjani, P., Pickrell, J., Mullikin, J.C., Vohr, S.H., Green, R.E., Hellmann, I., Johnson, P.L.F., Blanche, H., Cann, H., Kitzman, J.O., Shendure, J., Eichler, E.E., Lein, E.S., Bakken, T.E., Golovanova, L.V., Doronichev, V.B., Shunkov, M.V., Derevianko, A.P., Viola, B., Slatkin, M., Reich, D., Kelso, J., Pääbo, S., 2014. The complete genome sequence of a Neanderthal from the Altai Mountains. Nature 505, 43–49.

Ramsøe, A., van Heekeren, V., Ponce, P., Fischer, R., Barnes, I., Speller, C., Collins, M.J., 2020. DeamiDATE 1.0: Site-specific deamidation as a tool to assess authenticity of members of ancient proteomes. J. Archaeol. Sci. 115, 105080.

Reich, D., Green, R.E., Kircher, M., Krause, J., Patterson, N., Durand, E.Y., Viola, B., Briggs, A.W., Stenzel, U., Johnson, P.L.F., Maricic, T., Good, J.M., Marques-Bonet, T., Alkan, C., Fu, Q., Mallick, S., Li, H., Meyer, M., Eichler, E.E., Stoneking, M.,

Richards, M., Talamo, S., Shunkov, M.V., Derevianko, A.P., Hublin, J.-J., Kelso, J., Slatkin, M., Pääbo, S., 2010. Genetic history of an archaic hominin group from Denisova Cave in Siberia. Nature 468, 1053–1060.

Richards, M.P., Pettitt, P.B., Trinkaus, E., Smith, F.H., Paunović, M., Karavanić, I., 2000. Neanderthal diet at Vindija and Neanderthal predation: the evidence from stable isotopes. Proc. Natl. Acad. Sci. U. S. A. 97, 7663–7666.

Richards, M.P., Taylor, G., Steele, T., McPherron, S.P., Soressi, M., Jaubert, J., Orschiedt, J., Mallye, J.B., Rendu, W., Hublin, J.J., 2008. Isotopic dietary analysis of a Neanderthal and associated fauna from the site of Jonzac (Charente-Maritime), France. J. Hum. Evol. 55, 179–185.

Richter, K.K., Wilson, J., Jones, A.K.G., Buckley, M., van Doorn, N., Collins, M.J., 2011. Fish ’n chips: ZooMS peptide mass fingerprinting in a 96 well plate format to identify fish bone fragments. J. Archaeol. Sci. 38, 1502–1510.

Rizal, Y., Westaway, K.E., Zaim, Y., van den Bergh, G.D., Bettis, E.A., 3rd, Morwood, M.J., Huffman, O.F., Grün, R., Joannes-Boyau, R., Bailey, R.M., Sidarto, Westaway, M.C., Kurniawan, I., Moore, M.W., Storey, M., Aziz, F., Suminto, Zhao, J.-X., Aswan, Sipola, M.E., Larick, R., Zonneveld, J.-P., Scott, R., Putt, S., Ciochon, R.L., 2020. Last appearance of Homo erectus at Ngandong, Java, 117,000-108,000 years ago. Nature 577, 381–385.

Robinson, A.B., Rudd, C.J., 1974. Deamidation of glutaminyl and asparaginyl residues in peptides and proteins. Curr. Top. Cell. Regul. 8, 247–295.

Rybczynski, N., Gosse, J.C., Harington, C.R., Wogelius, R.A., Hidy, A.J., Buckley, M., 2013. Mid-Pliocene warm-period deposits in the High Arctic yield insight into camel evolution. Nat. Commun. 4, 1550.

Sawyer, S., Renaud, G., Viola, B., Hublin, J.-J., Gansauge, M.-T., Shunkov, M.V., Derevianko, A.P., Prüfer, K., Kelso, J., Pääbo, S., 2015. Nuclear and mitochondrial DNA sequences from two Denisovan individuals. Proc. Natl. Acad. Sci. U. S. A. 112, 15696–15700.

Schmitz, R.W., Serre, D., Bonani, G., Feine, S., Hillgruber, F., Krainitzki, H., Pääbo, S., Smith, F.H., 2002. The Neandertal type site revisited: interdisciplinary investigations

of skeletal remains from the Neander Valley, Germany. Proc. Natl. Acad. Sci. U. S. A. 99, 13342–13347.

Schroeter, E.R., Cleland, T.P., 2016. Glutamine deamidation: an indicator of antiquity, or preservational quality? Rapid Commun. Mass Spectrom. 30, 251–255.

Schurr, M.R., 1998. Using stable nitrogen-isotopes to study weaning behavior in past populations. World Archaeol. 30, 327–342.

Scotchler, J.W., Robinson, A.B., 1974. Deamidation of glutaminyl residues: dependence on pH, temperature, and ionic strength. Anal. Biochem. 59, 319–322.

Semal, P., Rougier, H., Crevecoeur, I., Jungels, C., Flas, D., Hauzeur, A., Maureille, B., Germonpré, M., Bocherens, H., Pirson, S., Cammaert, L., De Clerck, N., Hambucken, A., Higham, T., Toussaint, M., van der Plicht, J., 2009. New data on the late Neandertals: direct dating of the Belgian Spy fossils. Am. J. Phys. Anthropol. 138, 421–428.

Serdyuk, N., Zenin, A., 2014. Small mammals from the Paleolithic site Strashnaya cave (Russia, Altai). Scientific Annals of the School Of Geology, 102 (184).

Shoulders, M.D., Raines, R.T., 2009. Collagen structure and stability. Annu. Rev. Biochem. 78, 929–958.

Shunkov, M.V., Kozlikin, M.B., Derevianko, A.P., 2020. Dynamics of the Altai Paleolithic industries in the archaeological record of Denisova Cave. Quat. Int.

Shunkov, M.V., Kulik, N.A., Kozlikin, M.B., Sokol, E.V., 2018. The phosphates of Pleistocene–Holocene sediments of the Eastern Gallery of Denisova Cave. Dokl. Earth Sci. 559 (10), 34–46.

Sinet-Mathiot, V., Smith, G.M., Romandini, M., Wilcke, A., Peresani, M., Hublin, J.-J., Welker, F., 2019. Combining ZooMS and zooarchaeology to study Late Pleistocene hominin behaviour at Fumane (Italy). Sci. Rep. 9, 12350.

Vasiliev, S.K., Kozlikin, M.B., Shunkov, M.V. 2018. Megafaunal Remains from the Upper Portion of Pleistocene Deposits in South Chamber of Denisova Cave. Problems of Archaeology, Ethnography, Anthropology of Siberia and Neighboring Territories 569.

Slon, V., Hopfe, C., Weiß, C.L., Mafessoni, F., de la Rasilla, M., Lalueza-Fox, C., Rosas, A., Soressi, M., Knul, M.V., Miller, R., Stewart, J.R., Derevianko, A.P., Jacobs, Z., Li, B., Roberts, R.G., Shunkov, M.V., de Lumley, H., Perrenoud, C., Gušić, I., Kućan, Ž.,

Rudan, P., Aximu-Petri, A., Essel, E., Nagel, S., Nickel, B., Schmidt, A., Prüfer, K., Kelso, J., Burbano, H.A., Pääbo, S., Meyer, M., 2017a. Neandertal and Denisovan DNA from Pleistocene sediments. Science 356, 605–608.

Slon, V., Mafessoni, F., Vernot, B., de Filippo, C., Grote, S., Viola, B., Hajdinjak, M., Peyrégne, S., Nagel, S., Brown, S., Douka, K., Higham, T., Kozlikin, M.B., Shunkov, M.V., Derevianko, A.P., Kelso, J., Meyer, M., Prüfer, K., Pääbo, S., 2018. The genome of the offspring of a Neanderthal mother and a Denisovan father. Nature 561, 113–116.

Slon, V., Viola, B., Renaud, G., Gansauge, M.-T., Benazzi, S., Sawyer, S., Hublin, J.-J., Shunkov, M.V., Derevianko, A.P., Kelso, J., Prüfer, K., Meyer, M., Pääbo, S., 2017b. A fourth Denisovan individual. Sci Adv 3, e1700186.

Sponheimer, M., Robinson, T., Ayliffe, L., Roeder, B., Hammer, J., Passey, B., West, A., Cerling, T., Dearing, D., Ehleringer, J., 2003. Nitrogen isotopes in mammalian herbivores: hair $\delta^{15}N$ values from a controlled feeding study. International Journal of Osteoarchaeology. 13 (1-2), 80–70.

Strohalm, M., Hassman, M., Kosata, B., Kodícek, M., 2008. mMass data miner: an open source alternative for mass spectrometric data analysis. Rapid Commun. Mass Spectrom. 22, 905–908.

Svyatko, S.V., Schulting, R.J., Mallory, J., Murphy, E.M., Reimer, P.J., Khartanovich, V.I., Chistov, Y.K., Sablin, M.V., 2013. Stable isotope dietary analysis of prehistoric populations from the Minusinsk Basin, Southern Siberia, Russia: a new chronological framework for the introduction of millet to the eastern Eurasian steppe. J. Archaeol. Sci. 40, 3936–3945.

Tahmasebi, F., Longstaffe, F.J., Zazula, G., 2018. Nitrogen isotopes suggest a change in nitrogen dynamics between the Late Pleistocene and modern time in Yukon, Canada. PLoS One 13, e0192713.

Tashak, V., 2003. Hearths at the Podzvonkaya Paleolithic Site: evidence suggestive of the spirituality of early populations of the Transbaikal region. Archaeology, Ethnology & Anthropology of Eurasia. 3, 70–80.

Tashak, V.I., 2014. Formation of the Early Upper Palaeolithic in Western Transbaikal (with particular reference to the Lower Complex of the Podzvonkaya site). Stratum Plus Journal 2014. 149–164.

Tashak, V.I., 2011. Chronology of the Early Upper Paleolithic of Western Transbaikalian (with particular reference to the materials of Podzvonkaya). Russian Archaeological Yearbook 1, 100–110.

Tashi, S., Singh, B., Keitel, C., Adams, M., 2016. Soil carbon and nitrogen stocks in forests along an altitudinal gradient in the eastern Himalayas and a meta-analysis of global data. Glob. Chang. Biol. 22, 2255–2268.

Tieszen, L.L., Boutton, T.W., 1989. Stable Carbon Isotopes in Terrestrial Ecosystem Research, in: Stable Isotopes in Ecological Research. Springer New York, p. 167–195.

Timoshok, E.E., Timoshok, E.N., Nikolaeva, S.A., Savchuk, D.A., Filimonova, E.O., Skorokhodov, S.N., Yu Bocharov, A., 2016. Monitoring of high-altitude terrestrial ecosystems in the Altai Mountains. IOP Conf. Ser.: Earth Environ. Sci. 48, 012008.

Tiunov, A.V., Dobrovoldskaya, M.V., 2011. Stable isotope (13c/12c and 15n/ 14n) evidence for mid-upper paleolithic hominines' palaeodiets in gorny altai. In Abstracts of Meeting of the European Society for the Study of Human Evolution. 23–24 September. Leipzig. p. 37.

Tsutaya, T., Yoneda, M., 2015. Reconstruction of breastfeeding and weaning practices using stable isotope and trace element analyses: A review. Am. J. Phys. Anthropol. 156 Suppl. 59, 2–21.

Turner, C.G., 1990. Palaeolithic Siberian dentition from Denisova and Okladnikov caves, Altaiskiy Kray, USSR. Current Research in the Pleistocene 7, 65–66.

van der Sluis, L.G., Hollund, H.I., Buckley, M., De Louw, P.G.B., Rijsdijk, K.F., Kars, H., 2014. Combining histology, stable isotope analysis and ZooMS collagen fingerprinting to investigate the taphonomic history and dietary behaviour of extinct giant tortoises from the Mare aux Songes deposit on Mauritius. Palaeogeogr. Palaeoclimatol. Palaeoecol. 416, 80–91.

van Doorn, N.L., Hollund, H., Collins, M.J., 2011. A novel and non-destructive approach for ZooMS analysis: ammonium bicarbonate buffer extraction. Archaeol. Anthropol. Sci. 3, 281.

van Doorn, N.L., Wilson, J., Hollund, H., Soressi, M., Collins, M.J., 2012. Site-specific deamidation of glutamine: a new marker of bone collagen deterioration. Rapid Commun. Mass Spectrom. 26, 2319–2327.

Vasiliev, S.K., 2008. Late Pleistocene Bison (Bison p. Priscus Bojanis, 1827) from the Southeastern Part of Western Siberia. Archaeology, Ethnology and Anthropology of Eurasia 34, 34–56.

Vasiliev, S.K., Shunkov, M.V., 2009. Large Pleistocene Mammals in the Southern Gallery of Denisova Cave. Problems of Archaeology, Ethnography, Anthropology of Siberia and Neighboring Territories XV, 63–69.

Vasiliev S.K., Shunkov M.V., Kozlikin M.B., 2017. Megafaunal Remains from the Eastern Chamber of Denisova Cave and Problems of Reconstructing the Pleistocene Environments in the Northwestern Altai. Problems of Archaeology, Ethnography, Anthropology of Siberia and Neighboring Territories XXIII.

Vasiliev, S.K., Shunkov, M.V., Kozlikin, M.B., 2013. Preliminary Results for the Balance of Megafauna from Pleistocene Layers of the East Gallery, Denisova Cave. Problems of Archaeology, Ethnography, and Anthropology of Siberia and Adjacent Territories 19, 32–38.

Vasiliev, S.K., Zenin, A.N., 2009. The faunistic remains from Strashnaya cave (North-west Altai) based on excavations 1988-2008. Problems of archeology, ethnography, anthropology, Siberia and adjacent territories. Novosibirsk: Institute archeology and ethnography, Siberian Branch RAS.

Ventresca Miller, A., Usmanova, E., Logvin, V., Kalieva, S., Shevnina, I., Logvin, A., Kolbina, A., Suslov, A., Privat, K., Haas, K., Rosenmeier, M., 2014. Subsistence and social change in central Eurasia: stable isotope analysis of populations spanning the Bronze Age transition. J. Archaeol. Sci. 42, 525–538.

Wadham, J.L., Hawkings, J., Telling, J., Chandler, D., Alcock, J., Lawson, E., Kaur, P., Bagshaw, E., Tranter, M., Tedstone, A., Others, 2016. Sources, cycling and export of nitrogen on the Greenland Ice Sheet. Biogeosci. 13, 6339–6352.

Welker, F., Hajdinjak, M., Talamo, S., Jaouen, K., Dannemann, M., David, F., Julien, M., Meyer, M., Kelso, J., Barnes, I., Brace, S., Kamminga, P., Fischer, R., Kessler, B.M., Stewart, J.R., Pääbo, S., Collins, M.J., Hublin, J.-J., 2016. Palaeoproteomic evidence identifies archaic hominins associated with the Châtelperronian at the Grotte du Renne. Proc. Natl. Acad. Sci. U. S. A. 113, 11162–11167.

Welker, F., Soressi, M.A., Roussel, M., van Riemsdijk, I., Hublin, J.-J., Collins, M.J., 2017. Variations in glutamine deamidation for a Châtelperronian bone assemblage as measured by peptide mass fingerprinting of collagen. STAR: Science & Technology of Archaeological Research 3, 15–27.

Welker, F., Soressi, M., Rendu, W., Hublin, J.-J., Collins, M., 2015. Using ZooMS to identify fragmentary bone from the Late Middle/Early Upper Palaeolithic sequence of Les Cottés, France. J. Archaeol. Sci. 54, 279–286.

Williams, M.W., Knauf, M., Cory, R., Caine, N., Liu, F., 2007. Nitrate content and potential microbial signature of rock glacier outflow, Colorado Front Range. Earth Surf. Processes Landforms 32, 1032–1047.

Wilson, J., van Doorn, N.L., Collins, M.J., 2012. Assessing the extent of bone degradation using glutamine deamidation in collagen. Anal. Chem. 84, 9041–9048.

Xing, S., Martinón-Torres, M., Bermúdez de Castro, J.M., Wu, X., Liu, W., 2015. Hominin teeth from the early Late Pleistocene site of Xujiayao, Northern China. Am. J. Phys. Anthropol. 156, 224–240.

Zanolli, C., Pan, L., Dumoncel, J., Kullmer, O., Kundrát, M., Liu, W., Macchiarelli, R., Mancini, L., Schrenk, F., Tuniz, C., 2018. Inner tooth morphology of Homo erectus from Zhoukoudian. New evidence from an old collection housed at Uppsala University, Sweden. J. Hum. Evol. 116, 1–13.

Zhang, D., Xia, H., Chen, F., Li, B., Slon, V., Cheng, T., Yang, R., Jacobs, Z., Dai, Q., Massilani, D., Shen, X., Wang, J., Feng, X., Cao, P., Yang, M.A., Yao, J., Yang, J., Madsen, D.B., Han, Y., Ping, W., Liu, F., Perreault, C., Chen, X., Meyer, M., Kelso, J., Pääbo, S., Fu, Q., 2020. Denisovan DNA in Late Pleistocene sediments from Baishiya Karst Cave on the Tibetan Plateau. Science 370, 584–587.

Zubova, A., Krivoshapkin, A.I., Shalagina, A.V., 2017. Human Teeth from Strashnaya Cave, the Altai Mountains, with Reference to the Dental Variation in Stone Age Siberia 45, 136–145.

Zwyns, N., Lbova, L.V., 2019. The Initial Upper Paleolithic of Kamenka site, Zabaikal region (Siberia): A closer look at the blade technology. Archaeological Research in Asia 17, 24–49.

Appendix 1 - Accepted publications

Manuscript A – 2019. Douka, K., Slon, V., Jacobs, Z., Ramsey, C.B., Shunkov, M.V., Derevianko, A.P., Mafessoni, F., Kozlikin, M.B., Li, B., Grün, R., Comeskey, D., Devièse, T., Brown, S., Viola, B., Kinsley, L., Buckley, M., Meyer, M., Roberts, R.G., Pääbo, S., Kelso, J., Higham, T. Age estimates for hominin fossils and the onset of the Upper Palaeolithic at Denisova Cave. Nature 565, 640–644.

LETTER

https://doi.org/10.1038/s41586-018-0870-z

Age estimates for hominin fossils and the onset of the Upper Palaeolithic at Denisova Cave

Katerina Douka[1,2]*, Viviane Slon[3], Zenobia Jacobs[4,5], Christopher Bronk Ramsey[2], Michael V. Shunkov[6,7], Anatoly P. Derevianko[6,8], Fabrizio Mafessoni[3], Maxim B. Kozlikin[6], Bo Li[4,5], Rainer Grün[9], Daniel Comeskey[2], Thibaut Devièse[2], Samantha Brown[1], Bence Viola[10], Leslie Kinsley[11], Michael Buckley[12], Matthias Meyer[3], Richard G. Roberts[4,5], Svante Pääbo[3], Janet Kelso[3] & Tom Higham[2]*

Denisova Cave in the Siberian Altai (Russia) is a key site for understanding the complex relationships between hominin groups that inhabited Eurasia in the Middle and Late Pleistocene epoch. DNA sequenced from human remains found at this site has revealed the presence of a hitherto unknown hominin group, the Denisovans[1,2], and high-coverage genomes from both Neanderthal and Denisovan fossils provide evidence for admixture between these two populations[3]. Determining the age of these fossils is important if we are to understand the nature of hominin interaction, and aspects of their cultural and subsistence adaptations. Here we present 50 radiocarbon determinations from the late Middle and Upper Palaeolithic layers of the site. We also report three direct dates for hominin fragments and obtain a mitochondrial DNA sequence for one of them. We apply a Bayesian age modelling approach that combines chronometric (radiocarbon, uranium series and optical ages), stratigraphic and genetic data to calculate probabilistically the age of the human fossils at the site. Our modelled estimate for the age of the oldest Denisovan fossil suggests that this group was present at the site as early as 195,000 years ago (at 95.4% probability). All Neanderthal fossils—as well as Denisova 11, the daughter of a Neanderthal and a Denisovan[4]—date to between 80,000 and 140,000 years ago. The youngest Denisovan dates to 52,000–76,000 years ago. Direct radiocarbon dating of Upper Palaeolithic tooth pendants and bone points yielded the earliest evidence for the production of these artefacts in northern Eurasia, between 43,000 and 49,000 calibrated years before present (taken as AD 1950). On the basis of current archaeological evidence, it may be assumed that these artefacts are associated with the Denisovan population. It is not currently possible to determine whether anatomically modern humans were involved in their production, as modern-human fossil and genetic evidence of such antiquity has not yet been identified in the Altai region.

Denisova Cave preserves the longest and most notable Palaeolithic sequence in northern Asia. It consists of three chambers: Main Chamber, East Chamber and South Chamber (Supplementary Information, section 1). Excavations at the site have so far yielded the remains of 12 hominins (Extended Data Fig. 1 and Supplementary Information, section 3); most of these remains are small and highly fragmentary. Despite this, the preservation of DNA in some of these remains is very good and has enabled genome-wide data to be obtained from both Neanderthal and Denisovan human remains, as well as from cave sediments, enabling comparisons to be made between the two hominin groups[1–8].

The chronology of the site and the age of the recovered human remains are key unresolved issues. Previous attempts at building a chronology at Denisova Cave have used radiocarbon dating in the uppermost sections, and thermoluminescence dating in the older layers[9]. More recently, radiocarbon dating from the uppermost Pleistocene layers in East Chamber revealed some age variations, which were ascribed to taphonomic mixing and carnivore bioturbation[2]. A set of optical ages[10] has been obtained from Pleistocene sedimentary layers in all three chambers.

Here we report 50 radiocarbon determinations from 40 samples, collected from the upper parts of the Pleistocene sequence (layers 9–12) in Main Chamber and East Chamber (Fig. 1 and Extended Data Table 1). A further 23 samples were processed but did not yield sufficient carbon for dating (Supplementary Information, section 2). We selected samples of charcoal, and humanly modified bone and artefacts (Extended Data Fig. 2 and Supplementary Information, section 2) from locations that were deemed during excavation to be undisturbed. Where possible, the samples were prepared using robust decontamination protocols, including collagen ultrafiltration and single amino acid extraction of hydroxyproline from bones and teeth, and acid-base-wet oxidation stepped-combustion (ABOx-SC) or acid-wet oxidation stepped-combustion (AOx-SC) for charcoal (Supplementary Information, section 2).

All samples from layers 11.3, 11.4 and 12 in East Chamber, as well as the directly dated Denisova 11 bone[11], pre-date the radiocarbon age limit. In layer 11.2, we found two age clusters: three samples have infinite ages, and three samples have finite calibrated ages (Extended Data Table 1). A horse tooth from layer 9.2 gave a result of 45,720–50,000 calibrated years before present (cal. years BP) (Oxford radiocarbon laboratory code OxA-29859). This date is statistically indistinguishable from the group of finite dates (treated with ultrafiltration and ABOx) from layer 11.2.

In Main Chamber, our radiocarbon ages reveal a depositional hiatus between layers 12 and 11.4. Samples from layer 12 (at the end of the Middle Palaeolithic) all gave infinite radiocarbon ages compared to samples from layer 11.4, which date to between approximately 35,000 and 40,000 cal. years BP (Fig. 1).

Four pendants made from red deer (*Cervus elaphus*) and elk (*Alces alces*) teeth—which are often associated with Upper Palaeolithic technocomplexes—provided results of ~32,000, ~40,000 and ~45,000 cal. years BP (Fig. 1 and Extended Data Fig. 2). The oldest of these dates (OxA-30963) is corroborated by a charcoal date (OxA-31506) from the same stratigraphic location and year of excavation, and is the earliest direct date for an artefact of this type in northern Eurasia.

[1]Department of Archaeology, Max Planck Institute for the Science of Human History, Jena, Germany. [2]Oxford Radiocarbon Accelerator Unit, Research Laboratory for Archaeology and the History of Art, University of Oxford, Oxford, UK. [3]Department of Evolutionary Genetics, Max Planck Institute for Evolutionary Anthropology, Leipzig, Germany. [4]Centre for Archaeological Science, School of Earth, Atmospheric and Life Sciences, University of Wollongong, Wollongong, New South Wales, Australia. [5]Australian Research Council (ARC) Centre of Excellence for Australian Biodiversity and Heritage, University of Wollongong, Wollongong, New South Wales, Australia. [6]Institute of Archaeology and Ethnography, Russian Academy of Sciences Siberian Branch, Novosibirsk, Russia. [7]Novosibirsk State University, Novosibirsk, Russia. [8]Altai State University, Barnaul, Russia. [9]Australian Research Centre for Human Evolution, Griffith University, Brisbane, Queensland, Australia. [10]Department of Anthropology, University of Toronto, Toronto, Ontario, Canada. [11]Research School of Earth Sciences, The Australian National University, Canberra, Australian Capital Territory, Australia. [12]Manchester Institute of Biotechnology, University of Manchester, Manchester, UK. *e-mail: douka@shh.mpg.de; thomas.higham@rlaha.ox.ac.uk

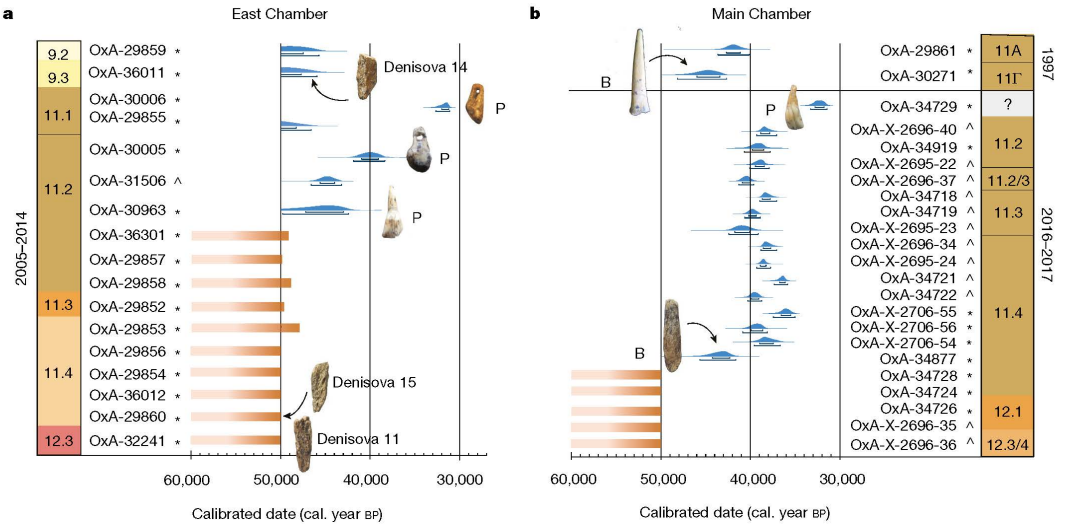

Fig. 1 | Radiocarbon age determinations from East Chamber and Main Chamber, Denisova Cave. Age determinations are given as dates in cal. years BP. The radiocarbon determinations ($n = 40$) are calibrated using OxCal 4.3 software[13] and the IntCal13 calibration curve[18], and are plotted in their respective stratigraphic sequence and chamber of origin. The finite probability distributions are in blue; error bars indicate the 68.2 and 95.4% highest posterior density ranges. Orange denotes measured ages that are beyond the radiocarbon limit (50,000 cal. years BP). Raw data are shown in Extended Data Table 1. **a**, East Chamber sequence and associated calibrated dates. **b**, Main Chamber sequence and associated calibrated dates. Number in the stratigraphic column on the left (**a**) or right (**b**) refers to the layer. *, bone sample; ^, charcoal sample. Images include the three directly dated human bone fragments (Denisova 11, Denisova 14 and Denisova 15), pendants (P) and bone points (B). Two much younger ages for layer 9.3 in Main Chamber are not shown. Artefacts and human bones are not shown to scale.

The younger determinations for some of these artefacts may be considered minimum ages owing to small sample sizes and marginal collagen yields (about 1 wt% collagen), which prevented the application of robust chemical pretreatment methods. Two bone points were dated to 42,660–48,100 and 41,590–45,700 cal. years BP (Fig. 2 and Extended Data Fig. 2), representing the earliest occurrence of such objects in northern Eurasia.

The radiocarbon ages for the oldest pendants and the bone points at Denisova Cave overlap with the directly dated anatomically modern human femur from Ust'-Ishim in western Siberia[12] (43,200–46,880 cal. years BP) (Fig. 2). This raises the possibility of a connection between the spread of modern humans and the emergence of innovative behaviours and symbolic artefacts across northern Eurasia at the start of the Initial Upper Palaeolithic, by 43,000–48,000 cal. years BP.

In an attempt to retrieve further human fossils from the site, we applied collagen peptide mass spectrometry fingerprinting (ZooMS) to 2,212 non-diagnostic bone fragments, and identified three specimens that contained peptides consistent with the Hominidae (Supplementary Information, section 8). The bones come from layers 9.3 (Denisova 14, ZooMS specimen code DC 3758) and 11.4 (Denisova 15, DC 3573) in East Chamber, and layer 9.1 (Denisova 16, DC 4114) in Main Chamber (Extended Data Fig. 3). Denisova 14 and Denisova 15 were directly dated and genetically analysed. The radiocarbon ages are close to or beyond the radiocarbon limit (Fig. 1 and Extended Data Table 1). No ancient hominin DNA was retrieved from Denisova 14, but Denisova 15 carries a mitochondrial genome of the Neanderthal type (Supplementary Information, section 5). Denisova 16 was too small for radiocarbon dating, and analyses of ancient DNA are ongoing.

Most directly dated human remains at the site yielded infinite radiocarbon ages and are associated, in most cases, with layers that are beyond the limit of this dating method. Finite ages for layers that contain human remains have been obtained using optical dating[10]; however, the association between these optically dated sediment samples and the human fossils is inferred, and the dated sediments do not immediately surround the fossils. Age estimates based on branch shortening of the nuclear genome have been published for Denisova 3, Denisova 5 and Denisova 11[3–5] (Supplementary Information, section 4) but these are sensitive to sequencing error and the date of the divergence between humans and chimpanzees (which is still debated). To exploit the different types of information—derived from radiocarbon and optical dating, stratigraphy and genetic analyses—that are available for Denisova Cave, we developed a Bayesian approach to generate robust age estimates for the human remains and to ameliorate the shortcomings of each technique and line of evidence when used individually.

We used OxCal v.4.3 software[13] to build Bayesian models that consist of several types of prior information: the stratigraphic position of all specimens (Fig. 3); the relative genetic ages for seven human remains (see below, Extended Data Fig. 4); the finite radiocarbon age for Denisova 14; a *terminus ante quem* boundary at 50,000 cal. years BP for all infinite radiocarbon ages; optical ages for layers 22.1 ($n = 2$) and 21 ($n = 3$) in Main Chamber and layers 12.3 ($n = 3$) and 11.2 ($n = 3$) in East Chamber (Supplementary Information, section 6); and a minimum uranium-series age of 67,500 ± 2,500 years for Denisova 11 (Supplementary Information, section 7).

The relative genetic ages of four Denisovans (Denisova 2, Denisova 3, Denisova 4 and Denisova 8) and two Neanderthals (Denisova 5 and Denisova 15)—as well as Denisova 11, who carries a Neanderthal mitochondrial genome—were derived from a multiple sequence alignment of their mitochondrial genome sequences. We achieved this by counting the number of substitutions on the branches that lead to each individual since the split from their most recent common ancestor with either the Sima de los Huesos individual[14], or with 19 Neanderthals from other archaeological sites and the Hohlenstein-Stadel Neanderthal (Extended Data Fig. 4). To convert these differences to time in years, we applied the mitochondrial mutation rate of 2.53×10^{-8} mutations per nucleotide position per year (95% highest posterior density $1.76–3.23 \times 10^{-8}$ mutations) inferred for modern humans[12]. We caution that this conversion to time assumes that the mutation rate in archaic humans is the same as that in modern humans, and that the approach

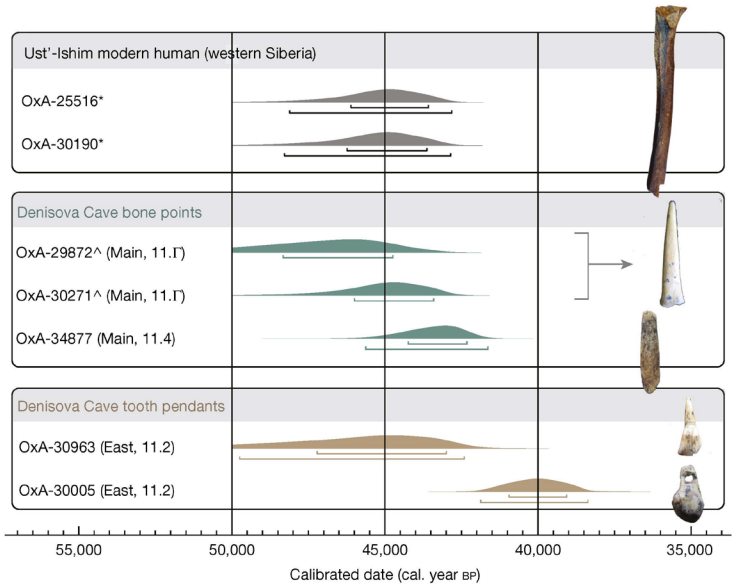

Fig. 2 | Comparison between the radiocarbon determinations obtained for the oldest bone points and tooth pendants from Denisova Cave and the two direct dates for the Ust'-Ishim modern human femur. The Ust'-Ishim femur has previously been published[12]. For each measurement, the laboratory code is indicated; for the artefacts from Denisova, the chamber and stratigraphic context are shown in parentheses. Error bars below the probability distributions indicate the 68.2 and 95.4% highest posterior density ranges. Error bars are not shown for age ranges predating the calibration limit of 50,000 cal. years BP. Dates marked with the same symbol (* or ^) were obtained from the same sample. Artefacts and human bone are not shown to scale.

cannot detect back-mutations and multiple substitutions that occur at the same position in the mitochondrial genome. The relative ages obtained using these assumptions were then included within the Bayesian model as relative constraints between the hominin remains. The split time estimates in the Denisovan and Neanderthal trees were treated as time differences, assuming an Erlang distribution.

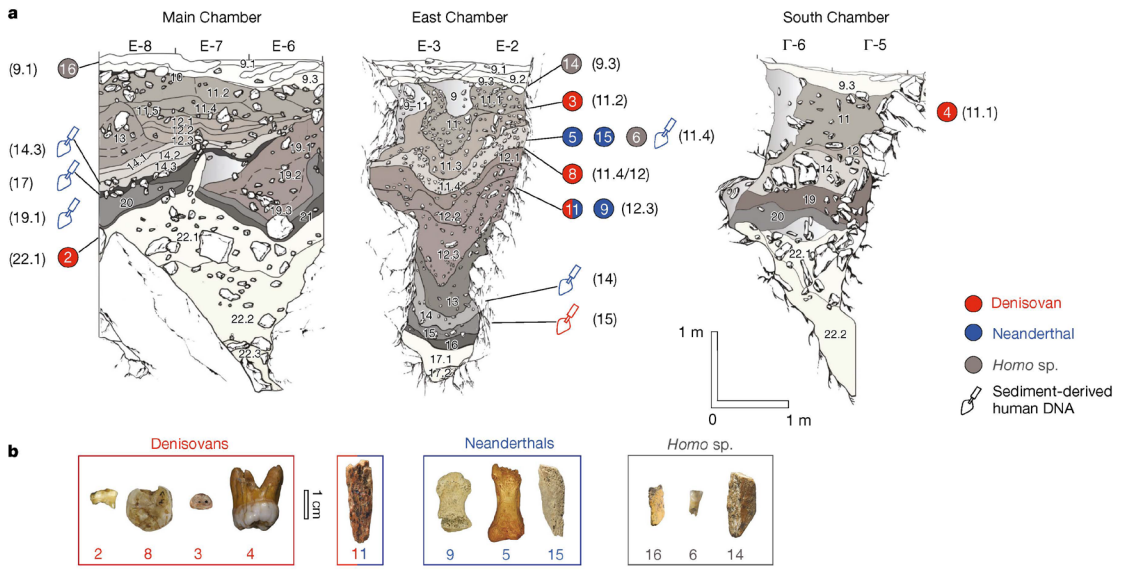

Fig. 3 | Stratigraphic sequences for the southeast profiles exposed in the three chambers at Denisova Cave and images of human fossil remains. **a**, Stratigraphic sequences. **b**, Human fossil remains. Circle, location of the human remains; trowel silhouette, sediment-derived human DNA. Red, Denisovans; blue, Neanderthals; grey, *Homo* sp. fossils for which no genetic data exist. Number in circle denotes the fossil number (for example, 2, Denisova 2). Number in parentheses refers to the layer in which the fossil or human DNA was found. Further information for each human fossil can be found in Extended Data Fig. 1 and Supplementary Information, section 3.

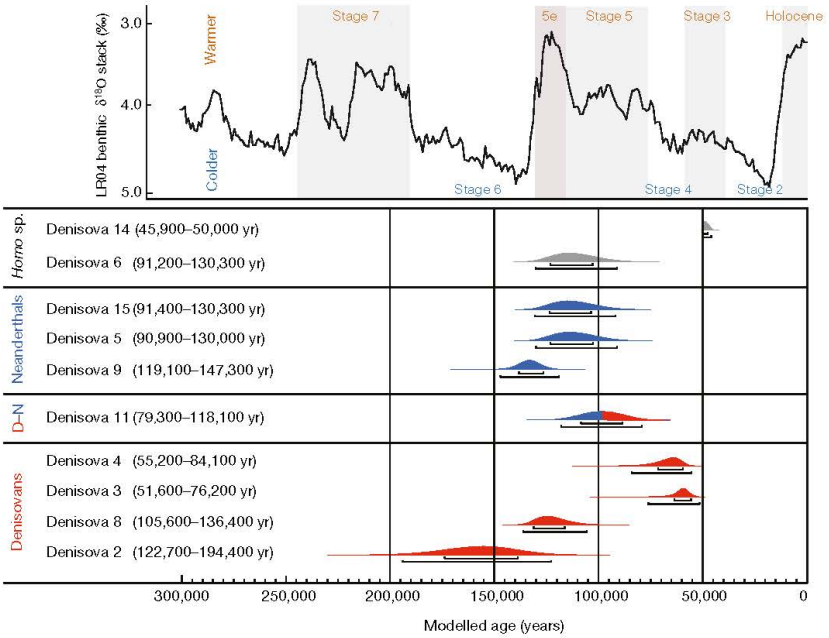

Fig. 4 | Age estimates for the human fossils from Denisova Cave as determined from Bayesian model 4, compared against the marine oxygen isotope curve from benthic $\delta^{18}O$ records. The probability distribution for Denisova 14 is the calibrated radiocarbon age obtained directly from the fossil; it extends beyond the range of the calibration curve and is therefore truncated at 50,000 cal. years BP. Error bars below the probability distributions indicate 68.2 and 95.4% highest posterior density ranges. Red, Denisovans; blue, Neanderthals; red and blue, Denisova 11 (direct offspring of a Denisovan and a Neanderthal (D–N)). No genetic data exist for Denisova 6 and Denisova 14; these specimens are attributed only to *Homo* sp. and are shown in grey. Stage refers to marine isotope stage; stage 5e, the warmest part of the last interglacial, is highlighted; benthic $\delta^{18}O$ data are from a previous publication[19]. See also Extended Data Fig. 6 and Supplementary Information, section 9.

We tested four separate Bayesian models (Extended Data Figs. 5, 6 and Supplementary Information, section 9). When the human remains are placed in their attributed stratigraphic positions (model 1), low model-agreement indices were obtained for Denisova 2 and Denisova 11; this suggests that these two fossils have moved post-depositionally. When we reassigned these two fossils to overlying layers (models 2–4), significantly higher overall model agreement indices were obtained (23.3% for model 1 versus 82.3–111% for models 2–4) (Extended Data Table 2). We also tested the results of all four models against ages derived using optical and genetic information only (Extended Data Fig. 7). The modelled age estimates for the human fossils that we report here derive from probability distribution functions using model 4 (Fig. 4, Extended Data Table 2 and Supplementary Information, section 9).

Denisova 2, the oldest Denisovan fossil, yielded a modelled age estimate of 122,700–194,400 years. Denisova 8, found at the interface between layers 11.4 and 12 of East Chamber, falls between 105,600 and 136,400 years. Denisova 3, the youngest Denisovan fossil (from layer 11.2 in East Chamber), yielded a modelled date of 51,600–76,200 years ago (at 95.4% probability). This is consistent with infinite radiocarbon dates of >48,600 ^{14}C years BP (OxA-29857) and >50,100 ^{14}C years BP (OxA-29858) that were obtained on two humanly modified bones collected from the same square and sector, and in the same year of excavation, as Denisova 3. The modelled age for Denisova 3 also overlaps with the age of 60,000–84,000 years estimated on the basis of branch shortening in the nuclear genome, when calculated using only transversion polymorphisms and assuming a divergence time between humans and chimpanzees of 13 million years[5] (Supplementary Information, section 4). Denisova 4 (layer 11.1, South Chamber) differs by only two mutations in its mtDNA compared to Denisova 3, and therefore has a similar age.

The two Neanderthals (Denisova 5 and Denisova 15) were found in similar stratigraphic positions in East Chamber (layer 11.4). Denisova 5 has a modelled date estimate of 90,900–130,000 years ago, which is consistent with the nuclear-genome branch-shortening age estimate (110,000–134,800 years)[5] (Supplementary Information, section 4). Denisova 15 differs by only a single mutation in its mtDNA compared to Denisova 5, and therefore yields an overlapping modelled age. No genetic information is available for Denisova 9 (layer 12.3); its modelled age (of 119,100–147,300 years) is based on the stratigraphic position of the fossil, and is constrained only by the optical ages from layer 12.3.

Denisova 11, also found in layer 12.3 in East Chamber, stratigraphically pre-dates Denisova 5. If this position is maintained (for example, as in model 2), Denisova 11 has an estimated age of 115,700–140,900 years, comparable to the modelled age estimate of all three Neanderthals (Denisova 5, Denisova 15, Denisova 9). However, genetic information—based on the differences in the number of mitochondrial substitutions and the sharing of nuclear substitutions with the high-coverage genome of Denisova 5—strongly suggests that Denisova 11 is younger than Denisova 5. To further explore this, we placed Denisova 11 above Denisova 5 in models 3 and 4. Both models yielded much higher agreement indices; this supports the notion that Denisova 11, which was discovered in the assemblage of unidentifiable bones from layer 12, is intrusive to this layer. This results in a younger final age estimate of 79,300–118,100 years for this specimen.

The age estimates for Denisova 11 and all Neanderthal remains from the site largely overlap (Fig. 4). Previous work[3] found Neanderthal and Denisovan DNA in underlying sediments in East Chamber (layers 14 and 15) and Neanderthal DNA in Main Chamber (layers 14, 17 and 19) (Fig. 3), which suggests that both groups were present in the cave before the earliest human fossils currently recorded there. The modelled ages for Neanderthal fossils found in East Chamber are consistent

with optical ages for sediments that contain Neanderthal DNA in Main Chamber. The earliest sediments with Neanderthal DNA (layer 14 in East Chamber) date to about 190,000 years ago[10]. This also overlaps with the optical age of sediments[10] from which Denisovan DNA was extracted (layer 15, East Chamber)[8], as well as with our modelled age for Denisova 2. The interstratification and temporal overlap of Denisovan and Neanderthal fossils and sedimentary DNA, as well as direct genetic evidence[4], suggest that both groups lived in the region, met and—on occasion—interbred over the course of approximately 150,000 years. The integration of all available data from Denisova Cave, and assuming ancient DNA retrieved from cave sediments is in situ, highlights the very early appearance of Neanderthals in Siberia, during the late part of warm marine isotope stage 7 (as early as 190,000 years ago); the majority of the specimens thus far recovered are from the last interglacial (marine isotope stage 5) (Fig. 4).

Denisovans at the site appear to have survived later than Neanderthals. Our modelled date estimate for the most recent Denisovan fossil (Denisova 3, 51,600–76,200 years ago) is earlier than published estimates of the date of Denisovan admixture into modern humans (44,000–54,000[15] and 31,000–50,000 years ago[16]). If these admixture estimates are robust, then the Altai Denisovans may not have been the latest-surviving population.

Our results also imply that all known Neanderthal and Denisovan fossils pre-date the appearance of the Initial Upper Palaeolithic (45,000–48,000 years ago) and the directly dated personal ornaments and bone points. The presence of anatomically modern humans to the northwest of Denisova Cave as early as 45,000 cal. years BP at Ust'-Ishim, synchronous with the dated pendants and bone points (Fig. 2), raises the possibility that modern humans may have been involved in the manufacture of these artefacts. However, given that previous work on the lithic evidence from Denisova Cave indicates that the Initial Upper Palaeolithic may have developed through a local Middle Palaeolithic substrate[17], and in the absence of modern human fossil or genetic evidence from the site, it is parsimonious at present to suggest that the makers of these artefacts may have been Denisovans. Future discovery of fossils from this site and others, and determination of their ages and genomes using a combination of methods, will shed further light on the relationships between archaic and modern humans and their associated material cultures.

Online content

Any methods, additional references, Nature Research reporting summaries, source data, statements of data availability and associated accession codes are available at https://doi.org/10.1038/s41586-018-0870-z.

Received: 12 May 2018; Accepted: 17 December 2018;
Published online 30 January 2019.

1. Krause, J. et al. The complete mitochondrial DNA genome of an unknown hominin from southern Siberia. *Nature* **464**, 894–897 (2010).
2. Reich, D. et al. Genetic history of an archaic hominin group from Denisova Cave in Siberia. *Nature* **468**, 1053–1060 (2010).
3. Prüfer, K. et al. The complete genome sequence of a Neanderthal from the Altai Mountains. *Nature* **505**, 43–49 (2014).
4. Slon, V. et al. The genome of the offspring of a Neanderthal mother and a Denisovan father. *Nature* **561**, 113–116 (2018).
5. Prüfer, K. et al. A high-coverage Neandertal genome from Vindija Cave in Croatia. *Science* **358**, 655–658 (2017).
6. Sawyer, S. et al. Nuclear and mitochondrial DNA sequences from two Denisovan individuals. *Proc. Natl Acad. Sci. USA* **112**, 15696–15700 (2015).
7. Slon, V. et al. A fourth Denisovan individual. *Sci. Adv.* **3**, e1700186 (2017).
8. Slon, V. et al. Neandertal and Denisovan DNA from Pleistocene sediments. *Science* **356**, 605–608 (2017).
9. Derevianko, A. P., Laukhin, S. A., Kulikov, O. A., Gnibidenko, Z. N. & Shunkov, M. V. First Middle Pleistocene age determinations of the Paleolithic in the Altai Mountains. *Dokl. Akad. Nauk* **326**, 497–501 (1992).
10. Jacobs, Z. et al. Timing of archaic hominin occupation of Denisova Cave in southern Siberia. *Nature* https://doi.org/10.1038/s41586-018-0843-2 (2019).
11. Brown, S. et al. Identification of a new hominin bone from Denisova Cave, Siberia using collagen fingerprinting and mitochondrial DNA analysis. *Sci. Rep.* **6**, 23559 (2016).
12. Fu, Q. et al. Genome sequence of a 45,000-year-old modern human from western Siberia. *Nature* **514**, 445–449 (2014).
13. Bronk Ramsey, C. Bayesian analysis of radiocarbon dates. *Radiocarbon* **51**, 337–360 (2009).
14. Meyer, M. et al. A mitochondrial genome sequence of a hominin from Sima de los Huesos. *Nature* **505**, 403–406 (2014).
15. Sankararaman, S., Mallick, S., Patterson, N. & Reich, D. The combined landscape of Denisovan and Neanderthal ancestry in present-day humans. *Curr. Biol.* **26**, 1241–1247 (2016).
16. Malaspinas, A.-S. et al. A genomic history of Aboriginal Australia. *Nature* **538**, 207–214 (2016).
17. Derevianko, A. P. *The Upper Paleolithic in Africa and Eurasia and the Origin of Anatomically Modern Humans* (in Russian) (SB RAS, Novosibirsk, 2011).
18. Reimer, P. J. et al. IntCal13 and Marine13 radiocarbon age calibration curves 0–50,000 years cal. BP. *Radiocarbon* **55**, 1869–1887 (2013).
19. Lisiecki, L. E. & Raymo, M. E. A Pliocene-Pleistocene stack of 57 globally distributed benthic $\delta^{18}O$ records. *Paleoceanography* **20**, PA1003 (2005).

Acknowledgements Funding for this research was received from the European Research Council (ERC) under the European Union's Seventh Framework Program (FP7/2007-2013); grant no. 324139 (PalaeoChron) awarded to T.H.; grant no. 715069 (FINDER) awarded to K.D.; grant no. 694707 (100 Archaic Genomes) awarded to S.P. The Max Planck Society provided support to S.P., V.S., F.M., M.M., J.K., K.D. and S.B. The Australian Research Council funded research fellowships to Z.J. (FT150100138), B.L. (FT14010038) and R.G.R. (FL130100116). The Royal Society funded a University Research Fellowship to M.B. B.V. was supported by the Social Sciences and Humanities Research Council (Canada). The archaeological field studies were funded by the Russian Science Foundation (project no. 14-50-00036 to A.P.D.) and the Russian Foundation for Basic Research (project no. 17-29-04206 to M.V.S. and M.B.K.). K.D., T.H. and T.D. thank Brasenose and Keble Colleges, University of Oxford, for funding and support. We thank staff at the Oxford Radiocarbon Accelerator Unit (ORAU), E. Gillespie and M. Higham Jenkins for their contribution to the radiocarbon dating and ZooMS work; and M. Ruddy for contributing to the marine oxygen isotope curve data used here (https://github.com/markruddy/ois5e-plot). D Challinor identified the charcoal before radiocarbon dating. I. Cartwright (University of Oxford) photographed Denisova 11, Denisova 14, Denisova 15 and Denisova 16. Y. Jafari, K. O'Gorman and T. Lachlan helped with optical-dating sample preparation and data analysis. S. Nagel, B. Nickel, B. Schellbach and A. Weihmann helped with DNA sample preparation; and A. Hübner gave input on the BEAST analysis.

Reviewer information *Nature* thanks R. Dennell, E. J. Rhodes and the other anonymous reviewer(s) for their contribution to the peer review of this work.

Author contributions K.D., V.S., Z.J., B.L., D.C., L.K., T.D., S.B., B.V. and M.B. performed the laboratory work; K.D., T.H., C.B.R., D.C. and T.D. obtained and analysed the radiocarbon data. V.S., F.M., J.K., M.M. and S.P. analysed the genetic data; C.B.R., K.D. and T.H. designed and tested the Bayesian models. S.B. and M.B. analysed the ZooMS samples. B.V. carried out morphological analyses of the fossils. Z.J., B.L. and R.G.R. analysed the optical dating data. L.K. and R.G. obtained and analysed the U-series data. A.P.D., M.V.S. and M.B.K. excavated the site and analysed all archaeological data. K.D., T.H. and Z.J. wrote the manuscript with input from all authors.

Competing interests The authors declare no competing interests.

Additional information
Extended data is available for this paper at https://doi.org/10.1038/s41586-018-0870-z.
Supplementary information is available for this paper at https://doi.org/10.1038/s41586-018-0870-z.
Reprints and permissions information is available at http://www.nature.com/reprints.
Correspondence and requests for materials should be addressed to K.D. or T.H.
Publisher's note: Springer Nature remains neutral with regard to jurisdictional claims in published maps and institutional affiliations.

METHODS

No statistical methods were used to predetermine sample size. The experiments were not randomized and investigators were not blinded to allocation during experiments and outcome assessment.

Radiocarbon dating and Bayesian modelling. Bones for dating were sampled using an NSK Elector drill with cleaned tungsten carbide drill bits. The routine ORAU chemical pretreatment protocols were applied[20]. A small number of samples was tested using compound-specific methods, in which underivatized amino acids were separated from hydrolysed bone collagen using preparative high-performance liquid chromatography[21]. Using this procedure, hydroxyproline was isolated and dated. Samples of charcoal were prepared for dating using ABA (acid–base–acid), ABOx-SC[22] or a modified AOx-SC preparation. OxCal v.4.3.2[13] and the IntCal13[18] calibration curve were used to calibrate the radiocarbon data and build Bayesian models that incorporated chronometric, stratigraphic and genetic relative dating.

ZooMS collagen fingerprinting analysis for hominin identification. Because about 95% of the bone assemblage from Denisova Cave is unidentifiable to the species or genus level, we applied ZooMS to identify human remains from the site. We analysed 2,212 non-diagnostic bone fragments using this technique (which was previously used to discover Denisova 11[4,11]), therefore bringing the total bones analysed from the site so far to 4,527 (Supplementary Information, section 8). Samples from bone fragments were cut and drilled at the University of Oxford, and processed for ZooMS analysis at the University of Manchester. This involved each bone sample being partially decalcified with 0.6 M HCl overnight (~18 h); then, 0.5 ml of solution from each sample was ultrafiltered twice (30 kDa molecular mass cut-off) into 50 mM ammonium bicarbonate. Then, 100 μl was then digested with sequencing grade trypsin at 37 °C overnight (~18 h) and 1-μl samples were spotted with 10 mg/ml α-cyano hydroxycinnamic acid matrix on a plate, following a previously published method[11], and allowed to air dry. Using a Brüker Ultraflex II matrix-assisted laser desorption/ionization-time of flight mass spectrometry (MALDI-ToF-MS) mass spectrometer, 2,000 laser acquisitions from random walking were acquired for each sample and the resulting spectra were screened for previously published hominin collagen peptide markers[11,23].

DNA sequencing and data processing. Bone powder was removed from the Denisova 14 and Denisova 15 bone fragments using a disposable dentistry drill. The bone powder samples were treated with 0.5% sodium hypochlorite before DNA extraction[24,25]. Twenty per cent of each DNA extract (that is, 10 μl) were converted into single-stranded DNA libraries[26] and indexed with two barcodes[27]. The DNA libraries were enriched for human mtDNA fragments using two rounds of an on-bead hybridization capture protocol[28]. The enriched DNA libraries were pooled with libraries generated as part of other projects, and sequenced on a MiSeq platform (Illumina) in 76-cycle paired-end runs[27]. Base calling was carried out using Bustard (Illumina) and de-multiplexing was performed by requiring exact matches to the expected barcode combinations. Overlapping paired-end reads were merged using leeHom[29]. Sequences were mapped to a reference genome using BWA[30] with parameters adapted to ancient DNA. PCR duplicates were collapsed into a single sequence using bam-rmdup (https://github.com/mpieva/biohazard-tools/). Only sequences longer than 35 bases and with a mapping quality higher than 25 were retained.

Reporting summary. Further information on research design is available in the Nature Research Reporting Summary linked to this paper.

Code availability. CQL codes for Bayesian analyses are included in the Supplementary Information, section 9. These can be imported and used in the OxCal platform[13].

Data availability

Raw radiocarbon determinations and associated chemical data, calibrated age ranges and CQL codes for the Bayesian models are included in the Supplementary Information. All MALDI-ToF-MS raw data for the ZooMS analyses are available from the corresponding authors upon request. The mtDNA capture data for Denisova 11, Denisova 14 and Denisova 15 are available in the European Nucleotide Archive under accession number PRJEB29061. The mtDNA sequence of Denisova 15 can be downloaded from GenBank (accession number MK033602). All other relevant data are available from the corresponding authors or are included in the Letter or its Supplementary Information.

20. Brock, F. et al. Current pretreatment methods for AMS radiocarbon dating at the Oxford Radiocarbon Accelerator Unit (ORAU). *Radiocarbon* **52**, 103–112 (2010).
21. Devièse, T., Comeskey, D., McCullagh, J., Bronk Ramsey, C. & Higham, T. New protocol for compound-specific radiocarbon analysis of archaeological bones. *Rapid Commun. Mass Spectrom.* **32**, 373–379 (2018).
22. Bird, M. I. et al. Radiocarbon dating of "old" charcoal using a wet oxidation, stepped-combustion procedure. *Radiocarbon* **41**, 127–140 (1999).
23. Buckley, M. & Kansa, S. W. Collagen fingerprinting of archaeological bone and teeth remains from Domuztepe, South Eastern Turkey. *Archaeol. Anthropol. Sci.* **3**, 271–280 (2011).
24. Dabney, J. et al. Complete mitochondrial genome sequence of a Middle Pleistocene cave bear reconstructed from ultrashort DNA fragments. *Proc. Natl Acad. Sci. USA* **110**, 15758–15763 (2013).
25. Korlević, P. et al. Reducing microbial and human contamination in DNA extractions from ancient bones and teeth. *Biotechniques* **59**, 87–93 (2015).
26. Gansauge, M. T. et al. Single-stranded DNA library preparation from highly degraded DNA using T4 DNA ligase. *Nucleic Acids Res.* **45**, e79 (2017).
27. Kircher, M., Sawyer, S. & Meyer, M. Double indexing overcomes inaccuracies in multiplex sequencing on the Illumina platform. *Nucleic Acids Res.* **40**, e3 (2012).
28. Fu, Q. et al. DNA analysis of an early modern human from Tianyuan Cave, China. *Proc. Natl Acad. Sci. USA* **110**, 2223–2227 (2013).
29. Renaud, G., Stenzel, U. & Kelso, J. leeHom: adaptor trimming and merging for Illumina sequencing reads. *Nucleic Acids Res.* **42**, e141 (2014).
30. Li, H. & Durbin, R. Fast and accurate long-read alignment with Burrows–Wheeler transform. *Bioinformatics* **26**, 589–595 (2010).

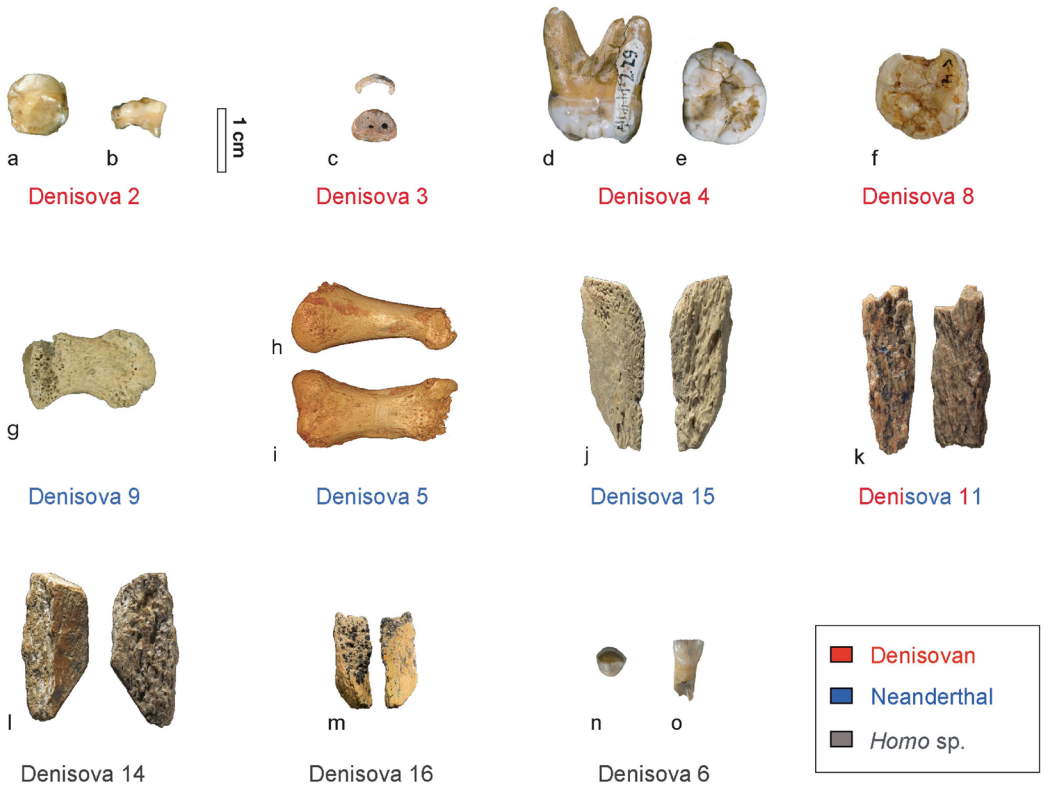

Extended Data Fig. 1 | Human remains from Denisova Cave. Red labels indicate Denisovans; blue labels indicate Neanderthals; and grey labels indicate *Homo* sp. bones that have not been assigned to a group. Denisova 11 is shown in red and blue. A further, unpublished Denisovan specimen (Denisova 13) is mentioned in the Supplementary Information, section 3. **a**, **b**, Denisova 2 in occlusal (**a**) and lingual (**b**) views. **c**, Denisova 3 in proximal view. **d**, **e**, Denisova 4 in mesial (**d**) and occlusal (**e**) views. **f**, Denisova 8 in occlusal view. **g**, Denisova 9 in palmar view. **h**, **i**, Renderings based on micro-computed tomography of Denisova 5 in lateral (**h**) and plantar (**i**) views. **j**, Denisova 15. **k**, Denisova 11. **l**, Denisova 14. **m**, Denisova 16. **n**, **o**, Denisova 6 in occlusal (**n**) and lingual (**o**) views.

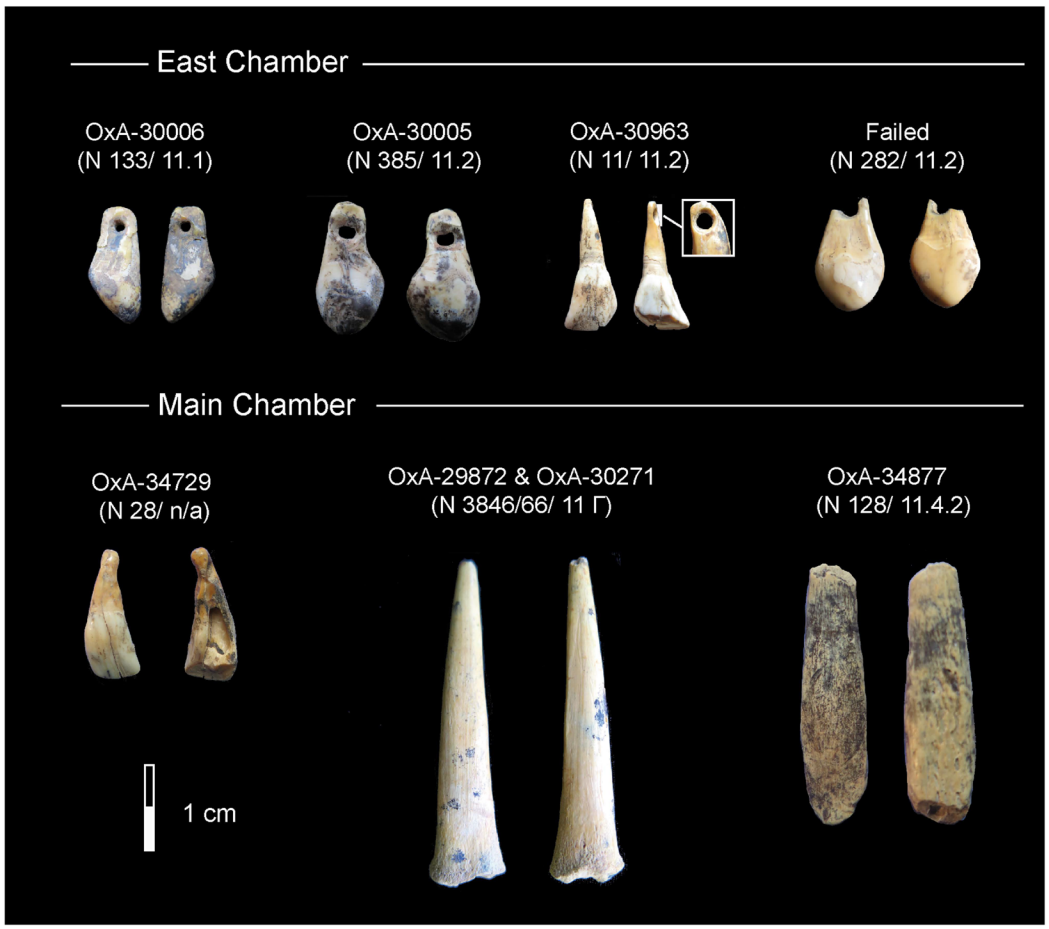

Extended Data Fig. 2 | Personal ornaments and bone points from Denisova Cave that were sampled for radiocarbon dating. N28 was discovered during section cleaning and is not assigned to a specific layer. N282 did not produce enough collagen, and was not dated. N3856/66 was dated twice. Direct dates are listed in Extended Data Table 1.

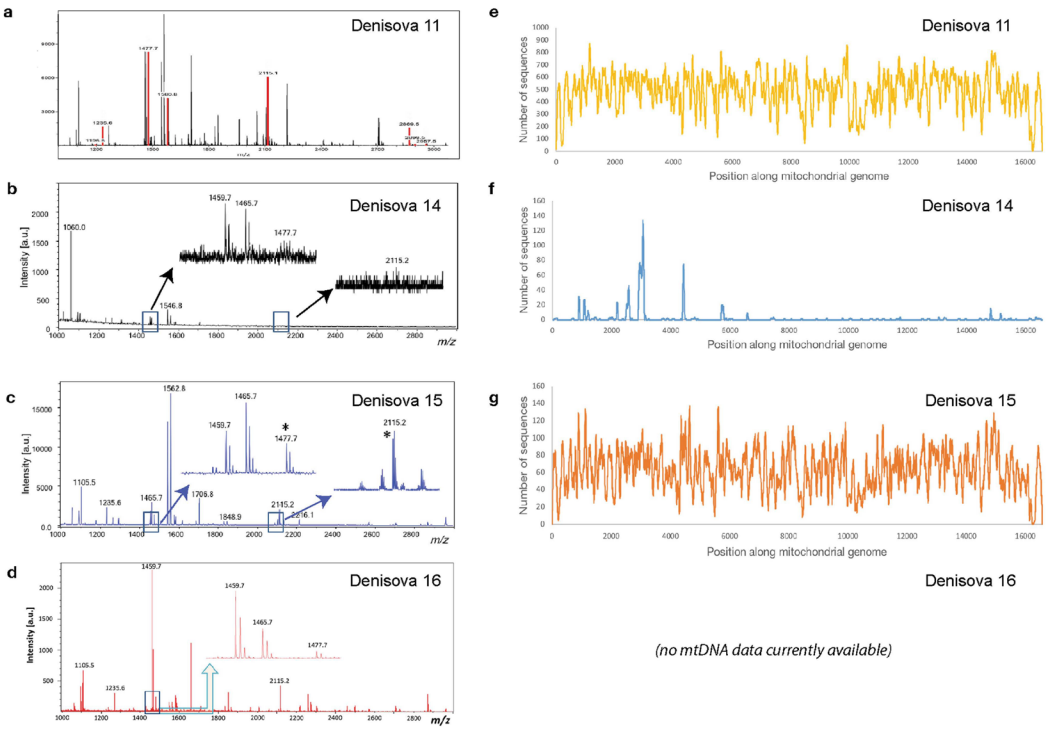

Extended Data Fig. 3 | Proteomic and genetic data for hominin bones discovered using ZooMS. a–d, Collagen fingerprinting MALDI-ToF-MS spectra for Denisova 11, Denisova 14, Denisova 15 and Denisova 16. **e–g**, Average coverage of the human mitochondrial reference genome for Denisova 11, Denisova 14 and Denisova 15. The average coverage of the mitochondrial genome is twofold for the sequences from Denisova 14, and 62.7-fold for Denisova 15. The low collagen preservation indicated for Denisova 14 on the basis of its peptide fingerprint correlates well with the poor recovery of ancient DNA from the same specimen.

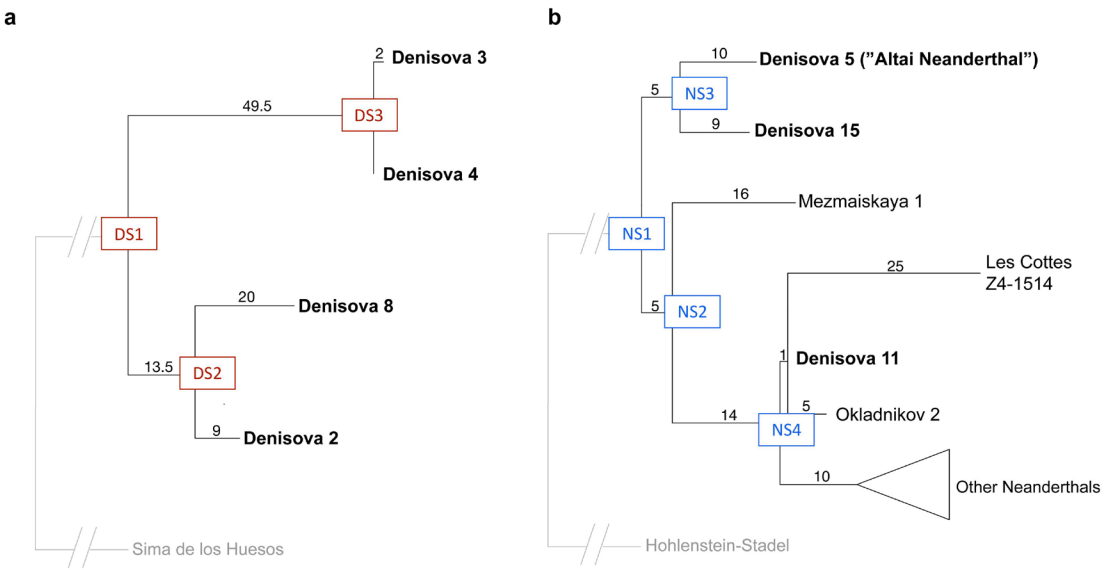

Extended Data Fig. 4 | Inferred number of substitutions that occur on branches that lead to the mtDNA genomes of Denisovan and Neanderthal individuals, since their split from the common ancestor that they share with other archaic individuals. Denisovan (DS) and Neanderthal (NS) split age estimates used in the Bayesian models to enable numerical calculation of the split times of the various points on this tree. Individuals from Denisova Cave are emphasized in bold. **a**, Denisovan mtDNA genomes (data taken from a previous publication[7]). **b**, Neanderthal mtDNA genomes; genomes used in this analysis are reported in Supplementary Table 6.

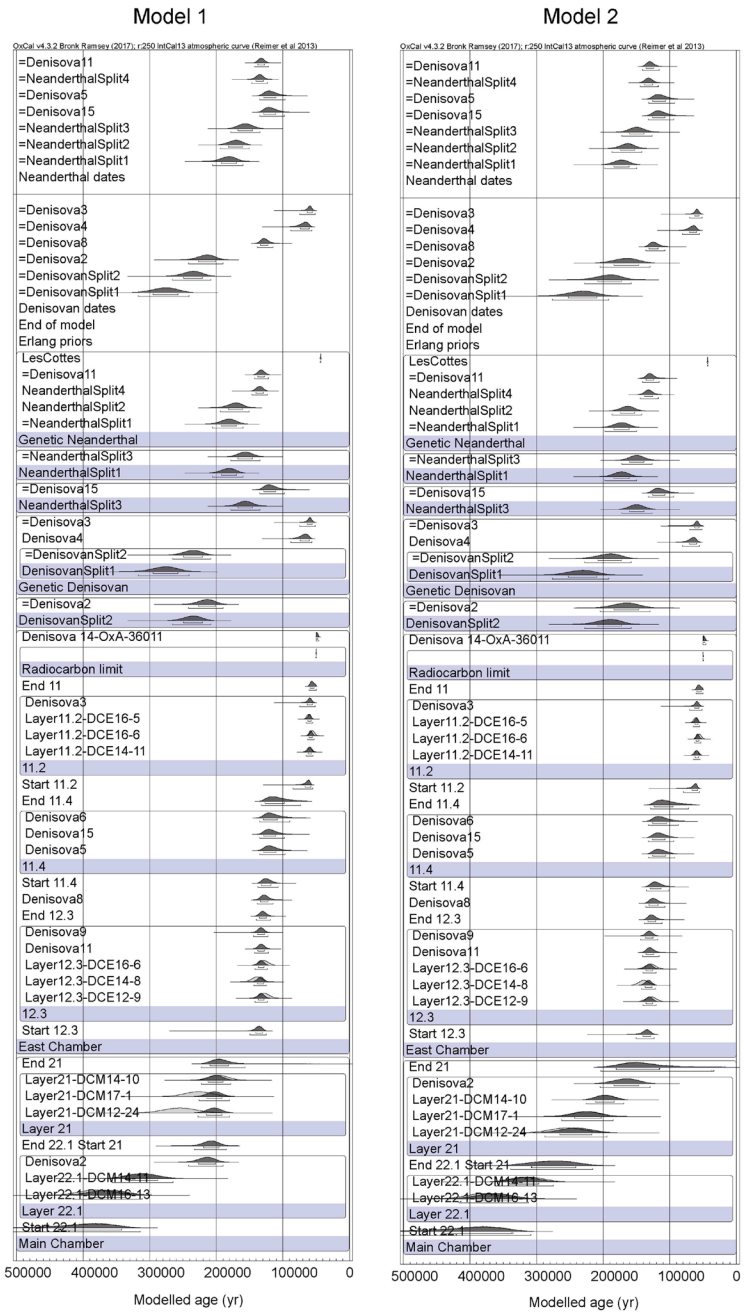

Extended Data Fig. 5 | Bayesian age models (models 1 and 2). Details of modelling are given in the Supplementary Information, section 9.

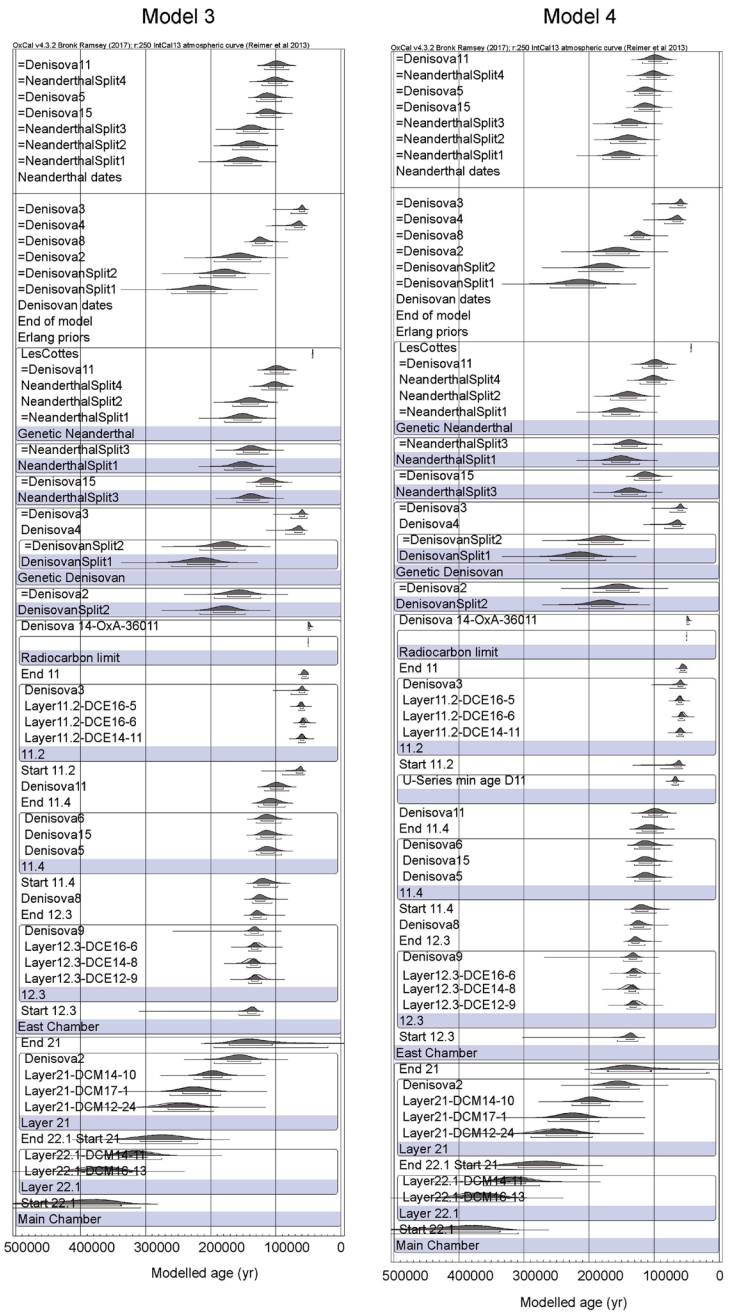

Extended Data Fig. 6 | Bayesian age models (models 3 and 4). Model 4 contains the most prior information and yielded very a high agreement index. We use this model to calculate and report the ages of the human fossils (Extended Data Table 2). Details of modelling are given in the Supplementary Information, section 9.

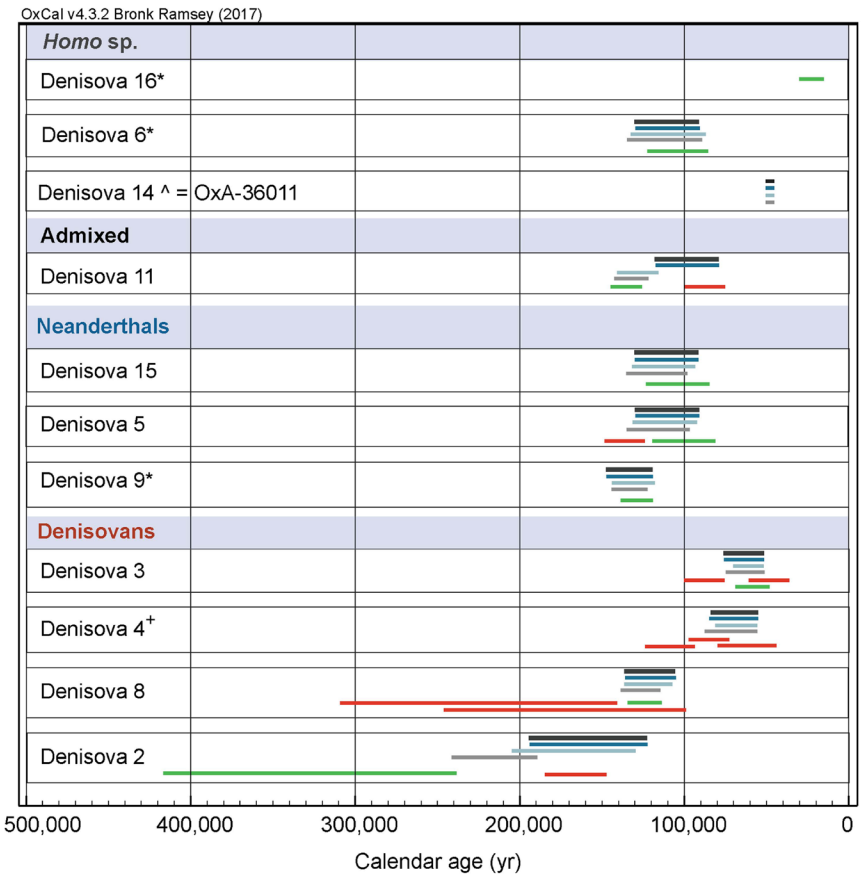

Bayesian model of all optical ages (data from ref. 10)

Genetic age estimates (previously published data in refs 2, 3, 4, 5, 6 and 7)

Bayesian model with a combination of optical, genetic and ^{14}C ages - Model 1

Bayesian model with a combination of optical, genetic and ^{14}C ages - Model 2

Bayesian model with a combination of optical, genetic and ^{14}C ages - Model 3

Bayesian model with a combination of optical, genetic and ^{14}C ages - Model 4

* No ^{14}C or aDNA data, only optical ages available

^ Direct ^{14}C date, same in all models

\+ No ^{14}C or optical dates available

Extended Data Fig. 7 | Comparison of hominin ages estimated on the basis of different types of data. Models 1 to 4 include stratigraphic information, mitochondrial mutation rates, radiocarbon dates and 11 optical ages, and are described in the Supplementary Information, section 9. The green bars show hominin ages derived from a model based on optical ages only (not presented here), which includes all data reported elsewhere[10]. The red bars show schematic age ranges that were estimated using both mitochondrial and nuclear DNA data. All ages are at 95.4% probability.

Extended Data Table 1 | Radiocarbon results from Denisova Cave

	OxA-	Material	Species ID	Layer	P-code	^{14}C yr BP	±	Calibrated yr BP			
								68.2%		95.4%	
East Chamber											
Excavations 2005-2014	29859	tooth	*Equus* cf. *hydruntinus*	9.2	AF	45500	2300	>50000	47400	>50000	45720
	36011	human bone	*Homo* sp. *Denisova 14*	9.3	AF	46300	2600	>50000	47680	>50000	45970
	30006	tooth (pendant)	*Cervus* sp.	11.1	AG	27820	340	32020	31230	32660	31100
	29855	bone	*Crocuta crocuta*	11.1	AF	47900	3100	>50000	48630	>50000	49780
	30005	tooth (pendant)	*Cervus* sp.	11.2	AG	35400	900	41000	39120	41900	38400
	33086	charcoal	not id-ed	11.2	ZR	40400	900	44760	43230	45670	42690
	31506				XR	41300	900	45560	44000	46450	43260
	30963	tooth (pendant)	*Alces alces*	11.2	AG	41300	2400	47200	43040	49710	42450
	36301	bone	not id-ed	11.2	AF	>49000					
	29857	bone	*Bison/Bos*	11.2	AF	>50100					
	29858	bone	*Capra sibirica*	11.2	AF	>48600					
	29852	bone	*Equus* cf. *hydruntinus*	11.3	AF	>49400					
	29853	bone	*Cervus elaphus*	11.4	AF	>47900					
	29856	bone	*Bison* sp.	11.4	AF	>49900					
	29854	bone	*Equus* cf. *hydruntinus*	11.4	AF	>50000					
	36012	human bone	Neanderthal *Denisova 15*	11.4	AF	>50200					
	29860	bone	*Capra sibirica*	11.4	AF	>50000					
	32241	human bone	Neanderthal/Denisovan *Denisova 11*	12	AF	>49900					
Main Chamber											
1997	29861	bone	*Ovis/Capra*	11A	AG	37500	1000	42720	41150	43680	40180
	29872	bone (point)	*Bison* sp.	11Г	AG	42900	2000	48300	44770	>50000	44000
	30271				AF	41200	1400	45980	43410	48100	42660
Excavation 2016	X-2696-20	charcoal	*Salix/ Populus*	9.2	YR	7255	35	8155	8015	8167	8001
	34713				XR	7209	35	8037	7970	8156	7956
	34729	Tooth (pendant)	*Alces alces*	Section cleaning	AG	28390	330	32800	31800	33280	31480
	X-2696-40	charcoal	*Salix/ Populus*	11.2	YR	33900	380	38850	37870	39290	37100
	34919	bone	*Capra* sp.	11.2	AF	34600	600	39800	38520	40670	37800
	X-2695-22	charcoal	Pinaceae	11.2	YR	34400	450	39440	38450	40070	37860
	X-2696-37	charcoal	Pinaceae	11.2-3	YR	35820	370	40900	40040	41310	39650
	34718	charcoal	*Abies/ Juniperus*	11.3	XR	33790	330	38670	37790	38970	37070
	34719	charcoal	Pinaceae	11.3	XR	35210	360	40220	39340	40660	38910
	X-2695-23	charcoal	Coniferous	11.3	YR	36300	900	41730	40030	42430	39080
	X-2696-34	charcoal	*Abies/ Juniperus*	11.4	YR	33380	260	38240	37260	38460	36780
	34717				XR	33720	300	38590	37780	38830	37100
	34918				ZR	33190	320	37960	36840	38370	36480
	X-2695-24	charcoal	*Abies/ Juniperus*	11.4	YR	33600	550	38580	37130	39150	36440
	34720				XR	34050	290	38890	38270	39290	37760
	34980				ZR	33600	550	38640	37090	39320	36410
	34721	charcoal	Pinaceae	11.4	XR	32530	260	36770	36120	37380	35830
	34722	charcoal	Coniferous	11.4	XR	34990	340	39920	39100	40310	38740
	34725	bone	*Ovis/Capra*	11.4	AF	32150	450	36550	35550	37410	35080
	X-2706-55				HYP	31730	330	36010	35250	36330	34900
	34727	bone	*Ovis/Capra*	11.4	AF	34750	600	39960	38670	40880	38160
	X-2706-56				HYP	33810	360	38750	37720	39140	36950
	34723	bone	*Ovis/Capra*	11.4.1	AF	33850	550	38980	37490	39600	36710
	X-2706-54				HYP	33230	350	38060	36870	38450	36440
	34877	Bone (point)	*Equus* sp.	11.4.2	AG	39300	1200	44260	42290	45700	41590
	34728	bone	*Bison/Bos*	11.4	AF	>50400					
	34724	bone	*Bison/Bos*	11.4	AF	>50300					
	34726	bone	*Bison/Bos*	12.1	AF	>50300					
	X-2696-35	charcoal	Deciduous	12.1	YR	>51600					
	X-2696-36	charcoal	Coniferous	12.3-4	YR	>55600					

OxA-, Oxford radiocarbon laboratory code. P-code, pretreatment method and dated material: AG, gelatinized bone collagen without ultrafiltration; AF, ultrafiltered bone collagen; HYP, single amino acid, hydroxyproline, from bone collagen; and ZR, XR and YR refer to ABA, ABOx-SC and AOx-SC methods, respectively (for charcoal samples). Samples highlighted in grey produced more than one radiocarbon determination, using different pretreatment methods.

Extended Data Table 2 | Comparison of the modelled age estimates for human fossils obtained from Bayesian models 1 to 4

	Model 1 (kyr)	Model 2 (kyr)	Model 3 (kyr)	Model 4 (kyr)
Model agreement index	23.3%	82.3%	111%	111%
Denisova 14	45.9–50	45.9–50	45.9–50	45.9–50
Denisova 6	89.5–135.1	87.0–132.3	91.2–130.1	91.2–130.3
Denisova 15	97.9–134.9	94.0–132.1	91.5–130.1	91.4–130.3
Denisova 5	96.4–134.8	92.8–132.0	91.0–129.8	90.9–130.0
Denisova 9	122.3–144.1	117.9–143.7	119.1–147.4	119.1–147.3
Denisova 11	121.8–142.5	115.7–140.9	79.2–117.5	79.3–118.1
Denisova 4	56.2–88.1	55.7–81.2	55.4–84.9	55.2–84.1
Denisova 3	51.7–75.1	51.9–70.3	51.6–76.9	51.6–76.2
Denisova 8	114.5–138.6	107.2–136.4	105.7–136.3	105.6–136.4
Denisova 2	189.9–241.7	129.5–204.5	122.8–194.4	122.7–194.4

Dates are given as thousands of years (kyr) ago. The agreement index for each model is shown in the second row. All age ranges are at 95.4% probability. The age listed for Denisova 14 is the direct radiocarbon age, and not a modelled estimate.

nature Y INFORMATION

Age estimates for hominin fossils and the onset of the Upper Palaeolithic at Denisova Cave

Katerina Douka[1,2]*, Viviane Slon[3], Zenobia Jacobs[4,5], Christopher Bronk ramsey[2], Michael V. Shunkov[6,7], Anatoly P. Derevianko[6,8], Fabrizio Mafessoni[3], Maxim B. Kozlikin[6], Bo Li[4,5], rainer Grün[9], Daniel Comeskey[2], thibaut Devièse[2], Samantha Brown[1], Bence Viola[10], Leslie Kinsley[11], Michael Buckley[12], Matthias Meyer[3], richard G. roberts[4,5], Svante Pääbo[3], Janet Kelso[3] & tom Higham[2]*

[1]Department of Archaeology, Max Planck Institute for the Science of Human History, Jena, Germany. [2]Oxford Radiocarbon Accelerator Unit, Research Laboratory for Archaeology and the History of Art, University of Oxford, Oxford, UK. [3]Department of Evolutionary Genetics, Max Planck Institute for Evolutionary Anthropology, Leipzig, Germany. [4]Centre for Archaeological Science, School of Earth, Atmospheric and Life Sciences, University of Wollongong, Wollongong, New South Wales, Australia. [5]Australian Research Council (ARC) Centre of Excellence for Australian Biodiversity and Heritage, University of Wollongong, Wollongong, New South Wales, Australia. [6]Institute of Archaeology and Ethnography, Russian Academy of Sciences Siberian Branch, Novosibirsk, Russia. [7]Novosibirsk State University, Novosibirsk, Russia. [8]Altai State University, Barnaul, Russia. [9]Australian Research Centre for Human Evolution, Griffith University, Brisbane, Queensland, Australia. [10]Department of Anthropology, University of Toronto, Toronto, Ontario, Canada. [11]Research School of Earth Sciences, The Australian National University, Canberra, Australian Capital Territory, Australia. [12]Manchester Institute of Biotechnology, University of Manchester, Manchester, UK. *e-mail: douka@shh.mpg.de; thomas.higham@rlaha.ox.ac.uk

SUPPLEMENTARY INFORMATION

1: STRATIGRAPHIC AND ARCHAEOLOGICAL BACKGROUND

M. Shunkov, A. Derevianko, M. Kozlikin

Denisova Cave (51°23'51.3"N, 84°40'34.3"E) is situated in the low and middle mountains of the northwest Altai mountains in the upper Anui Basin. The site is located on the right side of the Anui River (Figure S1). The left side is confined to the slopes of the Karakol Mountain (1315 m) and the right side to the slopes of the Sosnovaya Mountain (1112 m). The valley floor is about 120 m wide (Figure S2) and the river surface is 662 m above sea level.

The cave has formed in a large Silurian marbled coarse-grained limestone block. Its entrance is located in the ledge of a southwest facing sheer rock wall at 28 m above the modern-day river level (Figure S3). The cave consists of a system of short sub-horizontal chambers varying in size, which communicate through the Main Chamber (Figure S4), a vast arched room measuring 11m × 9m and about 10m in height. Two narrow dark chambers, the East Chamber and the South Chamber, stretch southeast deep into the karst massif, where they are completely filled by loose sediments[1].

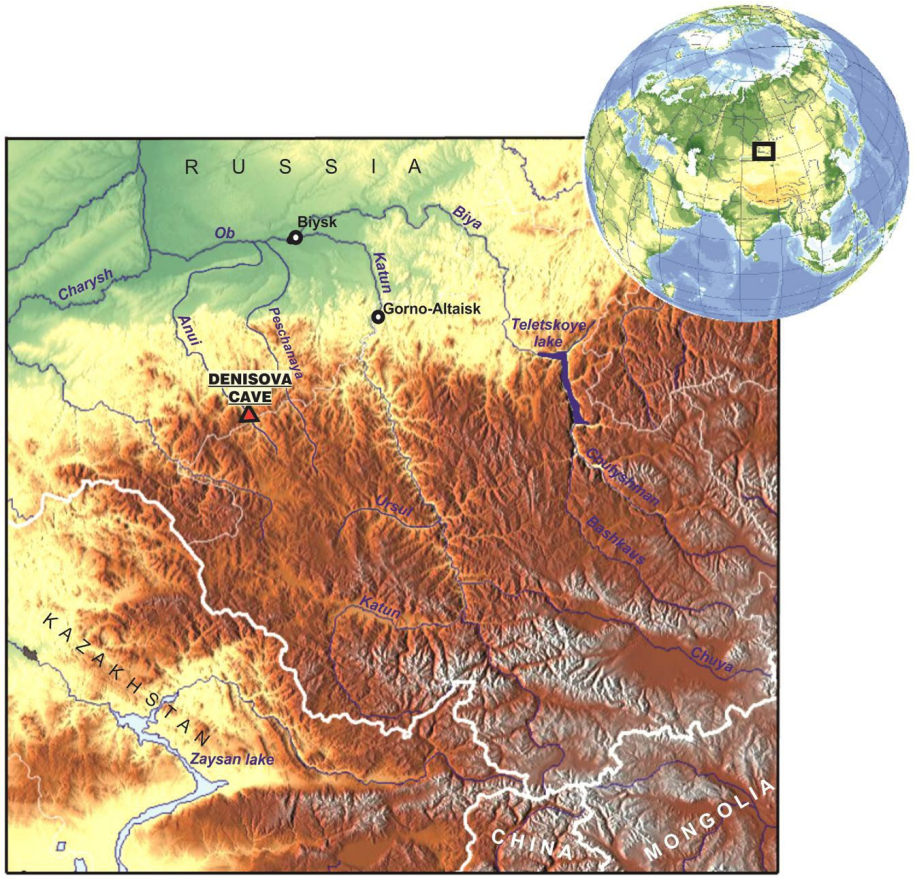

Figure S1. Location of Denisova Cave in the Altai region**.**

Denisova Cave was discovered in 1977 by N.D. Ovodov, a Russian palaeontologist[2]. Systematic investigations began in 1982. In 1982 and 1983, the Holocene deposits from the Main Chamber and the cave entrance were excavated[3]. In 1984, 1993–1995, 1997 and 2016, research focused on the Pleistocene deposits of the Main Chamber. The Pleistocene part of the cave entrance was excavated in 1990, 1991 and 1996 (Figure S4). Between 1999–2003, excavations were undertaken at the mouth of the South Chamber. In the 2004–2016 excavations revealed the Holocene and Pleistocene deposits in the East Chamber.

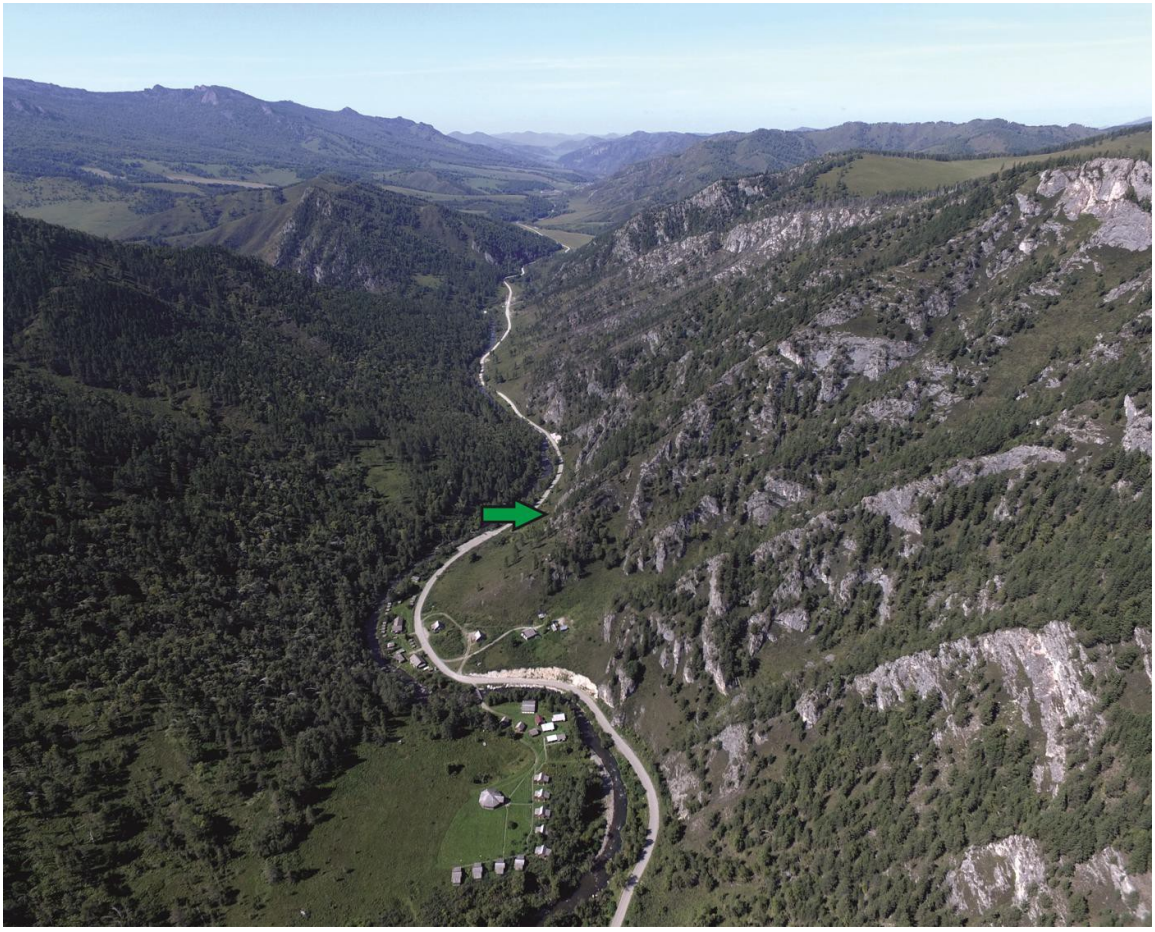

Figure S2. The Anui River valley in the vicinity of Denisova Cave (photograph by A. Postnov). The cave entrance is indicated by the green arrow. View to the north-northwest.

Figure S3. General view of Denisova Cave (photograph by S. Zelensky).

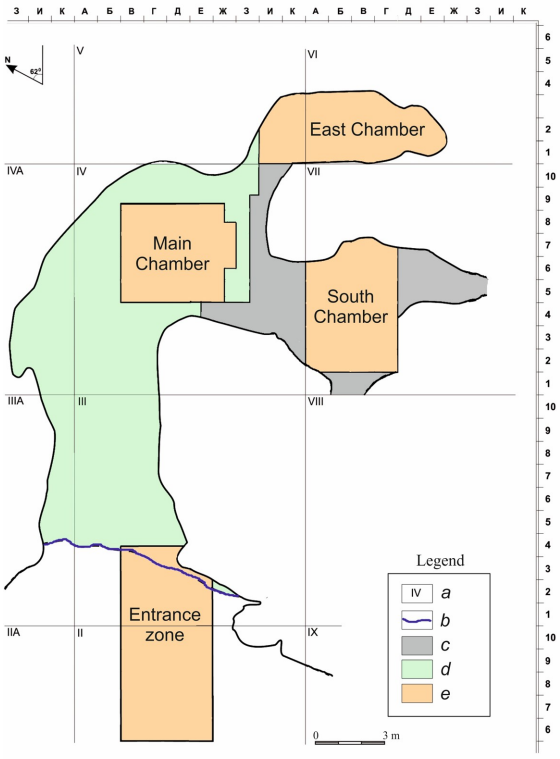

Figure S4. Denisova Cave plan showing excavated areas. Legend: a. sector number; b. cave dripline; c. Holocene surface; d. top of exposed Pleistocene deposits; e. excavation trenches in the Pleistocene deposits.

A. Stratigraphy

Main Chamber

In the Main Chamber, a total of 14 major lithological units (layers 9–22, from top to bottom) were recognised in the Pleistocene deposits of the stratigraphy. Based on a number of texture changes in the sediments, some layers (9, 11–14, 19, 22) were subdivided into additional stratigraphic horizons. Lens-shaped layers 15, 16 and 18 stretched locally in the middle portion of the deposits and were documented only in the sections produced in 1984. The 2016 excavation profile, from which the majority of samples for radiocarbon dating were collected, is shown in Figure S5[4].

The upper part of the Pleistocene deposits (layers 9.2 and 9.3) exposed during the 2016 excavations include light pale yellow loess loams with lenses and occasional inclusions of debris, finely broken stone and the new formations of whitish phosphate. Isolated burrows resulting from the activities of shrews have been identified.

The middle strata (layers 11.2–11.4, 12.1–12.3, 14, 19–21) consist of stratified lens-shaped multi-coloured loams with rubble and debris. The layers vary in thickness and reveal a sinuous shape; they show both well-defined boundaries, and indistinct ones in the form of a zone showing gradual transition.

The lower part (layers 22.1–22.3) of the stratigraphic section comprises heavy, pale ochred- yellow loams with eroded debris of different fractions, including isolated limestone blocks.

East Chamber

The East Chamber is a narrow sub-vertical fissure developed by karst processes formed by a system of steeply dipping fissures that appeared in the limestone massif. The chamber floor consists of alternate transversal rock projections and steeply dipping tunnel-shaped features[5].

Due to major differences in the composition and visual appearance of the sediments, it is not possible to make unambiguous correlation between the stratigraphic sections in the East Chamber and those exposed in the Main Chamber. Therefore, an independent stratigraphic numbering system was introduced for the deposits of the East Chamber. A total of 15 stratigraphic units were recognized in the Pleistocene part of the East Chamber (layers 9-17) (Figure S6)[6]. The deposition of loose sediments in the East Chamber indicates that this location underwent phases similar to those recognised in the Main Chamber. In general, the thick strata of sediments in the East Chamber consist, sedimentologically and lithologically, of three series of layers separated with well-defined depositional gaps.

The upper series (layers 9.1–9.3) comprises light loess loams with lenses and isolated inclusions of debris and finely broken stones. These loams are rich in organic matter resulting in severe chemical alteration of the sediments.

The middle series (layers 11.1–11.4, 12.1–12.3, 13–16) includes stratified lens-shaped rubbly material filled with multi-coloured light loams. Its formation occurred after the karst cavity opened up, in an environment of intense biogenic and anthropogenic impact and against a background of

increased local climatic fluctuations.

The lower series (layers 17.1 and 17.2) consists of loamy and heavy loamy deposits of ochre- yellow color, with inclusions of lime-rock particles and leached sinter deposits. It constitutes redeposited material typical of sealed karst cavities. This earliest depositional phase occurred when the cavity was closed to external influences.

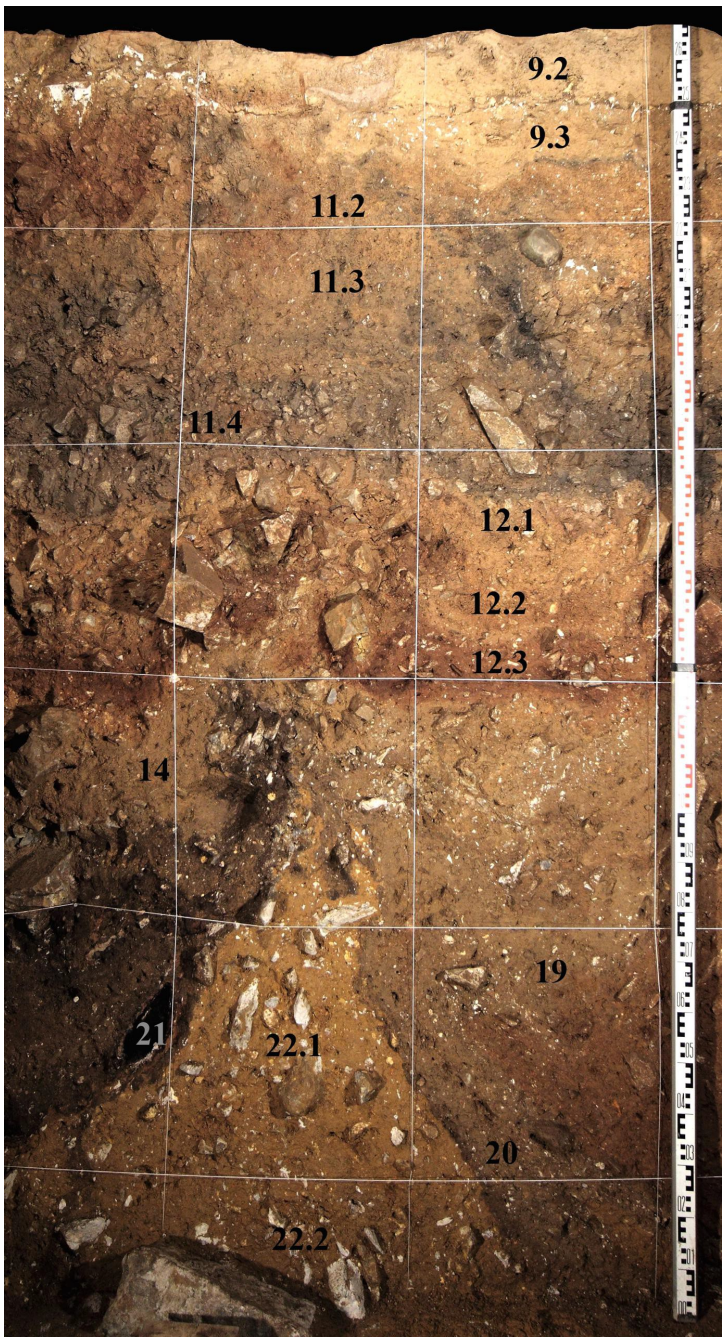

Figure S5. Southeast wall of the 2016 excavation trench in the Main Chamber showing numbers of lithological layers. Most charcoal for radiocarbon dating came from the upper part of this excavation profile.

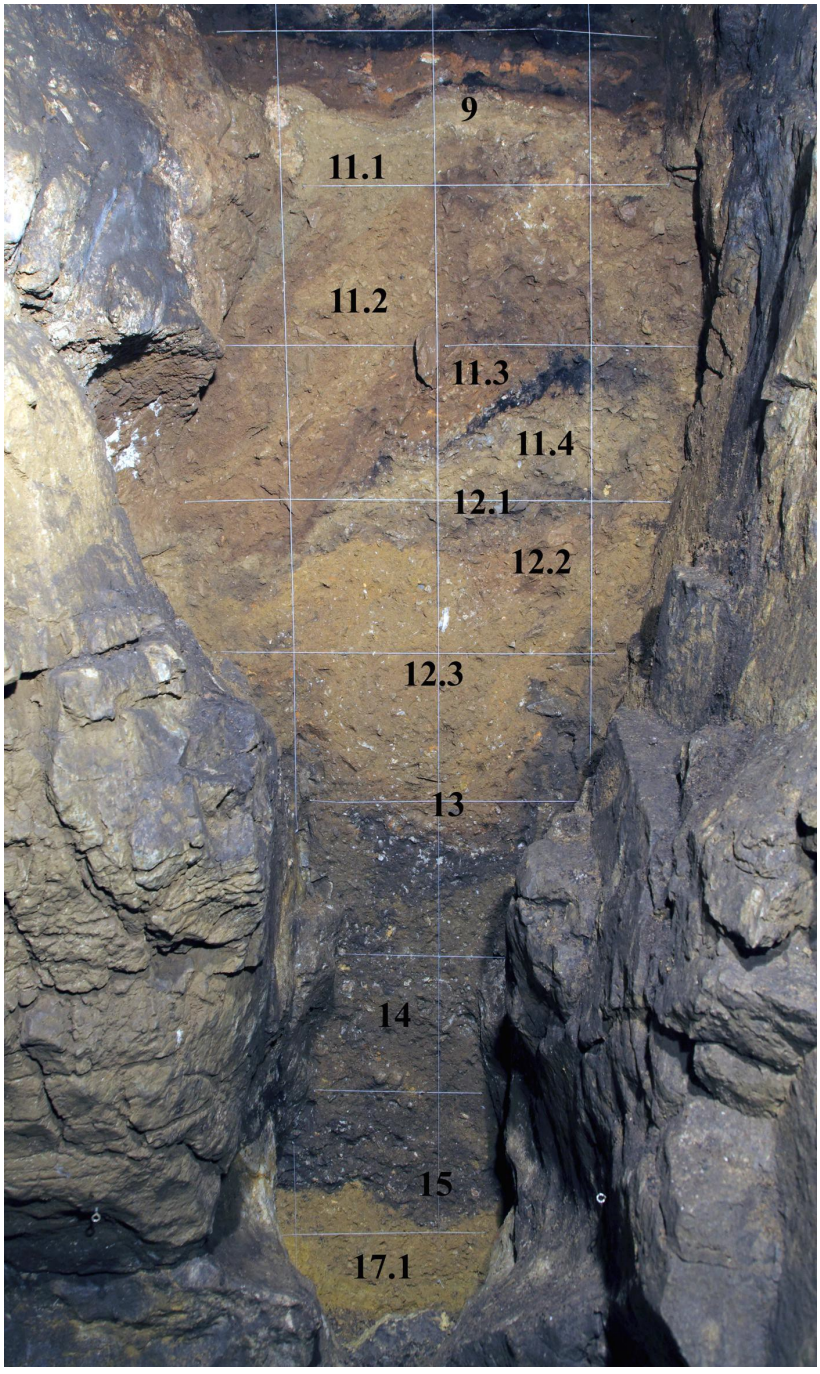

Figure S6. Southeast wall of the 2015 excavation trench in the East Chamber of Denisova Cave with numbers of lithological layers.

B. Archaeology

The upper part of layer 22 in the Main Chamber has yielded the earliest archaeological evidence at Denisova Cave. A small assemblage of lithic artefacts was recovered from this part of the section including a series of cores that indicate the use of parallel, radial and unsystematic flaking. The lithic assemblage is dominated by scrapers, denticulate, notched and spur-like tools. Levallois flakes have been also identified.

The lithic assemblage retrieved from lithological layers 21 and 20 in the Main Chamber and layers 15 and 14 in the East Chamber are attributed to the early Middle Palaeolithic. This is characterized by the use of radial cores and Kombewa-type cores. Levallois cores for the manufacture of flakes were also present. Here, similarly to the assemblage from layer 22, the tools include different types of denticulate, notched, spur-like tools and scrapers. Archaeological evidence from layers 19–12 in the Main Chamber and from layers 13–11.3 in the East Chamber are attributed to the middle and late Middle Palaeolithic. Flat parallel and radial cores, as well as Kombewa-type cores, are abundant among nucleuses found in the lithic industries recovered from this part of the excavation section. Levallois cores for manufacturing flakes and blades comprise a small sub-set. Isolated sub-prismatic cores are also documented. Here, compared to the preceding early Middle Palaeolithic assemblage, the proportion of elongated flakes in the flake industry increases and regular blades made their appearance. While different types of scrapers dominate the assemblage, a distinct notch-denticulate component remains. Levallois points occur in small numbers. Upper Palaeolithic artefacts, including such types as end-scrapers, burins, chisel-like tools and truncated flakes, appear in the record. Archaeological materials recovered from layer 11 in the Main Chamber, as well as from layers 11.2 and 11.1 in the East Chamber, are assigned to the “Initial Upper Palaeolithic”. The term is used here to denote an early Upper Palaeolithic assemblage with features of Levallois reduction and retouched Upper Palaeolithic components. The lithic assemblage is characterized by the use of cores that were used for both parallel and radial flaking. Volumetric and Levallois flaking was less common. Compared to the Middle Palaeolithic assemblages, the toolkit demonstrates a decrease in the percentage of flake tools resulting from Levallois flaking, and an increase in the proportion of blades. The composition of the Initial Upper Palaeolithic tool assemblage with signs of secondary reduction from the East Chamber and the Main Chamber shows similarities with the preceding Middle Palaeolithic industries. A number of typologically important tools are still based on various types of scrapers, denticulate, notched and spur-like tools. Levallois points are present and Upper Palaeolithic-type pieces constitute no more than 18% of the tools. Numerous objects linked with symbolic behaviour as well as bone tools were discovered alongside the lithic industry. A wide variety of pendants, tubular beads, beads and rings, were found, made of animal teeth and bones, mammoth ivory, ostrich eggshell, and ornamental stone. These were manufactured using techniques such as cutting, scraping, drilling, grinding and polishing. Local materials were used for the production of some ornaments, but exotic minerals

(serpentine, chloritolite) located 100–250 km from the cave were also used. Ostrich eggshell is likely to have been imported from modern-day Mongolia.

The archaeological record from layer 9 in the Main and East Chambers illustrates further development of the Upper Palaeolithic assemblages. During this time, the role of blade production increased and bladelet technology emerged. Tool assemblages contain very distinctive types of Upper Palaeolithic pieces, although scrapers are still common. Bone tools and ornaments produced from organic materials are also present.

Characteristic tool types from the Main And East Chambers are shown in Figures S7 and S8. According to the excavators, the Palaeolithic assemblages from Denisova Cave reflect a long-term process of progressive evolution in lithic industries, attesting to the continuity of technological traditions among humans inhabiting the site during the Middle and Upper Palaeolithic periods.

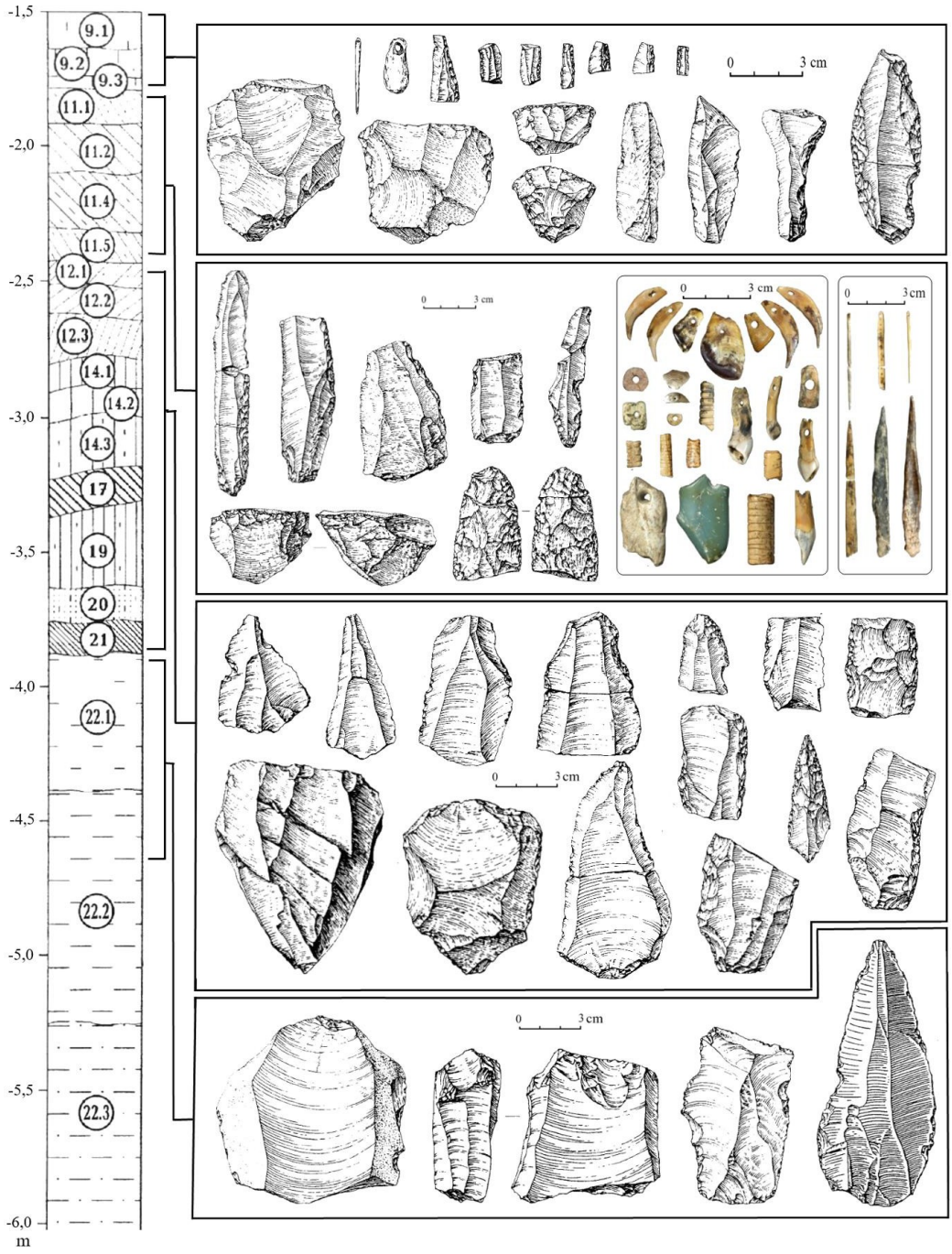

Figure S7. Artefacts from the Main Chamber of Denisova Cave.

Figure S8. Artefacts from the East Chamber of Denisova Cave.

B. Regional comparisons

In addition to Denisova Cave, eight cave sites and over ten open-air sites, with a total of over 70 occupation layers spanning the Middle and Upper Palaeolithic periods, have been discovered in the Altai Mountains[7,8]. Based on extensive evidence from fieldwork and laboratory studies from these sites, the excavators have argued that there is a uninteruptive evolutionary development of the Middle Palaeolithic industry with no easily discernible effect stemming from the infiltration of populations associated with a different cultural adaptation.

At the final stage of the Middle Palaeolithic (50–60,000 years ago), two variants in the production of lithic industries emerged in the Altai, the Kara-Bom and Karakol variants. These may represent different adaptive strategies by early Upper Palaeolithic hunter-gatherers; both however appear to emerge from a single Middle Palaeolithic tradition.

In areas where the Upper Palaeolithic is linked to the arrival of different human populations, the Middle and Upper Palaeolithic industries demonstrate sharp differences, and discontinuity in both primary and secondary reduction strategies. On the contrary, at sites where Upper Palaeolithic industries developed locally, it is possible to trace the evolutionary development through the Middle Palaeolithic industries. This is the case of Denisova Cave.

The lithic evidence from layer 11 in the Main Chamber and layers 11.2 and 11.1 in the East Chamber of Denisova Cave demonstrates the retention of Middle Palaeolithic elements in primary and secondary reduction, with the emergence of a techno-typological base characteristic of the Upper Palaeolithic.

Based on the lithic and bone industries, numerous non-utilitarian objects, economic strategies, and the presence of seemingly imported materials or finished pieces, the behaviour of populations who inhabited the Altai region is characteristic of that often associated with anatomically modern humans. However, recovery of mitochondrial and nuclear DNA from human fossils found associated with the Upper Palaeolithic layer 11.2 in the East Chamber and layer 11.1 in the South Chamber shows that these hominins were the *Denisovans*[9].

A human population with a distinct Mousterian-type lithic industry, associated with the Neanderthals, also inhabited the Altai region[10]. Evidence in support of this has been found in Okladnikov and Chagyrskaya caves. Materials recovered from these caves share similarities in major technological and typological features, which are not characteristic of other Palaeolithic assemblages in the region. This Mousterian-type industry is characterized by the dominance of radial technology that became the basis for the mass production of angled blanks. The assemblages from both Okladnikov and Chagyrskaya caves demonstrate identical features of secondary reduction. The toolkit includes a broad range of scrapers, points, notch-denticulate tools, retouched flakes and bifaces. A key feature of this industry is the presence of backed scraper knives, as well as various angled pieces including *déjeté* scrapers[11]. Very few and isolated Mousterian-type tools such as the ones discovered at Chagyrskaya and Okladnikov caves have been recognized in the Middle Palaeolithic layers of Denisova Cave, where Neanderthal remains

were recovered from layers 11.4 and 12 in the East Chamber and Neanderthal DNA was extracted

from the sediment of layers 11.4 and 14 in the East Chamber and layers 14, 17 and 19 in the Main Chamber[12-13].

One possibility to explain the archaeological evidence is that Denisovans were the producers of the Upper Palaeolithic technocomplexes in the Altai region between 50–35 ka. To date, there is no anthropological or genetic record of anatomically modern humans in the Altai during the late Pleistocene. The presence of the Ust-Ishim modern human in western Siberia at 45,000 cal BP[14], however, raises the possibility that modern humans who were present in the wider region may have also been the makers of the Upper Palaeolithic in the Altai. It is important to consider that our age estimate for *Denisova 3*, the most recent Denisovan fossil at the site pre-dates 50,000 BP and the direct date for Ust-Ishim. More human material is required to answer with more certainty questions regarding the link between hominins and lithic industries and other types of artefacts.

2: RADIOCARBON DATING

K. Douka, T. Higham, T. Devièse, D. Comeskey

A. Dated material

Samples for AMS ^{14}C dating were obtained either at the storage and museum facilities in Novosibirsk (bone and artefacts) or at the cave during, or shortly after, excavation (mainly charcoals). Four series of samples were selected for dating; human bones, cutmarked bones, tooth pendants, bone points and charcoal samples.

Below in brackets are the number of "individual samples"/ "total radiocarbon dates" obtained, per type of material. In some cases indivdual samples were dated more than once, in others they failed to procuded enough C for dating.

1. human bones (n=2/2), plus *Denisova 11* previously published.
2. cut-marked animal bones and teeth (n=23/21) (Figure S9)
3. tooth pendants (ornaments) (n=5/4) (Extended Data Figure 2)
4. bone points (n=2/3) (Extended Data Figure 2)
5. charcoal samples (n=31/20).

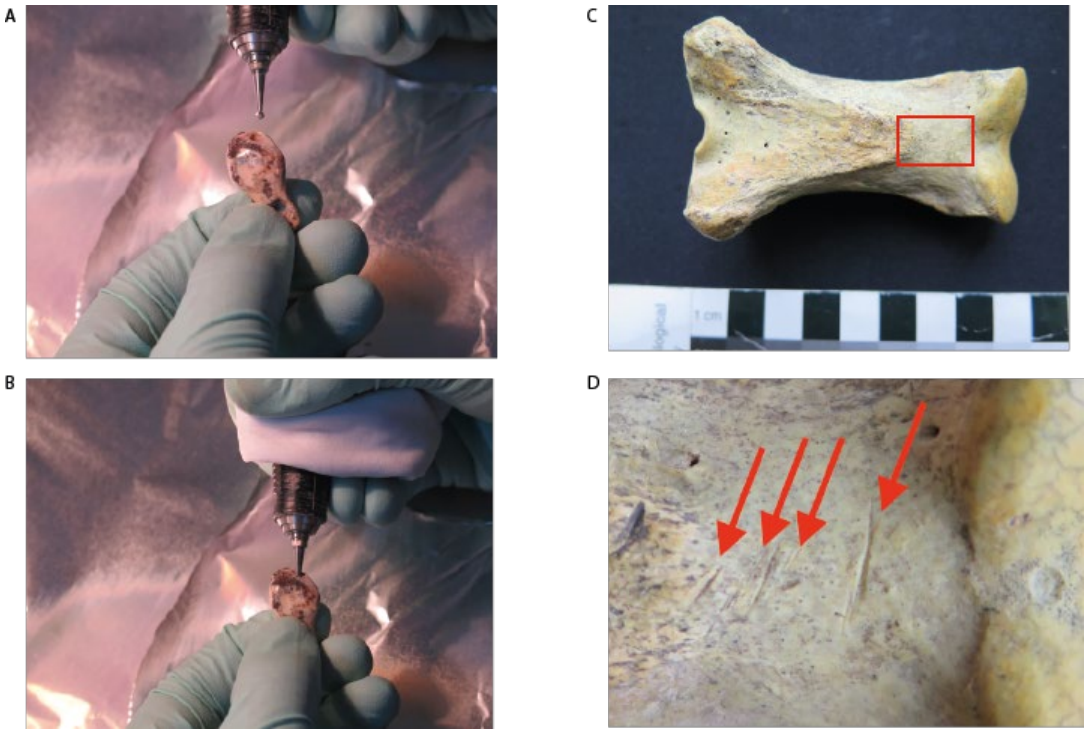

Figure S9: A-B: Tooth pendants from the East and Main Chambers were drilled using the ORAU's keyhole sampling method to minimise sample invasiveness and destruction. C-D: Cut-marked bone was selected for AMS dating; in this example a bone of *Equus cf hydruntinus* from Layer 11.3 (East Chmaber) was dated to >49,400 BP (OxA-29852) (D see inset of photograph C).

B. Charcoal Identification

Charcoal was taxonomically identified prior to radiocarbon dating by Dr Dana Challinor. The fragments were extremely small, with some less than 2mm in transverse section (the standard size required for identification). In all cases, however, it was possible to determine whether coniferous or deciduous wood was present. Identification was also hampered by high levels of vitrification and the inability to fracture without destruction. Standard identification procedures were followed based upon anatomical structure, with reference to modern specimens and reference texts. The material was held in a sand bath for examination.

At least three separate genera were positively distinguished; *Pinus* (pine), *Abies/Juniperus* (fir or juniper) and *Salix/Populus* (willow or poplar). In many cases, it was possible to say, on the basis of resin canal presence, that a member of the Pinaceae was represented, but closer identification was not possible. Only one fragment exhibited the large pitting typical of *Pinus*, but others with smaller pitting could be from a different pine species or from *Picea* (spruce). Notes on the identifications for each fragment are included in Table S1 below, but a couple of other anatomical observations are worth noting: no scalloped tori were visible; bi-seriate bordered pits were absent (which is typical of *Larix*, larch); and no spiral thickenings were observed (which rules out the presence of *Taxus,* yew), although some compression lines (indicating branchwood) were noted.

Table S1: Identifications for the charcoal samples dated from the Main Chamber. *P no*. denotes the Oxford sample reference number.

P no.	Identification	Identification notes
41823	*Abies/Juniperus*	No resin canals, taxadoid-cupressoid pits, single borded pits, uniseriate rays, no spirals. Vitrified.
41824	Pinaceae	Resin canals, single bordered pits, small ray pitting. Vitrified.
41825	Pinaceae	1 resin canal but too small to confirm other characteristics.
41826	Coniferous	Too small to identify further.
41827	Deciduous r-w	Diffuse porous but too small to confirm identify further.
41828	Coniferous	Poss resin canal, but unclear as very distorted.
41833	Pinaceae	Resin canals, single bordered pits so prob *Picea* or *Pinus* – but too small to see pitting
41839	*Abies/Juniperus*	As for <823> but crumbled.
41840	*Pinus* sp.	No resin canals visible, but definite large pitting – pinoid type.
41841	Pinaceae	1 resin canal observed in ray TLS but too small to see other characteristics. Vitrified

41842	Pinaceae	No resin canals but poor confition, vitrified. Taxodoid pits.
41843	*Salix/Populus*	Short radial files, uniseriate rays, distinctive pitting
41844	Deciduous	Diffuse porous but too small to take further.
41845	Coniferous	<1 growth ring. Compression lines
41846	*Abies/Juniperus*	No resin canals, uniseriate rays, single bordered pits, taxadoid to cuppresoid pitting
41847	cf. *Pinus* sp.	Resin canals (not traumatic), horizontal walls pitted, single row bordered pits, ray pitting unclear as small so cf. id. Compression lines
41849	Pinaceae	Possible resin canal, single row bordered pits, uniseriate rays, no spirals
41850	Coniferous	Single row bordered pits, no spirals

C. Radiocarbon dating methods

AMS sample pretreatment and measurment were performed at the Oxford Radiocarbon Accelerator Unit (ORAU), University of Oxford, UK. Bones for dating were sampled as unobtrusively as possible using an NSK micromotor drill with tungsten carbide and diamond drill bits. The samples underwent the routine ORAU chemical pretreatment protocol briefly described below.

Drilled or coarsely ground bone powder was immersed in solutions of 0.5 M HCl (3 washes over 18h at room temperature (RT)), 0.1M NaOH (30 minutes, at RT) and 0.5M HCl (~1 hour; at RT), interspersed with ultra-pure (MilliQ™) water rinses between each reagent. The extracted collagen was gelatinised in a pH 3 solution at 75 °C for 20 hours and filtered through previously- cleaned 9ml polyethylene Ezee-filters™ (Elkay, UK). The filtrate was transferred with glass pipettes into previously-cleaned ultrafilters (Sartorius Vivaspin™ 15–30kD MWCO) and centrifuged at 2500-3000rpm until 0.5–1.0mL of the >30kD gelatin fraction was left (~30-40 mins). The supernatant was collected using glass pipettes, placed into prebaked clean glass tubes, frozen at -18 °C, and freeze-dried for a minimum of 12 hours. Ezee-filters™ and ultrafilter precleaning steps are undertaken as outlined in Brock *et al*. (2010)[15]. For some bones, noted as AG in the pretreatment code column (Table S2), ultrafiltration was not applied due to low amount of recovered collagen.

For three bone samples from the Main Chamber (P 41851, P 41853 and P 41856) we also used the single amino acid radiocarbon dating method developed at the ORAU. This method involves separation of the underivatised amino acids from hydrolysed bone collagen samples using preparative High Performance Liquid Chromatography (Prep-HPLC)[16]. Using this procedure (coded HYP), hydroxyproline (Hyp), which essentially acts as a biomarker of bone collagen, was isolated and dated. This approach is the most efficient technique to remove contaminants including conservation materials.

Samples of charcoal were prepared for dating using three methods: the routine ABA (Acid-Base-Acid) method, the ABOx-SC preparation[17] as applied at Oxford[15] and a modified ABOx-SC preparation which excludes the base step (AOx-SC) (Douka et al. *in preparation*). This latter method has been shown to produce results indistinguishable to those obtained with the ABOx- SC method but without the extensive material loss associated with it. In Table S2, ABA is denoted as ZR, ABOx-SC as XR, AOx-SC as YR.

Gelatin, amino acids, or pre-combusted charcoal samples were analysed using a PDZ-Europa Robo-Prep combustion elemental analyser coupled to a PDZ-Europa 20/20 mass spectrometer operating in continuous flow mode using an He carrier gas. This enables the measurement of $\delta^{15}N$ and $\delta^{13}C$ values and N and C content, and calculation of C:N atomic ratios. VPDB is the standard for $\delta^{13}C$ values, AIR for the $\delta^{15}N$ values. Graphite was produced by reacting the sample CO_2 over an iron catalyst in an excess H_2 atmosphere at 560°C. AMS radiocarbon measurement was undertaken using the ORAU 2.5MV HVEE accelerator.

We used OxCal 4.3.2[18] and the IntCal13 calibration curve[19] to calibrate the radiocarbon data when these were within the working limit of the method, i.e. <50,0000 BP.

D. Radiocarbon dating results

Radiocarbon dates and all analytical data are reported in Table S2. The vast majority of bones were well preserved in terms of collagen, with only one yielding less than 1% wt. collagen (the effective threshold in the ORAU). We did, however, have some bone samples that failed to produce a collagen yield of significance, these failed samples are shown in Table S3. All other analytical parameters we measured, including the C/N atomic ratio, were within accepted ranges. The dates are corrected for routine procedures such as pre-treatment chemistry, combustion and graphitisation. For the HYP dates, the correction also includes the extraneous carbon added during the chromatographic separation[16]. The results obtained for the same sample using AF and HYP protocols are in statistical agreement.

The calibrated radiocarbon data of the finite ages, i.e. those within the limit of the method, are shown in Table S4 and Figure S10 below.

Table S2: New radiocarbon determinations from Denisova Cave. *OxA-* is the Oxford radiocarbon lab code, *P no*. denotes the Oxford sample reference number, *P code* denotes the pretreatment method and dated material used (AG is gelatinised filtered collagen without ultrafiltration for the low collagen bones; AF is ultrafiltered collagen; HYP is the single amino acid, hydroxyproline; ZR, XR and YR refer to ABA, ABOx-SC or AOx- SC methods, respectively, for charcoal samples). Samples highlighted in grey denote samples that produced more than one radiocarbon determination using different pretreatment methods.

	Radiocarbon results										Analytical data						
	OxA-	P no.	Material	Species ID	Layer	Year exc. Square, ID	^{14}C yrs BP	±	F^{14}C	±	δ^{13}C (‰)	N^{15}N (‰)	C:N	P code	Used mg	Yield mg (%)	%C
East Chamber																	
Excavations 2005-2014	29859	35677	tooth	*Equus* cf. *hydruntinus*	9.2	2008, n/a	45500	2300	0.00347	0.00099	-19.77	5.01	3.36	AF	790	12.81 (1.6)	40.3
	36011	43830	human bone	*Homo* sp.	9.3	DC 3758 *Denisova 14*	46300	2600	0.00313	0.00101	-18.82	16.49	3.25	AF	290	5.27 (1.8)	42.2
	30006	35672	tooth (pendant)	*Cervus* sp.	11.1	2007, E-4(B), N 133	27820	340	0.03134	0.00133	-19.30	9.72	3.47	AG	230	3.71 (1.6)	35.6
	29855	35673	bone	*Crocuta crocuta*	11.1	2005, B-2, N 382	47900	3100	0.00257	0.00099	-17.71	10.09	3.33	AF	840	97.60 (11.6)	42.7
	30005	35671	tooth (pendant)	*Cervus* sp.	11.2	2006, Г-2, N 385	35400	900	0.01213	0.00137	-18.96	8.91	3.46	AG	290	3.03 (1.0)	38.6
	33086	37599	charcoal	not id-ed	11.2	2014, A-2, N 195	40400	900	0.00655	0.00073	-23.20	0.00	n/a	ZR	52.7	2.73 (5.2)	60.8
	31506						41300	900	0.00586	0.00063	-21.98	0.00	n/a	XR	104	5.74 (5.5)	60.5
	30963	37598	tooth (pendant)	*Alces alces*	11.2	2014, A-2, N 11	41300	2400	0.00582	0.0017	-19.57	6.59	3.11	AG	225	2.22 (1.0)	37.6
	36301	43832	bone	not id-ed	11.2	2013, D, K-2,4	>49000		0.00020	0.00103	-20.5	5.1	3.20	AF	720	6.2 (0.8)	42.9
	29857	35675	bone	*Bison/Bos* sp.	11.2	2008, Δ-3, N 381	>50100		0.0000	0.00098	-19.38	4.66	3.30	AF	970	55.40 (5.7)	42.1
	29858	35676	bone	*Capra sibirica*	11.2	2008, Δ-2	>48600		0.00037	0.00099	-19.20	5.28	3.34	AF	760	32.40 (4.3)	40.2
	29852	35668	bone	*Equus* cf. *hydruntinus*	11.3	2009, Г-3, N 359	>49400		0.00019	0.00097	-20.34	6.72	3.31	AF	700	47.90 (6.8)	42.5
	29853	35669	bone	*Cervus elaphus*	11.4	2009, Г-2, N 615	>47900		0.0006	0.00098	-19.38	6.24	3.31	AF	830	31.70 (3.8)	41.7

	29856	35674	bone	*Bison* sp.	11.4	2011, Г-4, N 23	>49900		0.00002	0.00099	-18.90	12.78	3.34	AF	890	27.30 (3.1)	39.6
	29854	35670	bone	E*quus* cf. *hydruntinus*	11.4	2009, Г-3, N 381	>50000		0.0000	0.00099	-20.09	11.20	3.33	AF	990	37.70 (3.8)	41.8
	36012	43831	human bone	*Neanderthal*	11.4	DC 3573 *Denisova 15*	>50200		0.0000	0.00097	-18.6	12.67	3.17	AF	450	40.84 (9.1)	43.9
	29860	35679	bone	*Capra sibirica*	11.4	2009, Г-2, N 606	>50000		0.0000	0.00098	-19.00	6.05	3.37	AF	1020	45.90 (4.5)	41.3
	32241	39272	human bone	Neanderthal/ Denisovan hybrid	12	2014, A-2, DC 1227, *Denisova 11*	>49900		0.0000	0.001	-17.37	16.35	3.32	AF	290	13.20 (4.6)	43.1
Main Chamber																	
Excavation 1997	29861	35682	bone	*Ovis/Capra*	11A	1997, B-6, N 3846/77	37500	1000	0.00934	0.00117	-18.78	6.37	3.34	AG	240	6.65 (2.8)	41.7
	29872	35681	bone (point)	*Bison* sp.	11Г	1997, A-8, N 3846/66	42900	2000	0.00479	0.00116	-19.90	3.61	3.36	AG	250	24.80 (9.9)	41.3
	30271						41200	1400	0.00593	0.00103	-20.33	3.45	3.34	AF	19	n/a (11.8)	42.7
Excavation 2016	X-2696-20	41575	charcoal	*Salix/Populus*	9.2	2016, E-3	7255	35	0.40529	0.00176	-25.76	0.00	0.00	YR	91	7.16 (7.9)	73.3
	34713						7209	35	0.40763	0.00176	-25.46	0.00	0.00	XR	123	7.43 (6.1)	76.9
	34729	41859	tooth (pendant)	*Alces alces*	n/a	Section cleaning	28390	330	0.02918	0.00119	-18.94	7.36	3.16	AG	360	7.02 (2.0)	38.6
	X-2696-40	41843	charcoal	*Salix/Populus*	11.2	2016, SH-7/cut 12, N 9	33900	380	0.01469	0.00069	-24.70	0.00	n/a	YR	95	3.50 (3.7)	49.1
	34919	41858	bone	*Capra* sp.	11.2	2016, SH-7/cut 12, N 28	34600	600	0.01348	0.001	-18.39	5.47	3.18	AF	710	35.57 (5.0)	43.8
	X-2695-22	41842	charcoal	Pinaceae	11.2	2016, SH-7/cut 12, N 10	34400	450	0.01384	0.00079	-22.41	0.00	n/a	YR	71	11.3 (7.98)	47.8
	X-2696-37	41833	charcoal	Pinaceae	11.2-11.3	2016	35820	370	0.01157	0.00054	-23.38	0.00	n/a	YR	101	7.66 (7.5)	72.9

	34718	41839	charcoal	*Abies/ Juniperus*	11.3	2016, SH-1/cut 22	33790	330	0.01491	0.00061	-22.84	0.00	n/a	XR	87	10.22 (11.8)	71.1
	34719	41841	charcoal	Pinaceae	11.3	2016, SH-7, cut 14, N 13	35210	360	0.01248	0.00056	-22.30	0.00	n/a	XR	74	8.08 (10.9)	72.5
	X-2695-23	41845	charcoal	Coniferous	11.3	2016, SH-7/cut 13, N 12	36300	900	0.01094	0.00126	-21.46	0.00	n/a	YR	62	1.52 (2.5)	56.3
	X-2696-34	41823	charcoal	*Abies/ Juniperus*	11.4	n/a	33380	260	0.01568	0.00052	-22.76	0.00	n/a	YR	100	8.15 (8.2)	75.1
	34717						33720	300	0.01502	0.00055	-22.87	0.00	n/a	XR	136	7.86 (5.8)	76.7
	34918						33190	320	0.01605	0.00065	-23.02	0.00	n/a	ZR	22	7.16 (33.1)	57.2
	X-2695-24	41846	charcoal	*Abies/ Juniperus*	11.4	2016, SH-7/ cut 21, N 15	33600	550	0.01529	0.00101	-22.35	0.00	n/a	YR	84	6.53 (7.7)	41.1
	34720						34050	290	0.01443	0.00052	-23.21	0.00	n/a	XR	100	7.89 (7.9)	71.9
	34980						33600	550	0.01523	0.00109	-24.42	0.00	n/a	ZR	25	4.16 (16.8)	32.7
	34721	41849	charcoal	Pinaceae	11.4	2016, M-7/ cut 13, N 52, hearth	32530	260	0.01743	0.00057	-23.27	0.00	n/a	XR	112	9.03 (8.1)	71.7
	34722	41850	charcoal	Coniferous	11.4	2016, M-8/ cut 21, N 21	34990	340	0.01284	0.00054	-24.60	0.00	n/a	XR	89	3.51 (3.9)	70.0
	34725	41853	bone	*Ovis/Capra*	11.4	2016, M-7/cut 19, N 70	32150	450	0.01824	0.00099	-18.85	5.40	3.15	AF	700	28.21 (4.0)	44.7
	X-2706-55						31730	330	0.01926	0.00083	-23.6	6.7	4.8	HYP	1650	169.0 (10.2)	40.3
	34727	41856	bone	*Ovis/Capra*	11.4	2016, SH7/ cut 23, N 88	34750	600	0.01318	0.00099	-18.25	5.95	3.13	AF	720	27.23 (3.8)	44.0
	X-2706-56						33810	360	0.01486	0.00071	-22.7	7.2	5.0	HYP	1510	129.0 (8.5)	44.5

	34723	41851	bone	*Ovis/Capra*	11.4.1	2016, M-8/ cut 15, N 2143	33850	550	0.01477	0.001	-18.23	5.83	3.12	AF	690	31.73 (4.6)	43.9
	X-2706-54						33230	350	0.01598	0.00074	-22.0	7.1	4.7	HYP	1680	175 (10.4)	41.0
	34877	41860	bone (point)	*Equus* sp.	11.4.2	2016, M-8 (B)/ cut 14, N 128	39300	1200	0.00752	0.00115	-20.85	6.09	3.17	AG	300	10.72 (3.6)	40.8
	34728	41857	bone	*Bison/Bos* sp.	11.4	2016, SH-7/cut 20, N64	>50400		0.0000	0.00094	-20.16	7.02	3.12	AF	750	38.46 (5.1)	45.3
	34724	41852	bone	*Bison/Bos* sp.	11.4	2016, M-7/cut 21, N 70	>50300		0.00001	0.00095	-18.81	5.70	3.13	AF	730	25.06 (3.4)	45.0
	34726	41854	bone	*Bison/Bos* sp.	12.1	2016, SH-7/ cuts 24-25	>50300		0.0000	0.00095	-19.75	6.01	3.12	AF	630	71.16 (11.3)	44.0
	X-2696-35	41827	charcoal	Deciduous	12.1	n/a	>51600		0.00061	0.00051	-26.36	0.00	n/a	YR	63	9.12 (14.4)	65.3
	X-2696-36	41828	charcoal	Coniferous	12.3-12.4	interface of layers	>55600		0.00011	0.00043	-24.99	0.00	n/a	YR	93	10.24 (11)	74.1

Table S3. Samples that failed to produce enough carbon for radiocarbon dating.

	P no.	Material	Species	Layer	Year Excavated, Square, ID no	P. code	Comments
East Chamber							
Excavations 2007-13	35678	bone	Ungulate	9.3	2008, b-2	AF	Failed due to no collagen yield
	34815	charcoal	n/a	11.1	2013, K-4	XR	Failed due to no yield
	34814	bone	Large mammal	11.2	2013, D-4, N 87	AG	Failed due to low collagen yield
	41824	bone	Large mammal	11.2	2013, D-3, N 149	AG	Failed due to low collagen yield
	35667	bone	*Cervus elaphus*	11.2	2009, b-2, N 284	AF	Failed due to no collagen yield
	37206	tooth (pendant)	*Cervus* sp.	11.2	2007, N 282	AF	Failed due to no collagen yield
Main Chamber							
Excavation 2016	41824	charcoal	Pinaceae	11.3	2016	YR	Failed due to no yield
	41825	charcoal	Pinaceae	11.4	2016	YR	Failed due to no yield
	41826	charcoal	Coniferous	11.4	2016	YR	Failed due to no yield
	41829	charcoal	n/a	12.2	2016	n/a	Withdrawn, low starting mass
	41830	charcoal	n/a	11.3	2016	n/a	Withdrawn, low starting mass
	41831	charcoal	n/a	11.2	2016	YR	Failed due to low yield
	41832	charcoal	n/a	11.3	2016	YR	Failed due to no yield
	41834	charcoal	n/a	9.3	2016	YR	Failed due to no yield
	41835	charcoal	n/a	11.3	2016	YR	Failed due to no yield
	41836	charcoal	n/a	11.2	2016	YR	Failed due to no yield
	41837	charcoal	n/a	9.3	2016	YR	Failed due to low yield
	41838	charcoal	n/a	9.3	2016	YR	Failed due to low yield
	41840	charcoal	*Pinus* sp.	12.3	2016, Square 8/cut 30	YR	Failed due to low yield
	41844	charcoal	Deciduous	11.2	2016, Square 7/ cut 12	YR	Failed due to low yield
	41847	charcoal	cf. *Pinus* sp.	11.4	2016, Square 7/ cut 23, N 17	XR	Failed due to no yield
	41848	charcoal	n/a	11.4	2016, Square M-7/ cut 13, N 51, hearth	YR	Failed due to no yield
	41855	bone	n/a	11.2	2016, SH-7/ cut 8	AG	Failed due to no collagen yield

Table S4. Calibrated age ranges BP (68.2% and 95.4% probabilities) for the finite radiocarbon dates we obtained from Denisova Cave. Age ranges are rounded to the nearest 10 years. Samples in grey indicate samples with more than one radiocarbon date.

	Layer	from	to	from	to
East Chamber		**68.2%**		**95.4%**	
OxA-29859	9.2	>50000	47400	>50000	45720
OxA-36011	9.3	>50000	47680	>50000	45970
OxA-30006	11.1	32020	31230	32660	31100
OxA-29855	11.1	>50000	48630	>50000	49780
OxA-30005	11.2	41000	39120	41900	38400
OxA-33086	11.2	44760	43230	45670	42690
OxA-31506		45560	44000	46450	43260
OxA-30963	11.2	47200	43040	49710	42450
Main Chamber					
OxA-29861	11A =11.1?	42720	41150	43680	40180
OxA-29872	11Г = 11.4?	48300	44770	>50000	44000
OxA-30271		45980	43410	48100	42660
X-2696-20	9.2	8155	8015	8167	8001
34713		8037	7970	8156	7956
OxA-34729	n/a	32800	31800	33280	31480
OxA-X-2696-40	11.2	38850	37870	39290	37100
OxA-34919	11.2	39800	38520	40670	37800
OxA-X-2695-22	11.2	39440	38450	40070	37860
OxA-X-2696-37	11.2/11.3	40900	40040	41310	39650
OxA-34718	11.3	38670	37790	38970	37070
OxA-34719	11.3	40220	39340	40660	38910
OxA-X-2695-23	11.3	41730	40030	42430	39080
OxA-X-2696-34	11.4	38240	37260	38460	36780
OxA-34717		38590	37780	38830	37100
OxA-34918		37960	36840	38370	36480
OxA-X-2695-24	11.4	38580	37130	39150	36440
OxA-34720		38890	38270	39290	37760
OxA-34980		38640	37090	39320	36410
OxA-34721	11.4	36770	36120	37380	35830
OxA-34722	11.4	39920	39100	40310	38740
OxA-34725	11.4	36550	35550	37410	35080
OxA-X-2706-55		36010	35250	36330	34900
OxA-34727	11.4	39960	38670	40880	38160
OxA-X-2706-56		38750	37720	39140	36950
OxA-34723	11.4.1	38980	37490	39600	36710
OxA-X-2706-54		38060	36870	38450	36440

OxA-34877	11.4.2	44260	42290	45700	41590

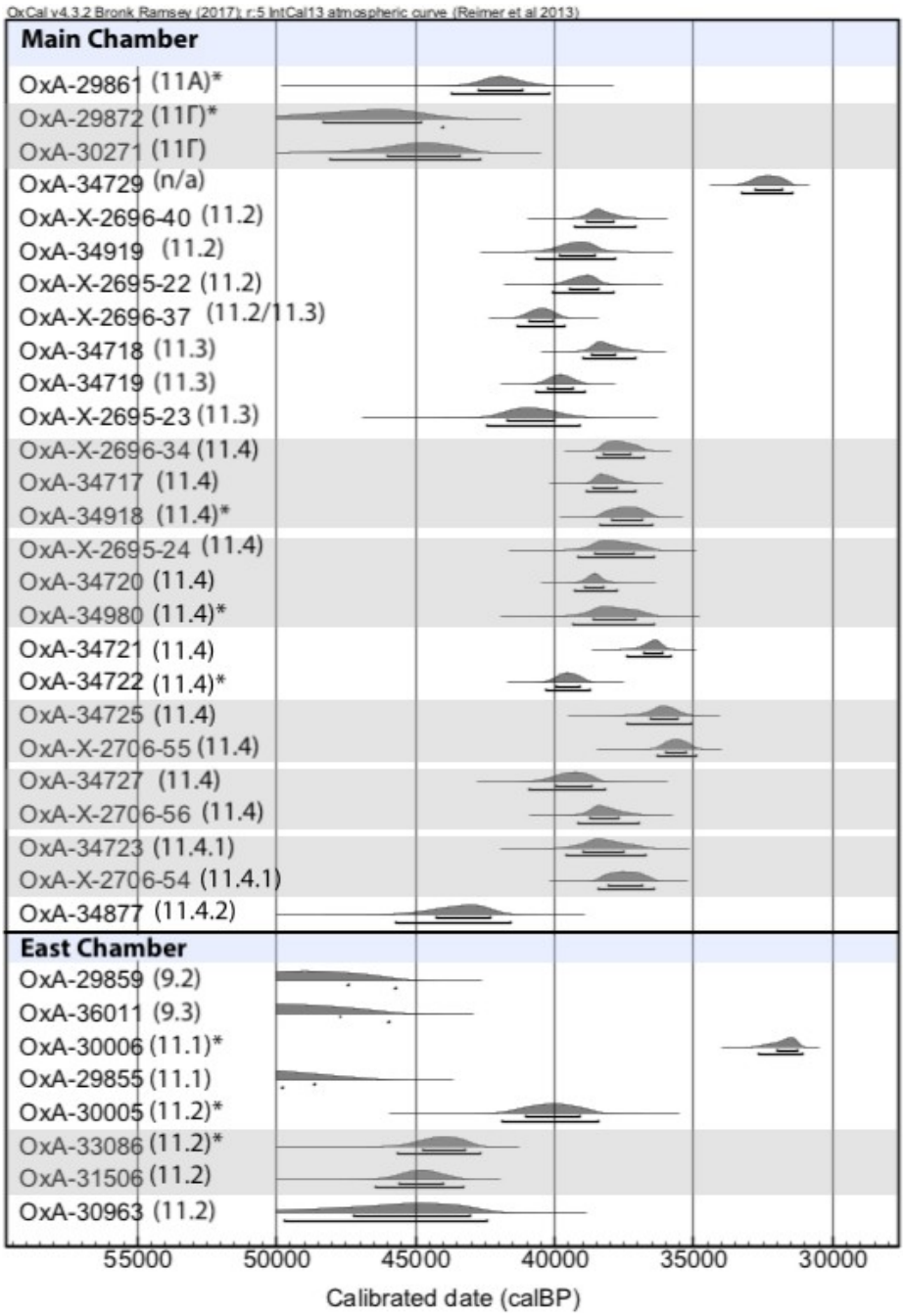

Figure S10. Calibrated dates from Denisova Cave using OxCal 4.3 and the IntCal13 calibration curve. Only the radiocarbon dates falling in the working limit of the method, i.e. <50,0000 BP, are included. The two Holocene dates from layer 9.2 in Main Chamber are not shown here. In grey are dates made on the same sample using different pretreatment protocols. The least reliable protocol (AG, gelatinization but no ultrafiltration for bone collagen; ZR, ABA for charcoals) is marked with an asterisk. In brackets are the layers for each sample. Numerical, raw and calibrated, data can be found in Table S2 and S4, respectively.

3. CATALOGUE OF HOMININ (OR PUTATIVE HOMININ) REMAINS FROM DENISOVA CAVE

B. Viola, K. Douka, T. Higham, M. Shunkov, J. Kelso

Denisova 1, incisor (non-human) (Figure S11 a- d)

1984, Main chamber, Sector 4, Sq. D7, Layer 12

Only the crown of this large incisor is preserved, with the root broken away at the level of the apical margin of the enamel on the labial face. Strong wear removed the crown down to the level of a few small grooves on the lingual margin, probably representing the *tuberculum dentale*.

The specimen was first described[20] as an upper left first incisor. Turner[20] described similarities with the Shanidar 2 upper incisors, but thought that the specimen did not show the typical shovelling seen in the Krapina material. In his opinion, the absence of a flat, or double shoveled labial surface supported European affinities. Later, Shpakova and Derevianko[21] and Shpakova[22] also compared the tooth to Shanidar 2, as well as Asian *Homo erectus*.

The similarities to Shanidar 2 described previously are not convincing. Shanidar 2, just like other Neanderthal upper first incisors[23] has a strongly rounded and convex labial surface, and exhibits both mesial and distal marginal ridges. This strongly contrasts with the morphology of *Denisova 1*, which has an extremely flat labial surface, and only a mesial marginal ridge (if interpreted as an upper left I^1).

The triangular outline in occlusal view and the rather abrupt angle between the mesial and labial surfaces is unlike the morphology usually seen in hominins. The enamel is also quite thin, and the L-shaped cross section of the pulp cavity, as evidenced by the secondary dentine, are all traits that raise questions with regards to the identification of this specimen as hominin. A more likely interpretation is that this is a very worn lower incisor of a large bovid, either *Bison priscus* or *Bos mutus*, both of which have been identified from Layer 12.

Denisova 2, left lower dm_2 (Denisovan) (Figure S11 e, f)

1984, Main chamber, Sector 4, Sq. B8, Layer 22.1

This specimen is a worn left lower second deciduous molar. Originally described by Turner[20] as a right lower dm_1, but the large size and the absence of the *tuberculum molare* make the identification as a dm_2 more plausible. The morphology of the specimen has been described in detail by Slon et al.[12] The morphology of the specimen does not allow assessment of its affinities

in detail, but both its mtDNA and nuclear DNA indicate that it belongs to the Denisovan lineage[12]. Female.

Denisova 3, proximal fragment of distal manual phalanx (Denisovan) (Figure S12 a)

2008, East Chamber, Sector 6, Sq. D-2/91, Layer 11.2

This small (7x5 mm) fragment of a distal hand phalanx does not preserve much morphological information. It derives from a subadult individual between about 7 and 13.5 years[9]. Short descriptions for the specimen were published previously. The mitochondrial DNA was published in 2010[24], the nuclear DNA was reported soon after[25]. Female.

Denisova 4, left upper $M^{2/3}$ (Denisovan) (Figure S11 f)

2000, South Chamber, Sq. G-2/29, Layer 11.1

A mostly complete upper molar, missing the distobuccal root and with slight wear. Morphology and mtDNA for this specimen is reported in 2010[9], 54.6 MB of nuclear DNA was analyzed in 2015[26]. The specimen is both morphologically and genetically distinct from Neanderthals, and a Denisovan. Male.

Denisova 5, proximal pedal phalanx (Neanderthal) (Figure S12 b, d)

2010, East Chamber, Sector 6, Sq. B-3, Subsq. G, Layer 11.4, sublevel (подуровень) 6

A relatively well preserved proximal pedal phalanx, with the trochlea missing and slight damage on the dorsal and medial margins of the proximal end. This specimen has been first published in 2011[27], describing the specimen as very robust and broad compared to Neanderthals. A high coverage nuclear and mitochondrial genome was published in 2014[28], both of which indicate that this specimen was a Neanderthal. Also known as the "Altai Neanderthal". Female.

Denisova 6, left lower second deciduous incisor (hominin indet.) (Figure S11 g, h)

2010, East Chamber, Sector 6, Sq. G-3, Subsq. G, Layer 11.4, sublevel (подуровень) 9

This specimen is a worn lower di_2 with about half of the root resorbed. The specimen has not

been sampled for ancient DNA due to its small size, a detailed description is in preparation.

Denisova 7, parietal fragment (non-human) (Figure S12 g, h)

2008, East Chamber, Sector 6, Sq. D-3, Layer 11.3

This specimen was originally identified as a hominin parietal fragment. Several features, such as the shape of the supposedly coronal suture, the curvature in the coronal plane, the lack of meningeal grooves as well as the marked and sharp edged digital impressions make this identification improbable, and a non-human, probably ursid origin of this specimen more likely. Unpublished ancient DNA analyses by E. Rogaev have found only cave bear DNA in this specimen.

Denisova 8, left upper $M^{2/3}$ (Denisovan) (Figure S11 k)

2010, East Chamber, Sector 6, Sq. G-4, Subsq. V/G, Interface between layer 11.4 and 12.

Recovered in several fragments, slightly above *Denisova 5*, this specimen preserves the almost complete crown of an upper second or more likely third molar. It is similar to Denisova 4 in its large size and complex occlusal morphology. Morphological, mtDNA and nuclear DNA data from this Denisovan individual was published in 2015[26]. Male.

Denisova 9, distal hand phalanx (Neanderthal) (Figure S12 f)

2011, East Chamber, Sector 6, Sq. G-3, Subsq. A, Layer 12.3, sublevel (подуровень) 4.

A relatively complete distal manual phalanx, damaged near the base. The specimen has been described[29] and ancient DNA analyses are in progress. Male.

Denisova 10, immature phalanx fragment (non-human) (Figure S12 c)

2011, East Chamber, Sector 6, Sq. G-2, Subsq. B, Layer 12, sublevel (подуровень) 1.

This specimen was originally identified as a hominin immature pedal phalanx. The specimen is rather well preserved, but is missing the yet unfused proximal epiphysis. In lateral view, this specimen shows a straight and horizontal plantar surface, and a concave dorsal surface. This, together with the very

rounded trochlea as well as the strong extensions of the distal articular

surface both medially and laterally on the plantar side are very unlike the toe morphology seen in hominins and fit much better with an identification as a middle pedal phalanx of a sub-adult bear.

Denisova 11, long bone fragment (Neanderthal/Denisovan offspring) (Figure S13 a)

2012, East Chamber, Sector 6, Sq. Д-2, Layer 12.3

This specimen was identified among bulk bone fragment collections using ZooMS (ZooMS ID: DC1227). Mitochondrial[30] and nuclear DNA[34] analyeses have been published, and further results are reported in Section 5. Female.

Denisova 12, molar fragment (non-human) (Figure S11 l)

2015, East Chamber, Sector 6, Sq. М-3, Layer 12, sublevel (подуровень) 9.

Originally identified as a human molar fragment. The thin enamel and the cusp morphology of this specimen make an identification as a lower deciduous molar of a cave bear more likely. Ancient DNA analyses support this conclusion.

Denisova 13, parietal fragment (hominin indet.)

2016, South Chamber, section cleaning, Layer 22?.

Two adjoining fragments of the posterior half of a hominin parietal. They were found during cleaning of the lower part of the stratigraphic section, hence tentatively attributed to Layer 22. Detailed morphological and ancient DNA analyses are in progress.

Denisova 14, long bone fragment (hominin) (Figure S13 b)

2012, East Chamber, Sector 6, Layer 9.3

This specimen was identified among the bulk fragment collection using ZooMS (ZooMS ID: DC3758) and is reported in this paper for the first time. Directly dated by AMS at 46,300 ± 2600 BP. Ancient DNA analyses failed to yield useable DNA (see Section 5 below).

Denisova 15, long bone fragment (Neanderthal) (Figure S13 c).

2012, East Chamber, Sector 6, Layer 11.4

This specimen was identified among the bulk fragment collection using ZooMS (ZooMS ID: DC3573) and is reported in this paper for the first time. Directly dated by AMS at >50,200 BP. MtDNA DNA analyses summarised in Section 5 below indicate this is a Neanderthal.

Denisova 16, bone fragment (hominin) (Figure S13 d).

2016, Central Chamber, Sector 4, Layer 9.1

This specimen was identified among the bulk fragment collection using ZooMS (ZooMS ID: DC4114) and is reported in this paper for the first time. Ancient DNA analyses are currently in progress. Due to small size of the bone radiocarbon dating was not performed.

Figure S11. Dental material from Denisova Cave. a-d: *Denisova 1* in occlusal (a), lingual (b), labial (c) and mesial (d) views. e,f: *Denisova 2* in occlusal (e) and lingual (f) views. g,h: *Denisova 6* in occlusal (g) and lingual (h) views. i,j: *Denisova 4* in mesial (i) and occlusal (j) views. k: *Denisova 8* in occlusal view. l: *Denisova 12* in occlusal view.

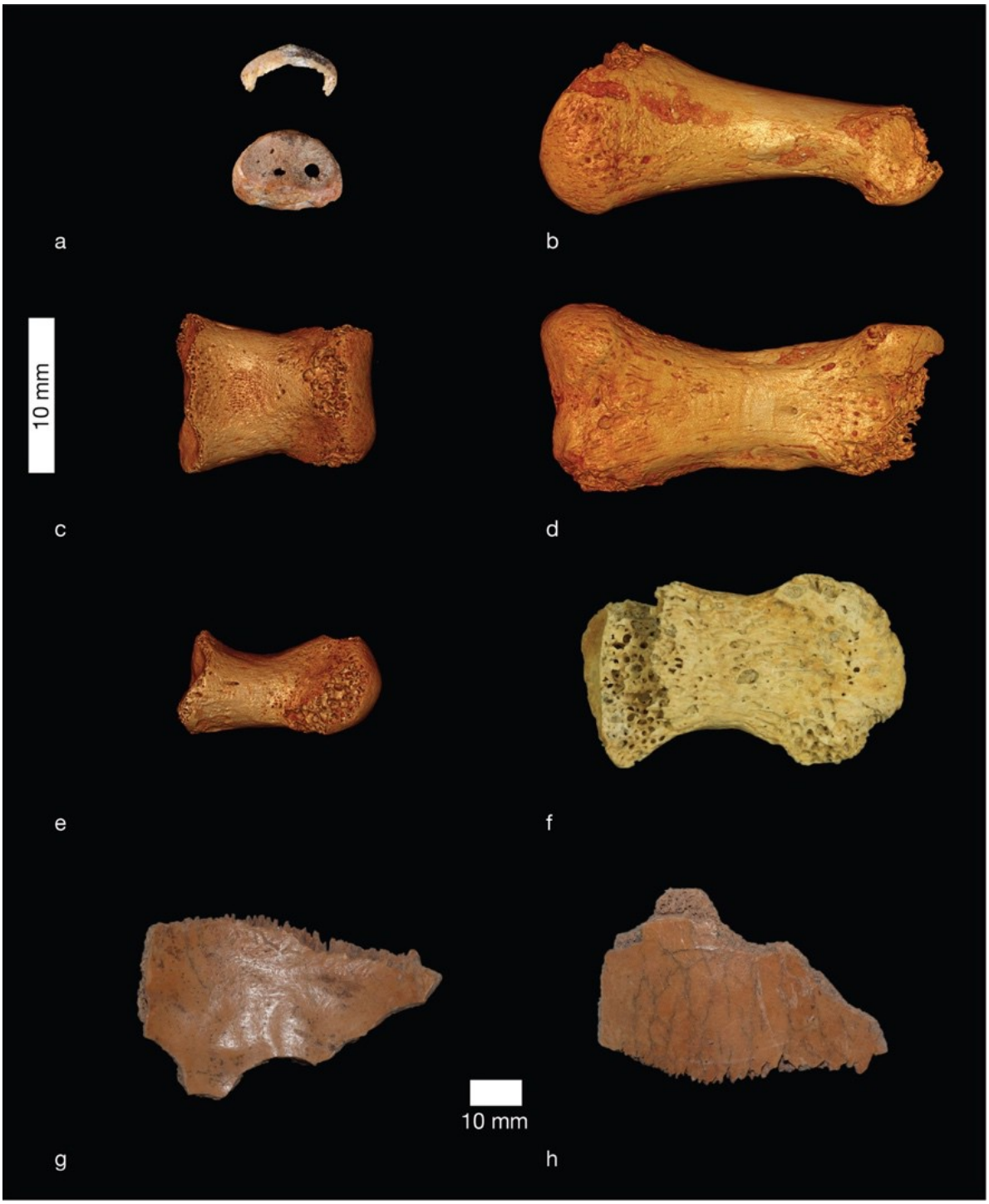

Figure S12. Cranial and postcranial remains from Denisova Cave. a. *Denisova 3* in proximal view. b, d: µCT based renderings of *Denisova 5* in lateral (b) and plantar (d) views. c,e: µCT based renderings of *Denisova 10* in dorsal (c) and lateral (e) views. f: *Denisova 9* in palmar view. g,h: Endocranial (g) and outside (h) views of *Denisova 7*.

Figure S13. Fragments of human remains from Denisova Cave identified using ZooMS. (a) *Denisova 11*[30,34], (b) *Denisova 14*, (c) *Denisova 15*, (d) *Denisova 16*.

4. GENETIC DATA

V. Slon, F. Mafessoni, J. Kelso, M. Meyer, S. Pääbo

A. Age estimates from nuclear DNA

Estimates of ages based on branch shortening have been made for the high-coverage genomes of *Denisova 3* and *Denisova 5* (the "Altai Neanderthal")[25,28,31] (Table S5). We caution that these estimates are sensitive to sequencing error and differ depending on whether all sites or only transversion polymorphisms are used to assess the branch shortening. It is also important to note that the conversion to absolute ages is influenced by whether the divergence from the common ancestor with the chimpanzee is assumed to be 6.5 million or 13 million years ago. In the calculations below we use a divergence of 13 million years, which corresponds to a mutation rate per year of 1.45 x 10-8 mutation per base pair per generation and a generation time of 29 years. This mutation rate is estimated from ancient DNA and from the sequencing of parent-offspring trios[14,32,33]. Although the absolute dates that we obtain using this approach are only approximate due to uncertainties in mutation rates and the generation times, these results indicate that *Denisova 5* is older than *Denisova 3*.

Additionally, the occurrence of admixture between Neanderthals and Denisovans provides an indication about the timing of Denisovan and Neanderthal presence in Denisova cave, and constrains the ages of some of the individuals from Denisova Cave. First, the genome of *Denisova 3* contains segments introgressed from a Neanderthal that is more closely related to *Denisova 5* than to *Vindija 33.19* from Croatia, whose genome has also been sequenced to high-coverage[31]. This admixture must have occurred after *Denisova 5* split from the most recent ancestor shared with *Vindija 33.19* (estimated to have been ~130-145ka) (Table S6), but before *Denisova 3* lived, therefore providing an upper limit on the age of *Denisova 3*. Second, comparisons of the low- coverage genome of *Denisova 11*, the F1-offspring of a Neanderthal mother and a Denisovan father, to the high-coverage Neanderthal and Denisovan genomes allowed us to estimate the times at which the parents of *Denisova 11* split from the lineages leading to *Denisova 3, Denisova 5* and *Vindija 33.19*[34] (Table S6). These provide upper limits on the age of *Denisova 11.* We estimate that *Denisova 11* separated from the lineage leading to *Vindija 33.19* ~40,000 *before Vindija 33.19* lived[31]*.* It was previously estimated that the common ancestor of *Vindija 33.19* and *Denisova 5* lived ~80,000 and ~20,000 after the separation from their common ancestor, respectively, thus we infer that *Denisova 11* lived no earlier than ~40,000 after the *Vindija 33.19- Denisova 5* split (*i.e.,* ~90-105ka)[34], at least 20ky after *Denisova 5*, and likely before *Denisova 3*. Note that the conversion of the split time to absolute ages is sensitive to all the above-mentioned caveats affecting the branch shortening estimates.

Table S5. Branch shortening and estimated ages of *Denisova 3* and *Denisova 5.* Data taken from Refs 28,31.

Specimen	Branch shortening	Estimated age (i)	Estimated age (ii)	Estimated age (iii)
Denisova 3	0.82% (0.74%-0.93%)	48-60 ka	76.6-92.4 ka	60-84 ka
Denisova 5	1.03% (0.96%-1.14)	62-74 ka	116.6-129.4 ka	110-134.8 ka

(i) Calculated on all sites and assuming a divergence time to the common ancestor of humans and chimpanzee of 6.5 million years; (ii) Calculated on all sites and assuming a human-chimpanzee divergence of 13 million years; (iii) Calculated using transversion polymorphisms only and assuming a divergence time to the common ancestor of humans and chimpanzee of 13 million years.

Table S6. Estimates of split times between Neanderthal and Denisovan lineages. Data taken from Refs [31,34].

Lineage 1	Lineage 2	Estimated split time (i)	Estimated split time (ii)
Denisova 5	*Vindija 33.19*	-	130-145 ka
Denisova 11 (Neanderthal parent)	*Denisova 5*	143-159 ka	142-158.5 ka
	Vindija 33.19	87-102 ka	82-97 ka
Denisova 11 (Denisovan parent)	*Denisova 3*	89-93 ka	76.5-80.5 ka

The conversion of split times into absolute dates takes into account the branch shortening estimates for the high-coverage genome, calculated (i) on all sites and assuming a human-chimpanzee divergence of 13 million years; or (ii) using transversion polymorphisms only and assuming a divergence time to the common ancestor of humans and chimpanzee of 13 million years.

B. Age estimates from mitochondrial DNA

(i) Estimating branch shortening by maximum parsimony

From a multiple sequence alignment of the mitochondrial genome sequences of the four Denisovans and the Middle Pleistocene *Sima de los Huesos* individual, we had previously inferred the number of substitutions on each branch since the split from the most recent common ancestor of all Denisovans using maximum parsimony (Figure S14A). We caution that back mutations and multiple substitutions occurring at the same position will not be accounted for, and may affect our inference of the number of substitutions occurring on the various branches. Nonetheless, this analysis suggested that *Denisova 2* is likely the oldest of the four Denisovans, followed by *Denisova 8* and then by the younger and possibly contemporaneous *Denisova 3* and *Denisova 4*[12]. **Error! Bookmark not defined.**

Similarly, we here inferred the number of substitutions on the branches relating the Neanderthal- like mtDNAs of *Denisova 5*, *Denisova 11* and *Denisova 15* with the mtDNA genomes of 19 other Neanderthals from other archaeological sites, using the divergent mtDNA of the *Hohlenstein- Stadel* Neanderthal as outgroup. We infer that since the split from the most recent ancestor shared with *Hohlenstein-Stadel*, a total of 15 and 14 substitutions occurred on the branches leading to *Denisova 5* and *Denisova 15*, respectively, suggesting that these two individuals were roughly contemporaneous; while 19 substitutions occurred on the branch leading to *Denisova 11*, suggesting that the latter individual is younger than *Denisova 5* and *Denisova 15* (Figure S14B).

We converted the differences in the number of inferred substitutions into differences in time by applying the mitochondrial mutation rate inferred for modern humans of 2.53×10^{-8} (95% HPD: $1.76\text{-}3.23 \times 10^{-8}$)[14] (Table S7). Note that this assumes that the mitochondrial mutation rate in archaic humans is the same as that in modern humans.

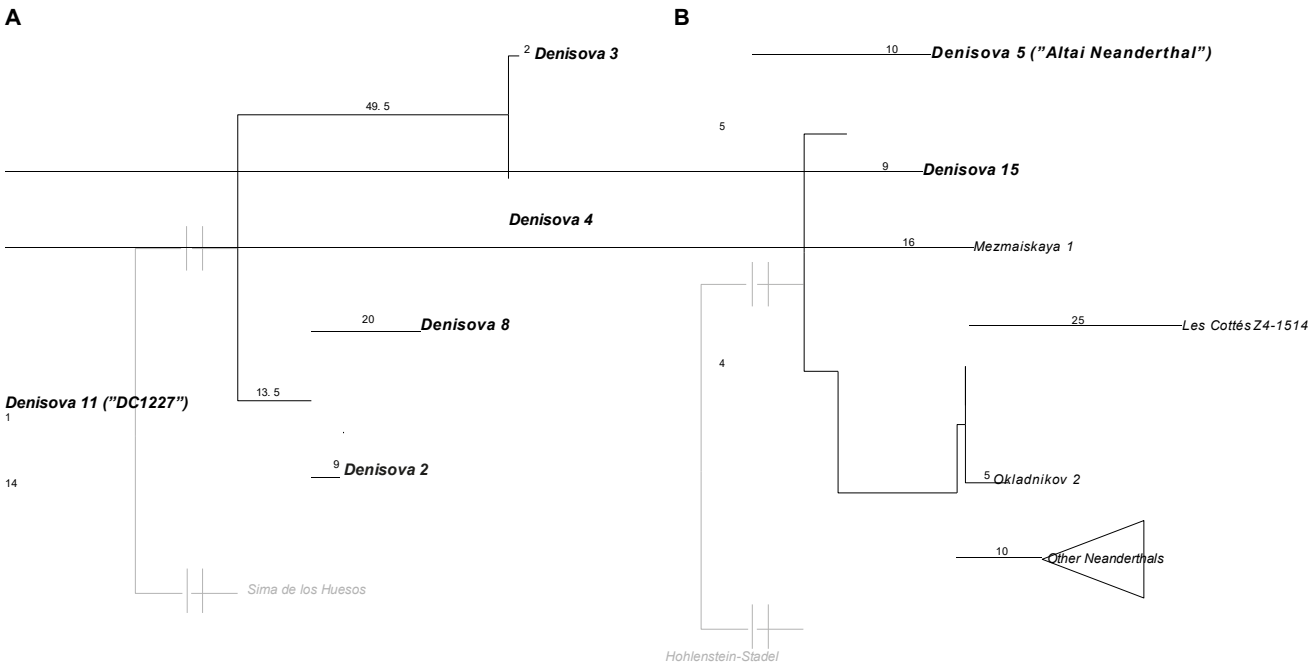

Figure S14. Inferred number of substitutions occurring on branches leading to the mtDNA genomes of individuals from Denisova Cave since their split from the common ancestor shared with other archaic individuals. Individuals from Denisova Cave are emphasized in bold. (A). Denisovan mtDNA genomes; data is taken from Ref. 12. (B) Neanderthal mtDNA genomes. The mtDNA genomes used in this analysis are reported in Table S10.

Table S7. Inferred number of substitutions on the branches leading to each Denisovan or Neanderthal mitochondrial DNA genome and the inferred relative age of each of the individuals.

mtDNA type	**Specimen**	**Substitutions since common ancestor**	**Inferred relative age** (Mutation rate: 2.53×10^{-8} (95% HPD: 1.76-3.23×10^{-8}))
Denisovan mtDNA	*Denisova 2*	22.5	54.2-99.4 ky older than *Denisova 3* 50.5-92.6 ky older than *Denisova 4* 20.6-37.7 ky older than *Denisova 8*
	Denisova 3	51.5	3.7-6.9 ky younger than *Denisova 4* 33.6-61.7 ky younger than *Denisova 8*
	Denisova 4	49.5	29.9-54.9 ky younger than *Denisova 8*
	Denisova 8	33.5	
Neanderthal	*Denisova 5*	15	7.5-13.7 ky older than *Denisova 11* 1.9-3.4 ky younger than *Denisova 15*
	Denisova 11	19	9.3-17.1 ky younger than *Denisova 15*

mtDNA	*Denisova 15*	14	

(ii) Estimating tip dates in a Bayesian framework

To estimate the tip dates of the Neanderthal mtDNA genomes of individuals from Denisova Cave (*Denisova 5*, *11* and *15*), we used the mtDNA sequences of 11 Neanderthals and 7 ancient modern humans, whose remains have been directly radiocarbon-dated, as calibration points for the rate of the molecular clock in a Bayesian phylogenetic analysis. The inferred ages of the three Neandertal mtDNA genomes are shown in Table S8. Note that this analysis is sensitive to the mutation rate inferred from the analysis (1.45×10^{-8}; 95% HPD: $1.05\text{-}1.88 \times 10^{-8}$). Although the point estimates suggest that *Denisova 5* and *Denisova 15* are nearly contemporaneous and both older than *Denisova 11* (in concordance with the previous analysis), we note that the HPD intervals of all three dates overlap. Note that the lack of directly-dated Denisovan remains that could be used as calibration points hinders attempts to perform a similar analysis to estimate the tip dates of Denisovan mtDNA genomes.

Table S8. Estimated tip dates for the coding region of the mtDNA genomes of three individuals from Denisova Cave.

mtDNA type	**Specimen**	**Inferred age** (mean [95% HPD])
Neanderthal mtDNA	*Denisova 5*	149.3 ka [91.3-214.8 ka]
	Denisova 11	107.8 ka [75.4-144.8 ka)
	Denisova 15	144.1 ka [87.2-209.4 ka]

5. SEQUENCING DATA FROM *DENISOVA 11*, *DENISOVA 14* AND *DENISOVA 15*

V. Slon, F. Mafessoni, J. Kelso, M. Meyer, S. Pääbo

Sample preparation: Following the abrasion of surface material, 19.4 mg and 17.7 mg of bone powder were removed from the *Denisova 14* and the *Denisova 15* bone fragments, respectively, using a disposable dentistry drill. The bone powder was treated with 0.5% sodium hypochlorite prior to DNA extraction[35,36]. 20% of each DNA extract (*i.e.*, 10µl) were converted into single- stranded DNA libraries[37] and indexed with two barcodes[38]. The DNA libraries were enriched for human mtDNA fragments using two rounds of an on-beads hybridization capture protocol[39] (with modifications in Ref. 13), using ~1µg and ~0.5µg DNA as input in the first and second round, respectively. Two DNA libraries prepared from the *Denisova 11* specimen previously[34] using similar methods (except using the single-stranded DNA library preparation protocol described in Ref 37) also underwent enrichment for human mtDNA fragments, in a single round of capture. One extraction blank and one library preparation negative control per setup were carried along (Table S9).

Sequencing and data processing: The enriched DNA libraries were pooled with libraries generated as part of other projects and sequenced on a MiSeq platform (Illumina) in 76-cycle paired-end runs[38]. Basecalling was carried out using Bustard (Illumina) and demultiplexing was performed by requiring exact matches to the expected barcode combinations. Overlapping paired-end reads were merged using leeHom[40]. Sequences were mapped to a reference genome using BWA[41] with parameters adapted to ancient DNA[25]. PCR duplicates were collapsed into a single sequence using bam-rmdup (https://github.com/mpieva/biohazard-tools). Only sequences longer than 35 bases and with a mapping quality higher than 25 were retained.

Table S9. Summary of the DNA extracts and DNA libraries used in the current study. Statistics are based on alignment of sequences to the rCRS. Negative controls are marked in gray.

Specimen	Extract	Bone powder (mg)	Indexed DNA library	Library enriched for human mtDNA	Reads sequenced	Unique mtDNA sequences (L≥35, MQ≥25)	C to T substitutions (%)	
							5'-end	3'-end
Denisova 11	E3652	29.0	R5780	R4290	1,222,917	143,553	38.3	40.7
	E3655	33.5	R5783	R4293	1,026,266	130,496	35.6	37.6
Controls	ENC	-	R5791	R4301	139,517	57	0.0	0.0
	LNC	-	R5792	R4302	146,807	13	0.0	0.0
Denisova 14	E4975	19.4	R6272	D8130	112,770	685	37.7	28.3
Denisova 15	E4976	17.7	R6273	D8131	120,182	18,905	46.9	37.2
Controls	ENC	-	R6277	D8135	12,832	60	20.0	0.0
	LNC	-	R6319	D8175	14,189	0	0.0	0.0

ENC: extraction negative control; LNC: library preparation negative control; L: length; MQ: mapping quality; C: cytosine; T: thymine. The extracts and indexed DNA libraries from *Denisova 11* were prepared elsewhere[34].

Assessing the preservation of ancient hominin mtDNA: Sequences were aligned to the revised Cambridge reference sequence (NC_012920.1) in order to evaluate the frequency of cytosine (C) to thymine (T) substitutions to the reference genome at terminal alignment positions, which are due to damage accumulating at the extremities of DNA fragments over time[42]. The elevated frequencies of terminal C to T substitutions in all four libraries are indicative of the presence of ancient DNA fragments in them (Table S9). For *Denisova 11*, this concurs with previous analyses showing that the preservation of ancient mtDNA of the Neanderthal type in this specimen[30].

To investigate the type of mtDNA fragments present in the data generated from *Denisova 14* and *Denisova 15*, we inspected the sequences that mapped to the human mitochondrial genome. We note that, unlike the sequences from *Denisova 15*, the sequences from *Denisova 14* did not map uniformly along the reference genome but rather tended to cluster in small regions (Figure S15), suggesting that some of the DNA fragments sequenced were not derived from human mtDNA[13]. To verify whether DNA from other mammals were present in the DNA libraries, we compared the DNA fragments to an in-house database of reference mammalian mitochondrial genome using MEGAN[43] with the parameters and thresholds described in Ref. 13. Of the 99 sequences from *Denisova 14* that could be identified at the family level, 59 were inferred to originate from hominins, 32 from hyaenids, and 8 from bovids. In comparison, all of the 15,804 identifiable sequences from *Denisova 15* originate from hominin mtDNA.

To further explore the possible presence of several taxa in the data from *Denisova 14,* we enriched the DNA library for mammalian mtDNA fragments[13,44] and compared them to the reference mammalian mtDNA database as above. We find that 2.1% of identifiable sequences (41 out of 1,937) came from hominin mtDNA fragments. Notably, these do not exhibit C to T substitutions to the rCRS to an extent expected from ancient DNA fragments (*i.e.,* at least 10% on both terminal ends[13,45]). In contrast, sequences attributed to other taxa present damage- derived substitutions typical of ancient DNA at their extremities. These include sequences attributed to bovids, hyaenids, equids and cervids, constituting 50.5%, 28.7%, 6.5% and 3.4% of identifiable fragments in the library, respectively. We conclude that no ancient hominin mtDNA is preserved in the *Denisova 14* specimen, and hypothesize that DNA from other taxa present in the environment contaminated the bone fragment.

To determine the type of ancient hominin mtDNA carried by *Denisova 15*, we evaluated the base presented by its sequences at the "diagnostic" positions for hominin mtDNA defined in Ref. **Error! Bookmark not defined.** following the approach in Ref. 46, *i.e.*, where changes are inferred to have specifically occurred in the mtDNA genomes of Neanderthals, of Denisovans, of modern humans, or of the *Sima de los Huesos* hominin. 95.6% of sequences match the Neanderthal-like state, compared to 1.0%, 2.3% and 1.3% matching the Denisovan, modern human and *Sima de los Huesos* states, respectively. We conclude that *Denisova 15* carries an mtDNA genome of the Neanderthal type.

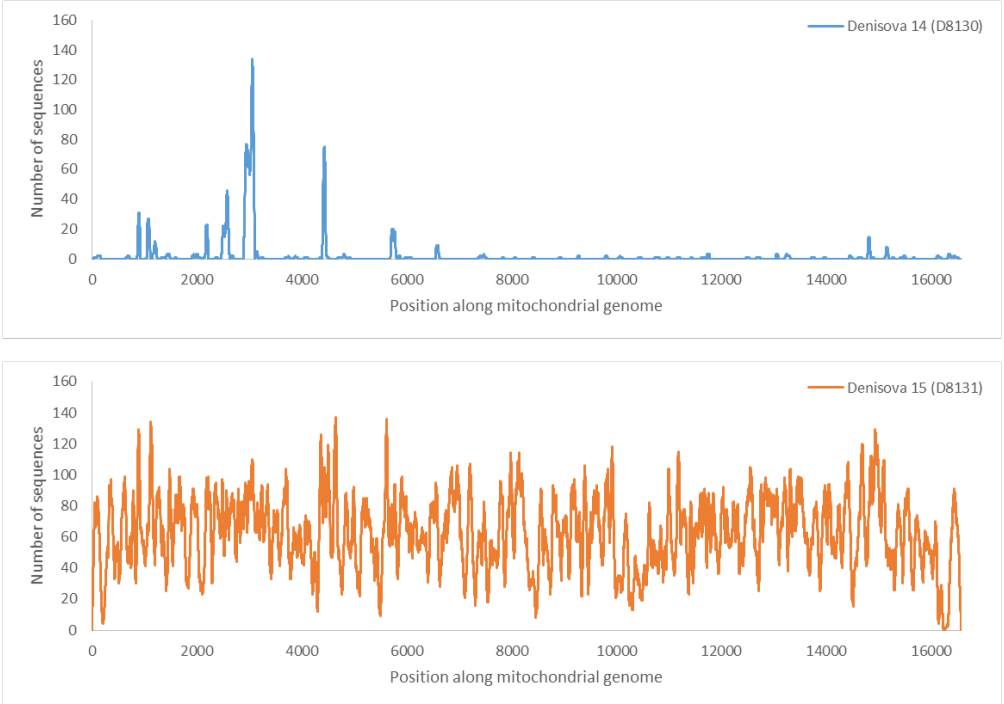

Figure S15. Average coverage of the human mitochondrial reference genome by sequences from *Denisova 14* (top) and *Denisova 15* (bottom). The average coverage of the mitochondrial genome is 2.0-fold for sequences from *Denisova 14* and 62.7-fold for those from *Denisova 15*.

Estimating contamination by present-day human mtDNA: To estimate the extent of contaminating present-day human DNA in the libraries prepared from *Denisova 11* and *Denisova 15*, we calculated the percentage of sequences carrying the base shared by a panel of 311 present-day human mtDNA genomes at 63 positions in the mitochondrial genome where these differ from Neanderthal mtDNAs[47]. To avoid damage-derived substitutions to affect these estimates, DNA strands incorporated in the library on the forward orientation were ignored where one of the two possible states is a C, and reverse strands were ignored at sites where one of the possible states is a G. For *Denisova 11,* we estimate that 0.3% (95% binomial CI: 0.2-0.5%) of the sequences in the two libraries originate from contamination. For *Denisova 15*, we estimate that contaminating present-day human mtDNA sequences constitute 0.4% (95% binomial CI: 0.1- 1.0%) of the data.

Reconstructing the mtDNA genomes of Denisova 11 and *Denisova 15:* Given that the mtDNA genomes of both *Denisova 11* and *Denisova 15* were established to be of the Neanderthal type, and in order to recover sequences that may be difficult to map because of their divergence to the human mtDNA genome, we re-aligned the sequences generated here to the Neanderthal mtDNA reference genome (NC_011137.1). To account for the circularity of the mitochondrial genome, 1000 bases from the start of the reference sequence were copied to its end[46]. Ts on forward strands and As on reverse ones at three terminal positions were converted to Ns to mitigate the effect of DNA damage on the consensus calling.

For *Denisova 11*, the sequences generated from the two DNA libraries were merged[48], yielding a total of 278,379 unique mtDNA sequences and resulting in an average mtDNA genomic coverage of 908.5-fold. The full mtDNA genome sequence of *Denisova 11* was reconstructed by calling bases by a majority vote while requiring each position to be covered by at least 5 sequences, 80% or more of which carry an identical base[46].

Given the lower average mtDNA coverage by sequences from *Denisova 15* (Figure S15), we relaxed the consensus calling criteria and required the presence of only 3 overlapping sequences, of which 67% or more carry the same base, to call a position[46]. We note that of the 55 sequences overlapping position 3829, 54.5% present a G and 45.5% present an A, and that both bases were seen multiple times in both sequence orientation. This suggests that *Denisova 15* had a heteroplasmy[49]. This position was left uncalled (N) in the consensus mtDNA genome sequence. A maximum-likelihood phylogenetic tree, computed in MEGA 6.0[50], relating the reconstructed mtDNA genomes of *Denisova 11* and *Denisova 15* with those of 25 ancient and present-day modern humans, 26 archaic hominins and a chimpanzee (Table S10) confirms that the mtDNA genomes of *Denisova 11* and *Denisova 15* fall within the known variation of Neanderthal-like mtDNA (Figure S16).

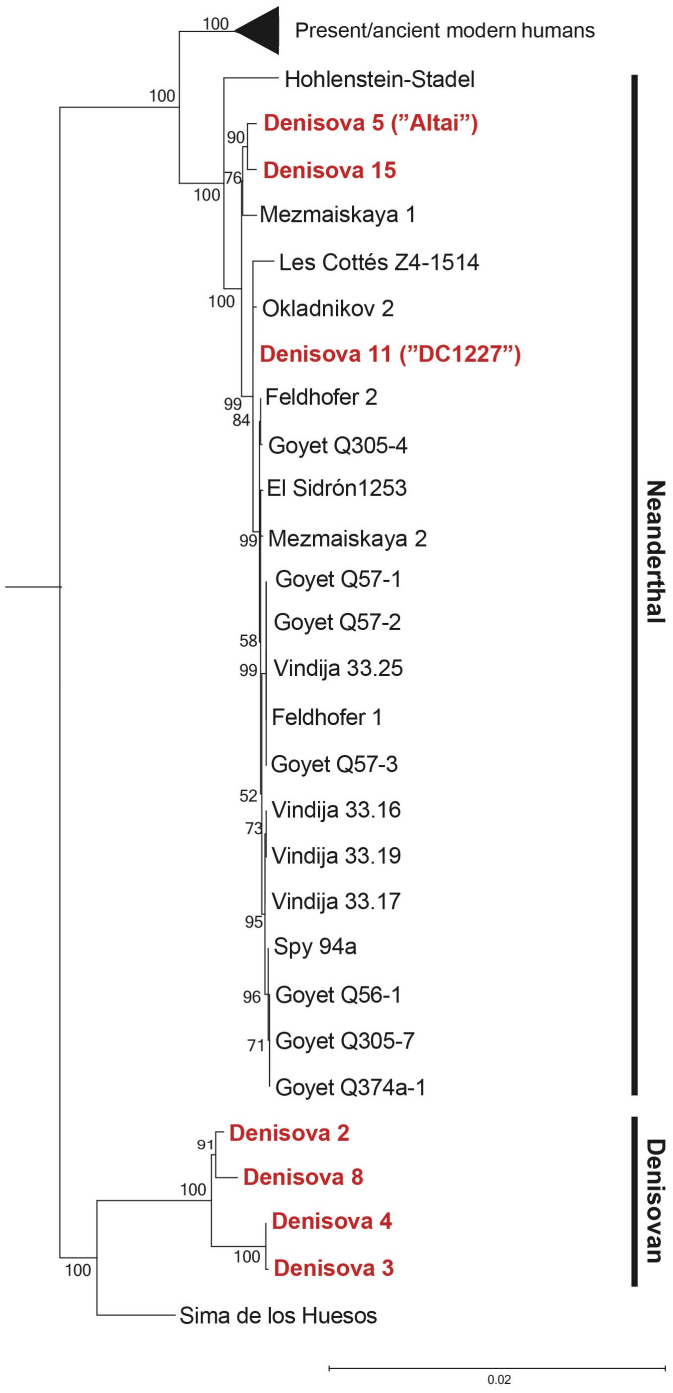

Figure S16. Maximum-likelihood phylogenetic tree relating the mtDNA genomes of individuals from Denisova Cave (in red) to that of other ancient and present-day individuals. The mtDNA types (Neanderthal- or Denisovan-like) are marked on the right. Missing bases and gaps in any of the mtDNA genomes were discarded from the entire dataset, and the mtDNA genome of a chimpanzee was used to root the tree. The Tamura-Nei substitution model with gamma distribution and allowing for invariable sites (TrN+G+I) was used. Branch lengths are scaled based on the number of substitutions per site, and support for each branch is based on 500 bootstrap replications.

Estimating the age of the Neanderthal-like mtDNA genomes from Denisova Cave: To estimate the relative ages of the individuals from Denisova Cave who carried a Neanderthal-like mtDNA, *i.e.*, *Denisova 5* ("*Altai Neanderthal*"), *Denisova 11* and *Denisova 15*, their mtDNA genome sequences were aligned to those of 20 other Neanderthals (Table S10) using MAFFT[51]. The number of base substitutions occurring on each branch leading to these mitochondrial genomes was inferred by parsimony in phangorn[52], with the divergent mtDNA genome of the *Hohlenstein-Stadel* Neanderthal[53] used as outgroup (Figure 14B). The differences in the inferred number of substitutions that occurred on each branch since the split from a common ancestor were converted into relative ages by applying the mitochondrial mutation rate calculated for modern humans of 2.53×10^{-8} (95% HPD: $1.76\text{-}3.23 \times 10^{-8}$)[14] (Table S7).

Additionally, we aimed to estimate the tip dates for these three mtDNA genomes. This was carried out in a Bayesian framework implemented in BEAST v1.8.4[54]. The three Neanderthal-like mtDNA genomes from Denisova Cave were aligned to those of 20 other Neanderthals, 22 ancient and present-day modern humans and one Denisovan to be used as outgroup (Table S10) using MAFFT[51]. Only the coding region of the mtDNA genome (positions 577-16,023 of the rCRS) was retained[55]. The Tamura-Nei substitution model[56] with invariable sites (TrN+I) was determined as the best-suited model using jModelTest v. 2.1.1[57]. The mitochondrial mutation rate of 2.53×10^{-8} was used as an initial prior for the molecular clock, which was allowed to vary between 1.0×10^{-6} and 1.0×10^{-10}. Priors given on the tip dates are shown in Table S10. The four possible combinations of constant population size or Bayesian skyline as tree model, and strict or uncorrelated relaxed lognormal clock, were tested by running 30,000,000 iterations with additional 1,000,000 iterations and sampling every 1,000 steps to compute the log marginal likelihood of each model using stepping-stone sampling. Comparisons were conducted using the difference between the log marginal likelihoods of the two models in each pairwise test (i.e., log10BF=log10(exp(log marginal likelihood for model A - log marginal likelihood for model B))). Using the scale defined in ref 58, the Bayesian skyline model was decisively better supported than the constant population size ($\log_{10}$BF>2.4); and the uncorrelated relaxed lognormal clock strongly supported compared to the strict one ($\log_{10}$BF=1.8). For these parameters, three chains of 75,000,000 iterations were combined after discarding 20% of the iterations as burn-in. The resulting estimated tip dates are shown in Table S8.

Table S10. Dataset of mtDNA genomes used in the genetic analyses. "Accession" refers to the mtDNA genome identifier in the NCBI database; "Date" corresponds to the prior used in the Bayesian analysis (direct radiocarbon-dates of the ancient specimens were calibrated using OxCal 4.3[59] with IntCal13[19], N/A indicates that the mtDNA genome was not used in that analysis); Ref. are references to the publication of the mtDNA genomes and, when relevant, of the radiocarbon date of the ancient individuals.

Individual	Accession	Date	Ref.	Individual	Accession	Date	Ref.
Ancient modern human mtDNA				**Denisovan mtDNA**			
Boshan 11	KC521454	8,234 (8,152-8,316)	[55]	Denisova 2	KX663333	N/A	[12]
Dolní Věstonice 13	KC521459	N/A	[55]	Denisova 3	NC_013993	55,000 (30,000-300,000)	[24]
Dolní Věstonice 14	KC521458	N/A	[55]	Denisova 4	FR695060	N/A	[9]
Iceman	EU810403	5,300 (5,275-5,325)	[60, 61]	Denisova 8	KT780370	N/A	[26]
Kostenki 14	FN600416	37,473 (36,262-38,684)	[62, 63]	**Neanderthal mtDNA**			
Loschbour	KC521455	8,054 (7,948-8,160)	[55, 64]	Denisova 5 ("Altai")	KC879692	55,000 (30,000-300,000)	[28]
Oberkassel 998	KC521457	N/A	[55]	Denisova 11	XXX	55,000 (50,000-300,000)	[30]
Saqqaq Eskimo	EU725621	4,504 (4,423-4,585)	[65, 66]	Denisova 15	XXX	55,000 (30,000-300,000)	This study
Tianyuan	KC417443	39,008 (37,761-40,254)	[39, 67]	El Sidrón 1253	FM865409	55,000 (30,000-300,000)	[68]
Ust'-Ishim	-	45,045 (43,212-46,878)	[14]	Feldhofer 1	FM865407	43,707 (42,670-44,744)	[68, 69]
Present-day modern human mtDNA				Feldhofer 2	FM865408	43,268 (42,193-44,342)	[68, 69]
Australian	AF346964	0 (0-100)	[70]	Goyet Q56-1	KX198082	42,515 (42,063-42,967)	[71]
Chinese	AF346973	0 (0-100)	[70]	Goyet Q57-1	KX198082	44,696 (43,834-45,558)	[71]
Filipino	AY289070	0 (0-100)	[72]	Goyet Q57-2	KX198088	41,185 (40,595-41,775)	[71]
Finland	AY195773	0 (0-100)	[73]	Goyet Q57-3	KX198083	42,407 (41,946-42,867)	[71]
Indian	AF382013	0 (0-100)	[74]	Goyet Q305-4	KX198087	44,236 (43,386-45,085)	[71]
Italian	AY882393	0 (0-100)	[75]	Goyet Q305-7	KX198086	55,000 (30,000-300,000)	[71]
Japan	AF346990	0 (0-100)	[70]	Goyet Q374a-1	KX198085	55,000 (30,000-300,000)	[71]
Mandenka	AF346995	0 (0-100)	[70]	Hohlenstein-Stadel	KY751400	55,000 (30,000-300,000)	[53]
Mbuti	AF346998	0 (0-100)	[70]	Les Cottés Z4-1514	MG025536	43,230 (42,720-43,740)	[76]
Native American	AY195748	0 (0-100)	[73]	Mezmaiskaya 1	FM865411	55,000 (30,000-300,000)	[68]
Pakistan	AY882380	0 (0-100)	[75]	Mezmaiskaya 2	MG025537	43,834 (42,038-45,630)	[76, 77]
Papua (Coast)	AY289082	0 (0-100)	[72]	Okladnikov 2	KF982693	55,000 (30,000-300,000)	[78]
Papua (Highlands)	AY289090	0 (0-100)	[72]	Spy 94a	MG025538	40,463 (39,840-41,085)	[76, 79]
San	AF347008	0 (0-100)	[70]	Vindija 33.16	NC_011137	43,707 (39,234-48,179)	[47, 80]
Spain	AY882392	0 (0-100)	[75]	Vindija 33.17	KJ533544	55,000 (30,000-300,000)	[81]
Chimpanzee mtDNA				Vindija 33.19	KJ533545	55,000 (50,000-300,000)	[31, 81]
-	NC_001643	N/A	[82]	Vindija 33.25	FM865410	55,000 (30,000-300,000)	[68]
Sima de los Huesos mtDNA							
Femur VIII	NC_023100	N/A	[46]				

6 . OPTICAL DATING OF SEDIMENT SAMPLES FROM DENISOVA CAVE

Z. Jacobs, B. Li, R. G. Roberts

Optical dating provides an estimate of the time since grains of luminescent minerals, such as quartz and potassium-rich feldspar (K-feldspar), were last exposed to sunlight[83,84,85,86,87,88]. The burial age is estimated by dividing the equivalent dose (D_e, a measure of the radiation energy absorbed by grains during their period of burial) by the environmental dose rate (the rate of supply of ionising radiation to the grains over the same period). The D_e is determined from laboratory measurements of the optically stimulated luminescence (OSL) from quartz or the infrared stimulated luminescence (IRSL) from K-feldspar, and the dose rate is estimated from field and laboratory measurements of environmental radioactivity, plus the small contribution from cosmic rays.

A large optical dating study has been conducted in all three chambers at Denisova Cave since August 2012, with the aim of obtaining a reliable chronology for all major Pleistocene sedimentary layers that contain artefacts (or are culturally sterile) and hominin fossils, as well as the remains of animals and plants. Finite ages for 103 sediment samples are presented in Jacobs *et al*.[89], together with full technical details associated with the measurement and calculation of the D_e values, environmental dose rates and optical ages. Ref. 89 also provides descriptions of the stratigraphic sequences and discussion of post-depositional integrity.

We note that the optical dating study of Jacobs *et al*.[89] and the present study, and their accompanying Bayesian age models, are complementary. One study does not supersede the other; rather, they serve different purposes. The chronological framework based on the optical ages provides a timeline for sediment deposition and, by association, a timeframe for cultural change and occupation of Denisova Cave by different hominin groups. Optical dating of single grains of quartz or K-feldspar enables issues of sediment mixing to be investigated and, hence, stratigraphic integrity examined. This approach may be sufficient to infer general patterns of change in stone-tool assemblages or environmental conditions through time, but it cannot be reliably extended to isolated teeth or bone fragments that may have been displaced since deposition by carnivore bioturbation, for example. A more robust age model for isolated human remains can be constructed by combining the available proxy evidence, including optical ages for sediment deposition, radiocarbon ages obtained for collagen from some of the human fossils, and relative genetic ages estimated for most of the fossils. This combined approach ameliorates the shortcomings specific to each of the methods.

In this study, we focus on the optical ages for four stratigraphic layers: layers 22.1 and 21 in the Main Chamber, to provide a maximum age constraint for hominin occupation of the site and for *Denisova 2* (which was recovered from layer 22.1); layer 12.3 in the East Chamber, to provide a

maximum age constraint for *Denisova 11* (layer 12.3), *Denisova 8* (interface of layers 12 and 11.4) and *Denisova 15* and *Denisova 5* (both from layer 11.4); and layer 11.2 in the East Chamber, from which *Denisova 3* was obtained. We include 11 optical ages from these layers in the Bayesian age models presented in Supplementary Information, Section 8.

Samples were collected at night (using dim red light for illumination), sealed in plastic bags and wrapped in black plastic to prevent light exposure during transport to the University of Wollongong. These sediment samples were used for OSL and/or IRSL measurements, to estimate the field water contents and to make laboratory measurements of the beta dose rate. Measurements of the *in situ* gamma dose rate were made at each sample location using a portable gamma-ray detector. In the laboratory, sand-sized grains of quartz and/or K-feldspar were extracted from the samples under dim red illumination using standard procedures[85]. Each sample was sieved to isolate quartz grains of 180–212 µm diameter and K-feldspar grains of 90– 212 µm diameter (Table S11), which were treated with solutions of 10% hydrochloric acid and 30% hydrogen peroxide to remove carbonates and organic matter, respectively. K-feldspar, quartz and heavy-mineral grains were separated from each other using solutions of sodium polytungstate and then etched in either 45% (quartz) or 10% (K-feldspar) hydrofluoric acid for 40 min (to clean the grain surfaces and remove, or greatly reduce in volume, the alpha-irradiated rinds), rinsed in hydrochloric acid (to remove any precipitated fluorides) and, finally, dried and sieved again.

Measurements of the beta dose rate were made on dried, homogenised and powdered portions of each sample using a low-level beta counting system[90] and the data-analysis procedures described in ref. 91. We used a 1-inch diameter NaI(Tl) detector and the 'threshold' technique[92] to estimate the gamma dose rates from the U and Th decay series and ^{40}K, with the detector calibrated using the doped concrete blocks at Oxford[93]. Cosmic-ray dose rates were estimated following ref. 94, taking into account the latitude, longitude and altitude of the site, the thickness and density of sediment overburden and bedrock shielding. The beta dose rates were attenuated for grain size, and the beta, gamma and cosmic-ray dose rates were corrected for long-term water content (Table S11). The total dose rates for K-feldspar grains also include an effective internal dose rate due to the decay of ^{40}K and ^{87}Rb inside the grains. We estimated the K content (12.8 ± 0.5%) from electron microprobe wavelength-dispersive X-ray spectroscopy measurements of 60 individual grains, and assumed a Rb concentration of 400 ± 100 µg/g (ref. 95).

We used a combination of quartz and K-feldspar grains to estimate depositional ages for layer 11.2 in the East Chamber and to test the sensitivity of these estimates to a variety of measurement conditions[89]. The ages for samples from layer 12.3 in the East Chamber and layers 21 and 22.1 in the Main Chamber were determined solely using K-feldspar grains, owing to

saturation of the quartz OSL signal. Single-grain analysis allows for grains with aberrant luminescence properties to be identified and rejected before age determination, and to address any issues of incomplete bleaching before deposition or stratigraphic disturbance after deposition[86,87,88,89,96]. A multiple-aliquot post-infrared IRSL (pIRIR) procedure was used to obtain D_e values for samples from layer 22.1 in the Main Chamber, but single-grain pIRIR measurements were also made for one of the samples (DCM16-13) from layer 22.1 to test the internal consistency of the methods. Samples were measured using automated Risø TL-DA-20 instruments equipped with infrared (870 nm) light emitting diodes for stimulation of multi-grain aliquots, and focussed green (532 nm) and infrared lasers (830 nm) for stimulation of individual quartz and K-feldspar grains, which were loaded on to custom-made discs[97]. The ultraviolet OSL and violet/blue IRSL emissions were detected by Electron Tubes Ltd 9235QA photomultiplier tubes fitted with either U-340 (OSL) or Schott BG-39 and Corning 7-59 (K-feldspar) filters, and beta doses were administered using calibrated $^{90}Sr/^{90}Y$ sources.

For single-grain measurements of quartz, we used a standard single-aliquot regenerative-dose procedure[98,99]. To measure the high-temperature pIRIR signals[100,101] from individual K-feldspar grains, we used a two-step, regenerative-dose pIRIR procedure[102] in which an initial infrared bleach at 200°C is followed by infrared stimulation of the dating signal at 275°C. K-feldspar D_e values were estimated using three methods:

1. Samples from layer 11.2 (East Chamber): projection of the sensitivity-corrected natural signal (L_n/T_n) on to the full dose-response curve regenerated for each grain.
2. Samples from layer 12.3 (East Chamber) and layer 21 (Main Chamber) and one of the samples from layer 22.1 (Main Chamber): projection of the weighted mean re-normalised L_n/T_n ratio for all grains used for D_e determination on to the standardised growth curve (SGC) for K-feldspar grains[103]. Full details and comparisons with other methods are provided in ref. 89.
3. Samples from layer 22.1 (Main Chamber): using a multiple-aliquot regenerative-dose (MAR) procedure[104], six aliquots of both samples were stimulated successively at 50, 100, 150, 200 and 275°C, and the re-normalised L_n/T_n ratios were projected on to a multiple-aliquot SGC to estimate the corresponding D_e values[89].

To determine appropriate D_e values for age determination, we examined each of the single-grain D_e or re-normalised L_n/T_n distributions (Fig. S17) for any patterns in the data, and calculated the extent of overdispersion (OD) for each distribution (i.e., the spread in values remaining after making allowance for measurement uncertainties) using the central age model (CAM)[98,105]. Each distribution was optimally fitted by a single component[105,106], so we used the CAM to estimate the weighted mean D_e values, after rejecting statistical outliers based on the normalised median absolute deviation[107,108].

The re-normalised L_n/T_n distributions for both of the multiple-aliquot samples are shown in Fig. S18. These data were obtained at the highest stimulation temperature (275°C). We have demonstrated that the samples suffer from negligible fading at this temperature[89], so their final ages were estimated from these data.

Optical ages and associated information are provided in Table S11; all uncertainties are reported at 1σ.

Ages for layers 22.1 and 21 in the Main Chamber are included in the Bayesian models (Supplementary Information, Section 8) to stratigraphically constrain *Denisova 2*. This Denisovan tooth was found near the top of layer 22.1 in square B8 during the 1984 excavation season (Fig. S4). This layer is easily recognisable in the Main Chamber as an ochre-coloured cave loam of considerable thickness at the base of the stratigraphic sequence (Fig. S5). Ages of 380 ± 26 kyr (DCM16-13) and 312 ± 24 kyr (DCM14-11) were obtained for layer 22.1. Layer 21 is a dark loam impregnated with organic ashes and fine biological detritus and has ages of 255 ± 25 (DCM12- 24), 227 ± 21 (DCM17-1) and 197 ± 15 kyr (DCM14-10). There is a clearly identifiable erosional unconformity between layers 22.1 and 21, with truncation of layer 22 prior to deposition of layer 21 (ref. 89).

Optical ages for layers 12.3 and 11.2 in the East Chamber are included in the Bayesian models (Supplementary Information, Section 8) to chronostratigraphically constrain the human remains recovered from this part of the sequence. Layer 12.3 is well represented throughout the East Chamber as a 50–60 cm-thick grey-brown medium loam. Three optical ages of 128 ± 8 (DCE12- 9), 139 ± 7 (DCE14-8) and 129 ± 7 kyr (DCE16-6) were obtained for this layer (Table S11). These ages are also well constrained by the optical ages for samples collected from layers directly above and below[89].

Layer 11.2 is one of the more complex layers at Denisova Cave, with clear evidence in places of bioturbation. It is a 30–50 cm-thick light loam, dark brown in colour with a reddish tint. The layer contains large amounts of angular limestone debris and has uneven and deformed boundaries due to post-depositional subsidence. Five sediment samples were dated from this layer; the D_e values for each sample were measured using both quartz and K-feldspar grains for comparison, and two grain-size fractions of K-feldspar were also measured separately for one sample (DCE16- 5). The quartz and K-feldspar ages for three of the samples are in good agreement (Table S11) and their D_e distributions show minimal evidence for large-scale mixing (Fig. S17). The combined quartz and K-feldspar ages for these three samples (Table S11) are 60 ± 3 (DCE14-11), 56 ± 3 (DCE14-14) and 61 ± 3 kyr (DCE16-5). The latter estimates are included in the Bayesian models (Supplementary Information, Section 8), as we have greatest confidence in the stratigraphic

integrity of these samples and their ages. The D_e distributions and optical ages of the other two samples from layer 11.2, one of which shows evidence of mixing, are discussed in ref. 89. Post- depositional disturbance of some parts of layer 11.2 is consistent with the previously published radiocarbon chronology for layer 11.2 (ref. 9) and with the new radiocarbon ages reported in this study (Supplementary Information, Section 2); the latter include samples with infinite ages and others with younger ages, which we presume are intrusive samples.

Table S11. Total dose rate, equivalent dose (D_e) and overdispersion (OD) values and optical ages for quartz (Q) and K-feldspar (KF) samples from layers 22.1 and 12 in the Main Chamber and layers 12.3 and 11.2 in the East Chamber. The age uncertainties represent the total (random plus systematic) uncertainties at 1σ. Ages shown in bold are the weighted mean ages with total (unshared plus shared) uncertainties at 1σ for the combined quartz and K-feldspar age estimates.

Sample	Layer	Mineral	Grain size	Water content (%)	Total dose rate (Gy/kyr)	D_e (Gy)	OD (%)	Optical age (kyr)
DCM16-13	22.1	KF	90-150	30 ± 6	2.66 ± 0.12	1011 ± 46	—	380.3 ± 25.5
DCM14-11	22.1	KF	125-212	30 ± 6	2.70 ± 0.14	842.6 ± 42.8	—	312.0 ± 23.5
DCM12-24	21	KF	180-212	50 ± 10	2.75 ± 0.13	698.9 ± 58.6	15.8 ± 1.91	254.6 ± 25.2
DCM17-1	21	KF	180-212	50 ± 10	2.18 ± 0.11	493.7 ± 36.4	13.1 ± 1.6	226.6 ± 20.5
DCM14-10	21	KF	125-212	60 ± 12	1.99 ± 0.13	391.6 ± 10.6	7.8 ± 1.0	196.9 ± 14.6
DCE12-9	12.3	KF	180-212	30 ± 6	2.50 ± 0.10	320.3 ± 12.7	13.3 ± 1.3	128.2 ± 7.6
DCE14-8	12.3	KF	180-212	30 ± 6	2.19 ± 0.19	304.5 ± 8.5	13.0 ± 0.9	139.0 ± 7.3
DCE16-6	12.3	KF	180-212	30 ± 6	2.33 ± 0.10	300.3 ± 9.2	16.5 ± 1.2	129.0 ± 7.1
DCE14-11	11.2	Q	180-212	20 ±	1.10 ± 0.04	65.2 ± 3.4	24.6 ± 4.5	59.5 ± 4.0
		KF			1.91 ± 0.08	113.1 ± 8.3	34.7 ± 5.7	59.1 ± 5.2
							Weighted mean	**59.9 ± 3.4**
DCE14-14	11.2	Q	180-212	20 ± 4	1.04 ± 0.05	62.7 ± 3.9	26.8 ± 5.3	60.3 ± 4.6
		KF	150-180		1.75 ± 0.08	92.7 ± 3.4	25.6 ± 3.1	53.0 ± 3.4
							Weighted mean	**55.7 ± 3.1**
DCE16-5	11.2	Q	180-212		0.99 ± 0.04	61.7 ± 3.6	31.8 ± 4.8	62.3 ± 4.6
		KF	150-180	20 ± 4	1.69 ± 0.07	100.9 ± 4.0	29.3 ± 3.2	59.6 ± 3.7
			125-150		1.55 ± 0.08	91.3 ± 3.9	31.7 ± 3.6	58.9 ± 4.2
							Weighted mean	**61.1 ± 2.9**

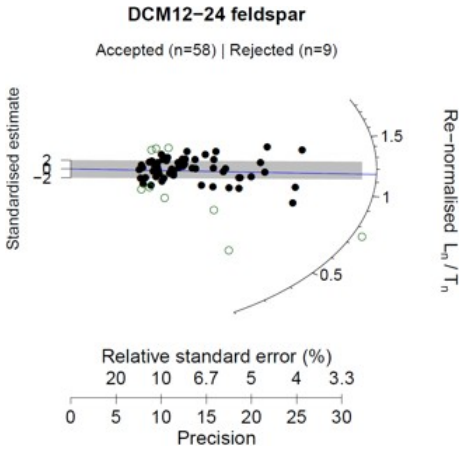
DCM12−24 feldspar
Accepted (n=58) | Rejected (n=9)
Standardised estimate
Re−normalised L_n / T_n
Relative standard error (%)
20 10 6.7 5 4 3.3
0 5 10 15 20 25 30
Precision

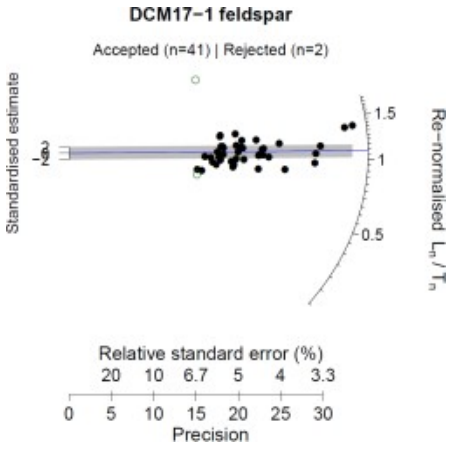
DCM17−1 feldspar
Accepted (n=41) | Rejected (n=2)
Standardised estimate
Re−normalised L_n / T_n
Relative standard error (%)
20 10 6.7 5 4 3.3
0 5 10 15 20 25 30
Precision

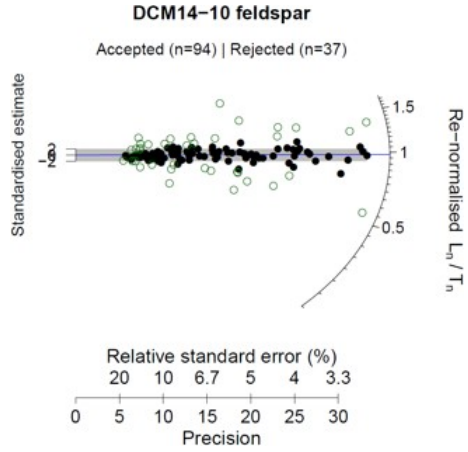
DCM14−10 feldspar
Accepted (n=94) | Rejected (n=37)
Standardised estimate
Re−normalised L_n / T_n
Relative standard error (%)
20 10 6.7 5 4 3.3
0 5 10 15 20 25 30
Precision

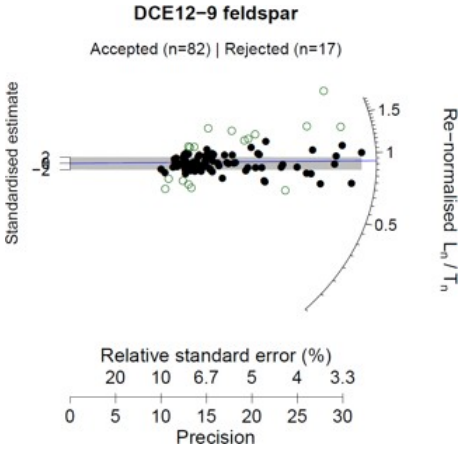
DCE12−9 feldspar
Accepted (n=82) | Rejected (n=17)
Standardised estimate
Re−normalised L_n / T_n
Relative standard error (%)
20 10 6.7 5 4 3.3
0 5 10 15 20 25 30
Precision

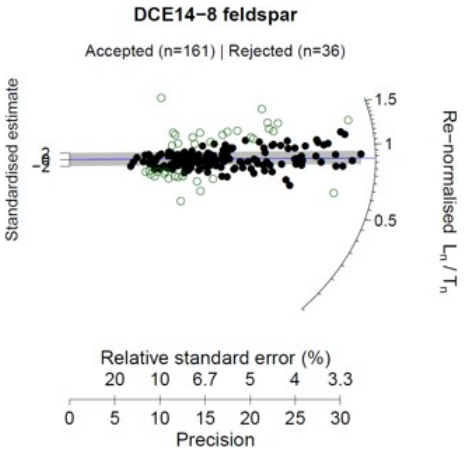
DCE14−8 feldspar
Accepted (n=161) | Rejected (n=36)
Standardised estimate
Re−normalised L_n / T_n
Relative standard error (%)
20 10 6.7 5 4 3.3
0 5 10 15 20 25 30
Precision

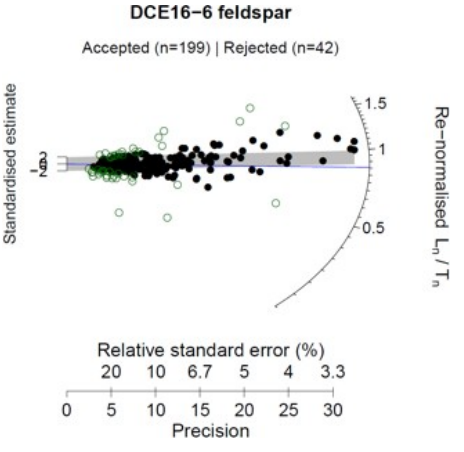
DCE16−6 feldspar
Accepted (n=199) | Rejected (n=42)
Standardised estimate
Re−normalised L_n / T_n
Relative standard error (%)
20 10 6.7 5 4 3.3
0 5 10 15 20 25 30
Precision

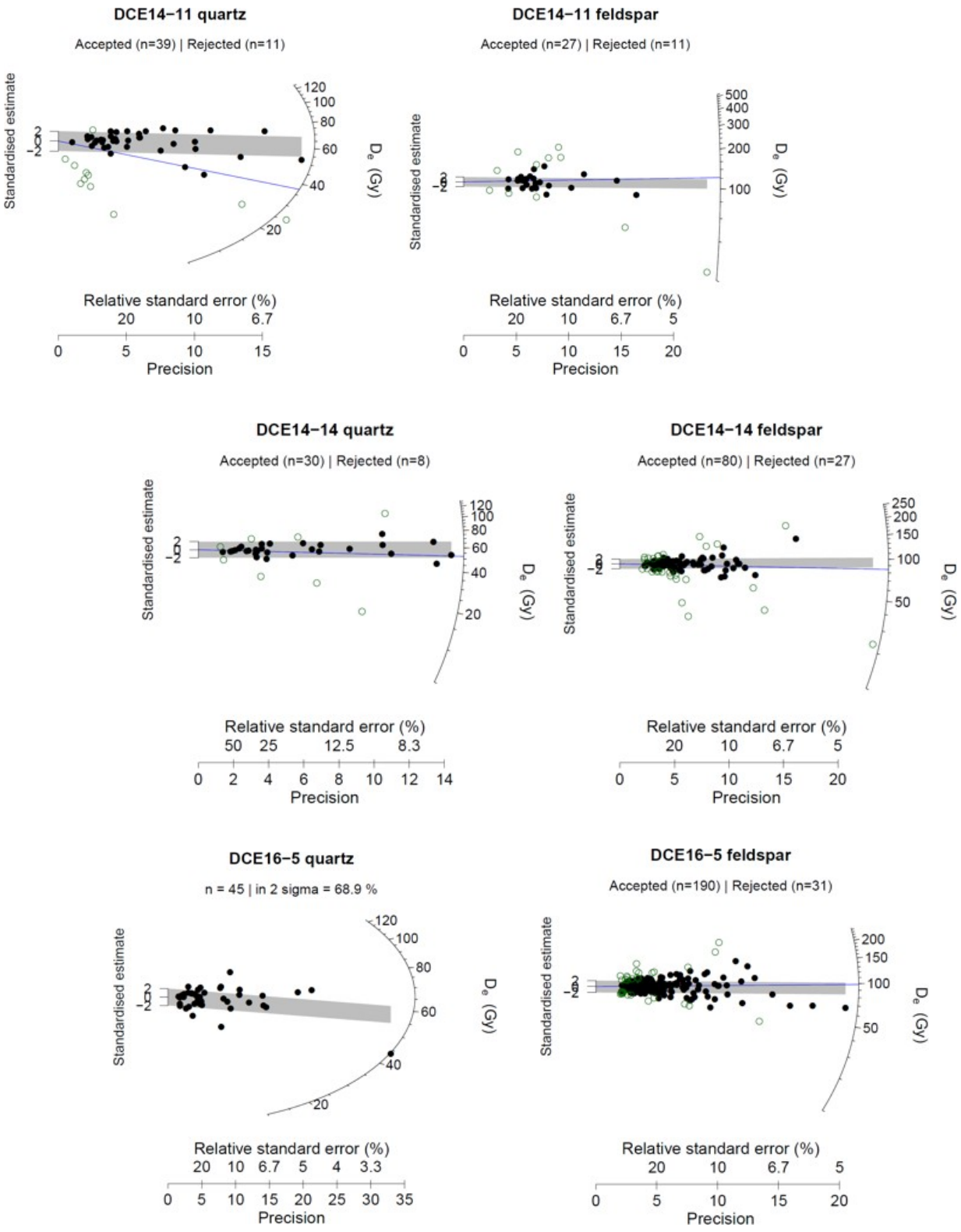

Figure S17. Distributions of D_e values and re-normalised L_n/T_n ratios for individual grains of quartz and K- feldspar from samples collected from layer 21 in the Main Chamber and layers 12.3 and 11.2 in the East Chamber. The grey band in each plot is centred on the weighted mean D_e value or re-normalised L_n/T_n

ratio determined using the CAM, after rejecting outliers (open circles). The blue lines indicate the CAM D_e values or re-normalised L_n/T_n ratios before outlier rejection. N represents the total number of single observations for each sample.

DCM14-11 DCM16-13

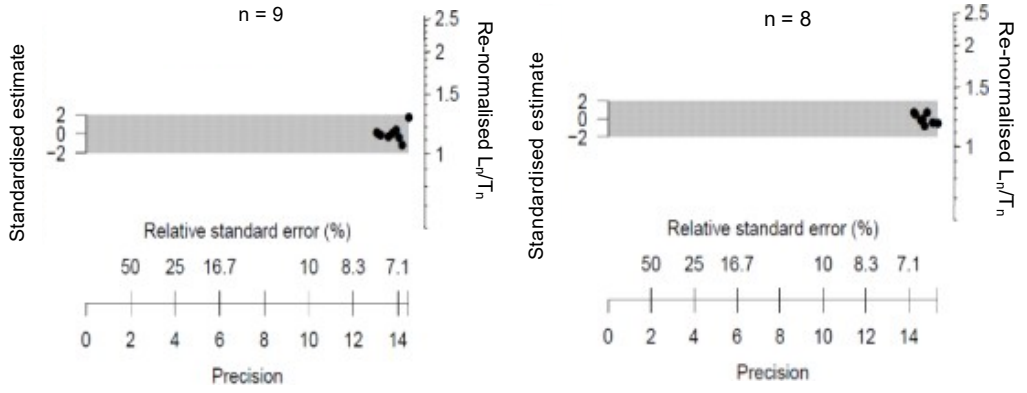

Figure S18. Re-normalised L_n/T_n ratios for two samples from layer 22.1 in the Main Chamber. Data were obtained using the MAR SGC procedure at a stimulation temperature of 275°C. The weighted mean L_n/T_n ratios (centred on the grey bands) were projected on to the MAR SGC to estimate the D_e values for age determination[89]. For DCM14-11, n=9; for DCM16-13, n=8 (where n is the total number of single observations for each sample).

7. URANIUM SERIES DATING OF *DENISOVA 11*

R. Grün, L. Kinsley

A fragment of bone remaining from radiocarbon and genetic analyses was analyses for its U content. We analysed the two cross sections (CC1 and CC2) of the bone as well as three tracks on the outside. The analyses followed the procedures which were described in detail by Grün et al.[109] and were carried out at three separate times. The "A" tracks on CC1 and CC2 were analysed in February 2018, the detailed analysis of CC2 ("B" tracks) and the surface in March 2018 and the detailed analysis of CC2 ("B" tracks) in May 2018. Spot analyses were carried out along 13 tracks on both cross sections of the bone and three tracks on the outer surface. Fig. S19 shows the positions of the analyses on the two cross sections and the three tracks on the outside of the bone and Tables S12 to S14 give all analytical data. The data in the table are shown for the tracks in Figure S19 from the left to the right and start on the outside of the bone. The three tracks on the surface (Fig. S19B) start at the base.

Results

A significant number of analyses show low U/Th ratios, particularly those carried out on the outside of the bone. This clearly demonstrates detrital contamination. To correct for this, U- concentrations were corrected for a Th/U ratio of 4.25, which represents the average value for the Earth's crust[110]. The net result is that the U-concentrations are reduced and assuming secular equilibrium in the detrital component, the $^{230}Th/^{234}U$ ratios decrease and the $^{234}U/^{238}U$ ratios increase, leading overall to younger apparent U-series ages (Fig. S20). For the following data analysis, we only used the corrected data.

Fig. S21 shows the results for the two cross sections, CC1 and CC2. CC1 shows a distinct U-concentration distribution with decreasing U-concentrations towards the outer surface (from around 1.5 ppm towards 0.5 ppm, Fig. S21A). Ages are generally in the range of around 30 to 40 ka, except close to the surface for tracks A1 and B1 to B5 (except B4, Fig. 21B). The older ages are associated with lower $^{234}U/^{238}U$ ratios (Fig. S21C). In contrast, CC2 has generally higher U- concentrations (0.8 to 1.7 ppm, Fig. S21D) without an obvious trend towards the surface of the bone. All ages fall between 25 and 45 ka, without any obvious trend (Figure S21E), the same applies to the $^{234}U/^{238}U$ values, one high data point has to be regarded an outlier (Track A2, 8th data point, Figure S21F), being more than 3-σ different to the surrounding data. The three tracks on the surface show decreasing U-concentrations towards CC2 (Fig. S22A) and increasing ages in tracks 2 and 3 towards CC1 (Fig. S22C).

Discussion

U-series ages are generally regarded as minimum age estimates as the uranium measured in the bones migrated into the skeletal tissue post mortem. Section CC2 shows that there was a major U-accumulation between about 25 and 45 ka, the age differences being due to somewhat delayed U uptake in the different domains of the bone. Cross section CC1 shows some significantly older ages. There is a clear trend between apparent age and U-concentration (Figure S23 top) and the question is whether leaching led to the older apparent ages. On the other hand the older ages are also associated with lower $^{234}U/^{238}U$ values (Fig. S24A). Leaching as such should not change the $^{234}U/^{238}U$ values. When plotting the apparent ages versus the initial $^{234}U/^{238}U$ values (Fig. S24B) any such trend disappears. This means that the source of the uranium in the sample remained with constant initial $^{234}U/^{238}U$ values of around 1.5, and the lower measured $^{234}U/^{238}U$ values in the domains with higher apparent ages are due to the fact that the uranium in these domains had a longer time to disintegrate. This may be due to the fact that these domains became a closed system earlier while the other domains still accumulated more uranium over time. The surface data show increasing apparent ages with increasing U- concentrations (Fig. S23C) and a lower $^{234}U/^{238}U$ values with increasing ages (Figure S24C). However, this trend disappears when the ages are plotted vs the initial $^{234}U/^{238}U$ ratios. Again the data point to the fact that some of the domains closer to the CC1 sections remained a closed system from an earlier time on.

While it is not possible to find an upper age limit for the bone with U-series analyses, its minimum age is in the range of 65 to 70 ka. We include this in the Bayesian modeling section below (Model 4).

Table S12. U-series results on cross section 1.

CC1	U (ppm)	Th (ppb)	U/Th	$^{230}Th/^{238}U$	$^{230}Th/^{238}U$ error	$^{234}U/^{238}U$	$^{234}U/^{238}U$ error	Age (ka)	Age error (ka)	Th-corr Age (ka)	Th-corr Age error (ka)
B1	0.48	182.06	2.6	0.7063	0.0392	1.3368	0.0350	78.8	7.0	71.7	6.1
	0.59	56.29	10.5	0.5859	0.0372	1.3721	0.0276	59.0	5.1	57.3	4.9
	0.98	21.91	44.7	0.4663	0.0240	1.4186	0.0169	42.6	2.7	42.2	2.7
	0.97	49.33	19.7	0.4547	0.0208	1.4104	0.0206	41.6	2.4	40.7	2.3
	1.26	22.12	56.9	0.4234	0.0266	1.4206	0.0190	37.9	2.9	37.6	2.8
	1.54	24.46	62.8	0.3500	0.0165	1.4254	0.0190	30.3	1.7	30.0	1.7
	1.84	11.20	164.5	0.3298	0.0149	1.4434	0.0168	27.9	1.5	27.8	1.5
	1.51	17.62	85.4	0.3603	0.0172	1.4157	0.0170	31.6	1.8	31.4	1.8
B2	0.67	127.36	5.3	0.5793	0.0311	1.3776	0.0275	57.8	4.3	54.4	4.0
	0.56	69.91	8.0	0.5829	0.0443	1.3394	0.0219	60.6	6.2	58.3	5.9
	0.79	35.28	22.4	0.5259	0.0301	1.3874	0.0298	50.7	3.9	49.9	3.8
	0.87	34.70	25.2	0.4957	0.0260	1.3855	0.0301	47.2	3.3	46.5	3.2
	1.28	27.17	47.2	0.4462	0.0224	1.4177	0.0220	40.4	2.5	40.0	2.5

	1.33	28.59	46.6	0.4060	0.0216	1.4133	0.0193	36.3	2.3	35.9	2.3
	1.21	36.52	33.1	0.4180	0.0196	1.4380	0.0322	36.8	2.3	36.3	2.2
	1.56	19.94	78.5	0.3789	0.0181	1.4546	0.0162	32.4	1.8	32.2	1.8
	1.65	19.78	83.5	0.3651	0.0157	1.4184	0.0241	32.0	1.7	31.8	1.7
	1.54	22.94	67.3	0.3475	0.0132	1.4348	0.0237	29.8	1.4	29.6	1.4
A1	0.49	87.38	5.6	0.6134	0.0318	1.3791	0.0269	62.2	4.5	59.0	4.2
	0.54	43.11	12.4	0.5913	0.0302	1.4083	0.0245	57.6	4.0	56.2	3.9
	0.71	35.63	20.0	0.5612	0.0188	1.4174	0.0182	53.5	2.4	52.6	2.4
	0.74	21.12	35.2	0.5306	0.0153	1.3999	0.0219	50.7	2.1	50.2	2.1
	1.32	19.01	69.2	0.4386	0.0131	1.4387	0.0162	38.9	1.5	38.6	1.5
	1.41	13.71	102.9	0.4086	0.0179	1.4496	0.0177	35.5	1.9	35.3	1.9
	1.47	18.79	78.4	0.4080	0.0147	1.4576	0.0196	35.2	1.6	35.0	1.6
	1.39	19.78	70.3	0.4056	0.0128	1.4583	0.0177	34.9	1.4	34.7	1.4
B3	0.87	72.17	12.1	0.4690	0.0260	1.4366	0.0224	42.2	2.9	40.8	2.8
	0.62	51.68	12.0	0.5725	0.0312	1.3796	0.0258	56.9	4.2	55.4	4.1
	0.60	27.58	21.8	0.5229	0.0360	1.3963	0.0346	49.9	4.6	49.1	4.5
	0.65	18.10	35.8	0.5081	0.0274	1.4101	0.0266	47.6	3.3	47.1	3.3
	1.17	15.36	76.4	0.4369	0.0198	1.4181	0.0248	39.4	2.3	39.2	2.3
	1.38	22.89	60.5	0.4243	0.0188	1.4519	0.0236	37.0	2.0	36.7	2.0
	1.20	15.50	77.7	0.4102	0.0211	1.4431	0.0255	35.8	2.3	35.6	2.3
	1.35	15.82	85.1	0.4009	0.0152	1.4270	0.0204	35.3	1.7	35.1	1.7
	1.48	14.89	99.5	0.3713	0.0169	1.4495	0.0232	31.8	1.8	31.6	1.7
	1.50	16.21	92.7	0.3567	0.0151	1.4304	0.0271	30.8	1.6	30.6	1.6
	1.41	24.05	58.5	0.3851	0.0158	1.4546	0.0201	33.0	1.6	32.7	1.6
	1.56	10.40	150.0	0.3468	0.0150	1.4240	0.0192	30.0	1.6	29.9	1.5
B4	0.64	292.17	2.2	0.7008	0.0315	1.3805	0.0195	74.3	4.9	66.0	4.2
	0.63	169.13	3.7	0.7152	0.0403	1.3786	0.0228	76.6	6.3	71.8	5.8
	0.63	27.37	23.1	0.5355	0.0356	1.3916	0.0362	51.7	4.6	50.9	4.6
	1.12	26.88	41.5	0.4909	0.0219	1.4250	0.0251	45.0	2.6	44.6	2.6
	1.31	27.73	47.3	0.4546	0.0187	1.4314	0.0295	40.8	2.3	40.5	2.2
	1.33	11.84	112.3	0.4406	0.0169	1.4474	0.0277	38.8	2.0	38.7	2.0
	1.27	22.74	55.6	0.3928	0.0191	1.4611	0.0175	33.6	1.9	33.3	1.9
	1.42	15.89	89.6	0.3921	0.0166	1.4339	0.0223	34.3	1.8	34.1	1.8
	1.34	17.02	78.5	0.3913	0.0185	1.4399	0.0253	34.0	2.0	33.8	2.0
	1.52	16.79	90.7	0.3793	0.0117	1.4566	0.0288	32.4	1.4	32.2	1.4
	1.35	12.28	109.5	0.3941	0.0192	1.4368	0.0324	34.4	2.1	34.2	2.1
	1.41	21.32	66.3	0.3644	0.0195	1.4409	0.0227	31.3	2.0	31.1	2.0
B5	0.58	113.15	5.1	0.6183	0.0387	1.4227	0.0315	60.2	5.2	56.8	4.8
	0.52	51.52	10.0	0.6423	0.0422	1.3875	0.0276	65.5	6.0	63.8	5.8
	0.72	31.86	22.5	0.5585	0.0304	1.4286	0.0260	52.6	3.8	51.8	3.7
	1.05	23.84	44.0	0.4801	0.0262	1.4173	0.0294	44.1	3.1	43.7	3.1
	1.03	19.71	52.0	0.4699	0.0282	1.4222	0.0259	42.8	3.2	42.5	3.2

	1.26	20.37	61.7	0.4401	0.0200	1.4419	0.0287	38.9	2.3	38.7	2.3
	1.06	16.50	64.4	0.4409	0.0238	1.4152	0.0178	39.9	2.6	39.7	2.6
	0.95	15.25	62.4	0.4130	0.0180	1.4278	0.0199	36.6	2.0	36.3	1.9
	1.49	18.33	81.1	0.3858	0.0210	1.4842	0.0374	32.3	2.2	32.1	2.2
	1.42	16.21	87.6	0.3845	0.0236	1.4433	0.0276	33.2	2.5	33.0	2.5
	1.63	17.44	93.4	0.3775	0.0186	1.4422	0.0232	32.6	1.9	32.4	1.9
	1.53	17.42	87.9	0.3687	0.0185	1.4313	0.0209	32.0	1.9	31.8	1.9
	1.47	20.42	71.9	0.3882	0.0177	1.4609	0.0262	33.1	1.9	32.9	1.9
B6	0.90	57.56	15.7	0.4350	0.0224	1.4555	0.0247	38.0	2.4	36.9	2.3
	0.63	40.20	15.7	0.5808	0.0304	1.4268	0.0278	55.4	3.9	54.3	3.8
	0.59	26.62	22.1	0.6015	0.0330	1.4512	0.0307	56.6	4.3	55.8	4.2
	1.23	40.58	30.3	0.4779	0.0231	1.4274	0.0296	43.5	2.8	42.9	2.7
	1.03	27.57	37.2	0.4586	0.0249	1.4339	0.0276	41.2	2.8	40.7	2.8
	1.37	19.28	71.2	0.4255	0.0206	1.4674	0.0330	36.6	2.3	36.4	2.3
	1.35	20.06	67.4	0.4169	0.0188	1.4549	0.0230	36.2	2.0	35.9	2.0
	1.18	11.30	104.1	0.4107	0.0238	1.4562	0.0233	35.5	2.5	35.3	2.5
	1.37	16.88	81.1	0.4102	0.0182	1.4524	0.0287	35.5	2.0	35.3	2.0
	1.44	21.81	66.2	0.3729	0.0207	1.4355	0.0334	32.3	2.2	32.0	2.2
	1.50	31.56	47.7	0.3969	0.0182	1.4436	0.0250	34.5	2.0	34.1	1.9
	1.44	17.88	80.6	0.3598	0.0176	1.4186	0.0245	31.4	1.9	31.2	1.9
	1.45	21.79	66.4	0.3960	0.0181	1.4521	0.0199	34.1	1.9	33.9	1.9
	1.59	31.14	51.1	0.3940	0.0207	1.4641	0.0258	33.6	2.2	33.3	2.1
A2	0.79	33.92	23.3	0.5061	0.0181	1.4118	0.0245	47.3	2.3	46.5	2.3
	0.93	26.27	35.3	0.5015	0.0164	1.4549	0.0190	45.0	1.9	44.5	1.9
	1.03	14.98	68.4	0.4543	0.0171	1.4622	0.0224	39.7	1.9	39.5	1.9
	0.99	14.13	69.7	0.4328	0.0139	1.4536	0.0149	37.8	1.5	37.6	1.5
	1.21	11.66	103.3	0.4090	0.0139	1.4322	0.0180	36.0	1.5	35.9	1.5
	1.32	11.34	116.4	0.3905	0.0126	1.4540	0.0167	33.5	1.3	33.4	1.3
	1.30	14.93	87.3	0.3859	0.0123	1.4418	0.0164	33.4	1.3	33.2	1.3
	1.30	13.53	96.1	0.3813	0.0107	1.4647	0.0130	32.3	1.1	32.2	1.1
	1.16	16.05	72.5	0.3972	0.0124	1.4616	0.0158	34.0	1.3	33.7	1.3
	1.28	16.85	75.9	0.3823	0.0102	1.4642	0.0135	32.5	1.1	32.2	1.0
B7	0.70	27.36	25.5	0.4841	0.0269	1.4580	0.0242	43.0	3.0	42.4	2.9
	0.81	19.17	42.3	0.5241	0.0229	1.4399	0.0284	48.1	2.9	47.7	2.8
	0.91	14.97	61.0	0.4665	0.0222	1.4489	0.0266	41.5	2.5	41.2	2.5
	1.27	13.35	95.3	0.4533	0.0209	1.4865	0.0361	38.8	2.4	38.7	2.4
	1.15	14.76	77.8	0.4343	0.0202	1.4450	0.0270	38.2	2.3	38.0	2.2
	1.19	16.04	74.2	0.4046	0.0181	1.4374	0.0272	35.4	2.0	35.2	2.0
	1.23	14.82	82.9	0.4060	0.0213	1.4571	0.0396	35.0	2.4	34.8	2.4
	1.22	14.46	84.6	0.4124	0.0183	1.4584	0.0372	35.6	2.1	35.4	2.1
	1.39	27.63	50.1	0.4064	0.0166	1.4512	0.0266	35.2	1.8	34.9	1.8
	1.38	12.49	110.7	0.4015	0.0151	1.4507	0.0170	34.7	1.6	34.6	1.6
	1.12	22.69	49.5	0.3826	0.0181	1.4555	0.0237	32.7	1.9	32.4	1.9
	1.38	14.65	94.1	0.3848	0.0176	1.4484	0.0223	33.1	1.8	32.9	1.8
	1.46	13.01	111.9	0.3804	0.0176	1.4489	0.0223	32.7	1.8	32.5	1.8

	1.45	10.24	142.0	0.3675	0.0125	1.4616	0.0285	31.1	1.4	31.0	1.4
B8	0.82	30.72	26.5	0.5251	0.0273	1.4397	0.0279	48.3	3.3	47.6	3.3
	1.01	19.31	52.4	0.4735	0.0239	1.4431	0.0246	42.4	2.7	42.1	2.7
	1.07	20.85	51.5	0.4830	0.0179	1.4544	0.0205	43.0	2.1	42.7	2.0
	1.10	16.09	68.1	0.4474	0.0197	1.4334	0.0204	40.0	2.2	39.7	2.2
	1.23	28.36	43.5	0.4357	0.0189	1.4443	0.0289	38.4	2.2	38.0	2.1
	1.30	13.88	93.4	0.4174	0.0201	1.4419	0.0290	36.6	2.2	36.4	2.2
	1.28	11.38	112.2	0.4188	0.0232	1.4515	0.0289	36.4	2.5	36.3	2.5
	1.39	12.95	107.1	0.3781	0.0165	1.4167	0.0191	33.3	1.8	33.2	1.7
	1.33	28.53	46.7	0.4033	0.0194	1.4605	0.0221	34.6	2.0	34.3	2.0
	1.36	11.80	115.3	0.3879	0.0169	1.4617	0.0226	33.1	1.8	32.9	1.8
	1.35	32.44	41.6	0.4049	0.0175	1.4424	0.0212	35.3	1.9	34.9	1.9
	1.32	19.96	66.1	0.4167	0.0211	1.4610	0.0233	35.9	2.2	35.7	2.2
	1.40	16.81	83.1	0.3827	0.0148	1.4483	0.0194	32.9	1.6	32.7	1.5
	1.47	33.85	43.3	0.3924	0.0158	1.4440	0.0273	34.0	1.8	33.6	1.7
B9	0.74	27.18	27.4	0.5304	0.0283	1.4607	0.0256	47.9	3.3	47.3	3.3
	0.83	26.60	31.2	0.5041	0.0255	1.4546	0.0288	45.3	3.0	44.8	3.0
	1.06	18.86	56.3	0.4581	0.0207	1.4170	0.0227	41.7	2.4	41.4	2.4
	1.16	16.37	70.7	0.4432	0.0198	1.4556	0.0212	38.8	2.2	38.6	2.1
	1.19	16.64	71.8	0.4236	0.0209	1.4357	0.0328	37.4	2.4	37.2	2.4
	1.26	22.64	55.5	0.4289	0.0188	1.4545	0.0191	37.4	2.0	37.1	2.0
	1.10	21.21	51.6	0.4196	0.0183	1.4460	0.0220	36.7	2.0	36.4	2.0
	1.20	13.47	88.8	0.4013	0.0135	1.4446	0.0315	34.9	1.6	34.7	1.6
	1.44	14.44	99.9	0.3926	0.0177	1.4166	0.0249	34.8	2.0	34.6	1.9
	1.31	23.26	56.4	0.4161	0.0171	1.4527	0.0271	36.1	1.9	35.8	1.9
	1.33	14.92	89.0	0.4112	0.0162	1.4528	0.0302	35.6	1.9	35.4	1.8
	1.51	24.25	62.3	0.4109	0.0158	1.4555	0.0174	35.5	1.7	35.3	1.7
	1.60	23.65	67.8	0.4002	0.0180	1.4546	0.0193	34.5	1.9	34.2	1.9
B10	0.94	25.86	36.4	0.4850	0.0265	1.4493	0.0232	43.4	3.0	43.0	2.9
	1.11	25.83	42.8	0.4938	0.0206	1.4356	0.0208	44.9	2.4	44.5	2.4
	0.98	28.78	33.9	0.4714	0.0238	1.4335	0.0259	42.6	2.7	42.1	2.7
	0.93	21.41	43.5	0.4738	0.0271	1.4746	0.0468	41.3	3.3	41.0	3.2
	1.29	19.25	67.0	0.4144	0.0219	1.4267	0.0299	36.8	2.5	36.5	2.4
	1.30	17.13	76.1	0.4306	0.0222	1.4224	0.0307	38.6	2.6	38.4	2.5
	1.41	19.00	74.3	0.4068	0.0215	1.4635	0.0233	34.9	2.2	34.7	2.2
	1.39	10.81	128.1	0.4193	0.0173	1.4561	0.0201	36.4	1.8	36.2	1.8
	1.39	12.39	112.5	0.4053	0.0156	1.4533	0.0195	35.0	1.7	34.9	1.6
	1.53	20.37	74.9	0.4138	0.0156	1.4358	0.0244	36.4	1.8	36.2	1.8
	1.37	15.64	87.7	0.4073	0.0158	1.4573	0.0208	35.1	1.7	34.9	1.7
	1.50	18.31	82.0	0.3881	0.0195	1.4765	0.0292	32.7	2.0	32.5	2.0
B11	0.96	48.86	19.7	0.4839	0.0255	1.4524	0.0303	43.2	3.0	42.3	2.9
	0.91	30.87	29.5	0.5199	0.0244	1.4313	0.0308	48.0	3.1	47.4	3.0
	0.92	20.85	44.2	0.4913	0.0258	1.4568	0.0229	43.8	2.9	43.4	2.9
	1.19	23.61	50.5	0.4515	0.0218	1.4521	0.0198	39.8	2.4	39.5	2.3
	1.39	26.38	52.7	0.4343	0.0202	1.4444	0.0268	38.3	2.3	37.9	2.2

	1.47	25.29	58.0	0.4176	0.0212	1.4287	0.0341	37.0	2.4	36.7	2.4
	1.53	21.57	70.9	0.4272	0.0187	1.4445	0.0191	37.5	2.0	37.3	2.0
	1.30	19.86	65.6	0.4245	0.0207	1.4469	0.0225	37.2	2.2	36.9	2.2

Table S13. U-series results on cross section 2

CC2	U (ppm)	Th (ppb)	U/Th	$^{230}Th/^{238}U$	$^{230}Th/^{238}U$ error	$^{234}U/^{238}U$	$^{234}U/^{238}U$ error	Age (ka)	Age error (ka)	Th-corr Age (ka)	Th-corr Age error (ka)
B1	1.77	119.22	80	0.3251	0.0114	1.4374	0.0224	27.6	1.2	26.4	1.1
	1.65	128.07	70	0.3482	0.0112	1.4517	0.0273	29.5	1.3	28.1	1.2
	1.70	94.36	90	0.3380	0.0157	1.4438	0.0174	28.7	1.6	27.7	1.5
	1.72	103.46	90	0.3639	0.0146	1.4437	0.0151	31.2	1.5	30.1	1.4
	1.67	109.26	80	0.3740	0.0140	1.4334	0.0158	32.5	1.5	31.3	1.4
	1.50	96.68	80	0.3860	0.0162	1.4371	0.0156	33.5	1.7	32.4	1.6
	1.58	62.84	130	0.3914	0.0118	1.4475	0.0150	33.8	1.2	33.1	1.2
	1.06	74.63	70	0.4214	0.0203	1.4371	0.0185	37.2	2.2	35.9	2.1
	0.80	69.23	60	0.4351	0.0177	1.4360	0.0255	38.6	2.0	37.1	1.9
	1.06	78.93	70	0.4255	0.0184	1.4079	0.0176	38.5	2.0	37.2	2.0
	1.14	92.17	60	0.4620	0.0183	1.4292	0.0193	41.7	2.1	40.3	2.0
	0.94	129.69	30	0.4979	0.0197	1.4104	0.0266	46.4	2.5	44.0	2.3
	0.94	201.68	20	0.5185	0.0212	1.4056	0.0217	49.0	2.7	45.2	2.4
	0.84	286.19	10	0.5049	0.0225	1.4330	0.0225	46.3	2.7	40.2	2.3
	0.84	396.91	10	0.4718	0.0226	1.4400	0.0205	42.4	2.5	33.9	2.0
B2	1.39	70.26	100	0.3601	0.0151	1.4332	0.0144	31.1	1.5	30.2	1.5
	1.57	73.28	110	0.3479	0.0141	1.4359	0.0176	29.8	1.4	29.0	1.4
	1.65	74.05	120	0.3335	0.0134	1.4399	0.0136	28.3	1.3	27.6	1.3
	1.57	129.32	60	0.3573	0.0147	1.4325	0.0186	30.8	1.5	29.4	1.4
	1.69	124.40	70	0.3668	0.0125	1.4495	0.0113	31.3	1.3	30.1	1.2
	1.62	80.44	100	0.3588	0.0128	1.4361	0.0159	30.9	1.3	30.0	1.3
	1.63	98.60	80	0.3677	0.0103	1.4270	0.0171	32.0	1.1	30.9	1.1
	1.31	136.37	50	0.4237	0.0145	1.4396	0.0200	37.3	1.6	35.5	1.5
	1.32	107.56	60	0.4052	0.0120	1.4295	0.0185	35.7	1.3	34.3	1.3
	1.38	117.16	60	0.4023	0.0145	1.4410	0.0204	35.1	1.6	33.6	1.5
	1.31	102.23	60	0.4443	0.0165	1.4144	0.0209	40.3	1.9	38.9	1.8
	1.18	127.78	50	0.4590	0.0234	1.4144	0.0257	41.9	2.7	40.0	2.6
	0.96	228.42	20	0.5023	0.0211	1.4092	0.0267	47.0	2.7	42.7	2.4
	1.07	434.22	10	0.4725	0.0200	1.4252	0.0151	43.0	2.3	35.7	1.8
	1.04	503.93	10	0.4867	0.0150	1.4513	0.0162	43.5	1.7	34.9	1.3
B3	1.45	190.70	40	0.4276	0.0313	1.3891	0.0324	39.4	3.6	37.0	3.3
	1.54	160.18	50	0.3637	0.0132	1.4435	0.0223	31.2	1.4	29.4	1.3
	1.64	54.09	160	0.3492	0.0146	1.4427	0.0157	29.8	1.5	29.2	1.4
	1.61	75.61	110	0.3506	0.0123	1.4537	0.0163	29.7	1.2	28.8	1.2
	1.49	99.10	80	0.3670	0.0132	1.4378	0.0147	31.7	1.4	30.5	1.3

	1.43	93.47	80	0.3823	0.0154	1.4496	0.0169	32.8	1.6	31.7	1.5
	1.35	89.86	80	0.3822	0.0141	1.4479	0.0185	32.9	1.5	31.7	1.4
	1.12	66.10	90	0.4067	0.0162	1.4132	0.0189	36.4	1.8	35.3	1.7
	1.11	54.34	110	0.4103	0.0173	1.4241	0.0184	36.4	1.9	35.6	1.8
	1.15	88.80	70	0.4306	0.0177	1.4544	0.0173	37.6	1.9	36.2	1.8
	1.08	122.60	40	0.4513	0.0199	1.4341	0.0276	40.4	2.3	38.4	2.2
	1.03	118.61	40	0.4535	0.0184	1.4312	0.0206	40.7	2.1	38.7	2.0
	0.87	123.49	30	0.5027	0.0215	1.4309	0.0211	46.1	2.5	43.6	2.4
	0.85	232.92	10	0.5147	0.0248	1.4361	0.0261	47.2	3.0	42.4	2.6
	0.98	220.26	20	0.3783	0.0140	1.4474	0.0215	32.5	1.5	28.6	1.3
A1	1.10	26.48	40	0.3438	0.0206	1.3837	0.0384	30.7	2.3	30.3	2.3
	1.21	25.00	40	0.3776	0.0182	1.4146	0.0175	33.3	1.9	33.0	1.9
	1.33	26.72	40	0.3653	0.0161	1.3957	0.0221	32.6	1.8	32.2	1.7
	1.56	18.25	80	0.3647	0.0153	1.4042	0.0170	32.3	1.6	32.1	1.6
	1.55	19.19	80	0.3570	0.0167	1.4298	0.0216	30.9	1.7	30.7	1.7
	1.56	16.61	90	0.3293	0.0153	1.4100	0.0226	28.6	1.6	28.4	1.6
	1.65	17.69	90	0.3486	0.0168	1.4317	0.0462	30.0	2.0	29.8	2.0
	1.64	14.85	110	0.3069	0.0145	1.4013	0.0224	26.6	1.5	26.5	1.5
	1.63	21.32	70	0.3214	0.0151	1.4261	0.0198	27.5	1.5	27.3	1.5
	1.72	15.19	110	0.3158	0.0159	1.4175	0.0171	27.1	1.6	27.0	1.6
	1.96	12.87	150	0.3075	0.0140	1.4184	0.0171	26.3	1.4	26.2	1.4
	1.74	15.15	110	0.3164	0.0172	1.4210	0.0185	27.1	1.7	27.0	1.7
	1.89	24.47	70	0.3641	0.0137	1.4232	0.0190	31.7	1.5	31.5	1.4
B4	1.54	87.84	90	0.3501	0.0125	1.4573	0.0176	29.5	1.3	28.5	1.2
	1.55	77.99	100	0.3454	0.0160	1.4427	0.0173	29.4	1.6	28.5	1.5
	1.57	105.66	80	0.3430	0.0148	1.4301	0.0253	29.5	1.6	28.3	1.5
	1.44	80.91	90	0.3460	0.0129	1.4427	0.0220	29.5	1.4	28.5	1.3
	1.52	77.44	100	0.3681	0.0122	1.4460	0.0204	31.5	1.3	30.7	1.3
	1.44	113.07	60	0.3667	0.0140	1.4385	0.0158	31.6	1.4	30.2	1.4
	1.35	85.01	80	0.3803	0.0126	1.4381	0.0196	33.0	1.4	31.9	1.3
	1.36	113.74	60	0.4123	0.0124	1.4468	0.0223	35.9	1.4	34.5	1.4
	1.46	93.78	80	0.4157	0.0178	1.4235	0.0156	37.0	1.9	35.9	1.8
	1.30	102.63	60	0.4201	0.0178	1.4387	0.0141	37.0	1.9	35.6	1.8
	1.39	76.14	90	0.4177	0.0162	1.4360	0.0173	36.8	1.8	35.9	1.7
	1.16	133.80	40	0.4615	0.0200	1.4441	0.0249	41.1	2.3	39.1	2.2
	0.88	119.39	40	0.4831	0.0163	1.4427	0.0235	43.5	2.0	41.1	1.9
	0.84	114.27	40	0.4652	0.0222	1.4365	0.0228	41.8	2.5	39.4	2.4
	1.06	226.63	20	0.3965	0.0164	1.4562	0.0181	34.1	1.7	30.4	1.5
B5	1.57	73.17	110	0.3505	0.0139	1.4647	0.0212	29.4	1.4	28.6	1.4
	1.54	93.17	90	0.3513	0.0146	1.4328	0.0263	30.2	1.6	29.2	1.5
	1.48	79.62	100	0.3547	0.0131	1.4176	0.0182	30.9	1.4	30.0	1.3
	1.56	89.83	90	0.3579	0.0120	1.4426	0.0226	30.6	1.3	29.6	1.2
	1.35	127.75	50	0.3843	0.0159	1.4679	0.0247	32.5	1.7	30.9	1.6
	1.39	94.68	80	0.3868	0.0132	1.4403	0.0148	33.5	1.4	32.4	1.3
	1.36	65.59	110	0.3690	0.0132	1.4316	0.0199	32.0	1.4	31.2	1.4

	1.41	102.85	70	0.3795	0.0144	1.4385	0.0282	32.9	1.6	31.6	1.6
	1.42	89.73	80	0.3979	0.0120	1.4394	0.0238	34.7	1.4	33.6	1.3
	1.39	147.67	50	0.4278	0.0155	1.4435	0.0227	37.6	1.7	35.8	1.6
	1.27	91.85	70	0.4250	0.0172	1.4298	0.0188	37.8	1.9	36.5	1.8
	1.27	140.59	40	0.4306	0.0170	1.4341	0.0228	38.2	1.9	36.3	1.8
	1.06	173.82	30	0.4655	0.0218	1.4388	0.0231	41.7	2.5	38.9	2.3
	1.20	230.15	20	0.4387	0.0147	1.4532	0.0213	38.4	1.7	35.1	1.5
	1.28	307.00	20	0.3789	0.0137	1.4280	0.0170	33.1	1.5	28.8	1.2
B6	1.46	100.55	70	0.3574	0.0196	1.4608	0.0286	30.1	2.0	29.0	1.9
	1.48	66.75	120	0.3712	0.0110	1.4499	0.0187	31.7	1.2	31.0	1.1
	1.34	89.59	80	0.3597	0.0120	1.4392	0.0175	30.9	1.3	29.7	1.2
	1.44	72.09	100	0.3603	0.0115	1.4414	0.0269	30.9	1.3	30.0	1.3
	1.43	85.10	90	0.3633	0.0179	1.4542	0.0237	30.9	1.8	29.8	1.8
	1.37	93.64	70	0.3817	0.0148	1.4358	0.0155	33.2	1.5	32.0	1.5
	1.36	71.03	100	0.3859	0.0182	1.4316	0.0185	33.7	1.9	32.8	1.8
	1.52	147.33	50	0.3864	0.0132	1.4365	0.0168	33.6	1.4	31.9	1.3
	1.40	134.75	50	0.4060	0.0171	1.4423	0.0257	35.4	1.9	33.7	1.8
	1.26	88.74	70	0.4109	0.0147	1.4324	0.0258	36.2	1.7	35.0	1.6
	1.15	101.79	60	0.4373	0.0166	1.4407	0.0181	38.7	1.8	37.1	1.7
	1.25	186.95	30	0.4379	0.0164	1.4422	0.0211	38.7	1.8	36.1	1.7
	1.25	302.71	20	0.4301	0.0173	1.4527	0.0225	37.6	1.9	33.3	1.7
	1.40	314.74	20	0.4111	0.0184	1.4449	0.0179	35.9	1.9	31.9	1.7
	1.28	458.80	10	0.4076	0.0162	1.4733	0.0245	34.7	1.7	28.4	1.4
B7	1.48	19.21	70	0.3905	0.0162	1.4261	0.0185	34.3	1.7	34.1	1.7
	1.50	13.47	110	0.3769	0.0151	1.4362	0.0232	32.7	1.6	32.5	1.6
	1.43	15.65	90	0.3895	0.0175	1.4379	0.0252	33.9	1.9	33.7	1.9
	1.48	13.99	100	0.3695	0.0148	1.4302	0.0137	32.1	1.5	31.9	1.5
	1.47	14.70	100	0.3655	0.0142	1.4165	0.0182	32.1	1.5	31.9	1.5
	1.34	13.65	90	0.3996	0.0162	1.4272	0.0156	35.2	1.7	35.0	1.7
	1.59	15.24	100	0.4087	0.0159	1.4485	0.0177	35.5	1.7	35.4	1.7
	1.40	15.00	90	0.4198	0.0170	1.4387	0.0243	36.9	1.9	36.7	1.9
	1.52	19.64	70	0.4397	0.0142	1.4155	0.0180	39.8	1.6	39.6	1.6
	1.45	21.00	60	0.4899	0.0207	1.4048	0.0302	45.7	2.7	45.5	2.6
	1.49	29.31	50	0.4722	0.0136	1.4092	0.0134	43.6	1.6	43.2	1.6
	1.36	86.64	10	0.4671	0.0130	1.4226	0.0198	42.5	1.6	41.4	1.6
B8	1.51	21.56	70	0.3665	0.0143	1.4471	0.0159	31.4	1.5	31.1	1.4
	1.45	23.01	60	0.3834	0.0142	1.4329	0.0214	33.4	1.5	33.1	1.5
	1.22	19.90	60	0.3833	0.0143	1.4494	0.0166	33.0	1.5	32.7	1.5
	1.48	14.72	100	0.3782	0.0159	1.4495	0.0196	32.4	1.7	32.3	1.6
	1.51	13.63	110	0.3887	0.0156	1.4491	0.0270	33.5	1.7	33.3	1.7
	1.39	17.28	80	0.3923	0.0134	1.4501	0.0225	33.8	1.5	33.6	1.5
	1.28	14.82	80	0.4008	0.0174	1.4297	0.0240	35.3	1.9	35.1	1.9
	1.36	21.11	60	0.4048	0.0163	1.4548	0.0192	34.9	1.7	34.7	1.7
	1.19	17.40	60	0.4368	0.0152	1.4427	0.0467	38.6	2.2	38.3	2.2
	1.44	36.23	30	0.4206	0.0158	1.4310	0.0175	37.3	1.7	36.8	1.7

B9	1.52	19.56	70	0.3862	0.0411	1.4505	0.0351	33.2	4.2	33.0	4.1
	1.49	17.64	80	0.3764	0.0145	1.4403	0.0190	32.5	1.5	32.3	1.5
	1.27	19.64	60	0.3663	0.0157	1.4462	0.0148	31.4	1.6	31.1	1.6
	1.50	19.44	70	0.3658	0.0128	1.4331	0.0188	31.7	1.4	31.4	1.3
	1.50	17.75	80	0.3949	0.0148	1.4403	0.0233	34.4	1.6	34.2	1.6
	1.48	15.11	90	0.3944	0.0153	1.4315	0.0200	34.6	1.7	34.4	1.6
	1.56	15.99	90	0.4029	0.0137	1.4310	0.0184	35.4	1.5	35.3	1.5
	1.42	27.29	50	0.4231	0.0176	1.4240	0.0198	37.7	2.0	37.4	1.9
	1.20	26.72	40	0.4438	0.0168	1.4237	0.0175	39.9	1.9	39.6	1.9
A2	1.48	29.99	40	0.3664	0.0177	1.4101	0.0197	32.3	1.9	32.0	1.8
	1.46	21.97	60	0.3402	0.0151	1.4134	0.0260	29.6	1.6	29.4	1.6
	1.80	15.21	110	0.3247	0.0166	1.4086	0.0293	28.2	1.8	28.1	1.7
	1.70	22.24	70	0.3295	0.0155	1.4013	0.0171	28.9	1.6	28.6	1.6
	1.79	15.53	110	0.3007	0.0120	1.4234	0.0276	25.6	1.3	25.4	1.3
	1.85	20.84	80	0.3154	0.0145	1.4461	0.0315	26.5	1.5	26.3	1.5
	1.69	20.98	80	0.3352	0.0128	1.4108	0.0175	29.2	1.3	29.0	1.3
	1.75	19.54	80	0.3445	0.0150	1.5351	0.0232	27.3	1.4	27.1	1.4
B10	1.63	16.81	90	0.3897	0.0118	1.4484	0.0220	33.6	1.3	33.4	1.3
	1.55	20.04	70	0.4098	0.0149	1.4382	0.0197	35.9	1.6	35.7	1.6
	1.72	16.64	100	0.3858	0.0177	1.4363	0.0252	33.6	1.9	33.4	1.9
	1.48	19.66	70	0.3822	0.0148	1.4343	0.0130	33.2	1.5	33.0	1.5
	1.59	18.73	80	0.4066	0.0147	1.4545	0.0221	35.1	1.6	34.9	1.6
	1.56	39.29	30	0.4302	0.0156	1.4403	0.0141	38.0	1.7	37.5	1.7
B11	1.50	18.33	80	0.3811	0.0137	1.4269	0.0184	33.3	1.5	33.1	1.5
	1.64	21.51	70	0.3812	0.0135	1.4393	0.0157	33.0	1.4	32.8	1.4
	1.45	20.01	70	0.3891	0.0169	1.4370	0.0215	33.9	1.8	33.6	1.8
	1.50	23.54	60	0.3842	0.0118	1.4483	0.0214	33.1	1.3	32.8	1.3
	1.40	26.90	50	0.4227	0.0149	1.4304	0.0212	37.5	1.7	37.2	1.7
	1.61	15.27	100	0.3693	0.0118	1.4526	0.0233	31.5	1.3	31.3	1.3

Table S14. U-series results on side tracks

Side	U (ppm)	Th (ppb)	U/Th	$^{230}Th/^{238}U$	$^{230}Th/^{238}U$ error	$^{234}U/^{238}U$	$^{234}U/^{238}U$ error	Age (ka)	Age error (ka)	Th-corr Age (ka)	Th-corr Age error (ka)
B1	0.73	416.30	1.76	0.5620	0.0259	1.3743	0.0185	55.8	3.4	45.1	2.6
	0.84	456.29	1.85	0.5809	0.0255	1.3826	0.0189	57.8	3.4	47.7	2.7
	0.81	338.49	2.39	0.6011	0.0252	1.3961	0.0329	59.6	3.8	52.0	3.2
	0.85	152.35	5.55	0.5649	0.0241	1.4134	0.0212	54.1	3.1	51.0	2.9
	0.86	123.33	6.95	0.5419	0.0247	1.4228	0.0201	50.9	3.0	48.4	2.8
	0.91	117.10	7.77	0.5278	0.0180	1.4095	0.0244	49.9	2.4	47.6	2.3
	0.93	130.06	7.18	0.5630	0.0238	1.4207	0.0201	53.5	3.0	51.1	2.9
	0.99	158.48	6.22	0.5788	0.0206	1.4115	0.0279	55.9	2.9	53.1	2.7
	1.10	139.48	7.87	0.5099	0.0224	1.3398	0.0247	51.1	3.1	48.7	2.9

	1.13	413.78	2.73	0.6300	0.0293	1.3897	0.0216	63.7	4.1	57.1	3.6
	1.28	467.09	2.74	0.6901	0.0300	1.4010	0.0152	71.2	4.4	64.7	3.8
	1.15	378.36	3.03	0.6541	0.0225	1.4151	0.0182	65.3	3.2	59.5	2.8
	1.07	423.02	2.53	0.6878	0.0340	1.4457	0.0230	67.8	4.7	60.9	4.1
	1.04	435.75	2.39	0.6780	0.0286	1.4301	0.0191	67.5	4.0	60.2	3.5
	1.18	612.17	1.92	0.7569	0.0461	1.4266	0.0175	78.8	6.9	69.7	5.8
B2	0.69	34.15	20.17	0.4056	0.0457	1.4214	0.0348	36.0	4.9	35.1	4.7
	0.80	50.53	15.88	0.4060	0.0227	1.4297	0.0273	35.8	2.5	34.7	2.4
	0.75	44.51	16.79	0.4211	0.0221	1.4241	0.0249	37.5	2.4	36.5	2.4
	0.68	54.73	12.46	0.4651	0.0231	1.4216	0.0306	42.3	2.8	40.9	2.7
	0.76	145.46	5.24	0.5135	0.0205	1.4161	0.0251	47.9	2.6	44.6	2.4
	0.87	74.37	11.65	0.5426	0.0257	1.4054	0.0225	51.8	3.3	50.3	3.1
	0.90	52.82	17.08	0.5697	0.0204	1.3937	0.0157	55.7	2.7	54.7	2.6
	1.00	82.08	12.14	0.6162	0.0226	1.3815	0.0222	62.4	3.3	61.0	3.2
	1.13	56.40	20.07	0.6244	0.0216	1.3924	0.0160	62.8	3.0	62.0	3.0
	1.28	49.02	26.12	0.5906	0.0247	1.3820	0.0165	59.0	3.3	58.4	3.3
	1.33	97.11	13.68	0.5967	0.0231	1.4084	0.0147	58.3	3.0	57.0	2.9
	1.17	165.75	7.07	0.5782	0.0235	1.4222	0.0183	55.3	3.0	52.8	2.8
	1.08	244.94	4.41	0.6027	0.0231	1.4243	0.0183	58.2	3.0	54.2	2.8
	1.06	234.13	4.52	0.6153	0.0244	1.4215	0.0222	59.9	3.3	56.0	3.1
	1.05	369.18	2.84	0.6605	0.0223	1.4123	0.0191	66.3	3.2	60.1	2.9
B3	0.69	39.06	17.58	0.3616	0.0214	1.4289	0.0387	31.3	2.3	30.3	2.3
	0.62	49.56	12.57	0.4003	0.0217	1.4359	0.0262	35.0	2.3	33.6	2.2
	0.70	63.00	11.17	0.3987	0.0203	1.4585	0.0216	34.2	2.1	32.7	2.0
	0.70	31.82	21.94	0.4003	0.0253	1.4384	0.0193	35.0	2.6	34.2	2.6
	0.72	37.71	19.20	0.4118	0.0263	1.4322	0.0296	36.3	2.9	35.4	2.8
	0.77	52.05	14.71	0.4385	0.0177	1.4384	0.0217	38.9	2.0	37.7	1.9
	0.85	64.67	13.07	0.5197	0.0232	1.4071	0.0207	49.1	2.9	47.7	2.8
	0.84	47.66	17.57	0.4360	0.0255	1.4153	0.0184	39.4	2.8	38.4	2.7
	0.91	56.09	16.25	0.4385	0.0166	1.4326	0.0215	39.1	1.9	38.0	1.8
	1.11	68.56	16.18	0.4498	0.0194	1.3992	0.0264	41.5	2.4	40.4	2.3
	1.06	80.72	13.17	0.5303	0.0255	1.4029	0.0274	50.5	3.3	49.2	3.2
	1.02	97.01	10.50	0.5210	0.0189	1.3930	0.0176	49.9	2.4	48.2	2.3
	0.94	79.30	11.81	0.4799	0.0171	1.4384	0.0163	43.3	2.0	41.8	1.9
	0.94	71.88	13.05	0.4491	0.0241	1.4309	0.0202	40.3	2.7	38.9	2.6
	1.05	66.60	15.74	0.5028	0.0193	1.4325	0.0228	46.0	2.3	44.9	2.3

A

B

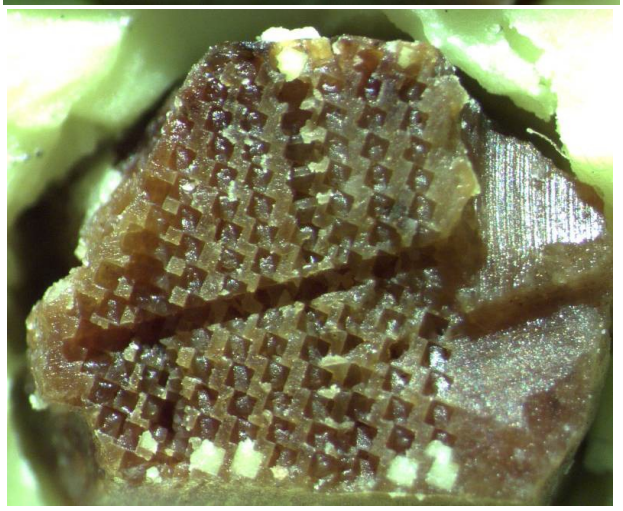

C

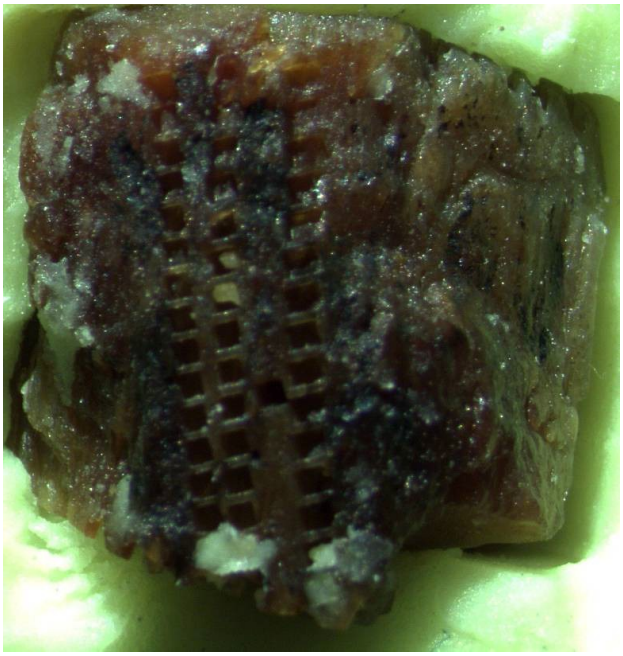

Figure S19. Position of laser spots. A: Cross section 1 (CC1), B: Cross section 2 (CC2), C: Bone surface. Scale, A = 6

mm in width, C = 6 mm in width.

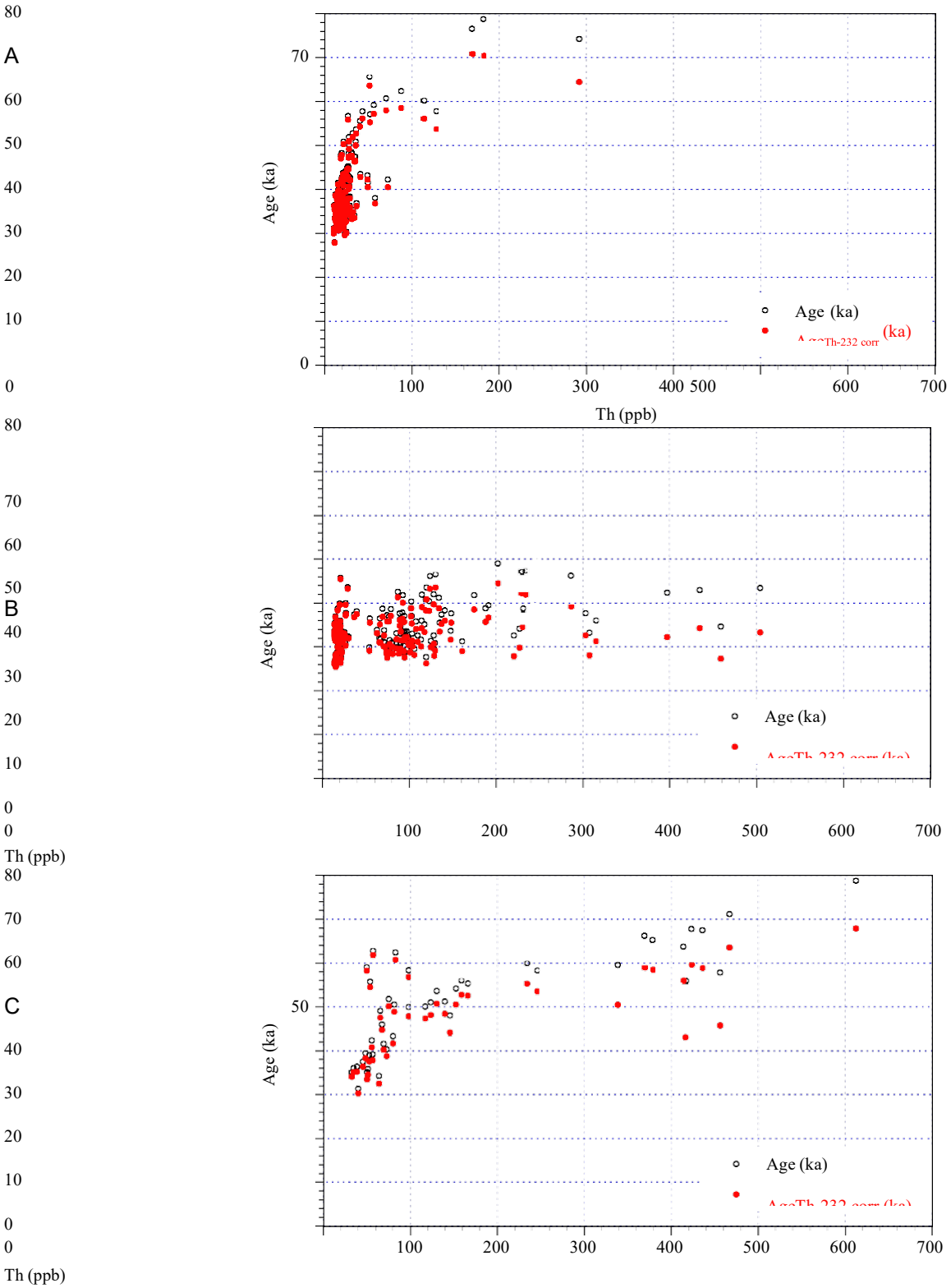
A
B
C
Age (ka)
Th (ppb)
Age (ka)
(ka)

Figure S20. Age and Th corrected age vs Th concentration for CC1 (A), CC1 (B) and the surface tracks (C).

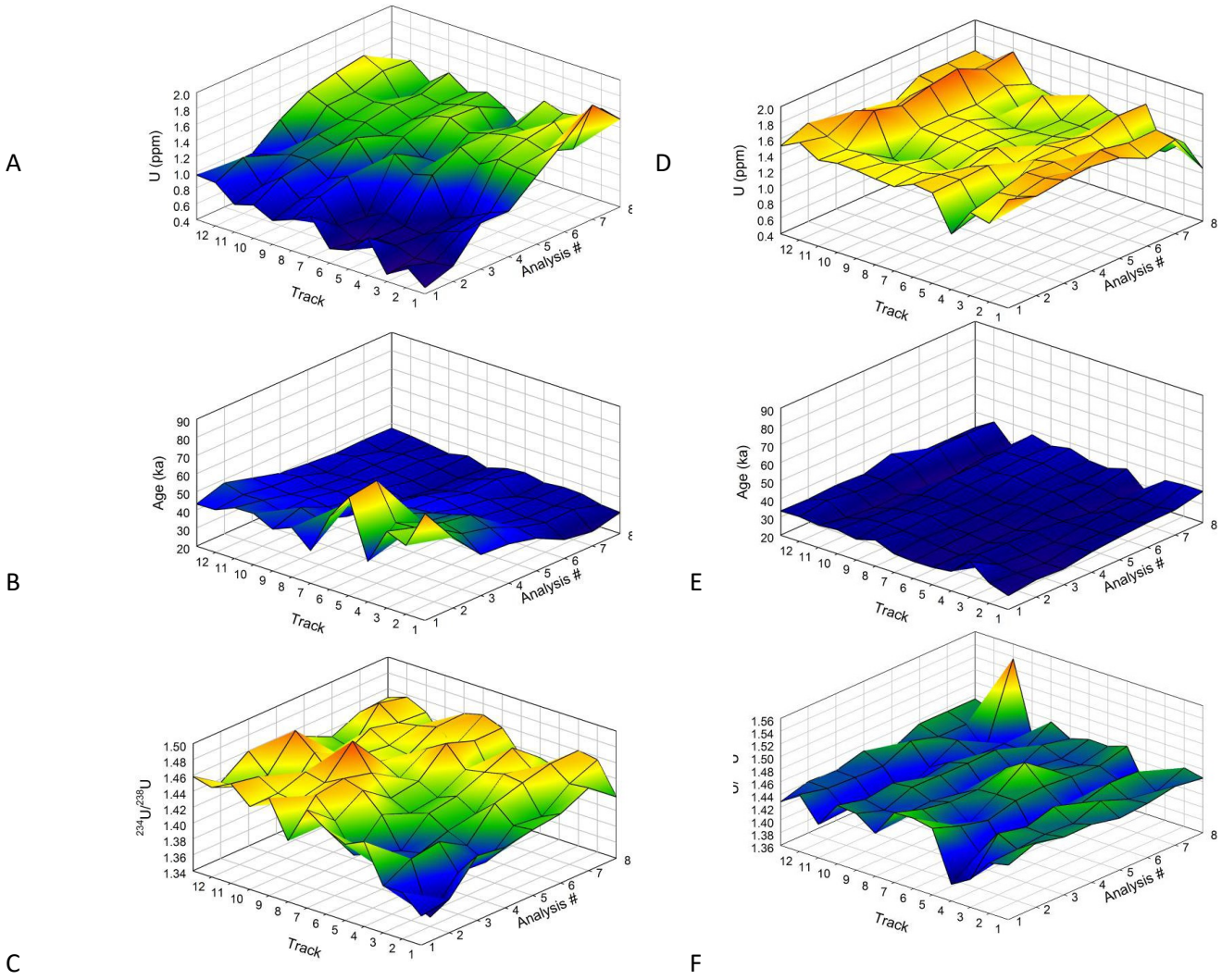

Figure S21. U-concentration (A,D), Age (B,E) and $^{234}U/^{238}U$ (C,F) for CC1 (A-C) and CC2 (D-F).

A

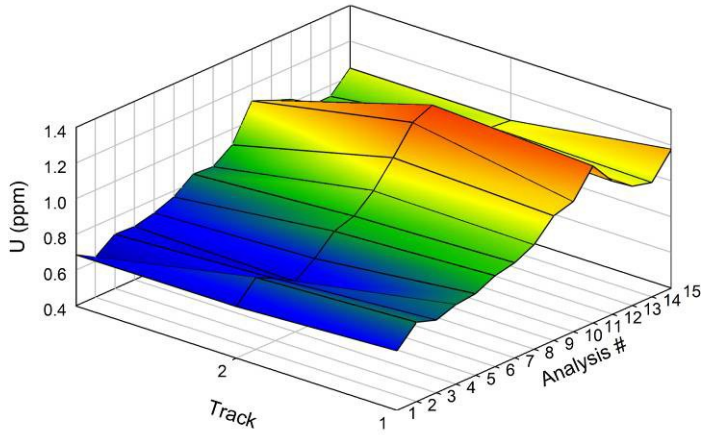

B

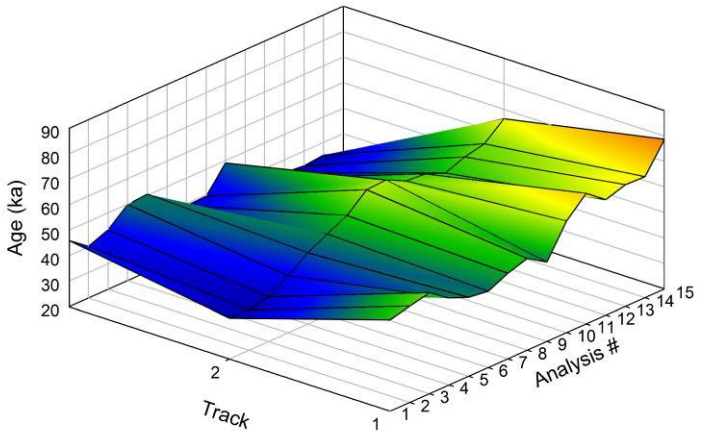

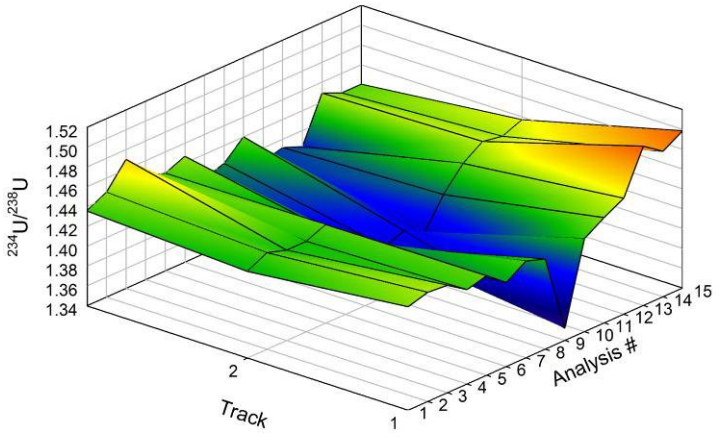

C

Figure S22. U-concentration (A), Age (B) and $^{234}U/^{238}U$ for the surface analyses.

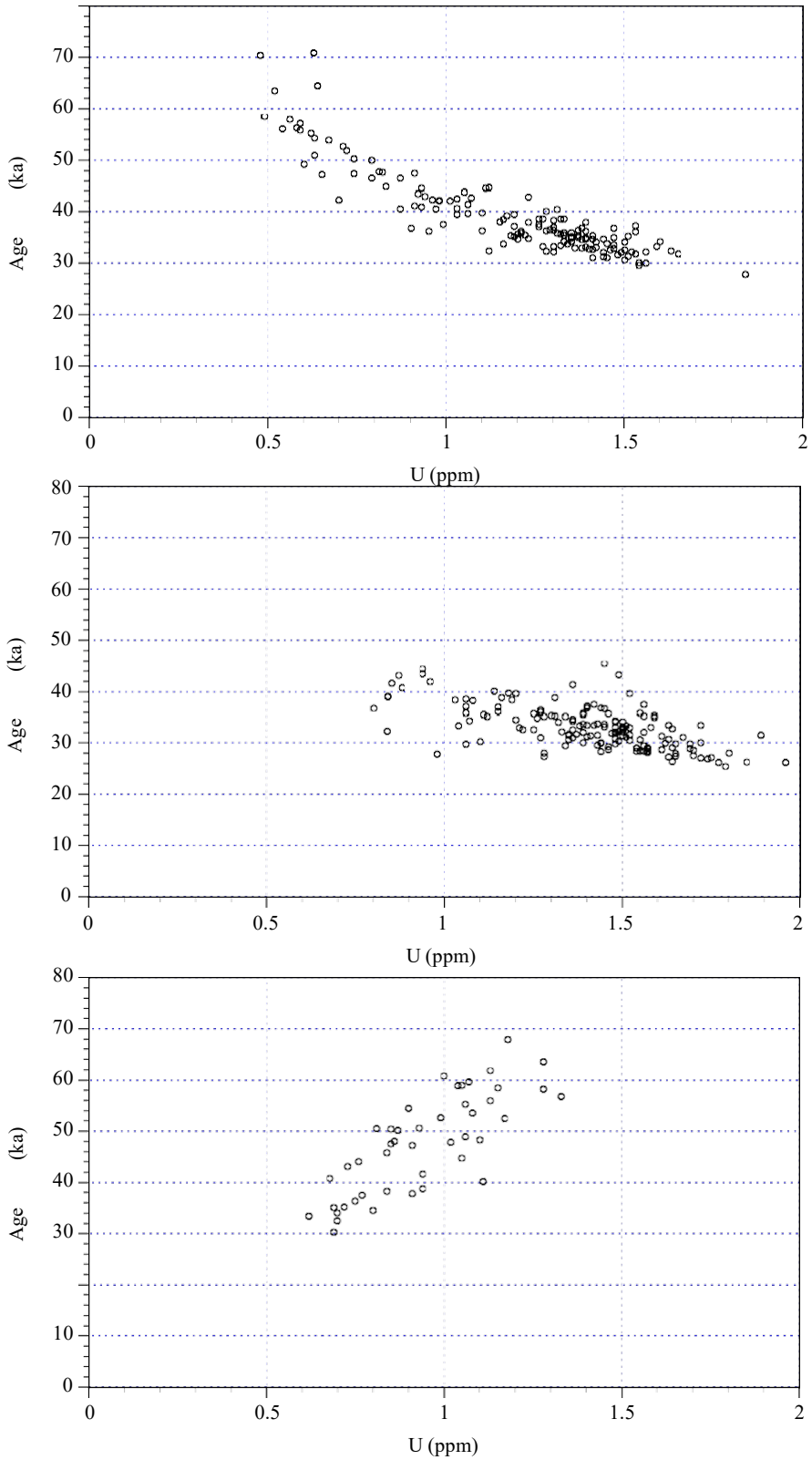

Figure S23. Th-corrected age vs U-concentration for CC1 (A), CC2 (B) and the surface analyses (C).

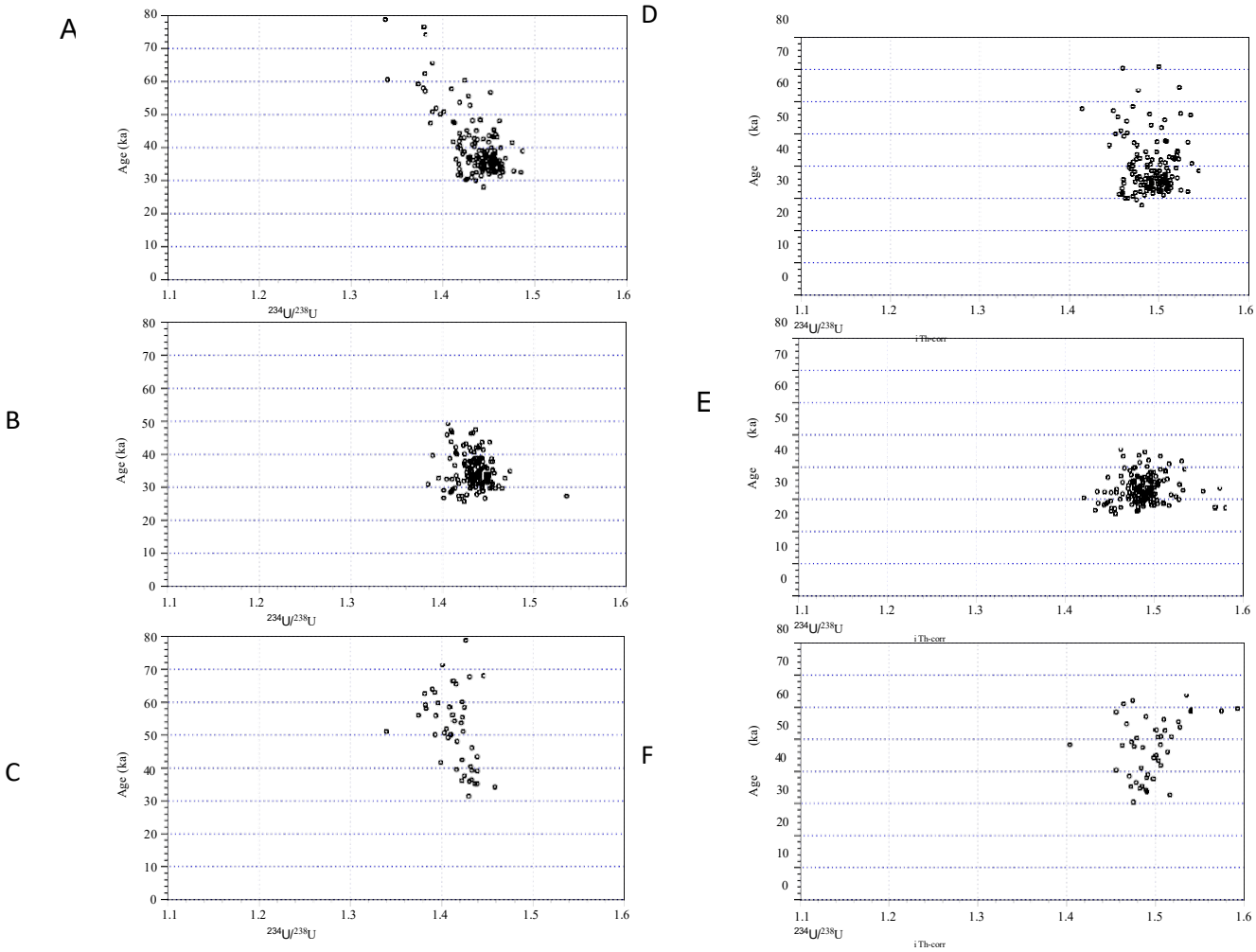

Figure S24. Apparent age vs measured $^{234}U/^{238}U$ ratio (A-C) and Th-corrected age versus initial corrected $^{234}U/^{238}U$ ratio (D-F) for CC1 (A, D), CC2 (B, E) and the surface analyses (C, F).

8. ZOOARCHAEOLOGY BY MASS SPECTROMETRY (ZOOMS)

S. Brown, M. Buckley

Zooarchaeology by Mass Spectrometry (ZooMS) was carried out on bone fragments accessed from the Institute of Archaeology and Ethnography in Novosibirsk. Samples of 2212 bones were analysed from across five layers: layer 9.1 (*n*= 31), layer 9.2 (*n*= 21), layer 9.3 (*n*= 310), layer 11.1 (*n*= 115), layer 11.2 (*n*= 557), layer 11.3 (*n*= 604), and layer 11.4 (*n*= 574). These were excavated during the 2005, 2007, 2009, and 2011 seasons at Denisova Cave. This brings the total to 4527 bones from Denisova Cave analysed using this method.

Samples were in general between 10-50mm in length and had been heavily fragmented, likely the result of taphonomic processes at the site and a high level of carnivore activity. The bone fragments were specifically chosen because they exhibited no diagnostic features which might make identification on the basis of morphology possible. Some however showed evidence of anthropic modification, such as burning and cutmarks.

ZooMS was carried out following the procedures described in Ref. 30 for the discovery of *Denisova 11*[34] (Figure S25a), using facilities at the University of Manchester and the ORAU, University of Oxford. A small fragment, between 20-50mg, was removed from each sample using a diamond disc drill bit. Each bone fragment was demineralised in 0.6M hydrochloric acid (HCl) for 18 hours at -4 ^{o}C. The supernatant was removed into 30 kDa molecular weight cut-off (MWCO) ultrafilters and centrifuged at 3700 rpm for 1 h, fragments were stored as backups at - 20 ^{o}C. The remaining residue was then rinsed twice with 500µl of 50 mM ammonium bicarbonate (AmBic), centrifuging at 3700 rpm for 30 mins after each rinse. An additional 200 µL of 50 mM AmBic was allowed to mix with the resulting supernatant, half of which was then stored at -20 ^{o}C as a backup. The remaining 100µl of eluted collagen was treated with 0.2 µg trypsin (sequencing grade; Promega UK) and incubated at 37 ^{o}C for 18 h.

Trypsinised samples were mixed with a matrix solution of 1µl α -cyano-4-hydroxycinnamic acid solution (10 mg/mL in 50% acetonitrile (ACN)/0.1% trifluoroacetic acid (TFA), spotted onto a ground steel target plate (Bruker MTP 384 Target Plate 8280784), and allowed to crystallise. Analysis was performed using a Bruker Ultraflex II (Bruker Daltonics, Bremen) MALDI-Tof/Tof- mass spectrometer. The resulting mass spectra were matched to a reference library of published peptide markers using FlexAnalysis software[111,112,113] resulting in the identification of the three hominin bones *Denisova 14, Denisova 15* and *Denisova 16* (Fig. S13 b,c,d). Additionally, large mammmals such as bovines (*Bos/Bison)*, sheep (*Ovis*), goats (*Capra*), horses (*Equus*), woolly

rhinoceros (*Rhinocerotidae*), mammoths (*Elephantidae*), hyaenas (*Crocuta*), bears (*Ursus*), and a number of small mammals were identified amongst the assemblage.
All radiocarbon dated bones were also analysed using ZooMS to taxonomically identify the bones.

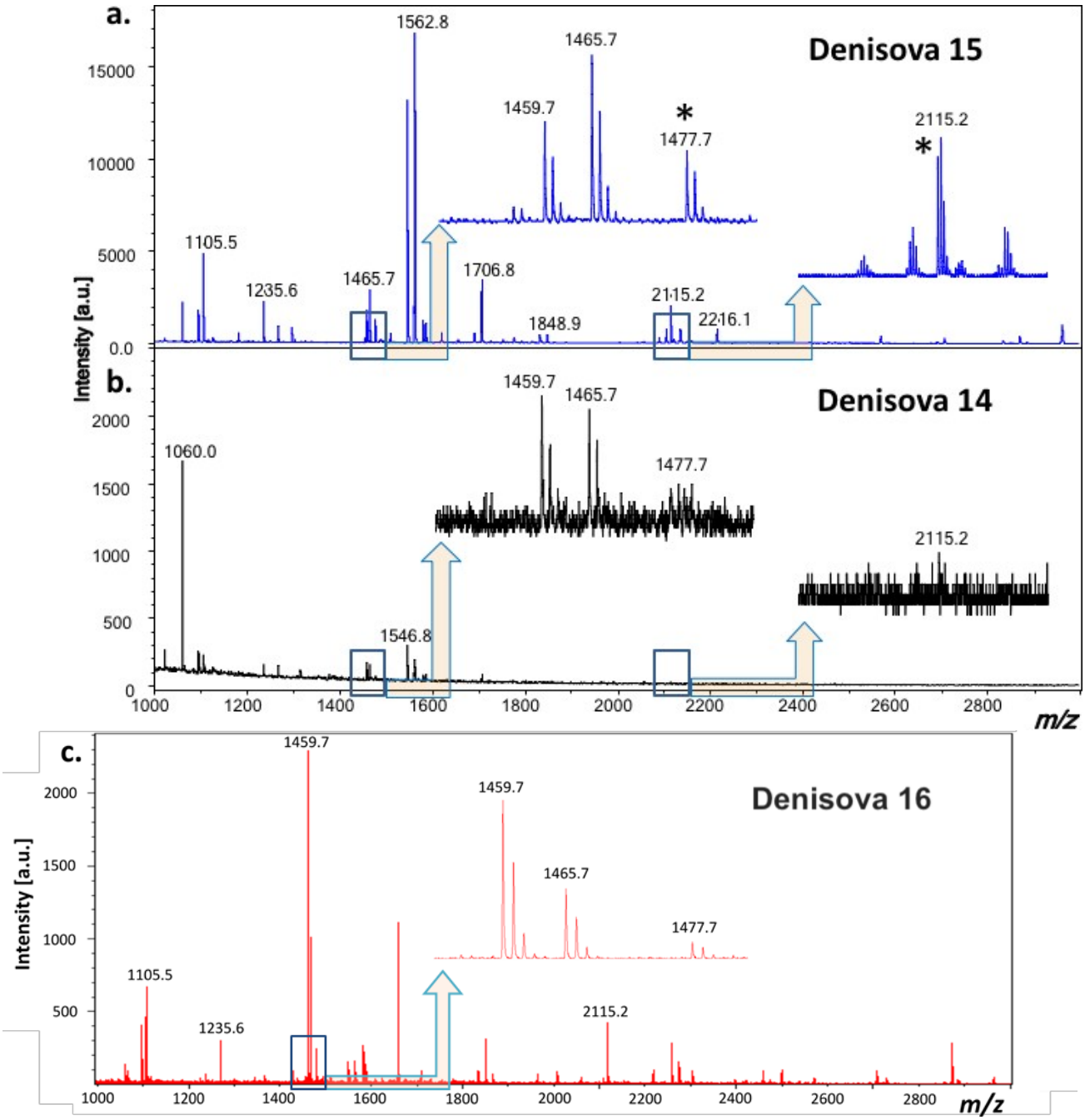

Figure S25. MALDI-ToF mass spectra of digested collagen from (a) *Denisova 15* (DC3753) (b) *Denisova 14* (DC 3758) and (c) *Denisova 16* (DC4114).

9. BAYESIAN AGE MODELLING

C. Bronk Ramsey, K. Douka, T. Higham

We built Bayesian age models to determine the chronometry of the site, and incorporated several different types of information within OxCal 4[18]. These included:

1. Radiocarbon dates calibrated against the IntCal13 calibration curve[19] (Section 2), including one direct radiocarbon age for *Denisova 14*, with the radiocarbon limit given as a *terminus ante quem*;
2. Eleven optical ages (Section 6);
3. Prior information in the form of age-ordering, either from direct stratigraphic constraints within the cave or as inferred from the mtDNA genetic tree;
4. Age differences between hominin remains as inferred from the number of substitutions observed (Section 4). Since this is the only unusual part of the age model, it is covered in more detail below.
5. A radiocarbon dated specimen from the site of Les Cottès (France)[76], dated between 43,740–42,720 cal BP (the actual radiocarbon date remains unpublished), which differs by 25 mutations to *Denisova 11*'s Neanderthal mother's mtDNA sequence.
6. A lower age limit for *Denisova 11* based on direct U-series analyses of the bone in the range of 65 to 70 ka (Section 7). It was inserted using Oxcal's 'Before' command.

We constructed a model for the age-difference between any two hominins based on:

a) The number of substitutions observed between them. The average time between substitutions is assumed to be τ years. The likelihood for the time difference δ between two hominins with k substitutions is assumed to be given by an Erlang distribution. We define $x = \delta/\tau$ (normalising to substitution time of 1) and then set:

$$x \sim x^{k-1} e^{-x}/(k-1)!$$

The mean of this distribution is k and so the mean likelihood estimate for δ is τk but with an uncertainty which tends to $\tau \sqrt{k}$ for high k values.

b) The mean time τ between each substitution is given a prior:

$$\tau \sim N(2649, 390^2)$$

The number of substitutions data is based on information described previously in Section 4 for the

mtDNA mutation rate (the data is contained in Table S7); L to H = 1.76 to 3.23×10^{-8}. Base-

pairs were taken to be: B = 16569. The time for one mutation was then taken to be in the range: 1/(BH) to 1/(BL), assuming a normal distribution for this with a mean: SubstT = (1/(BH) + 1/(BL))/2 and with a standard error of SubstTSigma = (1/(BL) - 1/(BH))/4. The figures give SubstT = 2649 yr and SubstTSigma = 390 yr.

We used these inferred number of substitutions occurring on branches leading to the mtDNA genomes of individuals from Denisova Cave since their split from the common ancestor shared with other archaic individuals to calculate posterior distribution functions (PDFs) in the age model for these nodal positions. Figure S26 shows the position of these nodal positions or split times in the mtDNA trees for Denisovans and Neanderthals.

Note that no nuclear DNA estimates or tip dates were included in any model.

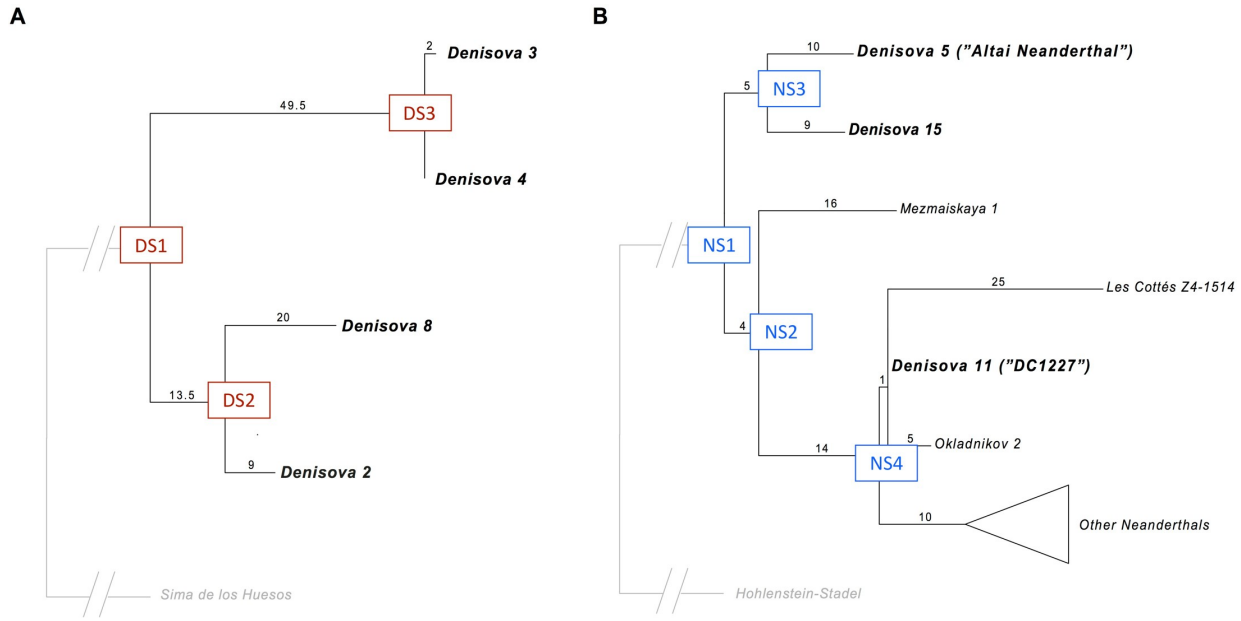

Figure S26. Inferred number of substitutions occurring on branches leading to the mtDNA genomes of individuals from Denisova Cave since their split from the common ancestor shared with other archaic individuals. DS and NS refer to Denisova and Neanderthal split age estimates we used in the Bayesian models to enable us to numerically calculate the split times of the various points on this tree.

In addition, we ran one of the models (Model 1, see below) using a non-informative uniform prior to enable it to find its estimated mutation rate based on the other data in the model (in this case taken over a range of possible values from 2000-10000 years). The result was 3600-8400 yr (at 95.4% probability), compared with the inferred rate of 2649 ± 390 yr.

All models were run with resolution of 250 up to 100k iterations (ie max. 10,000,000 iterations). Model codes are included below as CQL codes designed for OxCal 4.3.

A. Description of each model

Model 1

In this model we tied the age estimate for *Denisova 2* (the oldest Denisovan who lived 50,000– 100,000 years before *Denisova 3*) to two optical ages from layer 22.1 (Main Chamber), its original findspot and we included three optical ages in Layer 21 (Main Chamber). We also included three optical ages from layer 12.3 (East Chamber) and three from 11.2.

Results: Model agreement for Model 1 was 23.3% (it ought to be >60%). While the Agreement index for *Denisova 2* was acceptable, its range was to the very youngest end of the ages in Layer 22.1, and more similar to those from Layer 21. Optical dating of the sediments from layer 22.1 suggests deposition before 287,000 ± 41,000 years ago[89], which does not fit with the genetic age estimates (*Extended Data Figure 6*). *Denisova 2* fits better if instead it is derived from layer 21 (see Model 2). This model is shown in Figure S27.

Model 2

In this model, the parameters were the same but instead of tying *Denisova 2* to Layer 22.1 we placed it with the optical ages in the overlying Layer 21 (Main Chamber). All other parts of the model were the same. This model is shown in Figure S28.

Results: Model agreement was higher at 82.3%, indicating a much better fit between the priors and posterior parts of the model. The age of *Denisova 2* shifted from 189.9-241.7 ka cal BP (Model 1) to 129.5-204.5 ka cal BP. Generally, since Agreement indices are pseudo-Bayes factors, a higher Agreement is significant and suggests this is a more acceptable model than Model 1. The Bayesian model results are more parsimonious with *Denisova 2* being derived from layers overlying the erosional unconformity that separates layers 22.1 and 21.

Model 3

This model is the same as Model 2, the only difference being that *Denisova 11* was moved from Level 12.3 into a post-11.4 level (East Chamber). This was undertaken based on evidence derived from the mtDNA mutation rate estimates which suggests strongly that *Denisova 11* is younger than *Denisova 5*, despite seemingly being excavated from Layer 11.4 just below it. The genetic constraints therefore compel *Denisova 11* to be younger but the stratigraphic sequence priors constrain it to be older. The bone itself was recovered from a bag of small unidentified bones

found in the Layer 12 from the East Chamber, but it may be that it was originally deposited higher up in the stratigraphic sequence. This model is shown in Figure S29.

Results: The model produced an Agreement index of 111.0%; equal highest of all models. All posterior results are similar to Model 2, the only difference being the age for *Denisova 11* which ranges from 115-142 ka BP in Models 1-2 to ~79,200-117,500 cal BP for model 3.

Model 4

This model is the same as Model 3, the only difference being the addition of a U-series date for *Denisova 11* as a minimum age.

Results: The model produced an Agreement index of 111%; equal highest of all models. All posterior results are similar to Model 3, hence the addition of the U-series date does not change the resulting distributions in any significant manner. The age of Denisova 11 under Model 4 is 79,300-118,100 years. This model is shown in Figure S30. This is our favoured model.

The human fossil age estimates calculated for all models are shown in Table S15 for comparison. When we compare the branch shortening age estimates for the nuclear data from *Denisova 3* and *Denisova 5* (Table S5) determined using transversion polymorphisms only and assuming a divergence time to the common ancestor of humans and chimpanzee of 13 million years, with our age estimates (Table S15), we observe that Models 3 and 4 are in closest agreement.

Table S15. Comparisons of age estimates (in thousand years ago) returned for each of the Bayesian models we describe above. The agreement index of each model is shown in the second row. All ranges are at 95.4% probability. The age for Denisova 14 is not modelled, it is the result of the direct AMS date on it.

	Model 1 (ka)	**Model 2 (ka)**	**Model 3 (ka)**	**Model 4 (ka)**
Model agreement index %	*23.3*	*82.3*	*111*	*111*
Denisova 14	45.9–50	45.9–50	45.9–50	45.9–50
Denisova 11	121.8–142.5	115.7–140.9	79.2–117.5	79.3–118.1
Denisova 5	96.4–134.8	92.8–132.0	91.0–129.8	90.9–130.0
Denisova 15	97.9–134.9	94.0–132.1	91.5–130.1	91.4–130.3
Denisova 3	51.7–75.1	51.9–70.3	51.6–76.9	51.6–76.2
Denisova 4	56.2–88.1	55.7–81.2	55.4–84.9	55.2–84.1
Denisova 8	114.5–138.6	107.2–136.4	105.7–136.3	105.6–136.4
Denisova 2	189.9–241.7	129.5–204.5	122.8–194.4	122.7–194.4

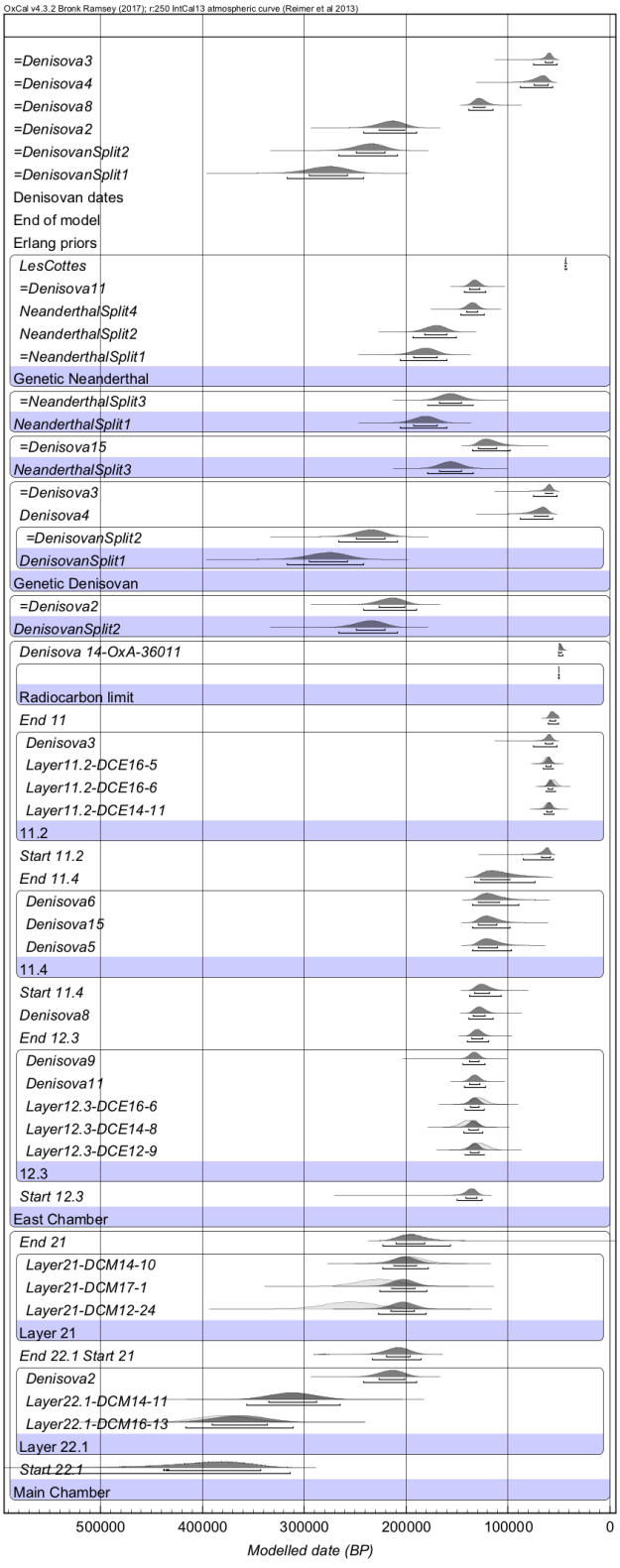

Figure S27. Bayesian age Model 1. Note the young age for *Denisova 2* compared with the optical ages in the same context.

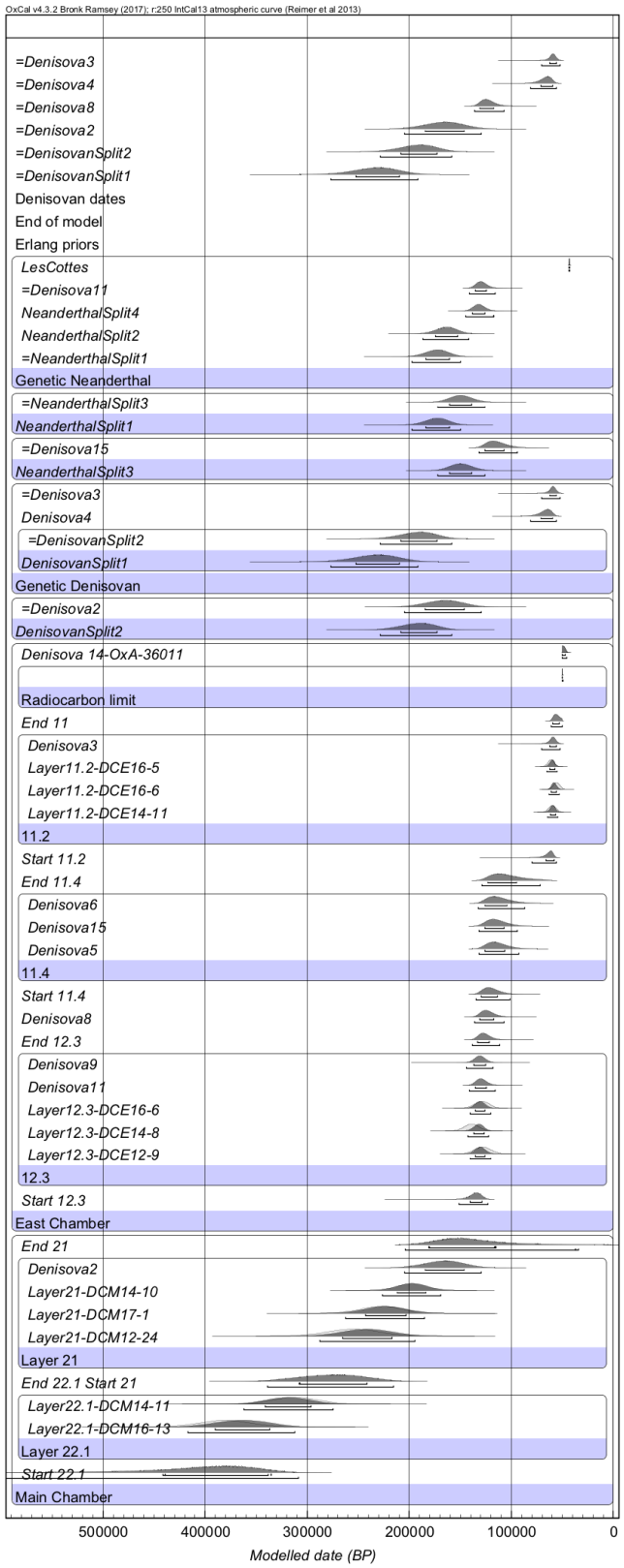

Figure S28. Bayesian age Model 2.

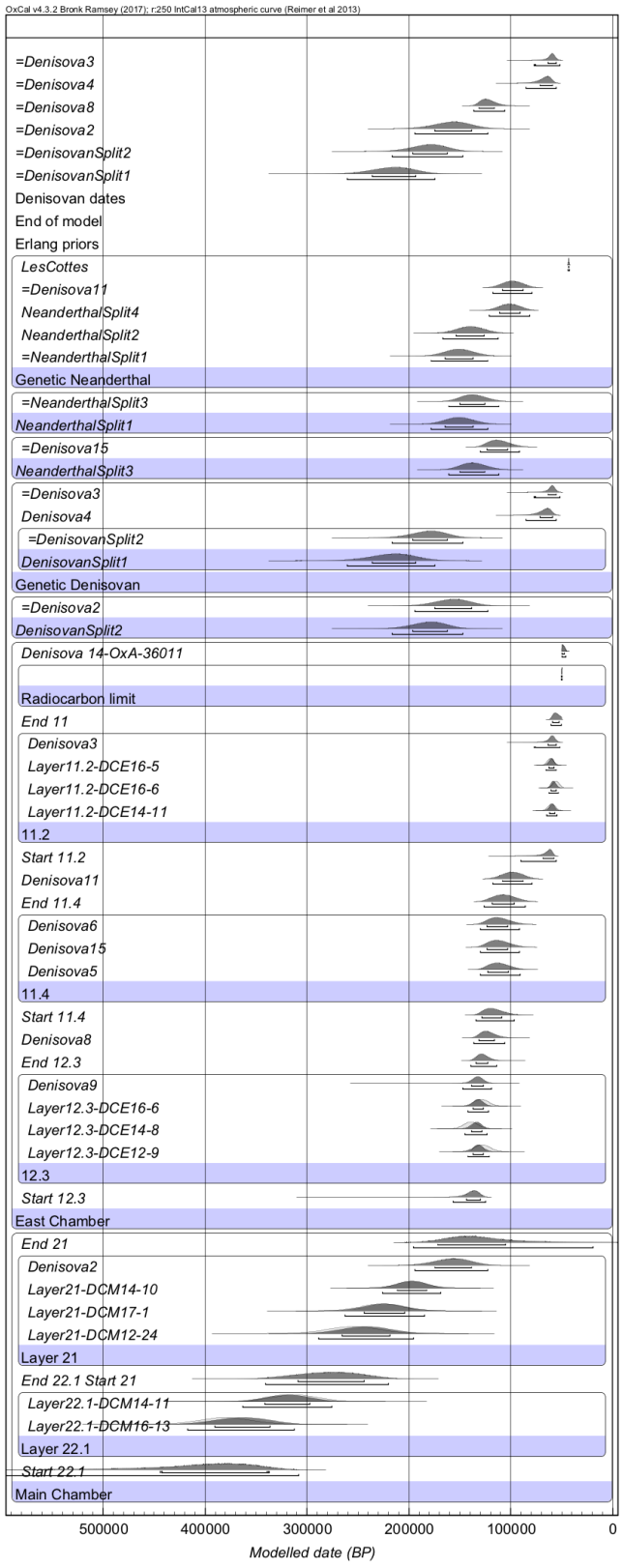

Figure S29. Bayesian age Model 3. In this model *Denisova 11* is moved to be later than the age for *Denisova 6, 15* and *5* in Layer 11.4.

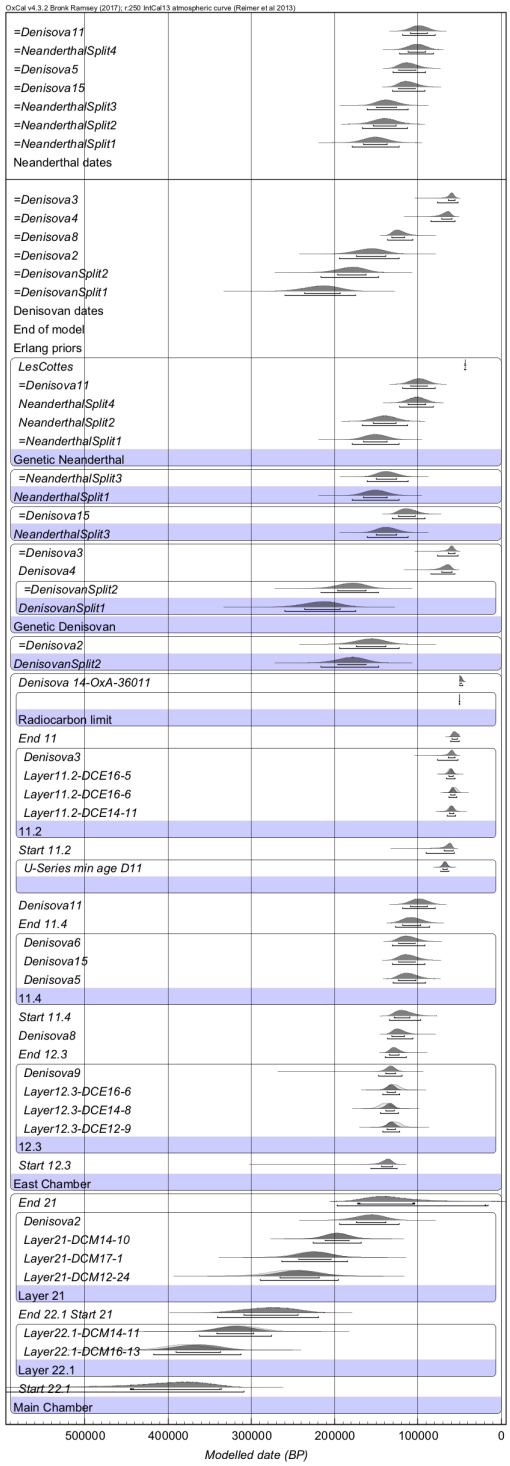

Figure S30. Bayesian age Model 4. In this model we added the Uranium series minimum age to *Denisova 11*.

CQL model code for the Bayesian models described above.

Model 1

```
Options()
{
Resolution=250;
kIterations=100;
};
/* For mitochondrial mutation rate taken to be in
95% range:
L to H = 1.76E-08 to 3.23E-08
Basepairs are taked to be:
B = 16569
Time for one mutation is then taken to be in the
range:
1/(BH) to 1/(BL)
We then assume a normal distribution for this
with a mean:
SubstT = (1/(BH) + 1/(BL))/2
and with a standard error of SubstTSigma
= (1/(BL) - 1/(BH))/4 The figures give
SubstT = 2649 yr and Subst_sigma = 390
yr.*/
Plot()
{
// substitution time
ST=N(2649, 390);
// site sequences Sequence("Main
Chamber")
{
Boundary("Start 22.1");
Phase("Layer 22.1")
{
Date("Layer22.1-DCM16-
13",N(calBP(380300),25500));
Date("Layer22.1-DCM14-
11",N(calBP(312000),23500));
Date("Denisova2");
};
Boundary("End 22.1 Start 21");
Phase("Layer 21")
{
Date("Layer21-DCM12- 24",N(calBP(254600),25200));
Date("Layer21-DCM17- 1",N(calBP(226600),20500));
Date("Layer21-DCM14- 10",N(calBP(196900),14600));
};
Boundary("End 21");
};
// site sequences Sequence("East
Chamber")
{
Boundary("Start 12.3");
Phase("12.3")
{
Date("Layer12.3-DCE12- 9",N(calBP(128200),7600));
Date("Layer12.3-DCE14- 8",N(calBP(139000),7300));
Date("Layer12.3-DCE16- 6",N(calBP(129000),7100));
Date("Denisova11");
Date("Denisova9");
};
Boundary("End 12.3");
Date("Denisova8")
{
};
Boundary("Start 11.4");
Phase("11.4")
{
```

```
Date("Denisova5");
Date("Denisova15");
Date("Denisova6");
};
Boundary("End 11.4");
Boundary("Start 11.2");
Phase("11.2")
{
Date("Layer11.2-DCE14-
11",N(calBP(59900),3400));
Date("Layer11.2-DCE16-
6",N(calBP(55700),3100));
Date("Layer11.2-DCE16-
5",N(calBP(61100),2900));
Date("Denisova3");
};
Boundary("End 11");
Before("Radiocarbon limit")
{
Date(N(calBP(50000),100,10));
};
R_F14C("Denisova 14-OxA-36011",
0.00313, 0.00101);
};
// genetic tree for Denisovans
Date("DenisovanSplit2",Denisova2-
ST*Prior("Erl9")); Sequence("Genetic
Denisovan")
{
Date("DenisovanSplit1",DenisovanSplit2-
ST*Prior("Erl13_5"));
Interval("DS1_to_4");
Date("Denisova4");
Interval("DS4_to_3");
Date("=Denisova3");
};

Difference("DS2_to_8","Denisova8","Denis
ovanSplit2");

// genetic tree for Neanderthals
Date("NeanderthalSplit3",Denisova15-
ST*Prior("Erl9"));

Date("NeanderthalSplit1",NeanderthalSplit 3-
ST*Prior("Erl5"));
Sequence("Genetic Neanderthal")
{
Date("=NeanderthalSplit1");
Interval("NS1_to_NS2");
Date("NeanderthalSplit2");
Interval("NS2_to_NS4");
Date("NeanderthalSplit4");
Interval("NS4_to_11"); Date("=Denisova11");
Interval("NS11_to_LesC");
Date("LesCottes",N(calBP(43230),255));
};

Difference("NS3_to_5","Denisova5","Neand
erthalSplit3");
Label("Erlang priors");
s1=DS1_to_4/ST;
Prior("=s1","Erl49_5"); s2=
DS4_to_3/ST;
Prior("=s2","Erl2"); s3=
DS2_to_8/ST;
Prior("=s3","Erl20"); s4=
NS1_to_NS2/ST;
Prior("=s4","Erl4"); s5=
NS2_to_NS4/ST;
Prior("=s5","Erl14"); s6=
NS4_to_11/ST;
Prior("=s6","Erl1"); s7=
NS3_to_5/ST;
Prior("=s7","Erl10"); s8=
NS11_to_LesC/ST;
Prior("=s8","Erl25");
Label("End of model");
```

```
Page();
Label("Denisovan dates"); Plot()
{
Date("=DenisovanSplit1");
Date("=DenisovanSplit2");
Date("=Denisova2");
Date("=Denisova8");
Date("=Denisova4");
Date("=Denisova3");
};
Line();
Label("Neanderthal dates"); Plot()
{
Date("=NeanderthalSplit1");
Date("=NeanderthalSplit2");
Date("=NeanderthalSplit3");
Date("=Denisova15");
Date("=Denisova5");
Date("=NeanderthalSplit4");
Date("=Denisova11");
};
};
```

Model 2

```
Options()
{
Resolution=250;
kIterations=100;
};
/* For mitochondrial mutation rate taken to be in
95% range:
L to H = 1.76E-08 to 3.23E-08
Basepairs are taked to be:
B = 16569
Time for one mutation is then taken to be in the
range:
1/(BH) to 1/(BL)
We then assume a normal distribution for this
with a mean:
SubstT = (1/(BH) + 1/(BL))/2
and with a standard error of
SubstTSigma = (1/(BL) - 1/(BH))/4
The figures give SubstT = 2649 yr and Subst_sigma
= 390 yr.*/
Plot()
{
// substitution time
ST=N(2649, 390);
Sequence("Main Chamber")
{
Boundary("Start 22.1");
Phase("Layer 22.1")
{
Date("Layer22.1-DCM16- 13",N(calBP(380300),25500));
Date("Layer22.1-DCM14- 11",N(calBP(312000),23500));
//  Date("Denisova2");
};
Boundary("End 22.1 Start 21");
Phase("Layer 21")
{
Date("Layer21-DCM12- 24",N(calBP(254600),25200));
Date("Layer21-DCM17- 1",N(calBP(226600),20500));
Date("Layer21-DCM14- 10",N(calBP(196900),14600));
Date("Denisova2");
};
```

```
Boundary("End 21");
};
// site sequences Sequence("East
Chamber")
{
Boundary("Start 12.3");
Phase("12.3")
{
Date("Layer12.3-DCE12-
9",N(calBP(128200),7600));
Date("Layer12.3-DCE14-
8",N(calBP(139000),7300));
Date("Layer12.3-DCE16-
6",N(calBP(129000),7100));
Date("Denisova11");
Date("Denisova9");
};
Boundary("End 12.3");
Date("Denisova8")
{
};
Boundary("Start 11.4");
Phase("11.4")
{
Date("Denisova5");
Date("Denisova15");
Date("Denisova6");
};
//Replaced Nuclear age estimate for D 3 with the
meaned OSL date from layer 11.2
Boundary("End 11.4");
Boundary("Start 11.2");
Phase("11.2")
{
Date("Layer11.2-DCE14-
11",N(calBP(59900),3400));
Date("Layer11.2-DCE16-
6",N(calBP(55700),3100));
Date("Layer11.2-DCE16-
5",N(calBP(61100),2900));
Date("Denisova3");
};
Boundary("End 11");
Before("Radiocarbon limit")
{
Date(N(calBP(50000),100,10));
};
R_F14C("Denisova14-OxA-36011",
0.00313, 0.00101);
};
// genetic tree for Denisovans
Date("DenisovanSplit2",Denisova2-
ST*Prior("Erl9")); Sequence("Genetic
Denisovan")
{
Date("DenisovanSplit1",DenisovanSplit2-
ST*Prior("Erl13_5"));
Interval("DS1_to_4");
Date("Denisova4");
Interval("DS4_to_3");
Date("=Denisova3");
};

Difference("DS2_to_8","Denisova8","Denis
ovanSplit2");
// genetic tree for Neanderthals
Date("NeanderthalSplit3",Denisova15-
ST*Prior("Erl9"));

Date("NeanderthalSplit1",NeanderthalSplit 3-
ST*Prior("Erl5"));
Sequence("Genetic Neanderthal")
{
Date("=NeanderthalSplit1");
Interval("NS1_to_NS2");
Date("NeanderthalSplit2");
Interval("NS2_to_NS4");
```

```
Date("NeanderthalSplit4");
Interval("NS4_to_11"); Date("=Denisova11");
Interval("NS11_to_LesC");
Date("LesCottes",N(calBP(43230),255));
};

Difference("NS3_to_5","Denisova5","Neand
erthalSplit3");
Label("Erlang priors");
s1=DS1_to_4/ST;
Prior("=s1","Erl49_5"); s2=
DS4_to_3/ST;
Prior("=s2","Erl2"); s3=
DS2_to_8/ST;
Prior("=s3","Erl20"); s4=
NS1_to_NS2/ST;
Prior("=s4","Erl4"); s5=
NS2_to_NS4/ST;
Prior("=s5","Erl14"); s6=
NS4_to_11/ST;
Prior("=s6","Erl1"); s7=
NS3_to_5/ST;
Prior("=s7","Erl10"); s8=
NS11_to_LesC/ST;
Prior("=s8","Erl25");
Label("End of model");
Page();
Label("Denisovan dates"); Plot()
{
Date("=DenisovanSplit1");
Date("=DenisovanSplit2");
Date("=Denisova2");
Date("=Denisova8");
Date("=Denisova4");
Date("=Denisova3");
};
Line();
Label("Neanderthal dates"); Plot()
{
Date("=NeanderthalSplit1");
Date("=NeanderthalSplit2");
Date("=NeanderthalSplit3");
Date("=Denisova15");
Date("=Denisova5");
Date("=NeanderthalSplit4");
Date("=Denisova11");
};
};
```

Model 3

```
Options()
{
Resolution=250;
kIterations=100;
};
/* For mitochondrial mutation rate taken to be in
95% range:
L to H = 1.76E-08 to 3.23E-08
Basepairs are taked to be:
B = 16569
Time for one mutation is then taken to be in the
range:
1/(BH) to 1/(BL)
We then assume a normal distribution for this
with a mean:
SubstT = (1/(BH) + 1/(BL))/2
and with a standard error of
SubstTSigma = (1/(BL) - 1/(BH))/4
```

```
The figures give SubstT = 2649 yr and Subst_sigma
= 390 yr.*/
Plot()
{
// substitution time
ST=N(2649, 390);
// site sequences Sequence("Main
Chamber")
{
Boundary("Start 22.1");
Phase("Layer 22.1")
{
Date("Layer22.1-DCM16-
13",N(calBP(380300),25500));
Date("Layer22.1-DCM14-
11",N(calBP(312000),23500));
};
Boundary("End 22.1 Start 21");
Phase("Layer 21")
{
Date("Layer21-DCM12-
24",N(calBP(254600),25200));
Date("Layer21-DCM17-
1",N(calBP(226600),20500));
Date("Layer21-DCM14-
10",N(calBP(196900),14600));
Date("Denisova2");
};
Boundary("End 21");
};
Sequence("East Chamber")
{
Boundary("Start 12.3");
Phase("12.3")
{
Date("Layer12.3-DCE12-
9",N(calBP(128200),7600));
Date("Layer12.3-DCE14-
8",N(calBP(139000),7300));
Date("Layer12.3-DCE16-
6",N(calBP(129000),7100));
Date("Denisova9");
};
Boundary("End 12.3");
Date("Denisova8")
{
};
Boundary("Start 11.4");
Phase("11.4")
{
Date("Denisova5");
Date("Denisova15");
Date("Denisova6");
};
Boundary("End 11.4");
Date("Denisova11");
Boundary("Start 11.2");
Phase("11.2")
{
Date("Layer11.2-DCE14-
11",N(calBP(59900),3400));
Date("Layer11.2-DCE16-
6",N(calBP(55700),3100));
Date("Layer11.2-DCE16-
5",N(calBP(61100),2900));
Date("Denisova3");
};
Boundary("End 11");
Before("Radiocarbon limit")
{
Date(N(calBP(50000),100,10));
};
R_F14C("Denisova 14-OxA-36011",
0.00313, 0.00101);
};
// genetic tree for Denisovans
Date("DenisovanSplit2",Denisova2-
ST*Prior("Erl9"));
```

```
Sequence("Genetic Denisovan")
{
Date("DenisovanSplit1",DenisovanSplit2-
ST*Prior("Erl13_5"));
Interval("DS1_to_4");
Date("Denisova4");
Interval("DS4_to_3");
Date("=Denisova3");
};

Difference("DS2_to_8","Denisova8",
"DenisovanSplit2");
// genetic tree for Neanderthals
Date("NeanderthalSplit3",Denisova15-
ST*Prior("Erl9"));

Date("NeanderthalSplit1",Neandert halSplit3-
ST*Prior("Erl5"));
Sequence("Genetic Neanderthal")
{
Date("=NeanderthalSplit1");
Interval("NS1_to_NS2");
Date("NeanderthalSplit2");
Interval("NS2_to_NS4");
Date("NeanderthalSplit4");
Interval("NS4_to_11"); Date("=Denisova11");
Interval("NS11_to_LesC");
Date("LesCottes",N(calBP(43230),255));
};

Difference("NS3_to_5","Denisova5",
"NeanderthalSplit3");
Label("Erlang priors");
s1=DS1_to_4/ST;
Prior("=s1","Erl49_5"); s2=
DS4_to_3/ST;
Prior("=s2","Erl2");
s3= DS2_to_8/ST;
Prior("=s3","Erl20"); s4=
NS1_to_NS2/ST;
Prior("=s4","Erl4"); s5=
NS2_to_NS4/ST;
Prior("=s5","Erl14"); s6=
NS4_to_11/ST;
Prior("=s6","Erl1"); s7=
NS3_to_5/ST;
Prior("=s7","Erl10"); s8=
NS11_to_LesC/ST;
Prior("=s8","Erl25");
Label("End of model"); Page();
Label("Denisovan dates"); Plot()
{
Date("=DenisovanSplit1");
Date("=DenisovanSplit2");
Date("=Denisova2");
Date("=Denisova8");
Date("=Denisova4");
Date("=Denisova3");
};
Line();
Label("Neanderthal dates"); Plot()
{
Date("=NeanderthalSplit1");
Date("=NeanderthalSplit2");
Date("=NeanderthalSplit3");
Date("=Denisova15");
Date("=Denisova5");
Date("=NeanderthalSplit4");
Date("=Denisova11");
};
};
```

Model 4

```
Options()
{
Resolution=250;
kIterations=100;
};
/* For mitochondrial mutation rate taken to be in
95% range:
L to H = 1.76E-08 to 3.23E-08
Basepairs are taked to be:
B = 16569
Time for one mutation is then taken to be in the
range:
1/(BH) to 1/(BL)
We then assume a normal distribution for this
with a mean:
SubstT = (1/(BH) + 1/(BL))/2
and with a standard error of
SubstTSigma = (1/(BL) - 1/(BH))/4
The figures give SubstT = 2649 yr and Subst_sigma
= 390 yr.*/
Plot()
{
// substitution time
ST=N(2649, 390);
// site sequences Sequence("Main
Chamber")
{
Boundary("Start 22.1");
Phase("Layer 22.1")
{
Date("Layer22.1-DCM16-
13",N(calBP(380300),25500));
Date("Layer22.1-DCM14-
11",N(calBP(312000),23500));
//  Date("Denisova2");
};
Boundary("End 22.1 Start 21");
Phase("Layer 21")
{
Date("Layer21-DCM12- 24",N(calBP(254600),25200));
Date("Layer21-DCM17- 1",N(calBP(226600),20500));
Date("Layer21-DCM14- 10",N(calBP(196900),14600));
Date("Denisova2");
};
Boundary("End 21");
};
Sequence("East Chamber")
{
Boundary("Start 12.3");
Phase("12.3")
{
Date("Layer12.3-DCE12- 9",N(calBP(128200),7600));
Date("Layer12.3-DCE14- 8",N(calBP(139000),7300));
Date("Layer12.3-DCE16- 6",N(calBP(129000),7100));
Date("Denisova9");
};
Boundary("End 12.3");
Date("Denisova8")
{
};
Boundary("Start 11.4");
Phase("11.4")
{
Date("Denisova5");
Date("Denisova15");
Date("Denisova6");
};
```

```
Boundary("End 11.4");
Date("Denisova11"); Before()
{
Date("U-Series min age
D11",N(calBP(67500),2500));
};
Boundary("Start 11.2");
Phase("11.2")
{
Date("Layer11.2-DCE14-
11",N(calBP(59900),3400));
Date("Layer11.2-DCE16-
6",N(calBP(55700),3100));
Date("Layer11.2-DCE16-
5",N(calBP(61100),2900));
Date("Denisova3");
};
Boundary("End 11");
Before("Radiocarbon limit")
{
Date(N(calBP(50000),100,10));
};
R_F14C("Denisova 14-OxA-36011",
0.00313, 0.00101);
};
// genetic tree for Denisovans
Date("DenisovanSplit2",Denisova2-
ST*Prior("Erl9")); Sequence("Genetic
Denisovan")
{
Date("DenisovanSplit1",DenisovanSplit2-
ST*Prior("Erl13_5"));
Interval("DS1_to_4");
Date("Denisova4");
Interval("DS4_to_3");
Date("=Denisova3");
};
Difference("DS2_to_8","Denisova8","Denis
ovanSplit2");
// genetic tree for Neanderthals
Date("NeanderthalSplit3",Denisova15-
ST*Prior("Erl9"));

Date("NeanderthalSplit1",NeanderthalSplit 3-
ST*Prior("Erl5"));
Sequence("Genetic Neanderthal")
{
Date("=NeanderthalSplit1");
Interval("NS1_to_NS2");
Date("NeanderthalSplit2");
Interval("NS2_to_NS4");
Date("NeanderthalSplit4");
Interval("NS4_to_11"); Date("=Denisova11");
Interval("NS11_to_LesC");
Date("LesCottes",N(calBP(43230),255));
};

Difference("NS3_to_5","Denisova5","Neand
erthalSplit3");
Label("Erlang priors");
s1=DS1_to_4/ST;
Prior("=s1","Erl49_5"); s2=
DS4_to_3/ST;
Prior("=s2","Erl2"); s3=
DS2_to_8/ST;
Prior("=s3","Erl20"); s4=
NS1_to_NS2/ST;
Prior("=s4","Erl4"); s5=
NS2_to_NS4/ST;
Prior("=s5","Erl14"); s6=
NS4_to_11/ST;
Prior("=s6","Erl1"); s7=
NS3_to_5/ST;
Prior("=s7","Erl10"); s8=
NS11_to_LesC/ST;
```

```
Prior("=s8","Erl25");
Label("End of model");
Page();
Label("Denisovan dates"); Plot()
{
Date("=DenisovanSplit1");
Date("=DenisovanSplit2");
Date("=Denisova2");
Date("=Denisova8");
Date("=Denisova4");
Date("=Denisova3");
};
Line();
Label("Neanderthal dates"); Plot()
{
Date("=NeanderthalSplit1");
Date("=NeanderthalSplit2");
Date("=NeanderthalSplit3");
Date("=Denisova15");
Date("=Denisova5");
Date("=NeanderthalSplit4");
Date("=Denisova11");
};
};
```

Erlang model

```
Plot()
{
P(Erl49_5, 0.1, 200, exp(48.5*ln(Erl49_5)-Erl49_5), 0.1);
P(Erl25, 0.1, 200, exp(24*ln(Erl25)-Erl25), 0.1);
P(Erl20, 0.1, 200, exp(19*ln(Erl20)-Erl20), 0.1);
P(Erl14, 0.1, 200, exp(13*ln(Erl14)-Erl14), 0.1);
P(Erl13_5, 0.1, 200, exp(12.5*ln(Erl13_5)-Erl13_5), 0.1);
P(Erl10, 0.1, 200, exp(9*ln(Erl10)-Erl10), 0.1);
P(Erl9, 0.1, 200, exp(8*ln(Erl9)-Erl9), 0.1);
P(Erl5, 0.1, 200, exp(4*ln(Erl5)-Erl5), 0.1);
P(Erl4, 0.1, 200, exp(3*ln(Erl4)-Erl4), 0.1);
P(Erl2, 0.1, 200, exp(1*ln(Erl2)-Erl2), 0.1);
P(Erl1, 0, 20, exp(-Erl1), 0.01);
};
```

SUPPLEMENTARY REFERENCES

1 Derevianko, A. P., Shunkov, M. V., Agadzhanyan, A. K., Baryshnikov, G. F., Malaeva, E. M., Ulianov, V. A., Kulik, N. A., Postnov, A. V., Anoikin, A. A. *Prirodnaya sreda i chelovek v paleolite Gornogo Altaya*. Novosibirsk: IAET SB RAS. 448 p. (in Russian) (2003).

2 Okladnikov, A. P. & Ovodov, N. D. Paleoliticheskaya stoyanka v Denisovoi peshchere na Altae.
Archaeological discoveries 1977. Moskow: Nauka Publ., pp. 266–268. (in Russian) (1978).

3 Derevianko, A. P. & Molodin, V. I. *Denisova peshchera*. Novosibirsk: Nauka Publ. Part 1. 262
p. (in Russian) (1994).

4 Ulianov, V. A., Kozlikin, M. B., Belousova, N. E., Shunkov, M. V. Stroenie pleistotsenovykh otlozhenii v tsentral'nom zale Denisovoi peshchery. *Problems of Archaeology, Ethnography, Anthropology of Siberia and Neighboring Territories*. Novosibirsk: IAET SB RAS. pp. 169–172. (in Russian) (2016).

5 Ulianov, V. A. & Shunkov, M. V. Nekotorye osobennosti sedimentogeneza v vostochnoi galeree Denisovoi peshchery. *Problems of Archaeology, Ethnography, Anthropology of Siberia and Neighboring Territories*. Novosibirsk: IAET SB RAS. pp. 159–162. (in Russian) (2013).

6 Ulianov, V. A., Kozlikin, M. B., Shunkov, M. V. Stroenie razreza pleistotsenovykh otlozhenii v vostochnoi galeree Denisovoi peshchery (po dannym raskopok 2015 goda). *Problems of Archaeology, Ethnography, Anthropology of Siberia and Neighboring Territories*. Novosibirsk: IAET SB RAS. pp. 157–160. (in Russian) (2015).

7 Derevianko, A. P. & Shunkov, M. V. Middle Palaeolithic industries with foliate bifaces in Altai Mountains. *Archaeology, Ethnology and Anthropology of Eurasia* **1**, 16–42 (2002).

8 Derevianko, A. P. & Shunkov, M. V. Formation of the Upper Palaeolithic Traditions in the Altai. *Archaeol. Ethnol. Anthropol. Eurasia* **3**, 12–40 (2004).

9 Reich, D., et al. Genetic history of an archaic hominin group from Denisova Cave in Siberia.
Nature **468**(7327), 1053–1960 (2010).

10 Viola, B. T, Markin, S. V., Buzhilova, A. P., Mednikova, M. B., Dobrovolskaya, M. V., Le Cabec, A., Shunkov, M. V., Derevianko, A. P., Hublin, J.-J. New Neanderthal remains from Chagyrskaya Cave (Altai Mountains, Russian Federation). *American Journal of Physical Anthropology* **147**(Suppl. 54), 293–294 (2012).

11 Derevianko, A. P., Shunkov, M. V. & Markin S. V. *The dynamics of the Palaeolithic industries in Africa and Eurasia in the Late Pleistocene and the issue of the* Homo sapiens *origin*. Novosibirsk: IAET SB RAS. 228 p. (2014).

12 Slon, V., et al. A fourth Denisovan individual. *Sci. Advances* **3**(7), p. e1700186 (2017).

13 Slon, V. et al. Neandertal and Denisovan DNA from Pleistocene sediments. *Science* **356**, 605–608 (2017).

14 Fu, Q., et al. Genome sequence of a 45,000-year-old modern human from western Siberia. *Nature* **514** (7523), 445–449 (2014).
15 Brock, F., Higham, T. F. G, Ditchfield, P., Ramsey, C. B. Current Pretreatment Methods for AMS Radiocarbon Dating at the Oxford Radiocarbon Accelerator Unit (ORAU). *Radiocarbon* **52**, 103–112 (2010).
16 Devièse, T., Comeskey, D., McCullagh, J., Ramsey,. C B., Higham, T. New protocol for compound specific radiocarbon analysis of archaeological bones. *Rapid Communications in Mass Spectrometry* **32**, 373-379 (2018).
17 Bird, M. I. *et al.* Radiocarbon Dating of 'Old' Charcoal Using a Wet Oxidation, Stepped- Combustion Procedure. *Radiocarbon* **41**, 127–140 (1999).
18 Ramsey, C. OxCal 4.2 Web Interface Build(78) (2013).
19 Reimer, P. J. *et al.* IntCal13 and Marine13 Radiocarbon Age Calibration Curves 0–50,000 Years cal BP. *Radiocarbon* **55**, 1869–1887 (2013).
20 Turner, C. G. in *Chronostratigraphy of the Palaeolithic in North, Central, East Asia and America*, A. P. Derevianko, Eds. (Novosibirsk: Institute of History, Philology and Philosophy, Siberian Branch of the USSR Academy of Sciences), pp. 239-243 (1990).
21 Shpakova, E. G. & Derevianko, A. P. The interpretation of odontological features of Pleistocene human remains from the Altai. *Archaeol. Ethnol. Anthropol. Eurasia* **1**, 125–138 (2000).
22 Shpakova, E. G. Paleolithic human dental remains from Siberia. *Archaeol. Ethnol. Anthropol. Eurasia* **4** (8), 64–76 (2001).
23 Bailey, S. Beyond shovel-shaped incisors: Neandertal morphology in a comparative context.
Periodicum Biologorum **108** (3), 253–267 (2006).
24 Krause, J., et al. The complete mitochondrial DNA genome of an unknown hominin from southern Siberia. *Nature* **464**(7290), 894–897 (2010).
25 Meyer, M., et al. A high-coverage genome sequence from an archaic Denisovan individual.
Science **338**(6104), 222–226 (2012).
26 Sawyer, S., et al. Nuclear and mitochondrial DNA sequences from two Denisovan individuals.
Proc. Natl. Acad. Sci. USA **112**(51), 15696–15700 (2015).
27 Mednikova, M. B. A. Proximal pedal phalanx of a Paleolithic hominin from Denisova Cave, Altai. *Archaeol. Ethnol. Anthropol. Eurasia* **39**, 129–138 (2011).
28 Prüfer, K., et al. The complete genome sequence of a Neanderthal from the Altai Mountains.
Nature **505**(7481), 43–49 (2014).
29 Mednikova, M. Distal Phalanx of the Hand of Homo from Denisova Cave Stratum 12: A Tentative Description. *Archaeol. Ethnol. Anthropol. Eurasia* **41**, 146–155 (2013).
30 Brown, S. et al. Identification of a new hominin bone from Denisova Cave, Siberia using collagen fingerprinting and mitochondrial DNA analysis. *Scientific Reports* **6**, doi:10.1038/srep23559 (2016).
31 Prüfer, K., et al. A high-coverage Neandertal genome from Vindija Cave in Croatia. *Science*

358(6363), 655–658 (2017).
32 Narasimhan, V.M, et al. Estimating the human mutation rate from autozygous segments reveals population differences in human mutational processes. *Nature Communications* **8** (1), 303 (2017).
33 Scally, A. & Durbin, R. Revising the human mutation rate: implications for understanding human evolution. *Nature Reviews Genetics* **13**, 745–753 (2012).
34 Slon, V., et al. The genome of the offspring of a Neandertal mother and a Denisovan father.
Nature **561**, 113–116 (2018).
35 Dabney, J., et al. Complete mitochondrial genome sequence of a Middle Pleistocene cave bear reconstructed from ultrashort DNA fragments. *Proc Natl Acad Sci USA* **110**(39), 15758– 15763 (2013).
36 Korlević, P., et al. Reducing microbial and human contamination in DNA extractions from ancient bones and teeth. *Biotechniques* **59**(2), 87–93 (2015).
37 Gansauge, M.T., et al. Single-stranded DNA library preparation from highly degraded DNA using T4 DNA ligase. *Nucleic Acids Res.* **45**(10): e79 (2017).
38 Kircher, M., S. Sawyer, and M. Meyer. Double indexing overcomes inaccuracies in multiplex sequencing on the Illumina platform. *Nucleic Acids Res.* 40(1): e3 (2012).
39 Fu, Q., et al., DNA analysis of an early modern human from Tianyuan Cave, China. *Proc Natl Acad Sci USA* **110**(6), 2223–2227 (2013).
40 Renaud, G., Stenzel, U. & Kelso, J. leeHom: adaptor trimming and merging for Illumina sequencing reads. *Nucleic Acids Res.* **42**(18), 141 (2014).
41 Li, H. & Durbin, R. Fast and accurate long-read alignment with Burrows-Wheeler transform.
Bioinformatics **26**(5), 589–595 (2010).
42 Briggs, A.W., et al. Patterns of damage in genomic DNA sequences from a Neandertal. *Proc Natl Acad Sci USA* **104**(37), 14616–14621 (2007).
43 Huson, D. H., et al. MEGAN analysis of metagenomic data. *Genome Res*. **17**(3), 377–386 (2007).
44 Slon, V., et al. Mammalian mitochondrial capture, a tool for rapid screening of DNA preservation in faunal and undiagnostic remains, and its application to Middle Pleistocene specimens from Qesem Cave (Israel). *Quaternary International* **398**, 210–218 (2016).
45 Prüfer, K. & Meyer, M. Comment on "Late Pleistocene human skeleton and mtDNA link Paleoamericans and modern Native Americans". *Science* **347**(6224), 835 (2015).
46 Meyer, M., et al. A mitochondrial genome sequence of a hominin from Sima de los Huesos.
Nature **505**(7483), 403-406 (2014).
47 Green, R. E., et al. A complete Neandertal mitochondrial genome sequence determined by high-throughput sequencing. *Cell* **134**(3), 416–426 (2008).
48 Li, H., et al. The Sequence Alignment/Map format and SAMtools. *Bioinformatics* 25(16), 2078–2079 (2009).
49 Li, M. K., et al. Detecting Heteroplasmy from high-throughput sequencing of complete human mitochondrial DNA genomes. *American Journal of Human*

Genetics **87**(2), 237–249 (2010).
50 Tamura, K., et al. MEGA6: Molecular Evolutionary Genetics Analysis version 6.0. *Mol Biol Evol*. 30(12), 2725–2729 (2013).
51 Katoh, K. & Standley, D. M. MAFFT multiple sequence alignment software version 7: improvements in performance and usability. *Mol Biol Evol* **30**(4), 772–780 (2013).
52 Schliep, K.P. phangorn: phylogenetic analysis in R. *Bioinformatics* **27**(4), 592–593 (2011).
53 Posth, C., et al. Deeply divergent archaic mitochondrial genome provides lower time boundary for African gene flow into Neanderthals. *Nature Communications* **8**, 16046 (2017).
54 Drummond, A. J. et al. Bayesian Phylogenetics with BEAUti and the BEAST 1.7. *Molecular Biology and Evolution* **29**(8), 1969–1973 (2012).
55 Fu, Q., et al. A revised timescale for human evolution based on ancient mitochondrial genomes. *Curr Biol* **23**(7), 553–559 (2013).
56 Tamura, K. & Nei, M. Estimation of the number of nucleotide substitutions in the control region of mitochondrial DNA in humans and chimpanzees. *Mol Biol Evol* **10**(3), 512–526 (1993).
57 Darriba, D., et al. jModelTest 2: more models, new heuristics and parallel computing. *Nat Methods* **9**(8), 772 (2012).
58 Kass, R. E. & Raftery, A. E. Bayes Factors. *Journal of the American Statistical Association* **90**(430), 773–795 (1995).
59 Bronk Ramsey, C. Methods for Summarizing Radiocarbon Datasets. *Radiocarbon* **59**(6), 1809–1833 (2017).
60 Ermini, L., et al., Complete mitochondrial genome sequence of the Tyrolean Iceman. Curr Biol, 18(21): p. 1687–1693 (2008).
61 Hedges, R.E.M., et al. Radiocarbon-Dates from the Oxford AMS System. Archaeometry Datelist 15. *Archaeometry* **34**, 337–357 (1992).
62 Krause, J., et al., A Complete mtDNA Genome of an Early Modern Human from Kostenki, Russia. *Current Biology* **20**(3): 231–236 (2010).
63 Marom, A., et al., Single amino acid radiocarbon dating of Upper Paleolithic modern humans. *Proceedings of the National Academy of Sciences of the United States of America* **109**(18): 6878–6881 (2012).
64 Delsate, D., Guinet, J. M. & Saverwyns, S. De l'ocre sur le crâne mésolithique (haplogroupe U5a) de Reuland-Loschbour (Grand-Duché de Luxembourg)? *Bull. Soc. Préhist. Luxembourgeoise* **31**, 7–30 (2009).
65 Gilbert, M. T., et al., Paleo-Eskimo mtDNA genome reveals matrilineal discontinuity in Greenland. *Science* **320**(5884), 178–179 (2008).
66 Rasmussen, M., et al., Ancient human genome sequence of an extinct Palaeo-Eskimo. Nature
463(7282), 757–762 (2010).
67 Shang, H., et al. An early modern human from Tianyuan cave, Zhoukoudian, China. *Proceedings of the National Academy of Sciences of the USA* **104**(16), 6573–6578 (2007).
68 Briggs, A.W., et al. Targeted retrieval and analysis of five Neandertal mtDNA genomes.
Science **325**(5938), 318–321

(2009).
69 Schmitz, R.W., et al. The Neandertal type site revisited: Interdisciplinary investigations of skeletal remains from the Neander Valley, Germany. *Proceedings of the National Academy of Sciences of the United States of America* **99**(20), 13342–13347 (2002).
70 Ingman, M., et al. Mitochondrial genome variation and the origin of modern humans. *Nature*
408(6813), 708–713 (2000).
71 Rougier, H., et al., Neandertal cannibalism and Neandertal bones used as tools in Northern Europe. *Scientific Reports* **6** (2016).
72 Ingman, M. & Gyllensten, U. Mitochondrial genome variation and evolutionary history of Australian and New Guinean aborigines. *Genome Res* **13**(7), 1600–1606 (2003).
73 Mishmar, D., et al. Natural selection shaped regional mtDNA variation in humans. *Proc Natl Acad Sci USA* **100**(1), 171–176 (2003).
74 Maca-Meyer, N., et al. Major genomic mitochondrial lineages delineate early human expansions. *BMC Genet* **2**, 13 (2001).
75 Achilli, A., et al. Saami and Berbers-an unexpected mitochondrial DNA link. *Am J Hum Genet*
76(5), 883–886 (2005).
76 Hajdinjak, M., et al. Reconstructing the Genetic History of Late Neandertals. *Nature* **555**, 652–656 (2018).
77 Pinhasi, R., et al. Revised age of late Neanderthal occupation and the end of the Middle Paleolithic in the northern Caucasus. *Proceedings of the National Academy of Sciences of the USA* **108**(21), 8611-8616 (2011).
78 Skoglund, P., et al. Separating endogenous ancient DNA from modern day contamination in a Siberian Neandertal. *Proc Natl Acad Sci USA* 111(6), 2229–2234 (2014).
79 Semal, P. et al. New Data on the Late Neandertals: Direct Dating of the Belgian Spy Fossils.
American Journal of Physical Anthropology 138(4), 421–428 (2009).
80 Serre, D. et al. No evidence of Neandertal mtDNA contribution to early modern humans. *Plos Biology* 2(3), 313–317 (2014).
81 Gansauge, M. T. & Meyer, M. Selective enrichment of damaged DNA molecules for ancient genome sequencing. *Genome Res*. **24**(9):1543–1549 (2014).
82 Horai, S., et al. Recent African origin of modern humans revealed by complete sequences of hominoid mitochondrial DNAs. *Proc Natl Acad Sci USA* **92**(2), 532–536 (1995).
83 Huntley, D. J., Godfrey-Smith, D. I. & Thewalt, M. L. W. Optical dating of sediments. *Nature*
313, 105–107 (1985).
84 Hütt, G., Jaek, I. & Tchonka, J. Optical dating: K-feldspars optical response stimulation spectra. *Quat. Sci. Rev.* **7**, 381–385 (1988).
85 Aitken, M. J. *An Introduction to Optical Dating: the dating of Quaternary sediments by the use of photon-stimulated luminescence* (Oxford Univ.

Press, Oxford, 1998).
86 Jacobs, Z. & Roberts, R. G. Advances in optically stimulated luminescence dating of individual grains of quartz from archeological deposits. *Evol. Anthropol.* **16**, 210–223 (2007).
87 Wintle, A. G. in *Treatise on Geochemistry*, 2nd ed. (eds Holland, H. D. & Turekian, K. K.), **14**, 17–35 (Elsevier, Oxford, 2014).
88 Roberts, R. G. *et al.* Optical dating in archaeology: thirty years in retrospect and grand challenges for the future. *J. Archaeol. Sci.* **56**, 41–60 (2015).
89 Jacobs, Z. *et al*. Timing of archaic hominin occupation of Denisova Cave in southern Siberia.
Nature (in press 2018).
90 Bøtter-Jensen, L. & Mejdahl, V. Assessment of beta dose-rate using a GM multicounter system. *Nucl. Tracks Radiat. Meas.* **14**, 187–191 (1988).
91 Jacobs, Z. & Roberts, R. G. An improved single grain OSL chronology for the sedimentary deposits from Diepkloof Rockshelter, Western Cape, South Africa. *J. Archaeol. Sci.* **63**, 175– 192 (2015).
92 Mercier, N. & Falguères, C. Field gamma dose-rate measurement with a NaI(Tl) detector: re-evaluation of the "threshold" technique. *Anc. TL* **25**, 1–4 (2007).
93 Rhodes, E. J. & Schwenninger, J. L. Dose rates and radioisotopes in the concrete calibration blocks at Oxford. *Anc. TL* **25**, 5–8 (2007).
94 Prescott, J. R. & Hutton, J. T. Cosmic ray contributions to dose rates for luminescence and ESR dating: large depths and long-term time variations. *Radiat. Meas.* **23**, 497–500 (1994).
95 Huntley, D. J. & Hancock, R. G. V. The Rb contents of the K-feldspars being measured in optical dating. *Anc. TL* **19**, 43–46 (2001).
96 Duller, G. A. T. Single-grain optical dating of Quaternary sediments: why aliquot size matters in luminescence dating. *Boreas* **37**, 589–612 (2008).
97 Bøtter-Jensen, L., Andersen, C. E., Duller, G. A. T. & Murray, A. S. Developments in radiation, stimulation and observation facilities in luminescence measurements. *Radiat. Meas.* **37**, 535–541 (2003).
98 Galbraith, R. F., Roberts, R. G., Laslett, G. M., Yoshida, H. & Olley, J. M. Optical dating of single and multiple grains of quartz from Jinmium rock shelter, northern Australia: Part I, experimental design and statistical models. *Archaeometry* **41**, 339–364 (1999).
99 Murray, A. S. & Wintle, A. G. Luminescence dating of quartz using an improved single- aliquot regenerative-dose protocol. *Radiat. Meas.* **32**, 57–73 (2000).
100 Thomsen, K. J., Murray, A. S., Jain, M. & Bøtter-Jensen, L. Laboratory fading rates of various luminescence signals from feldspar-rich sediment extracts. *Radiat. Meas.* **43**, 1474–1486 (2008).
101 Li, B., Jacobs, Z., Roberts, R. G. & Li, S. H. Review and assessment of the potential of post-IR IRSL dating methods to circumvent the problem of anomalous fading in feldspar luminescence. *Geochronometria* **41**, 178–201 (2014).

102 Blegen, N. *et al*. Distal tephras of the eastern Lake Victoria basin, equatorial East Africa: correlations, chronology and a context for early modern humans. *Quat. Sci. Rev.* **122**, 89– 111 (2015).

103 Li, B., Roberts, R. G., Jacobs, Z. & Li, S. H. Single-grain dating of potassium-rich feldspar grains: towards a global standardised growth curve for the post-IR IRSL signal. *Quat. Geochronol.* **45**, 23–36 (2018).

104 Li, B., Jacobs, Z. & Roberts, R. G. An improved multiple-aliquot regenerative-dose (MAR) procedure for post-IR IRSL dating of K-feldspar. *Anc. TL* **35**, 1–10 (2017).

105 Galbraith, R.F. & Roberts, R. G. Statistical aspects of equivalent dose and error calculation and display in OSL dating: an overview and some recommendations. *Quat. Geochronol.* **11**, 1–27 (2012).

106 Roberts, R. G., Galbraith, R. F., Yoshida, H., Laslett, G. M. & Olley, J. M. Distinguishing dose populations in sediment mixtures: a test of single-grain optical dating procedures using mixtures of laboratory-dosed quartz. *Radiat. Meas.* **32**, 459–465 (2000).

107 Powell, R., Hergt, J. & Woodhead, J. Improving isochron calculations with robust statistics and the bootstrap. *Chem. Geol.* **185**, 191–204 (2002).

108 Rousseeuw, P. J., Debruyne, M., Engelen, S. & Hubert, M. Robustness and outlier detection in chemometrics. *Crit. Rev. Anal. Chem.* **36**, 221–242 (2006).

109 Grün, R., Eggins, S., Kinsley, L., Mosely, H., Sambridge, M. Laser ablation U-series analysis of fossil bones and teeth. Palaeogeography, Palaeoclimatology, Palaeoecology **416**, 150- 167 (2014).

110 Paul, D., White, W.M., & Turcotte, D.L. Constraints on the $^{232}Th/^{238}U$ ratio (k) of the continental crust. Geochem. Geophys. Geosyst., **4**(12), 1102, 1-17 (2003).

111 Buckley, M., Collins, M., Thomas-Oates, J., Wilson, J.C. Species Identification by Analysis of Bone Collagen Using Matrix-Assisted Laser Desorption/ionisation Time-of-Flight Mass Spectrometry. *Rapid Communications in Mass Spectrometry*: RCM **23** (23), 3843–54 (2009).

112 Buckley, M., & Kansa Whitcher, S. Collagen Fingerprinting of Archaeological Bone and Teeth Remains from Domuztepe, South Eastern Turkey. *Archaeological and Anthropological Sciences* **3** (3), 271–280 (2011).

113 Kirby, D. P., Buckley, M., Promise, E., Trauger, S.A., Holdcraft, T.R. Identification of Collagen- Based Materials in Cultural Heritage. *The Analyst* **138** (17), 4849–58 (2013).

Manuscript B – 2020. Brown., S., Douka, K., Collins, M., Richter, K. On the standardization of ZooMS nomenclature. Journal of Proteomics.

On the Standardization of ZooMS Nomenclature

Journal of Proteomics

Authors

Samantha Brown*

Max Planck Institute for the Science of Human History, Jena, Germany

brown@shh.mpg.de

Katerina Douka

Max Planck Institute for the Science of Human History, Jena, Germany

douka@shh.mpg.de

Matthew Collins

Section for Evolutionary Genomics, University of Copenhagen, 1165 København

Department of Archaeology, University of Cambridge, Cambridge CB2 3DZ

matthew@palaeome.org

Kristine Korzow Richter*

Max Planck Institute for the Science of Human History, Jena, Germany

krichter@shh.mpg.de, kkrichter@palaeome.org

* Corresponding author

Acknowledgements

We would like to thank Frido Welker and Daniel Kirby for comprehensive discussions and feedback on multiple versions of the manuscript. We would like to thank the staff of the Department of Archaeology, Max Planck Institute for the Science of Human History, for facilitating this work, in particular Nicole Boivin. This work received support from the European Research Council (ERC) under the European Union's Horizon 2020 research and innovation program, grant agreement 715069-FINDER-ERC-2016-STG, awarded to Katerina Douka, and the Max Planck Society. We would like to thank Alberto Tauozzi, Theis Jensen, Abigail Desmond, Maria Codlin and Carli Peters for discussions surrounding issues with the previous nomenclature system.

On the Standardization of ZooMS Nomenclature

Abstract

Zooarchaeology by Mass Spectrometry (ZooMS) is rapidly becoming a staple in archaeological and cultural heritage science. Developed a decade ago, this peptide mass fingerprinting technique is expanding from a small group of researchers mainly involved in method development to a broader group of scientists using it as another tool in their toolboxes. With new researchers beginning to use the method, it is imperative that a user-friendly, standardized approach be established. A major barrier has been the often haphazard and changing nomenclature used to label peptide markers necessary for taxonomic identification. Consistent, reliable, and easy-to-understand nomenclature is key to the growth of ZooMS, particularly as the reference library continues to expand. We propose a new set of standardised guidelines for peptide markers based on their position in the type I collagen sequence from the beginning of the highly conserved, helical region. Since this region has no insertions or deletions over a wide range of taxonomic groups, the proposed nomenclature system can be used reliably and consistently across all vertebrate taxa. We propose to label ZooMS peptide markers with the gene, followed by the position of the first and last amino acid of the marker from the start of the helical region.

Significance Statement

We propose a standardised nomenclature system for ZooMS peptide markers that provides consistent labels across multiple, broad taxonomic groups. This system unambiguously locates the marker peptides in the type I collagen sequence, avoids duplication of marker names, and facilitates the creation of large ZooMS databases which can include all vertebrates.

Keywords

collagen, zooarcheology, peptide mass fingerprinting, MALDI-TOF-MS, ZooMS

Graphical Abstract:

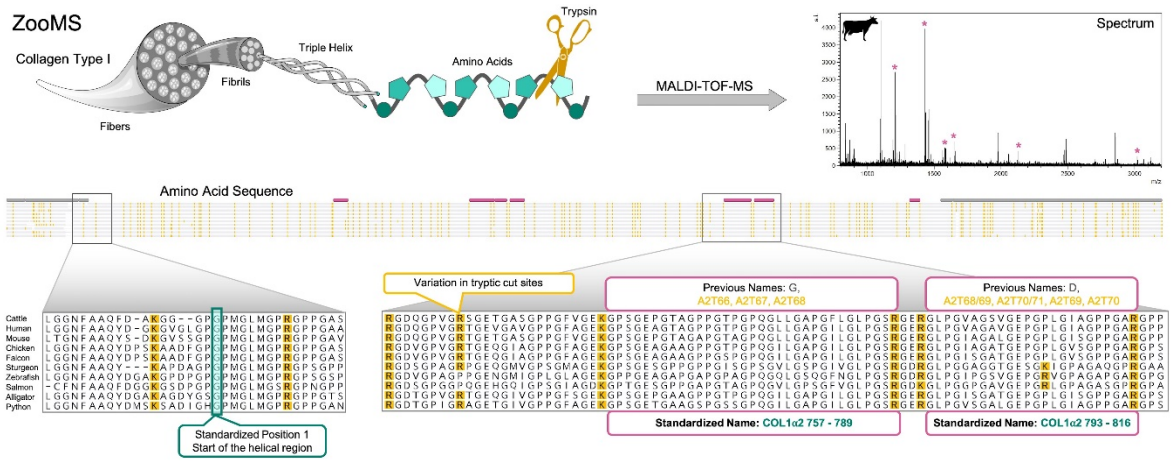

Introduction

Zooarchaeology by Mass Spectrometry (aka. ZooMS) is a form of peptide mass fingerprinting (pmf) using a MALDI-TOF-MS which allows for taxonomic identification through the analysis of trypsin-digested type I collagen [1] (Fig. 1). The method requires the development of a reference database against which the masses of tryptic peptides in an unknown sample are compared. Since the method was established, more than 200 publications have mentioned or applied ZooMS in their research (Fig. 2). The growth in the application of ZooMS, however, is apparent not only in the number of publications and the increasing spread of projects globally but also in the expansion of the reference database to include new markers and additional taxonomic groups. Recent publications have included the study of leather artefacts in Denmark [2,3], herding ecology in the Eurasian Steppe [4], hominin behaviour in Italy [5], ivory trade in Southern Africa [6], and salmon exploitation in the Pacific [7] to name only a handful of examples. Non-destructive and minimally destructive ZooMS protocols [8–10] and widespread applications of high-throughput protocols [5,11–13] have driven this expansion, highlighting the efficient and malleable nature of ZooMS.

With new labs and research groups beginning to use the method, it is imperative that a standardized approach to ZooMS work be established, similar to that which has been proposed for the broader field of palaeoproteomics [14]. At present, there is no centralised, open access reference library of previously established ZooMS markers. Instead researchers are left to individually compile their own lists as new peptide markers are published. While this is not inherently problematic, a major barrier to many new

researchers has been the often haphazard and ever changing nomenclature used to label peptide markers necessary for taxonomic identification. Creating a standardised system of nomenclature which allows for predictable and consistent naming of markers, particularly as the reference library continues to grow, is therefore crucial to the expansion of ZooMS. Here we propose a new set of guidelines for the standardised labelling of peptide markers based on the alignment of the type I collagen helix to a specific position, which is conserved across vertebrates.

Type I Collagen

A brief discussion of type I collagen (COL1), it's structure, and utility in ZooMS analysis is necessary before outlining our proposal for a cohesive nomenclature system. COL1 is the most abundant protein in tetrapods, comprising 95% of the entire collagen and 80% of all protein [15]. It is a fibrillar collagen composed of three, highly conserved alpha chains which form tightly packed, helical fibrils. The fibrils, connected by hydroxylysine cross-linkages, in turn, form fibers, which provide essential structural support in multiple tissues including bone, cartilage, and skin [16]. In tetrapods, the COL1 triple-helix is composed of two identical COL1α1 chains and one COL1α2 chain [15]. In a small number of species, the triple-helix is homo-trimeric and composed of three copies of one COL1 chain [17,18]. In many fish species, COL1 is composed of three different chains, COL1α1, COL1α2, and COL1α3, where COL1α3 is the result of a gene duplication of COL1α1 [18–20]. This allows for a higher degree of taxonomic separation for fish using pmf [7,21].

The helical nature of COL1 is generated by a repeating pattern of three amino acids, G-X-Y. Every third residue is the small and flexible amino acid glycine (G), while X and Y are often proline and hydroxyproline, respectively. Due to this highly stable and compact structure as well as the large starting volume, COL1 is particularly robust and can survive quite well on archaeological timescales in a variety of climates and conditions [22]. COL1 has been shown to have a longer preservation than other biomolecules, including DNA [14] with ZooMS being applied to bone remains as old as 3.4Ma [23]. Collagen preservation limits are potentially much older than this.

Each proto-COL1 protein chain is composed of a signal peptide (~20 amino acids) and N-terminal and C-terminal propeptides (~150-300 amino acids each) that flank the mature

peptide. The propeptides, responsible for nucleation or the start of the triple helix formation, are removed prior to fibrillogenesis. As they do not form part of the collagen network, they are not useful for identification purposes [16,24]. The mature peptide, which composes the collagen fibers, contains three regions. Two short non-helical regions, N-terminal and C-terminal telopeptides (~9-30 amino acids each) flank the longer helical region of 1014 amino acids which contain the highly conserved G-X-Y pattern. Individual triple helices nucleate from the C-terminus. The C-telopeptides are important in coordinating this process. Individual fibrils will self assemble into microfibrils which then further aggregate to ultimately form collagen fibrils of up to 1 cm in length. Fibrils aggregate in a quarter staggered arrangement in a unit cell of 5 triple helices, offset one from another by 234 residues. In order to maintain this structure COL1 has a highly conserved charge distribution resulting in a high degree of conservatism in the tryptic cleavage locations (arginine and lysine). While the slow mutation rate of COL1 relative to other proteins [25] and the high degree of conservation of tryptic sites is a drawback for its use in phylogenetic separation [26], it is an advantage for pmf. Once the pmf spectra from a number of taxonomically diverse mammals were analyzed it was clear that taxonomic differences could be identified and ZooMS was born [1].

ZooMS Nomenclature

Peptide markers suitable for taxonomic discrimination are identified through the comparison of reference MALDI-TOF MS spectra. They are then verified using MS/MS analyses. Initially, ZooMS was based on the presence/absence of seven tryptic peptide markers, labelled A-G, based upon increasing mass-to-charge (m/z) ratios in the MALDI spectra [1] (Table 1). These seven markers were chosen as they were reliably present within the 32 mammalian species analysed and showed differences between taxonomic groups in the 2009 study that established ZooMS [1]. Three of the ZooMS markers, A, F, and G, have two m/z values, subsequently named either A'/F'/G' or A2/F2/G2. This is due to a posttranslational modification in which proline converts to hydroxyproline for a mass difference of 16 daltons, commonly seen at the Y position of the repeating pattern of amino acids. This modification can be fixed, where all of the collagen chains have a hydroxyproline at the particular location, or variable, where both hydroxyproline and proline are present at the location in different chains [1].

While the lettering system provided an easy means of labelling these peptides, the letters do not identify which chain the peptides derived from, nor where the peptides are situated within the protein sequence. The lettering system also inherently hinders the possibility for incrementally labelling newly identified peptide markers which, for instance, could fall between the masses of B (typically m/z 1400-1500) and C (m/z 1500-1600). A case in point is the separation of cetacean and pinniped species, which relied on the adoption and identification of three new peptide markers [27]. These were labelled “Cet1”, “Cet2”, and “P” as they fell in between markers already labelled in the A-G lettering system. In subsequent research, Cet1 was renamed “P1”, Cet2 was renamed “P2”, and P was removed from newer ZooMS datasets entirely [12,28]. An additional concern is the application of the lettering system to new species groups which have different fundamental marker sets, such as birds or fish [7,29–32]. Clearly, the growth and naming of new peptide markers used in the pmf of COL1 could benefit from a standardized scheme replicable across taxonomic groups, independent of mass ranges and pre-existing marker names.

Key to being able to understand what the markers mean and predict if species can be separated is knowing the location and sequence of the peptide which corresponds to the marker. The most commonly used way of reporting the location is in relation to the tryptic digestion of COL1, where the protein is theoretically digested and each peptide fragment is given a sequential number (Fig 3). This takes advantage of the conserved locations of arginine and lysine residues. However, despite the fact that these residues are highly conserved across large taxonomic groups, they are not fixed. In addition, the same sequence/marker has been reported at several different locations. Marker A for instance, was initially reported in tryptic position COL1A2T80 [1] and more recently has been recorded at COL1A2T85 [33]. This does not reflect any difference in the sequence, rather it reflects disparity over the start of the labeling and the digestion parameters used for the theoretical digestion. The tryptic numbering system starts at the beginning of the mature protein (telopeptide) rather than the start of the protein sequence as reported in Uniprot, which contains the signal peptide and the propeptides. This allows for more consistency in the numbering system as the mature peptide is more conserved than the flanking propeptides.

However, programs for sequence alignments do not normally offer automatic numbering for trypsin digested peptides. This means either counting tryptic cut sites by hand on the alignment which is prone to mistakes or using a program or script which predicts the digestion pattern for individual sequences. Programs predicting tryptic cleavages have two settings for trypsin which will cause different numbering schemes due to the potential to exclude digestion when proline is after the tryptic cut site. Most importantly, names based on tryptic cut sites will differ between taxa which have single amino-acid polymorphisms at tryptic cut sites. This is particularly a problem for the analysis of fish, reptile, and amphibian COL1 [7], although there are rare examples in mammals. For example, based on our alignment of ~100 mammalian COL1 sequences, we observe unique amino acid substitutions for *Orycteropus after* (R>Q; GenBank: XP_007937996.1) and *Erinaceus europaeus* (GenBank: XP_007522561.1) and *Fukomys damarensis* (GenBank: XP_010601746.1) (both R>H) affecting tryptic cut sites. Without adequate reporting of how numbering was determined there is a high likelihood that additional discrepancies will appear between publications making it confusing for researchers trying to use ZooMS.

Several solutions to creating standardised nomenclature have been proposed. Labelling based on position from the start of the protein is a simple convention and easily conveys the meaning behind those labels. It would however result in a fluctuating labelling system between species as the N-terminal propeptide is highly variable in the number of amino acids between species. This variability, therefore, precludes the creation of large comparable databases for ZooMS analysis. Another proposed labelling system is using positional numbering from the start of the mature peptide. This is less straightforward but still quite easy to do using alignment software. It is advantageous over labelling based on the start of the protein as there will be fewer instances of variability between species, but large datasets of comparable peptide markers between vertebrates will still not be possible as the N-terminal telopeptide is still variable between different taxonomic groups. The most reliable method for nomenclature, and the method we propose here, is to name all peptide markers in reference to a single homologous position at the start of the highly conserved, helical region just after the N-terminal telopeptide (Fig. 3).

We aligned all vertebrate taxa for which COL1 sequences are available in NCBI or Uniprot (~150 mammals, ~30 birds, ~100 fish, and ~20 reptiles and amphibians) and identified the start of the helical region in COL1α1, COL1α2, and COL1α3 (see Supplementary Information for a subset of this alignment and annotated sequences). This corresponds to the start of the collagen-specific three letter repeating pattern (G-X-Y). For all assessed species, there were no insertions or deletions in the amino acid sequence in the helical region, meaning that the numbering system could be used consistently and reliably across all vertebrate taxa. In COL1α1, the start of the helical region is GPMGPXGPR (where X is variable) at position 178 in the *Bos taurus* reference sequence (UniProt: P02453) and 16 amino acids after the start of the mature peptide. In COL1α2, it is GPMGLMGPR, at position 89 in the *Bos taurus* reference sequence (UniProt: P024650) and 9 amino acids after the start of the mature peptide. In fish, the corresponding sequence in COL1α3 is GPXGPMGPR, at position 166 in the Danio rerio reference sequence (UniProt: Q6NZ15) and 16 amino acids after the start of the mature peptide.

We propose to label ZooMS peptide markers with the gene (COL1α1, COL1α2, or COL1α3), followed by the start position of the peptide in reference to the first amino acid of the helical region, followed by the end position of the peptide in reference to the first amino acid of the helical region (Table 1). While not the most intuitive or easiest labelling method, it will provide consistent nomenclature of peptide markers for all vertebrates, a significant advantage over the tryptic digestion and other positional labels. The position can easily be located using existing alignment software. Furthermore, the adoption of this method avoids the problem of duplicate names appearing in the literature and, unlike the letter-based nomenclature, allows markers to be named consecutively within the COL1 sequence.

An unavoidable, yet important, consequence of this proposed nomenclature is that it will only be applicable to markers which can be located within the COL1 sequence, usually through MS/MS confirmation. Markers which have been identified solely on the basis of pmf should be labelled as the m/z value only, omitting the COL1 label. This will allow for the straightforward means of identifying confirmed versus tentative markers in the ZooMS reference database, adding a further means of data quality control. In addition, there are some peptide markers which are composed of multiple COL1 peptides. Our proposed nomenclature would allow for these to be clearly indicated as being composed of multiple

peptides. These should be used with great caution for taxonomic identification using pmf as there is no way to deconvolute multiple peptides with the same mass without MS/MS analysis.

Another consideration is that pmf based methods are being developed for identification of other archaeological materials including eggshells [34,35], baleen [36], and hair and fur [37–39]. Similar considerations as presented here will need to be considered when developing nomenclature for the pmf identification of other proteins, especially keratins, in archaeological materials.

Conclusion

With the growth of ZooMS, a standardized, consistent, reliable, and adaptable marker nomenclature is essential. Standardizing the nomenclature to the position from the start of the highly conserved, G-X-Y, helical region provides a consistent naming system applicable to all vertebrates and avoids accidental duplication of names by different groups during marker development and publication. Additional markers that are not confirmed by MS/MS and therefore have not been located to a position in the COL1 sequence should be reported specifically for a particular taxonomic group using the m/z value of the marker only, omitting the COL1 label. This nomenclature allows easy access for all researchers to understand which markers have been confirmed, for which markers independent confirmation is still pending, and where the markers are positioned in the COL1 sequence. It also emphasizes the importance of using markers that are composed of a single peptide and allows for new markers to be developed. We encourage discussion within the community about nomenclature and until a standardized method is established, we believe the use of clear and reproducible reporting of what nomenclature system is being used is essential, especially as new markers are developed.

Tables

				Nomenclature						
						Start Position				
Sequence	**m/z**	**Oxidations**	**Gene**	**Letter**	**Tryptic**	**Whole Sequence**	**Mature Peptide**	**Helical Region**	**Proposed Full Name**	**Proposed "nickname"**
GVQGPPGPAGPR	1105	1	COL1α1	Cet1 / P1	A1T47	685	524	507	COL1α1 508-519	α1 508
GLTGPIGPPGPAGAPGDKGEAGPSGPAGPTGAR	2853 / 3869	2/3	COL1α1	F	A1T55/56	763	602	585	COL1α1 586-618	α1 586
GSTGEIGPAGPPGPPGLR	1648	2	COL1α2	Cet2 / P2	A2T26	380	301	292	COL1α2 292 - 309	α2 292
GEQGPAGPPGFQGLPGPAGTAGEAGKPGER	2792	3	COL1α2	E	A2T41/42	542	463	454	COL1α2 454 - 483	α2 454
GIPGEFGLPGPAGAR	1427	2	COL1α2	B	A2T43	572	493	484	COL1α2 484 - 498	α2 484
GPPGESGAAGPTGPIGSR	1580	1	COL1α2	C	A2T45	590	511	502	COL1α2 502 - 519	α2 502
GPSGEPGTAGPPGTPGPQGLLGAPGFLGLPGSR	3017 / 3033	4/5	COL1α2	G	A2T67	845	766	757	COL1α2 757 - 789	α2 757
GLPGVAGSVGEPGPLGIAGPPGAR	2131	3	COL1α2	D	A2T69	881	802	793	COL1α2 793 - 816	α2 793
IGQPGAVGPAGIR	1192 / 1208	0/1	COL1α2	A	A2T85	1066	987	978	COL1α2 978 - 990	α2 978

Table 1: Commonly used markers for ZooMS including the sequence and m/z values for *Bos taurus* (COL1α1 UniProt: P02453, COL1α2 UniProt: P024650), the number of prolines with an oxidation that are on the peptides, the m/z values visualized in the MALDI spectra, and the different nomenclature used including the proposed, standardized one. The marker at m/z 3017 is commonly reported for several taxa which have published

ZooMS reference spectra [1,12], but is greyed out here because it can be composed of multiple COL1 peptides in some taxonomic groups and therefore caution is advised when using it [40].

Figure Captions

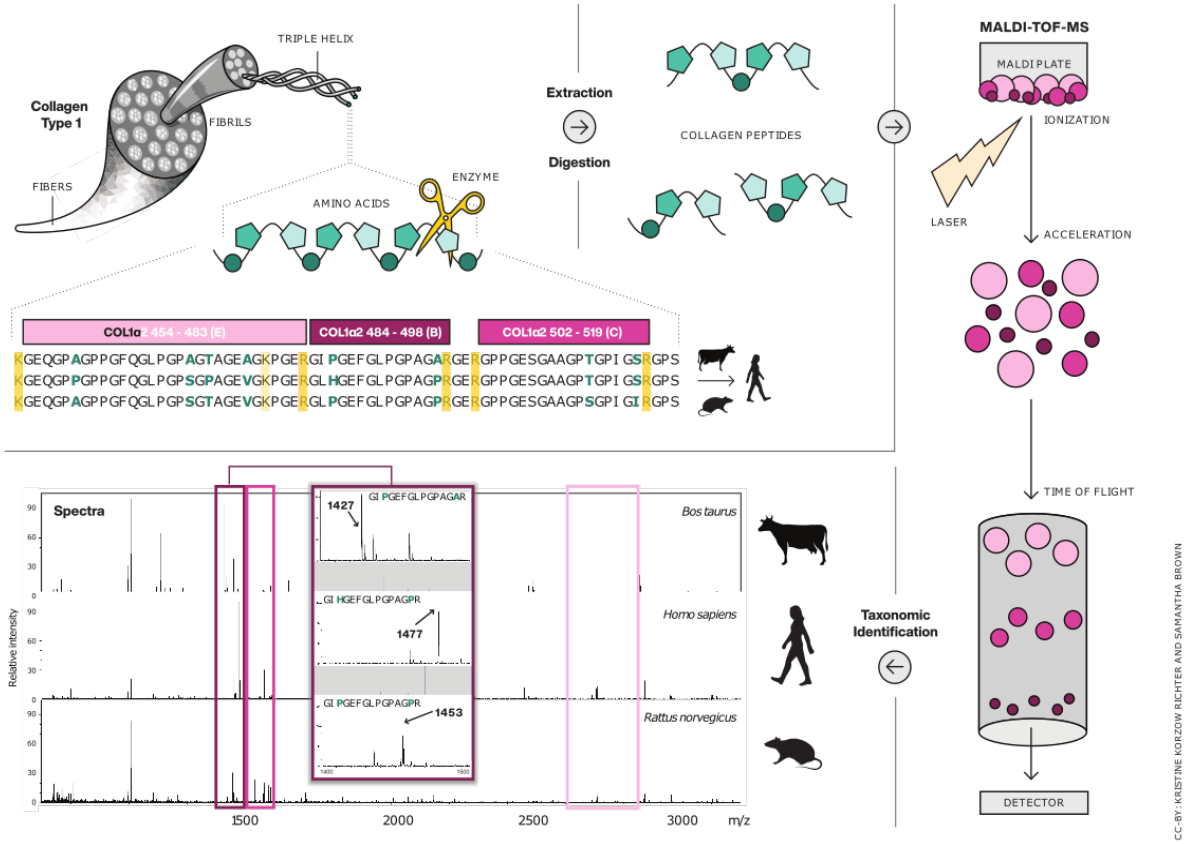

Figure 1: Schematic diagram of ZooMS and sequence alignment. ZooMS gelatinizes fibrillar collagen type I, which contains a characteristic three amino acid repeating pattern of G-X-Y (shaded green shapes). Digestion is typically conducted with the enzyme trypsin, which cuts on the C-terminal side of arginine and lysine (highlighted in yellow in the sequence data). Analysis by MALDI-TOF-MS results in spectra which can be identified based on unique patterns of peaks. The zoomed-in spectral images indicate differences between the three species in the marker COL1α2 484-498. Marker peptides are indicated in the sequence data, MALDI-TOF-MS and the spectra in shades of pink based upon mass. The sequence data is a partial alignment of COL1α2 from *Bos taurus* (UniProt: P024650), *Homo sapiens* (UniProt: P08123), and *Rattus norvegicus* (UniProt: P02466). Collagen image from smart.servier.com.

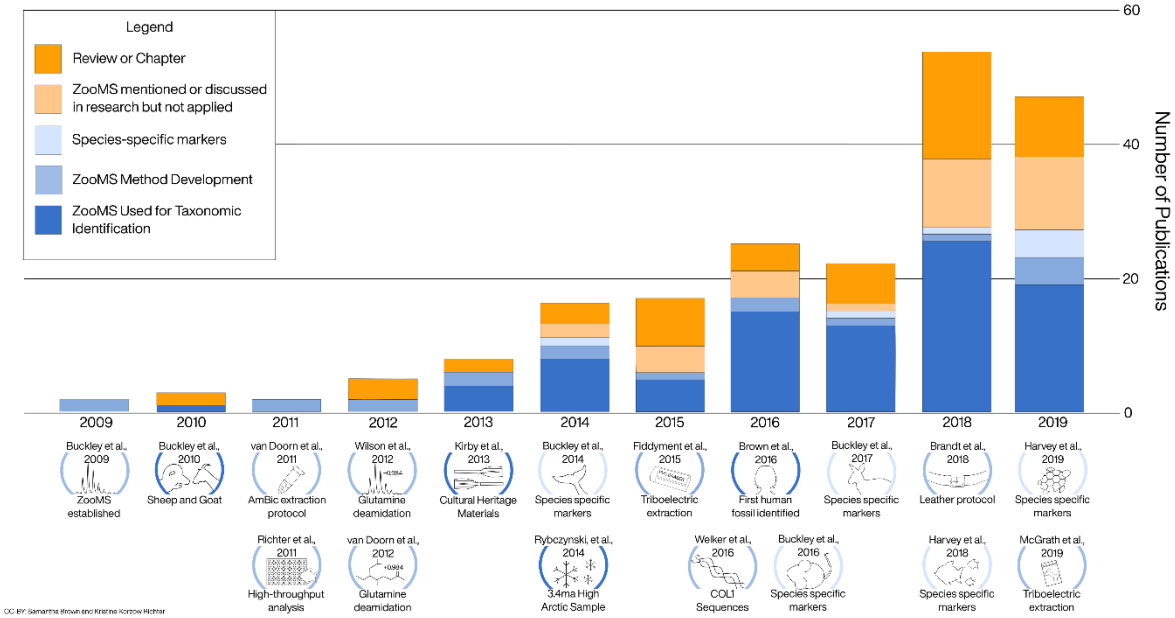

Figure 2: Number of papers which mention “Zooarchaeology by Mass Spectrometry” in the decade after the method was established according to Google Scholar. Major milestones for the method are referenced in circles below the year they were published [1,2,8–12,21,23,27,29,31,41–45].

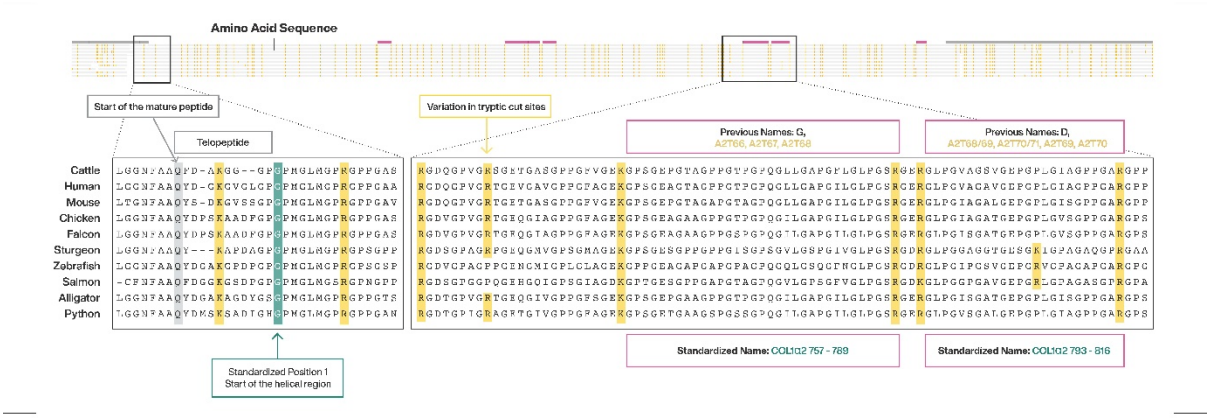

Figure 3: Alignment COL1A2 of mammals (*Bos taurus*, *Homo sapiens*, *Mus musculus* (UniProt: Q01149)), birds (*Gallus gallus* (UniProt: P02467), *Falco peregrinus* (GenBank: XP_005228841.1), fish (*Acipenser schrenckii* (GenBank: BAT51012.1), *Danio rerio* (GenBank: AAH71278.1), *Oncorhynchus mykiss* (GenBank: CDQ73303.1)), and reptiles (*Alligator mississippiensis* (GenBank: KYO26674.1), *Python bivittatus* (GenBank: XP_007425176.1)). Tryptic cut sites, arginine and lysine, are highlighted in yellow. While highly conserved they are not completely shared across all taxonomic groups. ZooMS markers are indicated by pink boxes. The zoomed in areas of the spectra show the start of the mature peptide, the N-terminal telopeptide, the start of the helical region, the letter nomenclature, the possible tryptic nomenclatures for the ten species listed, and our proposed standardized nomenclature.

References

[1] M. Buckley, M. Collins, J. Thomas-Oates, J.C. Wilson, Species identification by analysis of bone collagen using matrix-assisted laser desorption/ionisation time-of-flight mass spectrometry, Rapid Commun. Mass Spectrom. 23 (2009) 3843–3854.

[2] L.Ø. Brandt, K. Haase, M.J. Collins, Species identification using ZooMS, with reference to the exploitation of animal resources in the medieval town of Odense, Danish Journal of Archaeology. 7 (2018) 139–153.

[3] J.A. Ebsen, K. Haase, R. Larsen, D.V.P. Sommer, L.Ø. Brandt, Identifying archaeological leather – discussing the potential of grain pattern analysis and zooarchaeology by mass spectrometry (ZooMS) through a case study involving medieval shoe parts from Denmark, J. Cult. Herit. 39 (2019) 21–31.

[4] W.T.T. Taylor, J. Clark, J. Bayarsaikhan, T. Tuvshinjargal, J.T. Jobe, W. Fitzhugh, R. Kortum, R.N. Spengler 3rd, S. Shnaider, F.V. Seersholm, I. Hart, N. Case, S. Wilkin, J. Hendy, U. Thuering, B. Miller, A.R.V. Miller, A. Picin, N. Vanwezer, F. Irmer, S. Brown, A. Abdykanova, D.R. Shultz, V. Pham, M. Bunce, K. Douka, E.L. Jones, N. Boivin, Early Pastoral Economies and Herding Transitions in Eastern Eurasia, Sci. Rep. 10 (2020) 1001.

[5] V. Sinet-Mathiot, G.M. Smith, M. Romandini, A. Wilcke, M. Peresani, J.-J. Hublin, F. Welker, Combining ZooMS and zooarchaeology to study Late Pleistocene hominin behaviour at Fumane (Italy), Sci. Rep. 9 (2019) 12350.

[6] A.N. Coutu, G. Whitelaw, P. le Roux, J. Sealy, Earliest Evidence for the Ivory Trade in Southern Africa: Isotopic and ZooMS Analysis of Seventh–Tenth Century ad Ivory from KwaZulu-Natal, African Archaeological Review. 33 (2016) 411–435.

[7] K. Korzow Richter, K. McGrath, E. Masson-MacLean, S. Hickinbotham, A. Tedder, K. Britton, Z. Bottomley, K. Dobney, A. Hulme-Beaman, M. Zona, R. Fischer, M.J. Collins, C.F. Speller, What's the catch? Archaeological application of rapid collagen-based species identification for Pacific Salmon, J. Archaeol. Sci. 116 (2020) 105116.

[8] N.L. van Doorn, H. Hollund, M.J. Collins, A novel and non-destructive approach for ZooMS analysis: ammonium bicarbonate buffer extraction, Archaeol. Anthropol. Sci. 3 (2011) 281.

[9] S. Fiddyment, B. Holsinger, C. Ruzzier, A. Devine, A. Binois, U. Albarella, R. Fischer, E. Nichols, A. Curtis, E. Cheese, M.D. Teasdale, C. Checkley-Scott, S.J. Milner, K.M. Rudy, E.J. Johnson, J. Vnouček, M. Garrison, S. McGrory, D.G. Bradley, M.J. Collins, Animal origin of 13th-century uterine vellum revealed using noninvasive peptide fingerprinting, Proc. Natl. Acad. Sci. U. S. A. 112 (2015) 15066–15071.

[10] K. McGrath, K. Rowsell, C. Gates St-Pierre, A. Tedder, G. Foody, C. Roberts, C. Speller, M. Collins, Identifying Archaeological Bone via Non-Destructive ZooMS and the Materiality of Symbolic Expression: Examples from Iroquoian Bone Points, Sci. Rep. 9 (2019) 11027.

[11] S. Brown, T. Higham, V. Slon, S. Pääbo, M. Meyer, K. Douka, F. Brock, D. Comeskey,

N. Procopio, M. Shunkov, A. Derevianko, M. Buckley, Identification of a new hominin bone from Denisova Cave, Siberia using collagen fingerprinting and mitochondrial DNA analysis, Sci. Rep. 6 (2016) 23559.

[12] F. Welker, M. Hajdinjak, S. Talamo, K. Jaouen, M. Dannemann, F. David, M. Julien, M. Meyer, J. Kelso, I. Barnes, S. Brace, P. Kamminga, R. Fischer, B.M. Kessler, J.R. Stewart, S. Pääbo, M.J. Collins, J.-J. Hublin, Palaeoproteomic evidence identifies archaic hominins associated with the Châtelperronian at the Grotte du Renne, Proc. Natl. Acad. Sci. U. S. A. 113 (2016) 11162–11167.

[13] K. Douka, S. Brown, T. Higham, S. Pääbo, A. Derevianko, M. Shunkov, FINDER project: collagen fingerprinting (ZooMS) for the identification of new human fossils, Antiquity. 93 (2019). https://doi.org/10.15184/aqy.2019.3.

[14] J. Hendy, F. Welker, B. Demarchi, C. Speller, C. Warinner, M.J. Collins, A guide to ancient protein studies, Nat Ecol Evol. 2 (2018) 791–799.

[15] K. Henriksen, M.A. Karsdal, Type I collagen, Biochemistry of Collagens, Laminins and Elastin. (2019) 1–12. https://doi.org/10.1016/b978-0-12-817068-7.00001-x.

[16] M.D. Shoulders, R.T. Raines, Collagen structure and stability, Annu. Rev. Biochem. 78 (2009) 929–958.

[17] R.P. Boot-Handford, D.S. Tuckwell, Fibrillar collagen: the key to vertebrate evolution? A tale of molecular incest, Bioessays. 25 (2003) 142–151.

[18] G. Morvan-Dubois, D. Le Guellec, R. Garrone, L. Zylberberg, L. Bonnaud, Phylogenetic analysis of vertebrate fibrillar collagen locates the position of zebrafish alpha3(I) and suggests an evolutionary link between collagen alpha chains and hox clusters, J. Mol. Evol. 57 (2003) 501–514.

[19] A. Meyer, Y. Van de Peer, From 2R to 3R: evidence for a fish-specific genome duplication (FSGD), Bioessays. 27 (2005) 937–945.

[20] S. Kimura, Y. Ohno, Fish type I collagen: tissue-specific existence of two molecular forms, (α1)2α2 and α1α2α3, in Alaska pollack, Comparative Biochemistry and Physiology Part B: Comparative Biochemistry. 88 (1987) 409–413.

[21] K.K. Richter, J. Wilson, A.K.G. Jones, M. Buckley, N. van Doorn, M.J. Collins, Fish ’n chips: ZooMS peptide mass fingerprinting in a 96 well plate format to identify fish bone fragments, J. Archaeol. Sci. 38 (2011) 1502–1510.

[22] M. Buckley, Zooarchaeology by Mass Spectrometry (ZooMS) Collagen Fingerprinting for the Species Identification of Archaeological Bone Fragments, in: C.M. Giovas, M.J. LeFebvre (Eds.), Zooarchaeology in Practice: Case Studies in Methodology and Interpretation in Archaeofaunal Analysis, Springer International Publishing, Cham, 2018: pp. 227–247.

[23] N. Rybczynski, J.C. Gosse, C.R. Harington, R.A. Wogelius, A.J. Hidy, M. Buckley, Mid-Pliocene warm-period deposits in the High Arctic yield insight into camel evolution, Nat. Commun. 4 (2013) 1550.

[24] M. Saito, T. Higuchi, N. Uchida, Identification and primary structures of eel type I collagen proα1, proα2 and proα3, Fish. Sci. 80 (2014) 1323–1335.

[25] D.A. Stover, B.C. Verrelli, Comparative vertebrate evolutionary analyses of type I collagen: potential of COL1a1 gene structure and intron variation for common bone-related diseases, Mol. Biol. Evol. 28 (2011) 533–542.

[26] S. Presslee, G.J. Slater, F. Pujos, A.M. Forasiepi, R. Fischer, K. Molloy, M. Mackie, J.V. Olsen, A. Kramarz, M. Taglioretti, F. Scaglia, M. Lezcano, J.L. Lanata, J. Southon, R. Feranec, J. Bloch, A. Hajduk, F.M. Martin, R. Salas Gismondi, M. Reguero, C. de Muizon, A. Greenwood, B.T. Chait, K. Penkman, M. Collins, R.D.E. MacPhee, Palaeoproteomics resolves sloth relationships, Nat Ecol Evol. 3 (2019) 1121–1130.

[27] M. Buckley, S. Fraser, J. Herman, N.D. Melton, J. Mulville, A.H. Pálsdóttir, Species identification of archaeological marine mammals using collagen fingerprinting, J. Archaeol. Sci. 41 (2014) 631–641.

[28] S. Evans, I. Briz i Godino, M. Álvarez, K. Rowsell, P. Collier, R.N.P. de Goodall, J. Mulville, A. Lacrouts, M.J. Collins, C. Speller, Using combined biomolecular methods to explore whale exploitation and social aggregation in hunter–gatherer–fisher society in Tierra del Fuego, Journal of Archaeological Science: Reports. 6 (2016) 757–767.

[29] V.L. Harvey, M.J. LeFebvre, S.D. deFrance, C. Toftgaard, K. Drosou, A.C. Kitchener, M. Buckley, Preserved collagen reveals species identity in archaeological marine turtle bones from Caribbean and Florida sites, R Soc Open Sci. 6 (2019) 191137.

[30] T. Rick, V.L. Harvey, M. Buckley, Collagen fingerprinting and the Chumash billfish fishery, Santa Barbara Channel, California, USA, Archaeol. Anthropol. Sci. 11 (2019) 6639–6648.

[31] V.L. Harvey, L. Daugnora, M. Buckley, Species identification of ancient Lithuanian fish remains using collagen fingerprinting, J. Archaeol. Sci. 98 (2018) 102–111.

[32] L.G. van der Sluis, H.I. Hollund, M. Buckley, P.G.B. De Louw, K.F. Rijsdijk, H. Kars, Combining histology, stable isotope analysis and ZooMS collagen fingerprinting to investigate the taphonomic history and dietary behaviour of extinct giant tortoises from the Mare aux Songes deposit on Mauritius, Palaeogeogr. Palaeoclimatol. Palaeoecol. 416 (2014) 80–91.

[33] A. Desmond, N. Barton, A. Bouzouggar, K. Douka, P. Fernandez, L. Humphrey, J. Morales, E. Turner, M. Buckley, ZooMS identification of bone tools from the North African Later Stone Age, J. Archaeol. Sci. 98 (2018) 149–157.

[34] J.R.M. Stewart, R.B. Allen, A.K.G. Jones, K.E.H. Penkman, M.J. Collins, ZooMS: making eggshell visible in the archaeological record, J. Archaeol. Sci. 40 (2013) 1797–1804.

[35] J.R.M. Stewart, R.B. Allen, A.K.G. Jones, T. Kendall, K.E.H. Penkman, B. Demarchi, T. O'Connor, M.J. Collins, Walking on Eggshells: A Study of Egg Use in Anglo-Scandinavian York Based on Eggshell Identification Using ZooMS, International

Journal of Osteoarchaeology. 24 (2014) 247–255.

[36] C. Solazzo, W. Fitzhugh, S. Kaplan, C. Potter, J.M. Dyer, Molecular markers in keratins from Mysticeti whales for species identification of baleen in museum and archaeological collections, PLoS One. 12 (2017) e0183053.

[37] K. Hollemeyer, W. Altmeyer, E. Heinzle, Identification and quantification of feathers, down, and hair of avian and mammalian origin using matrix-assisted laser desorption/ionization time-of-flight mass spectrometry, Anal. Chem. 74 (2002) 5960–5968.

[38] C. Solazzo, M. Wadsley, J.M. Dyer, S. Clerens, M.J. Collins, J. Plowman, Characterisation of novel α-keratin peptide markers for species identification in keratinous tissues using mass spectrometry, Rapid Commun. Mass Spectrom. 27 (2013) 2685–2698.

[39] C. Solazzo, Follow-up on the characterization of peptidic markers in hair and fur for the identification of common North American species, Rapid Commun. Mass Spectrom. 31 (2017) 1375–1384.

[40] A. Janzen, K.K. Richter, O. Mwebi, S. Brown, M Onduso, F. Gatwiri, E. Ndiema, M. Katongo, S.T. Goldstein, K. Douka, N. Boivin, Distinguishing African bovids using Zooarchaeology by Mass Spectrometry (ZooMS): New peptide markers and assessments of Iron Age economies in Zambia, PLoS One. (n.d.).

[41] M. Buckley, S. Whitcher Kansa, S. Howard, S. Campbell, J. Thomas-Oates, M. Collins, Distinguishing between archaeological sheep and goat bones using a single collagen peptide, J. Archaeol. Sci. 37 (2010) 13–20.

[42] M. Buckley, R. Cosgrove, J. Garvey, G.J. Prideaux, Identifying remains of extinct kangaroos in Late Pleistocene deposits using collagen fingerprinting, J. Quat. Sci. 32 (2017) 653–660.

[43] M. Buckley, M. Gu, S. Shameer, S. Patel, A.T. Chamberlain, High-throughput collagen fingerprinting of intact microfaunal remains; a low-cost method for distinguishing between murine rodent bones, Rapid Commun. Mass Spectrom. 30 (2016) 805–812.

[44] J. Wilson, N.L. van Doorn, M.J. Collins, Assessing the extent of bone degradation using glutamine deamidation in collagen, Anal. Chem. 84 (2012) 9041–9048.

[45] N.L. van Doorn, J. Wilson, H. Hollund, M. Soressi, M.J. Collins, Site-specific deamidation of glutamine: a new marker of bone collagen deterioration, Rapid Commun. Mass Spectrom. 26 (2012) 2319–2327.

Appendix 2 – Submitted manuscripts

Manuscript C - submitted. Brown, S., Massilani, D., Kozlikin, M., Shunkov, M., Derevianko, A., Stoessel, A., Jope-Street, B., Meyer, M., Kelso, J., Pääbo, S., Higham, T., Douka, K. The earliest Denisovans and their cultural adaptation. Nature Ecology and Evolution.

The earliest Denisovans and their cultural adaptation

Samantha Brown[1*§], Diyendo Massilani[2§], Maxim B. Kozlikin[3], Michael V. Shunkov[3,4], Anatoly P. Derevianko[3], Alexander Stoessel[1,2,5], Blair Jope-Street[1], Matthias Meyer[2], Janet Kelso[2], Svante Pääbo[2], Thomas Higham[6], Katerina Douka[1*]

[1] Max Planck Institute for the Science of Human History, Jena, Germany.

[2] Max Planck Institute for Evolutionary Anthropology, Leipzig, Germany.

[3] Institute of Archeology and Ethnography of the Siberian Branch of the Russian Academy of Sciences, Novosibirsk, Russia.

[4] Novosibirsk State University, Novosibirsk, Russia.

[5] Institute of Zoology and Evolutionary Research, Friedrich Schiller University Jena, Erbertstraße 1, 07743, Jena, Germany.

[6] Oxford Radiocarbon Accelerator Unit, RLAHA, University of Oxford, Oxford OX13QY, UK.

*Correspondence to: Samantha Brown and Katerina Douka

Email: brown@shh.mpg.de, douka@shh.mpg.de
[§]These authors contributed equally to this work

Keywords

Denisovan; Neanderthal; ZooMS; mtDNA; Asia; Palaeolithic archaeology

Abstract

Since the initial identification of the Denisovans a decade ago, only a handful of their physical remains have been discovered. Here, we analyse ~3800 non-diagnostic bone fragments using collagen peptide mass fingerprinting to locate new hominin remains from Denisova Cave (Siberia, Russia). We identify five new hominin bones, four of which contained sufficient DNA for mitochondrial analysis. Three carry mtDNA of the Denisovan type and one is found to carry mtDNA of the Neanderthal type. The former come from the same archaeological layer, near the base of the cave's sequence and are the oldest securely dated evidence of Denisovans, at 200 ka (205-192 ka at 68.2% or 217-187 ka at 95% probability). The stratigraphic context in which they were located contains a wealth

of archaeological material in the form of lithics and faunal remains, allowing us to determine the material culture associated with these early hominins and explore their behavioural and environmental adaptations. Technologically, a close counterpart is found in the Near East associated with the Acheulo-Yabrudian technocomplex. The combination of targeted collagen fingerprinting applications and genetic analyses has so far more-than-doubled the number of hominin bones at Denisova Cave and has expanded our understanding of Denisovan and Neanderthal interactions as well as their archaeological signatures.

Text

The identification and analysis of Pleistocene hominin remains form the basis for unraveling the processes governing human evolution, interaction, and adaptation, yet discovery of new human fossils continues to present a significant hurdle. Recent developments in excavation practices and archaeological sciences cannot subvert an unavoidable problem; that human remains are rarely discovered, especially in prehistoric contexts where formal burials were not observed. This is particularly true for the Denisovans, a sister population to the Neanderthals, whose discovery fundamentally changed our understanding of hominin diversity in the Pleistocene.[1,2] The high-coverage nuclear genome of a Denisovan individual (Denisova 3) showed that they diverged from a common ancestor with Neanderthals between 440-390 ka (thousand years ago).[3] The identification of Denisovan ancestry in indigenous peoples of Australia and Papua New Guinea and in East and South East Asians has led to the inference that modern humans met and admixed with at least two distinct populations of Denisovans in the Upper Pleistocene.[4,5] This raises the possibility that Denisovans may have been widespread across continental Asia, island southeast Asia and near Oceania.

So far, only five small and highly fragmented fossils, all discovered at Denisova Cave (Russian Altai, Siberia, Russia), have been identified as Denisovans on the basis of DNA analyses.[1,2,6–8] The fossils for Denisovans identified at the site so far include worn and incomplete molars (Denisova 2, Denisova 4, and Denisova 8), partial phalanges (Denisova 3), and small bone chips (Denisova 11). Only one (Denisova 3) has yielded enough DNA for whole genome sequencing[9] as poor DNA preservation and modern contamination has thus far impeded nuclear genome analyses of the other specimens. Outside Denisova Cave, a mandible from Baishiya Cave (Xiahe, China) was tentatively assigned to Denisovans on the basis of proteomic evidence.[10]

Advances in proteomic research, in particular the increasingly common application of peptide mass fingerprinting (or ZooMS; Zooarchaeology by Mass Spectrometry),[11] has been shown to be an efficient way for determining hominin presence at archaeological sites through the taxonomic identification of bone based on collagen characterization.[12] It is most reliable in assigning a genus or family-level identification and, in some instances, species-specific determinations are possible.[13] The highly time- and cost-efficient nature of ZooMS, its reproducibility, and the long-term preservation of collagen compared with other biomolecules, including DNA, make it an invaluable screening tool for the identification of fragmentary, morphologically non-diagnostic bones. ZooMS has been used to successfully identify hominin remains in large assemblages of bones[12,14–17] including Denisova 11, a female individual with a Neanderthal mother and a Denisovan father.[7,12]

Here we present a high-throughput application of peptide mass fingerprinting to unidentified bones from Denisova Cave. Located in the northwest Altai mountains, Denisova Cave preserves the longest archaeological sequence in northern Eurasia dating from the Middle Pleistocene to the Holocene.[16,18] The cave contains a rich stratigraphic

record, most notable for its Middle and Upper Palaeolithic cultural, faunal and fossil remains.[19–22] It is the only site where the presence of Denisovans and Neanderthals has been determined on the basis of DNA recovery from both human fossils and cave sediments[23] in several layers throughout the sequence. The combination of good biomolecular preservation, rich archaeological assemblages, and the presence of multiple hominin groups makes Denisova Cave one of the most informative archaeological sites for Pleistocene Eurasia.

Non-diagnostic bone fragments, an important untapped source of potential human fossils, represent 95% of the bones excavated at Denisova Cave.[24] We applied ZooMS to 3,791 bones from the East Chamber, one of the three explored galleries of the cave. The fragments were specifically chosen for their lack of diagnostic features which precluded macroscopic identification. The bones came from each of the archaeological layers of the East Chamber, layers 9, 11, 12, 13, 14, and 15, and layer 17 which contains no archaeological evidence for hominin occupation (layers 10 and 16 are sterile; Table S2). The majority of analyzed bones were excavated from layers 14 and 15 from which no hominin bones were previously found, although layer 15, the lowermost archaeological layer of the East Chamber, has previously yielded Denisovan sediment DNA.[23] From each bone, a chip of approximately 20mg was removed and, following established protocols,[14,25,26] collagen was extracted and analyzed in order to carry out taxonomic identification (Materials and Methods). The vast majority of the analyzed bones were assigned to large herbivores (Bos/Bison, Equidae and Cervidae) and carnivores, in reasonable agreement with fauna previously identified at the site through morphological analysis[18,24,27] (Fig. S1).

Five bones generated peptide mass fingerprints with characteristic markers corresponding to the Hominidae (Fig. 1b, Table S1, Dataset S1).[11,28] Four of them come from layer 15 (DC7277, DC7795, DC8591, and DC8846) and one from layer 12 (DC4969). Given that no great apes are known from the region these bones almost certainly belong to humans. Human fossils identified using ZooMS now account for the majority of the hominin bones discovered at Denisova Cave (nine of the 17 fossils; 52%).

To digitally preserve the morphology of the bone fragments, four of the five new specimens were scanned with a microCT system (BrukerTM SkyScan 2211 X-ray Nanotomograph). We used image spatial resolutions ranging between 0.020 and 0.023 mm, following the recommendations of Immel et al.[29] to avoid degrading effects of X-ray irradiation on ancient DNA (Materials and Methods). 3D surfaces of the fossil bones were extracted from the microCT scans (Fig. S2; Dataset S2).

Since peptide mass fingerprinting cannot be used for a more specific taxonomic assignation than Hominidae, we used DNA analysis to identify the groups these five bones belonged to on the basis of mitochondrial (mt)DNA sequences. Extraction, sequencing and authentication of ancient hominin DNA from each bone followed

published procedures (Materials and Methods). Using a mtDNA enrichment approach we isolated sufficient ancient hominin DNA and reconstructed the mitochondrial genomes of four of the five specimens; Denisova 17 (DC4969), Denisova 19 (DC8846), Denisova 20 (DC7795) and Denisova 21 (DC8591). These were sequenced to an average coverage of 2,695-fold, 15-fold, 31-fold and 28-fold, respectively. Pairwise differences and phylogenetic analyses showed that the mtDNA of Denisova 17 falls within the diversity of Neanderthal mtDNAs, while the mtDNAs of Denisova 19, Denisova 20 and Denisova 21 fall within the diversity of Denisovan mtDNAs (Fig. 2). Denisova 18 contains too few ancient DNA fragments to securely associate its mtDNA with a hominin group (Materials and Methods and Supplementary Information).

The presence of Neanderthals in the Altai was originally identified in Okladnikov Cave, a site located 50km to the north of Denisova Cave, on the basis of mtDNA evidence.[30] Further archaeological and genetic data suggests that Neanderthals were in Siberia on several separate occasions.[31,32] They appear at Denisova Cave (layer 12, East Chamber) at least ~150-130 ka.[16,18] Five Neanderthal fossils have been found in the East Chamber so far, of which three are from layer 12 (Denisova 9, 11, 17) and two from the overlying layer 11.4 (Denisova 5, 15) (Fig. 3a). A single sediment sample from layer 14 of the East Chamber yielded Neanderthal DNA[23], but further work is required to replicate and confirm this signal. The mtDNA of the newly identified Neanderthal Denisova 17 is not closely related to the mtDNAs of any other Neanderthals from Denisova Cave analyzed to date, whereas Denisova 5 and Denisova 15 are closely related to one another (Fig. 2a) (Supplementary Information, Fig. S4 and Table S5). In contrast, Denisova 11 mtDNA is more closely related to the mtDNAs of Neanderthals from western Eurasia and to other Siberian Neanderthals, such as those from Okladnikov Cave and Chagyrskaya Cave (Fig. 2a).[31,33] Gene flow between Neanderthals and Denisovans provides additional indirect evidence of earlier interactions between the two groups. Analysis of the genome of a female Denisovan individual (Denisova 2), for example, has revealed that she had Neanderthal ancestry deriving from an introgression ~1500 years before she lived.[32] Two other Denisovans from higher up the stratigraphic sequence (Denisova 8 and 3) also show Neanderthal introgression from two different Neanderthal populations.[32] Although it is not possible to tell where these interbreeding events occurred, they provide evidence for potential co-habitation and frequent interactions between the two hominin populations from >200 ka until their disappearance from the Altai around 50 ka. Neanderthal presence, while more pronounced during the Last Interglacial period at Denisova Cave (MIS5) (Fig. 3b), is discontinuous within the Altai region[34] and may reflect occasional eastward migration of Neanderthal groups across large tracts of Eurasia. Since no gene flow from Denisovans to late European Neanderthals has been identified so far, these interactions seem most likely to have occurred in northeastern Eurasia. The Altai, in particular, appears to be an overlapping zone for both Denisovan and Neanderthal groups for over 150,000 years, witnessing population admixture as well as sustaining distinct hominin populations over this long period.

The specimens with the Denisovan mtDNAs (19, 20 and 21) all come from layer 15 of the East Chamber. The mitochondrial sequences of Denisova 19 and 21 are identical indicating that they may belong to the same individual or be maternal relatives. They differ by 4 substitutions from Denisova 20. In phylogenetic trees, the mtDNAs of the newly identified Denisovans form a clade with the mtDNAs of Denisova 2 (layer 22.1, Main Chamber) and Denisova 8 (layer 11.4, Easter Chamber) from which they differ by 20 and 30 substitutions, respectively (Fig. 2b and Fig. S3 and S6). Parsimony analyses are consistent with Denisova 19, 20 and 21 being of similar age or slightly older than Denisova 2, and substantially older than Denisova 8 and the later Denisova 3 and Denisova 4 (layer 11.2, East Chamber, and layer 11.1, South Chamber, respectively).

The mtDNA age estimates for the newly-identified specimens (Supplementary Information, Table S6) and their relationship to Denisova 2 agrees with the overall stratigraphic context and previous attempts to cross-correlate the three Chambers of Denisova Cave on the basis of age, archaeological sequence and hominin groups.[18,24] Previously, the earliest Denisovan (Denisova 2) was estimated to date to 122-194 ka using a Bayesian approach incorporating optical, genetic and stratigraphic data[18] (Fig. 3b). That specimen was discovered in 1984 in the Main Chamber and its contextual integrity has been questioned, whereas the new fossils reported here were excavated in 2012-13 from a secure context in the East Chamber. Layer 15 is the oldest archaeological layer of the East Chamber and is estimated to date to ~200 ka based on Bayesian modelling of optical ages (205-192 ka at 68.2% probability, or 217-187 ka at 95.4% probability)[18] (Fig. 3a). Both the mtDNA age estimates and the established chronology for layer 15 render Denisova 19, 20, 21 or their maternal relatives as the oldest Denisovans currently documented (Supplementary Information, Fig. S3).

The distribution of Denisovan DNA in present-day humans suggests that Denisovans were widely dispersed throughout Asia, and that there was spatial and temporal structure in their population.[4,5,31,33] Present-day humans from Siberia, East Asia, and indigenous Americans carry at least two Denisovan DNA components, one of which is more closely related to the genome of Denisova 3.[4,5] Characterization of the nuclear DNA of the Denisova 19, 20 and 21 individuals is required to determine whether these early Denisovans are more closely related to the Denisovans that admixed with the ancestors of present-day humans living in Island Southeast Asia and New Guinea.[5]

The presence of individuals carrying Denisovan mtDNA in the lowermost archaeological layer 15 of the East Chamber offers us an opportunity to consider the wider archaeological and subsistence context of this group of hominins. So far this has not been possible because the first Denisovan fossils identified either derived from layers impoverished in archaeological material or from layers where Neanderthal cohabitation could not be excluded.[7,12,23] The first evidence for Denisovan presence in the form of the mtDNAs of Denisova 19, 20 and 21 at the site falls in the Penultimate Interglacial (MIS 7) (Fig. 3b); a warm climatic period with comparable conditions to today that would have rendered the Altai a favorable location for hominin expansion and intensified occupation.

During this phase, a mosaic of landscapes can be detected in the vicinity of the cave, including both broad-leaved forests and open steppe landscapes.[20] Both traditional zooarchaeological and ZooMS analyses reveals that the inhabitants of the cave targeted a variety of taxa living in these environments, including interglacial forest and forest-steppe species, such as roe deer (*Capreolus pygargus*), Siberian red deer (*Cervus elaphus*), and giant deer (*Megaloceros giganteus*), as well as species typical of more open country, such as horse (*Equus ovodovi* and *Equus ferus*), bison (*Bison priscus*), woolly rhinoceros (*Coelodonta antiquitatis*), and Mongolian gazelle (*Gazella guttursza*)[18,24,27] (Fig. S1). Frequent anthropogenic impacts on bones, including splitting, burning and butchery cut-marks, confirm that these species were regularly procured. Humans appear not to have been the only occupants of Denisova Cave during this period, however. About a quarter of the macroscopically-identified faunal assemblage from layer 15 comprised carnivore remains, predominantly *Canis lupus* and *Cuon alpinus*.[18,24] This high proportion of carnivore taxa suggests that humans may have been actively competing with these predators over resources and perhaps the cave itself.

Archaeologically, layers 15 and 14 of the East Chamber contain the highest frequency of stone artifacts in the entire sequence of the cave, with more than 3,000 pieces per $1m^2$.[21] The lithic assemblage comprises discoidal, Levallois, and parallel cores to produce flakes using primary reduction techniques. Scrapers are the dominant tool type, including those shaped by steep Quina-type retouch, as well as spur-like, denticulate, and notched forms. Large ventrally thinned and basally truncated flakes, or truncated-faceted flakes, are typical pieces (Fig. S7, SI Section 4). A small number of blades with a longitudinal dorsal scar pattern are also present. Analyses of organic residues collected from a retouched flake from Layer 15 revealed saturated and unsaturated fatty acids and, alongside the absence of bone and plant micro-residues, its proposed use was for animal skin processing activities, such as scraping, cutting, and/or sawing.[35]

Based on its techno-typological characteristics and chrono-stratigraphic position, the lithic assemblage of layers 14 and 15 is attributed to an Early Middle Palaeolithic stone tool industry that has no direct counterparts in North and Central Asia. If we were to look further afield, the closest parallel is the Acheulo-Yabrudian cultural complex (AYCC) from the Near East, identified at several cave and open-air sites such as Tabun, Qesem, Hayonim, Misliya and dating to between 350-250 ka.[36] This is a period of major transformations in hominid adaptive and cognitive abilities that marks the transition from the Lower to Middle Palaeolithic. Techno-typological similarities between the AYCC with Denisova Cave include comparable forms of ventrally thinned and basally truncated flakes, and the presence of Quina scrapers, denticulate and notched tools. There are no bifacial tools in the Denisova assemblage; bifaces are a typical element of the Acheulean variant of the AYCC, but are rare or absent in the other two facies of the complex.

In the Levant, the shift from the Lower Palaeolithic Acheulean technological system dominated by handheld tools, such as flakes and bifaces, to lithic industries grouped under the AYCC, with a focus on the production of Quina scrapers and some blades, has

been linked to a series of major technological and subsistence innovations and adaptation strategies.[37] These include, among others, the habitual use of fire and the systematic hunting and butchering of medium-size ungulates, such as fallow deer. Interestingly, charcoal micro-residues were found in layers 15 and 14 of the East Gallery,[38] and cervids were clearly favoured by the early inhabitants of Denisova Cave, a practice that remains in stark contrast to the faunal record for all subsequent layers of the site.[18] There are at least two possibilities to explain the similarities between the AYCC and Denisova's Early Middle Palaeolithic stone assemblage. First, the origin of the Denisova lithic industries may be linked to the migration of hominins from West Asia, bringing with them the AYCC tradition. The biological affiliation of these hominins is unknown but likely predates the split between Neanderthals and Denisovans around 400 ka;[3] we may hypothesize that they belonged to late *Homo heidelbergensis*. Second, there is convergence at play in the development of the lithic adaptation in these two regions in which similar characteristics have appeared superficially as a result of environmental conditions or pressures. Since there are no intermediate occurrences of similar traditions in Central Asia as yet, and no intermediate forms of hominins that could be directly linked to Denisovans, further work is required to resolve this important question. The application of state-of-the-art biomolecular approaches therefore holds great potential in finding new hominin fossils dating back to the Middle Pleistocene, such as the ones we report here, and provides an opportunity to calibrate past demographic and dispersal events and elucidate the lifeways of early hominins.

Materials and Methods

Zooarchaeology by Mass Spectrometry (ZooMS). Analysis was carried out at the ZooMS facility of the Department of Archaeology at the Max Planck Institute for the Science of Human History, Jena, Germany. We followed established protocols.[25,26] In brief, from each bone approximately 10-20mg was removed using a circular diamond drill-bit. Samples were rinsed in ammonium bicarbonate overnight and incubated for 1h at 65℃. The supernatant was treated with 1µl trypsin (Thermo Scientific Pierce ™ Trypsin Protease) and allowed to digest at 37℃ for 18h. The incubated samples were concentrated and desalted using C18 ZipTips (Thermo Scientific Pierce™ C18 Tips) and eluted in a final solution of 50µl of 50% acetonitrile and 0.1% TFA. 0.5µl of the resulting solution was mixed with 0.5µl of α -cyano-4-hydroxycinnamic acid solution (10 mg/mL in 50% acetonitrile (ACN) and 0.1% trifluoroacetic acid (TFA) and allowed to crystallize. The samples were analysed using a MALDI TOF/TOF (Bruker Autoflex Speed LRF) mass spectrometer. The resulting spectra were screened for diagnostic markers using flexAnalysis 3.4 (Bruker Daltonics) and mMass software.[39] The spectra were compared against a reference library of known peptide markers[11,14,28] in order to identify any Hominidae bones amongst the assemblage.

MicroCT Scanning. Prior to sampling for aDNA analysis, the five bones identified as Hominidae using ZooMS, were scanned with image spatial resolutions ranging between

0.020 and 0.023 mm using the BrukerTM SkyScan 2211 X-ray Nanotomograph housed at MPI-SHH in Jena, Germany. Following the recommendations of Immel et al.[29] for avoiding degrading effects of X-ray irradiation, we strictly limited the scan image spatial resolution to 0.020 mm although smaller voxel sizes could have been achieved. We used a 0.5 mm titanium filter to remove the lowest energies of the X-ray spectrum. All scans were done applying a source voltage of 110 kV and a source current of 170 µA. Using the 'Isosurface' module the Avizo™ 9.4 (Visualization Science Group), we extracted 3D surfaces of the fossil bones from the microCT scans.

Mitochondrial DNA Analysis

DNA extraction and library preparation

After the removal of approximately 1 mm of surface material using a sterile dentistry drill, multiple small samples of ~7 to ~21mg of bone powder were obtained from each specimen. DNA was extracted from each sample (or a sub-sample thereof, not using more than 15 mg bone powder) with a method that uses silica-coated magnetic particles for the retrieval of short DNA molecules on an automated liquid handling platform.[40] Due to the low quantities of material that were removed, the volume of lysis buffer was reduced to 300µl, of which 150 µl were used for DNA extraction.

For Denisova 18, 19, 20 and 21, additional sampling of 9 mg to 17 mg of bone powder was performed and the samples were pre-treated with 0.5% sodium hypochlorite (bleach) solution following the protocol developed by Korlević et al.[41] DNA was extracted from the bleach treated samples following the same silica-based protocol as for non-bleached samples. The entire DNA extracts were converted into single-stranded DNA libraries.[42] Extraction and library negative controls were carried through all steps of the experiments. The libraries were amplified according to a double indexing scheme[43] and purified as described in the aforementioned library preparation protocol.[42]

A total of 29 single stranded DNA libraries were made for the 5 samples, including 9 for which extracts were pre-treated with bleach (Table S3). Using quantitative qPCR, we estimated the number of DNA molecules incorporated in each library between $1.6x10^{10}$ and $5.6x10^{9}$ for non-bleached samples and between $1.8x10^{9}$ and $1.5x10^{8}$ for bleached samples, which is on average higher than for libraries prepared from negative controls. Unfortunately, we found that the bleach treatment greatly reduced the amount of the endogenous DNA, making it unsuitable for these samples.

Mitochondrial DNA captures and sequencing

Each amplified library was enriched for human mitochondrial DNA (mtDNA) in two consecutive rounds of hybridization capture with a probe set covering the full human mitochondrial genome.[44,45] The enriched libraries were pooled and sequenced on a MiSeq (Illumina) in 76-cycle paired-end run.

Data processing and Mapping to a reference genome

Base calling was performed using Bustard (Illumina) and sequences that did not exactly match the expected index combinations were discarded. Adapter sequences were removed and overlapping paired-end reads were merged using leeHom with the parameter « --ancientdna ».[46] Overlap-merged sequences were mapped to the human

mitochondrial revised Cambridge reference sequence (rCRS) using Burrows-Wheeler Aligner (BWA)[47] with parameter « -n 0.01 –o 2 –l 16500 ».[9] PCR duplicates were collapsed into single sequences by consensus calling using bam-rmdup (https://github.com/mpieva/biohazard-tools). Sequences shorter than 35 bases or with a mapping quality lower than 25 were discarded. Initial investigations based on the sharing of derived sites carried by sequences covering positions in the mtDNA genome that are diagnostic of modern humans, Neanderthals and Denisovans showed that the mtDNA of Denisova 17 is of Neanderthal type and that Denisova 18, 19, 20 and 21 are of Denisovan type. In order to recover sequences that may be difficult to map due to their divergence to the human reference mtDNA genome, we re-aligned the raw sequences of the DNA libraries of Denisova 18, 19, 20 and 21 to the mtDNA sequences of the Denisova 3[2] and the Denisova 8[8] individuals. Because sequences aligned to Denisova 8 mtDNA were slightly more numerous than the sequences mapped to the Denisova 3 mtDNA, we used them for subsequent analyses.

Reconstruction of mtDNA genome sequence

Data from different libraries of the same specimen were merged, and only sequences with a length greater than 35 base pair (bp) and a mapping quality of at least 25 were retained to call the mtDNA consensus sequences. Because of the level of present-day human DNA contamination in Denisova 19, 20 and 21, we restricted the analysis to sequences showing evidence of cytosine (C) to thymine (T) mismatches to the reference genome at the 3 first or last bases (deaminated sequences). Using deaminated sequences only, we called a consensus at each position covered by at least three sequences where at least 66% of the fragments carry the same base. The state of positions covered by two or fewer deaminated sequences were called using the alignment of all sequences when supported by more than 5 sequences for libraries with contamination estimate < 5%. For Denisova 17, we used all sequences and called a consensus at each position covered by at least 5 sequences where at least 80% of the fragments carry the same base. For all consensus sequences, manual correction of the alignment was necessary to confidently call certain positions, especially over cytosine homopolymer stretches.

Pairwise, phylogenetic analyses and relative molecular age estimates

For the phylogenetic analyses, the reconstructed mtDNA sequences of Denisova 17, 19, 20 and 21 were aligned to the mtDNA genomes of 26 Neanderthals,[12,34,48–56] four Denisovans,[2,6,8] the Middle Pleistocene Hominin from Sima de los Huesos,[57] six ancient modern humans,[44,58–62] six present-day humans[63] and a chimpanzee[64] using Clustal Omega[65] (Table S7). Pairwise differences between mitochondrial genomes and Neighbor Joining phylogeny were inferred using MEGA X.[66] Maximum Parsimony analyses were conducted in PAUP*[67] using minimization of F-value (MINF) as character-state optimization, gaps in the sequences were treated as “missing”. Optimal trees were generated by heuristic search method using a Nearest-neighbor interchange (NNI) branch swapping algorithm and consensus tree was called by 50% majority-rule method of several equally parsimonious trees. Relative molecular age of the Denisovan and

Neanderthal mtDNAs were estimated by inferring by parsimony the number of substitutions accumulated in each mtDNA sequences since the split from the mtDNA of the middle pleistocene hominin from Sima de los Huesos for Denisovans and since the split from the highly diverged mtDNA of the Hohlenstein Stadel individual for Neanderthals. We caution that back mutations and multiple substitutions occurring at the same position will not be accounted for and may affect our inferences.

References

1. Reich, D. *et al.* Genetic history of an archaic hominin group from Denisova Cave in Siberia. *Nature* **468**, 1053–1060 (2010).
2. Krause, J. *et al.* The complete mitochondrial DNA genome of an unknown hominin from southern Siberia. *Nature* **464**, 894–897 (2010).
3. Prüfer, K. *et al.* A high-coverage Neandertal genome from Vindija Cave in Croatia. *Science* **358**, 655–658 (2017).
4. Browning, S. R., Browning, B. L., Zhou, Y., Tucci, S. & Akey, J. M. Analysis of Human Sequence Data Reveals Two Pulses of Archaic Denisovan Admixture. *Cell* **173**, 53–61.e9 (2018).
5. Jacobs, G. S. *et al.* Multiple Deeply Divergent Denisovan Ancestries in Papuans. *Cell* **177**, 1010–1021.e32 (2019).
6. Slon, V. *et al.* A fourth Denisovan individual. *Sci Adv* **3**, e1700186 (2017).
7. Slon, V. *et al.* The genome of the offspring of a Neanderthal mother and a Denisovan father. *Nature* **561**, 113–116 (2018).
8. Sawyer, S. *et al.* Nuclear and mitochondrial DNA sequences from two Denisovan individuals. *Proc. Natl. Acad. Sci. U. S. A.* **112**, 15696–15700 (2015).
9. Meyer, M. *et al.* A high-coverage genome sequence from an archaic Denisovan individual. *Science* **338**, 222–226 (2012).
10. Chen, F. *et al.* A late Middle Pleistocene Denisovan mandible from the Tibetan Plateau. *Nature* **569**, 409–412 (2019).
11. Buckley, M., Collins, M., Thomas-Oates, J. & Wilson, J. C. Species identification by analysis of bone collagen using matrix-assisted laser desorption/ionisation time-of-flight mass spectrometry. *Rapid Commun. Mass Spectrom.* **23**, 3843–3854 (2009).
12. Brown, S. *et al.* Identification of a new hominin bone from Denisova Cave, Siberia using collagen fingerprinting and mitochondrial DNA analysis. *Sci. Rep.* **6**, 23559 (2016).
13. Buckley, M. *et al.* Species identification of archaeological marine mammals using collagen fingerprinting. *J. Archaeol. Sci.* **41**, 631–641 (2014).
14. Welker, F. *et al.* Palaeoproteomic evidence identifies archaic hominins associated with the Châtelperronian at the Grotte du Renne. *Proc. Natl. Acad. Sci. U. S. A.* **113**, 11162–11167 (2016).
15. Charlton, S. J. L., Alexander, M., Collins, M. J., Milner, N. & Craig, O. E. Finding Britain's last hunter-gatherers: A new biomolecular approach to 'unidentifiable' bone fragments utilising bone collagen. **73**, 55–61 (2016).
16. Douka, K. *et al.* Age estimates for hominin fossils and the onset of the Upper Palaeolithic at Denisova Cave. *Nature* **565**, 640–644 (2019).
17. Devièse, T. *et al.* Direct dating of Neanderthal remains from the site of Vindija Cave and implications for the Middle to Upper Paleolithic transition. *Proc. Natl. Acad. Sci. U. S. A.* **114**, 10606–10611 (2017).

18. Jacobs, Z. *et al.* Timing of archaic hominin occupation of Denisova Cave in southern Siberia. *Nature* **565**, 594–599 (2019).
19. Agadjanian, A. K. The dynamics of bioresources and activity of the paleolithic man, using the example of northwestern Altai Mountains. *Paleontol. J.* **40**, S482–S493 (2006).
20. Bolikhovskaya, N. S. & Shunkov, M. V. Pleistocene Environments of Northwestern Altai: Vegetation and Climate1. *Archaeology, Ethnology and Anthropology of Eurasia* **42**, 2–17 (2014).
21. Shunkov, M. V., Kozlikin, M. B. & Derevianko, A. P. Dynamics of the Altai Paleolithic industries in the archaeological record of Denisova Cave. *Quat. Int.* (2020) doi:10.1016/j.quaint.2020.02.017.
22. Derevianko, A. P., Shunkov, M. V. & Markin, S. V. *The dynamics of the Paleolithic industries in Africa and Eurasia in the Late Pleistocene and the issue of the Homo sapiens Origin*. (IAET SO RAN, 2014).
23. Slon, V. *et al.* Neandertal and Denisovan DNA from Pleistocene sediments. *Science* **356**, 605–608 (2017).
24. Vasiliev, S. K., Shunkov, M. V. & Kozlikin, M. B. Preliminary Results for the Balance of Megafauna from Pleistocene Layers of the East Gallery, Denisova Cave. *Problems of Archaeology, Ethnography, and Anthropology of Siberia and Adjacent Territories* **19**, 32–38 (2013).
25. van Doorn, N. L., Hollund, H. & Collins, M. J. A novel and non-destructive approach for ZooMS analysis: ammonium bicarbonate buffer extraction. *Archaeol. Anthropol. Sci.* **3**, 281 (2011).
26. Brown, S. *et al.* Zooarchaeology by Mass Spectrometry (ZooMS) for bone material - AmBiC protocol v1 (protocols.io.bffdjji6). (2020).
27. Brown, S. *et al.* Zooarchaeology through the lens of collagen fingerprinting at Denisova Cave. *in prep*.
28. Buckley, M. & Kansa, S. W. Collagen fingerprinting of archaeological bone and teeth remains from Domuztepe, South Eastern Turkey. *Archaeol. Anthropol. Sci.* **3**, 271–280 (2011).
29. Immel, A. *et al.* Effect of X-ray irradiation on ancient DNA in sub-fossil bones - Guidelines for safe X-ray imaging. *Sci. Rep.* **6**, 32969 (2016).
30. Krause, J. *et al.* Neanderthals in central Asia and Siberia. *Nature* **449**, 902–904 (2007).
31. Vernot, B. *et al.* Excavating Neandertal and Denisovan DNA from the genomes of Melanesian individuals. *Science* **352**, 235–239 (2016).
32. Peter, B. M. 100,000 years of gene flow between Neandertals and Denisovans in the Altai mountains. *bioRxiv* (2020).
33. Reich, D. *et al.* Denisova admixture and the first modern human dispersals into Southeast Asia and Oceania. *Am. J. Hum. Genet.* **89**, 516–528 (2011).
34. Mafessoni, F. *et al.* A high-coverage Neandertal genome from Chagyrskaya Cave. *Proc. Natl. Acad. Sci. U. S. A.* (2020) doi:10.1073/pnas.2004944117.
35. Bordes, L., Fullagar, R., Prinsloo, L. C. & Hayes, E. Raman spectroscopy of lipid micro-residues on Middle Palaeolithic stone tools from Denisova Cave, Siberia. *Journal of* (2018).
36. Zaidner, Y. & Weinstein-Evron, M. The end of the Lower Paleolithic in the Levant: The Acheulo-Yabrudian lithic technology at Misliya Cave, Israel. *Quat. Int.* **409**, 9–22 (2016).

37. Barkai, R. & Gopher, A. Cultural and Biological Transformations in the Middle Pleistocene Levant: A View from Qesem Cave, Israel. in *Dynamics of Learning in Neanderthals and Modern Humans Volume 1: Cultural Perspectives* (eds. Akazawa, T., Nishiaki, Y. & Aoki, K.) 115–137 (Springer Japan, 2013).
38. Morley, M. W. *et al.* Hominin and animal activities in the microstratigraphic record from Denisova Cave (Altai Mountains, Russia). *Sci. Rep.* **9**, 13785 (2019).
39. Strohalm, M., Hassman, M., Kosata, B. & Kodícek, M. mMass data miner: an open source alternative for mass spectrometric data analysis. *Rapid Commun. Mass Spectrom.* **22**, 905–908 (2008).
40. Rohland, N., Glocke, I., Aximu-Petri, A. & Meyer, M. Extraction of highly degraded DNA from ancient bones, teeth and sediments for high-throughput sequencing. *Nat. Protoc.* **13**, 2447–2461 (2018).
41. Korlević, P. *et al.* Reducing microbial and human contamination in DNA extractions from ancient bones and teeth. *Biotechniques* **59**, 87–93 (2015).
42. Gansauge, M.-T., Aximu-Petri, A., Nagel, S. & Meyer, M. Manual and automated preparation of single-stranded DNA libraries for the sequencing of DNA from ancient biological remains and other sources of highly degraded DNA. *Nat. Protoc.* (2020) doi:10.1038/s41596-020-0338-0.
43. Kircher, M., Sawyer, S. & Meyer, M. Double indexing overcomes inaccuracies in multiplex sequencing on the Illumina platform. *Nucleic Acids Res.* **40**, e3 (2012).
44. Fu, Q. *et al.* DNA analysis of an early modern human from Tianyuan Cave, China. *Proc. Natl. Acad. Sci. U. S. A.* **110**, 2223–2227 (2013).
45. Maricic, T., Whitten, M. & Pääbo, S. Multiplexed DNA sequence capture of mitochondrial genomes using PCR products. *PLoS One* **5**, e14004 (2010).
46. Renaud, G., Stenzel, U. & Kelso, J. leeHom: adaptor trimming and merging for Illumina sequencing reads. *Nucleic Acids Res.* **42**, e141 (2014).
47. Li, H. & Durbin, R. Fast and accurate short read alignment with Burrows-Wheeler transform. *Bioinformatics* **25**, 1754–1760 (2009).
48. Green, R. E. *et al.* A complete Neandertal mitochondrial genome sequence determined by high-throughput sequencing. *Cell* **134**, 416–426 (2008).
49. Prüfer, K. *et al.* The complete genome sequence of a Neanderthal from the Altai Mountains. *Nature* **505**, 43–49 (2014).
50. Rougier, H. *et al.* Neandertal cannibalism and Neandertal bones used as tools in Northern Europe. *Scientific Reports* vol. 6 (2016).
51. Briggs, A. W. *et al.* Targeted retrieval and analysis of five Neandertal mtDNA genomes. *Science* **325**, 318–321 (2009).
52. Gansauge, M.-T. & Meyer, M. Selective enrichment of damaged DNA molecules for ancient genome sequencing. *Genome Res.* **24**, 1543–1549 (2014).
53. Skoglund, P. *et al.* Separating endogenous ancient DNA from modern day contamination in a Siberian Neandertal. *Proc. Natl. Acad. Sci. U. S. A.* **111**, 2229–2234 (2014).
54. Posth, C. *et al.* Deeply divergent archaic mitochondrial genome provides lower time boundary for African gene flow into Neanderthals. *Nat. Commun.* **8**, 16046 (2017).
55. Hajdinjak, M. *et al.* Reconstructing the genetic history of late Neanderthals. *Nature* **555**, 652–656 (2018).
56. Peyrégne, S. *et al.* Nuclear DNA from two early Neandertals reveals 80,000 years of genetic continuity in Europe. *Sci Adv* **5**, eaaw5873 (2019).
57. Meyer, M. *et al.* A mitochondrial genome sequence of a hominin from Sima de los

Huesos. *Nature* **505**, 403–406 (2014).
58. Fu, Q. *et al.* Genome sequence of a 45,000-year-old modern human from western Siberia. *Nature* **514**, 445–449 (2014).
59. Fu, Q. *et al.* An early modern human from Romania with a recent Neanderthal ancestor. *Nature* **524**, 216–219 (2015).
60. Fu, Q. *et al.* The genetic history of Ice Age Europe. *Nature* **534**, 200–205 (2016).
61. Devièse, T. *et al.* Compound-specific radiocarbon dating and mitochondrial DNA analysis of the Pleistocene hominin from Salkhit Mongolia. *Nat. Commun.* **10**, 274 (2019).
62. Sikora, M. *et al.* Ancient genomes show social and reproductive behavior of early Upper Paleolithic foragers. *Science* **358**, 659–662 (2017).
63. Green, R. E. *et al.* A draft sequence of the Neandertal genome. *Science* **328**, 710–722 (2010).
64. Horai, S. *et al.* Man's place in Hominoidea revealed by mitochondrial DNA genealogy. *J. Mol. Evol.* **37**, 89 (1993).
65. Sievers, F. *et al.* Fast, scalable generation of high-quality protein multiple sequence alignments using Clustal Omega. *Mol. Syst. Biol.* **7**, (2011).
66. Stecher, G., Tamura, K. & Kumar, S. Molecular Evolutionary Genetics Analysis (MEGA) for macOS. *Mol. Biol. Evol.* **37**, 1237–1239 (2020).
67. Swofford, D. L. PAUP: phylogenetic analysis using parsimony, version 4.0 b10. (2002).
68. Lisiecki, L. E. & Raymo, M. E. A Pliocene-Pleistocene stack of 57 globally distributed benthic δ18O records. *Paleoceanography* **20**, (2005).

Acknowledgments

We would like to thank the European Research Council, the Max Planck Society, the Oxford Radiocarbon Accelerator Unit (ORAU), and the Institute of Archeology and Ethnography, Russian Academy of Sciences Siberian Branch for their ongoing support. Michelle O'Reilly from the Max Planck Institute for the Science of Human History and Ian Cartwright from the University of Oxford photographed the hominin fossils. We would like to thank in particular the volunteers who helped us sample the material, Miriam Jenkins, Esther Gillespie, Lauren Bell, Marine Caldarola, Raija Heikkila, Laura Doody, Saltanat Amirova, Geoff Church, Lucy Koster, Rachael Holmes, Luke Ghent, Phoebe Ewles-Bergeron, Nicholas Siemens, Marion Sandilands, and Julianna Zavodski as well as Viviane Slon, Elena Essel, Sarah Nagel and Julia Richter from the Max Planck Institute for Evolutionary Anthropology for discussions and laboratory work. This work has received funding from the ERC under the European Union's Horizon 2020 Research and Innovation Programme, grant agreement no. 715069 (FINDER) to KD and under the European Union's Seventh Framework Programme (FP7/2007–2013), grant agreement no. 324139 (PalaeoChron) to TH, and grant agreement no. 694707 (100 Archaic Genomes) to SP. The archaeological field studies were funded by the Russian Foundation for Basic Research (no. 18-09-40100 and no. 18-09-00404).

Author Contributions

SB, DM, BJ, AS performed the laboratory work; SB, DM, AS, MM, JK, SP, KD analyzed the data; MK, MS, AD provided samples and site-specific expertise; KD designed the study; SB, DM, TH, and KD wrote the paper with the assistance and input of all authors.

Additional Information

Supplementary Information is available for this paper.

Correspondence and requests for materials should be addressed to Samantha Brown (brown@shh.mpg.de) and Katerina Douka (douka@shh.mpg.de).

Figures

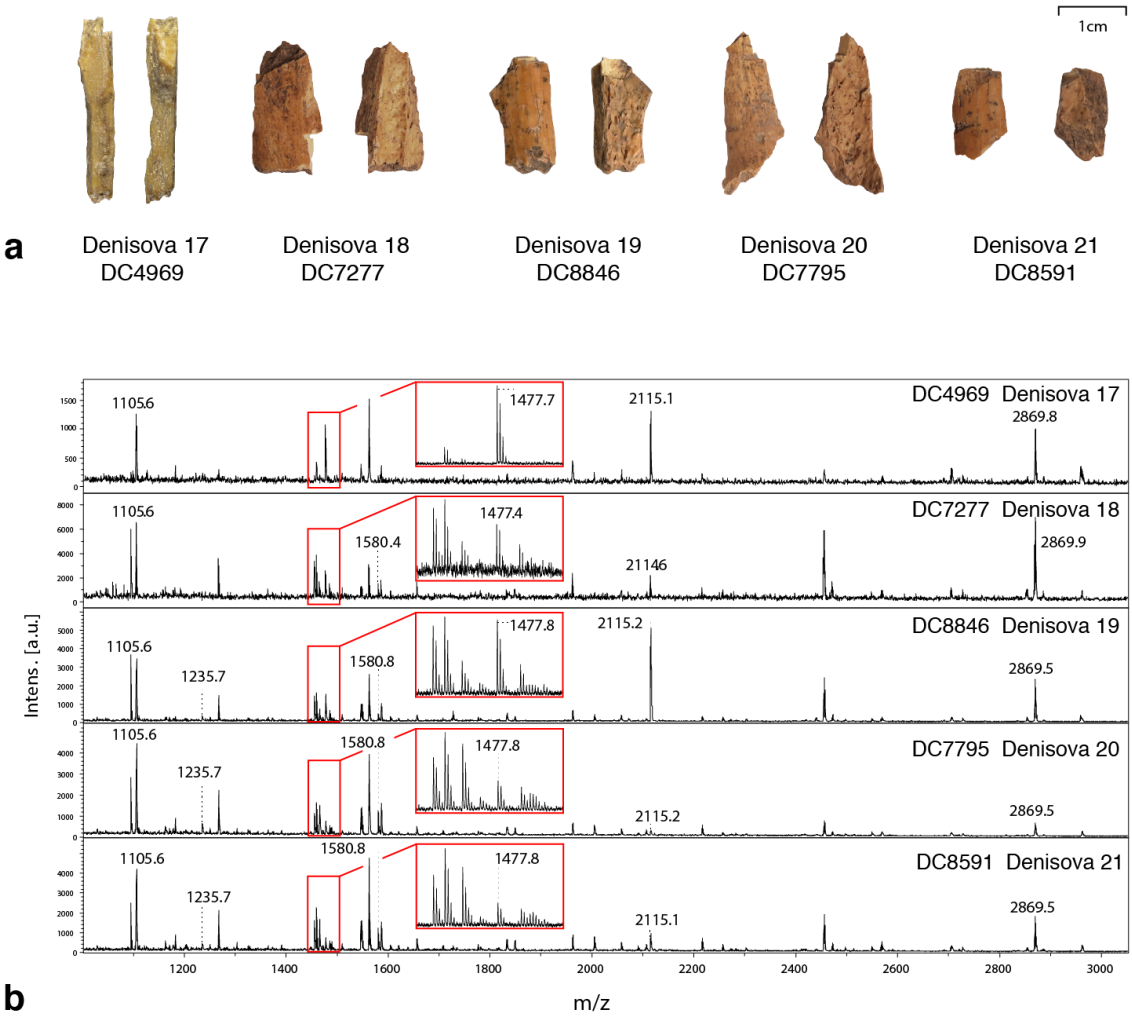

Figure 1. a. The five new hominin bones identified using ZooMS analysis. The two larger surfaces of each bone are shown. **b.** MALDI-TOF mass spectra for the five new identified Hominidae bones from Denisova Cave. Peptide mass fingerprints for Denisova 17 (DC4969), Denisova 18 (DC7277), Denisova 19 (DC8846), Denisova 20 (DC7795), Denisova 21 (DC8591). Labelled peaks are used as markers to identify these bones as Hominidae.[11,14]

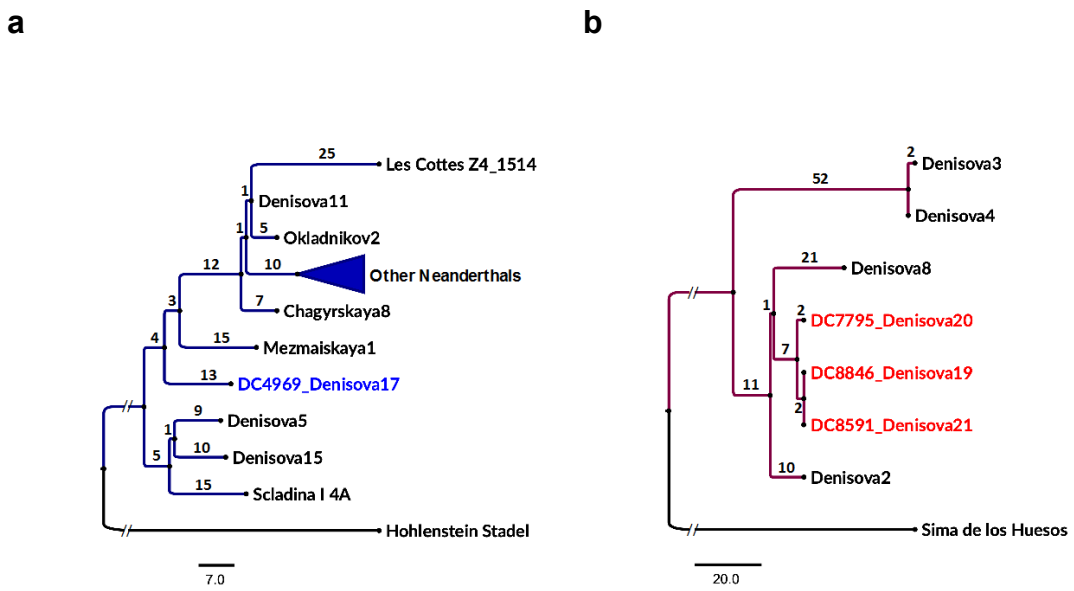

Figure 2. Mitochondrial (mt) DNA maximum parsimony phylogenetic trees. **a.** Neanderthal mtDNA parsimony phylogeny including Denisova 17 and 26 previously published Neanderthal mtDNAs. The mtDNA of Denisova 17 differs by 27, 26 and 28 substitutions from the mtDNA of Denisova 11, Denisova 5 and Denisova 15. The topology of the tree corresponds to the 50% majority-rule consensus of 16 equally parsimonious trees rooted using the highly divergent mtDNA of the Hohlenstein Stadel Neanderthal. **b.** Denisovan mtDNA parsimony phylogeny including Denisova 19, 20 and 21 and four previously published Denisovan mtDNAs. The tree is one of the two most parsimonious trees (Supplementary Information, Fig. S6) rooted using the mtDNA of the Middle Pleistocene Hominin from Sima de los Huesos. The trees are drawn to scale, with branch lengths computed in number of substitutions.

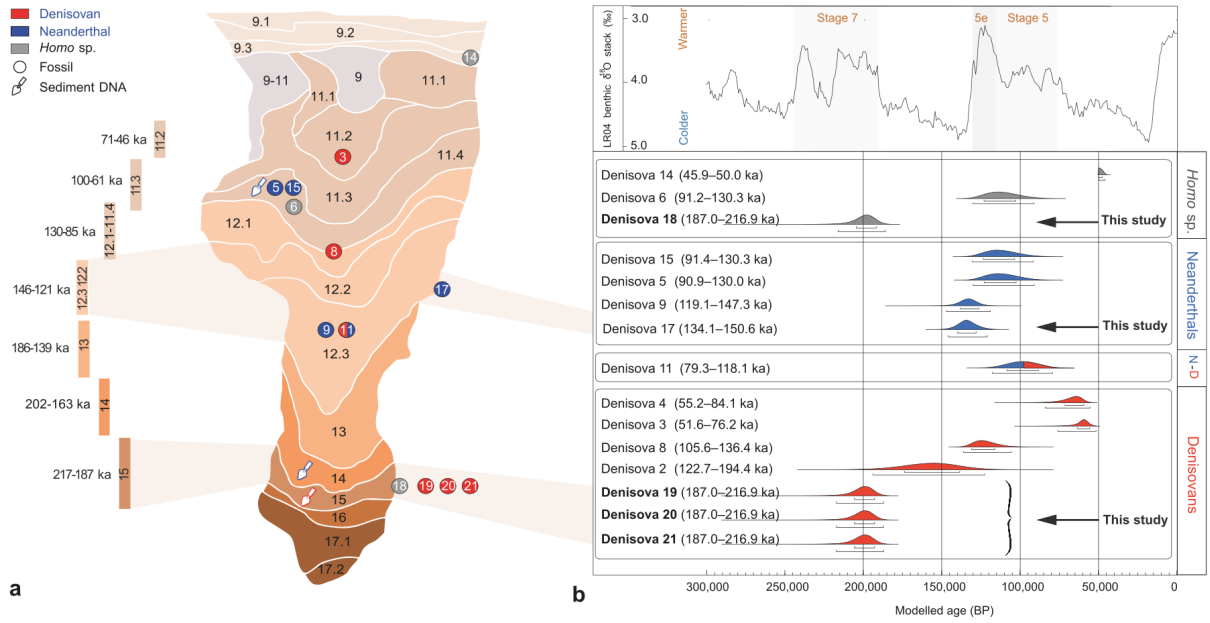

Figure 3. The hominin record at Denisova Cave **a.** Stratigraphy of the East Chamber of Denisova Cave. The position of hominin fossils (circles) and sediment DNA (trowel) is shown on the stratigraphic column whereas the newly identified hominin fossils, Denisova 17, Denisova 18, Denisova 19, Denisova 20, and Denisova 21 are shown next to the relevant stratigraphic layers. To the left, the colored bars and the numerals represent the age range in thousand years before present (ka BP) of each dated layer based on modelled optical ages.[18] **b.** Updated age ranges of all hominins from Denisova Cave, including the newly identified specimens. The ages for Denisova 17, 19, 20, 21 derive from the Bayesian statistical treatment of optical ages.[18] The ages for all other fossils derive from different Bayesian modeling described in Douka et al.[16] and which includes both genetic, radiocarbon and optical ages. The marine-oxygen isotope curve compiled from benthic δ18O records[68] is shown to the top; the Last and Penultimate Interglacials (Marine Isotope Stages 5 and 7) that were the warmest parts of the last 300 ka are highlighted.

Supplementary Information Text

1. Zooarchaeology by Mass Spectrometry (ZooMS)

ZooMS analysis was carried out for 3,791 samples from Denisova Cave's East Gallery.[1] All archaeological layers were investigated resulting in the identification of five Hominidae samples. The majority of bones studied were identified as Bos/Bison (23%), Cervidae/Gazella/Saiga (22%), and Equidae (10%; Fig. S1). 22% of the samples failed ZooMS analysis as a result of poor collagen preservation; these are not shown in Fig. S1. The results of the ZooMS-based fauna identification are in reasonable agreement with fauna previously identified at the site through traditional morphological analysis.[1-3] Trends linked to prevailing environmental conditions (interglacial versus glacial periods), ambient temperatures and plant coverage have been reconstructed, although a larger sample size is required to solidify these trends.

2. List of new hominin fossils

Denisova 17, bone fragment (Neanderthal) (Fig. 1).

2011, East Chamber, Sector 6, Layer 12

This specimen was identified among the bulk fragment assemblage from layer 12 of the East Chamber using ZooMS (ZooMS ID: DC4969) and is reported in this paper for the first time. MtDNA analysis, summarised in Section 3 of the Supplementary Text, indicates this individual carries Neanderthal mtDNA.

Denisova 18, bone fragment (Homo sp.) (Fig. 1).

2012-2013, East Chamber, Sector 6, Layer 15

This specimen was identified among the bulk fragment assemblage from layer 15 of the East Chamber using ZooMS (ZooMS ID: DC7277) and is reported in this paper for the first time. MtDNA analysis, summarised in Section 3 of the Supplementary Text, was inconclusive due to present-day human contamination and low aDNA preservation in the sample.

Denisova 19, bone fragment (Denisovan) (Fig. 1).

2012-2013, East Chamber, Sector 6, Layer 15

This specimen was identified among the bulk fragment assemblage from layer 15 of the East Chamber using ZooMS (ZooMS ID: DC8846) and is reported in this paper for the first time. MtDNA analysis, summarised in Section 3 of the Supplementary Text, indicates this individual carries Denisovan mtDNA. The Denisova 19 and 21 mitochondrial sequences are identical and may belong to the same individual or maternal relatives.

Denisova 20, bone fragment (Denisovan) (Fig. 1).

2012-2013, East Chamber, Sector 6, Layer 15

This specimen was identified among the bulk fragment assemblage from layer 15 of the East Chamber using ZooMS (ZooMS ID: DC3573) and is reported in this paper for the first time. MtDNA analysis, summarised in Section 3 of the Supplementary Text, indicates this individual carries Denisovan mtDNA.

Denisova 21, bone fragment (Denisovan) (Fig. 1).
2012-2013, East Chamber, Sector 6, Layer 15
This specimen was identified among the bulk fragment assemblage from layer 15 of the East Chamber using ZooMS (ZooMS ID: DC3573) and is reported in this paper for the first time. MtDNA analysis, summarised in Section 3 of the Supplementary Text, indicates this individual carries Denisovan mtDNA. The mitochondrial sequence of Denisova 21 and Denisova 19 identical and may belong to the same individual or maternal relatives.

3. Mitochondrial DNA analysis

Ancient DNA authenticity

Cytosine residues (C) close to the ends of ancient DNA molecules tend to become deaminated to uracils (U)[4] and are read by DNA polymerases as thymines (T). Thus we gauged the presence of ancient DNA in a sample based on the frequency of C to T mismatches to the reference at the extremities of the sequences.[5] After sequencing of the human mtDNA enriched libraries, the data were mapped to the human reference mtDNA sequence rCRS and 26 libraries show evidence for presence of ancient hominin mtDNA as their C to T frequencies at both the 5' and 3' ends are > 10% (between 19.7% and 53.2% at the 5' ends and between 10% and 47.8% at the 3'ends) (Table S3). 3 out of 5 libraries of Denisova 18 have C to T frequency <10% indicating that aDNA is less well preserved in that specimen in comparison to the others.

Determination of mtDNA hominin type

We determined the mtDNA hominin type of the mapped sequences in each library by estimating the frequency of sequences matching the modern human, Neanderthal or Denisovan states at "diagnostic" positions that discriminate each of the different hominin mtDNA lineages.[6] Considering only sequences carrying a C to T mismatch at one or the other end (deaminated sequences), the libraries of *Denisova 17* have a total of 4,990 deaminated sequences covering the Neanderthal mtDNA diagnostic positions and 94% of them match the Neanderthal state, indicating that the mtDNA of *Denisova 17* is of Neanderthal type. The deaminated sequences of the *Denisova 19, 20* and *21* libraries match the Denisovan state at 96% (250/260), 92% (425/463) and 87% (381/439), respectively, indicating that these specimens have a mtDNA of Denisovan type. The two libraries of *Denisova 18* with C to T frequencies >10% yield a total of only 248 deaminated sequences with 34 of them covering the diagnostic positions of the Denisovan mtDNA and matching at 70% the Denisovan state, 18 of them covering the diagnostic positions of Neanderthal mtDNA and matching at 0% the Neanderthal state and 8 of them covering the diagnostic positions of modern human mtDNA and matching at 62.5% the modern human state. It is likely that the

Denisova 18 specimen has a mtDNA of the Denisovan type, but due to the small number of mtDNA sequences we cannot rule out cross-contamination from the other Denisovan specimens during the DNA processing.

Re-alignment of the data

For *Denisova 18, 19, 20* and *21*, which were assigned to the Denisovan mtDNA type, we re-aligned all sequences to the mtDNA sequences of *Denisova 3* and *Denisova 8*[7] in order to recover sequences that might have been lost due to high divergence to the human reference mtDNA. Re-alignment to the *Denisovan 8* mtDNA recovered 4.4% to 9.2 % and 0.4% to 2.6% more mapped sequences than when the sequence of rCRS and the *Denisova 3* mtDNAs were used as reference. Similarly, we re-aligned sequences from the Denisova 17 libraries to the mtDNA of the Vindija 33.25 individual and recovered between 5.9% and 6.1% more mapped sequences than with the rCRS as reference. C to T frequencies for each library were computed based on the reference genome used (Table S4). After merging the sequences obtained from different libraries from the same specimen, we have 907,043 unique mtDNA sequences longer than 35 bp for *Denisova17*, and 22,215, 20,741, 40,284, and 41,434 unique mtDNA sequences longer than 35 bp for *Denisova 18, 19, 20* and *21*, respectively. The average rate with which identical sequences were observed was ~2-fold for *Denisova 17* and over 12-fold for the others, indicating that the libraries have been sequenced deeply (Table S4).

Present-day human mitochondrial contamination

We estimated the mitochondrial contamination by determining the proportion of sequences that share the derived modern human states at positions where 311 present-day humans from around the world differ from all Neanderthals and Denisovans. We estimated the average contamination among the libraries prepared from *Denisova 17* to 0.89%, and the average contamination for *Denisova 18, 19, 20* and *21* to 65.9%, 9.4%, 13.4% and 31.9%. Because of the contamination estimates of *Denisova 18, 19, 20* and *21*, we used only deaminated fragments to reconstruct their mtDNA genome sequences.

Mitochondrial genome consensus

Depending on the modern human contamination estimates we used either all sequences or only deaminated sequences to reconstruct mtDNA consensus sequences. Using all sequences we call a mtDNA consensus sequence for *Denisova 17* to an average coverage of 2,695-fold. Complete consensus mtDNAs of *Denisova 20, 21* were called using only deaminated sequences to an average coverage of 31-fold and 28-fold, respectively. For *Denisova 19*, we have an average coverage of 15-fold with three positions that could not be called confidently. The mtDNA consensus of *Denisova 18* could not be called.

Phylogenetic analyses

Pairwise differences (Fig. S3) and phylogenetic analyses (Fig. S4) support the assignment of the mtDNA of *Denisova 17* within the diversity of Neanderthal mtDNAs and the assignment of the mtDNA of Denisova 19, 20 and 21 within the diversity of Denisovan mtDNAs. The *Denisova 17* mtDNA sequence

differs from the mtDNAs of other Neanderthals from Denisova Cave - *Denisova 5, 15* and *11*- by 26, 27 and 28 substitutions, respectively (Fig. S3). Sixteen equally parsimonious trees with an equal length of 253 substitutions can be generated for our dataset of 27 Neanderthal mtDNAs. We called a consensus tree using the 50% majority-rule method (Fig. S5) and counted the number of substitutions accumulated in each mtDNA of the Neanderthal from Denisova cave since they split from their most recent ancestor to the exclusion of the Hohlenstein-Stadel Neanderthal. Since they diverged from their last common ancestor, *Denisova 5, 15, 17* and *11* have accumulated 15, 16, 17 and 21 substitutions, respectively (Fig. S5). *The Denisova 17* mtDNA accumulated 4 substitutions less than the mtDNA of *Denisova 11* and 1 and 2 substitutions more than the mtDNAs of *Denisova 15* and *Denisova 5*, respectively. Using the mitochondrial mutation rate inferred for modern humans of 2.53x10-8 (95% HPD: 1.76-3.23 x 10-8) (Table S5) under the assumption that the mitochondrial mutation rate in archaic humans is the same as that in modern human, we estimate that the molecular age of the mtDNA of *Denisova 17* is about 7-14 ky older than *Denisova 11*, 2-3 ky younger than *Denisova 15* and 4-7 ky younger than *Denisova 5* (Table S5).

Excluding the three positions not covered in the mtDNA of the *Denisova 19* individual, its sequence is identical to the mtDNA sequence of *Denisova 21*. Both *Denisova 19* and *21* mtDNAs differ from *Denisova 20* mtDNA by 4 substitutions (Fig. S3). The phylogenetic relationship between the three new Denisovan mtDNAs and the previously published four Denisovan mtDNAs can be described by two equally parsimonious scenarios with a length of 274 substitutions (Fig. S6A and S6B). In both scenarios the 7 Denisovan mtDNAs are distributed in 2 main clades, one composed by the mtDNAs of the *Denisova 19, 20, 21, 2* and *8* individuals and the other composed by the mtDNAs of the *Denisova 3* and *4* individuals. The two maximum parsimony trees differ in their topology and the lengths of their branches. In the tree Fig. S6A, the mtDNAs of *Denisova 19, 20* and *21* group together in a clade including *Denisova 2* and *8* and the mtDNAs of *Denisova 19, 20, 21* and *2* accumulated 21 substitutions since their divergence from a common ancestor with *Denisova 3* and *Denisova 4*, and 33 substitutions since their divergence from a common ancestor with *Denisova 8*. *Denisova 19, 20, 21* and *2* are older since they accumulated 12 substitutions less than *Denisova 8* since they diverged from each other. The alternate tree in Fig. 6B suggests that the clade formed by *Denisova 2, 8, 19, 20* and *21* is more structured, with *Denisova 2* and *8* grouping together alongside the group formed by *Denisova 19, 20* and *21*. In this tree, the mtDNAs of *Denisova 19, 20* and *21* accumulated 6 and 18 substitutions fewer than the mtDNAs of *Denisova 2* and *Denisova 8*, respectively. Both scenarios show that the branch length leading to the mtDNA of *Denisova 3* and *Denisova 4* are the longest and that the mtDNA of *Denisova 3* and *Denisova 4* accumulated respectively 33 and 31 substitutions more than the mtDNA of *Denisova 19, 20* and *21* since they diverged from the common ancestor of Denisovan mtDNA. The estimates of the molecular ages of the mtDNAs suggest that *Denisova 19, 20* and *21* are of similar age or about 11-20 ky older than *Denisova 2*, about 22-62 ky older than *Denisova 8* and about 58-113 ky older than *Denisova 3* and *Denisova 4* (Table S6).

4. Archaeology

The oldest archaeological evidence from Denisova Cave was found in layer 22 of Main Chamber, with an upper age limit of 287 ± 41 ka estimated using a series of optical ages[2]. It is overlain by layers 21 and 20, dated in around 250 ± 44 to 170 ± 19 ka. In the East Chamber, these deposits correspond to layers 15 and 14 dated between 203 ± 14 ka and 187 ± 14 ka during MIS 7[2].

Based on the chronostratigraphy of cave sediments and the techno-typological appearance of stone tool industries, the material culture from layers 15 and 14 in East Chamber is attributed to the Early Middle Palaeolithic. The stone tool industries of this period are characterized by the presence of discoid cores with unifacial and bifacial variations, as well as parallel unifacial single-platform cores that are mainly produced from massive flakes and larger pebbles or smaller boulders. Flakes are dominated by short pieces with a smooth or natural platform, showing evidence of longitudinal or multidirectional dorsal faceting. Blades are rare and have a smooth striking platform and a longitudinal dorsal scar pattern. Typologically stone artifacts made on standard blanks, such as single, oblique, transverse, convergent, and canted scrapers, including those shaped by stepped Quina-type retouch, as well as spur-like, denticulate and notched forms, are the most common in the lithic inventory. Of particular interest are the numerous ventrally thinned pieces that comprise large, massive flakes with the distal edge and one or two lateral edges intensively reduced by large flake removals on the ventral surface.

Another characteristic type of artifacts includes basally truncated and truncated-faceted flakes, showing indications of ventral or, rarely, dorsal truncation. In addition, the tool assemblage contains naturally backed knives, transverse burins on blade, angle burins on massive flakes, as well as elongated Levallois points with a faceted medially convex striking platform, and flake-blades with occasional retouch.

The Early Middle Paleolithic stone tool assemblages associated with the lower part of Pleistocene deposits from Denisova Cave constitute original lithic industries with no direct equivalents in North and Central Asia. Their closest counterparts may be found in the Early Middle Paleolithic assemblages from the Near East, namely the Acheulo-Yabrudian cultural complex (AYCC) dating back between 350–250 ka. The AYCC has been recovered from caves and open-air sites, such as Tabun, Qesem, Bezez, Hayonim, Azraq, Misliya, Zuttiyeh, Yabrud I, Masloukh, Jerf Ajla, and others. Techno-typological features of these industries and those of the early Middle Paleolithic assemblage from Denisova Cave show great similarities in comparable forms of ventrally thinned and basally truncated flakes, Quina scrapers, denticulate and notched tools. The stone tool industry found at Denisova Cave differs principally from the Near Eastern assemblages in the lack of bifacial tools in its composition.

The Early Middle Paleolithic industry of Tabun D-type contains a significant number of single-platform unifacial cores for the manufacture of elongated blanks, including lamellar and pointed pieces. Flakes and shorter points with a wide base were detached from double-platform cores. It seems that the Early Middle Paleolithic industries existed in the Levant for about 100,000 years. During this long time period both Levallois and non-Levallois reduction techniques were employed disproportionately, whereas blades and flakes were used as blanks. These differences seem to be associated with changes in adaptation strategies of early hominins living in new diverse environments.[8]

One hypothesis for the transmission of these technologies sees late *H. heidelbergensis* migrating eastward from the Levant to Central Asia after 400 ka and then to southern Siberia. These hominins, while dispersing across Central and North Asia, gave rise to a new taxon, the Denisovans, who began to occupy Denisova Cave in the Altai.

The next development phase of the Middle Paleolithic in the East Chamber is associated with the late Middle and early Upper Pleistocene deposits corresponding to MIS 6–4. This period is represented by stone tool industries from layers 13–11.3 and dates to between 156 ± 15 ka and 70 ± 8 ka[2]. The Middle Paleolithic lithic reduction systems involved radial and parallel flaking; furthermore, edge-faceted and volumetric sub-prismatic cores made on large cobbles and boulders, rarely on large flakes, were also reduced using the same methods. Levallois flaking technique is also present in the assemblage. Scrapers of different modifications were found to be the most typologically diverse tools in the lithic inventory. In additions denticulate, notched, and spur-like pieces are interesting types of tools. Mousterian points, Levallois points and blades, ventrally thinned flakes, and Upper Paleolithic tools, such as end- and canted scrapers, angle burins, borers and truncated flakes, constitute small but rather distinctive groups of the lithic toolkit.
In general, as we move up the sequence the Middle Paleolithic industries show expansion in typological diversity of cores and a percentage increase of blades in flakes, whereas the lithic inventory composition shows an increase in the share of Upper Paleolithic tools against the background of a reduction in the Levallois and notch-denticulate components. Despite gaps in the Pleistocene sedimentary sequence, archaeological evidence from the stratified Middle Paleolithic complex of Denisova Cave shows the development of technologies in a wide time range spanning MIS 9–4, from the early Middle Paleolithic through its final stages,demonstrating the continuity of the Middle Paleolithic traditions without abrupt changes in the composition of stone tool industries.

Supplementary Figures

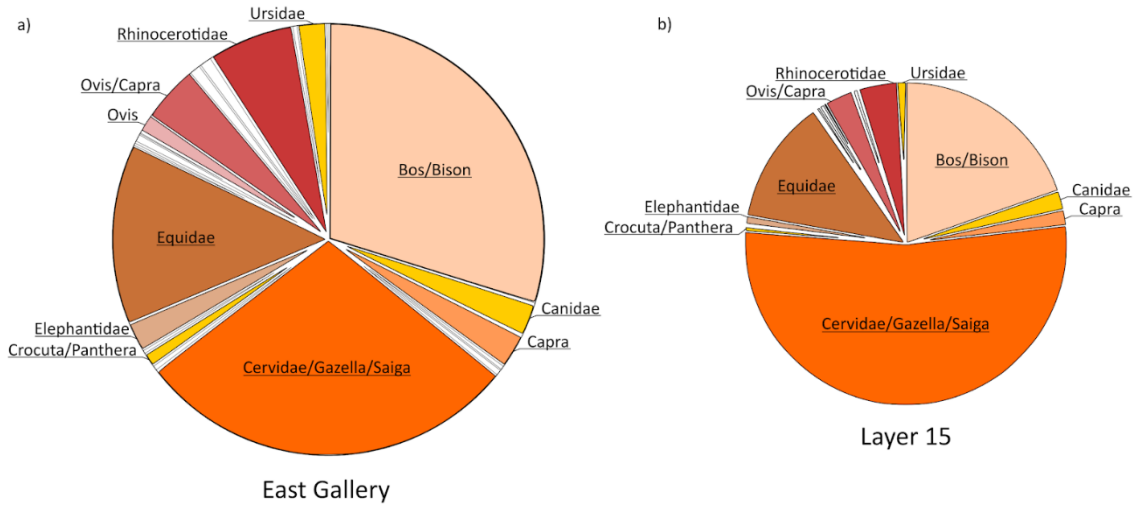

Fig. S1. Pie chart for the largest faunal groups present in the unidentified bone assemblage identified using ZooMS. Graph a) shows the total percentages of fauna identified for all bones analysed for the East Chamber of Denisova Cave, b) shows the total percentage of fauna identified for Layer 15 of the East Gallery only[3].

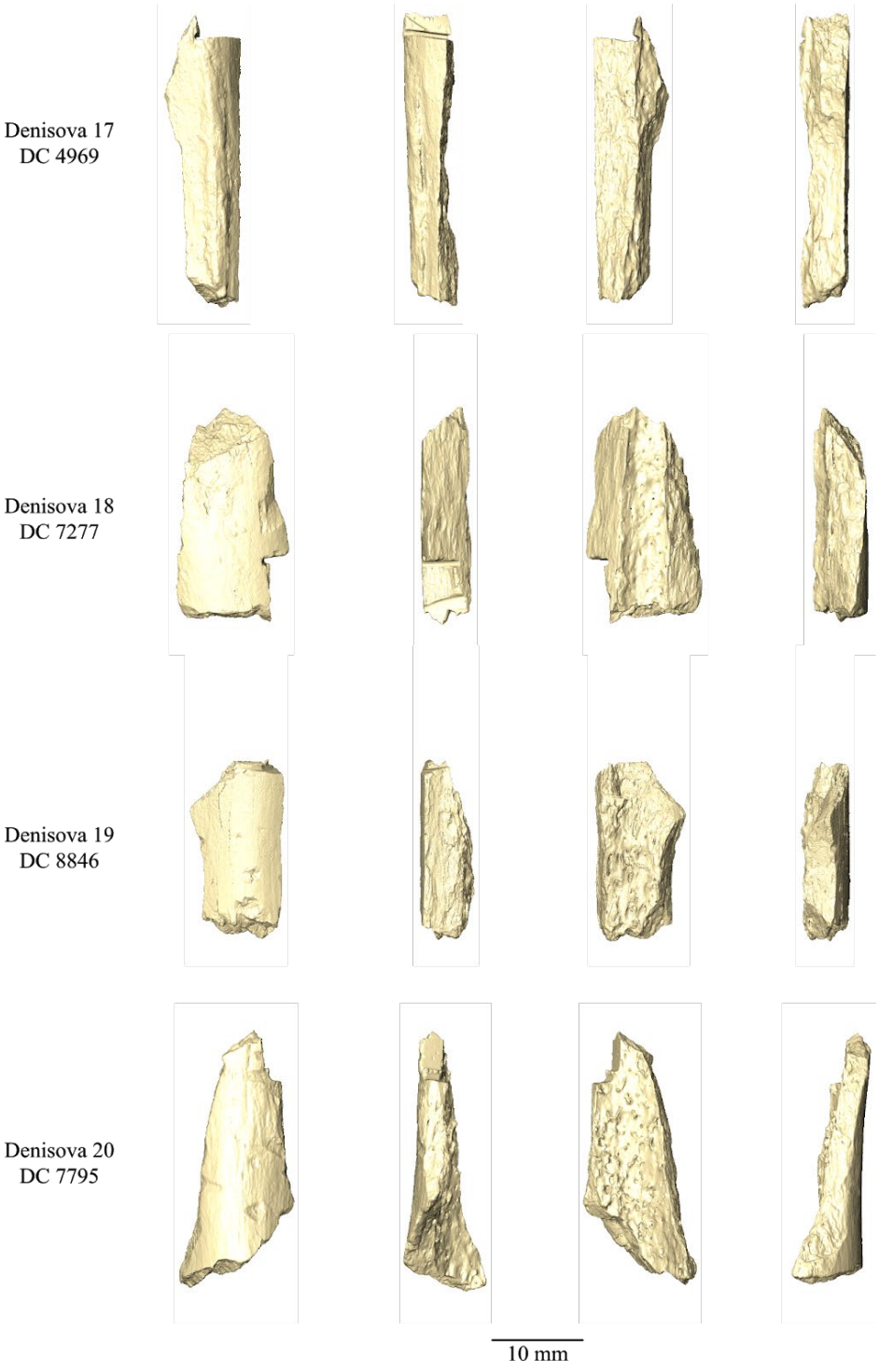

Fig. S2. 3D surface renderings retrieved from the microCT scanning performed for Denisova 17, 18, 19 and 20 (DC4969, DC7277, DC8846, and DC7795).

A)

	Denisova2	Denisova19	Denisova21	Denisova20	Denisova8	Denisova4	Denisova3
Denisova2		20	20	20	29	69	71
Denisova19	20		0	4	29	67	69
Denisova21	20	0		4	30	67	69
Denisova20	20	4	4		30	67	69
Denisova8	29	29	30	30		83	85
Denisova4	69	67	67	67	83		2
Denisova3	71	69	69	69	85	2	

B)

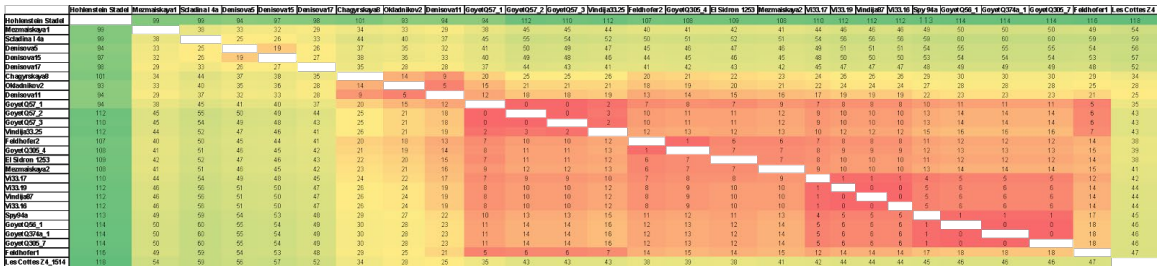

Fig. S3. Number of pairwise nucleotide differences between the mtDNAs of A) 8 Denisovan individuals and B) 27 Neanderthals individuals. Positions containing gaps and missing data between each pair were excluded from the analysis

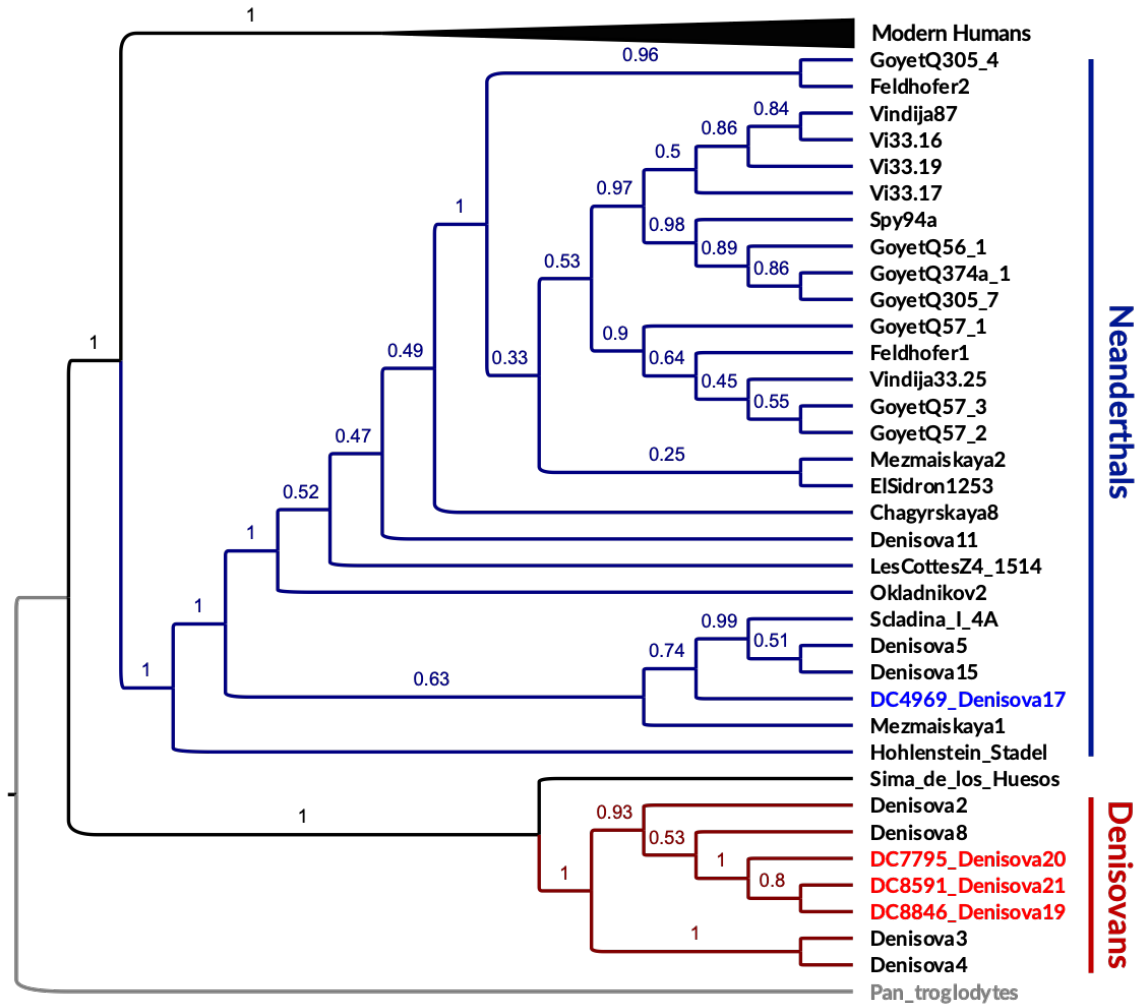

Fig. S4. Neighbor-joining tree relating the mtDNA of Denisova 17, 19, 20 and 21 to other ancient and present-day hominin mtDNAs. The mtDNA of chimpanzee was used as an outgroup. The percentage of replicate trees in which the associated taxa clustered together in the bootstrap test (100 replicates) are shown next to the branches.

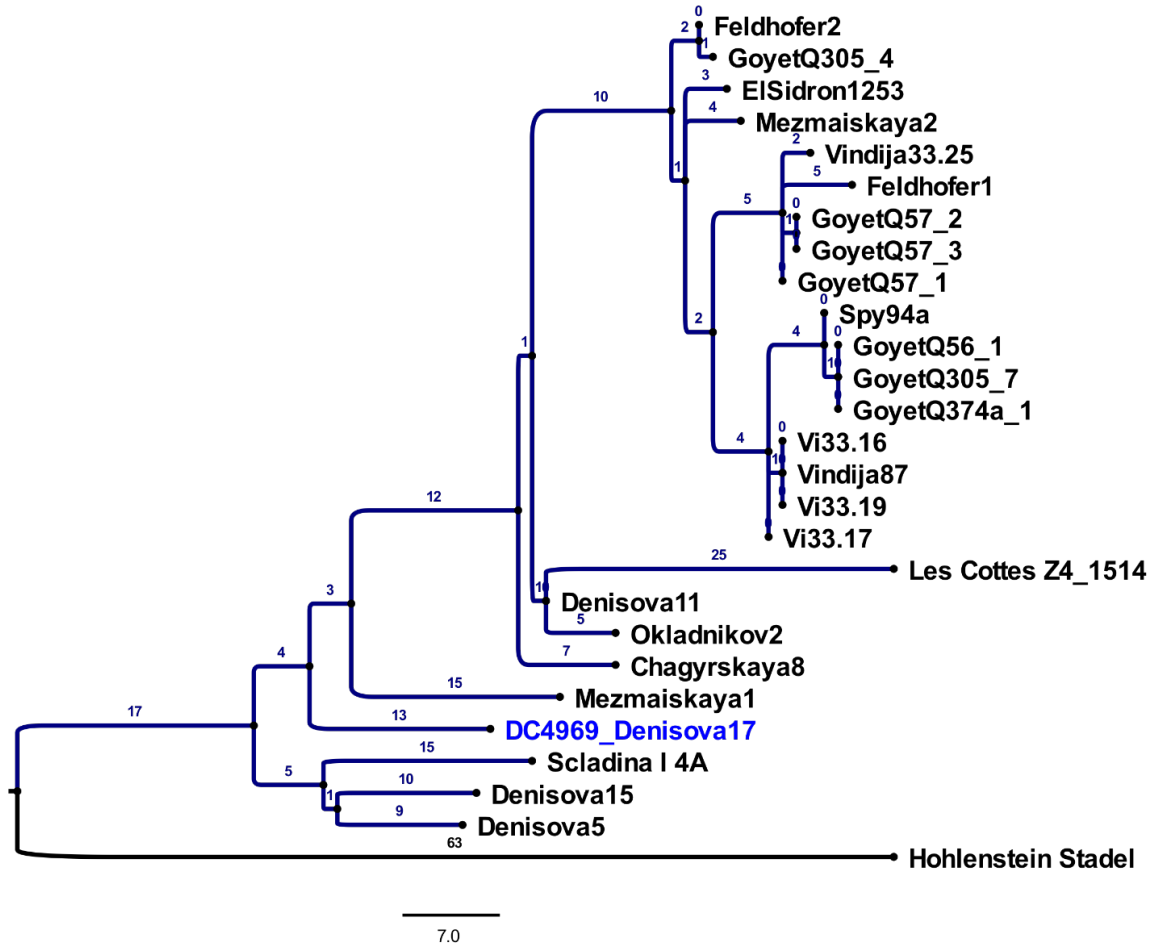

Fig. S5. Consensus parsimony tree obtained by 50% majority rule of 16 equally parsimonious trees relating the mtDNA of Denisova 17 to 26 other Neanderthal mtDNAs. The highly divergent mtDNA of the Hohlenstein Stadel Neanderthal was used as an outgroup. The tree is drawn to scale, with branch lengths computed in number of substitutions.

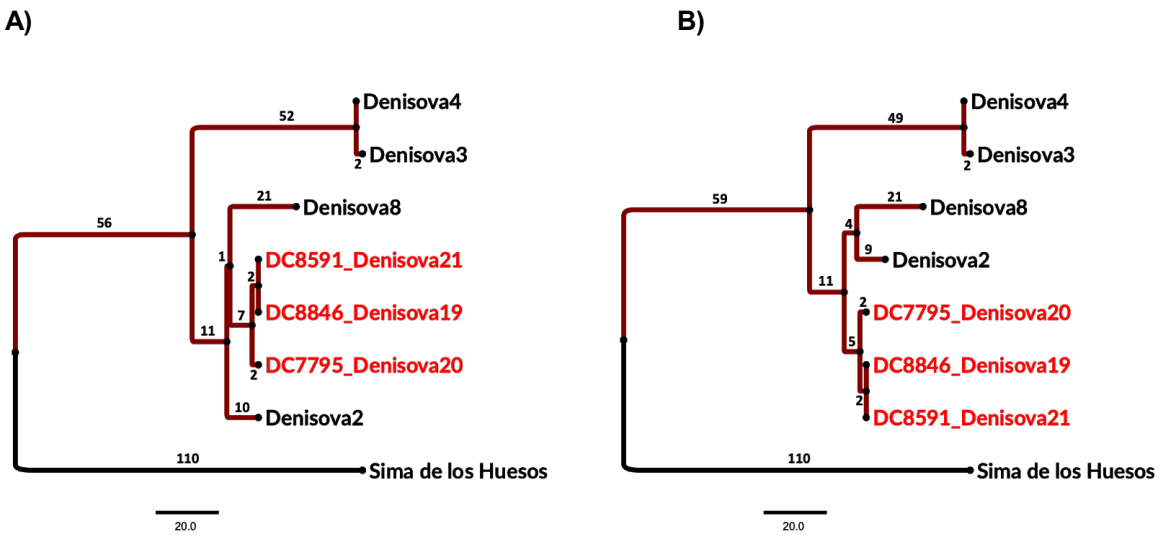

Fig. S6. The two equally parsimonious trees relating the mtDNA of Denisova 19, 20 and 21 to 4 other Denisovan mtDNAs. The mtDNA of the Middle Pleistocene hominin from Sima de los Huesos was used as an outgroup. The trees are drawn to scale, with branch lengths computed in number of substitutions.

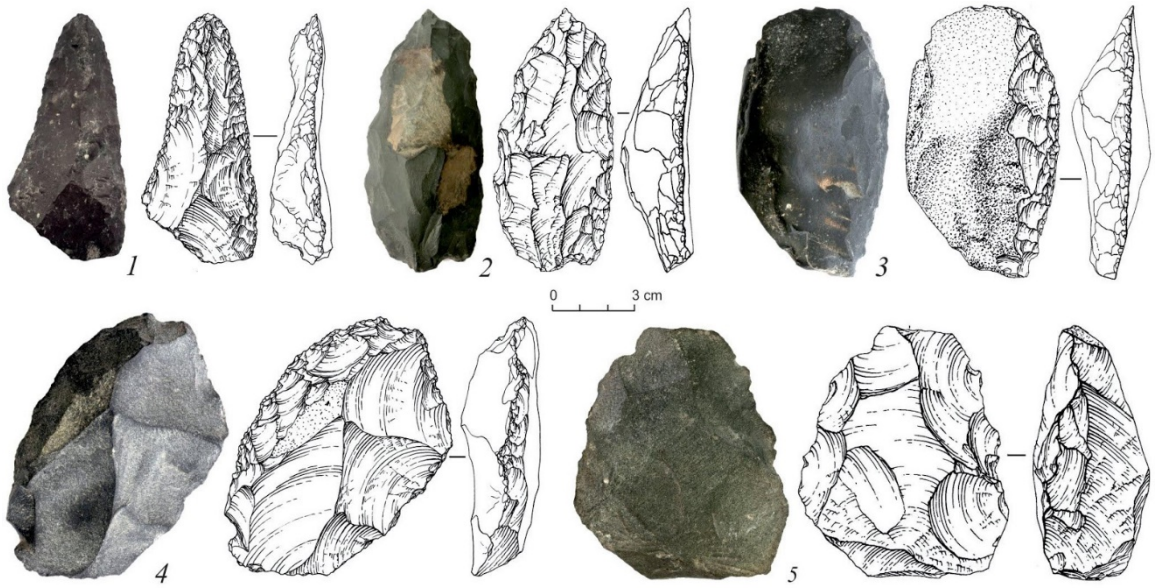

Fig. S7. Illustrations and photographs of artifacts recovered from the Early Middle Paleolithic layers 15-14 attributed to the arrival of Denisovans at Denisova Cave.

Table S1. Peptide markers used to identify DC4969, DC7277, DC7795, DC8846, and DC8591 as Hominidae.

DC #	ID	P1	A	A'	B	C	P2	D	E	F	F'	G	G'
4969	Denisova 17	1105.6			1477.7			2115.1		2869.8	2885.3		
7277	Denisova 18	1105.6			1477.4	1580.4		2114.6		2869.9	2885.2		
7795	Denisova 20	1105.6		1235.7	1477.8	1580.8		2115.2		2869.5	2885.5		
8846	Denisova 19	1105.6		1235.6	1477.8	1580.8		2115.2		2869.5	2885.4	2957.6	
8591	Denisova 21	1105.6		1235.6	1477.8	1580.8	1619.8	2115.1		2869.5	2885.4		

Table S2. Number of bones analysed per stratigraphic layer of the East Chamber of Denisova Cave.

Stratigraphic Layer	Number of fragmented bones analysed
9.2	89
9.3	196
11.2	566
11.3	20
11.4	353
12	425
13	27
14	1096
15	967
17.1	52
Total	3791

Table S3. Summary of the sequence data generated from the libraries that were enriched for hominin mtDNA. The statistics are based on alignment of sequences to the human mtDNA reference sequence (rCRS). Negative controls are included at the bottom of the table.

DC ID	Specimen ID	Sample ID	Extract ID	Library ID	Bleach pre-treated	#library molecules	Unique Mapped fragments >= 35 bp	Duplication rate	5' C to T frequency	3' C to T frequency
DC4969	Denisova 17	SP9673	E16281	B31446	No	1.9E+09	216,937	2.22	32.9	26.4
DC4969	Denisova 17	SP9673	E16282	B31447	No	1.1E+10	341,557	1.78	31.8	25.9
DC4969	Denisova 17	SP9673	E16283	B31448	No	5.6E+09	296,352	1.95	32.8	26.5
DC7277	Denisova 18	SP9674	E16285	B31449	No	3.4E+10	8,493	31.69	9.0	5.8
DC7277	Denisova 18	SP9674	E16286	B31450	No	2.7E+10	4,513	41.57	20.6	12.3
DC7277	Denisova 18	SP9674	E17773	B35203	Yes	1.8E+08	3,352	40.53	0.8	0.7
DC7277	Denisova 18	SP9674	E17774	B35204	Yes	1.6E+08	5,343	64.43	1.5	1.2
DC7277	Denisova 18	SP9674	E17775	B35205	No	2.3E+10	330	1.63	34.3	17.9
DC8846	Denisova 19	SP9677	E16293	B31457	No	8.0E+09	3,294	76.55	40.9	30.6
DC8846	Denisova 19	SP9677	E16294	B31458	No	8.0E+09	6,025	58.19	37.2	29.4
DC8846	Denisova 19	SP9677	E16295	B31459	No	1.3E+10	6,525	31.66	42.3	29.0
DC8846	Denisova 19	SP9677	E17785	B35215	Yes	5.5E+08	371	16.87	31.6	38.8
DC8846	Denisova 19	SP9677	E17786	B35216	Yes	1.6E+08	794	36.07	46.1	41.4
DC8846	Denisova 19	SP9677	E17787	B35217	No	6.4E+09	2,518	1.91	38.0	35.7
DC7795	Denisova 20	SP9675	E16287	B31451	No	1.5E+10	5,323	43.92	43.5	35.4
DC7795	Denisova 20	SP9675	E16288	B31452	No	1.4E+10	8,247	35.57	39.7	31.6
DC7795	Denisova 20	SP9675	E16289	B31453	No	1.6E+10	18,675	15.76	43.6	36.6
DC7795	Denisova 20	SP9675	E17776	B35206	Yes	1.1E+09	853	10.61	52.7	46.2
DC7795	Denisova 20	SP9675	E17777	B35207	No	1.6E+10	2,670	1.79	52.0	47.8
DC7795	Denisova 20	SP9675	E17778	B35208	Yes	3.6E+08	203	21.25	43.8	30.0
DC7795	Denisova 20	SP9675	E17779	B35209	No	8.6E+09	459	1.39	51.2	43.2

DC7795	Denisova 20	SP9675	E17780	B35210	Yes	1.9E+09	255	5.79	20.5	10.0
DC7795	Denisova 20	SP9675	E17781	B35211	No	1.5E+10	1,047	2.18	53.2	47.0
DC8591	Denisova 21	SP9676	E16290	B31454	No	1.6E+10	11,261	30.76	23.5	17.4
DC8591	Denisova 21	SP9676	E16291	B31455	No	1.1E+10	17,626	12.05	45.0	37.6
DC8591	Denisova 21	SP9676	E16292	B31456	No	1.0E+10	8,005	16.43	19.7	12.6
DC8591	Denisova 21	SP9676	E17782	B35212	Yes	3.8E+08	493	35.25	32.0	18.9
DC8591	Denisova 21	SP9676	E17783	B35213	Yes	2.1E+08	262	94.23	50.0	38.2
DC8591	Denisova 21	SP9676	E17784	B35214	No	8.6E+09	1,305	2.68	45.4	32.2
control	control	control	E17788	B35218	Yes	1.3E+08	73	4.42	0	0
control	control	control	-	B31445	No	8.0E+07	209	342.01	0	5.9

Library molecules = qPCR estimates of the number of unique molecules in each library; Unique mapped fragments = number of DNA sequences with a map quality score of 25 or greater retained after duplicate removal; Duplication rate = Average number of duplicates per unique sequence

Table S4. Summary of the sequence data used to call the mtDNA consensus sequences of *Denisova 17, 18*, 1*9, 20* and *21*.

DC ID	Sample ID	Library ID	ref. sequence	Unique Mapped fragments >= 35 bp	Duplication rate	mtDNA coverage (x)	Human Contamination Estimate	5' C to T frequency	3' C to T frequency	#deaminated fragments	mtDNA coverage deaminated (x)
DC4969	Denisova 17	B31446	Vindija3325	231,199	2.2	774	2.5%	32.9	26.1	46583	165
DC4969	Denisova 17	B31447	Vindija3325	361,920	1.8	1238	0.1%	31.6	25.4	69016	256
DC4969	Denisova 17	B31448	Vindija3325	313,924	2.0	1060	0.1%	32.8	26.2	61211	221
DC7277	Denisova 18	B31449	Denisova8	8,777	31.8	33	68.6%	11.9	8	676	2.5
DC7277	Denisova 18	B31450	Denisova8	4,634	39.6	19	37.6%	23	12.6	488	1.8
DC7277	Denisova 18	B35203	Denisova8	3,270	40.1	14	87.8%	2.4	3.1	118	0.5
DC7277	Denisova 18	B35204	Denisova8	5,211	63.1	20	89.4%	3.4	2.9	201	0.8
DC7277	Denisova 18	B35205	Denisova8	323	1.6	1	45.9%	35.5	15.7	51	0.2
DC8846	Denisova 19	B31457	Denisova8	3,576	74.4	12	0.0%	43.1	30.5	855	3.1
DC8846	Denisova 19	B31458	Denisova8	6,327	57.8	23	0.0%	38.4	28.5	1392	5.1
DC8846	Denisova 19	B31459	Denisova8	7,073	31.2	25	6.5%	42.4	29.8	1622	5.8
DC8846	Denisova 19	B35215	Denisova8	383	16.1	1	34.1%	36.6	41.9	96	0.3
DC8846	Denisova 19	B35216	Denisova8	821	35.0	3	10.9%	46.1	38.4	251	0.9
DC8846	Denisova 19	B35217	Denisova8	2,561	1.9	9	4.8%	38.6	34.8	636	2.4
DC7795	Denisova 20	B31451	Denisova8	5,814	43.3	19	8.6%	44.2	34.7	1508	4.9
DC7795	Denisova 20	B31452	Denisova8	8,696	35.3	29	5.1%	41.4	33.3	2197	7.3
DC7795	Denisova 20	B31453	Denisova8	20,233	15.6	67	2.9%	46	38.2	6252	21.2
DC7795	Denisova 20	B35206	Denisova8	860	10.1	3	1.1%	51	49.1	291	0.9
DC7795	Denisova 20	B35207	Denisova8	2,719	1.8	8	4.0%	53.3	47.5	1006	3.1
DC7795	Denisova 20	B35208	Denisova8	204	20.7	1	21.7%	45.2	35.5	61	0.2
DC7795	Denisova 20	B35209	Denisova8	462	1.4	1	0.0%	55.7	41.7	144	0.4

DC7795	Denisova 20	B35210	Denisova8	243	5.7	1	62.4%	26.1	15.3	39	0.1
DC7795	Denisova 20	B35211	Denisova8	1,053	2.1	3	14.8%	53.9	49.4	360	1.1
DC8591	Denisova 21	B31454	Denisova8	11,874	30.9	46	30.2%	26.3	19.6	1649	6.1
DC8591	Denisova 21	B31455	Denisova8	19,149	12.1	65	0.1%	45.6	38.1	5351	19.1
DC8591	Denisova 21	B31456	Denisova8	8,339	16.3	33	48.9%	24.1	14.7	1089	4.0
DC8591	Denisova 21	B35212	Denisova8	495	33.7	2	39.0%	32.8	15.4	73	0.2
DC8591	Denisova 21	B35213	Denisova8	266	93.5	1	45.3%	48.3	45.5	73	0.2
DC8591	Denisova 21	B35214	Denisova8	1,311	2.6	4	27.8%	44.2	32.7	332	1.1

Unique mapped fragments = number of DNA sequences with a map quality score of 25 or greater retained after duplicate removal; Duplication rate

= Average number of duplicates per unique sequence

Table S5. Inferred number of substitutions on the branches leading to the mtDNA sequences of Neanderthals individuals from Denisova Cave since their last common to the exclusion of the mtDNA of the *Hohlenstein Stadel* Neanderthal and their approximate relative molecular ages.

mtDNA type	Specimen	Substitutions since common ancestor	Comparison of inferred molecular age (Mutation rate: 2.53x10-8 (95% HPD: 1.76x10-8 - 3.23x10-8))
Neanderthal mtDNA	***Denisova 17***	17	3.7-6.8 ky younger than *Denisova 5* 1.9-3.4 ky younger than *Denisova 15* 7.4-13.7 ky older than *Denisova 11*
	Denisova 5	15	1.9-3.4 ky older than *Denisova 15* 11.2-20.5 ky older than *Denisova 11*
	Denisova 15	16	9.3-17.1 ky older than *Denisova 11*
	Denisova 11	21	-

Table S6. Inferred number of substitutions on the branches leading to the mtDNA sequences of Denisovan individuals since their last common ancestor to the exclusion of the mtDNA of the Middle Pleistocene Hominin from Sima de los Huesos and their approximate relative molecular ages.

mtDNA type	Specimen	Substitutions since common ancestor		Comparison of inferred molecular age (Mutation rate: 2.53x10-8 (95% HPD: 1.76x10-8 - 3.23x10-8))	
		Scenario 2	Scenario 1	Scenario 2	Scenario 1
Denisovan mtDNA	***Denisova 19***	21	18	similar age to DC7795 *Denisova 20* similar age to DC8591 *Denisova 21* similar age to *Denisova 2* 22.4-41.1 ky older than *Denisova 8* 57.9-106.3 ky older than *Denisova 4* 61.6-113.2 ky older than *Denisova 3*	similar age to DC7795 *Denisova 20* similar age to DC8591 *Denisova 21* 11.2-20.6 ky older than *Denisova 2* 33.6-61.7 ky older than *Denisova 8* 57.9-106.3 ky older than *Denisova 4* 61.6-113.2 ky older than *Denisova 3*
	Denisova 20	21	18	similar age to DC8591 *Denisova 21* similar age to *Denisova 2* 22.4-41.1 ky older than *Denisova 8* 57.9-106.3 ky older than *Denisova 4* 61.6-113.2 ky older than *Denisova 3*	similar age to DC8591 *Denisova 21* 11.2-20.6 ky older than *Denisova 2* 33.6-61.7 ky older than *Denisova 8* 57.9-106.3 ky older than *Denisova 4* 61.6-113.2 ky older than *Denisova 3*
	Denisova 21	21	18	similar age to *Denisova 2* 22.4-41.1 ky older than *Denisova 8* 57.9-106.3 ky older than *Denisova 4* 61.6-113.2 ky older than *Denisova 3*	11.2-20.6 ky older than *Denisova 2* 33.6-61.7 ky older than *Denisova 8* 57.9-106.3 ky older than *Denisova 4* 61.6-113.2 ky older than *Denisova 3*
	Denisova 2	21	24	22.4-41.1 ky older than *Denisova 8* 57.9-106.3 ky older than *Denisova 4* 61.6-113.2 ky older than *Denisova 3*	22.4-41.1 ky older than *Denisova 8* 46.7-85.7 ky older than *Denisova 4* 50.4-92.6 ky older than *Denisova 3*
	Denisova 8	33	36	35.5-65.2 ky older than *Denisova 4* 39.2-72.0 ky older than *Denisova 3*	24.3-44.6 ky older than *Denisova 4* 28.0-51.4 ky older than *Denisova 3*
	Denisova 4	52	49	3.7-6.8 ky older than *Denisova 3*	3.7-6.8 ky older than *Denisova 3*
	Denisova 3	54	51	-	-

Table S7. Mitochondrial DNA genomes used for the genetic analyses. The age in CalBP corresponds to the radiocarbon date of the specimen as reported in the corresponding reference.

Sample	Accession Number	Hominin	Origin (country)	Age in CalBP (95% CI)	References
Pan troglodytes	NC_001643	Chimpanzee	-	-	Horai & al, 1992
German	AF346983	Modern Human	Germany	0	Ingman & al, 2000
Japan	AF346990	Modern Human	Japan	0	Ingman & al, 2000
Mbuti	AF346999	Modern Human	Africa	0	Ingman & al, 2000
Yoruba	AF347014	Modern Human	Africa	0	Ingman & al, 2000
Morocco	AF381988	Modern Human	Morocco	0	Maca-Meyer & al, 2001
NativeAmerican	AY195748	Modern Human	North America	0	Mishmar & al, 2003
Pakistan	AY882379	Modern Human	Pakistan	0	Achilli & al, 2005
Spain	AY882392	Modern Human	Spain	0	Achilli & al, 2005
Kostenki14	FN600416	ancient Modern Human	Russia	37,473 (36,262-38,684)	Fu & al, 2016; Orlando & al, 2014
Oase	Fu & al. 2014	ancient Modern Human	Romania	39,536 (41,761 - 37,311)	Fu & al, 2015
Salkhit	MT561166	ancient Modern Human	Mongolia	34,425 (33,900 - 34,950)	Deviese & al, 2019
Sunghir3	Sikora & al. 2017	ancient Modern Human	Russia	34,093 (33,031 - 35,154)	Sikora & al, 2017
Tianyuan	KC417443	ancient Modern Human	China	39,008 (37,761-40,254)	Fu & al, 2013
Ust_Ishim	Fu & al. 2015	ancient Modern Human	Russia	45,045 (43,212-46,878)	Fu & al, 2014
Chagyrskaya8	MK388903	Neandertal	Russia	NA	Mafessoni & al, 2020
Denisova5	KC879692	Neandertal	Russia	NA	Prüfer & al, 2014
Denisova11	KU131206	Neandertal	Russia	NA	Brown & al, 2016
Denisova15	MK033602	Neandertal	Russia	NA	Douka & al, 2019
Denisova17	MT576650	Neandertal	Russia	NA	This study
ElSidron1253	FM865409	Neandertal	Spain	NA	Briggs & al, 2009
Feldhofer1	FM865407	Neandertal	Germany	43,707 (42,670-44,744)	Briggs & al, 2009; Schmitz & al, 2002
Feldhofer2	FM865408	Neandertal	Germany	43,268 (42,193-44,342)	Briggs & al, 2009; Schmitz & al, 2002
GoyetQ305_4	KX198087	Neandertal	Belgium	44,236 (43,386-45,085)	Rougier & al, 2016
GoyetQ305_7	KX198086	Neandertal	Belgium	NA	Rougier & al, 2016
GoyetQ374a_1	KX198085	Neandertal	Belgium	NA	Rougier & al, 2016
GoyetQ56_1	KX198082	Neandertal	Belgium	42,515 (42,063-42,967)	Rougier & al, 2016
GoyetQ57_1	KX198082	Neandertal	Belgium	44,696 (43,834-45,558)	Rougier & al, 2016
GoyetQ57_2	KX198088	Neandertal	Belgium	41,185 (40,595-41,775)	Rougier & al, 2016

GoyetQ57_3	KX198083	Neandertal	Belgium	42,407 (41,946-42,867)	Rougier & al, 2016
Hohlenstein_Stadel	KY751400	Neandertal	Germany	NA	Peyrégne & al, 2019
LesCottesZ4_1514	MG025536	Neandertal	France	43,230 (42,720-43,740)	Hajdinjak & al, 2018
Mezmaiskaya1	FM865411	Neandertal	Russia	NA	Briggs & al, 2009
Mezmaiskaya2	MG025537	Neandertal	Russia	43,834 (42,038-45,630)	Hajdinjak & al, 2018; Pinhasi et al, 2011
Okladnikov2	KF982693	Neandertal	Russia	NA	Skoglund & al, 2014
Scladina_I_4A	MK123269	Neandertal	Belgium	NA	Peyrégne & al, 2019
Spy94a	MG025538	Neandertal	Belgium	40,463 (39,840-41,085)	Hajdinjak & al, 2018; Semal & al, 2008;
Vindija33.16	NC_011137	Neandertal	Croatia	43,707 (39,234-48,179)	Green & al, 2008; serre & al, 2004
Vindija33.17	KJ533544	Neandertal	Croatia	NA	Gansaugue & al, 2014
Vindija33.19	KJ533545	Neandertal	Croatia	NA	Gansaugue & al, 2014; Prüfer & al, 2014
Vindija33.25	FM865410	Neandertal	Croatia	NA	Briggs & al, 2009
Vindija87	MG025539	Neandertal	Croatia	NA	Hajdinjak & al, 2018
Denisova2	KX663333	Denisovan	Russia	NA	Slon & al, 2017
Denisova3	NC_013993	Denisovan	Russia	NA	Krause & al, 2010
Denisova4	FR695060	Denisovan	Russia	NA	Reich & al, 2010
Denisova8	KT780370	Denisovan	Russia	NA	Sawyer & al, 2015
Denisova19	MT576651	Denisovan	Russia	NA	This study
Denisova20	MT576652	Denisovan	Russia	NA	This study
Denisova21	MT576653	Denisovan	Russia	NA	This study
Sima de los Huesos	NC_023100	Sima de los Huesos	Spain	NA	Meyer & al, 2014

Dataset S1.

Raw MALDI-TOF files from ZooMS analysis of the hominin bones DC4969 (Denisova 17), DC7277 (Denisova 18), DC8846 (Denisova 19), DC7795 (Denisova 20), and DC8591 (Denisova 21) converted to open source format. Files have been uploaded to: https://dx.doi.org/10.17617/3.44

Dataset S2.

MicroCT Scan files of the hominin bones DC4969 (Denisova 17), DC7277 (Denisova 18), DC8846 (Denisova 19), and DC7795 (Denisova 20). Files have been uploaded to: https://dx.doi.org/10.17617/3.45

SI References

1. Brown, S. *et al.* Zooarchaeology through the lens of collagen fingerprinting at Denisova Cave.
2. Vasiliev, S. K., Shunkov, M. V. & Kozlikin, M. B. Preliminary Results for the Balance of Megafauna from Pleistocene Layers of the East Gallery, Denisova Cave. *Problems of Archaeology, Ethnography, and Anthropology of Siberia and Adjacent Territories* **19**, 32–38 (2013).
3. Jacobs, Z. *et al.* Timing of archaic hominin occupation of Denisova Cave in southern Siberia. *Nature* **565**, 594–599 (2019).
4. Briggs, A. W. *et al.* Patterns of damage in genomic DNA sequences from a Neandertal. *Proc. Natl. Acad. Sci. U. S. A.* **104**, 14616–14621 (2007).
5. Krause, J. *et al.* A complete mtDNA genome of an early modern human from Kostenki, Russia. *Curr. Biol.* **20**, 231–236 (2010).
6. Slon, V. *et al.* Neandertal and Denisovan DNA from Pleistocene sediments. *Science* **356**, 605–608 (2017).
7. Slon, V. *et al.* A fourth Denisovan individual. *Sci Adv* **3**, e1700186 (2017).
8. Derevianko, A. P. The Middle Paleolithic of the Levant. *Arheol. ètnogr. antropol. Evrazii* **44**, 3–36 (2016).

Appendix 3 - Manuscripts ready for submission

Manuscript D - in prep. Brown, S., Wang, N., Oertle, A., Comeskey, D., Jope-Street, B., Harvey, V., Pal Chowdury, M., Kozlikin, M., Shunkov, M., Derevianko, A., Buckley, M., Higham, T., Douka, K. Zooarchaeology through the lens of collagen fingerprinting at Denisova Cave.

Zooarchaeology through the lens of collagen fingerprinting at Denisova Cave

Samantha Brown[1]*, Naihui Wang[1], Annette Oertle[1], Daniel Comeskey[2], Blair Jope-Street[1], Virginia L. Harvey[3,4], Manasij Pal Chowdhury[3,4], Maxim B. Kozlikin[5], Michael V. Shunkov[5,6], Anatoly P. Derevianko[4], Michael Buckley[3,4], Thomas Higham[2], Katerina Douka[1]*

Affiliations:

[1]Max Planck Institute for the Science of Human History, Jena, Germany.

[2]Oxford Radiocarbon Accelerator Unit, RLAHA, University of Oxford, Oxford OX13QY, UK.

[3]The University of Manchester, Department of Earth and Environmental Sciences, School of Natural Sciences, Manchester, M13 9PL, UK

[4]Manchester Institute of Biotechnology, The University of Manchester, 131 Princess Street, Manchester, M1 7DN, UK

[5]Institute of Archeology and Ethnography of the Siberian Branch of the Russian Academy of Sciences, Novosibirsk, Russia.

[6]Novosibirsk State University, Novosibirsk, Russia.

*Correspondence to: brown@shh.mpg.de, douka@shh.mpg.de

Abstract

Denisova Cave, a Pleistocene site in the Altai Mountains of Russian Siberia, has yielded significant fossil and lithic evidence for the Pleistocene in Northern Asia. Abundant animal and human bones have been discovered at the site, however, these tend to be highly fragmented, necessitating new approaches to identifying the important hominin and faunal fossils. Here we report the results for,253 bones taxonomically identified using ZooMS. Through the integration of the ZooMS-based data with the macroscopically-identified fauna we aim to create a holistic picture of the zooarchaeological record of the site. Where morphological analysis of bones from the site have identified a high proportion of carnivore bones (30.2%) we find they account

for only 7.6%, with large mammals between 3-5 more abundant in the ZooMS identified bone assemblage. Our analysis reveals a cyclical pattern in fragmentation of bones with hominins using percussive based tools and carnivores likely furthering this initial fragmentation through gnawing and digestion. highlights trends associated with climate variability throughout the Middle and Upper Pleistocene, elucidating the reasons behind the high degree of bone fragmentation at Denisova Cave.

Main Text

Fragmentation of bones poses a particular problem when studying archaeological and paleontological assemblages. Robust enough that they can survive a range of depositional environments, bones are still susceptible to numerous taphonomic processes. Freezing and thawing, weathering, trampling, gnawing, and the role of humans modifying and processing bones, either for subsistence reasons (e.g. bone marrow exploitation) or for the production of osseous tools, are some of the key influences that may alter a bone's physical integrity.[1,2] As a result, it is estimated that only a third of bones located in Pleistocene archaeological contexts can be identified using visual inspection.[3,4] Without a reliable means of taxonomically identifying these remains, they are often disregarded and in some instances, especially in the past, they have been discarded altogether.

The rarity of Pleistocene archaeological sites necessitates an economical approach to the study of the fossil record. Prior to the 21st Century, bones with intact morphological features have been key to unravelling evolutionary pathways, hunting and subsistence strategies, and facilitating environmental reconstructions, among others. Recently, however the potential of highly fragmented bone assemblages which cannot be identified on the basis of morphology has been explored through the use of peptide mass fingerprinting, specifically using ZooMS (Zooarchaeology by Mass Spectrometry).[5] ZooMS provides an efficient means of screening assemblages of fragmented bone and taxonomically identifying them. The method has been applied to large Pleistocene assemblages,[6–8] including the Middle to Late Pleistocene site, Denisova Cave.[9,10]

Denisova Cave, situated in the Altai Mountains of Russian Siberia, is unique in its hominin record as the only site where both Neanderthal and Denisovan fossils have

been identified.[11–14] Despite particularly favorable conditions that ensure a high degree of biomolecular preservation at the site, less than 5% of bones excavated from Denisova Cave can be macroscopically identified[15–21] thus making the cave a good candidate for the application of peptide mass fingerprinting. ZooMS analysis of fragmented bones at Denisova Cave has so far resulted in the identification of nine new hominin remains,[9,10,22] including two Neanderthals (Denisova 15 and Denisova 17), three Denisovans (Denisova 19, Denisova 20, and Denisova 21), and the offspring of a Neanderthal mother and a Denisovan father (Denisova 11).[9,23] In the course of identifying these individuals a large assemblage of fauna has been identified which has not been discussed thus far.

Here we report the results for 8,253 fragmented bones from the Denisova Cave that were analysed using ZooMS. This fragmented assemblage can be studied within a broader framework following the recent publications detailing the chronology of the site,[10,19] zooarchaeological findings,[15–20] and palaeoenvironmental reconstructions.[21,24].

The incorporation of ZooMS-based determinations into more traditional zooarchaeological analysis is inherently complicated, particularly when analysing morphologically non-diagnostic bones. A first limitation stems from the broad taxon groupings created through ZooMS analysis which do not match the often more detailed macroscopic identifications. For large mammals, ZooMS is typically only able to make genus level identifications, with some exceptions in which species can be identified.[25] Second, because NISP (Number of Individual Specimens) is the only reliable measurement through which these highly fragmentary bones can be counted, this inevitably leads to an overestimation of the presence/absence of fauna.[3,4] Using different approaches we detail below, we aim to use ZooMS-identified bones to create a holistic view of fauna at Denisova Cave and determine broad trends in the ratios of faunal remains and their variation through time.

Materials and Methods

We analyse 8,253 non-diagnostic bone fragments which were excavated from all three chambers of Denisova Cave, the majority of which come from the East Chamber (n= 6,308), followed by the Main (n=1,123) and South (n=822) chambers (Supplementary

Information). Bones were specifically chosen as they could not be identified on the basis of morphology and, where possible, bones larger than 2 cm were preferentially selected as smaller bones would not allow for on-going destructive analyses like radiocarbon dating and genetic analysis. Samples were drilled in preparation for analysis and from each bone approximately 20 mg was removed using a diamond covered disc. Care was taken between drilling samples to clean equipment to minimise cross-contamination between fossils.

Analyses were carried out at the ZooMS facility of the Department of Archaeology at the Max Planck Institute for the Science of Human History (MPI-SHH), Jena, Germany and the Manchester Institute of Biotechnology at the University of Manchester, UK. Samples analysed at the MPI-SHH followed published protocols using ammonium bicarbonate as the means of collagen extraction.[7,26,27] Samples analysed at the University of Manchester followed published acid soluble protocols.[9,28] The resulting spectra were screened for diagnostic markers using flexAnalysis 3.4 (Bruker Daltonics) and mMass software.[29] The spectra were compared against a reference library of known peptide markers[5,7,30] which was informed by previous zooarchaeological analysis carried out at Denisova Cave.[15–20]

In order to directly compare our ZooMS-based determinations with the morphologically identified bones from zooarchaeological analysis carried out over the last decades we have converted those zooarchaeological records into datasets compatible with ZooMS identifications. Additionally, we examine the ZooMS-IDed component through the incorporation of body class size, fragmentation patterns, and chronologically, based on the marine oxygen isotope stages (MIS) they belong to.

Results

Overall, of the 8,253 analysed bones, 74% were taxonomically assigned to a specific ZooMS taxon and an additional 5% could only be identified to family or order level due to low quality spectra (Supplementary Information). The South Chamber had a high rate of samples which failed to produce enough collagen for taxonomic identification (28%), in comparison with lower rates of failure for the East (16%) and Main (17%) chambers.

In total we identify 18 ZooMS taxa (Table 1). A ZooMS taxon is defined here as the most specific identification ZooMS is able to provide, generally to a genus or family level. For instance, several Canids have been identified within the morphological assemblage at Denisova Cave, including *Canis lupus* (wolf), *Vulpes corsak* (corsak fox), *Cuon alpinus* (dhole), and *Alopex lagopus* (arctic fox), all of which could only be identified to 'Canidae' through ZooMS analysis as their peptide mass fingerprints are identical. *Vulpes vulpes* (red fox) is the only Canid that can be differentiated using ZooMS, as it's (Supplementary Table 1). The assemblage is dominated by large vertebrates, with small vertebrates and birds accounting for less than 1% of the identified material examined. This is likely in part as a result of our selection of bones about 2cm in length.

In order to compare the ZooMS identified fauna with previously-published zooarchaeological datasets from Denisova Cave we have compiled those datasets, referred to as the 'morphological assemblage', from the literature and converted them into ZooMS-style datasets which can then be directly compared with the new results we present here. In our discussion of percentages, we have excluded samples which failed ZooMS analysis or those which could not be assigned to the most specific ZooMS taxon possible with the exception of Ovis/Capra and Crocuta/Panthera in order to make them more compatible with zooarchaeological results. We have also excluded small vertebrates as they were not identified in sufficient numbers for direct comparison with the morphological assemblage. While some results are not included in our discussions and comparisons with the zooarchaeological datasets, all results are reported in the supplementary information (Supplementary Table 2, 3, 4; External Database 1).

We use the term "predator", rather than "carnivore", to group the activity of hominins, Canidae, Crocuta/Panthera, Ursidae and *V. vulpes*, who have varied diets, whereas the term "herbivores" includes Bos/Bison, Capra, Cervidae/Gazella/Saiga, Elephantidae, Equidae, Ovis, and Rhinocerotidae.

East Chamber

ZooMS analysis was carried out on 6,308 bone fragments from all archaeological layers of the East Chamber (Table 1; Supplementary Table 2). Predators account for

20% of the morphological assemblage of the East Gallery, in comparison with only 7.7% of the ZooMS-IDed assemblage. The overall proportion of predator remains do not vary significantly throughout the layers of the East Chamber in the morphological assemblage, however cave hyaena (*Crocuta crocuta spelaea*) are the dominant predators between layers 9–13, alongside smaller numbers of Panthera, Canidae, and Felidae.[16,19] Their behaviours are particularly visible in the archaeological record between layers 9–11 where a large number of other fossils have clearly passed through the digestive tracts of hyaenas and wolves, leaving acid corrosion marks on bones and dissolving the enamel on teeth.[16,19] While Crocuta/Panthera are visibly the dominant predator(s) within the morphological assemblage, in the ZooMS-IDed component they are present in relatively low numbers, accounting for approximately 1.9% of bones (Figure 1). Rather it is Canidae which are consistently the dominant predator group in the ZooMS-IDed component for each of the studied layers of the East Chamber. Within the morphological assemblage, Canidae only exceed Crocuta/Panthera for layers 15–17[16,19] during which forest species like *Capreolus pygargus* (Siberian roe deer) and *Cervus elaphus* (red deer) are the major herbivore groups present in the assemblage (see below). In the ZooMS-IDed fauna, Canidae account for 2.7% of all the bones studied within the East Chamber.

The two most significant herbivore taxa in the ZooMS-IDed component for the East Chamber are Cervidae/Gazella/Saiga and Bos/Bison. Cervidae/Gazella/Saiga includes *C. pygargus*, *C. elaphus*, *Megaloceros giganteus* (Irish elk), *Alces alces (elk)*, *Saiga tatarica borealis* (saiga antelope), and *Gazella guttursza*. The only cervid species present at Denisova Cave which can be separated from this group is the Siberian roe deer which can be differentiated from Cervidae/Gazella/Saiga on the basis of their COL1α2 757–789 (α2 757)[31] marker. The α2 757 marker for Siberian roe deer is present at m/z 3043.4/3059.4 and present at m/z 3017.5/3033.5 for Cervidae/Gazella/Saiga. Since this differentiation is based on a single marker it is possible that many of the generically identified Cervidae/Gazella/Saiga are actually Siberian roe deer which were missing their α2 757 marker in poorer preserved specimens. The α2 757 marker is easily lost as a result of collagen degradation, a common problem for instance in the separation of *Ovis* and *Capra* which is done on the basis of the same marker.[32] Cervidae/Gazella/Saiga bones account for 54% of the

ZooMS-IDed component for layer 15. This number declines significantly in the overlying archaeological layers. In comparison, Bos/Bison, a taxonomic group that contains the remains of steppe bison (*Bison priscus*) and the less common Baikal yak (*Poëphagus mutus*), continue to increase by percentage throughout the stratigraphic layers. Bos/Bison eventually account for 70% of the ZooMS IDed fauna in layer 9.2[10] (Figure 2; Supplementary Table 2).

Main Chamber

We carried out ZooMS analysis for 1,123 bones from layers 9–12 of the Main Chamber (Table 1; Supplementary Table 3). Predators dominate the morphological assemblage, accounting for more than 30% of all identifiable bone for layers 9–12. In comparison, the dominant predators, Canidae, Crocuta/Panthera, and Ursidae, make up only 5.5% of the ZooMS-IDed component. Crocuta/Panthera, likely including *C. spelaea* although *Panthera spelaea* are also present in the earliest Pleistocene layers of the Main Chamber and dominate the morphological assemblage for layers 9–11, accounting for 9.4% of identifiable bones (Figure 1).[19] In the ZooMS-IDed component, Crocuta/Panthera account for 1.68% of the fragmented bones for layers 9–11 making them the most identified predator for these contexts. The morphological assemblage identifies Canidae as the major predator group in layer 12,[19,20] however none were identified within the ZooMS-IDed component for this context.

The major herbivore groups do not differ significantly between the morphological and ZooMS identified fauna. Equidae, Ovis/Capra, and Cervidae/Gazella/Saiga are present in relatively large numbers in each dataset. Bos/Bison remains increase significantly within the ZooMS-IDed fauna, accounting for 35% of the assemblage, more than four times the amount identified within the morphological bones (8.35%).

South Chamber

We analysed 822 bones from the South Chamber using ZooMS (Table 1; Supplementary Table 4). Crocuta/Panthera, Canidae, and Ursidae are the dominant predator groups identified in the ZooMS fauna in this Chamber. They account for only 10.5% of this assemblage, three times less than predators in the morphological assemblage (Figure 1). Ursidae (*Ursus (Spelaearctos) savini*) account for 9.7% of the

ZooMS-IDed fauna for layer 11. Previous zooarchaeological analysis suggested the cave may have been used for hibernation by the small cave bear (*U. spelaearctos*)[17] which could explain the unusually high number of bear bones. In comparison, Crocuta/Panthera were the dominant predator group for the ZooMS-IDed fauna in layer 12, accounting for 2.7% of the assemblage which is largely in line with dominant predator groups identified in the morphological assemblage. Bos/Bison (36.6%) and Equidae (10.3%) were the most common herbivores present within the ZooMS-IDed component.

Zooarchaeological analysis of bones from the South Chamber[17,18] suggests intense predator occupation for layers 9–12, particularly for Crocuta/Panthera. Their bones are disproportionately represented in the morphologically identifiable bones for South Gallery (n=255), second only to *Capra* remains, which are identified as the likely prey for cave hyena and snow leopard.[17,18] Fragments of cave hyena coprolites were identified throughout layers 9–12 of the South Chamber and many of the bones from prey taxa show traces of acid corrosion, indicating that they have passed through the digestive tracts of predators[17,18] It is noteworthy that only 3.7% of bones recovered from this part of the cave are larger than 5 cm.[18] We may hypothesize that this large degree of fragmentation is due to predation. In turn, such a high concentration of carnivore processing could explain the low level of protein preservation in this section of the cave; 28% of the fragmented remains analysed using ZooMS failed to produce enough collagen for identification as opposed to 17% and 16% for the East and Main Chambers, respectively (Table 1; Supplementary Table 4).

Discussion

ZooMS has previously been applied to larger microfauna assemblages and older individual faunal samples,[33,34] yet this is the largest application of ZooMS to an assemblage of fragmented bones with an archaeological association. The oldest archaeological layers we study here (Layers 14 and 15) date to between 217–163 ka.[19] For Layer 15, from which we analysed nearly 1,000 bones, the success rate was 86% (Supplementary Table 2). This is particularly encouraging and paves the way for the analysis of bone assemblages of similar, or greater, antiquity from other sites with comparable biomolecular preservation.

Our ZooMS results provide interesting insights on the microenvironment and diagentic factors affecting biomolecular preservation at the site. Significant differences in success rates were observed across layers and the three non-connecting chambers. Bones from the East Gallery were the most successful, with 84% producing enough collagen for ZooMS analysis. The oldest context studied from the East Chamber, layer 17.1, had the highest number of failed samples (64%), followed by the youngest Pleistocene contexts, layers 9.2 (33%) and 9.3 (37%). The high failure rate for the latter is likely due to the heavy phosphatisation in the soil[24,35] which has previously impeded OSL, radiocarbon dating, and genetic analyses for these layers.[10,19] In the Main Chamber, 17% of samples failed ZooMS analysis and 28% of samples failed for the South Chamber.

At Denisova Cave a high degree of bone fragmentation is observed. Of the 177,000 bones excavated at the East Chamber more than 95% were less than 2–5 cm in length and could not be identified macroscopically.[16,19] In contrast, on average 74% of the fragmented bones we analysed could be assigned to a specific ZooMS taxon and an additional 5% of samples that produced low quality spectra could be identified to family or order levels. This contrast in identification success (<5% which have been identified morphologically versus ~80% based on fragmented bones analysed using ZooMS) highlights once again the merits of large scale application of ZooMS on highly fragmented archaeological assemblages.

ZooMS data sheds light on the post-depositional processes and taphonomic agents responsible for the accumulation, as well as state of preservation, of a bone assemblage. By comparing the results of the zooarchaeological analysis against the results of ZooMS analysis we are able to assess the extensive fragmentation we observe throughout the sequence. The majority of bones from the ZooMS-IDed component were the remains of prey, suggesting that the accumulation of the assemblage is not entirely relegated to equifinality and that some processes of the accumulation can be unravelled.[36,37] There is evidence for intensive hominin processing of carcasses, particularly in the earliest archaeological layers 14 and 15,[22,24] and gnawing and digestion of bones in the Upper Palaeolithic layers by hyenas, panthers, leopards, and wolves.[16,18,24] Based on this evidence, the

fragmented bone assemblage appears to reflect intense occupation of the site and the hunting practices of humans and carnivores alike.

Recent analysis of the microstratigraphy of Denisova Cave has shown that due to slow sedimentation accumulation rates it is currently not possible to identify when predators like bears, wolves, and hyaenas were occupying the cave as opposed to hominin groups like Denisovans and Neanderthals.[21] Rather, it seems that many groups were alternating, or were possibly in competition, as the site's main occupants throughout the Pleistocene.[17,21] Early evidence suggests that at times they may have even benefited from each other's presence. The close stratigraphic relationship between carnivores and hominins at Denisova Cave and the inability to specifically discern when these groups were dominant at the site may indicate the role scavenging played at Denisova Cave, particularly in regards to cave hyaenas and wolves who were taking advantage of the intensive hunting practices of Denisovans and Neanderthals.[21] Additionally, cut marked carnivore bones, particularly of red and polar foxes,[38] as well as limited evidence for skinning of wolves and bears, suggests hominins might have been targeting them for their fur. This practice is common in other Pleistocene sites in Russia, such as in the Kostenki region.[39,40]

The most notable difference between the morphological assemblage and the ZooMS-IDed component of Denisova Cave is the abundance of predators in comparison with herbivores. In the morphological assemblage of all three chambers, on average, predator groups account for 30.2% of all identified bones,[15–20] in comparison with the ZooMS-IDed component where predators account for only 7.6%. This discrepancy informs us of the main factor influencing fragmentation rates at the site. Carnivores were the driving force behind the high rate of herbivore bone fragmentation, however, their bones are less likely to suffer similar fragmentation activity caused by carcass processing by hominins and other predators at the site. Given that the hominin bones recovered so far from the site are similarly fragmented (none exceed a few cm in length), we hypothesize that although humans were the main agent responsible for the accumulation and initial dismembering, butchering, and fragmentation of (most) animal bones in the cave, a secondary agent, that is carnivores such as hyenas, caused further processing and reduction in size of both animal and human bone deposited at the site.

Recent work on building chronologies for the site using radiocarbon and optical dating[10,19] has enabled the three chambers of Denisova Cave to be securely dated and cross-correlated. As a result of these publications, stratigraphic contexts from separate sections of the site can now be can now be attributed to specific MIS stages and compared to one another. We can identify several trends in the ZooMS-IDed component with reference to depositional age and the environmental conditions prevailing at the time. We note, for instance, that despite the wide variety of taxa Cervidae/Gazella/Saiga, they remain in relatively low abundance throughout the majority of the Pleistocene, except for the earliest layers which correspond to MIS 9–7 (337–191 ka). The majority of bones from this phase were excavated in layer 15 which is attributed to MIS 7 and the Penultimate Interglacial, and coincides with the arrival of the first Denisovans to the site.[22,24,41] Layers 15 and 14 have the highest abundance of stone tools for any other phase at Denisova Cave and a large proportion of humanly modified bone.[22,24] The morphological assemblage for this layer is dominated by the remains of Siberian roe deer (19%) and red deer (10%).[16,19] Cervids were clearly favoured by these early inhabitants of the cave, an observation which remains in stark contrast to the faunal record of all later phases documented at the site.

Bos/Bison, likely steppe bison (*Bison priscus*) and the less common Baikal yak (*Poëphagus mutus*), are the most abundant fauna for almost all subsequent (post MIS 7) periods documented at Denisova Cave. The two groups cannot be separated using peptide mass fingerprinting and therefore are grouped together in the ZooMS results. *B. priscus* are likely the major contributors to this group, as they dominate the morphological assemblage, *P. mutus* are also present throughout the Pleistocene layers albeit in much smaller numbers.[15–20] Steppe bison and Baikal yak are known to have favoured steppe and forest-steppe environments.[16,42] However, despite the expansion of forests during interglacial periods their remains continue to dominate the ZooMS-IDed component at 39% (MIS 3) and 31% (MIS 5). This suggests that rather than the environment being a driving force behind the abundance of fragmented Bos and Bison bones, predators, likely hominins, were preferentially targeting them, mirroring a trend identified in other large Pleistocene ZooMS assemblages.[6]

Regarding predators in the ZooMS-IDed component, Canidae are the dominant group for the majority of the Pleistocene layers studied. From MIS 9–4 their bones account for approximately 5% of the identified remains in our study. They are identified alongside smaller numbers of other predators, including Felidae and *V. vulpes*. Crocuta/Panthera remains are first identified in the ZooMS-IDed component in layer 15 and they have been macroscopically identified in the morphological assemblage in layers covering the entire Pleistocene. The majority of these bones are probably cave hyaena, however, smaller numbers of snow leopard and Eurasian cave lion are present throughout the stratigraphy.[15–20] Crocuta/Panthera remains become more common than Canidae during MIS 5-3, alongside archaeological evidence of intensive carnivore occupation during the same period, particularly in the South Chamber. Bear remains are identified throughout the Pleistocene layers of Denisova Cave both in the ZooMS-IDed component and the morphological assemblage. The extinct cave bears, *U. savini*, were mostly vegetarian, and used the cave for hibernation.[17,18]

Body mass and size class, assigned based on previously published data,[43] probably play a disproportionate role in the taxa identified using ZooMS analysis. For instance, Elephantidae, Bos/Bison, and Rhinocerotidae remains, all within body class size 6, are 3–5 times more abundant in the ZooMS-IDed component than the morphological dataset (Figure 1). Bos/Bison remains are the most sensitive to this shift, accounting for only 6.3% of the morphological assemblage[15–20] in comparison with 31% of the ZooMS-IDed component. Even the bones of mammoths, which were likely only present in the Altai region in small numbers and are not considered to have been a major contributor to hominin diet,[44] are three times more abundant by percentage in the ZooMS identified fauna (3.84% versus 1.08%). The only exception to this is the ratio of horse bones, for which no significant change in the percentage of their remains exists between the zooarchaeological dataset[15–20] and the ZooMS-IDed component. With these factors in mind, any tentative predictive model for the abundance of large herbivores within a fragmented bone assemblage should take into account both body class size and the likelihood that some taxa were targeted by hominins who were processing carcasses using percussive instruments.

Conclusion

The application of ZooMS at Denisova Cave highlights the potential of the method to elucidate early hunting practices and adaptation to new environments. The new data has significantly improved our understanding of the site's faunal record and taphonomy and the high success rate is illustrative of the potential of the method to other sites and regions with comparable biomolecular preservation and to material of the same or even greater antiquity extending further back into the Middle Pleistocene. Aside from its effectiveness in screening large numbers of bones for the identification of specific taxa, e.g. hominin fossils, the method is complementary to traditional zooarchaeological practices allowing a large part of the morphologically non-identifiable component to be diagnosed taxonomically using ZooMS. This is particularly true at Denisova Cave where traditional osteological practices have identified less than 5% of the excavated fauna versus ~80% identification success using ZooMS in this study. The new data are also useful for elucidating the taphonomic history of the bones recovered from a site. In our case, this is shown by the differences in prey-predator ratios in the ZooMS-IDed versus the morphologically-identified assemblages which highlight that the main influence in the fragmentation of herbivorous/prey bones at Denisova was two-fold and operated at different levels. Hominin processing of carcasses was the main factor for the deposition and initial fragmentation of many of the herbivore and some of the carnivore bones recovered at the site. This was followed by secondary and more extreme fragmentation of both animal and human bones as a result of predator scavenging.

Methods

Analysis was carried out at the ZooMS facility of the Department of Archaeology at the Max Planck Institute for the Science of Human History (MPI-SHH), Jena, Germany and the Manchester Institute of Biotechnology at the University of Manchester, UK. Samples analysed at the MPI-SHH followed established ammonium bicarbonate buffer protocols[7,26,27]. In brief, Samples were rinsed in ammonium bicarbonate overnight and incubated for 1 h at 65 ℃. The supernatant was treated with 0.4µg trypsin (Thermo Scientific Pierce ™ Trypsin Protease) and allowed to digest at 37 ℃ for 18 h. The incubated samples were concentrated and desalted using C18 ZipTips

(Thermo Scientific Pierce™ C18 Tips) and eluted in a final solution of 50 µl of 50% acetonitrile and 0.1% TFA. 0.5 µl of the resulting solution was mixed with 0.5 µl of α cyano-4-hydroxycinnamic acid solution (10 mg/mL in 50% acetonitrile [ACN] and 0.1% trifluoroacetic acid [TFA]) and allowed to crystallise. The samples were analysed using a Bruker Autoflex Speed LRF MALDI ToF/ToF mass spectrometer.

Samples analysed at the University of Manchester were done so using established acid soluble protocols.[9,28] Samples were demineralised in 0.6 M hydrochloric acid (HCl) for 18 h. The supernatant was removed into 30 kDa molecular weight cut-off (MWCO) ultrafilters and centrifuged at 3,700 rpm for 1 h. The filtrate was then twice washed through with 500 µL of 50 mM ammonium bicarbonate (AmBic) and further centrifuged at 3700 rpm for half an hour after each treatment. The final residue was resuspended with additional AmBic (200 µL), half of which was removed to create a backup sample set before digestion. The remaining 100 µL was then treated with 0.2 µg trypsin (sequencing grade; Promega UK) and incubated at 37 °C for 18 h. The resulting solution was then diluted to 1:10 using TFA and mixed with a matrix solution of 1 µl of α-cyano-4-hydroxycinnamic acid solution (10 mg/mL in 50% ACN/0.1% TFA), allowed to crystallise and analysed using a Bruker Ultraflex II MALDI ToF/ToF mass spectrometer. For samples identified as ovicaprids, the tryptic peptide solution was further purified and fractionated using C18 Ziptips into 10% ACN and 50% ACN fractions (both in 0.1% TFA) and further analysed using MALDI as described above.

Acknowledgements: We would like to thank the European Research Council, the Max Planck Society, the Oxford Radiocarbon Accelerator Unit (ORAU), the University of Manchester and Manchester Institute of Biotechnology, and the Institute of Archeology and Ethnography, Russian Academy of Sciences Siberian Branch for their ongoing support. We would like to thank Miriam Jenkins, Esther Gillespie, Lauren Bell, Marine Caldarola, Raija Heikkila, Laura Doody, Saltanat Amirova, Geoff Church, Lucy Koster, Rachael Holmes, Luke Ghent, Phoebe Ewles-Bergeron, Nicholas Siemens, Marion Sandilands, and Julianna Zavodski who helped us sample the material as well as Sandra Heberstreit, Jana Zech, and Kristine Richter from the Max Planck Institute for the Science of Human History for discussions and laboratory work.

Author Contributions: SB, NW, AO, DC, BJS, VLH, MB performed the laboratory work; SB, NW, AO, BJS, VLH, MPC analyzed the data; MK, MS, AD provided the samples and site-specific expertise; KD and TH designed the study; SB and KD wrote the manuscript with the assistance and input of all authors.

Funding: This work has received funding from the ERC under the European Union's Horizon 2020 Research and Innovation Programme, grant agreement no. 715069 (FINDER) to KD and under the European Union's Seventh Framework Programme (FP7/2007–2013), grant agreement no. 324139 (PalaeoChron) to TH. The archaeological field studies were funded by the Russian Foundation for Basic Research (no. 18-09-40100 and no. 18-09-00404). Many thanks also go to the University of Manchester for Dean's Award Scholarship funding to VLH.

References

1. Madgwick, R. & Mulville, J. Investigating Variation in the Prevalence of Weathering in Faunal Assemblages in the UK: A Multivariate Statistical Approach: Investigating Variation in Weathering in UK Faunal Assemblages. *Int. J. Osteoarchaeol.* **22**, 509–522 (2012).

2. Madgwick, R. & Mulville, J. Reconstructing depositional histories through bone taphonomy: extending the potential of faunal data. *J. Archaeol. Sci.* **53**, 255–263 (2015).

3. Morin, E., Ready, E., Boileau, A., Beauval, C. & Coumont, M.-P. Problems of Identification and Quantification in Archaeozoological Analysis, Part I: Insights from a Blind Test. *Journal of Archaeological Method and Theory* **24**, 886–937 (2017).

4. Morin, E., Ready, E., Boileau, A., Beauval, C. & Coumont, M.-P. Problems of Identification and Quantification in Archaeozoological Analysis, Part II: Presentation of an Alternative Counting Method. *Journal of Archaeological Method and Theory* **24**, 938–973 (2017).

5. Buckley, M., Collins, M., Thomas-Oates, J. & Wilson, J. C. Species identification by analysis of bone collagen using matrix-assisted laser desorption/ionisation time-of-flight mass spectrometry. *Rapid Commun. Mass Spectrom.* **23**, 3843–3854 (2009).

6. Sinet-Mathiot, V. *et al.* Combining ZooMS and zooarchaeology to study Late Pleistocene hominin behaviour at Fumane (Italy). *Sci. Rep.* **9**, 12350 (2019).

7. Welker, F. *et al.* Palaeoproteomic evidence identifies archaic hominins associated with the Châtelperronian at the Grotte du Renne. *Proc. Natl. Acad. Sci. U. S. A.* **113**, 11162–11167 (2016).

8. Prüfer, K. *et al.* A high-coverage Neandertal genome from Vindija Cave in Croatia. *Science* **358**, 655–658 (2017).

9. Brown, S. *et al.* Identification of a new hominin bone from Denisova Cave, Siberia using collagen fingerprinting and mitochondrial DNA analysis. *Sci. Rep.* **6**, 23559 (2016).

10. Douka, K. *et al.* Age estimates for hominin fossils and the onset of the Upper Palaeolithic at Denisova Cave. *Nature* **565**, 640–644 (2019).

11. Prüfer, K. *et al.* The complete genome sequence of a Neanderthal from the Altai Mountains. *Nature* **505**, 43–49 (2014).

12. Krause, J. *et al.* A complete mtDNA genome of an early modern human from Kostenki, Russia. *Curr. Biol.* **20**, 231–236 (2010).

13. Reich, D. *et al.* Genetic history of an archaic hominin group from Denisova Cave in Siberia. *Nature* **468**, 1053–1060 (2010).

14. Mednikova, M. B. A proximal pedal phalanx of a Paleolithic hominin from denisova cave, Altai. *Archaeology, Ethnology and Anthropology of Eurasia* **39**, 129–138 (2011).

15. Vasiliev S.K., Shunkov M.V., Kozlikin M.B. Megafaunal Remains from the Eastern Chamber of Denisova Cave and Problems of Reconstructing the Pleistocene Environments in the Northwestern Altai. *Problems of Archaeology, Ethnography, Anthropology of Siberia and Neighboring Territories* **XXIII**, (2017).

16. Vasiliev, S. K., Shunkov, M. V. & Kozlikin, M. B. Preliminary Results for the Balance of Megafauna from Pleistocene Layers of the East Gallery, Denisova Cave. *Problems of Archaeology, Ethnography, and Anthropology of Siberia and Adjacent Territories* **19**, 32–38 (2013).

17. Vasiliev, S. K. & Shunkov, M. V. Large Pleistocene Mammals in the Southern Gallery of Denisova Cave. *Problems of Archaeology, Ethnography, Anthropology of Siberia and Neighboring Territories* **XV**, 63–69 (2009).

18. Vasiliev, S.K., Kozlikin, M.B., Shunkov, M.V. Megafaunal Remains from the Upper Portion of Pleistocene Deposits in South Chamber of Denisova Cave. *Problems of Archaeology, Ethnography, Anthropology of Siberia and Neighboring Territories* **569**, (2018).

19. Jacobs, Z. *et al.* Timing of archaic hominin occupation of Denisova Cave in southern Siberia. *Nature* **565**, 594–599 (2019).

20. Agadjanian, A. K. & Serdyuk, N. V. The history of mammalian communities and paleogeography of the Altai Mountains in the Paleolithic. *Paleontol. J.* **39**, 645–821 (2005).

21. Morley, M. W. *et al.* Hominin and animal activities in the microstratigraphic record from Denisova Cave (Altai Mountains, Russia). *Sci. Rep.* **9**, 13785 (2019).

22. Brown, S. *et al.* Earliest evidence for Denisovans identified using peptide mass fingerprinting and mitochondrial DNA analysis. submitted.

23. Slon, V. *et al.* The genome of the offspring of a Neanderthal mother and a Denisovan father. *Nature* **561**, 113–116 (2018).

24. Shunkov, M. V., Kozlikin, M. B. & Derevianko, A. P. Dynamics of the Altai Paleolithic industries in the archaeological record of Denisova Cave. *Quat. Int.* **559** (10) 34– 46 (2020).

25. Buckley, M. *et al.* Species identification of archaeological marine mammals using collagen fingerprinting. *J. Archaeol. Sci.* **41**, 631–641 (2014).

26. van Doorn, N. L., Hollund, H. & Collins, M. J. A novel and non-destructive approach for ZooMS analysis: ammonium bicarbonate buffer extraction. *Archaeol. Anthropol. Sci.* **3**, 281 (2011).

27. Brown, S. *et al.* Zooarchaeology by Mass Spectrometry (ZooMS) for bone material - AmBiC protocol v1 (protocols.io.bffdjji6). (2020).

28. van der Sluis, L. G. *et al.* Combining histology, stable isotope analysis and ZooMS collagen fingerprinting to investigate the taphonomic history and dietary behaviour of extinct giant tortoises from the Mare aux Songes deposit on Mauritius. *Palaeogeogr. Palaeoclimatol. Palaeoecol.* **416**, 80–91 (2014).

29. Strohalm, M., Hassman, M., Kosata, B. & Kodícek, M. mMass data miner: an open source alternative for mass spectrometric data analysis. *Rapid Commun. Mass Spectrom.* **22**, 905–908 (2008).

30. Buckley, M. & Kansa, S. W. Collagen fingerprinting of archaeological bone and teeth remains from Domuztepe, South Eastern Turkey. *Archaeol. Anthropol. Sci.* **3**, 271–280 (2011).

31. Brown, S., Collins, M., Douka, K. & Korzow Richter, K. On the standardization of ZooMS nomenclature. *Journal of Proteomics*. (2020).

32. Buckley, M. *et al.* Distinguishing between archaeological sheep and goat bones using a single collagen peptide. *J. Archaeol. Sci.* **37**, 13–20 (2010).

33. Buckley, M., Harvey, V. L. & Chamberlain, A. T. Species identification and decay assessment of Late Pleistocene fragmentary vertebrate remains from Pin Hole Cave (Creswell Crags, UK) using collagen fingerprinting. *Boreas* **46**, 402–411 (2017).

34. Rybczynski, N. *et al.* Mid-Pliocene warm-period deposits in the High Arctic yield insight into camel evolution. *Nat. Commun.* **4**, 1550 (2013).

35. Shunkov, M. V., Kulik, N. A., Kozlikin, M. B. & Sokol, E. V. The phosphates of Pleistocene–Holocene sediments of the Eastern Gallery of Denisova Cave. *Dokl. Earth Sci.* (2018).

36. Rogers, A. R. On Equifinality in Faunal Analysis. *Am. Antiq.* **65**, 709–723 (2000).

37. Lyman, R. L. *Vertebrate Taphonomy*. (Cambridge University Press, 1994).

38. Vasil'ev, S. A. Faunal exploitation, subsistence practices and Pleistocene extinctions in Paleolithic Siberia. *Deinsea* **9**, 513–556 (2003).

39. Vereshchagin, N. K. & Kuzmina, I. E. Remains of mammals from the Palaeolithic sites on the Don and upper Desna. *Trudy Zoologicheskogo instituta AN SSSR* **72**, 77–110 (1977).

40. Borgia, V. Hunting High and Low: Gravettian Hunting Weapons from Southern Italy to the Russian Plain. *Open Archaeology* **3**, 376–391 (2017).

41. Slon, V. *et al.* Neandertal and Denisovan DNA from Pleistocene sediments. *Science* **356**, 605–608 (2017).

42. Vasiliev, S. K. Late Pleistocene Bison (Bison p. priscus Bojanis, 1827) from the Southeastern Part of Western Siberia. *Archaeology, Ethnology and Anthropology of Eurasia* **34**, 34–56 (2008).

43. Smith, F. A. *et al.* Body mass of late Quaternary mammals. *Ecology* **84**, 3402 (2003).

44. Agadjanian, A. K. & Shunkov, M. V. Late Pleistocene Mammals of the Northwestern Altai: Report 2. Charysh Basin. *Paleontol. J.* **52**, 1461–1472 (2018).

45. Lisiecki, L. E. & Raymo, M. E. A Pliocene-Pleistocene stack of 57 globally distributed benthic δ18O records. *Paleoceanography* **20**, (2005).

Tables

Table 1: The results of ZooMS analysis of 8,253 fragmented bones from Denisova Cave.

ZooMS Taxon	East Chamber	Main Chamber	South Chamber	Total
Bos/Bison	1631	320	221	2172
Canidae	142	11	8	161
Capra	205	71	32	308
Cervidae	16			16
Cervidae/Gazella/Saiga	1187	34	33	1254
Crocuta/Panthera	99	22	20	141
Elephantidae	182	39	35	256
Equidae	677	119	60	856
Felidae	7	1		8
Hominin	6	1		7
Leporidae	2			2
Muridae	2			2
Mustelidae	2			2
Ovis	152	108	43	303
Ovis/Capra	302	62	47	411
Rangifer	33	3	1	37
Rhinocerotidae	387	97	46	530
Ursidae	125	18	33	176
Vulpes vulpes	17			17
Bird	10	1		11
Capra/Rangifer	11	2	5	18
Cervidae/Gazella/Saiga/Equidae	14			14
Crocuta/Panthera/Mustelidae	11	3	3	17
Equidae/Rhinocerotidae		1		1
Felidae/Crocuta/Panthera	1			1
Felidae/Crocuta/Panthera/Mustelidae	2			2
Felidae/Ursidae	18	3	2	23
Ovis/Capra/Cervidae/Gazella/Saiga	26	2		28
Ovis/Capra/Rangifer	2		2	4
Ovis/Cervidae/Gazella/Saiga	28	5		33
Unknown	19	3	3	25
Failed	992	197	228	1417
Total	**6308**	**1123**	**822**	**8253**

Figures

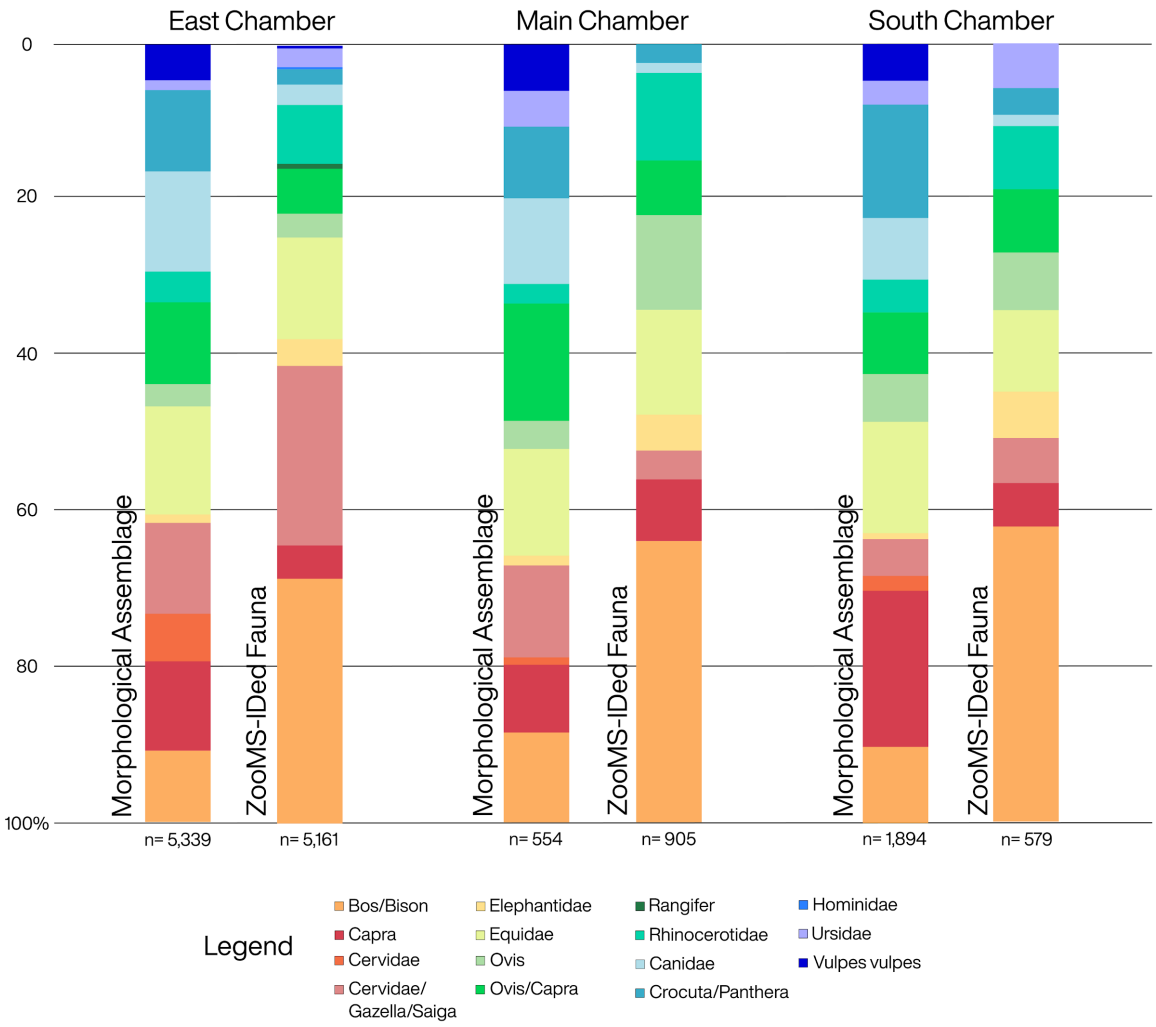

Figure 1: Comparison of the overall abundance of fauna between the morphological assemblage and the ZooMS-IDed fauna for the three chambers of Denisova Cave. Only the largest faunal groups have been included. Small mammals from both the morphological assemblage and ZooMS-IDed component, samples which failed ZooMS analysis, and “Unknown” spectra were removed.

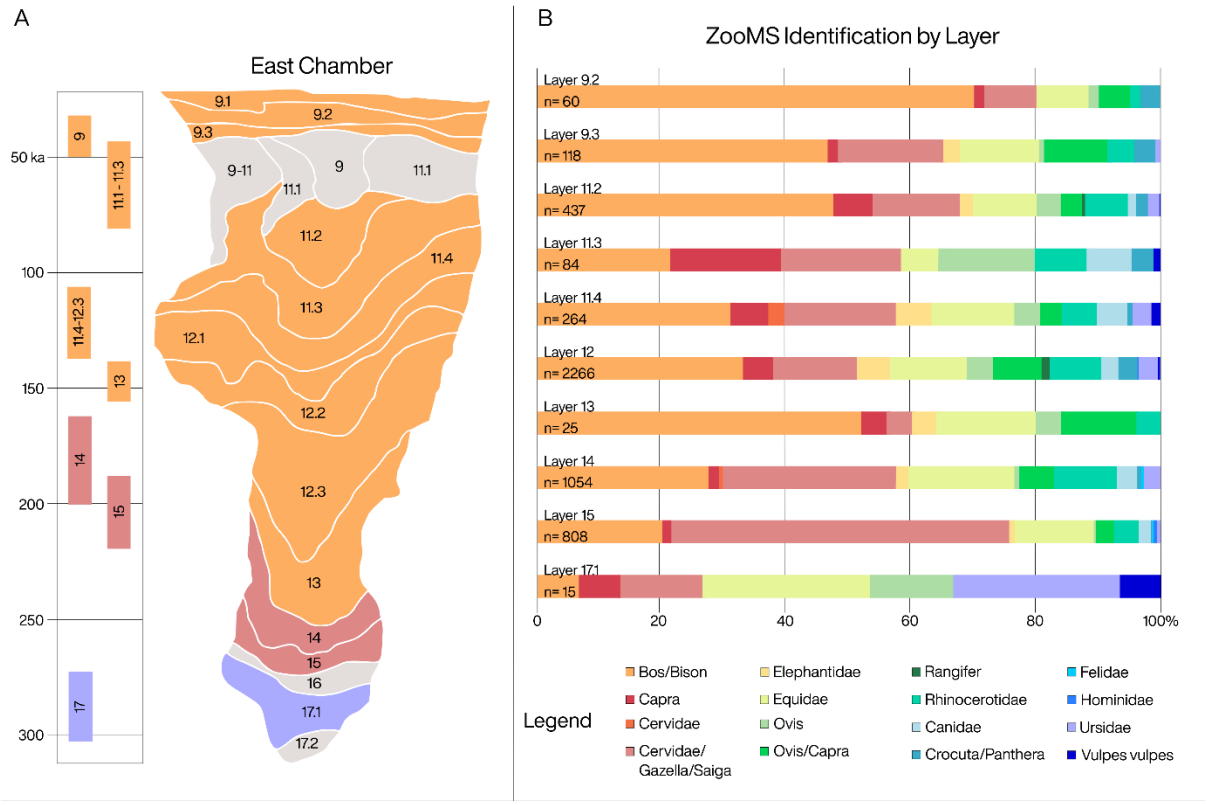

Figure 2: Relative abundance of fauna identified using ZooMS per layer of the East Chamber of Denisova Cave. Each bar depicts the major taxa identified, excluding small mammals, “Unknown” identifications, and failed samples. The stratigraphy (left) is highlighted with the most abundant fauna for each layer. Layers in grey were not included in this study.

Supplementary Text

Several important qualifying factors are necessary in understanding the ZooMS results presented in this study. Small vertebrates, for instance, are unlikely to be identified through the use of ZooMS in this case, in part because the current established ZooMS reference library largely excludes important taxa for the Altai, including the Sciuridae, Dipodidae, and Spalacidae families, and in part because of our preferential selection of bones larger than 2 cm. The spiral horned antelope (*Spirocerus kiakhtensis*) is the only medium-large vertebrate which does not currently have markers in the ZooMS reference library. *S. kiakhtensis* were found throughout Northern and Central Asia until the Late Pleistocene[31] and appear in small numbers at Denisova Cave.[15–21] Until a full proteomic analysis of securely attributed *S. kiakhtensis* remains is completed it is not clear which markers should be expected for this taxon. Several samples did not match taxa in the ZooMS reference library and have been reported in our results as being "Unknown" (Table 1; Supplementary Table 2, 3, 4).

ZooMS Analysis Results

6,308 samples were analysed from all archaeological layers of the East Chamber, including layer 9.2 (n= 89), 9.3 (n= 196), 11.2 (n= 620), 11.3 (n= 95), 11.4 (n= 353), 12 (n= 2311), 12.3 (n= 165), 13 (n= 28), 14 (n= 1381), 15 (n= 967), 17.1 (n= 53). An additional 50 samples were excavated at the interface between layers 12.1 and 12.2. 82% of the samples analysed from the East Gallery could be assigned to a specific ZooMS taxon and an additional 2% of samples produced low quality spectra which could only be identified to family or order. 16% of samples failed ZooMS analysis meaning that overall, the East Gallery had the lowest percentage of samples which failed to produce enough collagen for taxonomic identification (Supplementary Table 2; Supplementary Data 1).

1,123 samples were analysed from the Main Chamber, the majority of which were excavated during the 2006 season. These come from Middle-Upper Palaeolithic and Upper Palaeolithic contexts, layers 9.1 (n= 36), 9.3 (n= 83), 10 (n= 10), 11.1 (n= 115), 11.2 (n= 176), 11.3 (n= 139), 11.4 (n= 527). An additional 36 samples were found at the interface between layers 9.3 and 11.2 (n= 6) as well as layers 11.4 and

12 (n= 30). Overall, a high level of identification was possible for this layer with 75% of samples assigned to a specific ZooMS taxon and an additional 7% of samples producing low quality spectra which could be identified to family or order. 17% of samples failed to produce enough collagen for taxonomic identification, the majority of which were excavated from layers 9.1, 9.3 and 10 (Supplementary Table 3; Supplementary Data 1).

822 samples were analysed from the South Chamber, the majority from recent excavations of layers 11 (n= 461) and 12 (358). An additional three samples for layer 21 were analysed, one failed and the other two were identified as Bos/Bison and Cervidae/Gazella/Saiga. 65% of samples could be identified using ZooMS and an additional 7% of samples produced low quality spectra and could not be assigned to a single ZooMS taxon. The South Gallery produced the highest number of failed samples, with 28% of samples failing to produce enough collagen for taxonomic identification (Supplementary Table 4; Supplementary Data 1).

Supplementary Tables

Supplementary Table 1: Species identified in the morphological datasets from Denisova Cave which have been grouped under the most precise ZooMS identification taxon possible, their "ZooMS taxon". Taxa and body class size information compiled from previously published data[1–8].

ZooMS taxon	Body class size	Family	Genus	Species
Leporidae	-	Leporidae	Lepus	*Lepus tanaiticus*
	3.2	Leporidae	Lepus	*Lepus tolai*
Ochotonidae	-	Ochotonidae	Ochotona	*Ochotona* sp.
Cricetidae	2.71	Cricetidae	Cricetus	*Cricetus* sp.
Castoridae	4.28	Castoridae	Castor	*Castor fiber*
Vulpes vulpes	3.77	Canidae	Vulpes	*Vulpes vulpes*
Canidae	4.23	Canidae	Canis	*Canis lupus*
	-	Canidae	Vulpes	*Vulpes corsak*
	4.11	Canidae	Cuon	*Cuon alpinus*
	3.54	Canidae	Vulples	*Alopex lagopus*
Ursidae	5.14	Ursidae	Ursus	*Ursus (Spelaearctos) savini*
Mustelidae	-	Mustelidae	Martes	*Martes zibellina*
	-	Mustelidae	Gulo	*Gulo gulo*
	-	Mustelidae	Mustela	*Mustela erminea*
	-	Mustelidae	Mustela	*Mustela nivalis*
	-	Mustelidae	Mustela	*Mustela sibirica*
	-	Mustelidae	Mustela	*Mustela altaica*
	-	Mustelidae	Mustela	*Mustela eversmanni*
Crocuta	4.8	Hyaenidae	Crocuta	*Crocuta crocuta spelaea*
Panthera	-	Felidae	Panthera	*Panthera spelaea*
	4.65	Felidae	Panthera	*Uncia uncia*
Felidae	4.25	Felidae	Lynx	*Lynx lynx*
	3.54	Felidae	Otocolobus	*Felis manul*
Elephantidae	6.74	Elephantidae	Mammuthus	*Mammuthus primigenius*
Equidae	5	Equidae	Equus	*Equus (Equus) ferus*
	5	Equidae	Equus	*Equus (Sussemionus) ovodovi*
	5	Equidae	Equus	*Equus hydruntinus*
Rhinocerotidae	6	Rhinocerotidae	Coelodonta	*Coelodonta antiquitatis*
Rangifer	4.93	Cervidae	Rangifer	*Rangifer tarandus*
Cervidae	-	Cervidae	Capreolus	*Capreolus pygargus*
Cervidae/Gazella/Saiga	5.19	Cervidae	Cervus	*Cervus elaphus*
	5.9	Cervidae	Megaloceros	*Megaloceros giganteus*
	5.55	Cervidae	Alces	*Alces* cf. *alces*
	4.46	Bovidae	Saiga	*Saiga tatarica borealis*
	4.45	Bovidae	Gazella	*Gazella guttursza*
	4	Bovidae		*Gazella / Saiga*
Bos/Bison	5.95	Bovidae	Bison	*Bison priscus*

	-	Bovidae	Bos	*Poëphagus mutus*
Capra	5.11	Bovidae	Capra	*Capra sibirica*
Ovis	5.26	Bovidae	Ovis	*Ovis ammon*
Unknown	-	Sciuridae	Pteromys	*Pteromys volans*
	2.2	Bovidae	Spirocerus	*Spirocerus kiakhtensis*
	1.93	Sciuridae	Spermophilus	*Spermophilus sp.*
	-	Sciuridae	Marmota	*Marmota baibacina*
	2.37	Dipodidae	Allactaga	*Allactaga sp.*
	2.35	Spalacidae	Myospalax	*Myospalax myospalax*

Supplementary Table 2: Results of ZooMS analysis carried out for the East Chamber of Denisova Cave separated by layer.

ZooMS Taxon	Stratigraphic layers for the East Chamber of Denisova Cave												
	9.2	9.3	11.2	11.3	11.4	12	12.1-12.2	12.3	13	14	15	17.1	Grand Total
Bird			1	1		6		1		1			10
Bos/Bison	42	55	208	18	82	708	16	36	13	290	162	1	1631
Canidae			6	6	13	59	2	4		34	16	2	142
Capra	1	2	26	15	16	98	1	12	1	19	13	1	205
Cervidae			1		7	1	1			6			16
Cervidae/Gazella/Saiga	5	20	61	16	47	291	5	11	1	291	437	2	1187
Crocuta/Panthera	2	4	8	3	2	70	1	1		7	1		99
Elephantidae		3	9		15	106	1	19	1	21	7		182
Equidae	5	15	45	5	35	256	5	20	4	180	103	4	677
Felidae										5	2		7
Hominin						2					4		6
Leporidae				1		1							2
Muridae						1				1			2
Mustelidae						1	1						2
Ovis	1	1	17	13	11	92		6	1	8	2		152
Ovis/Capra	3	12	15		9	159	6	14	3	58	23		302
Rangifer			2			26		3		1	1		33
Rhinocerotidae	1	5	30	7	15	174		16	1	106	32		387
Ursidae		1	8		8	69		2		28	5	4	125
Vulpes vulpes			1	1	4	8		2				1	17
Capra/Rangifer		1			4					6			11
Cervidae/Gazella/Saiga/Equidae		2	1			2				5	4		14
Crocuta/Panthera/Mustelidae			1		3	4				2	1		11
Felidae/Crocuta/Panthera											1		1
Felidae/Crocuta/Panthera/Mustelidae			2										2
Felidae/Ursidae			4		1	1				7	3	2	18
Ovis/Capra/Cervidae/Gazella/Saiga		2	1		5	3				14	1		26
Ovis/Capra/Rangifer										1		1	2
Ovis/Cervidae/Gazella/Saiga			5		1					18	4		28
Unknown					**3**	**7**			**1**	**5**	**2**	**1**	**19**
Success	**60**	**123**	**452**	**86**	**281**	**2145**	**39**	**147**	**26**	**1114**	**824**	**19**	**5316**
Failed	**29**	**73**	**168**	**9**	**72**	**166**	**11**	**18**	**2**	**267**	**143**	**34**	**992**
Grand Total	**89**	**196**	**620**	**95**	**353**	**2311**	**50**	**165**	**28**	**1381**	**967**	**53**	**6308**

Supplementary Table 3: Results of ZooMS analysis carried out for the Main Chamber of Denisova Cave separated by layer.

ZooMS Taxon	Stratigraphic layers for the Main Chamber of Denisova Cave										
	9.1	**9.2**	**9.3**	**9.3/ 11.2**	**11**	**11.1**	**11.2**	**11.3**	**11.4**	**11.4/12**	**Grand Total**
Bird								1			1
Bos/Bison	4	1	19	1	2	49	40	36	159	9	320
Canidae			2			1	2	3	3		11
Capra			1			2	17	13	37	1	71
Cervidae/Gazella/Saiga	1		4		1	4	4	5	14	1	34
Crocuta/Panthera			2			5	5	3	7		22
Elephantidae	1		1			5	9	9	14		39
Equidae	4		3			4	21	12	71	4	119
Felidae									1		1
Hominin	1										1
Ovis	2		6	2	3	9	15	19	48	4	108
Ovis/Capra	1		6		2	11	8	9	22	3	62
Rangifer									3		3
Rhinocerotidae	1		6	1	1	10	20	3	53	2	97
Ursidae			2	1		2	3	4	6		18
Capra/Rangifer							1		1		2
Crocuta/Panthera/Musteli dae							1		2		3
Equidae/Rhinocerotidae						1					1
Felidae/Ursidae							1		2		3
Ovis/Capra/Cervidae/ Gazella/Saiga								1	1		2
Ovis/Cervidae/Gazella/Saiga	1						1	1	2		5
Unknown								**1**		**2**	**3**
Success	**16**	**1**	**52**	**5**	**9**	**102**	**144**	**120**	**446**	**26**	**926**
Failed	**20**		**30**	**1**	**2**	**12**	**28**	**19**	**81**	**4**	**197**
Grand Total	**31**	**1**	**82**	**6**	**11**	**115**	**176**	**139**	**527**	**30**	**1123**

Supplementary Table 4: Results of ZooMS analysis carried out for the South Chamber of Denisova Cave separated by layer.

ZooMS Taxon	Stratigraphic layers for the South Chamber of Denisova Cave			
	11	**12**	**21**	**Grand Total**
Bos/Bison	91	129	1	221
Canidae	5	3		8
Capra	20	12		32
Cervidae/Gazella/Saiga	14	18	1	33
Crocuta/Panthera	12	8		20
Elephantidae	12	23		35
Equidae	29	31		60
Ovis	20	23		43
Ovis/Capra	31	16		47
Rangifer	1			1
Rhinocerotidae	23	23		46
Ursidae	29	4		33
Capra/Rangifer		5		5
Crocuta/Panthera/Mustelidae	1	2		3
Felidae/Ursidae	2			2
Ovis/Capra/Rangifer	2			2
Unknown	**2**	**1**		**3**
Success	**294**	**298**	**2**	**594**
Failed	**167**	**60**	**1**	**228**
Grand Total	**461**	**358**	**3**	**822**

External Database:

External Database 1: ZooMS Spectra files
ZooMS spectra for each of the samples analysed is included in this database.
https://data.mendeley.com/datasets/mzt6zspjbp/draft?a=3a091eb7-a728-45a3-a04b-aa52adefa997

https://data.mendeley.com/datasets/f2454wydnv/draft?a=41974958-608e-48c9-90f2-3d844135b2d4

Supplementary References

1. Morley, M. W. *et al.* Hominin and animal activities in the microstratigraphic record from Denisova Cave (Altai Mountains, Russia). *Sci. Rep.* **9**, 13785 (2019).
2. Vasiliev, S. K., Shunkov, M. V. & Kozlikin, M. B. Preliminary Results for the Balance of Megafauna from Pleistocene Layers of the East Gallery, Denisova Cave. *Problems of Archaeology, Ethnography, and Anthropology of Siberia and Adjacent Territories* **19**, 32–38 (2013).
3. Vasiliev S.K., Shunkov M.V., Kozlikin M.B. Megafaunal Remains from the Eastern Chamber of Denisova Cave and Problems of Reconstructing the Pleistocene Environments in the Northwestern Altai. *Problems of Archaeology, Ethnography, Anthropology of Siberia and Neighboring Territories* **XXIII**, (2017).
4. Vasiliev, S. K., Kozlikin, M.B., Shunkov, M. V. Megafaunal Remains from the Upper Portion of Pleistocene Deposits in South Chamber of Denisova Cave. *Problems of Archaeology, Ethnography, Anthropology of Siberia and Neighboring Territories* **569**, (2018).
5. Jacobs, Z. *et al.* Timing of archaic hominin occupation of Denisova Cave in southern Siberia. *Nature* **565**, 594–599 (2019).
6. Vasiliev, S. K. & Shunkov, M. V. Large Pleistocene Mammals in the Southern Gallery of Denisova Cave. *Problems of Archaeology, Ethnography, Anthropology of Siberia and Neighboring Territories* **XV**, 63–69 (2009).
7. Agadjanian, A. K. & Serdyuk, N. V. The history of mammalian communities and paleogeography of the Altai Mountains in the Paleolithic. *Paleontol. J.* **39**, 645–821 (2005).
8. Smith, F. A. *et al.* Body mass of late Quaternary mammals. *Ecology* **84**, 3402 (2003).

Manuscript E – in prep. Brown, S., Wang, N., Oertle, A., Jope-Street, B., Kozlikin, M., Shunkov, M., Derevianko, A., Higham, T., Douka, K., Richter, K. Examining collagen preservation through glutamine deamidation at Denisova Cave.

Examining collagen preservation through glutamine deamidation at Denisova Cave

Samantha Brown[1], Maxim Kozlikin[2], Michael Shunkov[2,3], Anatoly Derevianko[2], Thomas Higham[4], Katerina Douka[1], Kristine Korzow Richter[1,5].

[1]Max Planck Institute for the Science of Human History, Jena, Germany.
[2]Institute of Archeology and Ethnography of the Siberian Branch of the Russian Academy of Sciences, Novosibirsk, Russia.
[3]Novosibirsk State University, Novosibirsk, Russia.
[4]Oxford Radiocarbon Accelerator Unit, RLAHA, University of Oxford, Oxford OX13QY, UK.
[5]Department of Anthropology, Harvard University, Cambridge, MA, USA

Abstract

The use of glutamine deamidation has been proposed as a means of measuring relative decay in archaeological bones using peptide mass fingerprinting data. If reliable, it could be used to identify intrusive fossils in stratigraphic layers and relatively date unprovenanced remains. Here we analyse glutamine deamidation in 2,501 fossils from the East Chamber of Denisova Cave, a site for which robust chronological studies have been carried out and burial conditions are well understood. We then compare these results with an additional 15 fossils measured using tandem mass spectrometry and the recently published deamiDATE. Our results reveal that intra and inter layer variability is too high to be able to detect a pattern of deamidation at the site, suggesting caution should be applied when attempting to link deamidation with relative decay or chronological age.

Keywords

Collagen, peptide mass fingerprinting, deamidation, glutamine, chronology, Denisova Cave

Introduction

Providing secure and reliable chronologies for Pleistocene-age fossils is crucial for addressing questions surrounding human evolution, human-animal-climate interactions, and ecological reconstructions. Despite major developments in the direct dating of fossils using radiometric methods (radiocarbon, uranium thorium, electron spin resonance dating) and through approximations from genetic-based estimates or optically stimulated luminescence (OSL), the process is often riddled with complexity. The analysis of protein degradation, specifically collagen, has been proposed as an alternative dating approach (van Doorn et al., 2012; Welker et al., 2017). Amino acid racemization for instance, has been used for decades to date geological samples containing proteins by analyzing the L/D amino acid ratio (Demarchi and Collins, 2013). Recently, the deamidation of collagen has been proposed as a method of relative dating and a way of identifying rates of relative decay within archaeological bone assemblages (Chen et al., 2019; Ramsøe et al., 2020; van Doorn et al., 2012; Wilson et al., 2012). Since it is not an absolute dating method and, as of yet, lacks research on calibrating the deamidation values to an absolute age in a way that has been done for other forms of protein degradation like amino acid racemization (Demarchi and Collins, 2013), deamidation rates are unable to provide the direct age of a fossil. Instead, deamidation has been proposed as a means of assessing the chronological relationship between stratigraphic layers, homogeneity of an assemblage, and the decay rate and state of preservation of collagenous samples (Chen et al., 2019; Sinet-Mathiot et al., 2019; Welker et al., 2017).

Using deamidation rates is particularly attractive because they can be calculated from the same mass spectral data used for other analyses, predominantly peptide mass fingerprints (PMF) generated from Matrix-Assisted Laser Desorption/Ionization - Time of Flight Mass Spectrometry (MALDI-TOF-MS) and shotgun palaeoproteomics data generated from Liquid Chromatography Mass Spectrometry (LC-MS/MS). PMF data of collagenous materials (bone, antler, hide, scales, and ivory) can be used for taxonomic identifications (ZooMS - Zooarchaeology by Mass Spectrometry) (Brandt et al., 2018; Buckley et al., 2009; Coutu et al., 2016; Richter et al., 2011) and LC-MS/MS data from collagen has been used, for instance, to reconstruct phylogenies and for taxonomic identifications (Kumazawa et al., 2016; Welker, 2018; Welker et al., 2015).

While both methods allow for assessing deamidation, the generation of LC-MS/MS data is more time consuming and expensive in comparison with PMF. LC-MS/MS data however, provides much higher resolution, including in relation to deamidation rates within a sample. Here we compare deamidation rates from different stratigraphic layers of the East Gallery of Denisova Cave to assess the reliability of both methods for relative dating.

Deamidation

Collagen, specifically type I collagen (COL1), is a particularly useful protein in archaeological sciences as it is the single most abundant protein in vertebrates and has been shown to be highly stable (Henriksen and Karsdal, 2019). The robusticity of COL1 is the result of its fibrillar structure, which is composed of triple helices made up of three tightly packed alpha chains connected to one another by hydroxylysine cross-linkages. Multiple helices form fibrils and then fibers which provide essential structural support for many biological tissues (Shoulders and Raines, 2009). The helical structure is generated by a repeating pattern of three amino acids, G-X-Y, in which every third residue is the small and flexible amino acid glycine (G), while X and Y are often proline and hydroxyproline, respectively (Henriksen and Karsdal, 2019; Shoulders and Raines, 2009). This robusticity and flexibility allows COL1 to remain stable over archaeological timescales in a variety of climates and conditions (Buckley, 2018); PMF of COL1 has been successful on bone remains as old as 3.4 ma (Rybczynski et al., 2013).

Following protein synthesis, *in vivo* (biologically-derived) post-translational modifications (PTMs) increase the functional diversity of the proteome. After the death of the organism additional chemical modifications, some of which are identical to the *in vivo* PTMs, occur as part of the degradation processes. Deamidation, the conversion of glutamine and asparagine to glutamic acid and aspartic acid respectively through the removal of an amide functional group (Figure 1a), is the most common diagenetic PTM identified in COL1 (Cleland et al., 2015). Spontaneous deamidation of asparagine has been used as a molecular clock for *in vivo* biological processes such as aging and development (Delmar et al., 2019; Hao et al., 2017; Tyler-Cross and Schirch, 1991).

Spontaneous deamidation occurs through two different mechanisms: formation of a cyclical intermediate (Figure 1a) and direct hydrolysis of the side chain. The formation of the cyclical intermediate has an overall faster reaction rate than direct hydrolysis. Under neutral and basic conditions asparagine will form the cyclical intermediate, and under acidic conditions (below pH 5) direct hydrolysis is favored (Catak et al., 2009). The mechanisms for glutamine deamidation have been less well studied, but under neutral conditions it is likely that direct hydrolysis is responsible for most of the deamidation (Joshi et al., 2005; Riggs et al., 2019) aside from when the glutamine is followed by a small, flexible glycine residue when the preferred pathway is likely the cyclical intermediate (Riggs et al., 2019). Asparagine, therefore, is much more sensitive to deamidation than glutamine (Daniel et al., 1996; Robinson et al., 2004; Terwilliger and Clarke, 1981; Wilson et al., 2012) making glutamine a far more suitable amino acid for measuring the thermal history of collagen over long time periods.

The rate at which deamidation occurs at a particular amino acid location is influenced by the local environment of the protein and amino acid including the primary amino acid sequence and the higher level structure (Delmar et al., 2019; Tyler-Cross and Schirch, 1991). In archaeological samples, the rate at which deamidation occurs is also heavily influenced by the thermal history of the bones (van Doorn et al., 2012; Wilson et al., 2012) including, climate and temperature of the burial environment, pH of the soil, ionic strength, and water availability (Robinson and Rudd, 1974; Scotchler and Robinson, 1974). Finally, the choice of methods for protein extraction and processing can induce deamidation (Hao et al., 2017). The single largest of these factors is the amino acid that follows the glutamate or aspargine with the small, flexible amino acid glycine providing the fastest rates and the bulky, structurally constrained amino acid proline providing the slowest rates (Robinson et al., 2004). As both of these amino acids are present in high percentages in collagen the variability between different locations within the protein is expected to be high.

Observing deamidation in LC-MS/MS data is relatively straightforward through the identification of the +0.984 Da mass shift of deamidated amino acids. Converting that data into a relative age can be done using deamiDATE (Ramsøe et al., 2020) which

takes into account the amino acid pattern before and after the deamidation site. The identification of deamidation sites in PMF data is more difficult. The mass shift must be measured through the deconvolution of the overlapping peptide peaks from the deamidated and non-deamidated peptides (Figure 1b) (Brown et al., 2020a; van Doorn et al., 2012; Wilson et al., 2012). For ZooMS identifications, the peptide COL1α1 508-519 is common and conserved across mammalian species making it highly diagnostic and a good indicator of collagen preservation (van Doorn et al., 2012; Wilson et al., 2012). The peptide, which contains one glutamine that can deamidate, is identified at m/z 1105.5 (non-deamidated) and m/z 1106.5 (deamidated). Therefore the ratio of the intensities between the peaks at 1105.5 and 1106.5 has been proposed as a way of quantifying the relative level of deamidation in a sample and thus its relative age (van Doorn et al., 2012; Wilson et al., 2012).

The applicability of relative decay rates observed through glutamine deamidation however has been challenged, with empirical data indicating that the variation observed within a bone assemblage from the same or similar contexts is too high (Pal Chowdhury et al., 2019; Schroeter and Cleland, 2016). As the method continues to be used in order to determine the antiquity of unprovenanced fossils (Chen et al., 2019), understanding the limitations and utility of collagen deamidation data from PMF spectra is of increasing importance. In this study we obtain and examine the deamidation values of 2,501 bones from multiple, well-dated stratigraphic layers at a single archaeological site (Denisova Cave, Russia) in order to assess the validity of deamidation as an age-predictor using both PMF and LC-MS/MS methods.

Materials

We have included 2,501 archaeological samples from Denisova Cave, Siberia, Russian Altai in our analysis of glutamine deamidation, utilising data sets which have previously been published (Supplementary Data 1; (Brown et al., in prep)). Denisova Cave has the longest archaeological sequence in Eurasia spanning ~300 ka (thousand years) (Douka et al., 2019; Jacobs et al., 2019). Large assemblages of bone have been excavated from all layers at the site, brought and deposited there by its hominin inhabitants as well as other predators. The assemblages have been extensively researched, from both a zooarchaeological and a palaeoproteomic perspective (Brown et al., 2016; in prep.; Douka et al., 2019; Jacobs et al., 2019;

Vasiliev, et al., 2018; Vasiliev et al., 2013). As the average ambient temperature inside the cave fluctuates a few degrees above 0℃, fossils excavated from the site typically have a high level of biomolecular preservation.

Bones excavated from Denisova Cave also have the benefit of a well-documented life history based on detailed studies of the sedimentology and microstratigraphy of most parts of the cave (Douka et al., 2019; Jacobs et al., 2019; Morley et al., 2019; Shunkov et al., 2020, 2018). While occasional instances of disturbance and movement of bones throughout the strata have been identified, overwhelmingly the chronological studies reveal that the stratigraphy is largely intact and areas of disturbance can be identified and excluded from further studies (Douka et al., 2019; Jacobs et al., 2019). The bones included in this study were excavated within the last decade from the East Chamber. All layers found in the East Chamber of Denisova Cave were sampled, namely layers 9 (n= 169), 11 (n= 518; ~107-46 ka), 12 (n= 296; ~146-107 ka), 13 (n= 76; ~156-146 ka), 14 (n= 688; ~202-163 ka), 15 (n= 743; ~217-187 ka), and 17.1 (n= 11; ~305-284 ka) (Figure 2a). Following excavation, all bones were stored in the same place, the Institute for Archeology and Ethnography of the Siberian branch of the Russian Academy of Sciences, and have not been treated with conservation products. The large assemblage of well-preserved material, from a secure stratigraphic sequence with a similar life history makes the bones from Denisova cave ideal candidates for assessing the relationship between relative age and glutamine deamidation.

Methods

In order to ensure only well preserved samples with low amount of artificial, lab-based deamidation were included in this study several qualifying factors were used to include/exclude samples. The first was the extraction protocol utilised. While multiple methods have been used to extract collagen for PMF at Denisova Cave (Brown et al., 2016; in prep.; Douka et al., 2019), only collagen which was extracted using an ammonium bicarbonate protocol, which is specifically designed to avoid artificially deamidating peptides (Brown et al., 2020b; van Doorn et al., 2011), were included in this study. Secondly, only samples which could be taxonomically identified using PMF analysis were included (Brown et al., in prep). Thirdly, only samples for which all three replicate spectra produced deamidation measurement were included. In total 2,501

ZooMS samples qualified for this study, spanning seven archaeological layers of the site's East Chamber and ~240 thousand years (ka) (Figure 2a) (Douka et al., 2019; Jacobs et al., 2019).

All peptide mass fingerprints analysed here were obtained from previously published studies (Brown et al., in prep), collagen for LC-MS/MS analysis was extracted using ammonium bicarbonate extraction protocols (Brown et al., 2020b; van Doorn et al., 2011) (Supplementary Information). To determine if patterns of glutamine deamidation could be identified in our dataset, deamidation was measured using two methods. Deamidation from the PMF spectra was measured using the Q2E package (Wilson et al., 2012). As soft ionisation mass spectrometry is unable to deconvolute the overlapping non-deamidated (m/z 1105.5) and deamidated (m/z 1105.6) peak for peptide COL1α1 508-519, Q2E uses a genetic algorithm to achieve this. This is done by comparing the theoretical distribution for the non-deamidated peptide against the MALDI-TOF data (Figure 1b) (Wilson et al., 2012). A peptide which appears to have no deamidation returns a score (Est%Gln) of 1 while an entirely deamidated peptide returns a score of 0 (Wilson et al., 2012) (Supplementary Data X).

Additionally, bulk site specific measurements of asparagine and glutamine deamidation were made using LC-MS/MS data and the recently published deamiDATE (Ramsøe et al., 2020) which provides a much higher degree of precision and resolution than those derived from the MALDI-TOF spectra only. For bulk measurements the ratio of non-deamidated asparagine and glutamine position is compared with the number of their deamidated forms to create a relative remaining intensity. Site specific deamidation looks at both the sequence-dependent deamidation rate of each occurrence of asparagine and glutamine within a sample, as well as the relative intensity of the deamidating protein, in a similar manner to the bulk measurement. We used 15 of the same samples that were included in the PMF dataset (Supplementary Information).

Results

Peptide Mass Fingerprinting Results

In total, 2,501 archaeological samples (7,503 replicates) from layers 9, 12, 13, 14, 15 and 17.1 of the East Chamber of Denisova Cave were analysed for glutamine deamidation using PMF (Figure 2a, Supplementary Data 1). Large variations in the deamination rate of COL1α1 508-519 are observed within each archaeological layer studied (Figure 2b). This is particularly true for the youngest layer studied, the Upper Pleistocene layer 9 (~45-50 ka) (Douka et al., 2019), which includes samples that appear almost completely deamidated (eg. DC10383, Est%GI= 0.09) and samples that appear almost completely non-deamidated (eg. DC7952, Est%GI= 0.98).

In order to exclude outliers, detect any subgroups, and identify average trends, we analysed our data using a Grubbs test (p= 0.05) and converted it into box-and-whisker plots (Figure 2c). The Grubbs test did not identify any outliers; however, when compiled into box-and-whisker plots outliers were detected for layers 11 (n=4), 12 (n=3), 14 (n=1), and 15 (n=2). Excluding layer 9 which had the highest variability and level 17.1 for which a significantly smaller number of bones were available for study than the other layers, a slight age-related trend is observed for layers 11-15 (Figure 2b). However, the intralayer variation is larger than the interlayer variation which results in overlapping distributions between the layers and very wide upper and lower quartiles. We then conducted a Kruskal-Wallis test (significance value 0.05) to determine if the slight trend visible in box-and-whisker plots was statistically significant and if layers were actually different from one another. Our analysis determined that there is no statistically significant difference between layers 11-15 (adjusted H= 1066.542; d.f= 4; p= 1.35e-229).

LC-MS/MS and deamiDATE Results

15 samples were analysed using LC-MS/MS and deamiDATE; these included two samples for layers 9, 11, 12, 13, 15 and 17.1 and three samples for layer 14. Bulk measurements of collagen using deamiDATE revealed that all of the bones fall below the expected thresholds for modern samples, in both their asparagine (N) and glutamine (Q) deamidation (Figure 4). As with measurements from MALDI-TOF spectra, bones from layers 9 (~45-50 ka) were significantly more deamidated than the

Middle Palaeolithic layers for the East Chamber (~50-217 ka). Layer 17.1 (~284-305 ka) appears to have higher levels of deamidation than younger layers, which was not necessarily the case in PMF data. Preservational factors are clearly apparent in bones from layer 9 where glutamine is more deamidated than asparagine. As asparagine typically deamidates faster than glutamine, the chemical environment of the soil could be responsible for a bias toward the cyclic intermediate for glutamine, a change in the activation energy of the reaction, and/or the presence of a catalyst present in the sediment of layer 9. In layers 11-15, glutamine deamidation generally increases as we move down the stratigraphy, with the exception of a single sample (DC8219) from layer 12 that is much more deamidated than other samples of a similar age. Unless DC8219 has been moved post-depositionally, this highlights that the high level of variability of samples even within the same context observed in the PMF results is also observed in the LC-MS/MS data.

Site specific deamidation, plotted against deamidation “half-times”, i.e. values estimated to be ~100 days for asparagine deamidation and more than 60 times as long for glutamine deamidation (Robinson et al., 2004) (Figure 4), identified no overall pattern in deamidation rates between layers. In fact, high variability was identified between stratigraphic layers but also within the same sample. While the bulk values were successful in validating that the samples are in fact ancient, the use of “half times” appears to be of little use for identifying a specific pattern for deamidation in bones of this antiquity.

Discussion

The most interesting result was the large intra-layer variability. To explore this further, we considered possible confounding factors that might result in artificially increased variability. Microstratigraphy analysis and OSL measurements have shown that the majority of the East Gallery has high levels of stratigraphic integrity, meaning there is very limited evidence of mixing of soils or fossils through contexts (Jacobs et al., 2019; Morley et al., 2019). While it is possible that some fossils may have moved through the stratigraphy the hypothetical extent to which this must have been occurring to result in the levels of intra-layer variability, evident in glutamine deamidation values, would be completely out of step with all other chronological and stratigraphic studies

carried out for the site (Douka et al., 2019; Jacobs et al., 2019; Morley et al., 2019; Shunkov et al., 2020).

To explain the inter-layer variability we also considered the role in which the treatment of bones prior to burial may have played on deamidation values. These effects include going through the digestive tract of predators and processing and cooking of bones by hominins. This was achieved by looking for differences between deamidation rates in bones from herbivores and predators (hominins, Canidae, Crocuta, Panthera, and Ursidae). The term “predator” is used here to include Ursidae remains which preferred vegetarian or omnivorous diets and used the cave for hibernation as they were unlikely to be targets of predation (Vasiliev, et al., 2018; Vasiliev et al., 2013). Herbivores were likely targets of both hominins and predators, suffering a variety of butchering practices and, while evidence for the use of fire is limited at Denisova Cave (Morley et al., 2019), processes of cooking were likely at play as well. Limited targeting of predators is evident at Denisova Cave, where hominins were exploiting their fur and hide. The extent to which hominins may have been actively hunting and processing the bones of other predators however is far lower, in comparison with the targeting of herbivores. As a result, if treatment of the bones prior to burial can result in significantly shifting deamidation values we would expect to see carnivores trending with lower levels of deamidation than herbivores. When comparing the two datasets by layer there is no statistical difference between the deamidation values for predators and herbivores (Supplementary Figure 1). In fact both datasets appear almost identical in the variability of deamidation rates. It therefore seems unlikely that these short term treatments of bone prior to burial plays as significant a role in their deamidation than long term burial conditions. Although it should be noted that burning, either from hearth firing or environmental fires, will preferentially destroy collagen meaning that they are unlikely to have passed the qualifying factors used to include/exclude data from this study. We would also discourage the use of deamidation rate relative dating on obviously burned bones even if there was enough preserved collagen.

When comparing the deamidation results using the two forms of measurement, the same general trends appear in the bulk deamidation analysis of the LC-MS/MS data

and the large MALDI-TOF (PMF) dataset. There is a slight (but sadly insignificant and with high intra-layer variability) trend between layers 11 and 15. However the oldest and youngest layers do not follow this trend in both datasets. The results of layer 9 are likely the result of preservational issues (discussed below). Bones from layer 17.1, the oldest layer of the East Chamber, are at least 50 ka older than those from layer 15. In initial taxonomic identification of bones from layer 17.1 (Brown et al., in prep), 64% of those analysed failed to produce enough collagen for taxonomic identification (Brown et al., in prep). The 11 samples that are included in this study represent the absolute best preservation particularly in the PMF markers used for identification and therefore, the PMF results are likely skewed towards lower levels of deamidation for layer 17.1 (Figure 2), although the two samples chosen for LC-MS/MS analysis do follow the slight trend seen in layers 11-15. In comparison, a much larger sample size was available for layer 15 (n= 743). Layers 11 is over 80 ka younger than level 15, mirrorring the relative difference between layers 15 and 17.1. In both the PMF and bulk LC-MS/MS results layer 15 showed higher levels of deamidation than layer 11. (Douka et al., 2019; Jacobs et al., 2019). For layers 12-15 which span approximately 70 ka of the Pleistocene, each consecutive layer has an overlapping distribution in the PMF data (Figure 2) and very little distinction in rates of deamidation is possible using LC-MS/MS data outside of an assertion that these are ancient samples (Figure 3).

Layer 9 contains the largest inter-layer variability as well as samples with the least and most deamidation values for the PMF analysis. While bones attributed to layer 9 are at least 230 ka younger than those from layer 17.1, 34% of samples appear more deamidated than the most deamidated sample from layer 17.1 (DC10782, Est%Gln= 0.43). The massive inter-layer variability in the PMF glutamine deamidation results for layer 9 matches what is known archaeologically for the context. Layer 9 is an Upper Palaeolithic layer; however, its sedimentology mirrors the overlying Holocene stratigraphy (Shunkov et al., 2018). The layer is comprised of a light loess loam with isolated inclusions of finely crushed stone (Douka et al., 2019; Jacobs et al., 2019; Shunkov et al., 2020). In the uppermost Holocene layers of the East Chamber, a high saturation of organic matter has triggered chemical transformations of the underlying layers, including layer 9, resulting in heavy phosphatization of sediments (Shunkov et

al., 2020, 2018). As a result there are no reliable OSL dates for the Upper Pleistocene layers (Jacobs et al., 2019) and the only reliable radiocarbon age comes from a hominin fossil identified within layer 9.3, Denisova 14 (50 - 45.9 ka) (Douka et al., 2019). ZooMS analysis performed on bones from layer 9 had a high rate of samples which could not be taxonomically identified, with more than 34% failing to produce enough collagen (Brown et al., in prep). It is therefore not surprising that glutamine deamidation is so varied within this context (Kato et al., 2019), highlighting a need for a good understanding of the thermal and chemical history of the bones before any type of relative age estimate based upon deamidation can be conducted. Interestingly, the phosphatisation of soils for layer 9 and the resulting acceleration in deamidation caused a flip in the expected relationship between glutamine and asparagine, with asparagine less deamidated than glutamine (Figure 3). This reversal in expected values could provide an important indicator for artificial or chemical deamidation as a result of specific burial conditions which would bias toward a different type of reaction or indicate the presence of a catalyst. These deamidation values reinforce the preservational issues surrounding samples from layer 9 and the likelihood that on-going proteomic and genetic analyses of bones from this layer will continue to be challenging.

In terms of determining an overall pattern of deamidation that corresponds to relative age for the site, our results highlight that some of the major problems with this dating approach. As mentioned above, the fact that deamidation rates are highly dependent on environmental factors means that intercomparison between sites will be extraordinarily difficult. Even when assessing differences within a site, as we have done here over hundreds of thousands of years, no significant differences between the layers were identified.

While age related trends in deamidation were able to be identified, the problems encountered with layer 17.1 led us to explore how the inclusion of fewer samples would affect the clarity of the trend. To demonstrate this, we randomly subsampled the Q2E results from the PMF data from layers 11-15 where the trend was clearest, using 10 samples from each layer four times (Supplementary Info). In each scenario, the layers were once again plotted against one another using box-and-whisker plots. The

resulting box-and-whisker plots (Figure 5) highlight the difficulty in securely identifying a trend in collagen preservation at the site when big data is not available. Overall, samples from layer 11 displayed a highly level of collagen preservation and performed the best in all but scenario C. The highest variation was displayed by layer 13 data which, in scenarios A and D, displayed lower levels of collagen preservation than older stratigraphic contexts. Where scenario B displayed the ideal relative decay rates between stratigraphic layers, scenario D reveals the problem of working with individual or small groups of samples.

Although the number of samples is smaller for the LC-MS/MS, there are dozens or hundreds of measurements per sample. Including all of the replicates from each layer, there is a small age-related trend. However, of the eleven samples from layers 11-15, three (one each from layers 11, 12, and 14) deviate from the trend. Making being able to assign relative ages to the different layers based upon either Q2E or deamiDATE deamidation rates problematic.

Additionally, this experiment highlights the difficulty of using deamidation rates to identify a single sample. Given that the level of intra-layer variability prevents the discrete separation of layers, trying to match an unknown sample to a particular layer based upon the deamidation values is not possible even, with a reference of hundreds of samples per layer (something which is not common for most sites). This also mostly precludes the identification of outlying or intrusive fossils into overlying or underlying layers.

We used two large data methods to analyze deamidation rates for layers 11-15: hundreds of samples with single PMF measurements and two or three samples with hundreds of measurements from LC-MS/MS data. In all cases our samples were clearly more deamidated than published modern material indicating our samples are indeed archaeological. Yet the results show no statically significant age related patterns between the layers and demonstrate that the results are highly variable when sub-samples are used. This may act as a cautionary warning to researchers applying relative age dating based upon deamidation results to other sites especially when using a small sub-sample of a layer's bone assemblage. At the very least, we strongly recommend, simulation studies of optimal sample size for a specific assemblage be

performed to assure that enough samples are used for analysis to identify any trends. Finally we remain sceptical on the value of the method in assessing real age trends in an assemblage as a whole, relative age trends between sites, or assigning single find within an assemblage given that many variables (thermal history, exact burial conditions, pre- and post-burial diagenesis) affecting bone collagen preservation remain unknown.

Finally, our research demonstrates the need for more research into the age limits of deamidation-based relative ages. Most of the published work has been on samples which are either much younger than the samples we tested here or where the differentiation needed was between modern and archaeological. The lack of a clear trend in the site specific deamidation analysis, when our dataset includes multiple examples of the extreme rates of deamination due to the high percentage of glycine and proline in collagen, as well as the reversal of the glutamine and asparagine deamidation levels in one of the layers highlights that better understanding of the factors that are driving deamidation over long timescales is needed. Only once these factors are better understood and accounted for in the models can the limits of how using deamination for relative age be determined.

Conclusion

The results of bulk collagen deamidation measurements from PMF spectra from Denisova Cave show that while large numbers of samples show a pattern of decreasing preservation across the site, that pattern is not statistically significant or distinct enough to make relative assessment of the age of bones possible. Similarly, identifying intrusive elements into a stratigraphic layer is likely not possible given the variability of collagen preservation within a single layer, despite the large chronological difference between archaeological contexts in the East Chamber. Measurements of collagen deamidation made using LC-MS/MS data confirmed that the samples were ancient, but were unable to detect a pattern in their overall preservation status based on provenance and/or age. Furthermore, sections of the cave which suffer from high levels of phosphatisation have caused and even greater variability in the youngest Pleistocene samples. Without a complete understanding of a bone's thermal history it would be easy to assume that remains excavated from this layer were potentially much

older or have a large amount of mixing with older layers based on their relative deamidation rate compared to other samples from the same site.

Deamidation measured through PMF spectra provides an overall means for assessing collagen preservation and, for instance in bones from layer 9, could be useful in identifying bones which are likely to be successful in other biomolecular methods such as DNA analysis or radiocarbon dating. Caution, however should be taken when attempting to connect these results with relative decay rates or an assessment of relative age.

Figures

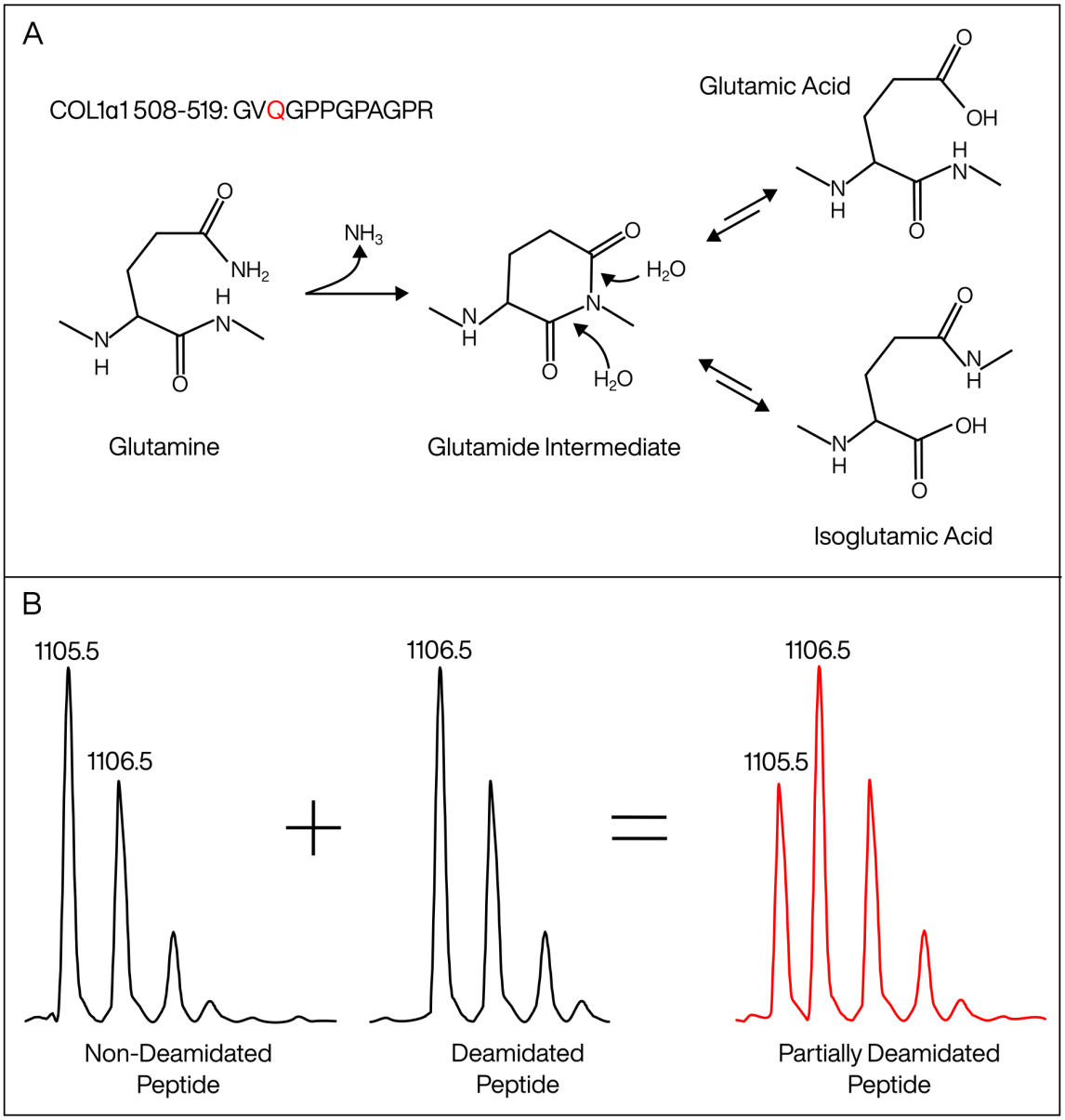

Figure 1: **1a** graphical illustration of glutamine deamidating into glutamic acid through a cyclical glutarimide intermediate, adapted (Li et al., 2010). Although it is more common for glutamine deamidation to proceed through direct hydrolysis, when followed in the sequence by a glycine (G) the mechanism likely proceeds through the cyclical intermediate as shown here. **1b** illustration of deamidation effects identified in a MALDI-TOF spectrum. The non-deamidated peak (COL1α1 508-519) is measured at 1105.6 m/z and the deamidated peak is measured at 1106.5 m/z. This theoretical distribution of COL1α1 508-519 is used to determine the extent of glutamine

deamidation in PMF spectra. The final “partially deamidated peptide” displays the overlapping distribution of COL1α1 508-519 when there are both non-deamidated and deamidated state peptides present.

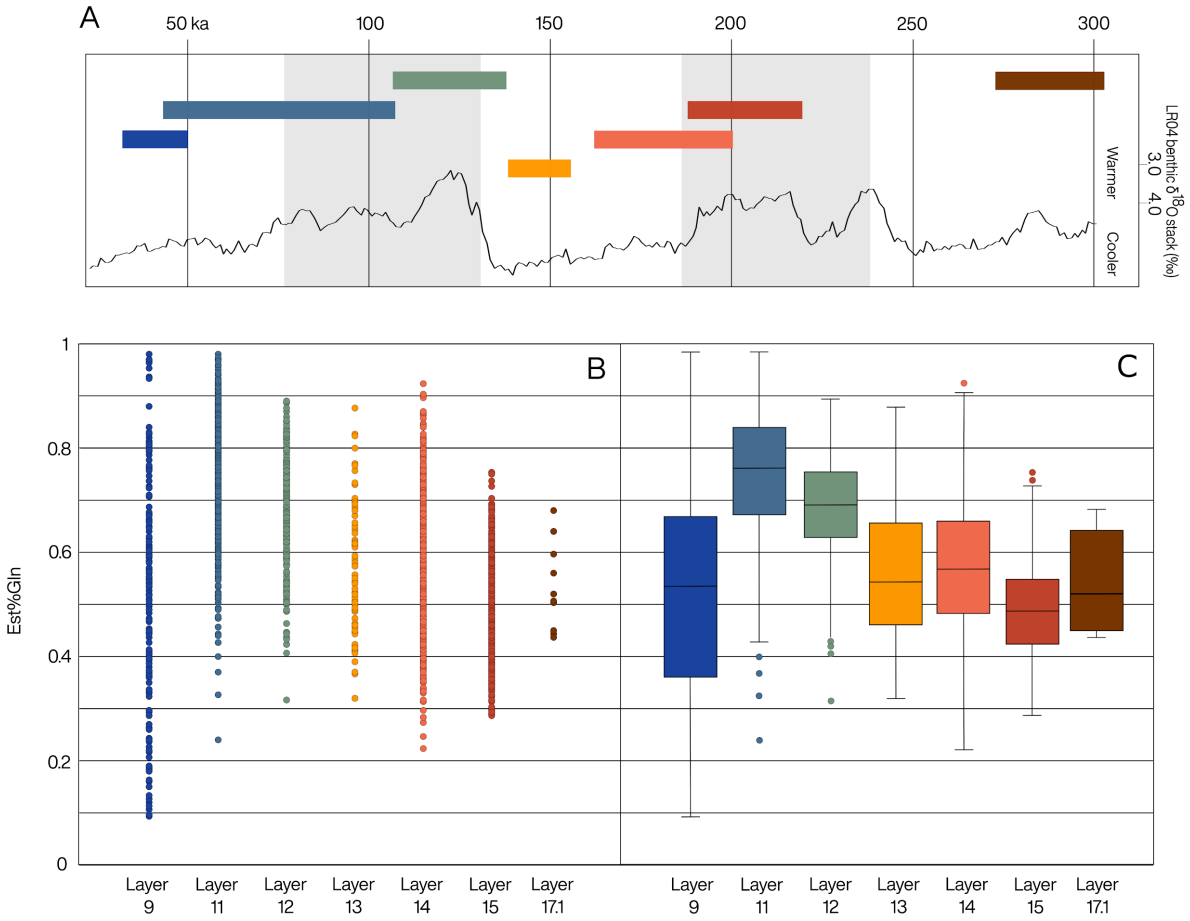

Figure 2: Results of glutamine deamidation measurements for the East Gallery of Denisova Cave. Glutamine deamidation measurements by layer using PMF spectra and Q2E (Wilson et al., 2012), an entirely non-deamidated value is represented by 1, and a completely deamidated value is represented by 0. 1a: The marine-oxygen isotope curve compiled from benthic δ18O records (Lisiecki and Raymo, 2005); the Last and Penultimate Interglacials (Marine Isotope Stages 5 and 7) that were the warmest parts of the last 300 ka are shown in grey. The age range for each of the layers included in this study are shown as coloured bars corresponding to the graphs (1b and 1c) below. 1b: individual bone measurements of glutamine deamidation using Q2E for layers 9 (n=169), 11 (n=518), 12 (n=296), 13 (n=76), 14 (n=688), 15 (n=743), and 17.1 (n=11). 1c: box-and-whisker plots for all PMF measurements by layer, identifying outliers for layers 11, 12, 14, and 15.

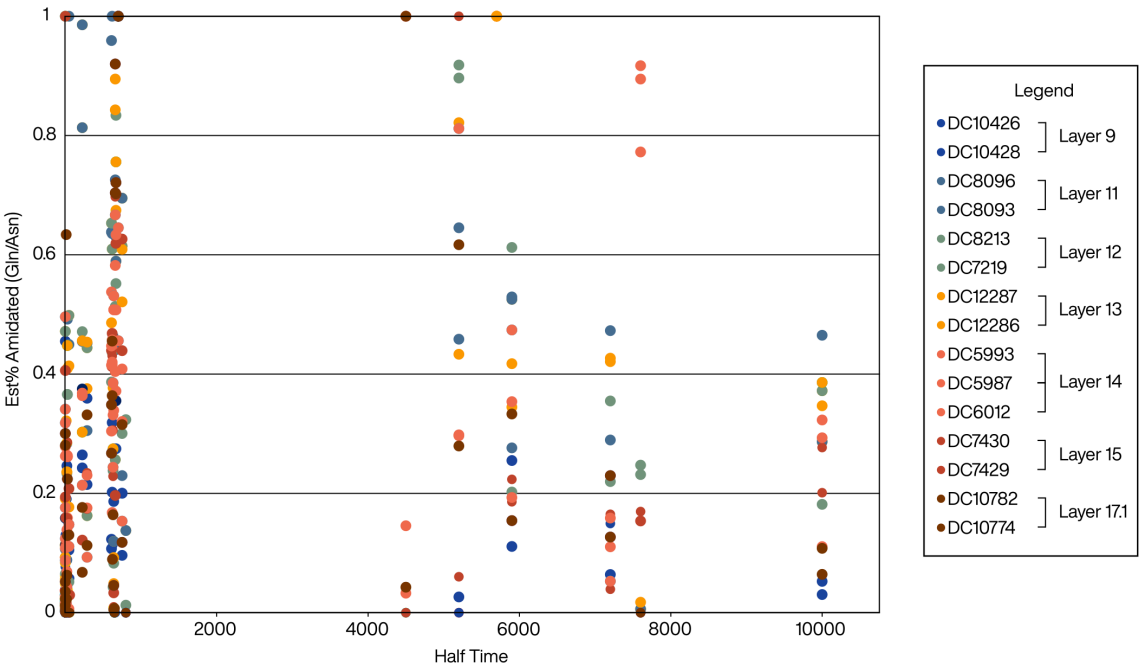

Figure 3: Site specific deamidation identified using LC-MS/MS data and measured using deamiDATE. An entirely non-deamidated value is represented by 1, and a completely deamidated value is represented by 0. Deamidation is measured against half time, taking into account both deamidated residues (glutamine and asparagine) and their local environment. Asparagine half time is estimated to be ~100 days for asparagine deamidation and more than 60 times as long for glutamine deamidation (Robinson et al., 2004).

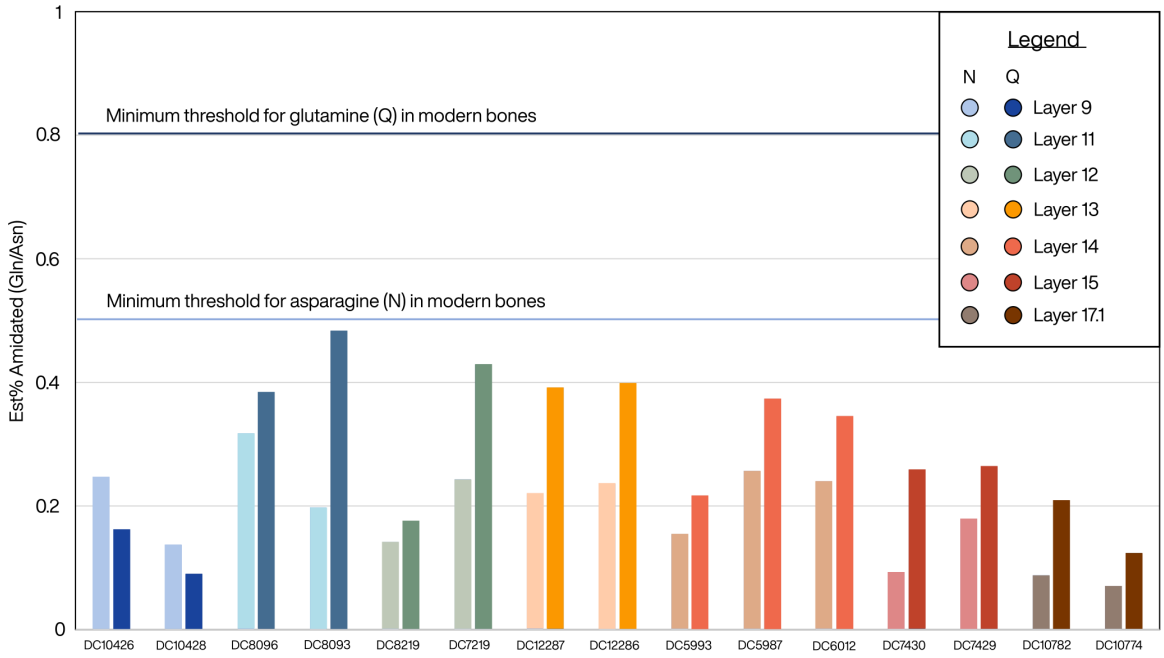

Figure 4: Bulk deamidation measured using LC-MS/MS data with deadmiDATE against modern collagen preservation levels reported in Ramsøe et al. (2020). An entirely non-deamidated value is represented by 1, and a completely deamidated value is represented by 0. All samples fall below the expected values for glutamine and asparagine deamidation for modern samples.

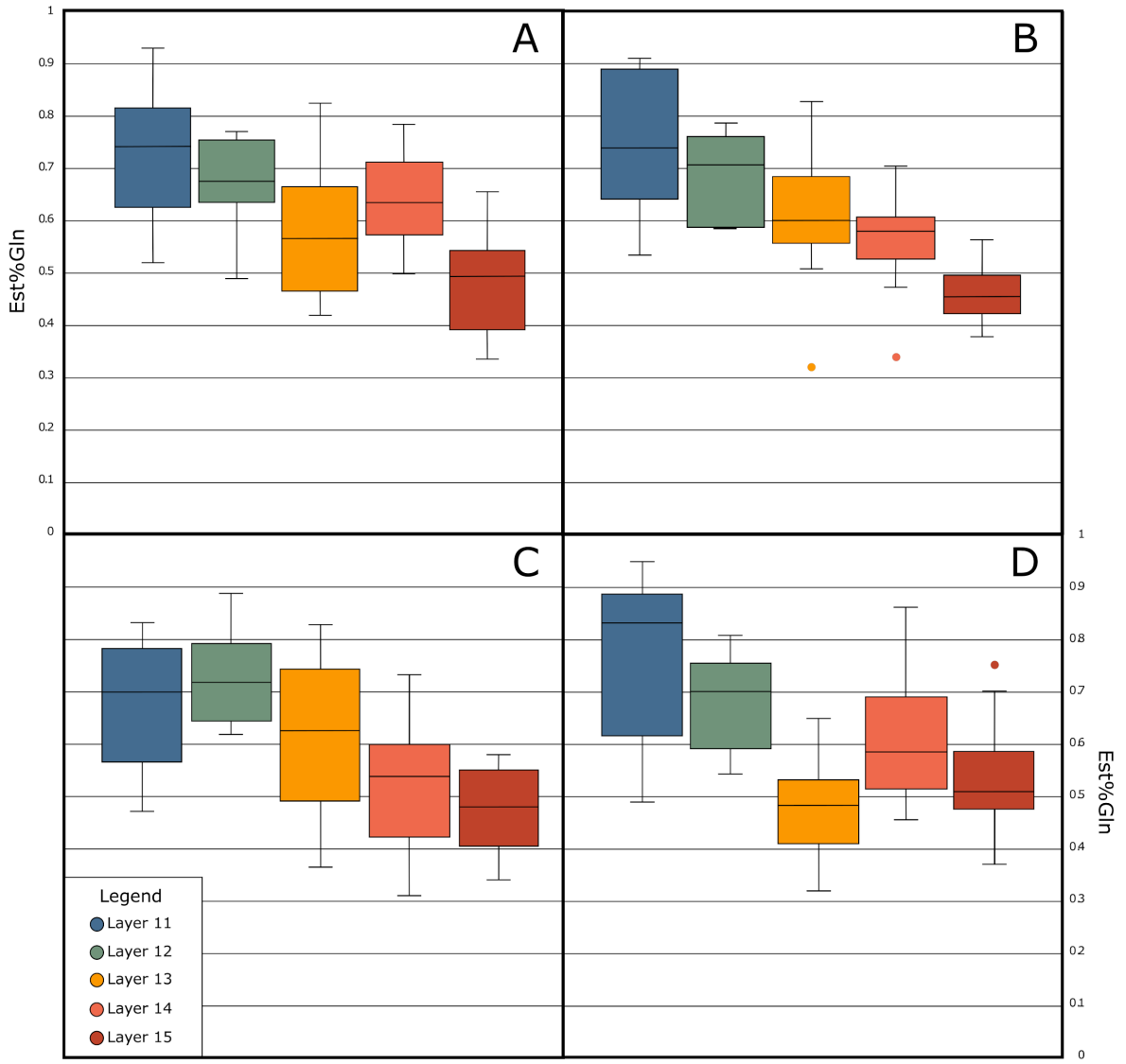

Figure 5: Four scenarios plotted for bulk deamidation measurements from MALDI TOF/TOF spectra using Q2E (Wilson et al., 2012). In each scenario, 10 samples were chosen per layer using a random number generator and then measured for their bulk glutamine (Est%Gln). Results were plotted using box-and-whisker plots in order to identify any underlying patterns of collagen preservation within the data.

References

Brandt, L.Ø., Haase, K., Collins, M.J., 2018. Species identification using ZooMS, with reference to the exploitation of animal resources in the medieval town of Odense. Danish Journal of Archaeology 7, 139–153.

Brown, S., Douka, K., Collins, M., Richter, K.K., 2020a. On the standardization of ZooMS nomenclature. J. Proteomics 104041.

Brown, S., Hebestreit, S., Wang, N., Boivin, N., Douka, K., Richter, K., 2020b. Zooarchaeology by Mass Spectrometry (ZooMS) for bone material - AmBiC protocol v1 (protocols.io.bffdjji6).

Brown, S., Higham, T., Slon, V., Pääbo, S., Meyer, M., Douka, K., Brock, F., Comeskey, D., Procopio, N., Shunkov, M., Derevianko, A., Buckley, M., 2016. Identification of a new hominin bone from Denisova Cave, Siberia using collagen fingerprinting and mitochondrial DNA analysis. Sci. Rep. 6, 23559.

Brown, S., Wang, N., Oertle, A., Comeskey, D., Jope, B., Harvey, V., Pal Chowdhury, M., Kozlikin, M., Shunkov, M.V., Derevianko, A., Buckley, M., Higham, T., Douka, K., in prep. Zooarchaeology through the lens of collagen fingerprinting at Denisova Cave.

Buckley, M., 2018. Zooarchaeology by Mass Spectrometry (ZooMS) Collagen Fingerprinting for the Species Identification of Archaeological Bone Fragments, in: Giovas, C.M., LeFebvre, M.J. (Eds.), Zooarchaeology in Practice: Case Studies in Methodology and Interpretation in Archaeofaunal Analysis. Springer International Publishing, Cham, pp. 227–247.

Buckley, M., Collins, M., Thomas-Oates, J., Wilson, J.C., 2009. Species identification by analysis of bone collagen using matrix-assisted laser desorption/ionisation time-of-flight mass spectrometry. Rapid Commun. Mass Spectrom. 23, 3843–3854.

Catak, S., Monard, G., Aviyente, V., Ruiz-López, M.F., 2009. Deamidation of asparagine residues: direct hydrolysis versus succinimide-mediated deamidation mechanisms. J. Phys. Chem. A 113, 1111–1120.

Chen, F., Welker, F., Shen, C.-C., Bailey, S.E., Bergmann, I., Davis, S., Xia, H., Wang, H., Fischer, R., Freidline, S.E., Yu, T.-L., Skinner, M.M., Stelzer, S., Dong, G., Fu, Q., Dong, G., Wang, J., Zhang, D., Hublin, J.-J., 2019. A late Middle Pleistocene Denisovan mandible from the Tibetan Plateau. Nature 569, 409–412.

Cleland, T.P., Schroeter, E.R., Schweitzer, M.H., 2015. Biologically and diagenetically derived peptide modifications in moa collagens. Proc. Biol. Sci. 282, 20150015.

Coutu, A.N., Whitelaw, G., le Roux, P., Sealy, J., 2016. Earliest Evidence for the Ivory Trade in Southern Africa: Isotopic and ZooMS Analysis of Seventh–Tenth Century ad Ivory from KwaZulu-Natal. African Archaeological Review 33, 411–435.

Daniel, R.M., Dines, M., Petach, H.H., 1996. The denaturation and degradation of stable enzymes at high temperatures. Biochem. J 317 (Pt 1), 1–11.

Delmar, J.A., Wang, J., Choi, S.W., Martins, J.A., Mikhail, J.P., 2019. Machine Learning Enables Accurate Prediction of Asparagine Deamidation Probability and Rate. Mol Ther Methods Clin Dev 15, 264–274.

Demarchi, B., Collins, M., 2013. Amino Acid Racemization Dating, in: Rink, W.J.,

Thompson, J. (Eds.), Encyclopedia of Scientific Dating Methods. Springer Netherlands, Dordrecht, pp. 1–22.
Douka, K., Slon, V., Jacobs, Z., Ramsey, C.B., Shunkov, M.V., Derevianko, A.P., Mafessoni, F., Kozlikin, M.B., Li, B., Grün, R., Comeskey, D., Devièse, T., Brown, S., Viola, B., Kinsley, L., Buckley, M., Meyer, M., Roberts, R.G., Pääbo, S., Kelso, J., Higham, T., 2019. Age estimates for hominin fossils and the onset of the Upper Palaeolithic at Denisova Cave. Nature 565, 640–644.
Hao, P., Adav, S.S., Gallart-Palau, X., Sze, S.K., 2017. Recent advances in mass spectrometric analysis of protein deamidation. Mass Spectrom. Rev. 36, 677–692.
Henriksen, K., Karsdal, M.A., 2019. Type I collagen. in Biochemistry of Collagens, Laminins and Elastin. p. 1–12.
Jacobs, Z., Li, B., Shunkov, M.V., Kozlikin, M.B., Bolikhovskaya, N.S., Agadjanian, A.K., Uliyanov, V.A., Vasiliev, S.K., O'Gorman, K., Derevianko, A.P., Roberts, R.G., 2019. Timing of archaic hominin occupation of Denisova Cave in southern Siberia. Nature 565, 594–599.
Joshi, A.B., Sawai, M., Kearney, W.R., Kirsch, L.E., 2005. Studies on the mechanism of aspartic acid cleavage and glutamine deamidation in the acidic degradation of glucagon. J. Pharm. Sci. 94, 1912–1927.
Kato, K., Nakayoshi, T., Kurimoto, E., Oda, A., 2019. Computational Studies on the Nonenzymatic Deamidation Mechanisms of Glutamine Residues. ACS Omega 4, 3508–3513.
Kumazawa, Y., Taga, Y., Iwai, K., Koyama, Y.-I., 2016. A Rapid and Simple LC-MS Method Using Collagen Marker Peptides for Identification of the Animal Source of Leather. J. Agric. Food Chem. 64, 6051–6057.
Lisiecki, L.E., Raymo, M.E., 2005. A Pliocene-Pleistocene stack of 57 globally distributed benthic δ18O records. Paleoceanography 20.
Li, X., Lin, C., O'Connor, P.B., 2010. Glutamine deamidation: differentiation of glutamic acid and gamma-glutamic acid in peptides by electron capture dissociation. Anal. Chem. 82, 3606–3615.
Morley, M.W., Goldberg, P., Uliyanov, V.A., Kozlikin, M.B., Shunkov, M.V., Derevianko, A.P., Jacobs, Z., Roberts, R.G., 2019. Hominin and animal activities in the microstratigraphic record from Denisova Cave (Altai Mountains, Russia). Sci. Rep. 9, 13785.
Pal Chowdhury, M., Wogelius, R., Manning, P.L., Metz, L., Slimak, L., Buckley, M., 2019. Collagen deamidation in archaeological bone as an assessment for relative decay rates. Archaeometry 61, 1382–1398.
Ramsøe, A., van Heekeren, V., Ponce, P., Fischer, R., Barnes, I., Speller, C., Collins, M.J., 2020. DeamiDATE 1.0: Site-specific deamidation as a tool to assess authenticity of members of ancient proteomes. J. Archaeol. Sci. 115, 105080.
Richter, K.K., Wilson, J., Jones, A.K.G., Buckley, M., van Doorn, N., Collins, M.J., 2011. Fish 'n chips: ZooMS peptide mass fingerprinting in a 96 well plate format to identify fish bone fragments. J. Archaeol. Sci. 38, 1502–1510.
Riggs, D.L., Silzel, J.W., Lyon, Y.A., Kang, A.S., Julian, R.R., 2019. Analysis of Glutamine Deamidation: Products, Pathways, and Kinetics. Anal. Chem. 91, 13032–13038.
Robinson, A.B., Rudd, C.J., 1974. Deamidation of glutaminyl and asparaginyl

residues in peptides and proteins. Curr. Top. Cell. Regul. 8, 247–295.
Robinson, N.E., Robinson, Z.W., Robinson, B.R., Robinson, A.L., Robinson, J.A., Robinson, M.L., Robinson, A.B., 2004. Structure-dependent nonenzymatic deamidation of glutaminyl and asparaginyl pentapeptides. Journal of Peptide Research. 63(5), 426–436.
Rybczynski, N., Gosse, J.C., Harington, C.R., Wogelius, R.A., Hidy, A.J., Buckley, M., 2013. Mid-Pliocene warm-period deposits in the High Arctic yield insight into camel evolution. Nat. Commun. 4, 1550.
Schroeter, E.R., Cleland, T.P., 2016. Glutamine deamidation: an indicator of antiquity, or preservational quality? Rapid Commun. Mass Spectrom. 30, 251–255.
Scotchler, J.W., Robinson, A.B., 1974. Deamidation of glutaminyl residues: dependence on pH, temperature, and ionic strength. Anal. Biochem. 59, 319–322.
Shoulders, M.D., Raines, R.T., 2009. Collagen structure and stability. Annu. Rev. Biochem. 78, 929–958.
Shunkov, M.V., Kozlikin, M.B., Derevianko, A.P., 2020. Dynamics of the Altai Paleolithic industries in the archaeological record of Denisova Cave. Quat. Int. 559(10), 34–46.
Shunkov, M.V., Kulik, N.A., Kozlikin, M.B., Sokol, E.V., 2018. The phosphates of Pleistocene–Holocene sediments of the Eastern Gallery of Denisova Cave. Dokl. Earth Sci. 478, 46–50.
Sinet-Mathiot, V., Smith, G.M., Romandini, M., Wilcke, A., Peresani, M., Hublin, J.-J., Welker, F., 2019. Combining ZooMS and zooarchaeology to study Late Pleistocene hominin behaviour at Fumane (Italy). Sci. Rep. 9, 12350.
S.K. Vasiliev, M.B. Kozlikin, M.V. Shunkov, 2018. Megafaunal Remains from the Upper Portion of Pleistocene Deposits in South Chamber of Denisova Cave. Problems of Archaeology, Ethnography, Anthropology of Siberia and Neighboring Territories 569.
Terwilliger, T.C., Clarke, S., 1981. Methylation of membrane proteins in human erythrocytes. Identification and characterization of polypeptides methylated in lysed cells. J. Biol. Chem. 256, 3067–3076.
Tyler-Cross, R., Schirch, V., 1991. Effects of amino acid sequence, buffers, and ionic strength on the rate and mechanism of deamidation of asparagine residues in small peptides. J. Biol. Chem. 266, 22549–22556.
van Doorn, N.L., Hollund, H., Collins, M.J., 2011. A novel and non-destructive approach for ZooMS analysis: ammonium bicarbonate buffer extraction. Archaeol. Anthropol. Sci. 3, 281.
van Doorn, N.L., Wilson, J., Hollund, H., Soressi, M., Collins, M.J., 2012. Site-specific deamidation of glutamine: a new marker of bone collagen deterioration. Rapid Commun. Mass Spectrom. 26, 2319–2327.
Vasiliev, S.K., Shunkov, M.V., Kozlikin, M.B., 2013. Preliminary Results for the Balance of Megafauna from Pleistocene Layers of the East Gallery, Denisova Cave. Problems of Archaeology, Ethnography, and Anthropology of Siberia and Adjacent Territories 19, 32–38.
Welker, F., 2018. Palaeoproteomics for human evolution studies. Quat. Sci. Rev. 190, 137–147.
Welker, F., Collins, M.J., Thomas, J.A., Wadsley, M., Brace, S., Cappellini, E.,

Turvey, S.T., Reguero, M., Gelfo, J.N., Kramarz, A., Burger, J., Thomas-Oates, J., Ashford, D.A., Ashton, P.D., Rowsell, K., Porter, D.M., Kessler, B., Fischer, R., Baessmann, C., Kaspar, S., Olsen, J.V., Kiley, P., Elliott, J.A., Kelstrup, C.D., Mullin, V., Hofreiter, M., Willerslev, E., Hublin, J.-J., Orlando, L., Barnes, I., MacPhee, R.D.E., 2015. Ancient proteins resolve the evolutionary history of Darwin's South American ungulates. Nature 522, 81–84.

Welker, F., Soressi, M.A., Roussel, M., van Riemsdijk, I., Hublin, J.-J., Collins, M.J., 2017. Variations in glutamine deamidation for a Châtelperronian bone assemblage as measured by peptide mass fingerprinting of collagen. STAR: Science & Technology of Archaeological Research 3, 15–27.

Wilson, J., van Doorn, N.L., Collins, M.J., 2012. Assessing the extent of bone degradation using glutamine deamidation in collagen. Anal. Chem. 84, 9041–9048.

Collagen extraction procedures

No samples were extracted for PMF measurement for this study, instead previously published data was utilised (Brown et al., in prep). As the extraction protocol is important when considering deamidation ratios a description of the extraction protocol carried out in Brown et al., 2020 is included here. The same extraction protocol was also used in preparing samples for LC-MS/MS analysis. In brief, 10-20mg of bone was rinsed in 0.5M ammonium bicarbonate (AmBic) overnight at room temperature. This was removed and the sample was incubated for 1 hour at 65°C in an additional 100µl of AmBic. The supernatant underwent digestion with 1µl trypsin (Thermo Scientific Pierce ™ Trypsin Protease) and was incubated at 37℃ for 18h. The samples were concentrated and desalted using C18 ZipTips (Thermo Scientific Pierce™ C18 Tips) and eluted in a final solution of 50µl of 50% acetonitrile and 0.1% TFA (Brown et al., 2020; van Doorn et al., 2011).

Peptide Mass Fingerprinting

For PMF measurement (Brown et al., in prep) 0.5µl of the resulting solution was mixed with 0.5µl of α -cyano-4-hydroxycinnamic acid solution (10 mg/mL in 50% acetonitrile (ACN) and 0.1% trifluoroacetic acid (TFA), was then spotted on a steel plate and was allowed to crystallise. The samples were analysed using a MALDI TOF/TOF (Bruker Autoflex Speed LRF) mass spectrometer. The resulting mass spectra were screened for diagnostic markers using the FlexAnalysis 3.4 software (Bruker Daltonics).

LC-MS/MS

15 samples were then measured using LC-MS/MS analysis, which was performed on a Q Exactive HF mass spectrometer (Thermo Scientific) equipped with a Digital PicoView source (New Objective) and coupled to an M-Class UPLC (Waters).
Solvent composition at the two channels was 0.1% formic acid for channel A and 0.1% formic acid, 99.9% acetonitrile for channel B. Column temperature was 50 °C. For each sample 4 µl of peptides were loaded on a commercial ACQUITY UPLC M-Class Symmetry C18 Trap Column (100 Å, 5 µm, 180 µm × 20 mm, Waters) followed by ACQUITY UPLC M-Class HSS T3 Column (100 Å, 1.8 µm, 75 µm × 250 mm, Waters).

The peptides were eluted at a flow rate of 300 nl min–1 by a gradient from 5 to 40% B in 120 min. Column was cleaned after the run by increasing to 98% B and holding 98% B for 5 min before re-establishing loading condition. Samples were acquired in a randomized order. The mass spectrometer was operated in data-dependent mode (DDA), acquiring a full-scan MS spectrum (350−1,500 m/z) at a resolution of 120,000 at 200 m/z after accumulation to a target value of 3,000,000, and a maximum injection time of 50 ms followed by higher-energy
+collision dissociation fragmentation on the 12 most-intense signals per cycle. Higher-energy collision dissociation spectra were acquired at a resolution of 30,000 using a normalized collision energy of 28 and a maximum injection time of 50 ms. The automatic gain control was set to 100,000 ions. Charge state screening was enabled. Singly, unassigned and charge states higher than eight were rejected. Only precursors with intensity above 90,000 were selected for MS/MS. Precursor masses previously selected for MS/MS measurement were excluded from further selection for 30 s and the exclusion window was set at 10 ppm. The samples were acquired using internal lock mass calibration on m/z 371.1012 and 445.1200.

LC-MS/MS Data Processing

Spectral data was processed using Byonic (Protein Metrics Inc., Cupertino, California, United States, version 3.2.0) with a database consisting of swissprot and the published proteomes for *Bos taurus* (UP000009136), *Capra hircus* (UP000291000), *Cervus elaphus* (UP000242450), *Equus caballus* (UP000002281), and *Ursus maritimus* (UP000261680). The parameters were set as follows: tryptic-specific digestion with 3 missed cleavages; a precursor mass tolerance of 5ppm; a fragment mass tolerance of 0.05Da; no fixed modifications; variable rare modifications (1 allowed): Gln -> pyroGlu N-term, ammonia loss N-term; variable common modifications (2 allowed): oxidation (M, K, P), deamidation (N, Q); common modifications. Proteins were filtered for 1% FDR and peptides were filtered for a PEP2D score of 0.001.

A focused database from the combined results of all of the proteins which were identified in the Byonic searches was produced. COL1 proteins were removed from the focused database and the curated COL1 sequences from the species of interest

were added: *Bos taurus* (COL1α1 UniProt: P02453, COL1α2 UniProt: P02465), *Capra hircus* (COL1α1 XP.017920382.1, COL1α2 XP_005678993.1), *Cervus elaphus* (COL1α1 MKHE01000005, COL1α2 CM008025), *Equus caballus* (COL1α1 XP.023508478.1, COL1α2 XP.001492989.1), *Ursus arctos* (COL1α1 XP.026368914.1), and *Ursus maritimus* (COL1α2 XP.008684476.1).

In order to use deamiDATE, the data was then processed using the focused database in MaxQuant (Cox and Mann, 2008) with the following parameters: trypsin specific digestion with 3 missed cleavages; a precursor mass tolerance of 5ppm; a fragment mass tolerance of 0.05Da; no fixed modifications; variable modifications (6 allowed): oxidation (M), hydroxyproline, deamidation (N, Q). The results were filtered for both a protein and peptide FDR of 1%. The results were filtered for peptides that were matched to any of the COL1 proteins and these results were then used as the input for deamiDATE which was run and results graphed as described in (Ramsøe et al., 2020). All data from Byonic and MaxQuant is uploaded to ProteomeXchange.

External database: File containing Q2E measurements of glutamine deamidation housed on Mendeley Data
https://data.mendeley.com/datasets/crb7jn6zmv/draft?a=a8925608-6caa-40fd-b362-f58a50c58bf6

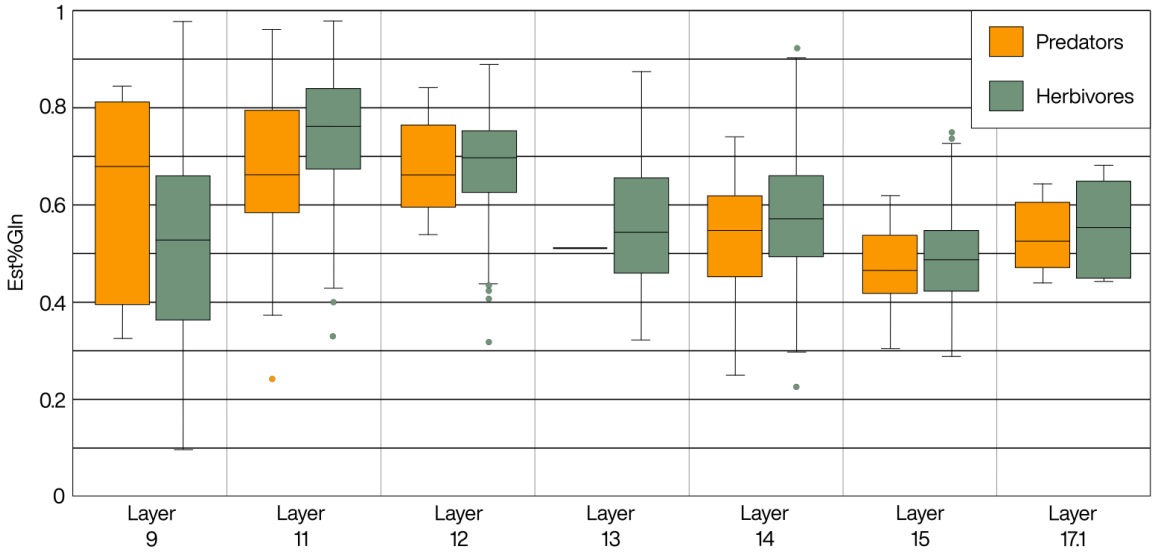

Supplementary Figure 1: Comparison of the glutamine values measured using PMF data by layer and separated into herbivore and predator categories. Measurements were made using Q2E (Wilson et al., 2012). Values have been placed into box-and-whisker plots, except for layer 13 in which only one predator was measured.

Supplementary References

Brown, S., Hebestreit, S., Wang, N., Boivin, N., Douka, K., Richter, K., 2020. Zooarchaeology by Mass Spectrometry (ZooMS) for bone material - AmBiC protocol v1 (protocols.io.bffdjji6).

Brown, S., Wang, N., Oertle, A., Comeskey, D., Jope, B., Harvey, V., Pal Chowdhury, M., Kozlikin, M., Shunkov, M.V., Derevianko, A., Buckley, M., Higham, T., Douka, K., in prep Zooarchaeology through the lens of collagen fingerprinting at Denisova Cave.

Cox, J., Mann, M., 2008. MaxQuant enables high peptide identification rates, individualized p.p.b.-range mass accuracies and proteome-wide protein quantification. Nat. Biotechnol. 26, 1367–1372.

Ramsøe, A., van Heekeren, V., Ponce, P., Fischer, R., Barnes, I., Speller, C., Collins, M.J., 2020. DeamiDATE 1.0: Site-specific deamidation as a tool to assess authenticity of members of ancient proteomes. J. Archaeol. Sci. 115, 105080.

van Doorn, N.L., Hollund, H., Collins, M.J., 2011. A novel and non-destructive approach for ZooMS analysis: ammonium bicarbonate buffer extraction. Archaeol. Anthropol. Sci. 3, 281.

Wilson, J., van Doorn, N.L., Collins, M.J., 2012. Assessing the extent of bone degradation using glutamine deamidation in collagen. Anal. Chem. 84, 9041–9048.

Manuscript F – in prep. Brown, S., Larsen, T., Roberts, P., Comeskey, D., Kozlikin, M., Shunkov, M., Derevianko, A., Higham, T., Douka, K. Isotopic evidence for the diets of Neanderthals and Denisovans in Siberia.

Manuscript F - in prep. Brown, S., Larsen, T., Roberts, P., Comeskey, D., Kozlikin, M., Shunkov, M., Derevianko, A., Higham, T., Douka, K. Isotopic evidence for the diets of Neanderthals and Denisovans in Siberia

Elevated stable carbon and nitrogen isotope values at Denisova Cave and Siberian palaeoenvironments

Samantha Brown[1], Thomas Larsen[1], Patrick Roberts[1], Maxim Kozlikin[2], Michael Shunkov[2,3], Anatoly Derevianko[2], Thomas Higham[4], Katerina Douka[1]

[1]Max Planck Institute for the Science of Human History, Jena, Germany.
[2]Institute of Archeology and Ethnography of the Siberian Branch of the Russian Academy of Sciences, Novosibirsk, Russia.
[3]Novosibirsk State University, Novosibirsk, Russia.
[4]Oxford Radiocarbon Accelerator Unit, RLAHA, University of Oxford, Oxford OX13QY, UK.

Abstract

Biomolecular studies of diet for Neanderthals and early modern humans have allowed for important insights into the subsistence strategies, ecological niches and adaptability of the two populations. While this work focused necessarily on Europe, recent discoveries of new hominin remains from the same period, particularly Denisovans, present a new opportunity to compare these Pleistocene hominin groups. Here, we study seven hominin fossils from Denisova Cave using bulk carbon and nitrogen values and compound specific isotope analysis. Additionally, we determine the bulk carbon and nitrogen values of 263 fauna from Middle and Late Pleistocene layers. We identify three individuals with the highest C and N values for Pleistocene hominins anywhere. Single amino acid data help us rule out aquatic resources in the hominin diet as the reason behind this isotopic elevation. Instead our data suggests that shifts between glaciation and meltwater/permafrost thaw during interglacial periods in high altitude environments may be elevating dramatically the hominin stable isotope values, by as much as 5‰ more elevated than the average for their European contemporaries. Further, we identify early evidence for differentiation in behaviours between populations living in the region. This study represents the first study of Denisovan dietary isotopes and highlights the need for robust environmental baselines in isotopic studies.

Introduction

The study of past human diets through the application of stable isotope analysis of bone collagen is a powerful and well-established tool in deciphering human adaptation to new and diverse environments. When applied to Pleistocene populations, these biomolecular markers have been used to assess mobility, subsistence strategies, ecological adaptations and niche construction (1–5). The study of Neanderthal carbon and nitrogen isotopic values was used as a means of understanding why Neanderthal populations disappeared while modern humans continued to spread across Europe (4, 6, 7). The high level of biomolecular preservation and the relatively sizable number of hominin fossils in Europe has allowed for this research to flourish for European assemblages and fossils, where broad environmental and faunal baselines have also been established (8, 9). In comparison, Siberia which is of singular importance in our understanding of Denisovans, has been under-studied. This is due to the difficulties in the identification of human remains large enough for such analysis as well as the lack of systematic research surrounding this aspect of Siberian hominins.

Denisovans, a sister group to Neanderthals, diverged from their common ancestor ~390 ka (thousand years ago) (10, 11). They likely lived throughout Asia but the majority of evidence for Denisovans comes from the eponymous site, Denisova Cave, in the northern lowlands of the Russian Altai Mountains. The cave is unique in its long stratigraphic record for the Eurasian Pleistocene. It has yielded evidence for the occupation of the site by both Neanderthals and Denisovan groups and for overlapping periods when the two groups met and interbred (10–15).

The Altai Mountains were a constantly transforming landform throughout the Pleistocene. Repeated glacial and interglacial periods carved out valleys and rivers (16). Within the mountains, mixed and coniferous forests during interglacial periods provided ideal conditions for people moving into the region, facilitating the arrival of the first Denisovans more than 200 ka and later Neanderthal groups around 130 ka (13, 14, 17–20). To the north, glaciers retreated from the Ob River valley during the Middle Pleistocene, making way for the formation of ice bound lakes, and an extensive permafrost tundra (21–23). While vegetation is assumed to have been scarce across these frozen tundras, the remains of mammoths, horses, and reindeer have been excavated from Pleistocene loess, the remnants of these monolithic permafrosts (22–

24), indicating that primary production was high enough to support certain faunal species.

The biomolecular study of ancient diet typically focuses on which dietary sources and trophic pathways would lead to particular bulk $\delta^{13}C$ and $\delta^{15}N$ values in the bone collagen of individuals. Measurements of $\delta^{13}C$ are typically used to assess the kinds of plant resources either being directly consumed by an individual or indirectly by their prey, whether environments were open or under the canopy effect, as well as changing temperatures and aridity (25–29). $\delta^{15}N$ values are typically used to indicate an individual's trophic position within a food web, where consumers will exhibit an elevation of ~1 — 6‰ over the consumed (25–27). These values also become elevated via breastfeeding or weaning, consumption of aquatic resources, and nutritional stresses like starvation or illness (30–35). The $\delta^{15}N$ baseline of an ecosystem is controlled by environmental conditions and nutrient sources (29), which can be impacted by pressures such as aridity. This too has had a measurable, if minor, effect on the stable isotopes of Pleistocene individuals (36–39). The creation of an appropriate faunal baseline, and where possible an environmental baseline, is therefore necessary to identify any factors which might be elevating or depleting isotopic values. Recently, compound specific isotope analysis (CSIA) has been used to refine these models. CSIA allows for the quantification of terrestrial, marine, and freshwater inputs into diet and has been used successfully to assess the inclusion (or not) of freshwater and marine resources from diets of prehistoric people (40–44).

To date, stable isotopes have only been measured in a handful of Pleistocene-age individuals from the Altai. These include hominins from Denisova Cave, Okladnikov Cave, and Ust'-Ishim. Denisova 11 (D11; ~120-90 ka), an individual with a Neanderthal mother and a Denisovan father (15), has the most elevated carbon ($\delta^{13}C$) and nitrogen ($\delta^{15}N$) values for any measured Middle Palaeoltihc hominin, at -17.6‰ and 16.6‰ respectively. Neanderthals from Okladnikov Cave (~44-33 ka) and the modern human (~45 ka) located at Ust'-Ishim display similar, if less elevated $\delta^{15}N$ values of between 13.4 to 14.2‰ (45, 46).

To create a robust faunal baseline to contextualise hominin subsistence strategies in the Altai Mountains, we analysed 270 bones from key archaeological layers from

Denisova Cave. CSIA analysis was used to identify the major protein sources exploited by the hominins. In conjunction, the two methods allow for a methodical reconstruction of diet in the Pleistocene Altai Mountains, in order to understand how hominin populations were adapting to environments in Siberia.

Materials

Rather than using the morphological zooarchaeological assemblage from Denisova Cave, which would limit this to a handful of individuals per species and require destructive sampling, we utilised assemblages of non-diagnostic bone fragments which account for more than 95% of bone excavated at the site (14, 47). Faunal remains from layer 12 were previously published in zooarchaeological analysis of Denisova Cave (48) and measured for stable isotope analysis in this study. Faunal remains for layers 11 and 9 were identified using ZooMS first and then measured for their bulk carbon and nitrogen values.

Hominin remains were identified in previously published studies, including Denisova 11 (D11) the half Neanderthal and half Denisovan individual (15, 49); two Neanderthals, Denisova 15 (D15) and Denisova 17 (D17) (13, 48); three Denisovans, Denisova 19 (D19), Denisova 20 (D20), and Denisova 21 (D21) (48); and three individuals for whom it has not been possible to attribute a single population, Denisova 14 (13), Denisova 18 (D18) (48) and Denisova 7 (D7). The latter is a parietal fragment, which was initially identified as possibly human, then as a bear fossil, however it exhibits unusually high $\delta^{13}C$ and $\delta^{15}N$ values (45, 50), making its attribution as a non-hominin unlikely (13). Using ZooMS analysis we determined D7 to belong to a hominin.

Methods

Extraction of collagen

In order to minimise destructive sampling, collagen which had previously been extracted and lyophilised for the radiocarbon dating of D11 and D15 was utilized (13, 49). Very little bone or collagen remains from the initial analysis of D14 and so the isotopic measurements produced by that previous study are used here (13). Collagen was extracted for these samples following standard radiocarbon protocols (51).

Variation between extraction protocols and analyses is expected to be low following previously reported comparability studies (52).

Collagen from hominin remains, D7, D17, D18, D19, D20, D21, was extracted using a modified version of recently published protocols which require only 100mg of bone (53). For these, bone chips were demineralised in 0.5M HCl for 1-2 days. The demineralised bone chips were then rinsed in ultrapure water, treated with NaCl and rinsed again. The HCl supernatant was ultra-filtered in 30 kda filters with ultrapure water. The ultra-filtered supernatant was added to the rinsed and demineralised bone chip and the entire sample was incubated at 70°C. Samples were run through an Ezee filter and freeze dried in order to lyophilise collagen.
Collagen from all other fossils was extracted following standard isotopic analysis protocols (54). Samples were demineralised in 0.5M HCl for a period of 1-5 days, rinsed in Milli Q water, treated with pH 3 water, and demineralised at 70℃ for 24 hours. The resulting supernatant was filtered using Ezee Filters and freeze dried in order to lyophilise the collagen.

ZooMS analysis

ZooMS analysis was carried out following established protocols (55). 0.1mg of lyophillised collagen was eluted in 50µl 0.5M ammonium bicarbonate (AmBic) and was incubated for 1 hour at 65℃ in an additional 100µl of Ambic. The supernatant was then incubated with 1µl trypsin (Thermo Scientific Pierce ™ Trypsin Protease) at 37℃ for 18h. The incubated samples were concentrated and desalted using C18 ZipTips (Thermo Scientific Pierce™ C18 Tips) and eluted in a final solution of 50µl of 50% acetonitrile and 0.1% TFA. 0.5µl of the resulting solution was mixed with 0.5µl of α-cyano-4-hydroxycinnamic acid solution (10 mg/mL in 50% acetonitrile (ACN) and 0.1% trifluoroacetic acid (TFA) and allowed to crystallise. The samples were analysed using a MALDI-TOF (Bruker Autoflex Speed LRF) mass spectrometer. The resulting spectra were screened for diagnostic markers using flexAnalysis 3.4 (Bruker Daltonics) software. The resulting mass spectra were screened for diagnostic markers using the FlexAnalysis software and compared against a reference library (Buckley et al. 2009; Buckley & Kansa 2011; Richter et al. 2011; Welker et al. 2015).

Bulk Isotope Analysis

In total 270 bones were measured for their collagen bulk carbon and nitrogen isotope values. Analyses were performed at the Isotope Laboratory, MPI-SHH, Jena using a Thermo Scientific Flash 2000 Elemental Analyser coupled to a Thermo Delta V Advantage mass spectrometer. Isotopic values are reported as the ratio of the heavier isotope ($^{13}C/^{12}C$ or $^{15}N/^{14}N$) as δ values in parts per mill (‰) relative to international standards, VPDB for $\delta^{13}C$ and atmospheric N2 (AIR) for $\delta^{15}N$. Results were calibrated against international standards of (IAEA-CH-6: $\delta^{13}C = -10.80 \pm 0.47‰$, IAEA-N-2: $\delta^{15}N = 20.3 \pm 0.2‰$, and USGS40: $\delta^{13}C = -26.38 \pm 0.042‰$, $\delta^{15}N = 4.5 \pm 0.1‰$) and a laboratory standard (fish gelatin: $\delta^{13}C = \sim -15.1‰$, $\delta^{15}N = \sim 14.3‰$). Based on replicate analyses, long-term machine error over a year is ±0.2‰ for $\delta^{13}C$ and ±0.2‰ for $\delta^{15}N$. Overall measurement precision was studied through the measurement of repeats of fish gelatin (±0.2‰ for $\delta^{13}C$ and ±0.2‰ for $\delta^{15}N$). The faunal (n = 263) and hominin (n = 7) bone collagen results from are presented in Supplementary Table 2. Samples with a C/N ratio between 2.9–3.6 were carried forward for interpretation.

Compound Specific Isotope Analysis

Previously extracted and lyophilised bone collagen samples were hydrolyzed and derivatized prior to analyzing the individual AAs. We hydrolyzed between 0.5 and 2.2 mg collagen in 1 mL 6M HCl at 110 °C for 20 h in 13 x 100 mm Pyrex tubes. The hydrolysates were subsequently lipid-extracted with a n-hexane and dichloromethane mixture (6:5 *v:v*) and dried them down under N_2. The hydrolyzed AAs were then derivatized to N-acetyl methyl esters (NACME) in 4 ml dram vials following (43, 56). In short, we methylated the AAs with acidified methanol during a 75 °C incubation for 1 h. Next, the methylated AAs were dried under N_2 and acetylated with acetic anhydride, triethylamine and acetone (1:2:5, *v:v:v*) at 60 °C for 8 min. The derivatized AA were dried under N_2, and then restituted in 2 ml ethyl acetate and washed with a 1 ml saturated NaCl. After evaporating the ethyl acetate under N_2, the derivatized AA were dissolved in 0.3 ml ethyl acetate and stored at -20°C until analysis.

The GC-C-IRMS analyses were performed at the Biochemistry Laboratory, MPI-SHH, Jena using an Elementar AnthrovisION isotope ratio mass spectrometer. To separate

and combust the compounds, the derivatized AA were injected onto a InertCap 35ms GC column (60 m x 0.32 mm x 0.50 µm) in an Agilent 7890B GC and routed through a GC5 furnace system with a quartz micro-bore furnace. The CO_2 gas were then introduced into a isoprime visION stable isotope analyzer to determine stable isotope ratios, which we report in delta notation ($\delta^{13}C$ values) with units of per mil (‰), using calibrated CO_2 gas as the proximal reference material for Vienna Pee Dee Belemnite. The software ionOS (version 3.6, Elementar) was used to integrate the peaks of the different ion masses - see example chromatogram in Supplementary Fig. S1. To correct for isotopic drift and check for analytical consistency, we injected an in-house reference n-alkane mixture with *n*-decane, *n*-undecane, and *n*-dodecane with known $d^{13}C$ values between samples. To correct for carbon added during methylation and acetylation, we prepared an external reference containing a mix of commercial AAs (AA-S-18, Sigma-Aldrich) with known $\delta^{13}C$ values that were derivatized with the sample reagents. The external n-alkane or AA references were alternately injected after every 8 sample injections. We used norleucine and caffeine as internal reference compounds.

We obtained reliable chromatography for the following AAs (listed according to their retention times): alanine (Ala), glycine (Gly), valine (Val), leucine (Leu), isoleucine (Ile), threonine (Thr), serine (Ser), aspartic acid (Asx), proline (Pro), glutamic acid (Glx), phenylalanine (Phe), hydroxyproline (Hyp) and lysine (Lys). We use the notations Asx and Glx rather than Asp and Glu to signify that asparagine and glutamine are converted to aspartic acid and glutamic acid during acid hydrolysis. The analytical uncertainty across 4-6 injections per sample was 0.35‰ per amino acid ranging from 0.13‰ for hydroxyproline to 0.93‰ for threonine (see the analytical results in Supplementary Dataset 3).

Statiscal Analysis of Compound Specific Isotope Analysis

All statistical analyses were performed in R version 3.6.3. We used literature $\delta^{13}C_{AA}$ values of collagen from consumers with well-established diets to predict whether the hominins fed on freshwater, marine, and terrestrial sources (41, 42, 57–59). Rather than the common approach of using pairwise ^{13}C offsets in collagen between valine and phenylalanine ($\delta^{13}C_{Val\text{-}Phe}$) for freshwater vs. marine resources (60), and glycine

and phenylalanine ($\delta^{13}C_{Gly\text{-}Phe}$) for marine vs. terrestrial resources (61), we instead used linear discriminant function analysis (LDA, R: MASS [25]) to create a classification model from literature $\delta^{13}C_{AA}$ data of archaeological hominin and fauna collagen (41, 42, 57–59). We only used training data generated with a continuous flow setup with an HPLC coupled to an IRMS system because these data have less analytical uncertainties compared to data generated with GC-C-IRMS systems where samples are derivatized prior to analysis. To calculate the probability of group membership of the classifier samples, we used a leave-one-out cross-validation approach. We applied multivariate analysis of variance (MANOVA) in conjunction with Pillai's trace to test the null hypothesis that the dietary groups have a common centroid in a dependent variable vector space. A rejection of this hypothesis entails that the groups have significantly different $\delta^{13}C_{AA}$ patterns. To compare significant differences among groups or sediment strata, we first checked for normality and homogeneity of variance assumptions. If these assumptions were met, we used parametric tests such as the Student's t-test, ANOVA (type I error) or ANCOVA (type III error).

Results

Zooarchaeology by Mass Spectrometry (ZooMS)

154 samples from layers 9.3 (n= 53) and 11.4 (n=101) and the candidate hominin (D7) were analysed using ZooMS. In total, eight samples failed to produce enough collagen for taxonomic identification and a further eight samples produced low quality collagen which could only be assigned to family or order. These 16 samples were removed from further analysis (Supplementary Table 1). D7 bore all of the peptide markers used in the identification of a Hominidae (Supplementary Table 1) and has been reassigned as a human fossil. Genetic analysis is currently underway to assign it to a specific population; for now it is listed as *Homo sp.*

Added to these results are the previously identified hominin remains (D11, D15, D17, D18, D19, D20, and D21) (13, 49) and 118 faunal bones identified for layer 12.3 (48). All were analysed for their bulk carbon and nitrogen values.

Isotopic Analysis of Bulk Carbon and Nitrogen

In total, 270 fossils were measured for their bulk isotope values. Seven samples were excluded from further analysis as their C/N ratio was outside the accepted range ((62, 63); Supplementary Table 2). One of the hominin bones, D17 failed to produce any collagen therefore its stable isotopes could not be measured.

The $\delta^{13}C$ values for hominins varied by only 2‰, with D11 the most elevated at -17.6‰ and D7 the most depleted at -19.6‰ (Figure X; Supplementary Table X). The range in $\delta^{15}N$ was far larger, with 5‰ separating the most elevated (D11; 16.6‰) from the most depleted (D20; 11.6‰). D7, D11, and D14 have the most elevated $\delta^{15}N$ values at 16.3, 16.6, and 16.5‰ respectively. Two of the ~200 ka hominins, D18 and D20, exhibit the most depleted $\delta^{15}N$ values at 11.6 and 11.7‰ respectively. The mitochondrial DNA for D19 and D21 was almost identical, suggesting the two fossils belonged to the same individual or were maternal relatives. Their almost identical $\delta^{13}C$ and $\delta^{15}N$ results further suggest that they were the same individual (Figure 1).

Carnivores exhibit variable isotopic values. Crocuta/Panthera, which likely represents *Crocuta crocuta spelaea*, *Panthera spelaea*, and *Uncia uncia*, had an average -18.5‰ (-17.6 – -19.8‰) and 9.8‰ (5.9 – 14.4‰) for their $\delta^{13}C$ and $\delta^{15}N$, respectively. Canidae, likely *Canis lupus*, *Vulpes corsak*, *Cuon alpinus*, and *Alopex lagopus*, showed an average $\delta^{13}C$ and $\delta^{15}N$ of -18.6‰ (-17.9 – -19.8‰) and 10.2‰ (8.4 – 14.2‰), respectively. One Felidae bone, which could be *Lynx lynx* or *Felis manul*, and two *Vuples vuples* bones had average values of -19.5‰ (-19.2 – -20.2‰) and 8.8‰ (7.4 – 9.9‰) for their $\delta^{13}C$ and $\delta^{15}N$, respectively. Carnivores showed similar $\delta^{15}N$ values in comparison with hominins, with the exception of D7, D11, and D14.

There is a large amount of variability in $\delta^{15}N$ and $\delta^{13}C$ values measured for herbivores. For instance, Bos/Bison remains from layer 11.3 exhibit $\delta^{15}N$ values ranging from 4.1 to 13.1‰ and Cervidae/Gazella/Saiga range from 4.4 to 12.2‰. Herbivores from each of the layers studied exhibit $\delta^{15}N$ values as elevated as their carnivore counterparts.

Compound Specific Isotope Analysis

The ^{13}CAA values of the Denisova hominins generally resembled those of the TP group (Fig. S2). To create a robust classification model from literature ^{13}CAA data (41, 42, 57–59), we first tested the power to discriminate among three consumers groups that predominantly fed high freshwater protein (HFP), high marine protein (HMP), or terrestrial protein (TP; from C3 vegetation habitats only) sources (see specimen list in

Table Sx). We first tested the model with 12 commonly reported AAs, Ala, Asx, Gly, Glx, Hyp, Leu, Lys Phe, Pro, Ser, Thr and Val. We found that Asx, Gly, Phe, Pro and Val were the most informative and robust (lowest intragroup ^{13}C variability) for distinguishing among the three dietary resources (Pillai's trace = 1.80, $F_{4,110}$ = 240.9; $p < .001$). Our results show that all seven hominins have $^{13}C_{AA}$ patterns closely resembling those of TP specimens falling well within the TP 95% prediction ellipse (Fig. 3).

Discussion

The average $\delta^{15}N$ value for Neanderthals in Europe is ~11‰ placing the Altai hominins well outside the expected range for individuals of a similar age (1, 44, 45, 64–72). There are several potential factors which could be influencing their stable isotope values elevating them beyond the expected range; however, the majority of these can be excluded. Breastfeeding and weaning for instance seem like an unlikely candidate. D11, the most elevated hominin in terms of both carbon and nitrogen, was determined to have been weaned at the time of her death. Analysis of the cortical bone thickness of the fragment indicates that she must have been at least 13 years of age (15). The Ust'-Ishim modern human (46) and Neanderthals from Okladnikov (45, 50) also belong to adult individuals, suggesting that this observed isotopic elevation is not a result of measurements from a series of breastfeeding/ weaning individuals.

Another oft-cited factor for the isotopic elevation of carbon and nitrogen values is the consumption of aquatic resources. We explored this possibility through the CSIA analysis of seven hominin fossils and found no indication of aquatic dietary input. This is in line with other archaeological data;

despite the presence of a small number of freshwater fish remains in the Denisova zooarchaeological collection, there is no evidence for the consumption of aquatic resources at the site, or elsewhere in the Altai, during the Pleistocene. The accumulation of fish remains is considered accidental (otter spraint, bird pellets) rather than anthropogenic introduction to the site.

The initial dietary research into the Ust'-Ishim femur speculated the elevated $\delta^{15}N$ was the result of freshwater fish consumption (46). However, our novel CSIA analysis of all hominins from Denisova revealed that they fall well within the expected range for those with a purely terrestrial diet, highlighting the necessity of applying this method

in similar contexts and other hominins to pull apart factors influencing isotopic variation.

One of the peculiarities of our current dataset is the unusually elevated carbon and nitrogen isotope values in hominin as well as herbivore remains analysed. This observation makes it necessary to consider the possibility that the entire ecosystem had elevated isotope values. All of the hominins investigated in this study lived throughout interglacial or interstadial periods, perhaps with the exception of D7 who was found in a layer not yet dated precisely and which covers the interglacial MIS 5 and the glacial MIS 4 periods (Figure 1). The interstadial periods which all other hominins date to represent periods in which forests begin to expand in the Altai (16, 73). During these periods humid conditions allowed for the meltwater from glaciers and permafrost to move into the Altai Mountains and the Ob River Valley. As a result, rain would have become more common, replacing frequent snowfall during the cold and arid glacial periods.

Water locked in glaciers and permafrost has a high nitrogen content, trapped in glacial ice either through the atmosphere or through microbial weathering processes (74, 75). During thawing, meltwater provides important nutrients to plant life and aquatic systems, supporting life in a variety of landscapes. Measurable increases in nitrogen subsidies from rivers and tundras, fed by glacial and permafrost water can be observed today in places like the Arctic, Switzerland, and Tibet where regular thaw cycles provide nutrients to ecosystems (76–80). Experimental studies for permafrost regions in the Yukon provide important insights and potentially a parallel to Pleistocene Altai. In a recent study, measurements of frozen ground squirrel nests excavated from permafrost revealed a ~2.8‰ elevation in $\delta^{15}N$ for plants growing in ice-rich loess deposits between the Late Pleistocene and modern day (81).

Throughout the Pleistocene, glaciers would have been a permanent fixture for the Altai Mountains. During interglacial and interstadial periods, meltwater would have fed plant life in the mountains and valleys, as well as the many rivers which moved through the region, potentially raising nitrogen levels in soil and plants and triggering oxidation. Permafrost in the lowlands and the Ob River valley would have also promoted this, fueling tundras with their own meltwater. Increasing oxidation in soils would also have promoted the release of methane (82, 83). Increasing methane release from in soils

can be correlated with measurable ^{13}C enrichment elevations in the remaining soil organic matter $\delta^{13}C$ and this may explain the slight increase in $\delta^{13}C$ we observe in the Altaian hominins in our study. Unfortunately, as measurements of soils today are unlikely to capture Pleistocene isotopic glacial conditions, and as it is not possible to measure plants from this period from the Altai Mountains, we must rely on faunal baselines and the elimination of all other factors which may have contributed to the unusual $\delta^{15}N$ and $\delta^{13}C$ measurements.

The elevated isotope values of the fauna and hominins may also be attributed to the altitude and topography of the Altai Mountains. Measurements of soil and plants in the Dongling Mountains and the Himalayas have recorded increasing $\delta^{15}N$ and $\delta^{13}C$ values with altitude (84, 85). Increasing altitude coupled with forested environments with nutrient rich soils was found to increase $\delta^{15}N$ values at elevations above 1350m a.s.l. (height above sea level). Present-day forests and tundra forests in the Altai Mountains are situated as high as 2300-2500 a.s.l (86). Denisova Cave itself however, sits at 700m a.s.l. Nonetheless, it is not improbable that some of the hominin groups occupying the cave may have been moving much higher into the Altai Mountains to hunt and forage (84). Over the past decade genetic evidence was brought forward to suggest that Denisovans may have been well adapted to higher altitudes based on the identification of the EPAS1 gene variant in their genome, a transcription factor that regulates the response to hypoxia, found today in modern Tibetans (87). Interestingly, the second occurence of Denisovans outside Denisova Cave is in Tibetan Plateau at 3820 m a.s.l. (88, 89).

Some of the measured Bos/Bison and Cervidae/Gazella/Saiga are as much as 4 — 5‰ more elevated in comparison with their European counterparts (Figure 4). This is the same rate of elevation for D7, D11, and D14 over the average $\delta^{15}N$ expected for European Pleistocene hominins (~11‰) (Figure 1b). Therefore, based on the environmental evidence for the region, isotopic measurements for fauna and hominins, and CSIA we suggest that high altitudes, coupled with increasing meltwater and soils nutrient accumulation during interglacial periods drove increasing $\delta^{15}N$ and $\delta^{13}C$ values in Pleistocene food webs in the Altai Mountains. Our results indicate that both Neanderthals and Denisovans were targeting terrestrial fauna; however, the variation in isotopic values suggests they may have been adapted to hunt in different types of

habitats. D7, D11, and D14 were likely targeting prey in regions where environmental pressures were more extreme, perhaps at high altitude where all of these factors, meltwater, altitude, and soil nutrient accumulation, may have come into play. As D11 had one Denisovan parent, and they have been tentatively tied to high latitude adaptations (87–89), it is tempting to suggest that this may reflect hunting in mountainous regions. D18 and D20 however have the most depleted $\delta^{15}N$, with their dietary isotopic values largely in line with European hominins. D20 carries mtDNA of the Denisovan type and, along with D18, appears to have been targeting prey in areas which are the least susceptible to the environmental variability exhibited by other individuals. These tentative results may indicate a change in behaviours over the course of the Pleistocene, however such an assumption would require further research in understanding Denisovan spatial-temporal spread and adaptations.

Conclusion

For the first time we are able to compare Neanderthals with another Pleistocene hominin group, Denisovans. While our results show both groups were targeting terrestrial fauna, they suggest the oldest Denisovans (D19, D20, and D21) and the Neanderthal, D15, may have been targeting prey in very different regions of the Altai Mountains in comparison with D7, D11, and D14.

The unprecedented isotopic values of herbivores measured from Denisova Cave, and the hominins which were targeting them, provide important evidence for the prevailing effect of the palaeoenvironment on dietary studies. We have attempted to explore and subsequently eliminate all other variables which may be driving isotopic values hence our results must reflect environmental pressures. Such research highlights the need to establish robust environmental baselines in dietary isotope studies. These may change over time following palaeoclimatic fluctuations therefore the measurement of fauna directly associated with hominin remains is necessary. Without the inclusion of CSIA carried out for the hominins from Denisova Cave, their unusual $\delta^{15}N$ values could have been interpreted as reflecting the inclusion of aquatic resources in their diet. Instead, we have identified the effects of a dynamic and changing environment in a highly glaciated area on the daily lives of hominins in the Altai Mountains.

Tables

ZooMS Identification	Layer 9.3	Layer 11.4	Layer 12	Total
Bos/Bison	29	38	1	68
Canidae		2	8	10
Capra	3	6	1	10
Capra/Rangifer		1		1
Cervidae (Capreolus, Odocoileus)	1	3		4
Cervidae/Gazella/Saiga	2	20	29	51
Crocuta/Panthera	1	6	6	13
Elephantidae	2	5	6	13
Equus	4	4	30	38
Failed	4	4		8
Felidae			1	1
Mustelidae/Crocuta/Panthera		3		3
Ovis	2	2	1	5
Ovis/Capra		3		3
Rangifer			5	5
Rhinocerotidae	5	2	20	27
Unknown		1		1
Ursus		1	8	9
Vulpes			2	2
Grand Total	53	101	118	272

Table 1: Summary of ZooMS Identifications by layer, including samples which were selected for layer 12 from previously published zooarchaeological analyses (48). Any samples which failed were removed from further analysis. Additionally, samples identified as Capra/Rangifer, Mustelidae/Crocuta/Panthera, and Ovis/Capra were removed from further analysis.

Figures

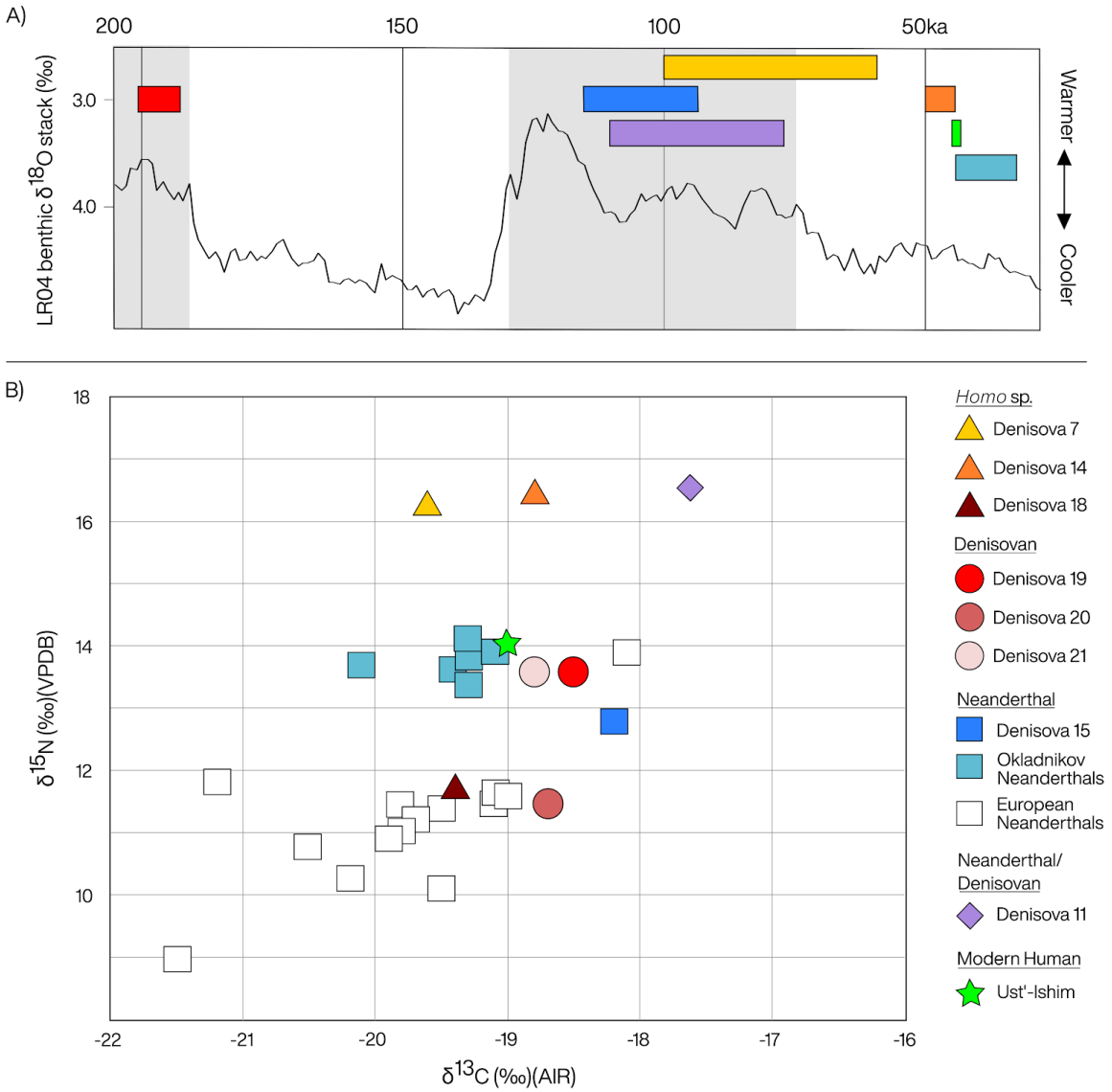

Figure 1: Measured dietary isotopes for Pleistocene hominins including three *Homo* sp. (D7, D14, and D18), three Denisovans (D19, D20, and D21), Neanderthals from Denisova Cave (D15), Okladnikov Cave, and Europe, the Neanderthal/Denisovan D11, and an early modern human (Ust'-Ishim). **1a**: The marine-oxygen isotope curve compiled from benthic $\delta_{18}O$ records (90); the Last and Penultimate Interglacial periods (Marine Isotope Stages 5 and 7) that include some of the warmest parts of the last 300 ka are highlighted. Coloured bars correspond to age estimations for the hominins included in Figure 1b (13, 46, 91). **1b**: $\delta_{13}C$ and $\delta_{15}N$ values for hominins from Europe and Siberia. The values for European Neanderthals were compiled from the literature (1, 44, 45, 64–72).

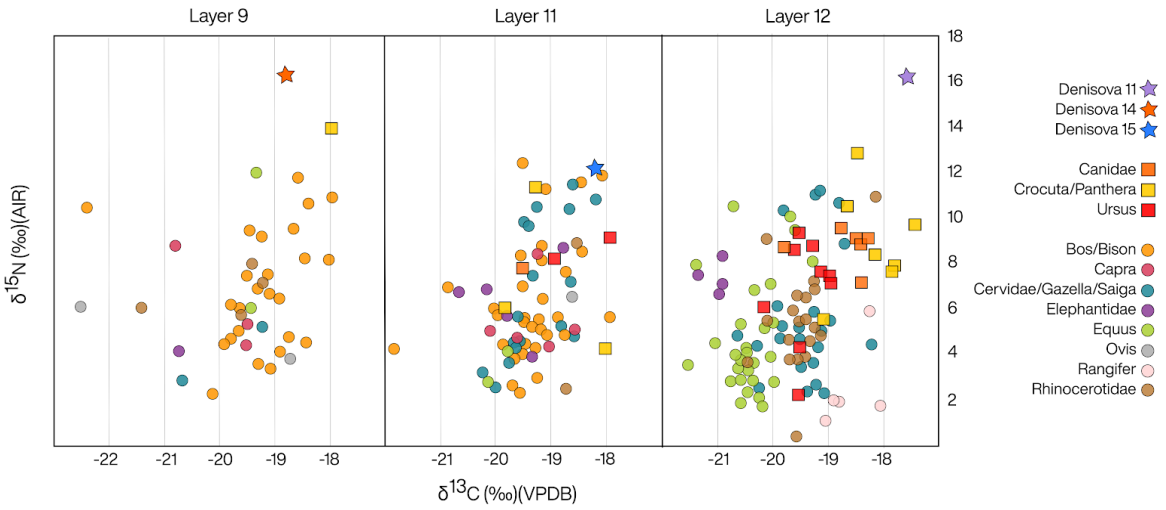

Figure 2: Bulk carbon and nitrogen measurements for layers 9, 11, and 12 including hominins which were identified within each of these layers.

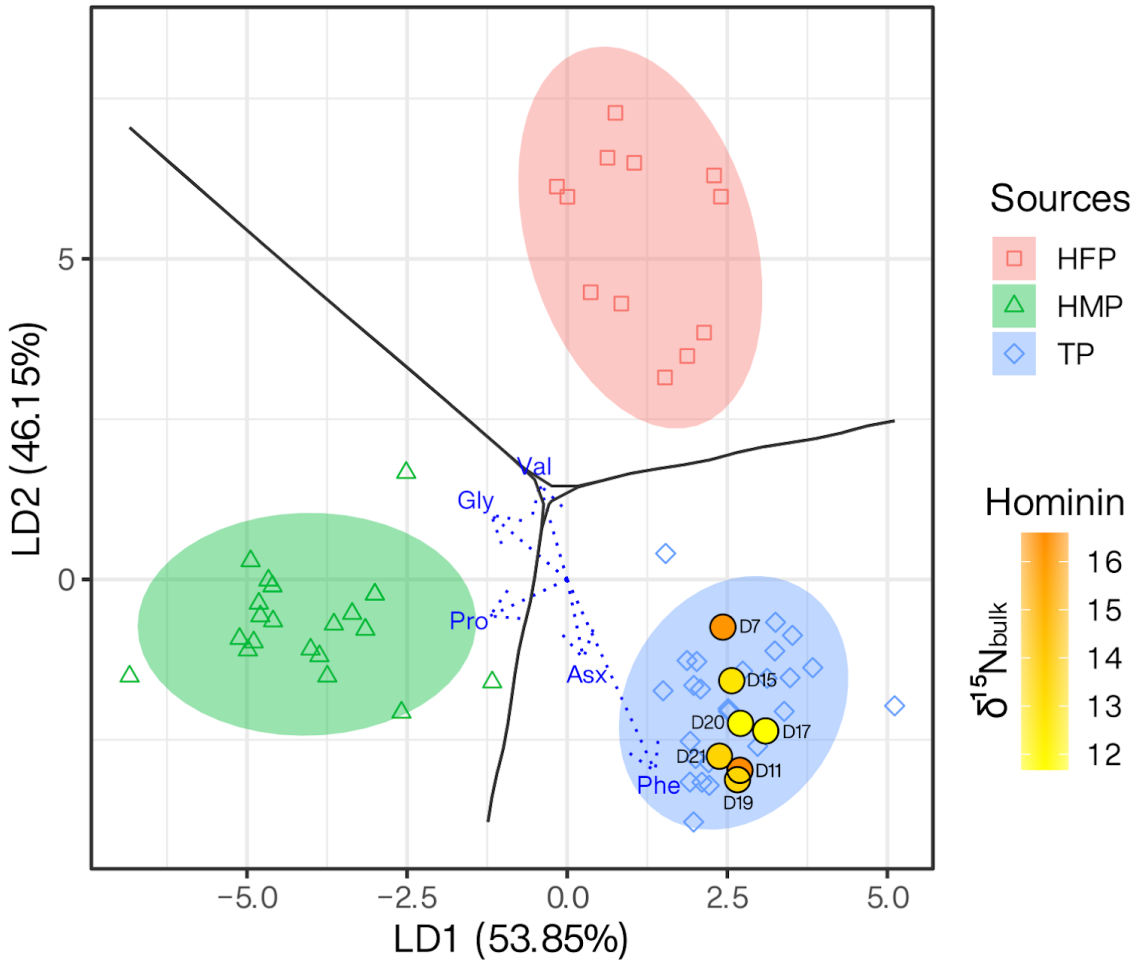

Figure 3: Linear discriminant function analysis based on $\delta^{13}C_{AA}$ values from collagen of archaeological hominins and fauna specimens predominantly feeding on high freshwater protein (HFP, n=12), high marine protein (HMP, n=20), or terrestrial protein (TP, n=26) sources (*4-8*). The predicted specimens, the Denisova hominins, are color coded according to their respective $\delta^{15}N$ values of bulk collagen. The values in parentheses are the percentage variations accounted by each linear discriminant score. The ellipses signify 95% confidence boundaries for each group, and the arrows represent the relative weightings of the independent variables, i.e. $\delta^{13}C_{AA}$ values, for creating the discriminant function. See Methods for the abbreviations of the amino acids.

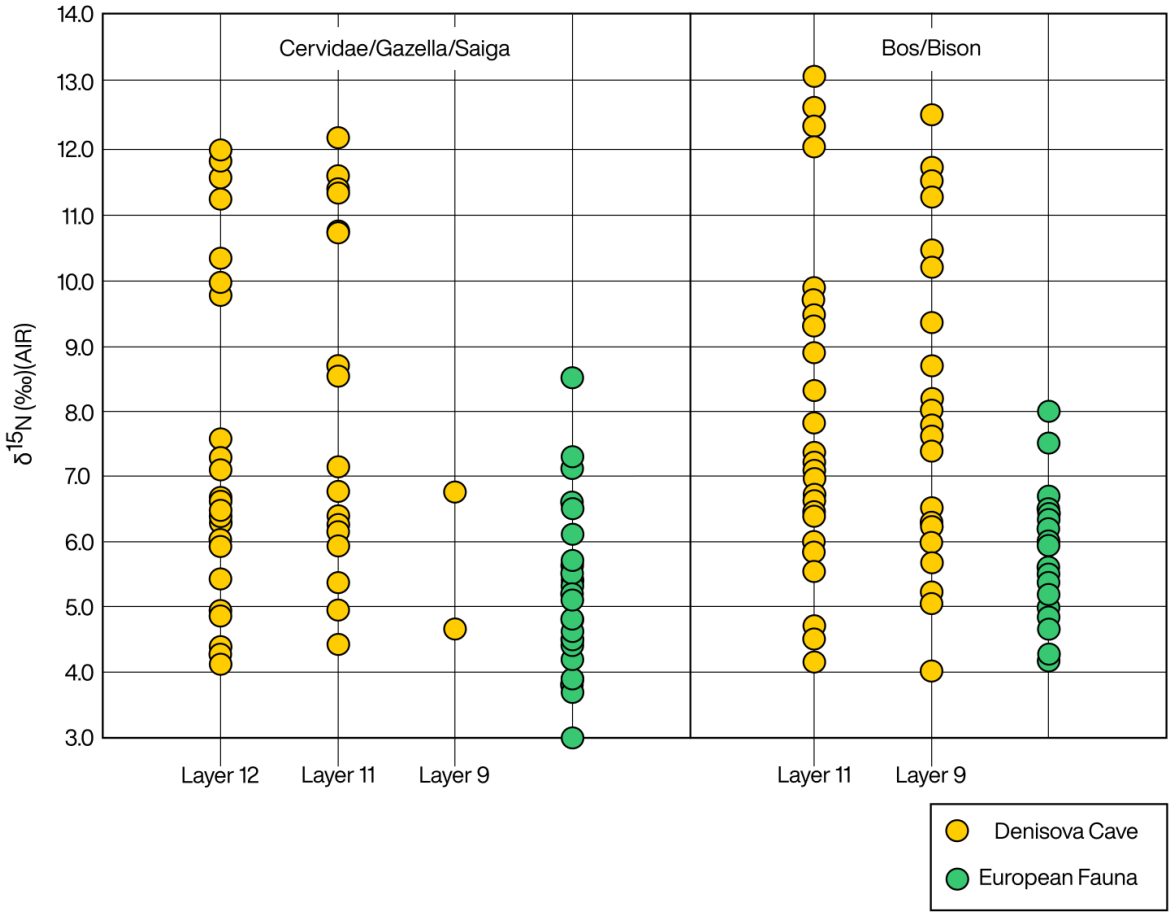

Figure 4: Comparison of fauna from Denisova Cave with their counterparts from European Pleistocene sites. European fauna was compiled from the literature (3, 37, 38).

References

1. M. P. Richards, *et al.*, Neanderthal diet at Vindija and Neanderthal predation: the evidence from stable isotopes. *Proc. Natl. Acad. Sci. U. S. A.* **97**, 7663–7666 (2000).

2. Y. I. Naito, *et al.*, Ecological niche of Neanderthals from Spy Cave revealed by nitrogen isotopes of individual amino acids in collagen. *J. Hum. Evol.* **93**, 82–90 (2016).

3. K. Britton, S. Gaudzinski-Windheuser, W. Roebroeks, L. Kindler, M. P. Richards, Stable isotope analysis of well-preserved 120,000-year-old herbivore bone collagen from the Middle Palaeolithic site of Neumark-Nord 2, Germany reveals niche separation between bovids and equids. *Palaeogeogr. Palaeoclimatol. Palaeoecol.* **333**, 168–177 (2012).

4. H. Bocherens, “Neanderthal Dietary Habits: Review of the Isotopic Evidence” in *The Evolution of Hominin Diets: Integrating Approaches to the Study of Palaeolithic Subsistence*, J.-J. Hublin, M. P. Richards, Eds. (Springer Netherlands, 2009), pp. 241–250.

5. O. E. Craig, *et al.*, Stable isotope analysis of Late Upper Palaeolithic human and faunal remains from Grotta del Romito (Cosenza), Italy. *J. Archaeol. Sci.* **37**, 2504–2512 (2010).

6. M. P. Richards, E. Trinkaus, Isotopic evidence for the diets of European Neanderthals and early modern humans. *Proc. Natl. Acad. Sci. U. S. A.* **106**, 16034–16039 (2009).

7. E. Morin, “Late Pleistocene population interaction in western Europe and modern human origins: New insights based on the faunal remains from Saint -Cesaire, southwestern France.” (2004) (January 5, 2020).

8. C. Wißing, *et al.*, Stable isotopes reveal patterns of diet and mobility in the last Neandertals and first modern humans in Europe. *Sci. Rep.* **9**, 4433 (2019).

9. D. Drucker, H. Bocherens, Carbon and nitrogen stable isotopes as tracers of change in diet breadth during Middle and Upper Palaeolithic in Europe. *Int. J. Osteoarchaeol.* **14**, 162–177 (2004).

10. D. Reich, *et al.*, Genetic history of an archaic hominin group from Denisova Cave in Siberia. *Nature* **468**, 1053–1060 (2010).

11. J. Krause, *et al.*, The complete mitochondrial DNA genome of an unknown hominin from southern Siberia. *Nature* **464**, 894–897 (2010).

12. M. V. Shunkov, M. B. Kozlikin, A. P. Derevianko, Dynamics of the Altai Paleolithic industries in the archaeological record of Denisova Cave. *Quat. Int.* (2020) https:/doi.org/10.1016/j.quaint.2020.02.017.

13. K. Douka, *et al.*, Age estimates for hominin fossils and the onset of the Upper Palaeolithic at Denisova Cave. *Nature* **565**, 640–644 (2019).

14. Z. Jacobs, *et al.*, Timing of archaic hominin occupation of Denisova Cave in southern Siberia. *Nature* **565**, 594–599 (2019).

15. V. Slon, *et al.*, The genome of the offspring of a Neanderthal mother and a Denisovan father. *Nature* **561**, 113–116 (2018).

16. J. Chlachula, Pleistocene climate change, natural environments and palaeolithic occupation of the Altai area, west-central Siberia. *Quat. Int.* **80-81**, 131–167 (2001).

17. F. Mafessoni, *et al.*, A high-coverage Neandertal genome from Chagyrskaya Cave. *Proc. Natl. Acad. Sci. U. S. A.* (2020) https:/doi.org/10.1073/pnas.2004944117.

18. K. A. Kolobova, *et al.*, Archaeological evidence for two separate dispersals of Neanderthals into southern Siberia. *Proc. Natl. Acad. Sci. U. S. A.* **117**, 2879–2885 (2020).

19. B. M. Peter, 100,000 years of gene flow between Neandertals and Denisovans in the Altai mountains. *bioRxiv* (2020).

20. S. Brown, *et al.*, Earliest evidence for Denisovans identified using peptide mass fingerprinting and mitochondrial DNA analysis.

21. A. V. Panin, *et al.*, Middle and Late Quaternary glacial lake-outburst floods, drainage diversions and reorganization of fluvial systems in northwestern Eurasia. *Earth-Sci. Rev.* **201**, 103069 (2020).

22. V. I. Astakhov, Late Pleistocene sedimentary environments in West Siberia. *Trudy Inst. Geol. and Geophys. , Siberian Branch Acad Sci. USSR*, 118–126 (1989).

23. V. I. Astakhov, The last glaciation in West Siberia. *Sveriges Geologiska Unders. okning, Ser. Ca* **81**, 21–30 (1992).

24. V. I. Astakhov, Evidence of Late Pleistocene ice-dammed lakes in West Siberia. *Boreas* (2006).

25. M. J. Schoeninger, M. J. DeNiro, H. Tauber, Stable nitrogen isotope ratios of bone collagen reflect marine and terrestrial components of prehistoric human diet. *Science* **220**, 1381–1383 (1983).

26. M. J. Schoeninger, M. J. DeNiro, Nitrogen and carbon isotopic composition of bone collagen from marine and terrestrial animals. *Geochimica et Cosmochimica Acta* **48**, 625–639 (1984).

27. M. Sponheimer, *et al.*, Nitrogen isotopes in mammalian herbivores: hair δ15N values from a controlled feeding study. *International Journal of Osteoarchaeology* **13**, 80–87 (2003).

28. N. J. Van der Merwe, E. Medina, The canopy effect, carbon isotope ratios and foodwebs in Amazonia. *J. Archaeol. Sci.* **18**, 249–259 (1991).

29. M. T. Rabanus-Wallace, *et al.*, Megafaunal isotopes reveal role of increased moisture on rangeland during late Pleistocene extinctions. *Nature Ecology & Evolution* **1** (2017).

30. J. Beaumont, J. Montgomery, The Great Irish Famine: Identifying Starvation in the Tissues of Victims Using Stable Isotope Analysis of Bone and Incremental Dentine Collagen. *PLoS One* **11**, e0160065 (2016).

31. H. Doi, F. Akamatsu, A. L. González, Starvation effects on nitrogen and carbon stable isotopes of animals: an insight from meta-analysis of fasting experiments. *R Soc Open Sci* **4**, 170633 (2017).

32. Y. I. Naito, Y. Chikaraishi, N. Ohkouchi, D. G. Drucker, H. Bocherens, Nitrogen isotopic composition of collagen amino acids as an indicator of aquatic resource consumption: insights from Mesolithic and Epipalaeolithic archaeological sites in France. *World Archaeol.* **45**, 338–359 (2013).

33. B. T. Fuller, *et al.*, Nitrogen balance and δ15N: why you're not what you eat during nutritional stress. *Rapid Commun. Mass Spectrom.* **19**, 2497–2506 (2005).

34. M. R. Schurr, Using stable nitrogen-isotopes to study weaning behavior in past populations. *World Archaeol.* **30**, 327–342 (1998).

35. T. Tsutaya, M. Yoneda, Reconstruction of breastfeeding and weaning practices using stable isotope and trace element analyses: A review. *Am. J. Phys. Anthropol.* **156 Suppl 59**, 2–21 (2015).

36. G. Hartman, Are elevated δ 15 N values in herbivores in hot and arid environments caused by diet or animal physiology? *Funct. Ecol.* **25**, 122–131 (2011).

37. D. G. Drucker, H. Bocherens, D. Billiou, Evidence for shifting environmental conditions in Southwestern France from 33 000 to 15 000 years ago derived from carbon-13 and nitrogen-15 natural abundances in collagen of large herbivores. *Earth Planet. Sci. Lett.* **216**, 163–173 (2003).

38. H. Bocherens, D. G. Drucker, S. Madelaine, Evidence for a 15N positive excursion in terrestrial foodwebs at the Middle to Upper Palaeolithic transition in south-western France: Implications for early modern human palaeodiet and palaeoenvironment. *J. Hum. Evol.* **69**, 31–43 (2014).

39. R. E. Stevens, R. E. M. Hedges, Carbon and nitrogen stable isotope analysis of northwest European horse bone and tooth collagen, 40,000 BP--present: Palaeoclimatic interpretations. *Quat. Sci. Rev.* **23**, 977–991 (2004).

40. C. L. Jarman, *et al.*, Diet of the prehistoric population of Rapa Nui (Easter Island, Chile) shows environmental adaptation and resilience. *Am. J. Phys. Anthropol.* **164**, 343–361 (2017).

41. E. C. Webb, *et al.*, Compound-specific amino acid isotopic proxies for detecting freshwater resource consumption. *J. Archaeol. Sci.* **63**, 104–114 (2015).

42. E. C. Webb, *et al.*, Compound-specific amino acid isotopic proxies for distinguishing between terrestrial and aquatic resource consumption. *Archaeol. Anthropol. Sci.* **10**, 1–18 (2018).

43. T. Larsen, *et al.*, Tracing carbon sources through aquatic and terrestrial food webs using amino acid stable isotope fingerprinting. *PLoS One* **8**, e73441 (2013).

44. K. Jaouen, *et al.*, Exceptionally high δ15N values in collagen single amino acids confirm Neandertals as high-trophic level carnivores. *Proc. Natl. Acad. Sci. U. S. A.* **116**, 4928–4933 (2019).

45. A. V. Tiunov, M. V. Dobrovoldskaya, Stable isotope (13c/12c and 15n/ 14n) evidence for mid-upper paleolithic hominines' palaeodiets in gorny altai (2011) (October 4, 2018).

46. Q. Fu, *et al.*, Genome sequence of a 45,000-year-old modern human from western Siberia. *Nature* **514**, 445–449 (2014).

47. S. K. Vasiliev, M. V. Shunkov, M. B. Kozlikin, Preliminary Results for the Balance of Megafauna from Pleistocene Layers of the East Gallery, Denisova Cave. *Problems of Archaeology, Ethnography, and Anthropology of Siberia and Adjacent Territories* **19**, 32–38 (2013).

48. S. Brown, *et al.*, in prep. Zooarchaeology through the lens of collagen fingerprinting at Denisova Cave.

49. S. Brown, *et al.*, Identification of a new hominin bone from Denisova Cave, Siberia using collagen fingerprinting and mitochondrial DNA analysis. *Sci. Rep.* **6**, 23559 (2016).

50. M. V. Dobrovolskaya, A. V. Tiunov, The Neanderthals of Okladnikov Cave Altai: Environment and Diet Based on Isotopic Analysis*. *Archaeology, Ethnology and Anthropology of Eurasia* **41**, 78–88 (2013).

51. F. Brock, T. Higham, P. Ditchfield, C. B. Ramsey, Current Pretreatment Methods for AMS Radiocarbon Dating at the Oxford Radiocarbon Accelerator Unit (Orau). *Radiocarbon* **52**, 103–112 (2010).

52. W. J. Pestle, B. E. Crowley, M. T. Weirauch, Quantifying inter-laboratory variability in stable isotope analysis of ancient skeletal remains. *PLoS One* **9**, e102844 (2014).

53. H. Fewlass, *et al.*, Pretreatment and gaseous radiocarbon dating of 40-100 mg archaeological bone. *Sci. Rep.* **9**, 5342 (2019).

54. R. Longin, New method of collagen extraction for radiocarbon dating. *Nature* **230**, 241–242 (1971).

55. A. N. Coutu, G. Whitelaw, P. le Roux, J. Sealy, Earliest Evidence for the Ivory Trade in Southern Africa: Isotopic and ZooMS Analysis of Seventh–Tenth Century ad Ivory from KwaZulu-Natal. *African Archaeological Review* **33**, 411–435 (2016).

56. L. T. Corr, R. Berstan, R. P. Evershed, Development ofN-Acetyl Methyl Ester Derivatives for the Determination of δ13C Values of Amino Acids Using Gas Chromatography-Combustion- Isotope Ratio Mass Spectrometry. *Analytical Chemistry* **79**, 9082–9090 (2007).

57. K. Choy, C. I. Smith, B. T. Fuller, M. P. Richards, Investigation of amino acid δ13C signatures in bone collagen to reconstruct human palaeodiets using liquid chromatography–isotope ratio mass spectrometry. *Geochimica et Cosmochimica Acta* **74**, 6093–6111 (2010).

58. N. V. Honch, J. S. O. McCullagh, R. E. M. Hedges, Variation of bone collagen amino acid δ13C values in archaeological humans and fauna with different dietary regimes: Developing frameworks of dietary discrimination. *Am. J. Phys. Anthropol.* **148**, 495–511 (2012).

59. M. Raghavan, J. S. O. McCullagh, N. Lynnerup, R. E. M. Hedges, Amino acid δ13C analysis of hair proteins and bone collagen using liquid chromatography/isotope ratio mass spectrometry: Paleodietary implications from intra-individual comparisons. *Rapid Communications in Mass Spectrometry: An International Journal Devoted to the Rapid Dissemination of Up-to-the-Minute Research in Mass Spectrometry* **24**, 541–548 (2010).

60. N. V. Honch, J. S. O. McCullagh, R. E. M. Hedges, Variation of bone collagen amino acid δ13C values in archaeological humans and fauna with different dietary regimes: developing frameworks of dietary discrimination. *Am. J. Phys. Anthropol.* **148**, 495–511 (2012).

61. L. T. Corr, J. C. Sealy, M. C. Horton, R. P. Evershed, A novel marine dietary indicator utilising compound-specific bone collagen amino acid δ13C values of ancient humans. *J. Archaeol. Sci.* **32**, 321–330 (2005).

62. M. J. Deniro, M. J. Schoeninger, C. A. Hastorf, Effect of heating on the stable carbon and nitrogen isotope ratios of bone collagen. *J. Archaeol. Sci.* **12**, 1–7 (1985).

63. S. H. Ambrose, L. Norr, “Experimental Evidence for the Relationship of the Carbon Isotope Ratios of Whole Diet and Dietary Protein to Those of Bone Collagen and Carbonate” in *Prehistoric Human Bone: Archaeology at the Molecular Level*, J. B. Lambert, G. Grupe, Eds. (Springer Berlin Heidelberg, 1993), pp. 1–37.

64. H. Bocherens, *et al.*, Isotopic biogeochemistry (13C,15N) of fossil vertebrate collagen: application to the study of a past food web including Neandertal man. *Journal of Human Evolution* **20**, 481–492 (1991).

65. H. Bocherens, *et al.*, New isotopic evidence for dietary habits of Neandertals from Belgium. *J. Hum. Evol.* **40**, 497–505 (2001).

66. P. Semal, *et al.*, New data on the late Neandertals: direct dating of the Belgian Spy fossils. *Am. J. Phys. Anthropol.* **138**, 421–428 (2009).

67. M. Fizet, B. Lange-Badré, δ13C et δ15N du collagène des mammifères:Reconstitution des relations trophiques et du paléoenvironnement du gisement de Marillac (France, Pléistocène supérieur). *Geobios* **28**, 167–181 (1995).

68. H. Bocherens, D. Drucker, D. Billiou, I. Moussa, Une nouvelle approche pour évaluer l'état de conservation de l'os et du collagène pour les mesures isotopiques (datation au radiocarbone, isotopes stables du carbone et de l'azote). *L'Anthropologie* **109**, 557–567 (2005).

69. C. Beauval, F. Lacrampe-Cuyaubère, B. Maureille, E. Trinkaus, Direct radiocarbon dating and stable isotopes of the neandertal femur from Les Rochers-de-Villeneuve (Lussac-les-Châteaux, Vienne). *Bulletins et mémoires de la Société d'Anthropologie de Paris, 18 (1-2) | 2006 2006(1-2)*, 35–42 (2006).

70. M. P. Richards, *et al.*, Isotopic dietary analysis of a Neanderthal and associated fauna from the site of Jonzac (Charente-Maritime), France. *J. Hum. Evol.* **55**, 179–185 (2008).

71. T. Higham, C. B. Ramsey, I. Karavanić, F. H. Smith, E. Trinkaus, Revised direct radiocarbon dating of the Vindija G1 Upper Paleolithic Neandertals. *Proc. Natl. Acad. Sci. U. S. A.* **103**, 553–557 (2006).

72. R. W. Schmitz, *et al.*, The Neandertal type site revisited: interdisciplinary investigations of skeletal remains from the Neander Valley, Germany. *Proc. Natl. Acad. Sci. U. S. A.* **99**, 13342–13347 (2002).

73. N. S. Bolikhovskaya, M. V. Shunkov, Pleistocene Environments of Northwestern Altai: Vegetation and Climate1. *Archaeology, Ethnology and Anthropology of Eurasia* **42**, 2–17 (2014).

74. B. T. Burpee, D. Anderson, J. E. Saros, Assessing ecological effects of glacial meltwater on lakes fed by the Greenland Ice Sheet: The role of nutrient subsidies and turbidity. *Arct. Antarct. Alp. Res.* **50**, S100019 (2018).

75. M. W. Williams, M. Knauf, R. Cory, N. Caine, F. Liu, Nitrate content and potential microbial signature of rock glacier outflow, Colorado Front Range. *Earth Surf. Processes Landforms* **32**, 1032–1047 (2007).

76. C. Mao, *et al.*, Permafrost nitrogen status and its determinants on the Tibetan Plateau. *Glob. Chang. Biol.* (2020) https:/doi.org/10.1111/gcb.15205.

77. F. Beermann, *et al.*, Permafrost thaw and liberation of inorganic nitrogen in eastern Siberia. *Permafrost Periglacial Processes* **28**, 605–618 (2017).

78. F. Keuper, *et al.*, Experimentally increased nutrient availability at the permafrost thaw front selectively enhances biomass production of deep-rooting subarctic peatland species. *Glob. Chang. Biol.* **23**, 4257–4266 (2017).

79. J. L. Wadham, *et al.*, Sources, cycling and export of nitrogen on the Greenland Ice Sheet. *Biogeosci. Discuss.* (2016).

80. H. Göransson, M. Welc, E. K. Bünemann, I. Christl, H. O. Venterink, Nitrogen and phosphorus availability at early stages of soil development in the Damma glacier forefield, Switzerland; implications for establishment of N2-fixing plants. *Plant Soil* **404**, 251–261 (2016).

81. F. Tahmasebi, F. J. Longstaffe, G. Zazula, Nitrogen isotopes suggest a change in nitrogen dynamics between the Late Pleistocene and modern time in Yukon, Canada. *PLoS One* **13**, e0192713 (2018).

82. P. Ambus, B. L. Andersen, M. Kemner, B. Sørensen, J. Wille, Natural carbon isotopes used to study methane consumption and production in soil. *Isotopes Environ. Health Stud.* **38**, 149–157 (2002).

83. J. Le Mer, P. Roger, Production, oxidation, emission and consumption of methane by soils: A review. *Eur. J. Soil Biol.* **37**, 25–50 (2001).

84. X. Liu, G. Wang, J. Li, Q. Wang, Nitrogen isotope composition characteristics of modern plants and their variations along an altitudinal gradient in Dongling Mountain in Beijing. *Sci. China Ser. D Earth Sci.* **53**, 128–140 (2010).

85. S. Tashi, B. Singh, C. Keitel, M. Adams, Soil carbon and nitrogen stocks in forests along an altitudinal gradient in the eastern Himalayas and a meta-analysis of global data. *Glob. Chang. Biol.* **22**, 2255–2268 (2016).

86. E. E. Timoshok, *et al.*, Monitoring of high-altitude terrestrial ecosystems in the Altai Mountains. *IOP Conf. Ser.: Earth Environ. Sci.* **48**, 012008 (2016).

87. E. Huerta-Sánchez, *et al.*, Altitude adaptation in Tibetans caused by introgression of Denisovan-like DNA. *Nature* **512**, 194–197 (2014).

88. D. Zhang, *et al.*, Denisovan DNA in Late Pleistocene sediments from Baishiya Karst Cave on the Tibetan Plateau. *Science* **370**, 584–587 (2020).

89. F. Chen, *et al.*, A late Middle Pleistocene Denisovan mandible from the Tibetan Plateau. *Nature* **569**, 409–412 (2019).

90. L. E. Lisiecki, M. E. Raymo, A Pliocene-Pleistocene stack of 57 globally distributed benthic δ18O records. *Paleoceanography* **20** (2005).

91. A. P. Derevianko, S. V. Markin, M. V. Shunkov, The Sibiryachikha Facies of the Middle Paleolithic of the Altai. *Archaeology, Ethnology and Anthropology of Eurasia* **41**, 89–103 (2013).

Acknowledgments

We would like to thank the European Research Council, the Max Planck Society, the Oxford Radiocarbon Accelerator Unit (ORAU), and the Institute of Archeology and Ethnography, Russian Academy of Sciences Siberian Branch for their ongoing support.
This work has received funding from the ERC under the European Union's Horizon 2020 Research and Innovation Programme, grant agreement no. 715069 (FINDER) to KD and under the European Union's Seventh Framework Programme (FP7/2007–2013), grant agreement no. 324139 (PalaeoChron) to TH. The archaeological field studies were funded by the Russian Foundation for Basic Research (no. 18-09-40100 and no. 18-09-00404). This research would not have been possible without the technical support of Jana Ilgner, Mary Lucas, Elsa Perruchini, Sandra Heberstreit, and Daniel Comeskey. We would also like to thank Phoebe-Hedell Stevens, Nils Vanwezer, and Ayushi Nayak for their input into project discussions and data interpretation.

Supplementary Information

Supplementary Data:

Supplementary Dataset 1: ZooMS Analysis Results
https://data.mendeley.com/datasets/dnpc9vn2wf/draft?a=8af55392-9296-4984-8874-f838e987257b

Supplementary Dataset 2: Isotope Results
https://data.mendeley.com/datasets/dnpc9vn2wf/draft?a=8af55392-9296-4984-8874-f838e987257b

Supplementary Dataset 3: CSIA Results
https://data.mendeley.com/datasets/26nmdjfnmy/draft?a=d79175ce-9df3-4640-b3b3-48fad6da9e71

Supplementary Figures:

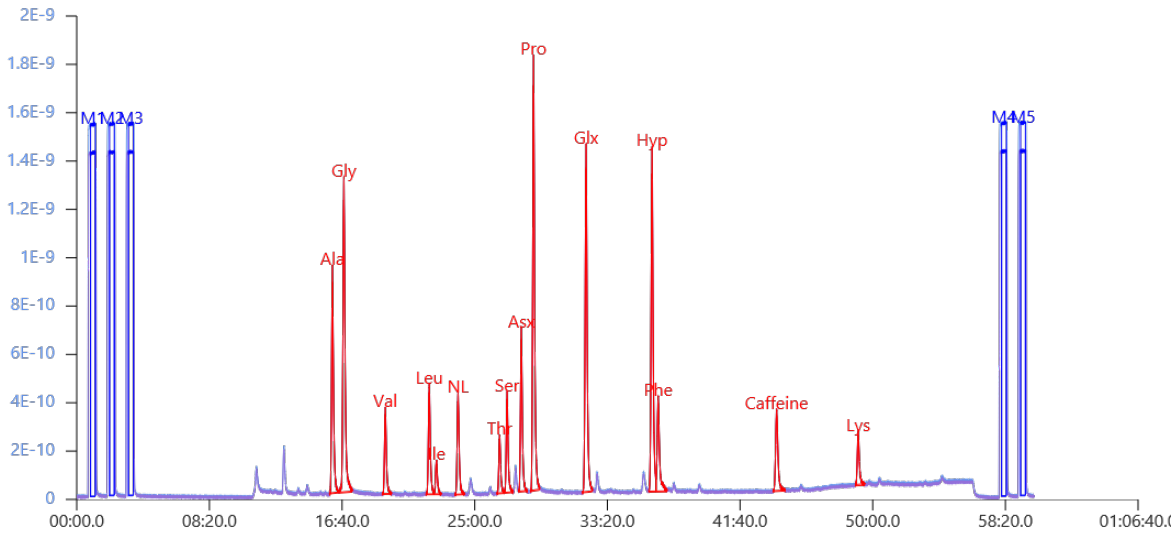

Supplementary Figure S1

Typical chromatogram of hominin bone collagen, here of the Denisova 15 specimen, on the Elementar GC-C-IRMS system. Norleucine (NL) and caffeine were added as internal standards. See Methods for the amino acid abbreviations.

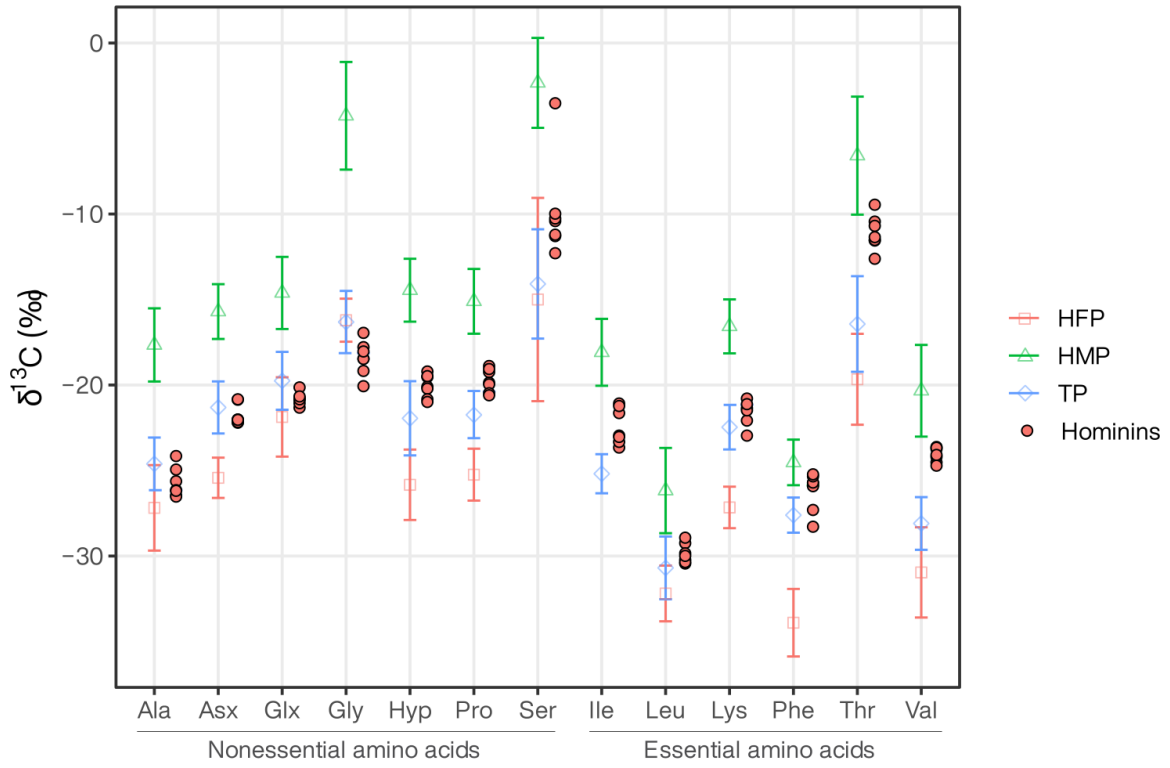

Supplementary Figure S2: The open symbols with error bars shows the mean±stdev of $\delta_{13}C_{AA}$ values of collagen from archaeological hominins and fauna predominantly feeding on high freshwater protein (HFP, n=12), high marine protein (HMP, n=20), or terrestrial protein (TP, n=26) sources (4-8). The filled symbols show the collagen $\delta_{13}C_{AA}$ values of the seven individual Denisova cave hominins. See Methods for the abbreviations of the amino acids.

Appendix 4 - Unpublished ZooMS results

Appendix 4.1 Supplementary Materials and Methods

Short descriptions of all of the other sites investigated as part of this dissertation are included below. All of the links to raw data and results tables can be found in Appendix 6.

Podzvonkaya

Podzvonkaya is situated in the valley along the Tamir River in the Kyakhta Region of the Buryatia Republic, Siberia (Figure 1). It is the collective name for four open air Palaeolithic sites, referred to as complexes (Antonova et al., 2020; Tashak, 2003, 2014, 2011). The fauna identified at the site through zooarchaeological analysis is dominated by horse, argali, bison, and Mongolian gazelle, highlighting the steppe landscape of the valley Podzvonkaya is located within. Bone fragments from the Eastern and Lower complexes were analysed in this study. The Eastern Complex is one of the larger sites of Podzvonkaya with rich assemblages of lithics and bones. Its Upper Palaeolithic assemblages are found in association with several hearths (Tashak, 2003). These have evidence for repeated use and were found covered with large stones, suggesting they were purposefully buried once exhausted. Alongside these hearths were the remains of animals which had been arranged in anatomical order. This is believed to reflect ritualistic behaviour by the inhabitants of these sites (Tashak, 2003). The Lower complex is a much smaller site, with only two cultural horizons. Both correspond to the Upper Palaeolithic however, fragments of Bronze and Iron age ceramics are present in the uppermost sections of the first horizon (Tashak, 2014).

Khotyk

Khotyk is an open air site in Western Transbaikal, Siberia (Kuzmin et al., 2006) Figure 1). Rich IUP assemblages of artefacts have been excavated from the site, including beads made of stone, bone, ivory, and shell; rings which have been drilled, carved and then polished; and a flute or whistle made from the cortical bone of a bird and etched with notches (Lbova, 2010).

Kamenka

Kamenka is an open-air site located 60km from Ulan-Ude, the capital of the Buryatia Republic, Siberia (Figure 1). The assemblages identified at Kamenka fall into complexes A-C and the site dates to between 41 - 24 ka (Lbova, 2008, 2000, 1999; Orlova et al., 2005; Zwyns and Lbova, 2019). As with other IUP sites in the region, Kamenka has a rich assemblage of stone and bone tools, alongside classic artefact types including beads, awls, and rings (Zwyns and Lbova, 2019). A worked fragment of goose bone, believed to be a whistle was also identified (Lbova, 2010; Lbova et al., 2010). This whistle from Kamenka and the flute identified at Khotyk are the earliest known examples of musical instruments in Siberia and add to the further evidence such as the flutes excavated from Aurignacian (43 - 35ka) sites in Germany (Conard et al., 2009; Higham et al., 2012).

Ust'-Karakol

Ust'-Karakol is an open-air site located 2 km upstream from Denisova Cave at the confluence of the Anui and Karakol rivers. It is a Middle-Upper Palaeolithic site with 19 cultural layers, revealing short term and repeated occupations until ~35 ka (Derevianko et al., 2005). The site has two excavation areas, Ust'-Karakol 1 and Ust'-Karakol 2. Most of the macroscopically identifiable fauna from the site are the remains of adult prey, with little evidence that hominins were targeting juvenile fauna (Derevianko et al., 2005). The presence of antler and deciduous teeth from horse and deer species suggests the site was used as a seasonal hunting camp (Baryshnikov, 1999).

Strashnaya Cave

Located in the Charysh River basin of the Northwest Altai, Strashnaya Cave is a stratified Middle-Upper Palaeolithic site (Zubova et al., 2017). Eight modern human teeth, all belonging to juveniles, were identified in the Upper Palaeolithic layers 3_1a (19,150 ± 80) (Zubova et al., 2017). These were found alongside blade and bladelet lithic technology, bone needles, a tool made from red deer antler, and pendants, buttons, and shells among others (Krivoshapkin et al., 2018). At present Strashnaya Cave represents the earliest securely known modern human site in the Altai Mountains. The Ust'-Ishim individual is significantly older (45 ka) (Fu et al., 2014),

however it is without an archaeological provenance. Excavations between 1988-2008 produced 102,000 bone fragments from the site, however more than 73% could not be identified on the basis of their morphology (Vasiliev and Zenin, 2009). Of those that could be identified, they represented 43 different mammal species, the majority of which are the remains of small vertebrates (Serdyuk and Zenin, 2014).

Appendix 4.2 Supplementary Results

Sites in the Transbaikal displayed varying levels of collagen preservation. Kamenka (n=341) produced the highest number of samples with enough collagen for taxonomic identification (83%). Unfortunately, at Podzvonkaya all but 7 of the samples from the Lower Complex (n= 36) failed to produce enough collagen for ZooMS identification. A much higher proportion of samples from the Eastern Complex of Podzvonkaya (n= 134) could be successfully identified (80%). At Khotyk (n= 224), 47% of samples failed ZooMS analysis.

The majority of samples which could be successfully identified for sites in the Transbaikal were Equidae, accounting for 33%, 25%, and 48% of the assemblages studied from Podzvonkaya, Khotyk, and Kamenka respectively. At Podzvonkaya and Kamenka, Cervidae/Gazella/Saiga were the next most abundant group (15% and 25%, respectively), likely reflecting the open steppe environments these sites are located within. At Khotyk, the second most abundant group was Rhinocerotidae (10%). Interestingly, an entire Rhino foot has been excavated from layer 3 of Khotyk (Lbova, 2010) which appears to have been an intentional burial, a common hallmark for symbolic behaviour of early modern humans in the IUP. The fragments of Rhinocerotidae bones identified within the ZooMS assemblage may be associated with this burial. Very few predators were identified within the fragmented assemblages, at Podzvonkaya one Canidae bone was identified within the East Complex; three Canidae and one Ursidae bone were identified at Khotyk; and a single Leporidae bone and two Ursidae bones were identified at Kamenka. Unusually, a single camel bone was identified at Kamenka and is currently undergoing further radiocarbon and genetic analysis. A single camel bone (Camelus sp.) had previously been identified at the site during excavations in 1993 (Germonpré and Lbova 1996). Camels were known in the deserts and steppes of Kazakhstan, Mongolia and China however their numbers have

significantly declined in the past century. The remains of camels have only been identified at two Pleistocene sites in the Transbaikal (Imetkhenov and Kalmykov, n.d.) but it is unclear if they were being exploited by humans (Germonpré and Lbova 1996).

In comparison with sites in the Transbaikal, the Altaian sites on average performed far better with 80% of samples from Ust'-Karakol (n= 107) and 91% of samples from Strashnaya Cave (n= 2,141) producing enough collagen for taxonomic identification using ZooMS.The majority of bones identified from Ust'-Karakol and Strashnaya Cave were Bos/Bison, at 23% and 34% respectively. At Strashnaya Cave, the high proportion of Bos/Bison bones, which likely represents *Bison priscus*, was identified alongside fairly even distributions of other major prey groups: Capra (8.6%), Cervidae/Gazella/Saiga (7.3%), Rhinocerotidae (6.2%), Equidae (5.9%), Elephantidae (5.5%), and Ovis (5.3%). Zooarchaeolgical analysis of the site had identified cave hyaena and wolves as the major predator groups for the site, and the likely contributors to the high rate of fragmentation at the site (Serdyuk and Zenin, 2014; Vasiliev and Zenin, 2009). Only two cave hyaena (Crocuta/Panthera) bones were identified for the site within the ZooMS assemblage, with Canidae (1.7%) and Ursidae (1.6%) dominating the ZooMS-IDed component. Ust'-Karakol had a much higher proportion of predators, with 9% of the assemblage identified as Canidae.

Appendix 5 - Catalogue of new hominin fossils from Denisova Cave

Denisova 7, parietal fragment (*Homo* sp.).

2008. East Chamber, Sector 6, Sq. D-3, Layer 11.3

This specimen was originally mis-identified as a cave bear parietal fragment. Several features, such as the shape of the supposedly coronal suture, the curvature in the coronal plane, the lack of meningeal grooves as well as the marked and sharp edged digital impressions made this non-human identification seem probable. ZooMS analysis however confirmed this fragment was a hominin (Manuscript F) and genetic analysis is currently underway.

Denisova 14, bone fragment (*Homo* sp.)

2012. East Chamber. Sector 6, Layer 9.3

This specimen was identified among the bulk fragment collection using ZooMS (ZooMS ID: DC3758) and is reported in this paper for the first time. Directly dated by AMS at 46,300 ± 2600 BP. Ancient DNA analyses failed to yield usable DNA (Manuscript A).

Denisova 15, bone fragment (Neanderthal)

2012. East Chamber, Sector 6, Layer 11.4

This specimen was identified among the bulk fragment collection using ZooMS (ZooMS ID: DC3573) and is reported in this paper for the first time. Directly dated by AMS at >50,200 BP. MtDNA DNA analyses indicate this is a Neanderthal (Manuscript A).

Denisova 16, bone fragment (*Homo* sp.)

2016. Main Chamber, Sector 4, Layer 9.1

This specimen was identified among the bulk fragment collection using ZooMS (ZooMS ID: DC4114) and is reported in this paper for the first time. Ancient DNA analyses failed to yield usable DNA (Manuscript A). Due to the small size of the bone radiocarbon dating was not performed.

Denisova 17, bone fragment (Neanderthal) (Fig. 1)

2011. East Chamber, Sector 6, Layer 12

This specimen was identified among the bulk fragment assemblage from layer 12 of the East Chamber using ZooMS (ZooMS ID: DC4969) and is reported in this paper for the first time. MtDNA analysis, summarised in Section 3 of the Supplementary Text, indicates this individual carries Neanderthal mtDNA.

Denisova 18, bone fragment (*Homo* sp.) (Fig. 1)

2012-2013. East Chamber, Sector 6, Layer 15

This specimen was identified among the bulk fragment assemblage from layer 15 of the East Chamber using ZooMS (ZooMS ID: DC7277) and is reported in this paper for the first time. MtDNA analysis, summarised in Section 3 of the Supplementary Text, was inconclusive due to present-day human contamination and low aDNA preservation in the sample.

Denisova 19, bone fragment (Denisovan) (Fig. 1)

2012-2013. East Chamber, Sector 6, Layer 15

This specimen was identified among the bulk fragment assemblage from layer 15 of the East Chamber using ZooMS (ZooMS ID: DC8846) and is reported in this paper for the first time. MtDNA analysis, summarised in Section 3 of the Supplementary Text, indicates this individual carries Denisovan mtDNA. The Denisova 19 and 21 mitochondrial sequences are identical and may belong to the same individual or maternal relatives.

Denisova 20, bone fragment (Denisovan) (Fig. 1)

2012-2013. East Chamber, Sector 6, Layer 15

This specimen was identified among the bulk fragment assemblage from layer 15 of the East Chamber using ZooMS (ZooMS ID: DC7795) and is reported in this paper for the first time. MtDNA analysis, summarised in Section 3 of the Supplementary Text, indicates this individual carries Denisovan mtDNA.

Denisova 21, bone fragment (Denisovan) (Fig. 1)

2012-2013. East Chamber, Sector 6, Layer 15

This specimen was identified among the bulk fragment assemblage from layer 15 of the East Chamber using ZooMS (ZooMS ID: DC8591) and is reported in this paper for the first time. MtDNA analysis, summarised in Section 3 of the Supplementary Text, indicates this individual carries Denisovan mtDNA. The mitochondrial sequence of Denisova 21 and Denisova 19 identical and may belong to the same individual or maternal relatives.

Appendix 6 - Supplementary Data

ZooMS Data

All of the data included in this dissertation can be downloaded at the below links. Each file contains raw m/z files and an associated ZooMS results file.

Denisova Cave:

https://data.mendeley.com/datasets/mzt6zspjbp/draft?a=3a091eb7-a728-45a3-a04b-aa52adefa997

https://data.mendeley.com/datasets/f2454wydnv/draft?a=41974958-608e-48c9-90f2-3d844135b2d4

Kamenka:

https://data.mendeley.com/datasets/y24f2wtj6z/draft?a=98146be8-7847-4d46-9bdc-e644cb4ed4eb

Khotyk:

https://data.mendeley.com/datasets/r8dfrnxgjv/draft?a=78d7d7ca-ef13-4d8d-ab81-7095553e3f6a

Podzvonkaya:

https://data.mendeley.com/datasets/72j2ddc4p5/draft?a=fad0788e-dfa4-475c-9c21-5338a943b166

Strashnaya Cave:

https://data.mendeley.com/datasets/zj6jh83r5r/draft?a=29e03d61-998f-45dc-9340-6cb8c511339c

Ust-Karakol:

https://data.mendeley.com/datasets/dsr5vcrmjm/draft?a=ccfe377c-0320-4e2f-a31b-be6c92ba89a2